NPQ in pennate diatoms : a simple phenomenon and tool to probe multi-level orchestration of photosynthetic regulations

Dany Croteau

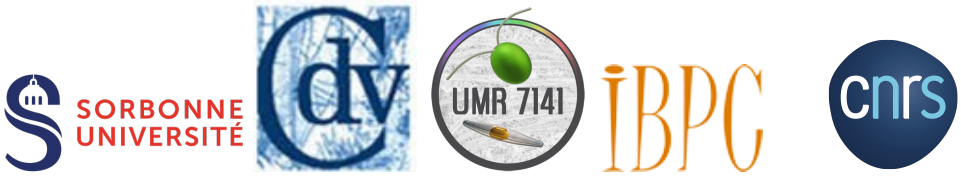

Sorbonne Université

Doctorate School: Complexity of Life Sciences (ED515)
CNRS - UMR7141 / Photobiology and Physiology of Plastids and Microalgae (P3M)

Ph.D. Thesis

NPQ in pennate diatoms: a simple phenomenon and tool to probe multi-level orchestration of photosynthetic regulations

Presented by Dany CROTEAU

Defended on the 22nd of October 2024,
at the Institute of Physico-Chemical Biology, Paris, France.

Ph.D. Jury:

President of the jury:	Stéphane LEMAIRE
Examinator:	Roberta CROCE
Examinator:	David KRAMER
Reviewer:	Stefania VIOLA
Reviewer:	Bernard LEPETIT
Supervisor:	Benjamin BAILLEUL
Invited member:	Johann LAVAUD

To the photosynthetic organisms
That have been cleaning our mess for the last 200 years.
And may they continue to do so
And preserve the beauty of the world in which Taluna will grow.

Remerciements

Les quatre années passées à Paris pour réaliser mon doctorat ont été remplies de beaucoup de changements, de progrès et de beaux moments, autant sur le plan académique que personnel. Plusieurs personnes ont participé à rendre cette expérience si mémorable et enrichissante. Ces prochaines lignes leur sont dédiées.

Tout d'abord, merci à mon superviseur Benjamin. Merci de m'avoir fait confiance, d'avoir offert cette opportunité à un jeune Québécois en sandales rencontré lors d'un congrès à Zagreb, d'avoir écouté mes arguments plus ou moins bien construits pour tester différentes hypothèses/manips, et de m'avoir permis de participer à autant de collaborations et de conférences, élargissant ainsi mes horizons scientifiques. Merci pour ton dévouement, ta disponibilité, ton enthousiasme et ta curiosité scientifique. Ce fut une véritable chance de grandir en tant que scientifique sous ta direction. Au plaisir de nos futurs échanges, autant en tant que collègues qu'amis.

Merci également à Angela et Marianne, qui ont permis de faire de cette thèse un véritable projet multidisciplinaire, intégrant biologie moléculaire et biochimie à l'approche principalement biophysique de Benjamin et moi. Merci d'avoir répondu à nos questions parfois naïves, et surtout à Marianne pour avoir accompli la tâche fastidieuse de m'apprendre à réaliser (ou du moins à essayer) des Western blots et des extractions d'ARN. Merci à Angela de m'avoir accueilli dans son laboratoire. Merci également à Alexandre pour son aide et sa patience pour répondre à nos questions de bioinformatique tout aussi naïves. Merci à Francis-André d'avoir enrichi mon expérience en partageant ses conseils, perspectives et connaissances, ainsi que pour ses relectures de mes travaux. Merci à Julien, qui arrivait toujours à la rescousse pour résoudre des problèmes techniques sur le JTS, problèmes dont je ne prenais conscience qu'après avoir centrifugé 1 L de culture ! Merci aussi à Wojciech. Les deux dernières années de thèse ont été rendues meilleures grâce à son arrivée au labo. Ce fut un plaisir de pouvoir discuter biophysique avec un ami, même si ce sont nos discussions sur la musique, la politique, l'économie, ainsi que les soirées passées ensemble, qui m'auront le plus marqués! Mon statut d'expatrié dans la labyrinthique administration française a mené à plus d'une situation abracadabrante. Je me dois de remercier encore une fois Angela et Benjamin, mais aussi Danielle et Yves, qui ont passé énormément de temps à me sortir de ces différentes embûches.

Merci à tous les membres de l'UMR7141, à la base de l'ambiance conviviale et unique du laboratoire. Ce fut un honneur de réaliser ma thèse dans ce laboratoire et cette institut si riches d'histoire. Merci à tous les "non-permanents" du labo dont les chemins ont croisé les miens (impossible de tous et toutes les nommer!), toujours partants pour organiser un pot et aller prendre un verre après le travail (et Sandrine et Stephan qui sont tout comme des "non-permanents" dans ces circonstances festives). Je dois admettre que l'ambiance du laboratoire me manque déjà, en dépit des réunions générales du jeudi matin ! Merci enfin à tous ces collègues qui m'ont permis de contribuer à leurs projets et d'aborder de nouvelles questions scientifiques.

Je tiens aussi à remercier Ian Probert et Martin Gachenot pour leur accueil à la Station

Biologique de Roscoff lors de notre campagne d'étude sur l'allélopathie à l'été 2021. Merci aux membres de mon comité de thèse, Bénédicte Charrier, Bernard Genty et Johann Lavaud, d'avoir suivi mon parcours, commenté mes avancements et de s'être déplacés à Paris pour les rencontres.

I would also like to thank all the members of my defense jury for reading my manuscript and providing their insightful comments, which have greatly enhanced this final version and the papers that will result from it. I am particularly grateful to the jury members for accepting our invitation to travel by train for environmental reasons, especially Bernard, who made the journey all the way from Rostock! It was an honor to defend my work before such a knowledgeable and distinguished jury.

Merci à toute la famille de la MEC, à l'origine de fous rires et de soirées inoubliables : Adrien, Henri, Fred, JF, Kyrian, Laurent, Rachèle, Sam, Thom et Thom. Merci également à France, la directrice de la MEC, qui a été d'une aide immense pour Nitaya et moi en nous accueillant pour une quatrième année et en permettant à Taluna de devenir la première résidente née à la MEC. Merci aux amis à la maison, qui s'ajustaient à notre agenda impossible pour passer un moment ensemble lorsque nous étions de passage, et à ceux qui sont venus nous visiter à Paris. Merci à ma famille, mes parents et mes sœurs, pour leur soutien inconditionnel et leurs encouragements. Merci particulier à ma mère, Douane et Caro, qui sont venues nous donner un coup de main en France à la suite de la naissance de Talu.

Enfin, merci à Nitaya de m'accompagner depuis le début de cette aventure en recherche et de lui donner son sens. Merci d'être venue avec moi dans "une ville de rêve" pour cette étape de nos parcours, d'être toujours là pour faire au moins semblant d'écouter mes problèmes de travail, et de ne pas trop juger mon horaire de fou. Merci d'avoir été partante pour toutes ces aventures, d'avoir traversé la frontière Albanaise sur le pouce 50°C, d'avoir parcouru le tour du Mont-Blanc en 8 jours et les falaises des Pays-Basques enceinte de 5 mois. Merci d'être ma meilleure amie, ma femme et la meilleure des mamans.

Contents

List of Figures

List of abbreviations

$\Delta\Psi$: Electric potential

ΔA : Absorption change

ΔpH : Proton concentration gradient

σ : Functional absorption cross-section

AA : Antimycin-A

AEF : Alternative Electron Flows

AOX : Alternative oxidase

ATP : Adenosine triphosphate

AX : Antheraxanthin

CBB : Calvin–Benson–Bassham cycle

CCM : Carbon Concentration Mechanisms

CEF : Cyclic Electron Flow

Chl : Chlorophyll

CS : Charge Separation

cyt. : Cytochrome

DCMU : N-(3,4-ichlorophenyl)-N-dimethylurea

DD : Diadinoxanthin

DD : De-Epoxidation State

DT : Diatoxanthin

DTT : Dithiothreitol

ECS : Electrochromic Shift

ETC : Electron Transport Chain

Fd : Ferredoxin

FCP : Fucoxanthin-Chl a/c-binding proteins

FNR : Fd:$NADP^+$ reductase

FPKM : Fragments Per Kilobase of transcript per Million mapped reads

FRET : Förster resonance energy transfer

LEF : Linear Electron Flow

LHC : Light-harvesting complex

MC : Metacluster

MGDG : Monogalactosyldiacylglycerol

$NADP^+$/NADPH : Nicotinamide adenine dinucleotide phosphate

NPQ : Non-Photochemical Quenching

OEC : Oxygen Evolving Complex

PC : Plastocyanin

PGR5 : Proton gradient regulation 5

PGRL1 : PGR5-like 1

pmf : Proton motive force

PQ/PQH_2 : Plastoquinone/Plastoquinol

PS : Photosystem

PsbS : Photosystem II Subunit S

Q : Quencher

Q_A/Q_B : Quinone A, Quinone B

qE : High-energy-dependent NPQ component

qI : Photoinhibition-dependent NPQ component

qT : State transition-dependent NPQ component

qZ : Xanthophyll-dependent NPQ component

PS : Photosystem

RC : Reaction centre

rETR : relative Electron Transport Rate

ROS : Reactive Oxygen Species

SHAM : Salicylhydroxamic acid

SP : Saturating pulse

SV : Stern-Volmer

TALEN : Transcription Activator-Like Effector Nucleases

TEF : Total Electron Flow

WT Wildtype

XC Xanthophyll Cycle

VDE : Violaxanthin De-Epoxidase

VX : Violaxanthin

ZX : Zeaxanthin

ZEP : Zeaxanthin Epoxidase

Abstract

Research on photosynthesis in marine microalgae has traditionally relied on models derived from studies of green organisms such as *Arabidopsis* and *Chlamydomonas*. However, these models do not fully account for the distinctions between primary and secondary endosymbionts. This divergence is evident in the study of non-photochemical quenching (NPQ) of chlorophyll *a* fluorescence, a key regulatory mechanism that protects photosystem II from excess light. In pennate diatoms, NPQ strictly depends on two key molecular components: the de-epoxidized xanthophyll pigment diatoxanthin (DT) and Lhcx family proteins, with Lhcx1 being the major constitutive one. Despite the clear link between NPQ and DT, several conflicting models of diatom NPQ exist, often unnecessarily borrowing the complexity of models from green organisms.

This thesis has two main objectives. First, it aims at understanding the nature and mechanism of NPQ in the model pennate diatom *Phaeodactylum tricornutum* by examining the roles of DT and Lhcx1. Second, it aims to provide a comprehensive understanding of the NPQ regulatory module: how NPQ influences the photosynthetic electron transfer chain and how this, in turn, affects NPQ.

In the first part of the study, 14 strains of *P. tricornutum*, including the wildtype and 13 mutated lines with variable Lhcx1 expression, were grown under two non-stressful light conditions. DT levels were modulated using short-term light stress, which allowed the creation of Lhcx1-DT matrices. These matrices demonstrated that NPQ is proportional to the product of Lhcx1 concentration and the proportion of DT in the xanthophyll pool. This suggests that the interaction between DT and Lhcx1, probably through DT binding to Lhcx1, forms a uniform Stern-Volmer quencher responsible for NPQ. Furthermore, the photosynthetic unit of pennate diatoms appears to follow a "lake" model, with discrepancies in the NPQ-photochemistry relationship potentially arising from unaccounted variables, such as cellular heterogeneity.

The second part of the thesis builds on these results to develop a "photoprotection dial" using various Lhcx1 mutants and adjusting high light exposure. This approach allows exploring how NPQ influences the photochemical phase of photosynthesis while holding other conditions constant. The results showed clear relationships between NPQ and the redox state of the photosynthetic electron transport chain, photoinhibition, and cyclic electron flow. The extent of NPQ was found to be linearly correlated with cyclic electron flow and inversely correlated with photoinhibition.

This approach is considered a preliminary step toward understanding the broader orchestration of photosynthetic regulatory modules, which represents a frontier in photosynthesis research. It allowed exploring how photosynthetic signals impact gene expression at a genome-wide scale, revealing that approximately half of the genes responded to high light conditions in a Lhcx1 (or NPQ)-dependent manner. Clustering these genes based on time of high light exposure and photoprotective capacity provided insights into groups with in-

variant expression (e.g., housekeeping and cell cycle genes), those significantly influenced by photoprotection (e.g., proteasomes, ribosomes, and photoprotection-related genes), and those regulated by light independently of Lhcx1 (e.g., genes related to light absorption and photosynthetic complexes).

Finally, a novel non-invasive method, based on the electrochromic shift of photosynthetic pigments, was developed to measure the absolute value of the proton motive force and its division into its electrical and osmotic components, ΔpH. This will facilitate studies of how the photosynthetic electron transfer chain affects the quantities and activities of molecular actors involved in NPQ via ΔpH, thus closing the loop of the NPQ regulatory module. Collaborative efforts also explored the interactions between photosynthesis, NPQ, and various aspects of diatom metabolism, including pH homeostasis, unique glycolysis-gluconeogenesis pathways, and circadian rhythms.

Résumé

Les recherches sur la photosynthèse des microalgues marines s'appuient traditionnellement sur des modèles dérivés d'études sur les plantes et microalgues vertes. Cependant, ces modèles ne distinguent pas entre endosymbiotes primaires et secondaires. Cette divergence est particulièrement criante dans l'étude de l'extinction non photochimique (NPQ) de la fluorescence de la chlorophylle *a*, un mécanisme de régulation essentiel qui protège le photosystème II de l'excès de lumière. Chez les diatomées pennées, le NPQ dépend strictement de deux composants moléculaires: le pigment xanthophylle déépoxydé diatoxanthine (DT) et les protéines de la famille Lhcx. Malgré le lien évident entre le NPQ et la DT chez les diatomées, plusieurs modèles contradictoires existent, souvent basé sur des modèles provenant d'organismes verts, inutilement complexes.

Cette thèse vise à atteindre deux objectifs principaux. Premièrement, elle vise à comprendre la nature et le mécanisme du NPQ chez la diatomée pennée modèle *Phaeodactylum tricornutum* en examinant les rôles de la DT et de Lhcx1. Deuxièmement, elle vise à fournir une compréhension globale de la manière dont le NPQ influence la chaîne de transfert d'électrons photosynthétique et comment celle-ci, à son tour, affecte la physiologie et le NPQ.

Dans la première partie de l'étude, 14 souches de *P. tricornutum*, dont le sauvage et 13 lignées mutantes avec une expression variable de Lhcx1, ont été étudiées. Les niveaux de DT ont été modulés par un stress lumineux de courte durée, permettant de créer des matrices Lhcx1-DT. Ces matrices ont démontré que le NPQ est proportionnel au produit de la concentration de Lhcx1 et de DT dans le pool de xanthophylles. Cela suggère que l'interaction entre la DT et Lhcx1, probablement via leur liaison, forme un "quencheur" Stern-Volmer homogène responsable du NPQ. De plus, l'unité photosynthétique des diatomées pennées semble suivre un modèle dit "lake", et les divergences dans la relation NPQ-photochimie proviennent potentiellement de variables non prises en compte, telles que l'hétérogénéité cellulaire.

La deuxième partie de la thèse s'appuie sur ces résultats pour développer un "contrôleur de photoprotection" en utilisant divers mutants Lhcx1. Cette approche permet d'explorer comment le NPQ influence la photochimie de la photosynthèse tout en maintenant les autres conditions constantes. Les résultats ont montré des relations claires entre le NPQ et d'autres processus photosynthétiques. Notamment, le NPQ était corrélé linéairement au flux cyclique d'électrons et inversement à la photoinhibition.

Cette approche peut être considérée comme une étape préliminaire vers la compréhension de l'orchestration plus large des modules régulateurs de la photosynthèse, une frontière dans la recherche sur la photosynthèse. Elle a permis d'explorer la manière dont les signaux photosynthétiques impactent l'expression des gènes à l'échelle du génome, révélant qu'environ la moitié des gènes réagissaient à des conditions de forte luminosité de manière dépendante du NPQ. Le regroupement de ces gènes en fonction du temps d'exposition à la lumière et du NPQ déployé a permis de distinguer les groupes à expression invariante (e.g. cycle

cellulaire), ceux significativement influencés par la photoprotection (e.g., ribosomaux et liés à la photoprotection) et ceux régulés strictement par la lumière (e.g., liés à l'absorption de la lumière).

Enfin, une nouvelle méthode non invasive a été développée pour mesurer la valeur absolue de la force motrice du proton et sa division en ses composantes électriques et osmotiques, ΔpH. Cette nouvelle méthode, basée sur le déplacement électrochromique des pigments photosynthétiques, facilitera les études sur la manière dont la chaîne électronique photosynthétique affecte les quantités et les activités des acteurs moléculaires impliqués dans le NPQ via le ΔpH, bouclant ainsi la boucle de rétroaction entre le NPQ et la photosynthèse. Des travaux collaboratifs ont également exploré les interactions entre la photosynthèse, le NPQ et divers aspects du métabolisme des diatomées, notamment l'homéostasie du pH, les voies de glycolyse-gluconéogenèse et les rythmes circadiens.

Chapter 1

Introduction

1.1 Diatoms' evolution, ecophysiology and contribution to global photosynthesis

When most people hear about photosynthesis, they think green, of trees and plants, of rain forests and flower fields. Indeed, human life is so deeply intertwined with terrestrial primary producers (if only through agriculture), that we easily forget that all the green surrounding us is in fact countless biological engines producing the oxygen we breathe. Plants and trees are also overwhelmingly abundant and store up to 90% of Earth's biomass (Bar-On et al., 2018). However, terrestrial ecosystems generate "only" 50% of global primary production, leaving an equal contribution up to marine ecosystems (Field et al., 1998). In the Ocean, most of photosynthesis is supported by extremely diverse unicellular microalgae (0.2 to 200 µm) communities, drifting with water masses, which form the phytoplankton and account for only $\approx$ 1% of global biomass. While green microalgae, the closest relatives to land plants[1] (Fig.1.1), are present in the phytoplankton they are not dominant. Rather, groups that evolved through secondary endosymbiosis; diatoms (part of Stramenopiles with brown algae), haptophytes and dinoflagellates, are dominant (Pierella Karlusich et al., 2020) and due to their carotenoid pigments, the world of marine photosynthesis is more brown than green. Therefore, understanding photosynthesis on a global scale and apprehending the consequences of anthropogenic climate perturbations requires a deep knowledge of the photophysiology of secondary endosymbionts[2], which we currently lack.

1.1.1 Evolution of the Chromista polyphyletic kingdom

The primary endosymbiosis event usually refers to the engulfment of a free-living cyanobacterium by a heterotrophic ancestor, which through genetic integration became the chloroplast in a eukaryotic cell and gave rise to Archaeplastida (land plants, green algae, rhodophytes (red algae) and glaucophytes) (Petersen et al., 2014). Secondary endosymbiosis refers to the engulfment of green and/or red algae which became the plastid (as opposed to the chloroplast

[1]Throughout this thesis, I refer to green algae as the microalgae representants of the Viridiplantae, including Ulvophyceae, Chlorophyceae, Trebouxiophyceae and prasinophytes. I use "green organisms" or "green lineage" to include land plants.

[2]Throughout this thesis, "secondary endosymbionts" refers to the microalgae capable of photosynthesis in the proposed polyphyletic kingdom of Chromista, to include haptophytes with the SAR supergroup comprising of Stramenopiles, Alveolates and Rhizaria.

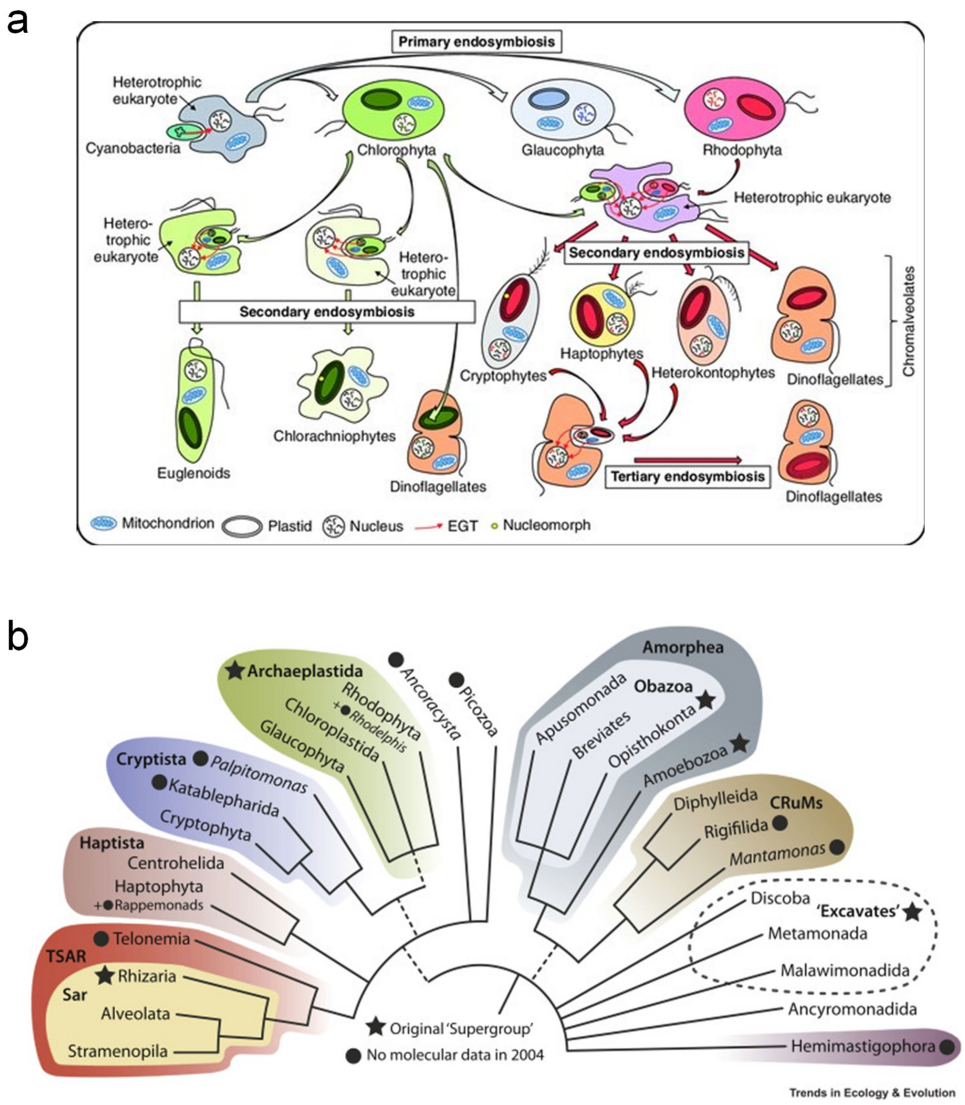

Figure 1.1: a) Schematic representation of primary, secondary and tertiary endosymbiotic events and endosymbiostic gene transfer (EGT) over microalgae evolution (from (Hopes and Mock, 2015)). b) Consensus of the "new" eukaryotic tree of life based on multiple recent phylogenomic studies (from (Burki et al., 2020)).

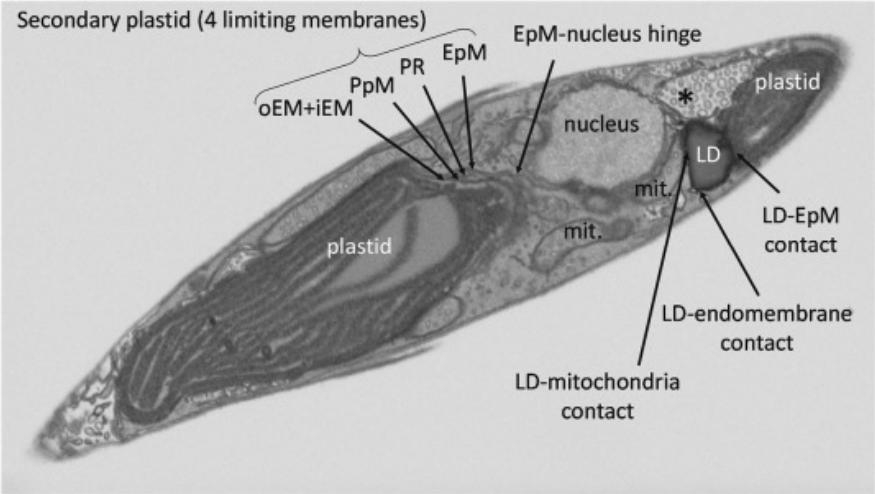

Figure 1.2: Cell of the model pennate diatom *Phaeodactylum tricornutum* under transmission electron microscopy, highlighting the four membranes around their secondary plastid, and showing other organelles and compartments (from Lupette et al., 2019). iEM, chloroplast inner envelope membrane; LD, lipid droplet; mit, mitochondria; PR, periplastid reticulum; PPM, periplastid membrane; oEM, chloroplast outer envelope membrane; EpM, epiplastid membrane; *, an uncharacterized endomembrane compartment.

which is strictly speaking for chlorophyll a/b containing plastids, found in the green lineage) of new phyla. Historically, a rather simple (single event) scheme was largely accepted, in which an engulfed red algae ancestor gave rise to the Chromealveolates group, comprising diatoms, haptophytes, dinoflagellates, and cryptophytes (Cavalier-Smith, 1998). However, the advent of genomic studies undermined the support for this hypothesis, arguing that several events of endosymbiosis with eukaryotic ancestors could have occurred (Moustafa et al., 2009, Stiller et al., 2014, Novák Vanclová et al., 2024), and that the Chromealveolates group is polyphyletic (now redefined as the Chromista kingdom which also includes heterotrophic and parasitic unicellular organisms like *Paramecium* and *Plasmodium*) (Burki et al., 2020) (Fig.1.1), with several taxa containing genes of both green and red origins (Dorrell and Smith, 2011), as well as bacterial genes acquired through horizontal gene transfers (Vancaester et al., 2020). In the case of dinoflagellates, tertiary endosymbiosis has also been an important evolutionary driver (Yoon et al., 2005). Endosymbiosis theory debates are beyond the scope of this thesis, but this complex evolutionary history gave rise to a diverse array of metabolic pathways used in the Chromista kingdom which is crucial to keep in mind when comparing functional photosynthesis between green organisms and secondary endosymbionts. For example, diatoms retained the urea cycle (absent in plants but present in animals and fungi) (A. E. Allen et al., 2011), which has deep implications for understanding their nitrogen and amino acids metabolism (Smith et al., 2019). Also, differently from most plants, the lower-half of the glycolysis-gluconeogenic pathway takes place in the plastid rather than in the cytosol in diatoms (Dorrell et al., 2024). Another crucial physiological consideration stemming from secondary endosymbiosis is that it led to four membranes, rather than two, enclosing the cytosol and plastid (Flori et al., 2016)(Fig.1.2). As of now, the implications of this increased compartmentalization regarding gas exchanges and molecular trafficking (just to cite a few) have been scarcely explored.

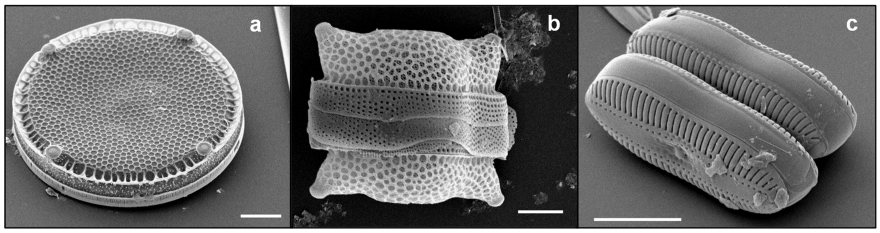

Figure 1.3: Electron micrographs of three diatom species, the centrics (Mediophyceae) a) *Eupodiscus radiatus* (20 µm scale bar) and b), *Biddulphia reticulata* (10 µm scale bar), and c), the raphid pennate *Diploneis* sp. (10 µm scale bar) (adapted from J. Bradbury, 2004).

1.1.2 Evolution of diatoms

From microfossil records and molecular arguments, the evolution of diatoms is believed to have happened about 200 million years ago (Nakov et al., 2018, Medlin, 2016), making them a relatively recent group with respect to the appearance of the first photosynthetic eukaryotes estimated at 1-to-2 billion years ago (Betts et al., 2018). Diatoms are typically separated into two main groups (Falciatore et al., 2020), initially defined on the basis of their cell symmetry. The centrics display radial symmetry and comprise the radial Coscinodiscaceae, from which evolved the bipolar Mediophyceae. The more recently evolved pennates show longitudinal symmetry and are split into subgroups depending on the presence of a raphe, a tiny slit in the frustule allowing mucilaginous material secretion, permitting motility. The evolution of the raphe approximately 120 million years ago is hypothesized to have spurred the niche expansion of raphid diatoms into a wide range of habitats, including some of the most hostile to photosynthetic growth, such as polar sea-ice brine channels and intertidal mudflats. The richness of the raphid species exploded about 75 million years ago and they are now more diverse than all other diatom subgroups combined (Nakov et al., 2018).

A hallmark morphological innovation of diatoms is their silica-made cell wall, the frustule, which creates beautiful and highly diverse patterns (Fig.1.3). The frustule of diatoms also has profound implications for biogeochemical cycles, it forms the largest pool of biological silicon on Earth and also accelerates the sinking of senescent cells in the water column, which favors diatoms' large contribution to the biological pump (P. J. Tréguer and De La Rocha, 2013). Frustules are also exceptionally well preserved in sediments, and a lot of what we know about the last few 100 million years of our planet, we owe to diatoms and other organisms forming biogenic silica structures. From a primary production perspective, diatoms are particularly important among secondary endosymbionts as they are estimated to be responsible for roughly 40% of marine, and therefore $\approx 20\%$ of global, primary productivity (P. Tréguer et al., 2018). A key phenological feature of some species that contribute disproportionately to the massive productivity of diatoms is their ability to come together and enter a phase of explosive growth, i.e., to bloom. Blooms tend to be triggered by the return of hospitable conditions (whether it is a drop in predation or an increase in resources) over the seasonal cycle of different ecosystems (Behrenfeld and Boss, 2014). The seasonal diatom bloom is vital to the integrity of many aquatic ecosystems as it represents the main annual carbon influx in the trophic chain.

Although diatoms are, unarguably, one of the most successful photosynthetic groups on Earth, there is still a lot to be learned about the most fundamental aspects of their physiology, including how they regulate photosynthesis. Actually, two basic observations motivate most of the work undertaken by my collaborators and myself over the course of my Ph.D. **i**)

How photosynthesis is modeled, studied and explained in diatoms (and other secondary endosymbionts) is often an extrapolation of what has been discovered over close to a century of work on green organisms (mainly *Arabidopsis thaliana*, common crops like tobacco, tomato or spinach and the green algae models, *Chlamydomonas reinhardtii* representing Chlorophyceae and *Chlorella sorokiniana*, representing Trebouxiophyceae). Which we described as the "green paradigm" of eukaryotic photosynthesis in (Croteau et al., 2024). **ii**) The radically different environments in which diatoms thrive compared to land plants impose different constraints on photosynthesis. When additionally considering divergent evolutionary histories and molecular heritages, different cellular architectures, and the implications of uni- versus multicellular organisms, the fact that land plants serve as the gold standard for studying photophysiology across the phytodiversity is perhaps better described as a "paradox" than a "paradigm". A lot of time was spent contemplating these questions during my Ph.D., which has culminated in the publication of two literature reviews which form the Chapter 2 of this thesis. These reviews represent an important portion of the theoretical background that supported my work regarding the regulation of photosynthesis. Therefore, some crucial mechanisms that demand a formal presentation in any thesis about photosynthesis regulation will be voluntarily left out of this Introduction chapter, and rather explored in depth in Chapter 2.

Moreover, to strive towards a goal as ambitious as challenging the "green paradigm" of eukaryotic photosynthesis we needed a particularly convenient model organism. An organism that would perfectly highlight an inclination my supervisor and I already had at the beginning of my Ph.D., i.e., that at many levels photosynthesis regulations appear "simpler" in diatoms (and perhaps most secondary endosymbionts?), or at the very least, more convenient to study, than in green organisms. To be able to further support our claim with molecular data, we decided to work on the model pennate diatoms *Phaeodactylum tricornutum* , shown in Fig. 1.2.

In order to have a better perspective on these considerations, to which I will comeback in the "Approach" Section 1.5.1, and the state-of-the-art knowledge of photosynthesis regulations reviewed in Chapter 2, I will first overview some fundamental aspects of photosynthesis, covering the crucial methods and approaches that led to much of those discoveries. Finally, I will delve into a detailed exploration of nonphotochemical quenching (NPQ)—a key regulatory mechanism that underpins the entire approach of my thesis, which was not addressed in the aforementioned reviews.

1.2 Photosynthesis, or how Life creates carbon bonds out of light and water

Photosynthesis is the process by which living organisms harvest light energy to extract electrons from an initial donor to fuel the incorporation of carbon from inorganic sources into carbohydrates. In nature, primary electron donors are diverse and include hydrogen, sulfide and organic substrates. These different photochemical reactions are collectively termed "anoxygenic photosynthesis" because they do not release oxygen in the process of reducing carbon molecules and are performed by different groups such as purple and green (sulfur or nonsulfur) bacteria. Colloquially, and for the remainder of this thesis, photosynthesis refers to "oxygenic photosynthesis". Important genera of cyanobacteria are crucial contributors to this type of photosynthesis (Flombaum et al., 2013), but eukaryotic microalgae and land plants realize the bulk of it on global scale. In this process, the primary electron donor is a

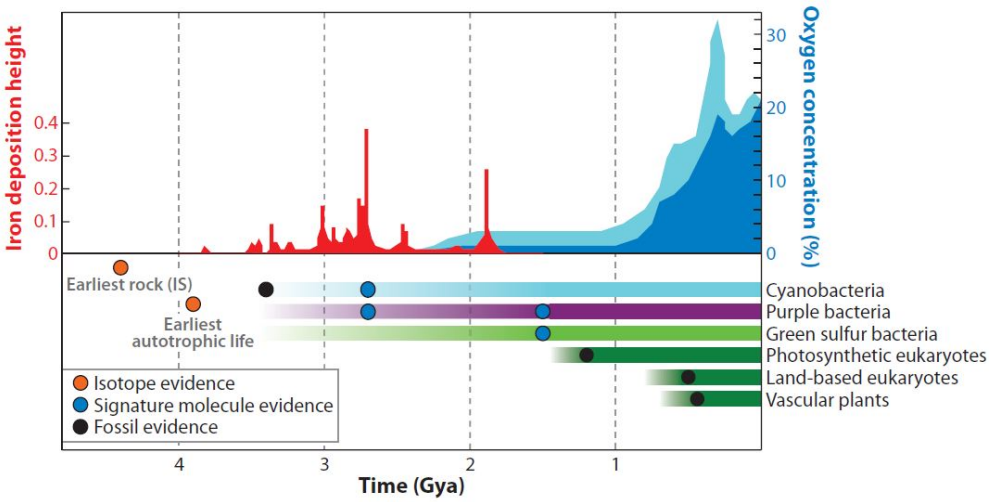

Figure 1.4: Evolution of diverse photosynthetic groups and the resulting consequences on the atmosphere composition over geological times, with a focus on the Great Oxygenation Event from (Hohmann-Marriott and Blankenship, 2011). The graph depicts the minimum (dark blue) and maximum (light blue) estimates of atmospheric oxygen concentration. Iron deposits are hypothesized to have buffered the initial rise of oxygen in the atmosphere, or as geological evidence of a form of anoxygenic photosynthesis. See reference for source data and further discussion. Gya; billion years ago.

water molecule; upon its photo-oxidation, electrons and protons are released and channeled into reducing power and the fuel for ATP synthesis, while O_2 release is a by-product (in the equation below, $h\nu$ is Planck's constant times the frequency of the photon).

$$6CO_2 + 6H_2O \xrightarrow{h\nu} C_6H_{12}O_6 + 6O_2 \tag{1.1}$$

The emergence of water photolysis is one of the most remarkable event in our planetary history and came about thanks to the evolution of type-II reaction centre (RC) bearing oxygen evolving complex (OEC) in an ancestral cyanobacteria lineage (Cardona, 2015). This biochemical innovation eventually led to the Great Oxygen Event (Fig. 1.4) which, by forcing a potent electron acceptor into forming $\approx 20\%$ of the atmosphere's composition, caused a mass extinction and, simultaneously, opened Earth's bioenergetic floodgates, which power the biodiversity as we know it today (Hohmann-Marriott and Blankenship, 2011). Quite wonderfully, water splitting is not only one of the most subverting evolutionary event to ever occurred but, also one of the most unlikely as it is extremely thermodynamically unfavorable with a Gibb's free energy of $\Delta G^\circ = 237.17$ kJ/mol.

1.2.1 The photochemical phase of photosynthesis and overview of the linear electron flow

Photosynthesis takes place in the plastid organelle (see the plastid of *P. tricorntutum* in Fig. 1.2), which is compartmentalized in the lumen and the stroma (in contact with the chloroplast outer envelope membrane), separated by the thylakoid membranes. Photosynthesis can be divided into a photochemical phase, which occurs in the thylakoid membranes and the lumen (see Fig. 1.1 in the review forming Section 2.2), and a non-photochemical phase, in which

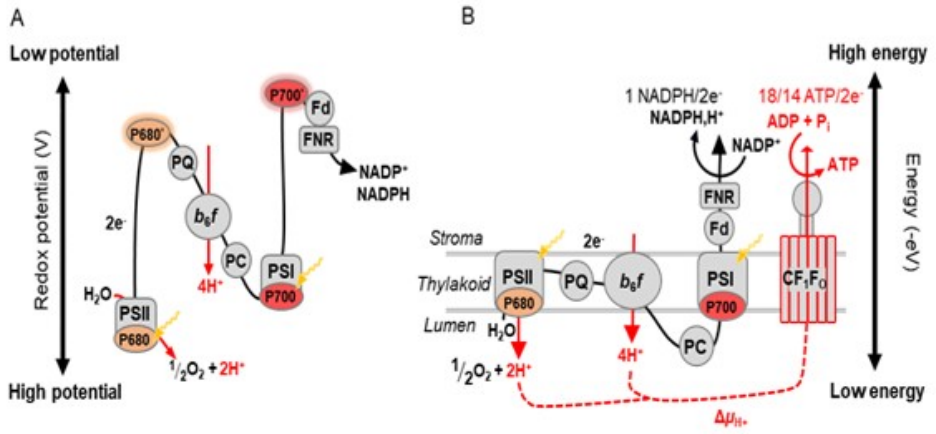

Figure 1.5: a) The LEF in the Z scheme of photosynthesis. b) Representation of the LEF in the thylakoid membranes (from Croteau et al., 2023). PSII, Photosystem II; PSI, Photosystem I; b_6f, cytochrome b_6f; CF_1F_O, CF_1F_O-ATPase; PC, plastocyanin; PQ, plastoquinol/plastoquinone; Fd, ferredoxin; FNR, Ferredoxin/NADP Reductase; $\Delta\mu H^+$, electrochemical proton gradient.

carbon reduction via the Calvin–Benson–Bassham (CBB) takes place in the stroma. The key distinction in the non-photochemical phase of photosynthesis between diatoms and green organisms are discussed in Croteau et al., 2024 (part of Chapter 2). Although there are countless crucial regulatory processes that influence the dynamics of the CBB, I will not be referring to those when "photosynthetic regulations" are discussed in my thesis, which focuses on the photochemical phase of photosynthesis. Therefore, the CBB will mainly be discussed from the perspective of the primary reducing power and ATP sink for the photochemical phase of photosynthesis.

The photochemical phase is driven by the concerted action of four major complexes embedded in the membranes of the thylakoids, which form sack-like structures (Fig. 1.1 in Section 2.2). Alike for the mitochondria electron transfer chain (ETC), it is the lipidic semi-permeable barrier between two aqueous compartments that permits to store the electrochemical proton gradient, or proton motive force (pmf), that fuels the conversion of ADP + P_i to ATP by the CF_1F_O-ATP synthase (the only of the four complexes that does not partake to electron transfer (Fig. 1.5). The two photosystems (PS) absorb light energy from photons, which excites electrons to higher energy states, enabling the PSs to carry out photochemical reactions. In the main linear electron flow (LEF), electrons extracted from water in the lumen at PSII are transferred along a redox cascade until reaching PSI, where a second photochemical step occurs to ultimately reduce $NADP^+$ to NADPH in the stroma. This is the classic Z-scheme first depicted by (Hill and Bendall, 1960) (Fig. 1.5a). The connection between the two PSs is made possible by two mobile shuttles. Downstream of PSII, electron transit through liposoluble plastoquinones (PQ), which form the PQ-pool together with its reduced form, plastoquinol (PQH_2). Upstream of PSI in the lumen, electrons are transported by the hydrophilic plastocyanin (PC), replaced by cytochrome (cyt.) c_6 in most diatoms (Groussman et al., 2015). The last photosynthetic complex, the cyt. b_6f makes possible the LEF (and most alternative electron flows (AEFs) extensively discussed in Section 2.1 and 2.2) and coordinates the activities of the two PSs. The oxidation of PQH_2 at the Q_O site of cyt. b_6f pumps two additional H^+ per electron transferred into the lumen (thanks

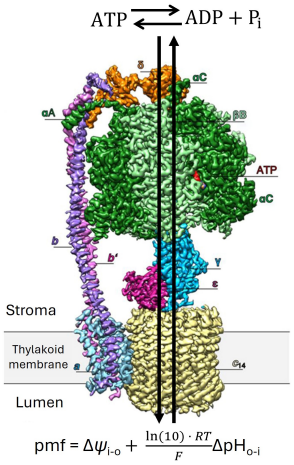

Figure 1.6: Representation of the proton motive force (pmf) driving the phosphorylation of ADP + P_i to ATP by the CF_1F_O-ATP synthase. See Hahn et al., 2018 for details about the crystal structure of the enzyme and Chapter 5 for details about the pmf partitioning between its osmotic (ΔpH) and electric gradient ($\Delta\psi$) components.

to the Q-cycle see Section 2.1) and is, most of the time, the kinetically determining step of the photosynthetic ETC with a turnover of ≈5-20 ms per electron transferred (Wilhelm and Wild, 1984, Sukenik et al., 1987). Two electrons are required to reduce NADPH and at least 3 H^+ are required per ATP molecule synthesized, so that the net equation of the photochemical phase of photosynthesis is usually written as:

$$2H_2O + 2NADP^+ + 3ADP + 3P_i + \xrightarrow{h\nu} 2NADPH + 3ATP + O_2 \tag{1.2}$$

Which, considering a maximal yield of 0.8 for PSII and of ≈1 for PSI, requires the absorption of 9 photons.

1.2.2 The coupling of electron transfer and proton pumping

We owe to Peter Mitchell the chemiosmotic theory (Mitchell, 1961) which provides the theoretical framing fpr how electron transfer (in the photosynthetic or mitochondrial ETC) is coupled to the pumping of proton into the lumen (or in the mitochondria intermembrane space), to ultimately produce ATP (Fig. 1.6). I will describe briefly the chemiosmotic theory in the case of oxygenic photosynthesis. Protons accumulating in the lumen, either via water photo-oxidation or the the cyt. b_6f turnover, store energy as an electrochemical proton gradient, or a proton motive force (pmf), that drives proton efflux through the CF_1F_O-ATP synthase and supplies the required energy for the phosphorylation of ADP+P_i to ATP (Mitchell and Moyle, 1967). Light energy is thus finally transduced into a chemical form, phosphodiester bonds, that is readily available for metabolic reactions. The pmf comprises two components: a chemical component, that depends on the proton concentration gradient between the two compartments (ΔpH) and an electric component, that depends on the difference in electric charge between the two membranes ($\Delta\psi$). Importantly, only protons participate to ΔpH, but all ions influence $\Delta\psi$ (Kramer et al., 2003, Armbruster et al., 2014). A key feature that sets the energy requirement for ATP production, is the stoichiometry of c subunits forming the rotor of the CF_1F_O-ATP synthase (Hahn et al., 2018). This feature varies among organisms of different origins (Turina et al., 2016) and considerations regarding

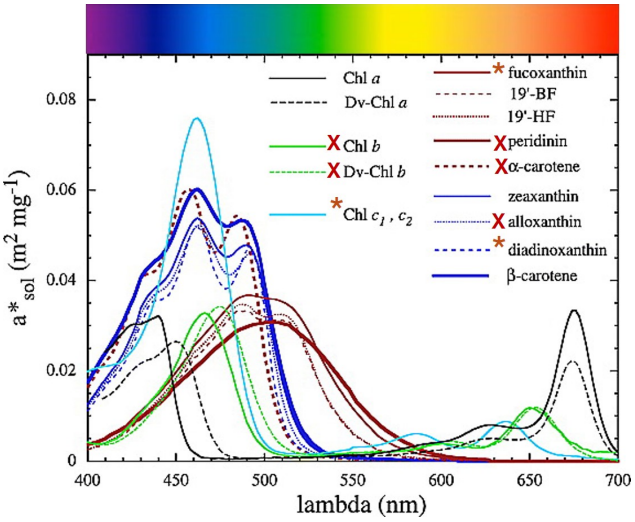

Figure 1.7: Estimated *in vivo* weight-specific absorption spectra of the main photosynthetic pigments $a^*_{\text{sol}}(\lambda)$ (in m^2 mg^{-1}) in phytoplanktonic samples collected in the water column of various regions. Adapted from (Bricaud et al., 2004), the brown asterisks indicate abundant pigments in diatoms used as markers of their presence and the red X are pigments not found in diatoms.

the H^+ catalytic requirements of the CF_1F_O-ATP synthase will be discussed from theoretical (Chapter 2) and experimental (Chapter 4) standpoints, later in my thesis. Another feature that I will discuss later, but that is useful to bear in mind from now, is that this reaction is reversible and depends upon the equilibration between the pmf and the $[ATP]/([ADP]+[P_i])$ ratio (see (Buchert et al., 2021) for instance).

1.2.3 Light absorption

Both PS comprise two functional parts. An intricate scaffold of proteins and light-absorbing pigments forms the light-harvesting complex (LHC), i.e., light harvesting antenna. In green organisms the main light-harvesting pigment is always chlorophyll (Chl) *a*, which has absorption peaks at 400-430 nm and around 678 nm. Red, ≈678 nm, photons have long been considered the energetic "red limit" of photosynthesis, but impressively some cyanobacteria evolved specialised red forms of Chl (e.g., *d* and *f*) and special protein-pigment organisation to extend the energetic limit of photosynthesis slightly beyond the visible spectrum (Nürnberg et al., 2018, Viola et al., 2022). In diatoms (and other secondary endosymbionts), a significant portion of pigments consists of various carotenoids, particular of the xanthophyll family, with fucoxanthin often found almost as abundant as Chl *a*. These green absorbing xanthophylls give the characteristic brown color to diatoms. Therefore, the light-harvesting complexes of diatoms are named fucoxanthin-Chl *a*/*c*-binding proteins (FCPs). FCPs contain other diatom-specific pigments, including various isoforms of the atypical, blue-green absorbing, Chl *c* (with no isoprenoid tail and in which porphyrin replaces the usual chlorin core) (Jiang et al., 2023), and no Chl *b* (abundant in plants) (Fig. 1.7). In all photosynthetic organisms, the structure, organisation and pigment content of the antenna determine its optical cross-section (optical-σ) (the wavelength-specific target area for absorbing incident photons). In natural conditions, or really in any conditions besides lab-maintained exponential growth, antenna content/organization, thus cross-section, is constantly adjusted in function of the

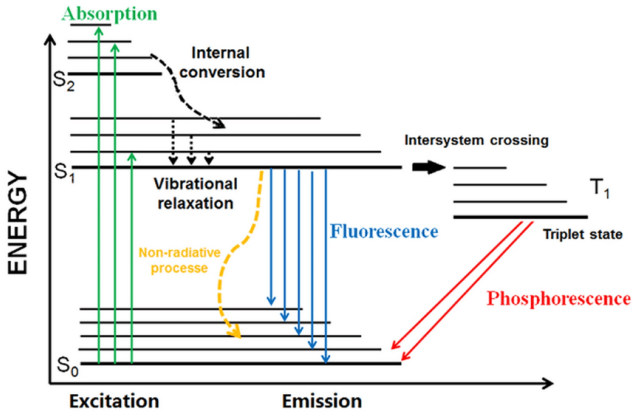

Figure 1.8: Representation of different excitation and de-excitation routes of a molecule in a Perrin-Jablonski diagram (from Schweizer et al., 2021).

light environment and the organism's metabolism over acclimation timescale (i.e., starting at the gene transcription level and which may only be completed after a few cellular divisions (discussed in more details in the introduction of Chapter 4).

When a photon is absorbed by a pigment, its energy is transferred by moving an electron from the ground (S_x) to an excited state (S_x). This exciton is highly unstable and its energy is transferred within the antenna via Förster resonance energy transfer (FRET) from one pigment to another in a close vicinity extremely quickly (ps scale) so that it is (at least partially) delocalized (Croce and Van Amerongen, 2014). The energy is eventually dissipated via one of three competitive processes **i**) Fluorescence, that is, the emission of a red-shifted photon, **ii**) Nonradiative decay pathways, mostly internal conversion and vibrational relaxation, which release heat. But, some nonradiative decay can also occur via intersystem crossing (electron spin flip), which has great biological implications as it generates triplet-state which can decay via phosphorescence but, are also highly susceptible to collisional quenching with O_2 leading to the formation of toxic reactive oxygen species (ROS) and, **iii**) The exciton is funneled to a "special" Chl pair in the RC of either PS (P680 and P700, see Fig. 1.5) and triggers charge separation (electron transfer) described in the next section (Fig. 1.8).

1.2.4 Photochemistry and water oxidation

The formation of radical pair and the physical separation of the positive and negative charges are made possible through a precise network of co-factors within PSII and PSI (see Fig. 1.9). When excitonic energy reaches the P680, or P700, radical pairs are formed, either $P680^+/Pheo^-$ (pheophytin) or $P700^+/F_X^-$. Through evolution, both PSs evolved to favor the *forward* transfer of the electron pulled from the special Chl pair, as opposed to futile back-reactions. This is possible thanks to the evolution of precise organisations between electron carriers in close proximity to each other and with increasing redox potentials (Rutherford et al., 2012). In PSI, electron can transit through either of the asymmetrical Chl *a*-phylloquinone branches to reduce the F_X-$F_A F_B$ iron-sulfur clusters. However, transfer through the B branch is roughly 20 times faster (15 versus 300 ns) (Santabarbara et al., 2015). Ferredoxin (Fd) is reduced by the F_X-$F_A F_B$ iron-sulfur cluster and plays the role of reducing power hub in the stroma (Fig. 1.9a). After photochemistry, $P700^+$ is rereduced by an electron from PC or cyt.c_6. PSII also has two branches located on the D1 and D2 core

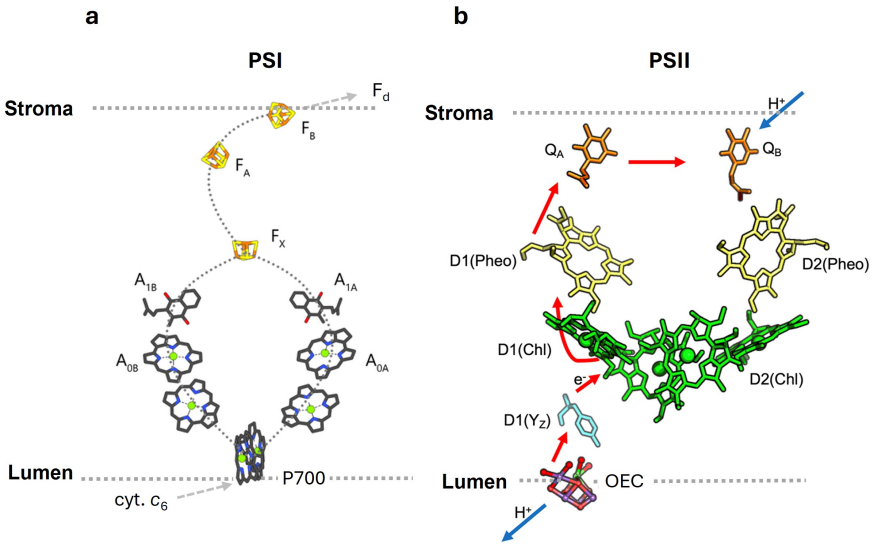

Figure 1.9: (a) The electron transport chain within PSI is depicted, starting from the luminal side with the P700 reaction centre, electrons are transferred a phylloquinone (A), to the iron-sulfur clusters (F_X-$F_A F_B$) and finally, to ferredoxin (F_d) on the stromal side, which is involved in the reduction of NADP+ to NADPH. (b) The electron transport within PSII starts at the oxygen-evolving complex (OEC), which oxidizes water, releasing protons into the lumen and transferring electrons first to a tyrosine residue in D1 (Y_Z), then to the P680 reaction centre. Following this, electrons pass to pheophytin (Pheo) and then to Q_A and ultimately Q_B, where protons are uptaken from the stroma, reducing a plastoquinone to plastoquinol (see (for more details, see Makita and Hastings, 2018) for PSI and (Kaur et al., 2021) for PSII).

sub-units, but electrons extracted from P680 only travel through the D1 branch, a structural adaptation to limit back-reactions and achieve the two-electron requirement for Q_A reduction (Rutherford et al., 2012). After photochemistry, $P680^+$ is rereduced by an electron from an intermediate tyrosine residue (Y_Z) which itself retrieves electrons from the OEC and its Mn_4CaO_5 cluster protruding in the lumen (Fig. 1.9b). The Mn_4CaO_5 acts as a capacitor and accumulates oxidative power with every electron given to Y_Z, cycling through 5 different states. When the Mn_4CaO_5 reaches four positive charges, it oxidizes two water molecules at once. While the oxidation-cycle of the Mn_4CaO_5 leading to O_2 evolution has been postulated 60 years ago (Joliot, 1965), the molecular intricacies of the reaction are still hotly debated in the photosynthesis community (Lubitz et al., 2019).

Thus, a given RC can only perform charge separation and participate in photochemistry if, when excitonic energy is received at the special Chl pair, it has access to an available electron donor and acceptor. When that is the case, we say that the RC is "open". Otherwise, it is "closed". Different spectroscopic methods exist to assess the proportion of open and closed RCs for PSI and PSII. PSII is open when P680 is reduced and Q_A is non-reduced, and PSI is open when P700 is reduced and the iron-sulfur clusters are oxidized.

1.3 Spectroscopic methods to study photosynthesis

When studying photosynthetic functioning, it is crucial to quantify its output. This can involve measuring various products, ranging from macro observations that integrate many variables, such as biomass accumulation or the incorporation of radio-labeled carbon, to more process-specific approaches like O_2 production by PSII. Nevertheless, the methods that were the most fruitful in the history of photosynthesis research are not intended to measure its products directly. Instead, they use specific absorption or emission spectral signatures to infer the activity of the different complexes of the ETC. The following sections describe two of the main methods that were extensively used over the course of my thesis and review key principles behind the use of these methods. One allows to probe the activity of PSII, with variable fluorescence, and the other, the activity of PSI, with P700 redox-dependent absorbance change.

1.3.1 Transient absorption spectroscopy and P700-related signals

The functioning of photosynthesis induces changes in the absorption of photosynthetic pigments. Those changes are small (variations of absorbance are typically of 0.01 to 0.1 %) but can be detected and provide important insights into photosynthesis. Two main features of photosynthesis functioning cause absorption changes (ΔA). First, the movement of electrons and protons across the thylakoid membranes generate an electric field which induces an electrochromic shift (ECS) of photosynthetic pigments, and changes in the absorption spectrum of the sample. Conversely, measuring these absorption changes due to ECS provides estimations of the electric potential component of the pmf, $\Delta\psi$, which is a very useful observable to study photosynthesis (Bailleul, Cardol, et al., 2010). ECS will not be presented in this section but rather in detail in the third experimental chapter of my thesis (Section 5.1) where it will be used extensively. Second, photosynthetic electron carriers are in turn reduced and oxidized. When their absorption spectra in the oxidized and reduced states are different, then any change in their redox state will give rise to an oxidized-minus-reduced ΔA that, again can be exploited to study the dynamics of specific steps of the photosynthetic electron transfer or to evaluate the redox state of various chemical species part of photosynthesis. Many molecules involved in the photosynthetic electron transfer undergo redox changes resulting in absorption changes but in this thesis, we will cover only the absorption changes related to the redox changes in the special pair of PSI, P700, and in the *c*-type cyt. involved in the electron transfer from the cyt. b_6f and PSI. In this section, I will describe P700-related signals, while *c*-type cytochrome signals will be described later (Section 4.2). In practice, both ECS and redox-dependent absorption changes are measured with the same device in our lab, the Joliot-type spectrophotometer (JTS-10, Biologic, France).

Compared to its reduced form, $P700^+$ absorption is decreased around 700 nm (and increased above 750 nm). Usually, the difference between 690-700 and 730-750 nm (or between 810-820 and 870-880 nm) is used to correct for the contributions of ferredoxin, plastocyanin (when present) and contributions from light scattering. In my work, I will be using 705 - 730 will (e.g., Godaux et al., 2015). The 810 - 870 method (e.g., (Klughammer and Schreiber, 1994) is the procedure used in the Walz systems, like the Dual-PAM-100 measuring system (Walz, Germany). Measuring the redox changes of P700 is a very efficient way to investigate PSI activity. Because the maximal quantum yield of PSI (ΦPSI) is $\approx$1 (Croce et al., 1996), redox-dependent absorbance change of P700, can be straightforwardly interpreted as changes in the concentration of "open" and "closed" RC (Klughammer and Schreiber, 1994). Indeed,

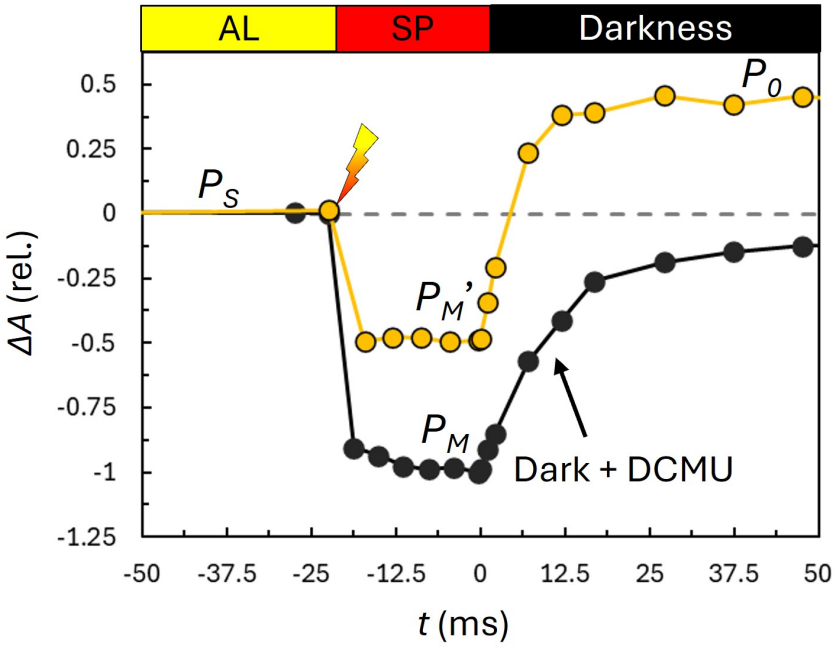

Figure 1.10: Typical P700 ΔA curves over a saturating pulse (SP) used to calculate the Φ of the different RCI populations under actinic light (AL) (570 µmol photons $m^{-}2\ s^{-}1$, yellow) or in darkness with DCMU (AL=0, black). The curves already have ΔA 730 nm substracted to the ΔA 705 nm signal, and Here, Ps has been arbitrarily set to 0 (baseline).

under a given actinic light intensity, the fraction of open RCI indicates the quantum yield (Φ) of PSI. Closed RCI can be either donor side limited by $P700^+$ (ΦND, which represents the amount of oxidized P700 under the actinic light exposure) or acceptor side limited by A_I^- (which regroups phylloquinones and F_X-$F_A F_B$) (ΦNA). By applying a short light saturating pulse (SP) (≈20 ms) on a dark-adapted sample, ideally supplemented with a PSII inhibitor like 3-(3,4-dichlorophenyl)-1,1-dimethylurea (DCMU) (which binds to PSII Q_B pocket), the maximal ΔA for fully oxidized $P700^+$ can be measured (P_M). Then, by exposing the same sample to actinic light, the steady-state absorption value can be measured (P_S, usually centered to 0). By superimposing a SP on the light-exposed sample, the minimal ΔA value can be measured; P_M' (which represents [photo-oxidable P700]) and the value to which ΔA returns in darkness shortly after the pulse is P_0 (which represents the concentration of P700 that were oxidized under illumination prior to the SP) (see Fig. 1.10). The sum of Φ for RCI in any of the three states must equal 1, therefore, Φ for each population can be calculated as:

$$\Phi\text{PSI} = \frac{P_S - P'_M}{P_0 - P'_M} \tag{1.3}$$

$$\Phi\text{ND} = -\frac{P0}{PM} \tag{1.4}$$

$$\Phi\text{NA} = 1 - \Phi\text{PSI} - \Phi\text{ND} \tag{1.5}$$

The relative electron transport rate of PSI ($rETR_I$) is calculated as $\Phi\text{PSI} \times E$. Absolute ETR per PSI can only be calculated if PSI antenna cross-section (σPSI) is measured, which is much more complicated than measuring yields (Flori et al., 2017).

While the calculation for ΦND is unanimously accepted, the calculation of ΦPSI remains debated in the community (two alternative methods are described in (Harbinson and Foyer, 1991) and (Klughammer and Schreiber, 1994)). In her thesis under Benjamin Bailleul's supervision, Suzanne Ferté demonstrated that these methods either overestimate ΦPSI by ignoring ΦNA (Harbinson & Foyer) or underestimate it by neglecting the effect of the SP in generating artefactual acceptor side-limitation (Klughammer & Schreiber). The "Ferte" calculation method used here was also validated using an alternative observable, ECS, and the reader is referred to her thesis for more details (Ferté, 2019). It is noteworthy that in diatoms, large acceptor side limitation is extremely rare, so that the three methods (Harbinson & Foyer, Klughammer & Schreiber or Ferté's method) give very similar results.

1.3.2 Variable chlorophyll *a* fluorescence as a probe of PSII activity

For any excited fluorophore (Chl *a* in solution for example), it is inevitable for a fraction of energy to be lost through non-radiative decay pathways (simplified as heat from now on) and fluorescence (F). For PSII antenna complex, an additional energy outlet is through photochemistry in the RCII (see Section 1.2.3). For PSII, the yield of energy lost as F (Φ_F) is relatively small and estimated between 2 and 8% (Trissl et al., 1993). But, as an observable, F is arguably the foundational phenomenon on which most of our understanding of photosynthesis is built. An inverse relationship between leaves F intensity and photosynthetic carbon assimilation has been observed since the earliest days of plant physiology research (Müller, 1874, Kautsky and Hilsch, 1931). Furthermore, a complementary relationship between F and photo-oxidation was also described more than 60 years ago (Delosme et al., 1959) and drove much of the research that led to the development of modern techniques using F as a window into PSII photochemistry.

Later, (Duysens and Sweer, 1963) hypothesized that F from photosynthetic material emanates from PSII and that its intensity/lifetime is correlated to the redox state of PSII first stable electron acceptor, Q_A (N.B., PSI fluorescence is believed *non-variable* and negligible by comparison, see Section 3.1). Therefore, F is maximal when all Q_A are reduced, and minimal when no Q_A is reduced (PSII donor side limitation is also rare in most conditions and seldom considered). This implies that the variations in energy lost as F and heat are always proportional and therefore that in photosynthetic organisms, variations in F can be seen as the inverse of variations in PSII photochemistry efficiency. Although, there are some criticisms/inconsistencies (Garab et al., 2023) and strong assumptions behind the Q_A-model of variable F (which I will discuss in Section 3.1), it is still extremely commonly used and almost universally accepted.

Considering a first-order kinetic competition model between F, intrinsic heat loss (H) and photochemistry (P), each process associated to its own constant rate (k)(Butler and Strasser, 1977), we obtain:

$$\Phi_F = \frac{k_F}{k_F + k_H + k_P[Q_A]} \tag{1.6}$$

$$\Phi_H = \frac{k_H}{k_F + k_H + k_P[Q_A]} \tag{1.7}$$

$$\Phi_P = \frac{k_P[Q_A]}{k_F + k_H + k_P[Q_A]} \tag{1.8}$$

By using a SP to fully reduced Q_A, P can be nullify to reach maximal Φ_F. Within this theoretical framework, F can be measured in different conditions to assess various photosynthetic parameters. For a given sample, F can be expressed as:

$$F = E \times \alpha \times \Phi_F \tag{1.9}$$

where E is the intensity of the light shone on the sample to induce F, α is a factor describing the instrument and sample, e.g., the geometry in the instrument, percentage of F detected, number of photosynthetic units and their average cross-section in the sample. The light used to probe fluorescence, the detecting light (DL), is said to be "non-actinic", i.e., its energy is too low to modify the redox state of PSII acceptors and its properties. Therefore, using a dark-adapted sample, for which it is usually assumed that Q_A=1, minimal fluorescence (F_0) can be probed by the DL. To measure maximal fluorescence (F_M), a SP (≈250 ms) is applied to reduce all PSII acceptors, Q_A=0, therefore photochemistry is abolished, before shining the DL. Both values allow calculating different parameters of PSII, like its maximum dark-adapted Φ (F_V/F_M), where F_V stands for *variable fluorescence* ($F_M - F_0$), is calculated as (see also Fig. 1.11):

$$F_V/F_M = \frac{F_M - F_0}{F_M} \tag{1.10}$$

This can be demonstrated as:

$$\frac{F_M - F_0}{F_M} = \left(\frac{k_F}{k_F + k_H} - \frac{k_F}{k_F + k_H + k_P[Q_A]}\right) \times \frac{k_F + k_H}{k_F} \tag{1.11}$$

from which we obtain,

$$\frac{F_M - F_0}{F_M} = 1 - \frac{k_F + k_H}{k_F + k_H + k_P[Q_A]} \tag{1.12}$$

then, replacing 1 by $\frac{\Sigma k}{\Sigma k}$ gives,

$$\frac{F_M - F_0}{F_M} = \frac{k_P[Q_A]}{k_F + k_H + k_P[Q_A]} = \Phi\text{PSII} \tag{1.13}$$

When the sample is exposed to the actinic light, minimal and maximal fluorescence are noted F and F_M', respectively, and ΦPSII is calculated as:

$$\Phi\text{PSII} = \frac{F'_M - F}{F'_M} \tag{1.14}$$

However, as the variable fluorescence method gained popularity, many experimenters reported a decrease in F_M' upon high light exposure, i.e., independent of Q_A redox state, which was termed *non-photochemical* quenching (NPQ) of PSII Chl *a* fluorescence. Different putative mechanisms were proposed to explain this phenomenon like an increase in non-radiative heat dissipation in the pigment bed (Krause, 1974, M. Bradbury and Baker, 1984, Demmig and Björkman, 1987, Genty et al., 1990), accumulation of altered PSIIs with distinct F properties (Weis and Berry, 1987), state transitions (Bilger and Schreiber, 1986) or a cyclic electron flow around PSII (Falkowski et al., 1986). We now know that, in most organisms, NPQ is a compound of processes (see Section 1.4), but for now, I will consider that NPQ is a heat dissipating mechanism, in kinetic competition with the other de-excitation pathways. Thus, I will simply consider NPQ as an additional outlet for exciton energy in a competition model, but for which the "constant rate" (k_{NPQ}) is variable. Hence, NPQ is understood

to provide photoprotection by increasing an alternative energy outlet for PSII when the availability of electron acceptors decreases, limiting the risk of generating highly unstable P680 triplet state, which can react with O_2 to form highly toxic $^1O_2$ (Krieger-Liszkay et al., 2008). In the presence of NPQ (under illumination or after light exposure in darkness during NPQ relaxation), equations 1.6 to 1.8 are rewritten accordingly:

$$\Phi_F = \frac{k_F}{k_F + k_H + k_{NPQ} + k_P[\mathrm{Q_A}]} \tag{1.15}$$

$$\Phi_H = \frac{k_H}{k_F + k_H + k_{NPQ} + k_P[\mathrm{Q_A}]} \tag{1.16}$$

$$\Phi_P = \frac{k_P[\mathrm{Q_A}]}{k_F + k_H + k_{NPQ} + k_P[\mathrm{Q_A}]} \tag{1.17}$$

$$\Phi_{NPQ} = \frac{k_{NPQ}}{k_F + k_H + k_{NPQ} + k_P[\mathrm{Q_A}]} \tag{1.18}$$

With ΦNPQ and ΦNO (regrouping Φ_F and Φ_H) always summing up to 1 with ΦPSII and calculated as:

$$\Phi\mathrm{NPQ} = \frac{F}{F'_M} - \frac{F}{F_M} \tag{1.19}$$

$$\Phi\mathrm{NO} = \frac{F}{F_M} \tag{1.20}$$

Similar to rETR in PSI, $\mathrm{rETR_{II}}$ under a given E can be calculated as:

$$\mathrm{rETR_{II}} = E \times \Phi\mathrm{PSII} \tag{1.21}$$

Beyond variable fluorescence being a more sensitive and user friendly method than absorption difference spectroscopy, two additional features of PSII have made the measurements of PSII ETR much more commonly used than $\mathrm{rETR_I}$ **i)** PSII photochemistry has a specific product in O_2 which can be used to validate the F measurements. A clear linear relationship has been observed between $\mathrm{rETR_{II}}$ and O_2 evolution in both plants (Genty et al., 1989, Harbinson et al., 1990, Krall and Edwards, 1990) and marine microalgae (including *P. tricornutum*) (Geel et al., 1997, Flameling and Kromkamp, 1998) under a wide range of light intensities (barring very limiting and supersaturating E) and growth conditions. **ii)** There is an accepted method to measure PSII antenna cross-section (σ_{PSII}) with fluorescence rise kinetics (Mauzerall and Greenbaum, 1989), which can be used to estimate absolute ETR and compared different samples/conditions or actinic light quality (colour).

All of these parameters and more (see reviews Kramer et al., 2004, Klughammer and Schreiber, 2008, Lazár, 2015, and also Appendix I at the end of Chapter 3) are now automatically calculated in commercially available fluorometers (Schreiber, 1986, Gorbunov and Falkowski, 2022, Kolber et al., 1998), and with this powerful and non-invasive method, measurements of ΦPSII and NPQ have become routine. Variable fluorescence is often used to take on macroscale questions and provide relative answers, like when monitoring phytoplankton productivity along certain hydrographical regions (Falkowski et al., 2017, Sezginer et al., 2023) or screening crop fitness to enlighten varieties selection (Baker and Rosenqvist, 2004, Harbinson et al., 2012). However, when, like in the case of my Ph.D., variable fluorescence is used to investigate photophysiology at the mechanistic level (Lavaud, Rousseau, van Gorkom,

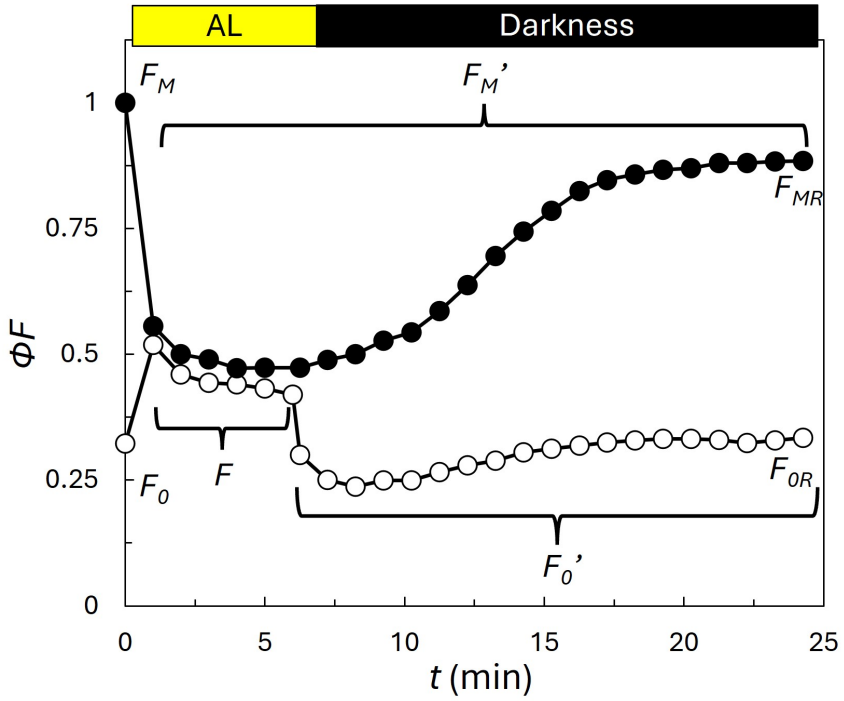

Figure 1.11: Typical protocol over which the induction of NPQ (under actinic light (AL)) and relaxation in darkness are monitored in *Phaeodactylum tricornutum* wildtype, to show the different fluorescence measurements used for the calculation of various PSII parameters (see text for details).

and Etienne, 2002, Giovagnetti and Ruban, 2017, Taddei et al., 2018, Buck et al., 2019, to cite only studies proposing a mechanistic model for pennate diatoms NPQ), one must be aware of the hypotheses and assumptions that birthed the development of user-friendly, "click and collect data", fluorometers and the limits that they bear.

Some of these assumptions became apparent with the early attempts to model NPQ. After observing a linear relationship between nonphotochemical fluorescence quenching and the concentration of the zeaxanthin (ZX) xanthophyll pigment in the evergreen shrub *Hedera canariensis*, (Bilger and Björkman, 1990) proposed that ZX could act similarly as a Stern-Volmer (SV) homogeneous quencher (Q). The SV-model was first introduced to describe *intermolecular* deactivation, as opposed to *intramolecular* deactivation processes like F and nonradiative pathways, for fluorophores in solution. Basically, relaxation to the ground state via heat release can be accelerated when another chemical species in the vicinity of the excited fluorophore interacts with it and therefore quenches F. The non-linear relationship between the concentration of a quencher $[Q]$ and F decrease was formulated by Stern and Volmer (1919) as:

$$\frac{F_i}{F_q} = 1 + k_{SV}[Q] \tag{1.22}$$

Where F_i and Fq are F intensity in the absence and the presence of Q respectively, and k_{SV} is a Stern-Volmer rate constant, which is the product of the chemical couple quenching rate and the fluorescence lifetime in the absence of the quencher. In plants, this model is now dismissed, but the mode of calculation of the NPQ parameter to quantify the process of regulated heat dissipation, remains influenced by the Stern-Volmer law:

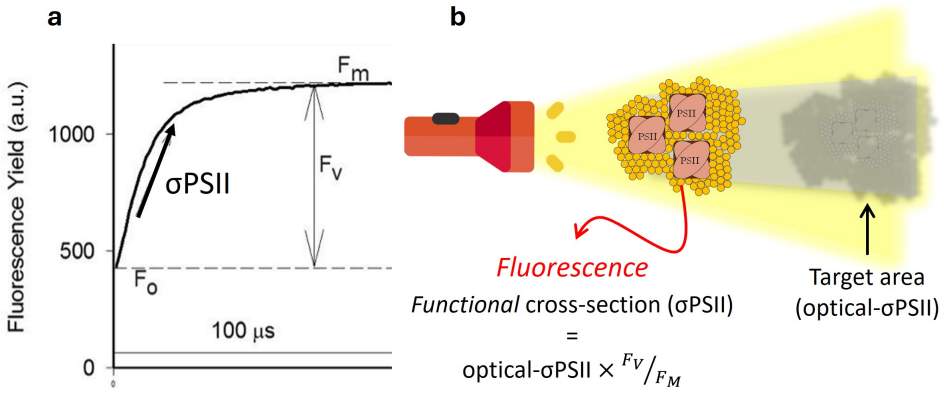

Figure 1.12: Typical fluorescence induction curve in a FIRe using single turnover flash (adapted from (Carvalho et al., 2016)) (A) and schematic representation of the difference between functional and optical σPSII (B) (see text for details).

$$\mathrm{NPQ} = \frac{F_M}{F'_M} - 1 \tag{1.23}$$

If one wants to quantify only the reversible part of NPQ (see Section 1.4 about NPQ mechanisms), the highest F_M' measured in the dark after relaxation (F_{MR}) can also be used as reference at the numerator (Fig. 1.11).

1.3.3 A quick word about the optical and functional cross-section of PSII

I previously referred to the optical-σPSII as the "wavelength-specific target area for absorbing impeding photons", which is an accurate definition, but an extremely impractical variable to measure in living systems. Instead, what is usually measured is the *functional* cross-section of PSII (σPSII), from fluorescence induction curves. Instead of measuring all photons absorbed by PSII antenna within a given photon flux, the rate at which absorbed photons lead to charge separation to generate Q_A^-, thus increasing fluorescence when the next photon is absorbed, is measured (Mauzerall and Greenbaum, 1989). In this case, σPSII is said to be *functional* because it depends upon the efficiency of PSII photochemistry as:

$$\sigma_{\mathrm{PSII}} = \mathrm{optical}\sigma_{\mathrm{PSII}} \times \frac{F_V}{F_M} \tag{1.24}$$

On a fluorescence induction curve, σPSII is inversely proportional to the area above the curve, or proportional to the velocity of the fluorescence rise (Fig. 1.12). This measurement can be made with any fluorometer and a DCMU poisoned sample (Malkin and Kok, 1966) or with a fluorometer equipped with extremely intense and short single turnover flash (which should reduce every Q_A only once). In my Ph.D., we took the latter approach by measuring σPSII with a Fluorescence Induction and Relaxation (miniFIRe) fluorometer (Gorbunov and Falkowski, 2022). However, the tricky part of calculating σPSII lies in the initial step of the induction curve which is largely affected by PSII connectivity (Stirbet, 2013). To limit the impact of this technical difficulty, the recommended approach is to measure σPSII once in the most stable, dark-adapted conditions, and then to assume the working hypothesis that any change in σPSII represents changes in ΦPSII rather than in the optical-σPSII. This is

not always true, for example in the case of state transitions for which some LHCs physically attached/detached from PSII (next Section 1.4). However, if NPQ arises only from variations in the magnitude of heat-dissipation processes in the antenna (like in the case of an SV-quencher), the same NPQ-dependencies is expected between σPSII and F'_V/F'_M (Mauzerall and Greenbaum, 1989, Gorbunov et al., 2001). Finally, it is also worth mentioning that the simple observation of a continuous fluorescence induction rise and the concept of σPSII is intrinsically incompatible with a perfect "lake model", whereby all RCIIs are sharing a common antenna. The lake model will be described in details in Section 3.1, where crucial assumptions behind the variable fluorescence model that may interfere with NPQ interpretations will be examined.

1.4 The different mechanisms and molecular actors of NPQ

I have now introduced NPQ as a *parameter* in the variable fluorescence model. However, NPQ is also broadly used to refer to the rapidly regulated biological *mechanism* by which photosynthetic organisms protect PSII from over-excitation when light absorption exceeds the rate at which reducing power can be consumed. This can create confusion as the NPQ *parameter*, by definition, refers to any decrease in maximal fluorescence compared to initial conditions. Therefore this includes, some processes like chloroplast movements (Kasahara et al., 2002), or Chl *a* bleaching and adjustment of pigment content which can occur over long experiments. Even technical bias, like cell sedimentation in a fluorometer cuvette, is strictly speaking "NPQ" if one talks about the *parameter*. However, when referring to NPQ the *mechanism*, what is meant is the sum of nonphotochemical processes that accelerates the decay of fluorescence lifetime in the photosynthetic antenna. In theory, NPQ provides photoprotection by decreasing exciton lifetimes, which decreases excitation pressure on PSII and limits the risks of generating toxic reactive oxygen species (ROS). NPQ is observed in virtually all phototrophs, but arises from collections of different components and their underlying mechanism, governed by a multitude of different molecular players and varying with acclimation conditions (Goss and Lepetit, 2015). Therefore, another difficulty in defining NPQ when doing comparison between organisms, or even between studies on a same organism, is the discrepancies in the nomenclature of the parameters and on what basis a given parameter is labeled. To add even more nuances, some processes like chloroplast movements mentioned above (Kasahara et al., 2002), and others described below, contribute to decreasing fluorescence *and* have photoprotective effects, but do not compete with photochemistry for excitons in PSII antenna, and therefore do not correspond to nonphotochemical quenching components *per se*. Historically, three NPQ components, mostly described in plants and green algae, were distinguished on the basis of their relative relaxation kinetics. Now, a mixture of distinctions founded on a molecular basis for model organisms and phenomenological resemblance to these components in less well-studied species is generally used. But the legacy of the three "historical" components by which NPQ = qT + qI + qE (explained below), still creates confusion.

1.4.1 The classical components of NPQ, from phenomenology to molecular actors

State transitions

State transitions refer to the migration of certain LHC from one PS to the other depending on the energetic state of the photosynthetic ETC. In *Chlamydomonas*, the redox state of the PQ-pool poise state transition by activating a specific kinase when it gets more reduced (Dumas et al., 2017). When the PQ-pool is oxidized, the system is described as in "State 1", upon increased reduction of the PQ-pool, LHCs typically associated to PSII are phosphorylated to PSI ("State 2") (Wollman, 2001). Functionally, state transitions redistribute energy between the two PSs(Nawrocki et al., 2016), which among others, alleviate the reduction pressure on PSII and increase the ATP/NADPH ratio output (by increasing cyclic electron flow discussed in Chapter 2) (J. F. Allen, 2003). Therefore, state transitions are a crucial feature of photosynthesis regulations, especially in organisms like green algae (Wollman, 2001, Lucker and Kramer, 2013) and cyanobacteria (Calzadilla and Kirilovsky, 2020) for which mixotrophic metabolism strongly interacts with the PQ-pool. However, the decrease in maximal fluorescence that comes with state transitions is due to a decrease of the optical-σPSII at the expense of increasing the optical-σPSI (included in α of Equation 1.9). Meaning that, although state transitions contribute to the NPQ *parameter*, they do not correspond to a nonphotochemical quenching process *per se*. Historically, state transitions were seen as the NPQ component relaxing under intermediate (min) scale and were labelled qT (Horton, 1996). Similar to state transitions (from State 1 to Sate 2), PSII-to-PSI spillover (Yokono et al., 2011), reduce pressure on PSII by transferring excitonic energy to PSI but without requiring physical movements of LHCs. So, PSII-to-PSI spillover also decreases fluorescence and can represent either *photochemical* or *nonphotochemical* quenching by PSI depending upon its open or closed state (closed PSI act as *nonphotochemical* quenchers (Butler, 1978)), but is rarely considered, perhaps wrongly, as NPQ. A huge advantage about working on NPQ with *P. tricornutum* (and possibly diatoms in general) is that these processes that complexify fluorescence data interpretation have never been reported. See (Owens, 1986) and discussion in (Lepetit et al., 2022) for state transitions and (Flori et al., 2017) for spillover.

Photoinhibition quenching

Historically distinguished by its long recovery time (up to hours) after intense light stress and requiring *de novo* synthesis of PSII core proteins D1 and D2 (Aro et al., 1993), photoinhibition quenching is termed qI. qI arises when PSII cores are photodamaged by one of two independent causes: **i)** Direct hit of the Mn_4CaO_5 cluster by blue/UV photons (Ohnishi et al., 2005), and **ii)** Photo-oxidation of amino acid residues in D1 or D2 proteins (Vass, 2012). Broken PSIIs can then act as non-photochemical quenchers. By definition, broken PSIIs also lose the ability to perform photochemistry. Therefore, distinguishing the "photoprotective" effect of broken PSIIs on remaining functioning PSIIs is a challenging task, especially considering the overlapping effects with other NPQ components, which has not been resolved yet. Additionally, there is a multi-step PSII repair cycle that counters the effects of photodamages on photochemistry by degrading broken PSIIs and restoring functional ones, which also influences fluorescence signals (Campbell and Tyystjärvi, 2012). As we learn more about the molecular actors of NPQ and the mechanism of qI at the molecular level (Nawrocki et al., 2021), it is likely that processes currently amalgamated with qI will be attributed to other mechanisms in the future. For example, the more recently identified qH component of NPQ relaxes on the same time scales as qI but relies on different molecular actors (with homologs

strictly associated with the green lineage for now) (Amstutz et al., 2020).

"High energy-dependent" quenching

The name "high energy-dependent" quenching (later termed qE) can be traced back to early observations of a correlation between the establishment of the transthylakoidal proton gradient (ΔpH) and fluorescence quenching (Krause, 1974). In most conditions and organisms, there is a ΔpH-dependent NPQ component that largely exceeds the others (barring massive photoinhibition) and is the "fastest" to relax. However, "qE" shows important differences between groups. For example, its typical relaxation half-time in darkness varies between $<$2 minutes in land plants (X.-P. Li et al., 2000) and $\approx$10-to-20 minutes in diatoms (see Fig. 1.11 for instance). This discrepancy reflects contrasts in processes involving distinct molecular actors, with overlapping effects in what the term qE encompasses. For most eukaryotic photosynthetic groups, the two most important categories of molecular actors involved in NPQ are **i)** Transmembrane LHC proteins of different families that directly react, through pH-sensing residues, to lower luminal pH and lead to an increase in fluorescence nonphotochemical quenching and, **ii)** Xanthophyll pigments that are part of swiftly regulated xanthophyll cycles (XC), where the accumulation of de-epoxidized species correlates with an increase of fluorescence nonphotochemical quenching. Addressing the roles of these molecular actors separately is challenging because they can have synergistic effects and both can be considered "high-energy-dependent" as they are regulated in some ways by luminal pH (Jahns and Holzwarth, 2012, Goss and Lepetit, 2015). Moreover, the kinetics of the XC can vary significantly between organisms and conditions. In plants, "high-energy-dependent" quenching strictly correlated to XC, and independent of direct ΔpH sensing by antenna proteins, exists but its kinetics are slow and can often be masked by qI. It was convincingly demonstrated only once mutants of the LHC involved in the faster and larger qE component were studied, and has been termed "qZ" (for zeaxanthin, see below) (Nilkens et al., 2010, Kress and Jahns, 2017). The importance of qZ in wildtype background is hard to determine, but it seems crucial to overcome harsh seasonal stress like cold-winter or dry periods in evergreen species, in which it is often termed "sustained NPQ" (Demmig-Adams et al., 2006, Verhoeven et al., 2018). In diatoms, the XC kinetics tend to be faster (Lavaud, Rousseau, and Etienne, 2002, Goss and Jakob, 2010), and NPQ dependent upon the accumulation of diatoxanthin is commonly termed qE. However, as we will see upon further examination of the characteristics of both molecular actor groups, it is likely that the major, and for some species/conditions the only, component of NPQ in diatoms is homologous to qZ, although it involves diatoxanthin. This is a central theme of my experimental work that will recur throughout this thesis.

1.4.2 The different xanthophyll cycles

In the 60s, building on the work of Yamamoto on spinach (H. Yamamoto et al., 1962), Hager began documenting xanthophyll (de-)epoxidation reactions characterized by the accumulation of the de-epoxidized xanthophyll forms under high light exposure and the reversal of these reactions in the dark, in diverse organisms, including the green lineage, but also in many secondary endosymbionts like diatoms, haptophytes, and dinoflagellates, among others (Hager, 1966, Stransky and Hager, 1970). By the time NPQ was discovered, much of the biochemistry of the "green lineage XC", or the violaxanthin-antheraxanthin-zeaxanthin cycle (VX, AX, ZX, VAZ-cycle), was elucidated (note that some green organisms also possess a lutein (Esteban et al., 2009) or loroxanthin cycle (Van den Berg and Croce, 2022)). Granted

the pH-dependence of the VX de-epoxidase (VDE), (H. Y. Yamamoto, 1979), it made ZX a natural molecular candidate for NPQ when it was observed in plants. This idea was reinforced by showing that, upon addition of dithiothreitol (DTT) to inhibit the VDE, NPQ is abolished (Demmig and Björkman, 1987, Bilger and Björkman, 1990).

In the **VAZ-cycle** (Fig. 1.13), the VDE catalyses both VX $\rightarrow$ AX and AX $\rightarrow$ ZX, starting from two epoxy groups on VX to finish with none on ZX. The VDE is located in the lumen, and is activated by dimerization upon acidification (with a pH optimum around 5.2) and requires ascorbate as co-factor (see XC reviews (Goss and Jakob, 2010, Goss and Lepetit, 2015)). Interestingly, the VDE is also redox-regulated via six disulfide bridges (the likely target for inactivation by DTT) (Simionato et al., 2015). Moreover, thylakoids regions enriched in the non-bilayer lipid monogalactosyldiacylglycerol (MGDG), forming inverted hexagon structures, are necessary to favour optimal de-epoxidation. The ZX epoxidase (ZEP), is a lipocalin protein, like VDE, but is located on the stromal side of the thylakoid. It catalyses the inverse reactions, epoxidizes ZX $\rightarrow$ AX and AX $\rightarrow$ VX, and utilises NADPH and O_2 as co-substrates. Typically, net epoxidation is seen in darkness or low light after light stress, although the ZEP is still active, but typically outrun by VDE, under light exposure (Küster et al., 2023). The regulation of the ZEP activity is source of debate, stromal pH (with its pH optimum at 7.5), phosphorylation, and redox control as potential regulators of its activity are suggested (Goss and Lepetit, 2015). However, some hypotheses are hard to reconcile with variations in ZEP rate under very low light and the strong buffering of stromal pH (Naranjo et al., 2016), and the apparent lack of effect of reducing agents on ZEP *in vitro* (Holzmann et al., 2022). Recently, downregulation by light-induced peroxidation has also been suggested (Holzmann et al., 2022). Beyond the green lineage, the VAZ-cycle is also associated with NPQ in many secondary endosymbiotic algae like multicellular brown algae, eustigmatophyceae and some dinoflagellates (T. Lacour et al., 2020).

In diatoms (and others), the XC mainly associated with NPQ is the diadinoxanthin **(DD)-DT cycle**, comprising only one de-epoxidation step from DD to DT. Some of the peculiarities of XC in diatoms include a more pH-sensitive VDE, already 50% active at pH 6.5, which can lead to strong DT accumulation even in the dark (Jakob et al., 2001, Croteau et al., 2021), due to ΔpH generation via ATP of mitochondrial origin hydrolysis by the plastidial CF_1F_O-ATP synthase/hydrolase (Bailleul et al., 2015). Another difference is the larger amplitudes in the light-dependent regulation of the catalytic rate of the ZEP (Blommaert et al., 2021). Like for plants, ZEP regulation is not elucidated in diatoms. But work on *P. tricornutum* led to the additional hindsight that uncouplers like NH_4Cl, usually interpreted to inactivate VDE by collapsing the ΔpH, actually increase ZEP activity rather than abolishing de-epoxidation (Blommaert et al., 2021). Recent findings could indicate that plants compensate damper regulations of ZEP rate by adjusting the total amount of the enzyme instead (Küster et al., 2023). Additionally, diatoms contained multiple genes encoding for both XC enzymes (annotated VDE and ZEP), one VDE, two VDE-like and one VDE-related, and three ZEPs. This expension of XC enzyme genes is in part due to the fact that diatoms contain both XC, although the VAZ-cycle is usually associated to the upstream biosynthesis pathway of the DD-DT cycle (Lohr and Wilhelm, 1999). The role of proteins associated with each gene is not resolved, but VDE and ZEP3 are associated to DD-to-DT interconversion (therefore NPQ), while ZEP2 appears to be involved in the VAZ-cycle (Giossi et al., 2024). Beyond implication in NPQ, xanthophylls have been associated to photoprotective functions such as antioxidant (Havaux et al., 2007) and modulators of thylakoid membrane fluidity in response to temperature (Bojko et al., 2019).

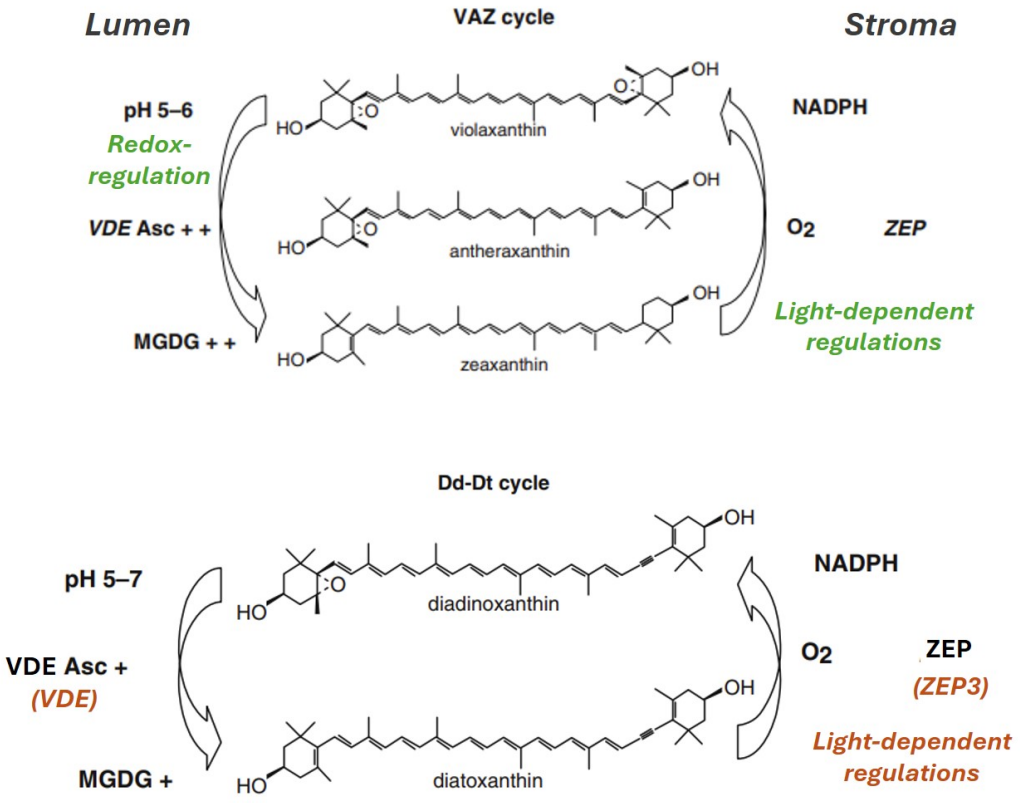

Figure 1.13: Reaction sequence and enzymes of the VAZ and the DD-DT cycles, showing the enzymes, their regulations and co-factors (with low (+) or high (++) requirement). This figure is adapted from (Goss and Jakob, 2010) to show recent discoveries/hypotheses in plants (green) and diatoms (brown). Redox-regulation was added to pH regulation for VDE, (only shown *in vitro* in plants but reducing agents also inhibits VDE in diatoms), the former "larger pH control" over diatoms' ZEP than for plants' ZEP, was changed to "light-dependent regulations" which encompass many hypotheses (including stromal pH), and the now known genes for VDE and ZEP involved in the DD-DT cycle of diatoms were added, see text and citations therein for details. Asc; Ascorbate, MGDG; Monogalactosyldiacylglycerol.

1.4.3 De-epoxidized xanthophylls as fluorescence quencher?

ZX was first proposed as an SV-quencher by Bilger and Björkman, 1990, who observed a linear relationship between NPQ and ZX (i.e., obeying Equation 1.22). This observation was soon replicated in the pennate diatom *P. tricornutum*, but the situation was more complex in the centric *Chaetoceros muelleri* (Olaizola et al., 1994, Olaizola and Yamamoto, 1994). A lot has happened since then, which I will not cover in depth, as this early phase of NPQ research is better understood through the lens of future discoveries, particularly the involvement of LHC proteins in NPQ (see below). Briefly, the early big picture that emerged in plants and green algae was that while the role of ZX was undeniable, the observed "qE" phenomenon was clearly more complex than the simple SV-model. The ideas of multiple quenching sites and the formation of LHC aggregates as quenchers were introduced (Baroli and Niyogi, 2000, Ruban et al., 2007, Jahns and Holzwarth, 2012). On the diatom side, the observation of simple NPQ/DT relationships was repeated (and continues to be) across a wide range of species, especially in pennates but also in some centrics (Lavaud, Rousseau, van Gorkom, and Etienne, 2002, Lavaud et al., 2004, Giovagnetti et al., 2014, Barnett et al., 2015, Blommaert et al., 2017, T. Lacour et al., 2020, Croteau et al., 2021). More complex observations in centrics usually manifest as a very fast relaxation component upon light shut-off (incompatible with epoxidation kinetics) (Grouneva et al., 2008) or significant changes in the slope of the NPQ/DT relationship between NPQ induction (under high light) and relaxation (under low light or in darkness) (Blommaert et al., 2017). Finally, to demonstrate a robust relationship between XC and NPQ, it is essential to account for the fact that there are at least three pools where DT and ZX can be found: associated with the PSII antenna, associated with the PSI antenna, and in the lipid phase (Lepetit et al., 2010, Goss and Lepetit, 2015).

1.4.4 Diverse, group-dependent, LHC proteins are crucial for NPQ

In plants (and mosses), **PsbS** is now unanimously described as the main/essential NPQ contributor (X.-P. Li et al., 2000, Xu et al., 2020). PsbS is a LHC protein that is not intrinsically part of the PSII complex, with four transmembrane helices, and that is constitutively accumulated (Fan et al., 2015). It triggers NPQ when upon a decrease in luminal pH (typically under high light), lumen-exposed glutamate residues are protonated, which appears to favour heat dissipation in the antenna (X.-P. Li et al., 2000, Nicol and Croce, 2021). PsbS does not have pigment binding sites, but surprisingly, the presence of pigments like ZX (Pinnola et al., 2013, Nicol and Croce, 2021, von Bismarck, Korkmaz, et al., 2023) or lutein (Mascoli et al., 2019) in the antenna seems to play a secondary fine-tuning role in NPQ, possibly by modulating PsbS pH-sensitivity and sometimes described as a molecular memory of past light stress (Kress and Jahns, 2017). I will return to a deeper discussion on the potential mechanisms of qE in Chapter 3. At the phenomenological level in non-model organisms, qE-like NPQ can be inferred from very fast relaxation kinetics and absence of, or nonlinear, relationships with de-epoxidized xanthophylls (although one must be careful about the different xanthophyll pools). *Chlamydomonas reinhardtii* has two PsbS genes, but protein accumulation is usually observed only transiently upon high light stress or together with **LHCSR** (see below) under other environmental triggers independently of excess light energy, like inorganic carbon availability (Redekop et al., 2022, Ruiz-Sola et al., 2023). A thorough understanding of PsbS contribution to NPQ and photoprotection in *C. reinhardtii* will require more investigation (Tibiletti et al., 2016, Redekop et al., 2020). Instead, the main molecular actor of NPQ in *C. reinhardtii* is **LHCSR3**. Strikingly, it is not constitutively expressed under constant

moderate light exposure, thus maximal qE capacities are only achieved after prolonged high light exposure in *C. reinhardtii* (Peers et al., 2009) or over a dynamic daily light regime (Nawrocki et al., 2020). A LHCSR1 homolog is also expressed under specific conditions and provides similar qE capacities (Dinc et al., 2016), but different interactions with carotenoids have been proposed (Perozeni et al., 2020). Differently from PsbS, LHCSR has three transmembrane helices and can bind pigments (Bonente et al., 2011). There is no doubt that the primary mode of action of LHCSR3 is, like PsbS, through pH-sensing. However, different views exist on whether ZX-dependent quenching also occurs (Troiano et al., 2021) or not (Tian et al., 2019). Very recently in *C. reinhardtii*, quenching was proposed to stem from a Chl *a* transferring its exciton to a lutein S_1 state (Zheng et al., 2024). A LHC subfamily of brown algae with highly conserved sequences with respect to LHCSR3 (Dittami et al., 2010), the **Lhcx** proteins, is essential for NPQ deployment in diatoms (Beer et al., 2006, Bailleul, Rogato, et al., 2010, Zhu and Green, 2010) (and some haptophytes (Pajot et al., 2022) and eustigmatophytes (Park et al., 2019)). Each species relies on a distinct array of Lhcx isoforms ranging among available genomes from 4 in *P. tricornutum* (Bowler et al., 2008) to 11 in the polar model species *Fragilariopsis cylindrus* (Mock et al., 2022), and 17 in the benthic *Seminavis Robusta* (Blommaert et al., 2020). Of its four Lhcx isoforms, *P. tricornutum* only expresses Lhcx1 constitutively (Bailleul, Rogato, et al., 2010), and Lhcx1-2-3 redundantly influence the level of NPQ a sample can deploy (Buck et al., 2019). In all species, the respective expression of the different Lhcx isoforms is adjusted in response to different environmental cues (Beer et al., 2011, Taddei et al., 2016, Mock et al., 2017, Bilcke et al., 2021, Buck et al., 2022, Pajot et al., 2022) and internal sensors such as the redox state of the PQ-pool (Lepetit et al., 2013, Agarwal et al., 2023). In *P. tricornutum*, Lhcx4 is expressed at night or during prolonged dark incubation (Nymark et al., 2013, Taddei et al., 2016) and does not rescue Lhcx knockout phenotype (Buck et al., 2021). Two crucial distinctions between pennate diatoms-NPQ and PsbS- or LHCSR-NPQ ought to be made **i)** In diatoms there is a strict requirement for the presence of both Lhcx1 and DT together for NPQ and, **ii)** The mutation of acidic residues exposed to the lumen does not knockout the NPQ-conferring capacity of Lhcx1 (Buck et al., 2021, Giovagnetti et al., 2022). Unlike for LHCSR3 (Bonente et al., 2011), there are no experimental demonstrations that Lhcx bind pigments. However, based on its similarities with LHCSR3 and the crystal structure of Lhcf4, a tryptophan residue in a pigment-binding like motif, in the close vicinity of a xanthophyll epoxy-group, was identified by Buck and collaborators. When this tryptophan residue was mutated, Lhcx1-2-3 lost their NPQ-conferring capacities. Moreover, this residue is natively absent in Lhcx4 which lacks the capacity to generate NPQ (Buck et al., 2021). More studies are needed to elucidate the role of Lhcx4, and isoforms in other species similarly lacking this tryptophan residue and showing nocturnal expression patterns (Blommaert et al., 2020, Pajot et al., 2022). All these observations make the term qZ more appropriate than qE to describe the main component of NPQ in *P. tricornuutm*, and likely most pennate diatoms (Blommaert et al., 2021). For the sake of scientific rigor, we tried to only describe a parameter as qZ when we could monitor and quantify the reversal of total NPQ, and otherwise use NPQ (which may include some small qI contributions).

1.5 Thesis goals and approach

1.5.1 The targeted mutagenesis revolution in support of physiology studies

In Section 1.2, I covered the main, vital, reactions which photosynthesis encompasses. Like in other fields, serendipity and rigorous bench-work, combining biochemistry and biophysics, were the reciprocal engines that drove much pioneer discoveries in photosynthesis (Kunkel, 1985). While we understand more at finer scales today, the original depictions of these processes remain impressively accurate, and the photosynthesis section of most undergraduate plant biology textbooks has barely changed in 50 years. The dominant trend of this era of photosynthesis research can be summarized as a "structure-function" investigation. Instead, recent efforts (covered in Chapter 2) revolved around uncovering segments of a complex web of interactions between cryptic "secondary" molecular actors which ensure the dynamic regulation and resilience of photosynthesis under varying natural conditions. Before presenting the experimental approach that was largely used during my Ph.D. research, it is useful to have a historical perspective on how most of this knowledge was acquired and the shift in scientific approach that catalyzed much of this progress. Indeed, regulatory reactions are particularly elusive to probe with traditional techniques because of their facultative nature and condition-dependent variations, their transient (or lack of) by-products, as well as redundancies and compensations between different pathways. In the last decades, a way out of this conundrum has often proven to be the reductionist approach enabled by the advent of molecular biology and reverse genetics.

Interest in mutants that display striking phenotypes is as old as agriculture and has always been part of the study of plant physiology. Moreover, random mutagenesis (*forward genetics*) has been used with great success for a long time by scientists, and is responsible for countless discoveries, supporting both improvement of "structure-function" knowledge (Chua and Bennoun, 1975, Bennoun et al., 1986) and the characterization of regulator actors (Fleischmann et al., 1999, Munekage et al., 2002). However, what bolstered a genuine revolution in the scientific approach for physiologists and microbiologists, is the rapid development of *targeted* mutagenesis techniques, including homologous recombination, interference RNA, TALENs (transcription activator-like effector nucleases) and finally, CRISPR/CAS systems (Shelake et al., 2019). The generation and characterization of loss-of-function mutants (e.g., knockouts) is now a staple of how physiological research questions are tackled. Naturally, investigating the effects of external factors on photosynthesis (and other biological processes), comparative studies investigating differences between ecotypes, species, and groups, and the use of exogenous drugs targeting specific reactions, remain part of the researcher's toolkit. But, increasing emphasis is put on linking regulatory functions to a specific gene and its encoded protein, as well as deciphering how they can modulate "basal photosynthesis functioning" and their expression patterns under different conditions. With their more complex molecular biology originating from a secondary endosymbiosis, and perhaps a seemingly more distant relationship to humans' interests than plants, the development of genetic tools in diatoms has lagged behind the ones in green organisms (Kindle, 1990; Pruitt and Meyerowitz, 1986). However, a lot of efforts and progress have been made in recent years. Twenty years after the publication of the first diatom genome (*T. pseudonana* (Armbrust et al., 2004)) and four years later the one of *P. tricornutum* (Bowler et al., 2008), generation of *P. tricornutum* knockout mutants has become almost routine (Serif et al., 2017) and at the basis of many

recent discoveries (see Croteau et al., 2024 in Section 2.2).

1.5.2 The limits of a reductionist approach in complex living systems

Nevertheless, despite the huge leap forward being made thanks to targeted mutagenesis, regulations do not happen in a vacuum and reductionism has intrinsic limits in complex living systems. In photosynthesis research, when mutagenesis allows establishing clear causal relationships between genotype and phenotype, it usually is for genes encoding proteins with a narrow scope of action, like in the case of AEFs mostly active under specific conditions (see below). By contrast, constitutive proteins are either vital, or operate nested in flexible modules where many actors can compensate for each other and lead to cascade signalling steering physiology reorganization to buffer the deleterious effects of a dysregulated gene, or organism death can occur (Munekage et al., 2004). All of the indirect and unforeseen effects of a mutation which limit our ability to draw strong conclusions regarding the role of the proteins can be described as "complex system problems": self-organisation and system history, non-linearity, response threshold, etc. This brings us to the contemporary era of "system biology", in which improving holistic understanding of regulations and their orchestrations at the organismal level, is the new grail of photosynthesis research. However, what will be the dominant approach looking forward is not yet clear. Definitely, the place of big data, whether through genome-scale modelling (Collakova et al., 2012, Broddrick et al., 2019) or broad-scale measurements on the field (Falkowski et al., 2017, Pierella Karlusich et al., 2020, Kanazawa et al., 2021) and via remote sensing (Krug et al., 2017), will keep on increasing. In parallel, if we want mutagenesis to synergize with these approaches and be part of the toolkit employed to tackle complex problems in photosynthesis regulations, creative approach and experimental design tailored to address these questions are needed. In my thesis, we introduced such an approach enabled by the simple photophysiology and NPQ dynamics of *P. tricornutum*.

1.5.3 A Lhcx1-molecular titration to address complex questions

How should we even begin to experimentally approach a goal as vast as "improving holistic understanding of photosynthesis regulations and their orchestrations at the organismal level"? Is it even feasible to provide answers to such a question within the intrinsic reductionist framework that lab-controlled conditions entail? Can mutating a single molecular actor be useful to address orchestration among a network of regulatory pathways? Actually, as mentioned above, because of the interactions and feedback loops between regulators, a mutation affecting only the function of interest would be the exception rather than the rule. Even targeted mutagenesis is almost *de facto* a tool leading to system-wide perturbations. The difficulty lies in quantifying these indirect effects with sufficient precision and adequate controls to pinpoint their underlying cause with reasonable certitude. First, selecting the right mutagenesis target is paramount. For one, meddling with the accumulation of the different major complexes of the photosynthetic ETC, would lead to drastic consequences. For example, decreasing the concentration of the CF_1F_O-ATP synthase and, therefore, proton efflux from the lumen, would lead to crippling effects caused by unbridled proton motive force deployment and electron bottlenecks in the ETC. To the point where the regulation processes that would be mobilised to alleviate such stress could be completely alien to "real world conditions". Therefore, inducing repercussions too complex to establish causal relationships. A case scenario in plants perfectly illustrates this point. In *Arabidopsis*, knocking

out the CF_1F_O-ATP synthase γ subunit is lethal (Dal Bosco et al., 2004), but still, a mutation "only" disabling the γ-subunit redox regulation has been reported to induce a 30% decrease in growth (Kohzuma et al., 2012).

Likewise, we reasoned that regulation mechanisms can be more informative mutation targets rather than obligatory complexes. However, we sought for three more characteristics for the perfect target **1)** It should be facultative and fully non-active in some growth conditions that are "real life relevant", allowing for similar initial state and system history between wildtype and mutant lines, **2)** It should have a regulatory role of primary importance under certain "real life relevant" perturbations and, **3)** Growth and experimental conditions where the target function is not compensated by redundant regulators can be found. To summarise these points, one should look for a system for which everything, but the magnitude of the regulation of interest, can be considered roughly equal among different mutant strains.

The case of NPQ is particularly interesting because of its ubiquitous role among the phytodiversity (Goss and Lepetit, 2015) to limit reducing pressure on PSII, and therefore on the PQ-pool and the cyt. b_6f under excessive illumination. This makes the regulatory role of NPQ obviously fundamental (checking Point 2 above), but is there a way to tinker with NPQ and respect the two other aforementioned criteria? In diatoms, one could target XC enzymes, but the consequences of a biosynthesis pathway dead-end can have complex and far-reaching effects, plus, xanthophylls possess indirect photoprotective roles (Havaux and Niyogi, 1999, Bojko et al., 2019, Giossi et al., 2024). Therefore, Lhcx proteins are better targets to achieve our goal of studying photosynthesis regulations orchestration, especially Lhcx1 which is the only isoform constitutively accumulated in *P. tricornutum* (Bailleul, Rogato, et al., 2010). At my arrival in the lab, there was already a series of *P. tricornutum* mutants displaying ranging Lhcx1 accumulation when grown under low light conditions (first published in (Giovagnetti et al., 2022)). In *P. tricornutum* the light-dependency of NPQ shows a sigmoidal behaviour with a strong sigmoidicity. This results in the complete absence of NPQ development in the low-light regime (Blommaert et al., 2021), therefore, conditions where Point 1 is respected can be found easily. One of the first objectives of my Ph.D. was to measure various physiological control (baseline) parameters to ensure that everything, but NPQ capacities *when* we induce a light stress, could be considered roughly equal between these mutants (see Chapter 3). Therefore, what remains to be considered is overlapping effects of other molecular actors and/or mechanisms (Point 3). In diatoms, Lhcx isoforms seem to redundantly provide NPQ capacities, but their gene transcription and subsequent synthesis respond to different signalling cues (Lepetit et al., 2013, Taddei et al., 2016, Buck et al., 2019). In our case, only Lhcx1 accumulates under low light growth conditions (Giovagnetti et al., 2022), but accumulation of other isoforms over experiments of compatible duration with gene expression and protein synthesis is something to keep in mind. Then, one may wonder how many components are involved in *P. tricornutum*'s NPQ? Previous reports suggested a simpler NPQ model in (pennate) diatoms than in green organisms, with a single qZ component under most conditions (see Section 1.4). In the first experimental Chapter of my thesis (Chapter 3), I am able to show that it is indeed the case. In this Chapter I also propose that this single component correspond to qZ and I was able to propose a working model for the role of Lhcx1 and DT .

This is extremely powerful as can be illustrated by comparing our approach to a similar one which has been used in *Arabidopsis* before. In that case, one WT, one PsbS Ko and two PsbS overexpressors lines were used (X.-P. Li et al., 2002). The authors reported no differences in growth, and in Chl *a* and *b* accumulation under low light conditions between genotypes. Under subsequent high light exposure, the authors showed that NPQ increases

and that photoinhibition susceptibility under high light decreases as a function of PsbS accumulation. Furthermore, among six Chl *a* fluorescence decay components, three displayed PsbS-dependent lifetimes (X.-P. Li et al., 2002). These results are impressive, and repeating them in diatoms would already provide much needed answers. For example, the photoprotective effect of NPQ on preventing D1 photodestruction has never been shown in diatoms without the untargeted effects of pharmacological inhibitors. However, we suspected that we could push this approach even further, thanks to the unusually simple photophysiology of *P. tricornutum*.

First, as mentioned in Section 1.4, plants have a more complex NPQ scheme. For instance, in the six fluorescence decay components reported by (X.-P. Li et al., 2002), could some have been influenced by varying qZ or qH levels? By state transitions? In fact, more than 20 years after (X.-P. Li et al., 2002), the quenching mechanism of NPQ in *Arabidopsis* is still source of much debate (Section 1.4). In the case of *P. tricornutum*, having a single NPQ component greatly facilitate data interpretation and allows to express other photosynthetic mechanisms as phenomenological relationships of qZ (rather than as a function of a compound of mechanisms represented by the term NPQ). Second, to enhance the resolution of phenomenological relationships between qZ and other mechanisms, we elected to use a larger span of 14 mutants with ranging constitutive Lhcx1 expression (one WT, one Lhcx1-Ko, and 12 Lhcx1-complemented lines). This Lhcx1 "molecular titration" enables us to evolve from a qualitative comparison between a few strains, to a quantitative analysis, in which we consider strains as coordinates on a continuous scale of Lhcx1 concentration or qZ magnitude. This experimental design provides us with more than a passive qZ gauge, but rather a "dial", by which we can select the more relevant range of qZ to explore to characterize a phenomenon of interest. By selecting the adequate mutants to observe a given range of qZ, in combination with other experimental dimensions; light intensity, time of high light exposure, etc, we are able to decipher intricate processes, like the role of Lhcx1 and DT in qZ (**Chapter 3**) or to distinguish between genes responding to direct light signalling from those triggered by qZ-dependent photosynthesis signals (**Chapter 4**). Additionally, this makes this approach incredibly robust to pleiotropic biases and able to detect potential non-linear and threshold responses, which are limitations of most experimental designs using mutagenesis (Fig. 1.14).

Considering that the overall objective of this thesis is to investigate the orchestration of photosynthetic regulations in diatoms, the ultimate (but out of reach for the moment) objective is obviously to build a model of regulations tailored to these important, but understudied, primary producers. Non-linear relationships can undermine modelling efforts, for example if the effect of a given regulation is erroneously extrapolated in the case of a threshold response, or even more inaccurately, in the case of non-monotone responses (Fig.1.14). Non-monotone functions typically characterize the temperature or pH optima of enzymes catalytic rate, or the growth rate of photosynthetic organisms as a function of light intensity and temperature. It is therefore not far-fetched to expect finding some variables responding to NPQ extent in non-monotone relationships. This is especially true if we recover thousands of variable with systemic 'omic approaches, which we will do in **Chapter 4** by characterizing how qZ extent modulates gene regulation over high light illumination. It is noteworthy, that Lhcx1 is by no means the only adequate target for a "molecular titration". I already discussed about (X.-P. Li et al., 2002), but see also other studies with PsbS mutants (Logan et al., 2008, Głowacka et al., 2018) or complemented mutants complemented in photorespiration enzymes for instance (von Bismarck, Wendering, et al., 2023). However, the incredibly simple qZ model and overall simple physiology of *P. tricornutum* as a model photosynthetic organism, is a really extraordinary opportunity to probe a complex systems with simple tools. Not without

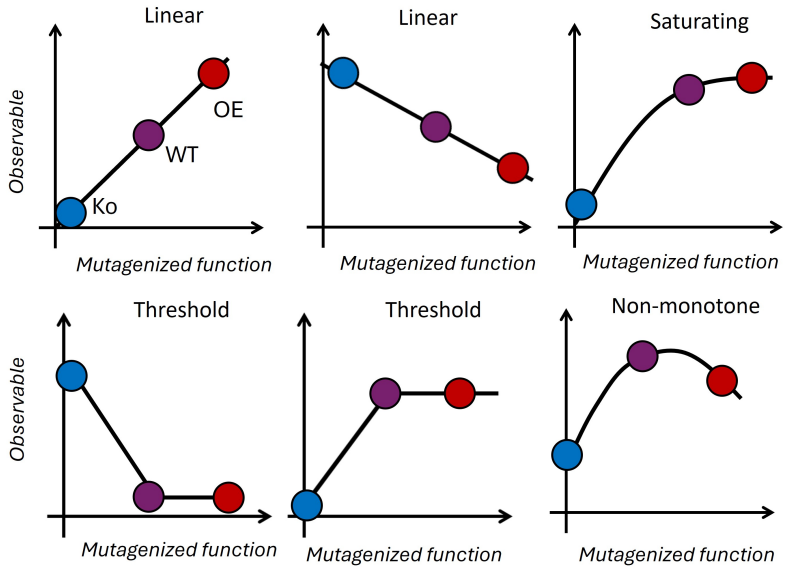

Figure 1.14: Schematic representation of different patterns of phenomenological relationship to expect between regulation mechanisms of interest and NPQ magnitude as the independent variable. The blue, purple and red dots represent a Lhcx1-Ko, the WT and a Lhcx1 overexpressing strain, respectively

tongue-in-cheek, we could say that the Lhcx1 "molecular titration" in *P. tricornutum* provides a holistic control to a reductionist approach to investigate photosynthesis regulations in diatoms.

Features of the simple NPQ/qZ model in pennate diatoms

1. A single NPQ component, qZ (**Chapter 3**).

2. A direct relationship between qZ and its molecular actors, Lhcx1 and DT, allows their rapid quantification with a non-invasive variable fluorescence probe (**Chapter 3**). This feature was already exploited by a past postdoc of my supervisor, Lander Blommaert, to decipher the kinetics of both XC enzymes in *P. tricornutum* (Blommaert et al., 2021).

3. The slow relaxation of qZ in the dark (≈10 min) allows to titrate qZ everything else being roughly equal within in a single strain, by measuring NPQ as a function of relaxation time (impracticable in PsbS/LHSCR3-qE, relaxing in 1-2 min) (**Chapter 3** and **4**).

4. Blommaert et al., 2021 also showed an important lag in the sigmoidal induction of NPQ as a function of light intensity in *P. tricornutum*, which allows to measure baseline parameters under low light exposure with no NPQ.

5. No state transitions muddle the estimation of NPQ. Even more importantly, this allows us to consider constant optical cross-section of both PS over the course of most experiments. We exploit these features, together with the preceding point, in **Chapter 4** to introduce a novel parameter estimating relative change in cyclic electron flow (cyclic electron flow pathways and regulations are discussed at length in **Chapter 2**).

Features making of *Phaeodactylum tricornutum* a simple model organism to represent secondary endosymbionts in photosynthesis studies

1. Easy to grow in lab, multiple biomolecular tools and the most in depth genome annotation among secondary endosymbionts (Falciatore et al., 2020).

2. We demonstrate in **Chapter 3** that the fate of photons absorbed by PSII in this species can be exceptionally accurately described by the theoretical lake model (defined in Section 3.1).

3. No apparent diffusion limitation to electron flow in the lumen (Flori et al., 2017 see also **Chapter 4**) by contrasts with plants (Kirchhoff et al., 2004), which helps when studying the high-potential chain.

4. Easier absorption difference signals to deconvolute with cyt. c_6 replacing plastocyanin (see for example in plants (Kramer and Sacksteder, 1998) or in cyanobacteria (Viola et al., 2019)).

5. A linear *and* a quadratic electrochromic shift (ECS) probes make the measurement of absolute values of transthylakoidal electric gradient possible (see **Chapter 5** and (Bailleul et al., 2015)).

6. No known redox regulation of the CF_1F_O-ATP synthase in diatoms.

1.5.4 Thesis outline

Before presenting the original research works undertaken during my Ph.D. (Fig. 1.15), I will describe the other photosynthesis dynamic mechanisms, that together with NPQ, form the complex web of processes that regulate photosynthesis. **Chapter 2** consists of two literature reviews published as book chapters focusing on alternative electron fluxes in the model green algae *Chalmydomonas reinhardtii* (Croteau et al., 2023) and the known differences in photosynthetic regulations between diatoms and green organisms (Croteau et al., 2024). In **Chapter 3** we use the "Lhcx1 molecular titration" to propose a simple model for NPQ in *P. tricornutum*, and possibly pennate diatoms altogether. We show strong evidence supporting a single qZ component and propose a working hypothesis accounting for the role of its two molecular actors, Lhcx1 and DT, which when together, acts as a Stern-Volmer-like quencher. Furthermore, we were able to demonstrate that the lake model is exceptionally accurate to describe the relationship between qZ and the quantum yield of PSII in *P. tricornutum* and a second pennate diatom. In **Chapter 4**, we used this simple model as a fulcrum to investigate higher levels of photosynthesis regulations. This includes the redox state of the intersystem electron chain, cyclic versus linear electron flow and the susceptibility to PSII photoinhibition and D1 photodestruction. Moreover, we combine our molecular titration with system biology to investigate how qZ influences the genome wide high light response of *P. tricornutum* via transcriptomics. **Chapter 5** includes an initial facet of my Ph.D. which could not be finalized on time for the writing of my thesis, which was the development of a novel ECS-based method to measure absolute pmf and transthylakoidal proton gradient (ΔpH) values. This method is theoretically possible thanks to the unusual quadratic ECS signal of diatoms. We planned on using this method to close the loop of NPQ regulations, by investigating how NPQ is itself regulated by the ΔpH, via the rates of XC enzymes (Goss

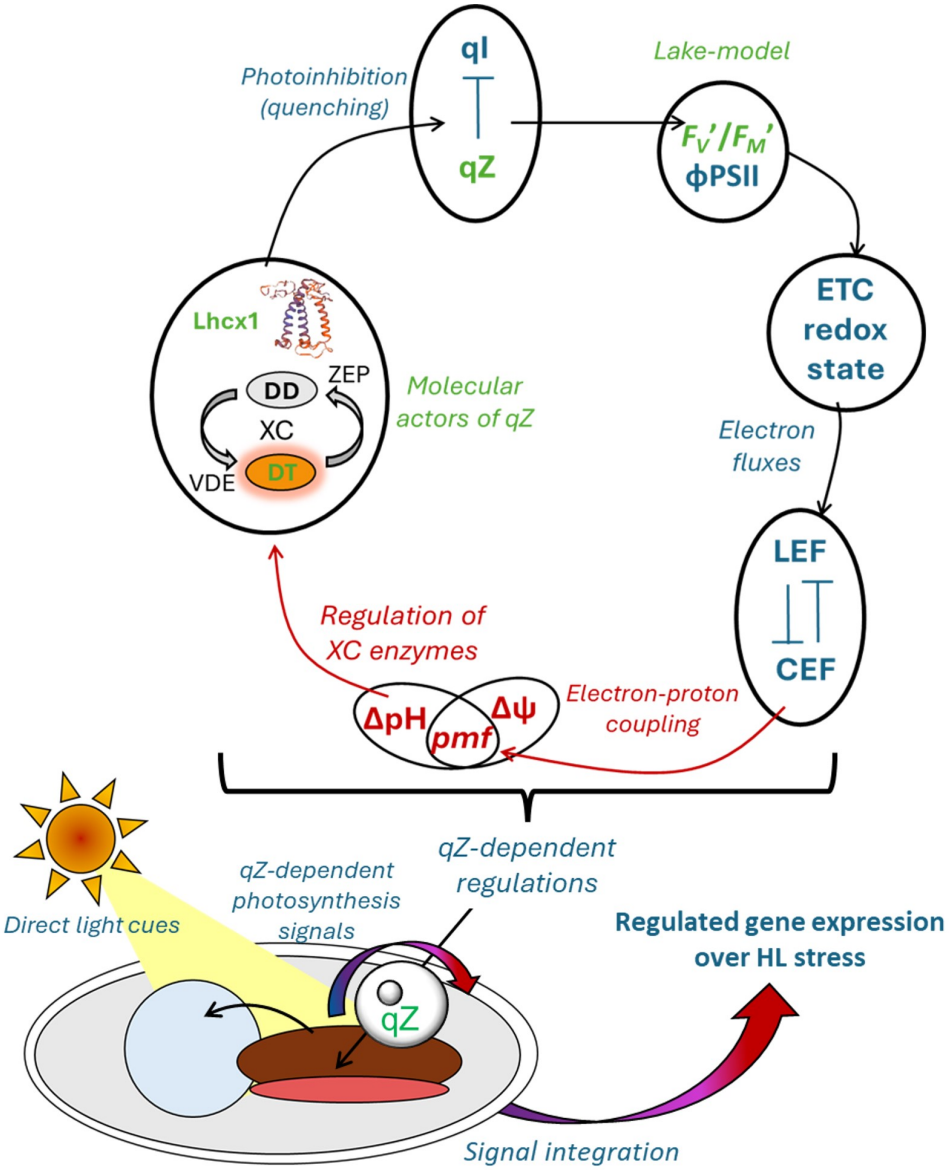

Figure 1.15: Scheme summarizing the original research works undertaken during my Ph.D. (excluding collaborations), and the photosynthesis regulation loop anchored on NPQ that we attempted to characterize. The color in which parameters, processes and concepts, are written represent the Chapter in which they are mainly address. Refer to text or abbreviations list for abbreviations.

and Jakob, 2010). We unfortunately could not adress this question in depth, but in **Chapter 5**, I present a proof of method suggesting that the method will be a powerful tool to do so in the near future. In **Chapter 5**, I also briefly overview the collaborative works to which I participated during my Ph.D. (one paper published (Dorrell et al., 2024), one in revision phase, and two manuscripts in preparation for submission in the coming months). My role in these collaborations was to use NPQ, and photophysiology at large, as powerful probes for phenotyping new *P. tricornutum* mutants and to investigate complex biotic interactions.

Chapter 2

Litterature reviews on photosynthesis regulations in diatoms and the green lineage

I focused a lot on NPQ in the introduction. Beyond countering ROS production, NPQ is a regulator of photosynthesis. By competing for exciton with photochemistry, it downregulates the reducing pressure on PSII and should allow a more oxidized PQ-pool, which is at the cross-roads of many interacting pathways. However, it is only one out of a vast network of processes that take place to regulate photosynthesis. The molecular actors of these pathways, their response to external conditions, and their redundant or synergistic interactions in the integrated regulation of photosynthesis, were intentionally left out of my Introduction, because they are covered here, in Chapter 2. From the beginning of my Ph.D., I had the opportunity, with my co-authors, to write two book chapters aimed at reviewing these mechanisms. These reviews form an important portion of the theoretical backbone to my original research endeavours, which will be presented in Chapter 3 and onward. Chapter 2 comprises these two literature reviews. The first chapter (Croteau et al., 2023) reviews the multiple regulatory processes in photosynthesis, including various electron flows, in the model green algae *C. reinhardtii*, and is part of the third edition of *The Chlamydomonas Sourcebook*. The second chapter (Croteau et al., 2024) highlights contrasts and similitude in photosynthesis regulations between diatoms and green lineage organisms and is part of *Diatom Photosynthesis: From Primary Production to High-Value Molecules*.

2.1 Review 1: The multiple routes of photosynthetic electron transfer in *Chlamydomonas reinhardtii*

Chapter 18: The multiple routes of photosynthetic electron transfer in *Chlamydomonas reinhardtii*

Dany Croteau[1], Jean Alric[2], Benjamin Bailleul[1]

[1] Institut de Biologie Physico-Chimique, Laboratory of Chloroplast Biology and Light Sensing in Microalgae, UMR 7141, Centre National de la Recherche Scientifique (CNRS), Sorbonne université, F-75005 Paris, France

[2] Aix Marseille Univ, CEA, CNRS, BIAM, UMR 7265, Photosynthesis and Environment, F-13108 Saint Paul-Lez-Durance, France

Non-print items - Abstract

Like all organisms performing oxygenic photosynthesis, *Chlamydomonas* captures light energy in two photochemical steps to drive linear electron flow from water to NADPH and to produce ATP. However, this process alone is not sufficient to drive CO_2 fixation in the Calvin-Benson Cycle and to respond to environmental and metabolic constraints, e.g. light availability or metabolic needs in term of ATP and NADPH. A complex network of alternative electron flows, comprises Cyclic Electron Flow around PSI and various water-to-water cycles that utilize O_2 as an alternative electron acceptor, provide an additional degree of freedom to face this challenge. The present chapter describes the various alternative routes of photosynthetic electron transfer in *Chlamydomonas*, describes how they are coordinated for optimization of photosynthesis and gives a retrospective on the early physiology work on those alternative electron flows among model photosynthetic organisms.

Non-print items – Keywords: Chlamydomonas, Alternative electron flows, photosynthesis, Mehler, flavodiiron proteins, PTOX, Cyclic Electron flow.

Abbreviations:

ETC: electron transport chain

PSI/PSII: Photosystem I / II

cyt. b_6f: cytochrome b_6f complex

LEF: linear electron flow

PQ/PQH_2: plastoquinone/plastoquinol

PC: plastocyanin

FNR: Ferredoxin:$NADP^+$ reductase

$NADP^+$/NADPH: dinucleotide phosphate

$\Delta\mu_{H+}$: electrochemical proton gradient

ΔpH: proton concentration gradient

Δψ: electric potential

CBC: Calvin-Benson Cycle

NPQ: Non-Photochemical Quenching of chlorophyll fluorescence

qT: state transition

qE: energy-dependent quenching

AEF: alternative electron flows

CEF: Cyclic Electron Flow

WWC: Water-to-Water Cycle

ROS: Reactive Oxygen Species

LHCII: Light Harvesting Complex II

PTOX: plastid terminal oxidase

Fd: ferredoxin

FQR: Fd-PQ oxidoreductase

PGR5: proton gradient regulation 5

PGRL1: PGR5-like 1

NDH: nucleotide dehydrogenase

WT: wild type

FLV: Flavodiiron protein

AsA: Ascorbate

MDA: monodehydroascorbate

PhQ: phylloquinones

AOX: Alternative Oxidase

CCM: carbon concentration mechanisms

GlcDH: glycolate dehydrogenase

NADP-MDH: NADP-malate dehydrogenase

Introduction

Like all organisms performing oxygenic photosynthesis, *Chlamydomonas* captures light energy in two photochemical steps to drive photosynthetic electron transport in the thylakoid membrane. Electron transport involves the action of three major molecular complexes embedded in the thylakoid lipid phase: the photosystems (PS) I and II (Vol 2, Chapter 16) and the cytochrome b_6f complex (cyt. b_6f, Vol 2, Chapter 17). In the main linear electron flow (LEF) pathway (Figure 1), the primary electron donor, water, is oxidized at the PSII reaction center. The two PS work in series (Hill & Bendall, 1960) transferring electrons along redox cascades. Between the photosystems, electrons transit through the cyt. b_6f complex via two mobile carriers, the hydrophobic and membrane soluble plastoquinone (PQ)-pool, which connects PSII to cyt. b_6f, and the water-soluble plastocyanin (PC) shuttle, in the thylakoid lumen, which connects cyt. b_6f to PSI. At the PSI acceptor side, Fd:$NADP^+$ reductase (FNR) accepts electrons from Fd to reduce dinucleotide phosphate ($NADP^+$) to NADPH. LEF allows water splitting on the PSII side of the electron transport chain, the production of reducing power on the PSI side, and the generation of an electrochemical proton gradient ($\Delta\mu_{H+}$) across the membrane. Proton accumulation in the lumen is coupled to both LEF through water splitting and the Q-cycle at cyt. b_6f (Joliot & Joliot, 2006). The proton-motive force $\Delta\mu_{H+}$ comprises two energetic components, a proton concentration gradient (ΔpH) and an electric potential ($\Delta\psi$), both driving the CF_1F_O-ATP synthase catalytic

rotation (Mitchell, 1966; Kramer *et al.*, 2003) (Vol 2, Chapter 17). The output molecules of LEF, NADPH and ATP, are the two energy sources that fuel the Calvin-Benson (CBC) cycle (Vol 2, Chapters 7 and 8).

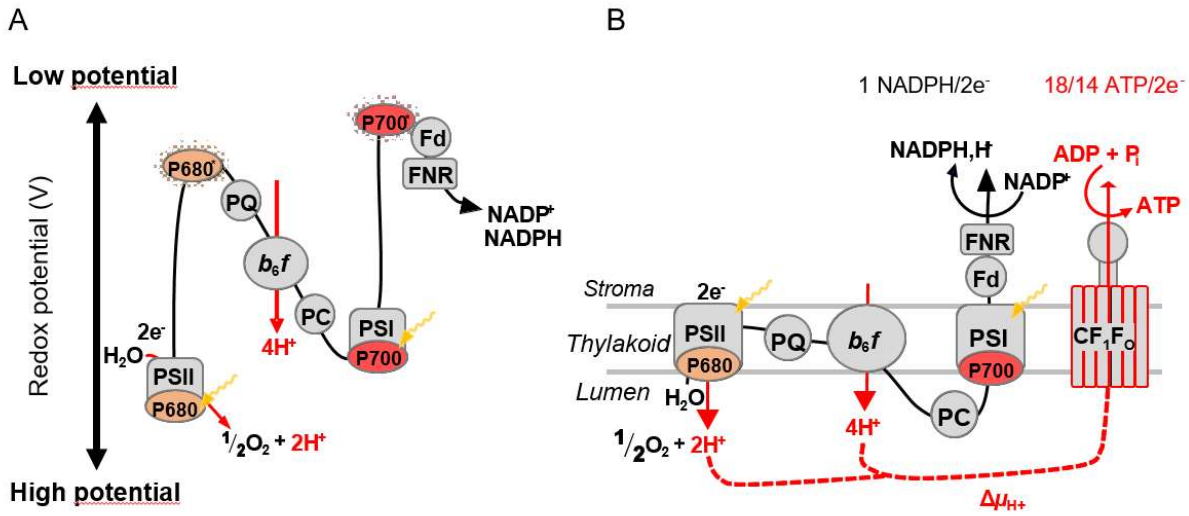

Figure 1: Photosynthetic Linear Electron Flow (LEF). **A**. LEF in the Z scheme depiction of photosynthesis. **B**. LEF with the disposition of the complexes in the thylakoid membranes. Abbreviations: PSII, Photosystem II; PSI, Photosystem I; *b*$_6$*f*, cytochrome *b*$_6$*f*; CF_1F_O, CF_1F_O ATP synthase; PC, plastocyanin; PQ, Plastoquinol/Plastoquinone; Fd: ferredoxin; FNR: Ferredoxin/NADP Reductase; $\Delta\mu_{H^+}$, electrochemical proton gradient. P680: special pair in the reaction center of PSII; P700: special pair in the reaction center of PSI. Black line: electron transport. Red dashed line: proton transport.

A description of the photosynthetic electron transport chain restricted to LEF would give an overly simplistic view of the photochemical phase of photosynthesis. LEF produces a fixed ratio of ATP and NADPH and, in the context where the light input and metabolic demands for ATP and NADPH are constantly changing, photosynthesis would be able to best utilize LEF if it functioned with some "degrees of freedom". Significant flexibility is incorporated into the biological regulation of light utilization by the two photosystems, through the non-photochemical

97 quenching (NPQ) at PSII (Chapter 25) or state transition (qT) (Vol 2, Chapter 24); the latter is
98 particularly important in *Chlamydomonas.* Another main mode of regulation of the photochemical
99 phase of photosynthesis relates to the flexibility of photosynthetic electron flows. In all organisms
100 performing oxygenic photosynthesis, LEF components (PSI, PSII, cyt. b_6f) are always involved in
101 a complex network of alternative electron flows (AEFs) which divert electron transport from the
102 production of NADPH or assimilation of CO_2. The present chapter focuses on those AEFs and is
103 structured as follows; in Section 1, we first explain the input and output constraints on LEF
104 operation (light availability and metabolic needs in term of ATP and NADPH) and how AEFs
105 provide an additional degree of freedom to face this challenge. Then we present the various AEFs
106 in Section 2, from the first experimental evidence to recent work more specific to *Chlamydomonas*.
107 We especially focus on the two main AEF modes (schematized in Figures 2 and 3); Cyclic Electron
108 Flow (CEF) around PSI, where electrons at the acceptor side of PSI are reinjected upstream of cyt.
109 b_6f, and the various water-to-water cycles (WWC) (or pseudo-cyclic electron fluxes), which utilise
110 O_2 as alternative electron acceptor instead of CO_2 (Curien *et al.*, 2016). In Section 3, we discuss
111 how the various AEFs coordinate to optimize photosynthesis in response to changes in
112 environmental conditions. Finally, in relation to the adaptive role of AEFs in green algae, this
113 review ends with a retrospective of the early physiology work on AEFs in various model
114 photosynthetic organisms.

115

116 ## 1. AEFs provide flexibility to the Linear Electron Flow

117 The operation of LEF, which uses light as a substrate and synthesizes ATP and NADPH
118 as end-products, is constrained at these two extremities of the pathway. First, when light fluctuates,

119 the absorption of light must be adjusted to the electron transport capacity; and second, the
120 ATP/NADPH ratio must adjust to the metabolic needs of the moment. All AEFs share some
121 common features: they play the role of valves, offering an outlet for an additional activity of one
122 photosystem or both. By doing so, they also allow the pumping of extra protons into the lumen,
123 thereby driving increases in the $\Delta\mu_{H+}$ and ATP production. In this first section we will describe
124 how common features of AEFs help the cells respond to light and metabolic constraints. Only in
125 Section 2, which describes the individual AEFs, will differences and specificities among them be
126 pointed out, e.g., maximal rate, protons pumped per electron transferred and ATP production.

127 Exposure to excess light can lead to over-reduction of PS acceptor-side electron carriers
128 (iron-sulfur centers, Fd and NADPH for PSI; Q_A, Q_B and the PQ pool for PSII), augmenting the
129 chances for excited chlorophyll *a* to transition into a highly unstable triplet state that reacts with
130 O_2. The latter can result in the production of Reactive Oxygen Species (ROS) and photooxidative
131 damage, including photoinhibition of the two PSs (Vol 2, Chapter 25). At PSII, the induction of a
132 series of mechanisms, collectively referred to as NPQ, allows for diminished light pressure on PSII
133 (Vol 2, Chapter 25). In *Chlamydomonas*, the major component of NPQ is energy-dependent
134 quenching (qE), which dissipates excess light energy harmlessly as heat and prevents
135 photoinhibition of both PS (Roach *et al.*, 2020). Another NPQ process particularly important in
136 *Chlamydomonas* is state transitions (qT), which induce a reversible kinase-dependent migration of
137 the light harvesting LHCII antennae from one photosystem to the other, thus modulating excitation
138 of PSII and PSI and thereby rebalancing energy fluxes (Vol 2, Chapter 24). The two processes are
139 regulated differently since qE depends on the lumenal pH whereas the activity of the kinase
140 involved in qT is regulated by the redox state of PQ at the Q_o site of cyt. b_6f (Wollman, 2001;
141 Dumas *et al.,* 2017). When considering necessary adjustments of light utilization by PSII to the

142 capacity for electron transfer, NPQ downregulates PSII photochemistry while AEFs provide
143 alternative routes for excess electrons, playing the role of redox exhaust valves and protecting the
144 PSs from photoinhibition.

145 In addition to response to changes in light levels, the photosynthetic electron transport
146 chain (ETC) faces a constraint related to the stoichiometry of NADPH and ATP. The LEF produces
147 ATP from H^+ accumulated in the lumen and NADPH from e^- transfer along the ETC. Because of
148 the H^+/e^- coupling, ATP/NADPH production is fixed in LEF. Water oxidation at the level of PSII
149 produces one proton in the lumen per electron transferred. At the level of the cyt. b_6f, 2 protons
150 are pumped per electron transferred along the chain towards PC, based on Q-cycle activity (Vol 2,
151 Chapter 17). Indeed, the reduction of plastoquinone (PQ) to plastoquinol (PQH_2) at the Q_B site of
152 PSII requires two protons from the stroma whereas the reoxidation of the PQH_2 at the lumen-
153 facing Q_o site of cyt. b_6f releases the two protons in the lumen. In contrast, the two electrons
154 released by PQH_2 oxidation at the Q_o site take bifurcated pathways. One electron follows the high
155 potential chain which includes the Rieske iron-sulphur protein and cyt. *f* and reduces PC. The
156 second electron follows the low potential chain via haem b_L and haem b_H. In Mitchell's original
157 proposal (1975), this electron in the low potential chain was used to reduce PQ to PQH_2 on the
158 stromal side of the membrane via an electron coming from PSII. However, based on work
159 performed with the respiratory cyt. bc_1 complex, a modified Q-cycle was proposed where the *b*
160 haems can act as an electron reservoir and one PQH_2 is regenerated after two cycles (Zhang *et al.*,
161 1998; Crofts *et al.*, 2003; Cramer *et al.*, 2011). The modified Q-cycle is constitutively functional
162 and transfers two protons per electron (Sacksteder *et al.,* 2000; but see section Cyclic Electron
163 Flow). Altogether, LEF produces 3 H^+ per electron but, from a metabolic perspective, what matters
164 is the relative amount of reducing power and ATP produced by the ETC, often reflected by the

ATP/NADPH ratio. Since two electrons are required to reduce $NADP^+$, this leads to a value of 6 protons per NADPH. The question mark lies in the proton requirement per ATP synthesized, which can vary between species depending on the stoichiometry of the subunits forming the membrane intrinsic *c*-ring of the CF_1F_O-ATP synthase (Petersen *et al.*, 2012; Turina *et al.*, 2016). For most researchers in the field, each proton crossing the CF_1F_O-ATP synthase induces a one incremental step rotation of the *c*-ring on the F_O sector of the complex, which is transduced via a central stalk into catalytic conformational changes of the $\alpha_3\beta_3$ subunits on the F_1 sector. Although it remains uncertain whether the work accomplished by each translocated proton is homogeneous (Turina *et al.*, 2016), the yield of 3 ATP molecules synthesized/hydrolysed per CF_1F_O 360º rotation is well established (Adachi *et al.*, 2007). There is no structural information about the CF_1F_O-ATP synthase of *Chlamydomonas* that establishes a definitive stoichiometry of protons translocated to ATP synthesized. The ratio of 14 H^+ per 3 ATP is usually used for eukaryotic photosynthetic organisms based on the 14 *c*-subunits of the ATP synthase rotor in spinach (Seelert *et al.*, 2000; Hahn *et al.*, 2018). Then the electron transfer from a water molecule to NADPH, which displaces 2 electrons and deposits 6 protons in the thylakoid lumen, would yield 1 NADPH and a 6/14 rotation of the ATP synthase, resulting in ~1.28 ATP per NADPH synthesized. This ratio is below the 3/2 requirement of the CBC (Allen, 2002). Consequently, without additional flexibility, LEF from water to inorganic carbon assimilation is predicted to accumulate NADPH until photosynthetic activity is fully arrested. AEFs permit an additional activity of the photosynthetic complexes that involves proton pumping and can include PSII and/or cyt. b_6f. From this perspective, AEFs can be seen as degrees of flexibility for electron transfer, allowing for proton pumping without net production of NADPH. This, in turn, generates extra ATP and addresses the issue of mismatch between the ATP and NADPH produced by photosynthetic electron transport and the

188 ATP/NADPH required to sustain inorganic carbon assimilation. Many reports aimed at calculating
189 the AEF activity required to adjust the ATP/NADPH ratio of the CBC (Allen, 2002; Amthor, 2010;
190 Alric *et al.,* 2010) have concluded that AEFs should accumulate one additional proton in the lumen
191 per NADPH produced by the LEF (6 +1 = 7 protons per NADPH would produce 1.5 ATP
192 molecules).

193 However, it would be naive to consider AEFs solely as a way to compensate for the
194 shortcomings of the 14 *c*-subunits of the CF_1F_O ATP synthase. In the stroma, reducing power in
195 the form of reduced ferredoxin or NADPH not only drives the CBC, but also fuels stromal enzymes
196 involved in essential metabolic pathways like nutrient assimilation (Vol 1, Chapter 4) and amino
197 acid biosynthesis. Moreover, substrate availability for photochemistry (light) and the CBC
198 (inorganic carbon) can largely and suddenly vary in the environment, limiting the general
199 relevance of such a statistical view. In low CO_2 conditions, carbon concentration mechanisms
200 (CCMs) are induced to generate a high CO_2 concentration around Rubisco, which is mostly
201 confined to the pyrenoid (reviewed in *Chlamydomonas* in (Wang *et al.*, 2015), also Vol 2, Chapter
202 7). Due to the ATP demand for operating CCMs, the ATP/NADPH ratio is further influenced by
203 CO_2 availability and inorganic carbon assimilation. The network of AEFs in organisms performing
204 oxygenic photosynthesis, including *Chlamydomonas*, reflect a dynamic flexibility of the ETC to
205 respond to changes in environmental conditions or metabolic needs. This flexibility fulfils three
206 major roles: (i) AEFs can dynamically optimize the ATP/NADPH ratio produced by
207 photosynthetic electron transport to the metabolic needs, and thereby avoid the ATP/NADPH
208 stoichiometric cul-de-sac intrinsic to a system that would solely use LEF; (ii) they offer electron
209 valves under conditions in which light absorption exceeds the capacity of LEF, preventing the

over-reduction of the ETC and the risk of photoinhibition; (iii) finally, by generating additional $\Delta\mu H^+$, AEFs participate in pH-mediated regulation of the ETC under saturating light conditions.

The pH control of the ETC comprises regulation of NPQ (Vol 2, Chapter 15, 25) and the so-called "photosynthetic control". Under conditions of an electron transfer limitation downstream of PSI (e.g., low temperature or low CO_2), PSI can be photoinhibited (Chaux *et al.,* 2015). The "photosynthetic control" (Vol 2, Chapter 17), which occurs when a low lumenal pH slows down PQH_2 oxidation at the Q_o site of cyt. b_6f (Bendall, 1982), prevents this harmful situation by moving the limiting step of the ETC upstream of PSI (Sukenik *et al.*, 1987). The redox regulation of the CF_1F_O-ATP synthase, which is not covered in this chapter (see Vol 2, Chapter 17), also plays a crucial role in modulating the ΔpH (Kramer *et al.*, 1990). The γ-subunit of the CF_1F_O-ATP synthase contains a cysteine pair that forms a disulfide bond under light conditions that decrease the $\Delta\mu_{H+}$ required for rotation of the CF_1F_O-ATP synthase (Junesch & Gräber, 1987). This mechanism is conserved and restricted to the green lineage, including *Chlamydomonas* (Buchert *et al*, 2017; Buchert *et al.*, 2021).

2. Diversity of AEFs in *Chlamydomonas*

With the definition used in this chapter for AEFs, i.e., electron routes involving photosynthetic complexes (PSII, PSI, cyt. b_6f) without resulting in CO_2 fixation, the diversity of AEFs in *Chlamydomonas* is large. Some of these pathways are already covered in other chapters and include the use of photosynthetically reduced ferredoxin or NADPH for nutrient assimilation, e.g., nitrogen or sulfur metabolism (Vol 2, Chapter 4) and for amino acid biosynthesis. This is also the case of the coupling between the photosynthetic ETC and the hydrogenase, which uses reduced ferredoxins as substrate under anaerobic conditions (Vol 2, Chapters 9 and 10). In a way, the

recombination events associated with photosynthetic reaction centers meet the definition, strictly speaking, but are covered already in the chapter dedicated to the photosystems (Vol 2, Chapter 16) and will not be considered here. This section will pay special attention to PSI CEF and the various WWCs but will start with the chlororespiratory pathway, a minimal respiratory chain in the thylakoid which is not strictly speaking an AEF but whose components are involved in PSI CEF and WWCs.

2.1 Chlororespiratory pathway

A minimal respiratory pathway exists in the thylakoids of most organisms performing oxygenic photosynthesis. The oxidation of PQH_2 in darkness was first reported by Diner and Mauzerall (1973), while Bennoun (1982) demonstrated that it was catalyzed by a plastid terminal oxidase (PTOX). PTOX, together with a NAD(P)H plastoquinone oxidoreductase, forms a chlororespiratory transport chain using electrons from NAD(P)H to reduce O_2 to H_2O (see review on PTOX (Nawrocki *et al.*, 2015)). In plants, PTOX was initially investigated to decipher its role in chloroplast development and carotenoids biosynthesis (Wu et al., 1999), presumably by regenerating (oxidized) PQ in darkness, which acts as an electron acceptor to activate the phytoene desaturase, an enzyme required for carotenoid biosynthesis (Carol & Kuntz, 2001; Bennoun, 2002). Two PTOX enzymes are expressed by *Chlamydomonas*, PTOX2 being the main oxidase with a rate that is ~10 fold faster than PTOX1 (4.5 vs. 0.4 $e^- PS^- s^{-1}$) (Houille-Vernes *et al.*, 2011). *Chlamydomonas* phytoene desaturase mutants show similar phenotypes to that of plant mutants with regards to carotenoid synthesis (McCarthy *et al.*, 2004; Couso *et al.*, 2011). However, the demonstration of PTOX involvement in this pathway remains inconclusive, notably because *ptox2* mutants of *Chlamydomonas* (see *Chlamydomonas* AEF mutants strains in Table 1) do not show changes in carotenoid content (Houille-Vernes *et al.*, 2011). This function could be fulfilled by

PTOX1 (Li *et al.*, 2020), as suggested for the green algae *Haematococcus pluvialis* (Wang *et al.*, 2009); however, two observations make the role of PTOX in carotenoid synthesis of green algae unclear. Not only is O_2 uptake by PTOX during the dark phase of the *Chlamydomonas'* diel cycle almost null (Strenkert *et al.*, 2019), but in contrast to plants, most carotenoids seem to be synthesized during the light period of the cycle in both *Chlamydomonas* (Janeiro & Barrnett, 1982) and *H. pluvialis* (Wang *et al.*, 2009).

In plants, the chlororespiratory pathway also involves a chloroplast nucleotide dehydrogenase (NDH) complex, called NDH-1. NDH-1 is closely related to mitochondrial respiratory complex I (Sazanov *et al.*, 1998), contains 11 subunits with multiple transmembrane domains and reduces quinones with electrons from reduced Fd. *Chlamydomonas* and other green algae possess instead the NAD(P)H dehydrogenase 2 (NDA2) (Jans *et al.*, 2008), which has a similar function to that of NDH-1 in cyanobacteria and higher plants. NDA2 also utilizes electrons from NAD(P)H to non-photochemically reduce the PQ-pool through its non-covalently bound flavin mononucleotide co-factor (Jans *et al.*, 2008; Desplats *et al.*, 2009). But it also shows important differences from NDH-1 (reviewed in (Peltier *et al.*, 2016)): NDA2 is a membrane-bound monomeric flavoenzyme on the stromal side of the thylakoids (Jans *et al.*, 2008) and it is non-electrogenic (Melo *et al.*, 2004), in contrast to NDH-1 (Strand *et al.*, 2017). Although *Chlamydomonas* NDA2 can utilize NADPH, it favors NADH as a substrate (Desplats *et al.*, 2009). Interestingly there is a chloroplast localized *Chlamydomonas* transhydrogenase that could convert NADPH to NADH (Mus *et al.*, 2007).

Although chlororespiration was initially proposed to generate an electrochemical proton gradient in *Chlamydomonas* (Bennoun, 2002), this model was later disproven. The electrochemical proton gradient in the dark stems from hydrolysis of ATP derived from respiratory metabolism by

278 the CF_1F_O-ATPase or by an ATP dependent ionic pump (Bennoun, 1994). Because of the absence
279 of electrogenicity of NDA2 and the position of PTOX on the stromal side of the thylakoid, the
280 chlororespiratory pathway is now considered non-electrogenic in *Chlamydomonas*. Strictly
281 speaking, chlororespiration cannot be considered a photosynthetic AEF because it does not involve
282 photochemical event. However, the two enzymes NDA2 and PTOX are independently involved in
283 CEF and WWC, respectively (see 2.2 and 2.3).

284 **2.2 Cyclic electron flow around PSI**

285 Like in other organisms, *Chlamydomonas* shows a fast ($t_{1/2}$ ~100ms) reduction of P_{700+} after
286 continuous illumination in the presence of DCMU (Maxwell & Biggins, 1976), but this phase is
287 largely slowed-down in the presence of a cyt. b_6f inhibitor (Canaani *et al.*, 1989). This was
288 considered evidence for electron transfer from the PSI acceptors in the stroma towards P_{700+} via
289 cyt. b_6f. Given that CEF around PSI is a process accepted by most researchers working on
290 *Chlamydomonas* (Finazzi *et al.,* 1999, Iwai *et al.,* 2010, Alric *et al.,* 2010), the question of the
291 electron transfer pathways from PSI acceptors to the cyt. b_6f, the identity of the molecular players
292 involved in these pathways and the maximal rate of CEF have all given rise to intense debate over
293 the last decades (recently reviewed in (Nawrocki *et al.,* 2019a)).

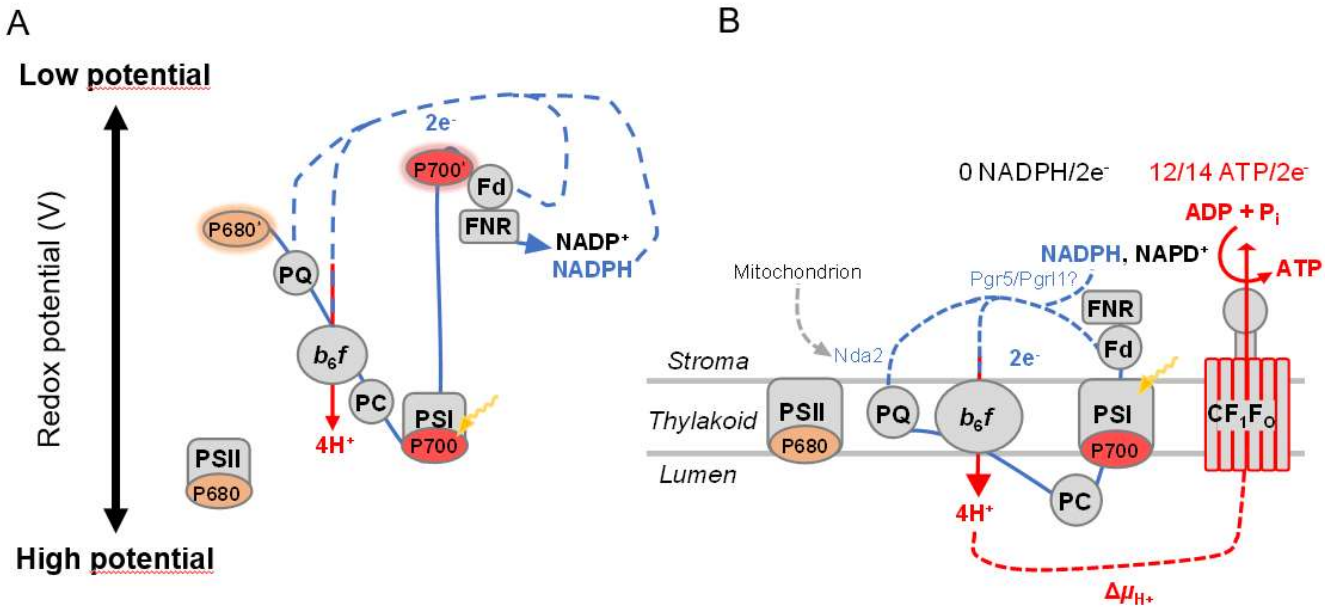

294

295 Figure 2: Cyclic Electron Flow (CEF) around Photosystem I. A. CEF in the Z scheme of photosynthesis.
296 B. Representation of the different routes of the CEF in the thylakoid membranes. Abbreviations: PSII,
297 Photosystem II; PSI, Photosystem I; b_6f, cytochrome b_6f; CF_1F_O, CF_1F_O ATPase; PC, plastocyanin; PQ,
298 Plastoquinol/Plastoquinone; Fd: ferredoxin; FNR: Ferredoxin/NADP Reductase; $\Delta\mu_{H^+}$, electrochemical
299 proton gradient; P680: special pair in the reaction center of PSII; P700: special pair in the reaction center
300 of PSI. Blue dashed line: electron transport. Red dashed line: proton transport.

301

302 ***The possible routes for CEF in Chlamydomonas***

303 Like in plants (Shikanai, 2007), two major CEF routes have been described in
304 *Chlamydomonas* (Figure 2). The "major one" corresponds to the original pathway postulated by
305 Arnon and co-workers (Arnon *et al.*, 1954) following the observation of light-dependent ATP
306 phosphorylation in isolated chloroplasts that is mediated by the stromal electron carrier ferredoxin
307 (Fd). A membrane-bound Fd-PQ oxidoreductase (FQR) was proposed to reinject electrons from
308 the PSI acceptor side to the inter-system ETC (Moss & Bendall, 1984; Bendall & Manasse, 1995).

309 This pathway was serendipitously "rediscovered" almost 50 years later in a screening for
310 *Arabidopsis* qE-defective mutants, lacking a small, stromal-soluble protein named PGR5 (for
311 *proton gradient regulation 5*) (see Table 1) (Munekage *et al.*, 2002). Shortly after, the molecular
312 partner of PGR5, PGRL1 (PGR5-like), was discovered, which is an integral thylakoid protein with
313 both termini stroma-exposed and six redox-active cysteine residues (DalCorso *et al.*, 2008). In
314 *Arabidopsis*, Hertle and co-authors (2013) (but see also (Szymańska *et al.*, 2011)) reported *in vitro*
315 FQR activity from PGRL1 (albeit on a non-physiological quinone species) which they attributed
316 to its redox-active cysteine residues presenting a binding site for a Fe-containing cofactor and
317 triggered by PGRL1 heterodimerization with PGR5 (however see (Strand *et al.*, 2016) for critical
318 discussion of this hypothesis). While both PGR5 and PGRL1 have been shown to modulate
319 *Chlamydomonas* CEF regulation (Alric, 2014; Johnson *et al.*, 2014; Jokel *et al.*, 2018; Buchert *et*
320 *al.*, 2020), their direct involvement in electron recycling from a PSI acceptor to the PQ-pool
321 remains debated (Nawrocki *et al.*, 2019a). Although this PGR5/PGRL1 pathway was sensitive to
322 inhibition by antimycin-A (a mitochondrial Complex III inhibitor) in plants, it is not the case in
323 *Chlamydomonas* (Iwai *et al.,* 2010, Antal *et al.,* 2013).

324 The second CEF pathway was first described in *Synechocystis* mutated in the membrane-
325 bound, nucleotide dehydrogenase (NDH) gene (Ogawa, 1991; Mi *et al.*, 1995). In the mutants the
326 PQ-pool remained oxidized after illumination in the presence of PSII inhibitor DCMU, as opposed
327 to the wildtype in which PQ re-reduction was attributed to NDH-1 (Mi *et al.*, 1995). In
328 *Chlamydomonas* and other green algae, the secondary CEF pathway involves a different NAD(P)H
329 dehydrogenase, NDA2 (Jans *et al.*, 2008), already described in the chlororespiratory section (see
330 2.1). In CEF, NDA2 utilizes electrons from NAD(P)H to non-photochemically reduce the PQ-pool

while *nda2* mutants show a shorter post-illumination fluorescence rise than wild-type because NAD(P)H can not be mobilized to reduce the PQ pool (Jans *et al.*, 2008).

The light sensitivity of *Arabidopsis* mutants lacking both NDH and PGR5/PGRL1 pathways confirmed the essential role of CEF in photosynthesis (Munekage *et al.*, 2004). It also suggested that these two routes, functionally redundant, represented the only possibilities for CEF in plants. However, emerging structural information on cyt. b_6f (Stroebel *et al.*, 2003; Malone *et al.*, 2019) suggests the presence of a third potential pathway for CEF in *Chlamydomonas.* In this model, CEF would be completed via direct reinjection of electrons to cyt. b_6f following the classic Q-cycle (Mitchell, 1975) from a stromal electron donor. This model, first proposed by Chain (1982) and reconsidered more recently based on kinetics studies (Joliot & Johnson, 2011; Nawrocki *et al.*, 2019a; Buchert *et al.*, 2020), does not involve lateral diffusion of PQ in the thylakoid membranes and supposes bifurcated reduction of the Q_i bound quinone, with one electron coming from a stromal reductant and the other from the low-potential chain (Vol 2, Chapter 17).

The maximal rate of CEF in Chlamydomonas

To evaluate the physiological importance of the CEF around PSI, it is important to determine the maximal rate of CEF relative to the maximal rate of LEF; this is a long-standing question. In *Chlamydomonas*, the maximal rate of LEF is usually 100-150 electrons per second per photosystem (Maxwell & Biggins 1976; Alric, 2010; Nawrocki *et al.*, 2019b). In the presence of DCMU, the rate of P_{700}^+ re-reduction following exposure to saturating light has been used as a direct measure of the rate of CEF and has provided typical values of 5-15 electrons per second per PSI under oxic conditions (Maxwell & Biggins, 1976; Alric *et al.,* 2010; Takahashi *et al*., 2013). This CEF rate would be insufficient to complement the ATP produced by LEF and sustain the

354 measured rates of carbon assimilation. However, CEF measurements in the presence of DCMU
355 are not always valid for estimating CEF rates under physiological conditions. If LEF and CEF are
356 in competition for a common substrate, whether oxidized PQ or reduced Fd, inhibition of LEF
357 would elevate CEF (Fan *et al.,* 2016). In contrast, CEF might be limited by the lack of reduced
358 Fd/NADPH (Alric *et al.*, 2010; Lucker & Kramer, 2013). This latter possibility is supported by
359 the occurrence of higher rates of CEF under anoxic conditions, where reducing equivalents from
360 glycolysis in the chloroplast would maintain elevated reduction of the ETC. Under these conditions
361 (DCMU plus anoxia), rates as high as 60 electrons per second per PSI were measured (Alric *et al.,*
362 2010), which was supported by measurements taken during the first seconds following a dark-to-
363 light transition in the absence of DCMU (Nawrocki *et al*, 2019b).

364 With this value in mind, it becomes possible to evaluate the relevance of the NDA2 and
365 PGR5/PGRL1 pathways for CEF on a kinetic basis. The slow rate of the NDA2 reaction under
366 aerobic conditions (2-4 $e^- PSI^{-1} s^{-1}$ (Houille-Vernes *et al.*, 2011) suggested that its role may be
367 restricted to chlororespiration (Nawrocki *et al.*, 2015). However, during N-deprivation, inhibition
368 of the CBC leads to elevated levels of stromal reductant and a doubling of the rate of NDA2-
369 dependent P_{700}^+ re-reduction that does not require PGR5/PGRL1 (Saroussi *et al.*, 2016). This
370 discrepancy could reflect a different redox state of stromal reductants in the two experiments: the
371 rate of NDA2 would be limited by NAD(P)H availability under oxic conditions. In
372 *Chlamydomonas*, *pgrl1* mutants were shown to transiently exhibit the same maximal CEF rate as
373 wild-type cells upon a dark-to-light shift (Nawrocki *et al.*, 2019b). This was also the case for *pgr5*
374 mutants of *Arabidopsis*; the maximal CEF rate was not affected relative to the wild- type plants
375 (Nandha *et al.*, 2007). In both cases, it was suggested that PGR5 and PGRL1 could play a
376 regulatory role in CEF, possibly via redox poising of the chloroplast, instead of playing a direct

377 FQR function. The supposed low rate reported for NDA2, together with the unchanged maximal
378 rate of CEF in *pgrl1* mutants, were taken as clues for the existence of another CEF pathway that
379 can deliver electrons to the Q_i site of cyt. b_6f, which would explain the high rates of CEF measured
380 in *Chlamydomonas*. We note, however, that compensation by NDA2 in the *Chlamydomonas pgrl1*
381 mutants cannot be fully excluded. Characterization of a *Chlamydomonas nda2*/*pgrl1* double
382 mutant would help determine if the NDA2 and PGR5/PGRL1 pathways are redundant or if neither
383 of these pathways represent major route of CEF.

384 ***A classical (Mitchellian) Q-cycle involved in CEF?***

385 Independent of the kinetic analyses discussed above, a renewed interest in the classical Q-
386 cycle mediated CEF model comes from crystallography and structural analyses of differences
387 between cyt. b_6f and cyt. bc_1 (Vol 2, Chapters 11 and 17). Notably, cyt. b_6f possesses three unique
388 prosthetic groups per monomer: one chlorophyll *a*, one β-carotene and one special haem c_i
389 (Stroebel *et al.*, 2003), which could be involved in direct electron transfer from reduced Fd to the
390 quinone in the Q_i site (Stroebel *et al.*, 2003; Malone *et al.*, 2019). Haem c_i is unique in its lack of
391 coordination of the haem iron (no amino acid axial ligand) and being covalently bound in the
392 vicinity of the high potential b_H at the Q_i site (Stroebel *et al.*, 2003; Alric *et al.*, 2005; Yamashita
393 *et al.*, 2007) yielding strong magnetic dipolar coupling between the two haems (Baymann *et al.*,
394 2007). Interestingly, FNR is known to interact with the cyt. b_6f stromal surface (Clark *et al.*, 1984;
395 Zhang *et al.*, 2001; Mosebach *et al.*, 2017) and FNR has been proposed to tether reduced Fd in the
396 proximity of the two high potential haems, enabling PQ reduction, which would attribute the FQR
397 function to cyt. b_6f (Joliot & Johnson, 2011; Goss & Hanke, 2014; Nawrocki *et al.*, 2019a). New
398 structural insights concerning cyt. b_6f seems to support this model (Malone *et al.*, 2019), which
399 resembles the Mitchellian Q cycle model with one electron coming from the stroma. Specifically,

400 the propionate of haem c_i can switch conformation upon PQ binding to the Q_i pocket, which could
401 reflect the previously documented decrease in c_i redox potential in dark-adapted algae (reducing
402 conditions) (Alric *et al.*, 2005) and provide a mechanistic basis for electron channelling from the
403 FNR:Fd complex to PQ mediated by haem c_i (Malone *et al.*, 2019). Highlighting the homodimer
404 structure of cyt. b_6f, its central cavity and the edge-to-edge distance that allows electron transfer
405 between opposing haems b_L (Lanciano *et al.*, 2013), Nawrocki et al. (2019a) proposed that
406 oxidized PQ in the Q_o site of one monomer could be shuttled to the Q_i site of the other monomer.
407 In this model, CEF and LEF would not compete for a common pool of oxidized PQ; instead PSII
408 would reduce the PQ pool that is freely diffusing in the thylakoid membranes, whereas CEF would
409 inject an electron into a PQ located in the cyt. b_6f cavity, allowing high CEF even under conditions
410 in which the PQ pool is highly reduced by LEF. Interestingly, a bound PQ molecule was observed
411 by cryo-electron microscopy between haems c_i and b_H of opposing cyt. b_6f monomers, which could
412 represent a glimpse at this putative trans-monomer shuttle (Malone *et al.*, 2019). By measuring
413 redox kinetics associated with the different haems of cyt. b_6f, Buchert et al. (2020) proposed that
414 the switch between the modified Q-cycle associated with LEF and a classical Q-cycle driving CEF
415 requires PGR5, explaining the different reports of CEF phenotypes in *pgr5* mutants (Munekage *et*
416 *al.*, 2002; Alric, 2014; Johnson *et al.*, 2014; Godaux *et al.*, 2015).

417 ***Influence of supercomplexes and state transitions on CEF***

418 Various early studies (Canaani *et al.*, 1989; Herbert *et al.*, 1990; Vallon *et al.,* 1991;
419 Majeran *et al.,* 2001; Finazzi *et al.*, 2002) have indicated a relationship between state transitions,
420 which regulate the attachment of LHCII to PSII (state 1) or PSI (state 2) (Vol 2, Chapter 24), and
421 CEF in *Chlamydomonas*. While PSII sets the redox poise of the ETC, only PSI participates in CEF.
422 Because the formation of state 2 increases the PSI antenna size, it would be expected to increase

PSI turnover and CEF if the latter is light-limited. During the formation of state 2, a fraction of the cyt. b_6f complex also moves from the PSII-enriched appressed regions of the thylakoid membrane to the stroma lamellae where PSI is localized (Vallon *et al.,* 1991).

Because the co-localization of PSI and cyt. b_6f and the increase of PSI antenna size coincide during the transition to state 2, the question of their relative effects on CEF was rather difficult to address. In 2010, Iwai and collaborators isolated a PSI-LHCI-LHCII-cytb_6f-PGRL1-FNR supercomplex (but lacking PGR5) under state 2. The transmembrane thylakoid phosphoprotein PETO, specific to green algae and interacts with the protein ANR1, was shown to be involved in the co-migration of PSI and cyt. b_6f. Furthermore, mutants of PETO displayed lower CEF under anoxiic conditions (Takahashi et al, 2016). Later reports (Buchert et al, 2018) failed to isolate supercomplexes containing PSI and cyt. b_6f but confirmed ANR1 and PETO as cyt. b_6f interactors. At first, the "Supercomplex model" proposed CEF activation upon a state 1 to state 2 transition, allowing for (i) compartmentalization between CEF and LEF, which would limit their competition for the mobile electron carriers (PQ, PC, Fd) (Joliot & Joliot, 2002; Alric *et al.*, 2010) and, (ii) tight interactions between Fd-FNR, cyt. b_6f and the PQ-pool, favoring fast electron transfer and high CEF rates *in vivo* (Iwai *et al.*, 2010; Joliot & Joliot, 2002; Alric *et al.*, 2010). However, those experiments could not disentangle the effect of state transitions per se, and that of the anaerobic treatment used for inducing the state transition (which would result in a decrease in the concentration of cellular ATP and an increase in reducing power). When a mutant specifically devoid of state transition was used as a control, the link between state transitions and increased CEF or supercomplex formation was ruled out: an increase in CEF and supercomplex formation is therefore induced by a redox trigger rather than state transitions (Lucker & Kramer, 2013; Takahashi *et al.*, 2013). Accordingly, whether involving the formation of supercomplexes or not,

446 the division of electron fluxes between LEF and the PGR5/PGRL1 CEF pathway seem to obey a
447 competition model that is regulated by the stromal ATP/NADPH ratio (Alric *et al.*, 2010; Johnson
448 *et al.*, 2014). Based on the absence of the PSI antennae subunits LHCA2 and LHCA9 in the
449 supercomplex, Steinbeck and collaborators (2018) recently proposed a mechanistical model for
450 CEF supercomplex assembly that is driven by the dissociation of these LHC under anoxia.
451 Remarkably, Δ*lhca2* knockout mutants exhibited a higher CEF rate under aerobic conditions than
452 wild-type cells under either aerobic or anaerobic conditions (Steinbeck *et al.*, 2018). In any case,
453 direct electron transfer from FNR:Fd to cyt. b_6f appears to be possible whether or not cyt. b_6f forms
454 a supercomplex with PSI. Furthermore, CEF rates in the supercomplexes remain to be measured
455 experimentally as *in vivo* experiments in yeast showed that the cyt. *bc1*-CcOx supercomplex does
456 not display faster kinetics of cytochrome *c* mediated electron transfer between the two complexes
457 (Trouillard *et al.*, 2011; see however Berndtsson *et al.*, 2020).

458 ***Proton pumping and regulatory role of CEF***

459 At present we can only speculate on the path of electrons in the CEF pathway, but through
460 the Q-cycle, it undoubtedly participates in the pumping of extra protons into the lumen. In plants,
461 the yield of protons pumped per electron recycled around PSI is different between PGR5/PGRL1
462 (2 H^+/e^-) and NDH-1 (3 or 4 H^+/e^-) pathways, due to the electrogenicity of the NDH-1 complex
463 (Strand *et al.,* 2017; Strand *et al.,* 2019). Because NDA2 is non-electrogenic (Melo *et al.*, 2004),
464 the NDA2 CEF pathway in *Chlamydomonas* participates in the $\Delta\mu_{H+}$ only to the same extent as
465 the PGR5/PGRL1 pathway or CEF based on the classical Q cycle, i.e. 2 H^+/e^-.

466 ## 2.3 Water-to-water cycles

Electrons extracted from water at PSII can be rerouted from LEF to various oxidases that utilise O_2 as electron acceptor and produce water (Curien *et al.*, 2016). This creates various AEFs linking the photo-induced oxidation of water to O_2 at one end of the ETC, to the reduction of O_2 to water at the other end, creating a WWC (or pseudo-cyclic electron fluxes).

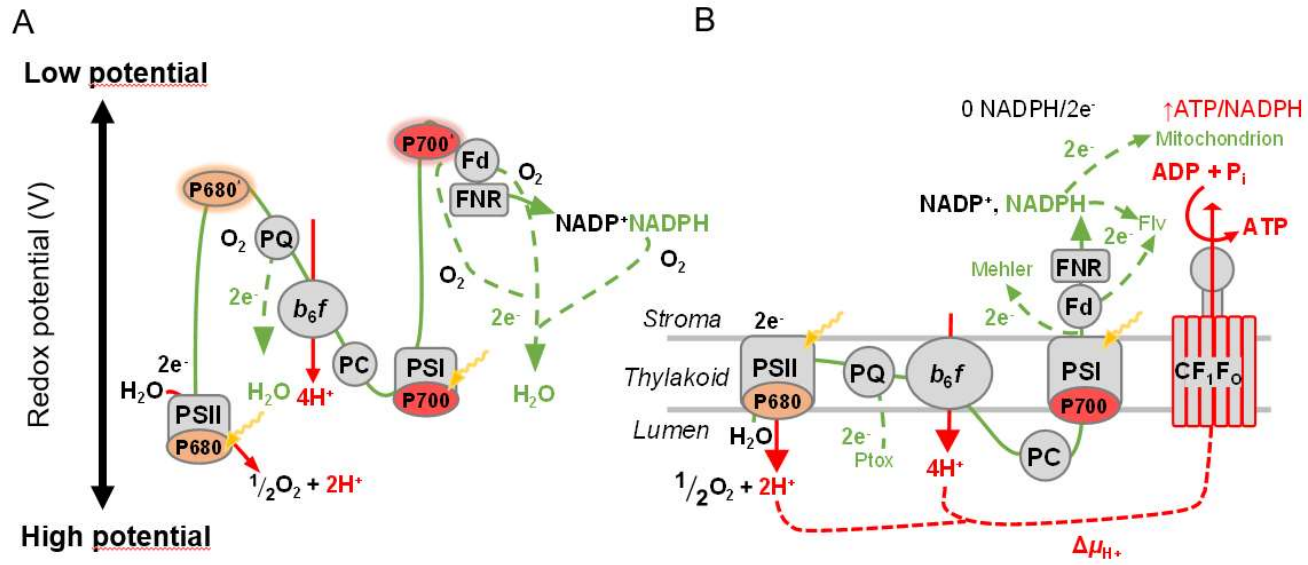

Figure 3: the Water-to-Water Cycles (WWC). A. Water-to-water cycles in the Z scheme of photosynthesis. B. Representation of the different WWCs in the thylakoid membranes. Abbreviations: PSII, Photosystem II; PSI, Photosystem I; b_6f, cytochrome b_6f; CF_1F_O, CF_1F_O ATPase; PC, plastocyanin; PQ, Plastoquinol/Plastoquinone; Fd: ferredoxin; FNR: Ferredoxin/NADP Reductase; $\Delta\mu_{H^+}$, electrochemical proton gradient; P680: special pair in the reaction center of PSII; P700: special pair in the reaction center of PSI. Green dashed line: electron transport. Red dashed line: proton transport.

PSII-PTOX pathway

By reoxidizing PQ, PTOX can divert electrons from the main electron transport chain. Therefore, it has been suggested to have a function as a safety-valve relieving excitation pressure on PSII under light exposure (Cournac *et al.*, 2000; Niyogi, 2000; McDonald *et al.*, 2011). It may indeed fulfill such a function in organisms that inhabit harsh environments and accumulate high levels of PTOX content (Stepien & Johnson, 2009; Laureau *et al.*, 2013; Ghotbi-Ravandi *et al.*,

484 2019). Supporting this, an important rerouting of electrons towards PTOX was reported in
485 cyanobacteria and prasinophytes (Bailey *et al.,* 2008; Cardol *et al.,* 2008). Because electrons are
486 initially extracted from H_2O at PSII in LEF, photo-induced oxidation of PQH_2 coupled to O_2
487 reduction by PTOX forms a WWC. However, a photoprotective role for PTOX seems conflicting
488 with its pro-oxidant activity (Heyno *et al.*, 2009; Krieger-Liszkay & Feilke, 2016), although we
489 cannot exclude that the ROS generated has signaling functions (Rea *et al.*, 2018). A putative
490 photoprotection role for PTOX is also hard to reconcile with its much slower rate compared to
491 PSII turnover under light intensities commonly experienced by *Chlamydomonas* (Houille-Vernes
492 *et al.*, 2011) and *Arabidopsis* (Joliot & Joliot, 2002). Indeed, comparable electron transport rates
493 measured between *Chlamydomonas* WT and *ptox2* mutants under steady illumination suggests
494 that the main function of PTOX is not as a photoprotective valve (Nawrocki *et al.*, 2019c).
495 Additional observations that WT and *ptox2* mutants have similar growth rates under continuous
496 illumination but that the growth rates of these mutants are severely impaired under intermittent
497 light, suggested that PTOX balances the redox state of the PQ-pool and PSI acceptors to optimize
498 photosynthesis upon dark-to-light transitions (Nawrocki *et al.*, 2019c) (see also (Houyoux *et al.*,
499 2011)). Heterotrophic and phototrophic metabolism intersect at the PQ-pool, a major hub of
500 regulation for electron transport. Therefore, the interplay between NDA2 and PTOX influences
501 the rates of LEF and CEF, respectively (Nawrocki *et al.*, 2019c), state transitions (Houille-Vernes
502 *et al.*, 2011) and metabolic exchanges (Wei *et al.*, 2014).

503 ***Flavodiiron proteins***

504 Flavodiiron proteins (FLV) were first identified in cyanobacteria (Helman *et al.*, 2003) but
505 have since been documented in all green lineages except angiosperms (Ilík *et al.,* 2017). The *FLV*
506 genes are absent in red and most brown algal genomes (see reviews (Peltier *et al.*, 2010; Alboresi

507 *et al.*, 2019)), with homologs reported in the genomes of the Symbiodiniaceae (dinoflagellates)
508 (Roberty *et al.,* 2014; Shimakawa *et al*., 2021). *Chlamydomonas* synthesizes both FLVA and
509 FLVB isoforms (homologous to Flv1 and Flv3, respectively, in cyanobacteria (Peltier *et al.*, 2010))
510 which are believed to associate in hetero-dimers to perform a WWC by photo-reducing O_2 at the
511 PSI acceptor side (Mustila *et al.*, 2016; Chaux *et al.*, 2017). So far, resolution of the Flv1 structure
512 has only been achieved for the two core domains (Flv1-ΔFlR) from *Synechocystis*, which doesn't
513 have the C-terminal NAD(P)H:flavin oxidoreductase extension (Borges *et al.*, 2019). Using *in*
514 *silico* modeling, Alboresi and co-authors (2019) suggested a distinct organisation of the catalytic
515 sites between FLVA and FLVB (in the bryophyte *Physcomitrella patens*), enabling activity of the
516 dimer, and a possible conformational change that allows for rapid regulation in response to external
517 cues like the stromal redox-state. The nature of the electron donor for the FLVs has been a matter
518 of debate in recent years. In *Synechocystis*, it was first proposed that the FLVs were able to receive
519 electrons directly from NAD(P)H via a C-terminal flavin oxidoreductase-like module (Vicente *et*
520 *al.*, 2002). However, FLVs were also reported to possibly interact with Fd in both *Chlamydomonas*
521 (Peden *et al.*, 2013) and *Synechocystis* (Cassier-Chauvat & Chauvat, 2014). It was recently
522 suggested that reduced Fd-PSI-F_AF_B - and not NADPH - is the redox partner of Flvs in
523 *Synechocystis* based on a comparative study of the re-oxidation kinetics of NADPH and of the iron
524 sulfur clusters of Fd, F_X and F_AF_B (terminal PSI acceptors) in wild type cells and *flv1*/*3* mutants
525 (Sétif *et al.*, 2020). Interestingly, for the P_{700} re-oxidation signal of *Chlamydomonas* wild-type
526 cells, *flv* and CEF mutants (Jokel *et al.*, 2018) have similar kinetics to those of *Synechocystis*
527 homologous strains (Sétif *et al.*, 2020), which possibly indicates that the *Chlamydomonas* FLVs
528 also receive electrons from reduced Fd-F_AF_B, as previously proposed by Jokel and co-authors
529 (2018).

Thus, the FLVs 'kick-start' linear electron transport, allowing for ATP production and alleviating limitations at the PSI acceptor side, while at steady-state, when the CBC enzymes are activated, the reducing equivalents are funnelled towards CO_2 reduction (Alboresi *et al.*, 2019). While the FLVs can serve as an extremely efficient immediate electron sink upon sudden light intensity shifts, their activity under steady state illumination was barely detected (Chaux *et al.*, 2017).

The Mehler reaction

The Mehler reaction was postulated following the observation that isolated pea thylakoids were able to photo-reduce O_2 to peroxide (H_2O_2) (Mehler, 1951). Subsequent seminal investigations by Asada and co-workers led to the identification of $O_2^{\bullet-}$ as the initial transient product generated by charge transfers from an internal PSI transporter on its acceptor side to O_2 (Asada & Kiso, 1973; Takahashi & Asada, 1988). The superoxide anion ($O_2^{\bullet-}$) is instantly disproportionated to H_2O_2 and O_2 by the thylakoid bound superoxide dismutase and both products are released in the stroma (Ogawa *et al.*, 1995). Although less toxic and a more efficient cellular messenger than $O_2^{\bullet-}$ (Rea *et al.*, 2018), H_2O_2 is harmful in excessive concentrations and is scavenged in the stroma by ascorbate peroxidase, which uses two ascorbate (AsA) molecules as electron donors to reduce H_2O_2 to two water molecules (making the Mehler reaction a WWC) and monodehydroascorbate (MDA) as products (Asada, 1999). Afterward, a MDA-reductase uses NADPH to recycle MDA back to AsA; this enzyme appears to play an important role in *Chlamydomonas*' photooxidative stress tolerance (Yeh *et al.*, 2019). Alternatively, MDA can spontaneously disproportionate to AsA and dehydroascorbate, which is converted to a supplemental AsA via the glutathione cycle, which also consumes NADPH (Lin *et al.*, 2018).

552 The PSI pigment-protein complex encompasses two symmetrical bifurcated electron
553 transfer chains spanning from P_{700} and converging on F_X, from phylloquinones (PhQ) A and B;
554 the latter are located respectively on the PsaA and PsaB subunits of the PSI heterodimer (Chapter
555 15). The classical view of the Mehler reaction is that reduced Fd is the sole electron donor to O_2
556 and that the reaction is favored by limited NADP+ availability (Furbank & Badger, 1983).
557 Recently, Kozuleva and co-authors (2021) proposed a novel mechanistic model for the Mehler
558 reaction after measuring the light-dependent second-order rate of O_2 photoreduction in various
559 *Chlamydomonas* PSI complexes with mutations in different electron carriers (see other crucial
560 work that led to the proposed model (Kozuleva & Ivanov, 2010; Kozuleva *et al.*, 2014;
561 Santabarbara *et al.*, 2015)). In this new model, F_AF_B participates to some extent in O_2
562 photoreduction, but its rate saturates under moderate irradiance intensities, and the major O_2
563 photoreduction site is associated with PhQ_A•- (Kozuleva *et al.*, 2021). Due to differences in the
564 protein scaffolds, the electron transfer to F_X is slower from PhQ_A than from PhQ_B, with lifetimes
565 of ~300 and ~15 ns respectively, making PhQ_A•- much more susceptible to transferring electrons
566 to exogenous O_2 and generating ROS (Cherepanov *et al.*, 2017). However, a mutation of a residue
567 that further delays PhQ_A•- decay, does not affect the quantum yield of PSI as the electron overflow
568 is redistributed to the PhQ_B branch of the reaction center (Santabarbara *et al.*, 2015).

569 While the Mehler reaction can contribute to the $\Delta\mu_{H+}$, quantifying this contribution *in vivo*
570 is challenging due to its transient products and interactions with other AEFs and electron flux
571 regulation mechanisms (see conflicting views on its significance in plants (Heber, 2002; Ort &
572 Baker, 2002)). For example, in *Chlamydomonas* exposed to high light intensity, it was
573 counterintuitive to find that the Mehler reaction was most active when the CO_2 concentration is
574 elevated and LEF is functioning optimally. When CO_2 is low, qE induction and state transitions

575 are sufficient to limit excitation pressure and H_2O_2 evolution (Roach *et al.*, 2015). Based on
576 experimental data and the thermodynamic parameters of electron transfers between PSI redox
577 carriers, Cherepanov and co-authors (2017) developed a model predicting that more than 0.3% of
578 total electron flux could be diverted to the Mehler reaction, although it is not clear how that electron
579 flux would be affected in the presence of FLV in *Chlamydomonas* (Chaux *et al.,* 2017). Likewise,
580 it is likely that some, if not most, of the light-dependent O_2 uptake attributed to the Mehler reaction
581 in previous studies of *Chlamydomonas* (Peltier & Thibault, 1985, Forti & Caldiroli, 2005, Franck
582 & Houyoux, 2008) was, in fact, due to the action of the - then unknown - FLVs (sometime called
583 Mehler-like reaction, as FLVs do not generate H_2O_2) (see section 3.1). Simultaneous quantification
584 of O_2 uptake and H_2O_2 evolution in FLV mutants will be necessary to determine how substantial
585 an electron sink the Mehler reaction can be in *Chlamydomonas*.

586 ***Other WWCs***

587 In photorespiration, O_2 rather than CO_2 enters Rubisco's catalytic site, which can trigger the
588 oxidation of ribulose 1,5 biphosphate (Rubisco oxygenase activity) and the synthesis of 3-
589 phosphoglycerate (3PGA) and 2-phophoglycolate (2PG). The subsequent suite of enzymatic
590 reactions that recycle these products (also called the C_2 cycle in reference to the two carbon
591 intermediates) is described in Vol 2, Chapters 7 and 8. A crucial trickle-down effect of recycling
592 2PG to 3PGA, is the regeneration of oxidized terminal electron acceptors like NADP+, NAD+,
593 oxidized Fd as well as ADP, fostering non-CO_2-assimilatory electron transport, which limits
594 overreduction of the ETC (reviewed in (Voss *et al.*, 2013)). Photorespiration is therefore a key
595 acclimation response in plants experiencing harsh conditions (chilling, high light, CO_2 limitation).

596 Rubisco's oxygenase activity is unavoidable, but its output tends to be limited in
597 microalgae due to the carbon concentration mechanisms (CCM) which consume ATP to generate

598 a high CO_2 concentration around Rubisco, which is mostly localized in pyrenoids (reviewed in
599 *Chlamydomonas* in (Wang *et al.*, 2015)) under low CO_2 conditions (Vol 2, Chapter 7). The
600 photorespiration pathway is conserved across photosynthetic phyla with two major divergences:
601 (i) reactions can be compartmentalized in different organelles including peroxisomes and
602 pyrenoids, which are not present in all taxa; *Chlamydomonas* possesses pyrenoids but no
603 peroxisomes (Goyal, 2002; see however Kong *et al.,* 2017) while vascular plants have no
604 pyrenoids; **(**ii) nature of the enzyme that oxidize glycolate to glyoxylate; *Chlamydomonas* (and all
605 Chlorophytes) has a glycolate dehydrogenase (GlcDH) similar to that in cyanobacteria (which
606 possess GlcDH and also glycolate oxidase (GOX)) while plants only have GOX (Esser *et al.*,
607 2014). *Chlamydomonas* GlcDH has three membrane spanning regions likely bound to the
608 mitochondrial membrane, and potentially feeds electrons to the ubiquinone pool of the respiratory
609 electron transport chain (Beezley *et al.*, 1976; Nakamura *et al.*, 2005; Aboelmy & Peterhansel,
610 2014). Cross-talk between photorespiration and mitochondrial activity was hypothesized to
611 explain the simultaneously increase in photorespiration and elevated mitochondria metabolism in
612 high light stress, which includes increased expression of genes encoding the key
613 photorespiratory enzymes, glycolate dehydrogenase and malate synthase, enzymes involved
614 in glyoxylate conversion to malate in the mitochondria (Davis *et al.*, 2013). A study by Nakamura
615 and co-workers (2005) strongly indicated that GlcDH supports photorespiratory function;
616 disruption of the *GlcDH* gene in *Chlamydomonas* led to a mutant requiring elevated levels of CO_2
617 for growth, which is phenotypically similar to higher plant mutants with photorespiratory defects.
618 Moreover, *GlcDH* mutants showed increased glycolate excretion into the medium (Nakamura *et*
619 *al.*, 2005). Although to a lesser extent, an increase in glycolate excretion was reported for
620 *Chlamydomonas* wild-type cells exposed to high light and low CO_2 when the photorespiration

621 pathway was inhibited (Moroney *et al.*, 1986; Nakamura *et al.*, 2005), and in immobilized cells
622 (for which diffusion of O_2 is low, resulting in an increase in the intracellular O_2 concentration as
623 the cells photosynthesize) (Garbayo *et al.*, 2005). However, increased extracellular glycolate
624 accumulation is often short-lived (Moroney *et al.*, 1986; Garbayo *et al.*, 2005; Günther *et al.*,
625 2012). This is possibly a consequence of overcompensation by enhanced induction of the CCM,
626 which limits photorespiratory carbon loss, as exemplified by the sustained up-regulation of CCM
627 genes compared to the transient increase observed for photorespiration genes following transfer of
628 the cells to low CO_2 (Tirumani *et al.*, 2019). In developing a system for sustained methane
629 bioproduction from glycolate, Wilhelm and co-workers (Günther *et al.*, 2012; Taubert *et al.*, 2019)
630 demonstrated low O_2/CO_2 acclimated *Chlamydomonas* cells shifted to low CO_2 conditions and
631 treated with the CCM and GlcDH inhibitor 6-ethoxy-2-benzothiazolesulfonamide, sustained
632 elevated production of glycolate for up to 21 d.

633 Another kind of WWC consists of cooperation between photosynthesis and respiration whereby
634 reducing power generated by photosynthetic electron transport is rerouted towards the
635 mitochondrial electron transfer chain, eventually fueling cytochrome oxidase (complex IV) and
636 Alternative Oxidase (AOX). Such WWCs, described in *Chlamydomonas* and plants (Lemaire *et*
637 *al*., 1988; Krömer & Heldt, 1991), involve the malate/oxaloacetate valve as well as other metabolic
638 shuttles that enable the transport of reducing power from the chloroplast to the mitochondrion via
639 the cytosol (Scheibe *et al*., 2005) (Vol 2, Chapter 8). The first enzyme of the malate valve is the
640 NADP-malate dehydrogenase (NADP-MDH), which is found only in the green lineage where its
641 activation is redox-regulated by thioredoxins (Selinski & Scheibe, 2019). In contrast to plants in
642 which NADP-MDH contains two disulfide bonds, *Chlamydomonas* NADP-MDH contains only
643 one disulfide bond at the C-terminal extension (Issakidis *et al.,* 1996; Lemaire et *al.,* 2005). The

644 plastidial isoform, MDH5, can use NADPH generated by photosynthesis to reduce oxaloacetate to
645 malate. The malate can then be transported to the cytosol/mitochondrion via specific transporters
646 localized in the chloroplast envelope. *Chlamydomonas* possesses three homologues of the
647 *Arabidopsis* chloroplastic 2-oxaloacetate/malate transporter, which exports malate and imports of
648 2-oxaloacetate (Weber *et al.,* 1995). Among them, LCI20 is found in the choroplast proteome and
649 was shown to be induced under low CO_2 conditions (Terashima *et al.,* 2011).

650 Additionally, extra ATP generated in the mitochondrion can be imported back to the chloroplast
651 through mitochondrial ATP/ADP translocators and potentially the DHAP/3-PGA shuttle
652 (Hoefnagel *et al*., 1998). Such cooperation can restore photoautotrophic growth to a
653 *Chlamydomonas* strain lacking the chloroplastic CF_1F_O-ATPase. Excess reducing power from the
654 chloroplast can be routed to the mitochondrion where it can be used for ATP synthesis, and this
655 mitochondrial ATP can then be used for CO_2 fixation in the chloroplast (Lemaire *et al.,* 1988).
656 The study of *Chlamydomonas* mutants affected in mitochondrial respiration indicate an important
657 role for energetic exchange between the organelles (Vol 2, Chapter 11). For examples, mutants of
658 the respiratory complexes (especially Complex III) show a decreased rate of photosynthesis, which
659 is even stronger when photosynthetic regulatory pathways are affected (e.g., *stt7* and *pgrl1*
660 background*)* (Massoz *et al.,* 2017; Massoz *et al.,* 2015; Cardol *et al.,* 2003, Cardol et al, 2009).
661 *Chlamydomonas* mutants of AOX also show an increased accumulation of ROS and degradation
662 of the photosynthetic machinery under high light conditions (Kaye *et al.,* 2019). This suggests that
663 the rerouting of photosynthetically derived electrons towards AOX plays a major role in high light
664 acclimation.

665 ## 3- An integrated and historical view of the AEFs

666 We will now discuss common, important functions of alternative electron transfer
667 pathways: poising the redox state of the electron transfer chain; playing the role of an exhaust
668 valves; increasing the $\Delta\mu_{H+}$ and ATP production. AEFs actions are integrated within a cohesive
669 response to bottlenecks in photosynthetic electron transport. In the last two decades, the extensive
670 use of mutants has revealed that AEFs allow for survival under conditions in which an excess of
671 absorbed light energy can cause cellular damage. The interplays and redundancies of AEF
672 networks provide the cell with a plasticity that allows them to accommodate changing
673 environmental conditions and metabolic demands.

674 Some redundancy between AEFs is indeed observed, especially in recent years between
675 CEF around PSI and WWCs mediated by FLVs. The introduction of *FLV* genes from the moss
676 *Physcomitrella patens* into *Arabidopsis* (Yamamoto *et al.*, 2016) or rice (Wada *et al.*, 2018) can
677 partially increase growth in *pgr5* mutants. In *P. patents***,** the *pgrl1 flvA* double mutant exhibited
678 exacerbated defects under fluctuating light compared to the *pgrl1* or *flvA* single mutants (Storti *et*
679 *al.*, 2019). The functional redundancy of these AEFs also was observed in *Chlamydomonas*, where
680 a deficiency in CEF in *pgrl1* mutants is compensated for by up-regulating of FLV synthesis (Dang
681 *et al.*, 2014). Light-dependent O_2 uptake was increased in this mutant, reflecting a higher FLV
682 activity, together with the energetic cooperation with mitochondrial metabolism (Dang *et al.*,
683 2014). Recently, it was shown that the rate of carbon fixation in *Chlamydomonas* decreased under
684 low inorganic carbon in *pgrl flv* double mutants compared to wild-type cells, but not in the
685 respective single mutants (Burlacot *et al*., 2021). This indicates that the supplementary ATP
686 demand for CO_2 concentrating mechanisms is met by the synergistic action of FLVs and PGRL1-
687 mediated CEF (Burlacot *et al*., 2021). Moreover, it is likely that accelerated CEF historically
688 reported for *Chlamydomonas* under anoxia is not only the result of a more reduced photosynthetic

689 electron transport chain (Alric *et al.,* 2010) but is also the consequence of decreased electron leaks
690 through FLV activity (Nawrocki *et al*., 2019b).

691 The discussion above raises questions of the relative importance of the different AEFs:
692 what are the rates of the different pathways under steady-state photosynthesis? How do they
693 change with environmental conditions (CO_2, temperature) or the metabolic status of the cell?
694 Because of this redundancy, comparing mutants of the different AEFs will not be sufficient to
695 answer such questions; methodological advances in measuring and distinguishing the different
696 electron transfer pathways in photosynthesis are needed to address these questions. During the
697 pioneering era of photosynthesis research, scientists were focused on making precise
698 measurements of the maximum quantum yield of the photosynthetic process. The number of
699 photons required for production of an O_2 molecule (or assimilation of a CO_2 molecule) is crucial
700 for understanding the molecular reactions/mechanisms used for converting light energy into
701 chemical energy. If we take the Emerson and Lewis value of 0.09 for the quantum yield (Emerson
702 & Lewis, 1943), it means that ~11 photons are needed (quantum requirement) to produce one
703 molecule of O_2 or to fix one molecule of CO_2. We now know that 8 electrons transferred linearly
704 through PSI and PSII are required for one O_2, that the quantum yield of PSI is close to 1 and that
705 of PSII is about 0.8, so there would be about 1-2 electrons rerouted to "alternative pathways". Now
706 that we know the molecular players involved in photosynthesis, and have mutants of AEFs, it
707 might be worth revisiting these studies; the maximum quantum yield of photosynthesis is expected
708 to depend both on the relative participation of the alternative pathways compared to linear electron
709 transfer, and on the energy-requirement of the CO_2-concentrating mechanism.

710 Another fundamental question relates to the kinetics of activation/deactivation of the
711 different AEFs in transitory conditions. While both the PGR5/PGRL1 and FLVs help limit PSI

712 photodamage during growth under rapidly fluctuating lights, FLVs have been shown to be
713 particularly crucial because of their more rapid induction compared to CEF (Jokel *et al.,* 2018).
714 Comparisons between *pgr5*, *pgrl1* and *flv Chlamydomonas* mutants showed that FLVs are essential
715 for survival under fluctuating light while the growth of *pgr5* and *pgrl1* single mutants was only
716 slowed-down (Jokel *et al.*, 2018). It was therefore posited that the FLVs act as a frontline defense
717 in the first few seconds of illumination, which also promotes the rapid formation of a ΔpH and the
718 development of NPQ (Chaux *et al.*, 2017), while it takes longer to reach high rates of CEF
719 following the onset of excess light (Jokel *et al.*, 2018; Storti *et al.*, 2019). As *Chlamydomonas* is a
720 soil-dwelling alga that may experience micro-oxic conditions in its natural environment, CEF may
721 sustain ATP production while FLVs may provide flexibility only at the onset of light. Another
722 example of the sequential coordination of the different AEFs is probably the dark-to-light
723 transition in anaerobic *Chlamydomonas* cells, which has been extensively studied for biohydrogen
724 production. In these conditions, the initial photosynthetic activity is entirely associated with
725 electron transfer from water oxidation at PSII to the hydrogenase, on the reducing side of PSI; this
726 activity is fully arrested in hydrogenase mutants (Godaux *et al.,* 2015; Burlacot *et al.,* 2021). The
727 electron flow from PSII to hydrogenase does not last for more than one or two minutes in wild-
728 type cells and is then replaced by other AEFs that play the role of accepting electrons in the gap
729 between the time at which hydrogenase activity declines and CO_2 fixation is initiated.
730 Interestingly, Godaux and collaborators, who measured PSI and PSII activity at the onset of light
731 but did not consider WWCs, concluded that CEF was the relay (Godaux *et al.,* 2015). Later,
732 Burlacot and collaborators performed a similar experiment that included measurements of light-
733 induced O_2 uptake (but no CEF measurements) in both wild-type cells and *flv* mutants and
734 concluded that the FLVs were the major components that fill the electron acceptor gap (Burlacot

735 *et al.,* 2018), as mentioned above. Concomitant measurements of CEF, H_2 production, CO_2 fixation
736 and FLV mediated O_2 uptake during the dark-to-light transitions would be useful to reconcile those
737 reports, which however suggest that, again, a synergic action of CEF and the FLVs allow the
738 transition from hydrogen production to carbon fixation.

739 How does *Chlamydomonas* relate to the great diversity of organisms performing oxygenic
740 photosynthesis with respect to the AEF circuitry? It is difficult to judge in which species or for
741 which kind of stress condition a particular pathway plays a more important role: why should a
742 regulatory pathway, identified as important for drought resistance in plants, be conserved in
743 oceanic algae that do not experience drought stress? Perhaps here we should recognize the
744 "chance" in the scientific approach: some AEFs have been identified and extensively studied in a
745 specific organism for practical or historical reasons. For example, genes of the chloroplast
746 NADPH:dehydrogenase complex involved in chlororespiration were identified in tobacco by
747 homology of the encoded proteins, derived from the sequence of the entire tobacco chloroplast
748 genome (Shinozaki *et al.,* 1986), with those of mitochondrial complex I (Matsubayashi *et al.,*
749 1987), and not because of studies focused on tobacco chlororespiration. Similarly, CEF around
750 PSI was not detected as a proton-motive force generator dependent on PSI excitation, but as a
751 process for ATP production in spinach thylakoid membranes (broken chloroplasts) reconstituted
752 with Fd (Tagawa *et al.,* 1963). In algae like *Chlamydomonas* (or *Chlorella*), the detection of AEFs
753 involving O_2 as a terminal electron acceptor instead of CO_2 was favored because (i) from an
754 experimental point of view, while it is difficult to assess the flow along a cyclic pathway where
755 the reaction intermediates do not change in concentration over time, it is relatively easy to measure
756 accumulation of an end-product of photosynthesis, like net O_2 evolution induced by continuous
757 illumination, (ii) they are aquatic species and detection of dissolved O_2 is easy and inexpensive,

758 and (iii) there is no, or little photorespiration (under high-CO_2 conditions or in low CO_2 with an
759 active CCM). *Chlamydomonas* is well suited for accurate and sensitive measurements of dissolved
760 O_2 using a polarographic method (Clark electrode), which is independent of the mass transfer of
761 O_2 between the liquid and the gas phase. These O_2 exchange measurements are done more cheaply
762 and easily in a liquid suspension of unicellular algae than on plant leaves where the gas flow
763 through a measuring chamber must be carefully controlled, and the detection of CO_2 is often
764 monitored using an infrared gas analyzer. In addition to the observation of the red drop (Emerson
765 & Lewis, 1943) and enhancement effect (Brody & Emerson, 1959), which suggested the existence
766 of two different photochemical centers, other observations, often based on the transient gush and
767 gulps of O_2, showed the existence of pools of carriers in the electron transport chain (Joliot 1965).
768 O_2 exchange was not only used to detect O_2 evolution but was also a pathfinder for O_2
769 photoreduction reactions. Perhaps the most illustrative example of the sensitivity of oxygen
770 exchange measurements in liquid suspensions was the observation of the "Kok effect" in the green
771 alga *Chlorella*, a break in the slope of the light-response curve of net O_2 exchange near the light
772 compensation point (Kok 1949). This finding suggested an inhibition of respiration under weak
773 illumination, a first insight into the interactions between photosynthesis and respiration. For O_2
774 exchange measurements, membrane inlet mass spectrometry (Hoch *et al.,* 1963) has allowed for
775 significant progress in identifying alternative electron transfer pathways based on discrimination
776 of different O_2 isotopes. The PSII-dependent oxygen evolution from water (E_O) is monitored at a
777 mass-to-charge ratio (m/*e* = 32, unlabeled $^{16}O_2$) while the oxygen uptake rate (U_O), corresponding
778 to mitochondrial respiration, photorespiration, chlororespiration and theMehler reaction, are
779 measured at m/e = 36 from labeled $^{18}O_2$ added to the sample before the measurement. These
780 experiments, more specific to respiration, confirmed the light-induced changes in O_2 exchange

781 observed earlier (Kok, 1949). In the case of *Scenedesmus*, O_2 photoreduction can compete with
782 CO_2 reduction to the point that it replaces it (Radmer & Kok, 1976); a similar phenomenon was
783 later observed for *Chlamydomonas* and hypothesized to contribute to the energy requirement of
784 the CO_2-concentrating mechanism (Sültemeyer *et al.,* 1993). We now know that high rates of O_2
785 photoreduction is dependent on the FLV proteins (Chaux *et al.,* 2017) and is mostly restricted to
786 terrestrial plants (gymnosperms), green algae (Chlorophyceae and Prasinophyceae), mosses and
787 cyanobacteria (Peltier *et al.,* 2010). Chlororespiration was also evidenced very early on using non-
788 labelled oxygen (Diner & Mauzerall, 1973), and later confirmed using membrane inlet mass
789 spectrometry (Peltier *et al.,* 1987, Vermeglio *et al.,* 1990, Cournac *et al.,* 2000).

790 Because the studies of AEFs among the different model species were partly a consequence
791 of "chance", a comparative approach may be required to understand the physiological roles of
792 alternative pathways within the context of photosynthetic diversity. It also suggests that
793 comparisons among model organisms or various species should not be restricted to concepts and
794 experimental results but should also take into account the materials and methods used in the work.

Table 1: Molecular actors of the Alternative Electron Flows.

Gene name, CreNumber, protein name and plastid localisation, mutant name, known environmental triggers for up-regulation of gene transcription in *Chlamydomonas* and important literature concerning the corresponding protein. One asterisks beside the literature reference indicates the first observation of the pathway, two asterisks indicates identification of the protein involved in the pathway, others represent ground-breaking results in *Chlamydomonas*. CEF PSI; cyclic electron transfer around photosystem I: WWC; water-water-cycle: HL; high light. The Mehler reaction, malate shuttle and photorespiration are excluded from water-to-water cycle (WWC) as they rely on a large suite of enzymes interacting with complete cell metabolism.**Literature:** 1: Arnon *et al.,* 1954, J. Am. Chem. Soc.; 2: Munekage *et al.,* 2002, Cell; 3: Johnson *et al.,*2014, Plant Physiol.; 4: Jokel *et al.,* 2018, Plant J.; 5: Dal'Corso *et al.,* 2008, Cell; 6: Petroustos *et al.,* 2009 J. Biol. Chem.; 7: Nawrocki *et al.,* 2019b, BBA-Bioenergetics; 8: Ogawa *et al.,* 1991 Proc. Natl. Acad. Sci.; 9: Jans *et al.,* 2009 Proc. Natl. Acad. Sci.; 10: Desplats *et al.,* 2009 J. Biol. Chem.; 11: Radmer & Kok, 1976 Plant Physiol.; 12: Helman *et al.,* 2003 Curr. Biol. ; 13: Chaux *et al.,* 2017 Plant Physiol.; 14: Diner & Mauzerall, 1973 BBA.; 15: Wu et *al.,* 1999 Plant Cell; 16: Houilles-Vernes *et al.,* 2011 Proc. Natl. Acad. Sci.; 17: Nawrocki *et al.,* 2019c Plant Physiol.

	Gene	Cre Locus ID	Protein	Protein localization	Mutants	Transcription up-regulation	Literature
CEF PSI	*PGR5*	Cre05.g242400	PGR5	Stroma	*Crpgr5*, *hpm91*	-Fe	1*, 2**, 3, 4
	PGRL1	Cre07.g340200	PGRL1	Thylakoid	*pgrl1*	-Fe	1*, 5**,6, 7
	NDA2	Cre19.g750547	NDA2	Thylakoid	Nda2-RNAi	-N, -S	8*, 9**,10
WWC	*FLVA*	Cre12.g531900	FLVA	Stroma	*flvB*	-CO_2, -S, HL	4, 11*,12**, 13
	FLV	Cre16.g691800	FLVB	Stroma	*flvB*	-CO_2, -S, HL	4, 11*,12**, 13
	PTOX1	Cre07.g350750	PTOX1	Thylakoid	*ptox1i*		14*,15**,16
	PTOX2	Cre03.g172500	PTOX2	Thylakoid	*ptox2, ptox2i*	-N	14*,15**,16,17

812 ## Acknowledgments

813 D.C. and B.B. acknowledge funding from the ERC Starting Grant
814 PhotoPHYTOMICS (ERC-2016-STG grant # 715579) and the “Initiative d’ Excellence” Program
815 from the French state (“DYNAMO” grant, ANR-11-LABX-0011-0). D.C., J.A. and B.B. also
816 acknowledge the Centre National de la Recherche Scientifique.

817

Bibliography

Aboelmy, M. H., & Peterhansel, C. (2014). Enzymatic characterization of *Chlamydomonas reinhardtii* glycolate dehydrogenase and its nearest proteobacterial homologue. *Plant Physiology and Biochemistry*, *79*, 25–30. https://doi.org/10.1016/j.plaphy.2014.03.009

Adachi, K., Oiwa, K., Nishizaka, T., Furuike, S., Noji, H., Itoh, H., … & Kinosita, K. (2007). Coupling of rotation and catalysis in F1-ATPase revealed by single-molecule imaging and manipulation. *Cell*, *130*(2), 309–321. https://doi.org/10.1016/j.cell.2007.05.020

Alboresi, A., Storti, M., Cendron, L., & Morosinotto, T. (2019). Role and regulation of class-C flavodiiron proteins in photosynthetic organisms. *Biochemical Journal*, *476*(17), 2487–2498. https://doi.org/10.1042/BCJ20180648

Allen, J. F. (2002). Photosynthesis of ATP-electrons, proton pumps, rotors, and poise. *Cell*, *110*(3), 273–276. https://doi.org/10.1016/S0092-8674(02)00870-X

Alric, J. (2014). Redox and ATP control of photosynthetic cyclic electron flow in *Chlamydomonas reinhardtii*: (II) Involvement of the PGR5-PGRL1 pathway under anaerobic conditions. *Biochimica et Biophysica Acta (BBA) - Bioenergetics*, *1837*(6), 825–834. https://doi.org/10.1016/j.bbabio.2014.01.024

Alric, J., Lavergne, J., & Rappaport, F. (2010). Redox and ATP control of photosynthetic cyclic electron flow in *Chlamydomonas reinhardtii* (I) aerobic conditions. *Biochimica et Biophysica Acta - Bioenergetics*, *1797*(1), 44–51. https://doi.org/10.1016/j.bbabio.2009.07.009

Alric, J., Pierre, Y., Picot, D., Lavergne, J., & Rappaport, F. (2005). Spectral and redox characterization of the heme Ci of the cytochrome b6f complex. *Proceedings of the National Academy of Sciences of the United States of America*, *102*(44), 15860–15865. https://doi.org/10.1073/pnas.0508102102

Amthor, J. S. (2010). From sunlight to phytomass: On the potential efficiency of converting solar radiation to phyto-energy. *New Phytologist*, *188*(4), 939–959. https://doi.org/10.1111/j.1469-8137.2010.03505.x

Antal, T. K., Kukarskikh, G. P., Bulychev, A. A., Tyystjärvi, E., & Krendeleva, T. (2013). Antimycin A effect on the electron transport in chloroplasts of two *Chlamydomonas reinhardtii* strains. *Planta*, *237*(5), 1241–1250. https://doi.org/10.1007/s00425-013-1843-y

Arnon, D.I., Whatley, F.R., & Allen M.B. (1954). Photosynthesis by Isolated Chloroplasts. II. Photosynthetic Phosphorylation, the Conversion of Light into Phosphate Bond Energy. *Journal of the American Chemical Society* 76: 6324–6329. https://doi.org/10.1021/ja01653a025

Asada, K. (1999). The water-water cycle in chloroplasts: Scavenging of active oxygens and dissipation of excess photons. *Annual Review of Plant Biology*, *50*, 601–639. https://doi.org/10.1146/annurev.arplant.50.1.601

Asada, K., & Kiso, K. (1973). The Photo-oxidation of epinephrine by spinach chloroplasts and Its inhibition by superoxide dismutase : Evidence for the formation of superoxide radicals in chloroplasts Kozi Asada and Kuniaki Kiso The Research for Food Science, Received The

857 divalent red. *Agricultural and Biological Chemistry*, *37*(2), 453–454. Retrieved from
858 http://joi.jlc.jst.go.jp/JST.Journalarchive/bbb1961/37.453

859 Bailey S., Melis A., Mackey K.R., Cardol P., Finazzi G., van Dijken G., Berg G.M., Arrigo K.,
860 Shrager J., & Grossman A (2008). Alternative photosynthetic electron flow to oxygen in
861 marine *Synechococcus*. *Biochimica et Biophysica Acta (BBA) - Bioenergetics*, 1;1777(3):269-
862 76. https://doi.org/10.1016/j.bbabio.2008.01.002

863 Baymann, F., Giusti, F., Picot, D., & Nitschke, W. (2007). The ci/bH moiety in the b6f complex
864 studied by EPR: A pair of strongly interacting hemes. *Proceedings of the National Academy*
865 *of Sciences of the United States of America*, *104*(2), 519–524.
866 https://doi.org/10.1073/pnas.0606369104

867 Beezley, B. B., Gruber, P. J., & Frederick, S. E. (1976). Cytochemical localization of glycolate
868 dehydrogenase in mitochondria of *Chlamydomonas*. *Plant Physiology*, *58*(3), 315–319.
869 https://doi.org/10.1104/pp.58.3.315

870 Bendall, D. S. (1982). Photosynthetic cytochromes of oxygenic organisms. *Biochimica et*
871 *Biophysica Acta (BBA) - Reviews On Bioenergetics*, *683*(2), 119–151.
872 https://doi.org/10.1016/0304-4173(82)90008-8

873 Bendall, D. S., & Manasse, R. S. (1995). Cyclic photophosphorylation and electron transport.
874 *Biochimica et Biophysica Acta (BBA) - Bioenergetics*, *8*. https://doi.org/10.1016/0005-
875 2728(94)00195-B

876 Bennoun, P. (1982). Evidence for a respiratory chain in the chloroplast. *Proceedings of the*
877 *National Academy of Sciences*, *79*(14), 4352–4356. https://doi.org/10.1073/pnas.79.14.4352

878 Bennoun, Pierre. (1994). Chlororespiration revisited: Mitochondrial-plastid interactions in
879 *Chlamydomonas*. *Biochimica et Biophysica Acta - Bioenergetics*, *1186*(1–2), 59–66.
880 https://doi.org/10.1016/0005-2728(94)90135-X

881 Bennoun, Pierre. (2002). The present model for chlororespiration. *Photosynthesis Research*, *73*(1–
882 3), 273–277. https://doi.org/10.1023/A:1020479920622

883 Berndtsson, J., Aufschnaiter, A., Rathore, S., Marin-Buera, L., Dawitz, H., Diessl, J., ... & Ott, M.
884 (2020). Respiratory supercomplexes enhance electron transport by decreasing cytochrome c
885 diffusion distance. *EMBO reports*, *21*(12), e51015.
886 https://doi.org/10.15252/embr.202051015

887 Borges, P. T., Romão, C. V., Saraiva, L. M., Gonçalves, V. L., Carrondo, M. A., Teixeira, M., &
888 Frazão, C. (2019). Analysis of a new flavodiiron core structural arrangement in Flv1-ΔFlR
889 protein from *Synechocystis* sp. PCC6803. *Journal of Structural Biology*, *205*(1), 91–102.
890 https://doi.org/10.1016/j.jsb.2018.11.004

891 Brody, M., & Emerson, R. (1959). The quantum yield of photosynthesis in *Porphyridium*
892 *cruentum*, and the role of chlorophyll a in the photosynthesis of red algae. *The Journal of*
893 *General Physiology*, *43*, 251–264. https://doi.org/10.1085/jgp.43.2.251

894 Buchert, F., Bailleul, B., & Hisabori, T. (2017). A γ-subunit point mutation in *Chlamydomonas*
895 *reinhardtii* chloroplast F1Fo-ATP synthase confers tolerance to reactive oxygen species.
896 *Biochimica et Biophysica Acta (BBA) - Bioenergetics*, *1858*(12), 966–974.

https://doi.org/10.1016/j.bbabio.2017.09.001

Buchert, F., Hamon, M., Gäbelein, P., Scholz, M., Hippler, M., & Wollman, F. A. (2018). The labile interactions of cyclic electron flow effector proteins. *Journal of biological chemistry*, *293*(45), 17559-17573. https://doi.org/10.1074/jbc.RA118.004475

Buchert, F., Bailleul, B., & Joliot, P. (2021). Disentangling chloroplast ATP synthase regulation by proton motive force and thiol modulation in *Arabidopsis* leaves. *Biochimica et Biophysica Acta (BBA) - Bioenergetics*, *1862*(8), 148434. https://doi.org/10.1016/j.bbabio.2021.148434

Buchert, F., Mosebach, L., Gäbelein, P., & Hippler, M. (2020). PGR5 is required for efficient Q cycle in the cytochrome b6f complex during cyclic electron flow. *Biochemical Journal*, *477*(9), 1631–1650. https://doi.org/10.1042/BCJ20190914

Burlacot, A., Dao, O., Auroy, P., Cuiné, S., Li-Beisson, Y., & Peltier, G. (2021). Alternative electron pathways of photosynthesis drive the algal CO2 concentrating mechanism. *bioRxiv*. https://doi.org/10.1101/2021.02.25.432959

Burlacot, A., Sawyer, A., Cuiné, S., Auroy-Tarrago, P., Blangy, S., Happe, T., & Peltier, G. (2018). Flavodiiron-mediated O2 photoreduction links H2 production with CO2 fixation during the anaerobic induction of photosynthesis. *Plant physiology*, *177*(4), 1639-1649

Canaani, O., Schuster, G., & Ohad, I. (1989). Photoinhibition in *Chlamydomonas reinhardtii*: Effect on state transition, intersystem energy distribution and Photosystem I cyclic electron flow. *Photosynthetic Research*, *20*, 129–146. https://doi.org/doi.org/10.1007/BF00034122

Cardol P., Gloire G., Havaux M., Remacle C., Matagne R., & Franck F. (2003). Photosynthesis and State Transitions in Mitochondrial Mutants of *Chlamydomonas reinhardtii* Affected in Respiration. *Plant Physiology* 133: 2010–2020. https://doi.org/ 10.1021/ja01653a025

Cardol, P., Alric, J., Girard-Bascou, J., Franck, F., Wollman, F. A., & Finazzi, G. (2009). Impaired respiration discloses the physiological significance of state transitions in Chlamydomonas. *Proceedings of the National Academy of Sciences*, *106*(37), 15979-15984. https://doi.org/10.1073/pnas.0908111106

Cardol P., Bailleul B., Rappaport F., Derelle E., Béal D., Breyton C., Bailey S., Wollman F.A., Grossman A., Moreau H., & Finazzi G. (2008) An original adaptation of photosynthesis in the marine green alga *Ostreococcus*. *Proceedings of the National Academy of Sciences, 3;* 105(22):7881-6. https://doi.org/10.1073/pnas.0802762105

Carol, P., & Kuntz, M. (2001). A plastid terminal oxidase comes to light: Implications for carotenoid biosynthesis and chlororespiration. *Trends in Plant Science*, *6*(1), 31–36. https://doi.org/10.1016/S1360-1385(00)01811-2

Cassier-Chauvat, C., & Chauvat, F. (2014). Function and regulation of ferredoxins in the cyanobacterium, *Synechocystis* PCC6803: Recent advances. *Life*, *4*(4), 666–680. https://doi.org/10.3390/life4040666

Chain, R. K. (1982). Evidence for a reluctant-dependent oxidation of chloroplast cytochrome b-563. *FEBS Letters*, *143*(2), 273–278. https://doi.org/10.1016/0014-5793(82)80115-4

935 Chaux, F., Burlacot, A., Mekhalfi, M., Auroy, P., Blangy, S., Richaud, P., & Peltier, G. (2017).
936 Flavodiiron proteins promote fast and transient O2 photoreduction in *Chlamydomonas*. *Plant*
937 *Physiology*, *174*(3), 1825–1836. https://doi.org/10.1104/pp.17.00421

938 Chaux, F., Peltier, G., & Johnson, X. (2015). A security network in PSI photoprotection:
939 Regulation of photosynthetic control, NPQ and O2 photoreduction by cyclic electron flow.
940 *Frontiers in Plant Science*, *6*:875. https://doi.org/10.3389/fpls.2015.00875

941 Cherepanov, D. A., Milanovsky, G. E., Petrova, A. A., Tikhonov, A. N., & Semenov, A. Y. (2017).
942 Electron transfer through the acceptor side of photosystem I: Interaction with exogenous
943 acceptors and molecular oxygen. *Biochemistry (Moscow)*, *82*(11), 1249–1268.
944 https://doi.org/10.1134/S0006297917110037

945 Clark, R. D., Hawkesford, M. J., Coughlan, S. J., Bennett, J., & Hind, G. (1984). Association of
946 ferredoxin-NADP+ oxidoreductase with the chloroplast cytochrome b-f complex. *FEBS*
947 *Letters*, *174*(1), 137–142. https://doi.org/10.1016/0014-5793(84)81092-3

948 Cournac, L., Redding, K., Ravenel, J., Rumeau, D., Josse, E. M., Kuntz, M., & Peltier, G. (2000).
949 Electron flow between photosystem II and oxygen in chloroplasts of photosystem I-deficient
950 algae is mediated by a quinol oxidase involved in chlororespiration. *Journal of Biological*
951 *Chemistry*, *275*(23), 17256–17262. https://doi.org/10.1074/jbc.M908732199

952 Couso, I., Vila, M., Rodriguez, H., Vargas, M. A., & León, R. (2011). Overexpression of an
953 exogenous phytoene synthase gene in the unicellular alga *Chlamydomonas reinhardtii* leads
954 to an increase in the content of carotenoids. *Biotechnology Progress*, *27*(1), 54–60.
955 https://doi.org/10.1002/btpr.527

956 Cramer, W. A., Hasan, S. S., & Yamashita, E. (2011). The Q cycle of cytochrome bc complexes:
957 A structure perspective. *Biochimica et Biophysica Acta (BBA) - Bioenergetics*, *1807*(7), 788–
958 802. https://doi.org/10.1016/j.bbabio.2011.02.006

959 Crofts, A. R., Shinkarev, V. P., Kolling, D. R. J., & Hong, S. (2003). The modified Q-cycle
960 explains the apparent mismatch between the kinetics of reduction of cytochromes c1 and bH
961 in the bc 1 complex. *Journal of Biological Chemistry*, *278*(38), 36191–36201.
962 https://doi.org/10.1074/jbc.M305461200

963 Curien, G., Flori, S., Villanova, V., Magneschi, L., Giustini, C., Forti, G., … & Finazzi, G. (2016).
964 The water to water cycles in microalgae. *Plant and Cell Physiology*, *57*(7), 1354–1363.
965 https://doi.org/10.1093/pcp/pcw048

966 DalCorso, G., Pesaresi, P., Masiero, S., Aseeva, E., Schünemann, D., Finazzi, G., … & Leister, D.
967 (2008). A complex containing PGRL1 and PGR5 is involved in the switch between linear
968 and cyclic electron flow in *Arabidopsis*. *Cell*, *132*(2), 273–285.
969 https://doi.org/10.1016/j.cell.2007.12.028

970 Dang, K.V., Plet, J., Tolleter, D., Jokel, M., Cuiné, S., Carrier, P., Auroy, P., Richaud, P., Johnson,
971 X., Alric, J. and Allahverdiyeva, Y., (2014). Combined increases in mitochondrial
972 cooperation and oxygen photoreduction compensate for deficiency in cyclic electron flow in
973 *Chlamydomonas reinhardtii. The Plant Cell, 26*(7), 3036-3050. https://doi.org/
974 10.1105/tpc.114.126375

975 Davis, M. C., Fiehn, O., & Durnford, D. G. (2013). Metabolic acclimation to excess light intensity
976 in *Chlamydomonas reinhardtii*. *Plant, Cell and Environment*, *36*(7), 1391–1405.
977 https://doi.org/10.1111/pce.12071

978 Desplats, C., Mus, F., Cuiné, S., Billon, E., Cournac, L., & Peltier, G. (2009). Characterization of
979 Nda2, a plastoquinone-reducing type II NAD (P) H dehydrogenase in *Chlamydomonas*
980 chloroplasts. *Journal of Biological Chemistry*, *284*(7), 4148–4157.
981 https://doi.org/10.1074/jbc.M804546200

982 Diner, B., & Mauzerall, D. (1973). Feedback controlling oxygen production in a cross-reaction
983 between two photosystems in photosynthesis. *Biochimica et Biophysica Acta (BBA) -*
984 *Bioenergetics*, *305*(2), 329–352. https://doi.org/10.1016/0005-2728(73)90180-1

985 Dumas, L., Zito, F., Blangy, S., Auroy, P., Johnson, X., Peltier, G., & Alric, J. (2017). A stromal
986 region of cytochrome b6f subunit IV is involved in the activation of the Stt7 kinase in
987 *Chlamydomonas*. *Proceedings of the National Academy of Sciences of the United States of*
988 *America*, *114*(45), 12063–12068. https://doi.org/10.1073/pnas.1713343114

989 Emerson, R., & Lewis, C. M. (1943). The dependence of the quantum yield of *Chlorella*
990 photosynthesis on wave lenghth of light. *American Journal of Botany*, *30*(3), 165.
991 https://doi.org/10.2307/2437236

992 Esser, C., Kuhn, A., Groth, G., Lercher, M. J., & Maurino, V. G. (2014). Plant and animal glycolate
993 oxidases have a common eukaryotic ancestor and convergently duplicated to evolve long-
994 chain 2-hydroxy acid oxidases. *Molecular Biology and Evolution*, *31*(5), 1089–1101.
995 https://doi.org/10.1093/molbev/msu041

996 Fan, D. Y., Fitzpatrick, D., Oguchi, R., Ma, W., Kou, J., & Chow, W. S. (2016). Obstacles in the
997 quantification of the cyclic electron flux around photosystem I in leaves of C3 plants.
998 *Photosynthesis Research*, *129*(3), 239–251. https://doi.org/10.1007/s11120-016-0223-4

999 Finazzi, G., Furia, A., Barbagallo, R. P., & Forti, G. (1999). State transitions, cyclic and linear
1000 electron transport and photophosphorylation in *Chlamydomonas reinhardtii*. *Biochimica et*
1001 *Biophysica Acta (BBA) - Bioenergetics*, *1413*(3), 117–129. https://doi.org/10.1016/S0005-
1002 2728(99)00089-4

1003 Finazzi, G., Rappaport, F., & Furia, A. (2002). Involvement of state transitions in the switch
1004 between linear and cyclic electron flow *Chlamydomonas reinhardtii*. *EMBO Reports*, *3*(3),
1005 280–285. https://doi.org/10.1093/embo-reports/kvf047

1006 Forti, G., & Caldiroli, G. (2005). State transitions in *Chlamydomonas reinhardtii*. The role of the
1007 Mehler reaction in state 2-to-state 1 transition. *Plant Physiology*, *137*(2), 492–499.
1008 https://doi.org/10.1104/pp.104.048256

1009 Franck, F., & Houyoux, P.-A. (2008). The Mehler reaction in *Chlamydomonas* during
1010 photosynthetic induction and steady-state photosynthesis in wild-type and in a mitochondrial
1011 mutant. *Photosynthesis. Energy from the Sun*, 581–584. https://doi.org/10.1007/978-1-4020-
1012 6709-9_131

1013 Furbank, R. T., & Badger, M. R. (1983). Oxygen exchange associated with electron transport and
1014 photophosphorylation in spinach thylakoids. *Biochimica et Biophysica Acta (BBA) -*

Bioenergetics s, *723*(3), 400–409. https://doi.org/10.1016/0005-2728(83)90047-6

Garbayo, I., Forján, E., Salguero, A., Cuaresma, M., Vega, J. M., & Vílchez, C. (2005). Enhancement of photorespiration in immobilized *Chlamydomonas reinhardtii* cells. *Biotechnology Letters*, *27*(4), 265–267. https://doi.org/10.1007/s10529-004-8352-9

Ghotbi-Ravandi, A. A., Shariati, M., Shobbar, Z. S., & Shahbazi, M. (2019). Expression pattern and physiological roles of Plastid Terminal Oxidase (PTOX) in wild and cultivated barley genotypes under drought stress. *Environmental and Experimental Botany*, *162*, 313–320. https://doi.org/10.1016/j.envexpbot.2019.03.007

Godaux, D., Bailleul, B., Berne, N., & Cardol, P. (2015). Induction of photosynthetic carbon fixation in anoxia relies on hydrogenase activity and proton-gradient regulation-like1-mediated cyclic electron flow in *Chlamydomonas reinhardtii*. *Plant Physiology*, *168*(2), 648–658. https://doi.org/10.1104/pp.15.00105

Goss, T., & Hanke, G. (2014). The end of the line: Can ferredoxin and ferredoxin NADP(H) oxidoreductase determine the fate of photosynthetic electrons? *Current Protein & Peptide Science*, *15*(4), 385–393. https://doi.org/10.2174/1389203715666140327113733

Goyal A. (2002). Glycolate metabolism in algal chloroplasts: Inhibition by salicylhydroxamic acid (SHAM). *Physiologia Plantarum* 116: 264–270. https://doi.org/ 10.1105/tpc.114.126375

Günther, A., Jakob, T., Goss, R., König, S., Spindler, D., Räbiger, N., … & Wilhelm, C. (2012). Methane production from glycolate excreting algae as a new concept in the production of biofuels. *Bioresource Technology*, *121*, 454–457. https://doi.org/10.1016/j.biortech.2012.06.120

Hahn, A., Vonck, J., Mills, D. J., Meier, T., & Kühlbrandt, W. (2018). Structure, mechanism, and regulation of the chloroplast ATP synthase. *Science*, *360*(6389). https://doi.org/10.1126/science.aat4318

Heber, U. (2002). Irrungen, Wirrungen? The Mehler reaction in relation to cyclic electron transport in C3 plants. In *Discoveries in Photosynthesis* (Vol. 103, pp. 551–559). Berlin/Heidelberg: Springer-Verlag. https://doi.org/10.1007/1-4020-3324-9_51

Helman Y, Tchernov D, Reinhold L, Shibata M, Ogawa T, Schwarz R, Ohad I, & Kaplan A. (2003). Genes encoding A-type flavoproteins are essential for photoreduction of O2 in cyanobacteria. *Current Biology* 13: 230–235. https://doi.org/ 10.1105/tpc.114.126375

Herbert, S. K., Fork, D. C., & Malkin, S. (1990). Photoacoustic measurements in Vivo of energy storage by cyclic electron flow in algae and higher plants. *Plant Physiology*, *94*(3), 926–934. https://doi.org/10.1104/pp.94.3.926

Hertle, A. P., Blunder, T., Wunder, T., Pesaresi, P., Pribil, M., Armbruster, U., & Leister, D. (2013). PGRL1 is the elusive ferredoxin-plastoquinone reductase in photosynthetic cyclic electron flow. *Molecular Cell*, *49*(3), 511–523. https://doi.org/10.1016/j.molcel.2012.11.030

Heyno, E., Gross, C. M., Laureau, C., Culcasi, M., Pietri, S., & Krieger-Liszky, A. (2009). Plastid alternative oxidase (PTOX) promotes oxidative stress when overexpressed in tobacco. *Journal of Biological Chemistry*, *284*(45), 31174–31180.

https://doi.org/10.1074/jbc.M109.021667

Hill, R., & Bendall, F. (1960). Function of the two cytochrome components in chloroplasts: A working hypothesis. *Nature*, *186*(4719), 136–137. https://doi.org/10.1038/186136a0

Hoch, G., Owens, O. v. H., & Kok, B. (1963). Photosynthesis and respiration. *Archives of Biochemistry and Biophysics*, *101*(1), 171–180. https://doi.org/10.1016/0003-9861(63)90547-2

Hoefnagel, M. H. N., Atkin, O. K., & Wiskich, J. T. (1998). Interdependence between chloroplasts and mitochondria in the light and the dark. *Biochimica et Biophysica Acta (BBA) - Bioenergetics*, *1366*(3), 235–255. https://doi.org/10.1016/S0005-2728(98)00126-1

Houille-Vernes, L., Rappaport, F., Wollman, F. A., Alric, J., & Johnson, X. (2011). Plastid terminal oxidase 2 (PTOX2) is the major oxidase involved in chlororespiration in *Chlamydomonas*. *Proceedings of the National Academy of Sciences of the United States of America*, *108*(51), 20820–20825. https://doi.org/10.1073/pnas.1110518109

Houyoux, P. A., Ghysels, B., Lecler, R., & Franck, F. (2011). Interplay between non-photochemical plastoquinone reduction and re-oxidation in pre-illuminated *Chlamydomonas reinhardtii*: A chlorophyll fluorescence study. *Photosynthesis Research*, *110*(1), 13–24. https://doi.org/10.1007/s11120-011-9686-5

Ilík, P., Pavlovič, A., Kouřil, R., Alboresi, A., Morosinotto, T., Allahverdiyeva, Y., … Shikanai, T. (2017). Alternative electron transport mediated by flavodiiron proteins is operational in organisms from cyanobacteria up to gymnosperms. *New Phytologist*, *214*(3), 967–972. https://doi.org/10.1111/nph.14536

Issakidis E, Lemaire M, Decottignies P, Jacquot JP, & Miginiac-Maslow M. (1996). Direct evidence for the different roles of the N- and C-terminal regulatory disulfides of sorghum leaf NADP-malate dehydrogenase in its activation by reduced thioredoxin. *FEBS Letters* 392: 121–124. https://doi.org/ 10.1016/0014-5793(96)00801-0

Iwai, M., Takizawa, K., Tokutsu, R., Okamuro, A., Takahashi, Y., & Minagawa, J. (2010). Isolation of the elusive supercomplex that drives cyclic electron flow in photosynthesis. *Nature*, *464*(7292), 1210–1213. https://doi.org/10.1038/nature08885

Janeiro, D. R., & Barrnett, R. (1982). Thylakoid membrane biogenesis in *Chlamydomonas reinhardtii* 137+: Cell-cycle variations in the synthesis and assembly of pigment. *Journal of Cell Biology*, *93*(2), 411–416. https://doi.org/10.1083/jcb.93.2.411

Jans, F., Mignolet, E., Houyoux, P. A., Cardol, P., Ghysels, B., Cuiné, S., … & Franck, F. (2008). A type II NAD(P)H dehydrogenase mediates light-independent plastoquinone reduction in the chloroplast of *Chlamydomonas*. *Proceedings of the National Academy of Sciences of the United States of America*, *105*(51), 20546–20551. https://doi.org/10.1073/pnas.0806896105

Johnson, X., Steinbeck, J., Dent, R. M., Takahashi, H., Richaud, P., Ozawa, S. I., … Alric, J. (2014). Proton gradient regulation 5-mediated cyclic electron flow under ATP- or redox-limited conditions: A study of ΔATPase pgr5 and ΔrbcL pgr5 mutants in the green alga *Chlamydomonas reinhardtii*. *Plant Physiology*, *165*(1), 438–452. https://doi.org/10.1104/pp.113.233593

Jokel, M., Johnson, X., Peltier, G., Aro, E. M., & Allahverdiyeva, Y. (2018). Hunting the main player enabling *Chlamydomonas reinhardtii* growth under fluctuating light. *Plant Journal*, *94*(5), 822–835. https://doi.org/10.1111/tpj.13897

Joliot, P. (1965). Cinétiques des réactions liées a l'émission d'oxygène photosynthétique. *Biochimica et Biophysica Acta (BBA) - Biophysics Including Photosynthesis*, *102*(1), 116–134. https://doi.org/10.1016/0926-6585(65)90207-4

Joliot, P., & Johnson, G. N. (2011). Regulation of cyclic and linear electron flow in higher plants. *Proceedings of the National Academy of Sciences of the United States of America*, *108*(32), 13317–13322. https://doi.org/10.1073/pnas.1110189108

Joliot, P., & Joliot, A. (2002). Cyclic electron transfer in plant leaf. *Proceedings of the National Academy of Sciences of the United States of America*, *99*(15), 10209–10214. https://doi.org/10.1073/pnas.102306999

Joliot, P., & Joliot, A. (2006). Cyclic electron flow in C3 plants. *Biochimica et Biophysica Acta (BBA) - Bioenergetics*, *1757*, 362–368. https://doi.org/10.1016/j.bbabio.2006.02.018

Junesch, U., & Gräber, P. (1987). Influence of the redox state and the activation of the chloroplast ATP synthase on proton-transport-coupled ATP synthesis/hydrolysis. *Biochimica et Biophysica Acta (BBA) - Bioenergetics*, *893*(2), 275–288. https://doi.org/10.1016/0005-2728(87)90049-1

Kaye Y, Huang W, Clowez S, Saroussi S, Idoine A, Sanz-Luque E, & Grossman A.R. (2019). The mitochondrial alternative oxidase from *Chlamydomonas reinhardtii* enables survival in high light. *Journal of Biological Chemistry* 294: 1380–1395. https://doi.org/10.1074/jbc.RA118.004667

Kok, B. (1949). On the interrelation of respiration and photosynthesis in green plants. *Biochimica et Biophysica Acta (BBA) - Bioenergetics*, *3*, 625–631. https://doi.org/10.1016/0006-3002(49)90136-5

Kozuleva, M. A., & Ivanov, B. N. (2010). Evaluation of the participation of ferredoxin in oxygen reduction in the photosynthetic electron transport chain of isolated pea thylakoids. *Photosynthesis Research*, *105*(1), 51–61. https://doi.org/10.1007/s11120-010-9565-5

Kozuleva, M. A., Petrova, A. A., Mamedov, M. D., Semenov, A. Y., & Ivanov, B. N. (2014). O2 reduction by photosystem i involves phylloquinone under steady-state illumination. *FEBS Letters*, *588*(23), 4364–4368. https://doi.org/10.1016/j.febslet.2014.10.003

Kozuleva, M., Petrova, A., Milrad, Y., Semenov, A., Ivanov, B., Redding, K. E., & Yacoby, I. (2021). Phylloquinone is the principal Mehler reaction site within photosystem I in high light. *Plant Physiology*, 1–11. https://doi.org/10.1093/plphys/kiab221

Kong F, Liang Y, Légeret B, Beyly-Adriano A, Blangy S, Haslam R.P., Napier JA, Beisson F, Peltier G, & Li-Beisson Y. (2017). *Chlamydomonas* carries out fatty acid β-oxidation in ancestral peroxisomes using a bona fide acyl-CoA oxidase. *Plant Journal* 90: 358–371. https://doi.org/ 10.1111/tpj.13498

Kramer, D. M., Cruz, J. A., & Kanazawa, A. (2003). Balancing the central roles of the thylakoid proton gradient. *Trends in Plant Science*, *8*(1), 27–32. https://doi.org/10.1016/S1360-

1135 1385(02)00010-9

1136 Kramer, D. M., Wise, R. R., Frederick, J. R., Alm, D. M., Hesketh, J. D., Ort, D. R., & Crofts, A.
1137 R. (1990). Regulation of coupling factor in field-grown sunflower: A Redox model relating
1138 coupling factor activity to the activities of other thioredoxin-dependent chloroplast enzymes.
1139 *Photosynthesis Research*, *26*(3), 213–222. https://doi.org/10.1007/BF00033134

1140 Krieger-Liszkay, A., & Feilke, K. (2016). The dual role of the plastid terminal oxidase PTOX:
1141 Between a protective and a pro-oxidant function. *Frontiers in Plant Science*, *6*(JAN2016),
1142 2015–2017. https://doi.org/10.3389/fpls.2015.01147

1143 Krömer, S., & Heldt, H. W. (1991). On the role of mitochondrial oxidative phosphorylation in
1144 photosynthesis metabolism as studied by the effect of oligomycin on photosynthesis in
1145 protoplasts and leaves of barley (*Hordeum vulgare*). *Plant Physiology*, *95*(4), 1270–1276.
1146 https://doi.org/10.1104/pp.95.4.1270

1147 Lanciano, P., Khalfaoui-Hassani, B., Selamoglu, N., & Daldal, F. (2013). Intermonomer electron
1148 transfer between the b hemes of heterodimeric cytochrome bc 1. *Biochemistry*, *52*(41), 7196–
1149 7206. https://doi.org/10.1021/bi400561e

1150 Laureau, C., De Paepe, R., Latouche, G., Moreno-Chacón, M., Finazzi, G., Kuntz, M., … & Streb,
1151 P. (2013). Plastid terminal oxidase (PTOX) has the potential to act as a safety valve for excess
1152 excitation energy in the alpine plant species *Ranunculus glacialis* L. *Plant, Cell and*
1153 *Environment*, *36*(7), 1296–1310. https://doi.org/10.1111/pce.12059

1154 Lemaire S.D., Quesada A., Merchan F., Corral J.M., Igeno M.I., Keryer E., Issakidis-Bourguet
1155 E, Hirasawa M, Knaff D.B., & Miginiac-Maslow M. (2005). NADP-malate dehydrogenase
1156 from unicellular green alga *Chlamydomonas reinhardtii*. A first step toward redox
1157 regulation? *Plant Physiology* 137: 514–521. https://doi.org/ 10.1104/pp.104.052670

1158 Lemaire, C., Wollman, F. A., & Bennoun, P. (1988). Restoration of phototrophic growth in a
1159 mutant of *Chlamydomonas reinhardtii* in which the chloroplast atpB gene of the ATP
1160 synthase has a deletion: an example of mitochondria-dependent photosynthesis. *Proceedings*
1161 *of the National Academy of Sciences*, 85(5), 1344-1348.

1162 Li, H., Zheng, C., Xiao, M., Huan, Q., Chen, J., Dong, M., … & Wang, J. (2020). Plastid terminal
1163 oxidases in *Chlamydomonas*: connections with astaxanthin and bio-hydrogen production.
1164 *Research Square,* 1–20. https://doi.org/doi.org/10.21203/rs.3.rs-21273/v1

1165 Lin, T. H., Rao, M. Y., Lu, H. W., Chiou, C. W., Lin, S. T., Chao, H. W., … & Lee, T. M. (2018).
1166 A role for glutathione reductase and glutathione in the tolerance of *Chlamydomonas*
1167 *reinhardtii* to photo-oxidative stress. *Physiologia Plantarum*, *162*(1), 35–48.
1168 https://doi.org/10.1111/ppl.12622

1169 Lucker, B., & Kramer, D. M. (2013). Regulation of cyclic electron flow in *Chlamydomonas*
1170 *reinhardtii* under fluctuating carbon availability. *Photosynthesis Research*, *117*(1–3), 449–
1171 459. https://doi.org/10.1007/s11120-013-9932-0

1172 Majeran W., Olive J., Drapier D., Vallon O., & Wollman F.A. (2001). The light sensitivity of ATP
1173 synthase mutants of *Chlamydomonas reinhardtii. Plant Physiology*, *126(1)*:421-33.
1174 https://doi.org/10.1104/pp.126.1.421

Malone, L. A., Qian, P., Mayneord, G. E., Hitchcock, A., Farmer, D. A., Thompson, R. F., … & Johnson, M. P. (2019). Cryo-EM structure of the spinach cytochrome b 6 f complex at 3.6 Å resolution. *Nature*, *575*(7783), 535–539. https://doi.org/10.1038/s41586-019-1746-6

Massoz, S., Hanikenne, M., Bailleul, B., Coosemans, N., Radoux, M., Miranda-Astudillo, H., ... & Remacle C. (2017). In vivo chlorophyll fluorescence screening allows the isolation of a *Chlamydomonas* mutant defective for NDUFAF3, an assembly factor involved in mitochondrial complex I assembly. *Plant Journal* 92(4): 584–595. https://doi.org/10.1104/pp.104.052670

Massoz S., Larosa V., Horrion B., Matagne R.F., Remacle C., & Cardol P. (2015). Isolation of *Chlamydomonas reinhardtii* mutants with altered mitochondrial respiration by chlorophyll fluorescence measurement. *Journal of Biotechnology* 215: 27–34. https://doi.org/10.1016/j.jbiotec.2015.05.009

Matsubayashi, T., Wakasugi, T., Shinozaki, K., Yamaguchi-Shinozaki, K., Zaita, N., Hidaka, T., … & Sugiura, M. (1987). Six chloroplast genes (ndhA-F) homologous to human mitochondrial genes encoding components of the respiratory chain NADH dehydrogenase are actively expressed: Determination of the splice sites in ndhA and ndhB pre-mRNAs. *MGG Molecular & General Genetics*, *210*(3), 385–393. https://doi.org/10.1007/BF00327187

Maxwell, P. C., & Biggins, J. (1976). Role of cyclic electron transport in photosynthesis as measured by the photoinduced turnover of P700 in vivo. *Biochemistry*, *15*(18), 3975–3981. https://doi.org/10.1021/bi00663a011

McCarthy, S. S., Kobayashi, M. C., & Niyogi, K. K. (2004). White mutants of *Chlamydomonas reinhardtii* are defective in phytoene synthase. *Genetics*, *168*(3), 1249–1257. https://doi.org/10.1534/genetics.104.030635

McDonald, A. E., Ivanov, A. G., Bode, R., Maxwell, D. P., Rodermel, S. R., & Hüner, N. P. A. (2011). Flexibility in photosynthetic electron transport: The physiological role of plastoquinol terminal oxidase (PTOX). *Biochimica et Biophysica Acta (BBA) - Bioenergetics*, *1807*(8), 954–967. https://doi.org/10.1016/j.bbabio.2010.10.024

Mehler, A. H. (1951). Studies on reactions of illuminated chloroplasts. II. Stimulation and inhibition of the reaction with molecular oxygen. *Archives of Biochemistry and Biophysics*, *34*(2), 339–351. https://doi.org/10.1016/0003-9861(51)90012-4

Melo, A. M., Bandeiras, T. M., & Teixeira, M. (2004). New insights into type II NAD (P) H: quinone oxidoreductases. *Microbiology and Molecular Biology Reviews, 68(4)*, 603-616.

Mi, H., Endo, T., Ogawa, T., & Asada, K. (1995). Thylakoid membrane-bound, nadph-specific pyridine nucleotide dehydrogenase complex mediates cyclic electron transport in the cyanobacterium *Synechocystis* sp. PCC 6803. *Plant and Cell Physiology*, *36*(4), 661–668. https://doi.org/10.1093/oxfordjournals.pcp.a078807

Mitchell, P. (1975). The protonmotive Q cycle: A general formulation. *FEBS Letters*. https://doi.org/10.1016/0014-5793(75)80359-0

Mitchell, P. (1966). Chemiosmotic coupling in oxidative and photosynthetic phosphorylation. *Biological Reviews*, *41*(3), 445–501. https://doi.org/10.1111/j.1469-185X.1966.tb01501.x

Moroney, J. V., Wilson, B. J., & Tolbert, N. E. (1986). Glycolate metabolism and excretion by *Chlamydomonas reinhardtii*. *Plant Physiology*, *82*(3), 821–826. https://doi.org/10.1104/pp.82.3.821

Mosebach, L., Heilmann, C., Mutoh, R., Gäbelein, P., Steinbeck, J., Happe, T., … & Hippler, M. (2017). Association of Ferredoxin:NADP+ oxidoreductase with the photosynthetic apparatus modulates electron transfer in *Chlamydomonas reinhardtii*. *Photosynthesis Research*, *134*(3), 291–306. https://doi.org/10.1007/s11120-017-0408-5

Moss, D. A., & Bendall, D. S. (1984). Cyclic electron transport in chloroplasts. The Q-cycle and the site of action of antimycin. *Biochimica et Biophysica Acta (BBA) - Bioenergetics*, *767*(3), 389–395. https://doi.org/10.1016/0005-2728(84)90036-7

Munekage, Y., Hashimoto, M., Miyake, C., Tomizawa, K. I., Endo, T., Tasaka, M., & Shikanai, T. (2004). Cyclic electron flow around photosystem I is essential for photosynthesis. *Nature*, *429*(6991), 579–582. https://doi.org/10.1038/nature02598

Munekage, Y., Hojo, M., Meurer, J., Endo, T., Tasaka, M., & Shikanai, T. (2002). PGR5 is involved in cyclic electron flow around photosystem I and is essential for photoprotection in *Arabidopsis*. *Cell*, *110*(3), 361–371. https://doi.org/10.1016/S0092-8674(02)00867-X

Mus, F., Dubini, A., Seibert, M., Posewitz, M. C., & Grossman, A. R. (2007). Anaerobic acclimation in *Chlamydomonas reinhardtii*: Anoxic gene expression, hydrogenase induction, and metabolic pathways. *Journal of Biological Chemistry*, *282*(35), 25475–25486. https://doi.org/10.1074/jbc.M701415200

Mustila, H., Paananen, P., Battchikova, N., Santana-Sánchez, A., Muth-Pawlak, D., Hagemann, M., … & Allahverdiyeva, Y. (2016). The flavodiiron protein Flv3 functions as a homo-oligomer during stress acclimation and is distinct from the Flv1/Flv3 hetero-oligomer specific to the O2 photoreduction pathway. *Plant and Cell Physiology*, *57*(7), 1468–1483. https://doi.org/10.1093/pcp/pcw047

Nakamura, Y., Kanakagiri, S., Van, K., He, W., & Spalding, M. H. (2005). Disruption of the glycolate dehydrogenase gene in the high-CO 2-requiring mutant HCR89 of *Chlamydomonas reinhardtii. Canadian Journal of Botany*, *83*(7), 820–833. https://doi.org/10.1139/b05-067

Nandha, B., Finazzi, G., Joliot, P., Hald, S., & Johnson, G. N. (2007). The role of PGR5 in the redox poising of photosynthetic electron transport. *Biochimica et Biophysica Acta (BBA) - Bioenergetics*, *1767*(10), 1252–1259. https://doi.org/10.1016/j.bbabio.2007.07.007

Nawrocki, W. J., Bailleul, B., Picot, D., Cardol, P., Rappaport, F., Wollman, F. A., & Joliot, P. (2019a). The mechanism of cyclic electron flow. *Biochimica et Biophysica Acta (BBA) - Bioenergetics*, *1860*(5), 433–438. https://doi.org/10.1016/j.bbabio.2018.12.005

Nawrocki, W. J., Bailleul, B., Cardol, P., Rappaport, F., Wollman, F. A., & Joliot, P. (2019b). Maximal cyclic electron flow rate is independent of PGRL1 in *Chlamydomonas*. *Biochimica et Biophysica Acta (BBA) - Bioenergetics*, *1860*(5), 425–432. https://doi.org/10.1016/j.bbabio.2019.01.004

Nawrocki, W. J., Buchert, F., Joliot, P., Rappaport, F., Bailleul, B., & Wollman, F.A. (2019c). Chlororespiration Controls Growth Under Intermittent Light. *Plant Physiology, 179*(2),

630–639. https://doi.org/10.1104/pp.18.01213

Nawrocki, W. J., Tourasse, N. J., Taly, A., Rappaport, F., & Wollman, F. A. (2015). The plastid terminal oxidase: Its elusive function points to multiple contributions to plastid physiology. *Annual Review of Plant Biology*, *66*(1), 49–74. https://doi.org/10.1146/annurev-arplant-043014-114744

Niyogi, K. K. (2000). Safety valves for photosynthesis. *Current Opinion in Plant Biology*, *3*(6), 455–460. https://doi.org/10.1016/S1369-5266(00)00113-8

Ogawa, T. (1991). A gene homologous to the subunit-2 gene of NADH dehydrogenase is essential to inorganic carbon transport of *Synechocystis* PCC6803. *Proceedings of the National Academy of Sciences of the United States of America*, *88*(10), 4275–4279. https://doi.org/10.1073/pnas.88.10.4275

Ogawa K., Kanematsu S., Takabe K., & Asada K. (1995). Attachment of CuZn-superoxide dismutase to thylakoid membranes at the site of superoxide generation (PSI) in spinach chloroplasts: Detection by immuno-gold labeling after rapid freezing and substitution method. *Plant and Cell Physiology* 36: 565–573. https://doi.org/10.1016/j.jbiotec.2015.05.009

Ort, D. R., & Baker, N. R. (2002). A photoprotective role for O2 as an alternative electron sink in photosynthesis? *Current Opinion in Plant Biology*, *5*(3), 193–198. https://doi.org/10.1016/S1369-5266(02)00259-5

Peden, E. A., Boehm, M., Mulder, D. W., Davis, R., Old, W. M., King, P. W., … & Dubini, A. (2013). Identification of global ferredoxin interaction networks in *Chlamydomonas reinhardtii*. *Journal of Biological Chemistry*, *288*(49), 35192–35209. https://doi.org/10.1074/jbc.M113.483727

Peltier, G., Aro, E.-M., & Shikanai, T. (2016). NDH-1 and NDH-2 plastoquinone reductases in oxygenic photosynthesis. *Annual Review of Plant Biology*, *67*(1), 55–80. https://doi.org/10.1146/annurev-arplant-043014-114752

Peltier, G., Ravenel, J., & Verméglio, A. (1987). Inhibition of a respiratory activity by short saturating flashes in *Chlamydomonas*: Evidence for a chlororespiration. *Biochimica et Biophysica Acta (BBA) - Bioenergetics*, *893*(1), 83–90. https://doi.org/10.1016/0005-2728(87)90151-4

Peltier, G., & Thibault, P. (1985). O 2 Uptake in the Light in *Chlamydomonas* : Evidence for Persistent Mitochondrial Respiration. *Plant Physiology*, *79*(1), 225–22530. https://doi.org/10.1104/pp.79.1.225

Peltier, G., Tolleter, D., Billon, E., & Cournac, L. (2010). Auxiliary electron transport pathways in chloroplasts of microalgae. *Photosynthesis Research*, *106*(1–2), 19–31. https://doi.org/10.1007/s11120-010-9575-3

Petersen, J., Förster, K., Turina, P., & Gräber, P. (2012). Comparison of the H+/ATP ratios of the H+-ATP synthases from yeast and from chloroplast. *Proceedings of the National Academy of Sciences of the United States of America*, *109*(28), 11150–11155. https://doi.org/10.1073/pnas.1202799109

Radmer, R. J., & Kok, B. (1976). Photoreduction of O 2 Primes and Replaces CO 2 Assimilation. *Plant Physiology*, *58*(3), 336–340. https://doi.org/10.1104/pp.58.3.336

Rea, G., Antonacci, A., Lambreva, M. D., & Mattoo, A. K. (2018). Features of cues and processes during chloroplast-mediated retrograde signaling in the alga *Chlamydomonas*. *Plant Science*, *272*(April), 193–206. https://doi.org/10.1016/j.plantsci.2018.04.020

Roach, T., Na, C. S., & Krieger-Liszkay, A. (2015). High light-induced hydrogen peroxide production in *Chlamydomonas reinhardtii* is increased by high CO2 availability. *Plant Journal*, *81*(5), 759–766. https://doi.org/10.1111/tpj.12768

Roach, T., Na, C. S., & Stöggl, W. (2020). The non-photochemical quenching protein LHCSR3 prevents oxygen-dependent photoinhibition in *Chlamydomonas reinhardtii*, *71*(9), 2650–2660. https://doi.org/10.1093/jxb/eraa022

Roberty, S., Bailleul, B., Berne, N., Franck, F., & Cardol, P. (2014). PSI Mehler reaction is the main alternative photosynthetic electron pathway in *Symbiodinium* sp., symbiotic dinoflagellates of cnidarians. *New Phytologist*, *204*(1), 81–91. https://doi.org/10.1111/nph.12903

Sacksteder, C. A., Kanazawa, A., Jacoby, M. E., & Kramer, D. M. (2000). The proton to electron stoichiometry of steady-state photosynthesis in living plants: A proton-pumping Q cycle is continuously engaged. *Proceedings of the National Academy of Sciences of the United States of America*, *97*(26), 14283–14288. https://doi.org/10.1073/pnas.97.26.14283

Santabarbara, S., Bullock, B., Rappaport, F., & Redding, K. E. (2015). Controlling electron transfer between the two cofactor chains of photosystem I by the redox state of one of their components. *Biophysical Journal*, *108*(6), 1537–1547. https://doi.org/10.1016/j.bpj.2015.01.009

Saroussi, S. I., Wittkopp, T. M., & Grossman, A. R. (2016). The Type II NADPH dehydrogenase facilitates cyclic electron flow, energy-dependent quenching, and chlororespiratory metabolism during acclimation of *Chlamydomonas reinhardtii* to nitrogen deprivation. *Plant Physiology*, *170*(4), 1975–1988. https://doi.org/10.1104/pp.15.02014

Sazanov, L. A., Burrows, P. A., & Nixon, P. J. (1998). The plastid ndh genes code for an NADH-specific dehydrogenase: Isolation of a complex I analogue from pea thylakoid membranes. *Proceedings of the National Academy of Sciences of the United States of America*, *95*(3), 1319–1324. https://doi.org/10.1073/pnas.95.3.1319

Scheibe, R., Backhausen, J. E., Emmerlich, V., & Holtgrefe, S. (2005). Strategies to maintain redox homeostasis during photosynthesis under changing conditions. *Journal of Experimental Botany*, *56*(416), 1481–1489. https://doi.org/10.1093/jxb/eri181

Seelert, H., Poetsch, A., Dencher, N. A., Engel, A., Stahlberg, H., & Müller, D. J. (2000). Proton-powered turbine of a plant motor. *Nature*, *405*(6785), 418–419. https://doi.org/10.1038/35013148

Sétif, P., Shimakawa, G., Krieger-Liszkay, A., & Miyake, C. (2020). Identification of the electron donor to flavodiiron proteins in *Synechocystis* sp. PCC 6803 by in vivo spectroscopy. *Biochimica et Biophysica Acta (BBA) - Bioenergetics*, *1861*(10), 148256.

https://doi.org/10.1016/j.bbabio.2020.148256

Shikanai, T. (2007). Cyclic Electron Transport Around Photosystem I: Genetic Approaches. *Annual Review of Plant Biology*, *58*(1), 199–217. https://doi.org/10.1146/annurev.arplant.58.091406.110525

Shimakawa, G., Shoguchi, E., Burlacot, A., Ifuku, K., Che, Y., Kumazawa, M., ... & Nakanishi, S. (2021). Coral symbionts evolved a functional polycistronic flavodiiron gene. *Photosynthesis Research*, 1-12. https://doi.org/10.1007/s11120-021-00867-7

Shinozaki, K., Ohme, M., Tanaka, M., Wakasugi, T., Hayashida, N., Matsubayashi, T., … & Sugiura, M. (1986). The complete nucleotide sequence of the tobacco chloroplast genome: Its gene organization and expression. *EMBO Journal*, *5*(9), 2043–2049. https://doi.org/10.1002/j.1460-2075.1986.tb04464.x

Steinbeck, J., Ross, I. L., Rothnagel, R., Gäbelein, P., Schulze, S., Giles, N., … & Hankamer, B. (2018). Structure of a PSI-LHCI-cyt b6f supercomplex in *Chlamydomonas reinhardtii* promoting cyclic electron flow under anaerobic conditions. *Proceedings of the National Academy of Sciences of the United States of America*, *115*(41), 10517–10522. https://doi.org/10.1073/pnas.1809973115

Stepien, P., & Johnson, G. N. (2009). Contrasting responses of photosynthesis to salt stress in the glycophyte *Arabidopsis* and the halophyte *Thellungiella*: Role of the plastid terminal oxidase as an alternative electron sink. *Plant Physiology*, *149*(2), 1154–1165. https://doi.org/10.1104/pp.108.132407

Storti, M., Alboresi, A., Gerotto, C., Aro, E. M., Finazzi, G., & Morosinotto, T. (2019). Role of cyclic and pseudo-cyclic electron transport in response to dynamic light changes in *Physcomitrella patens*. *Plant Cell and Environment*, *42*(5), 1590–1602. https://doi.org/10.1111/pce.13493

Strand, D. D., Fisher, N., Davis, G. A., & Kramer, D. M. (2016). Redox regulation of the antimycin A sensitive pathway of cyclic electron flow around photosystem I in higher plant thylakoids. *Biochimica et Biophysica Acta (BBA) - Bioenergetics*, *1857*(1), 1–6. https://doi.org/10.1016/j.bbabio.2015.07.012

Strand, D. D., Fisher, N., & Kramer, D. M. (2017). The higher plant plastid NAD(P)H dehydrogenase-like complex (NDH) is a high efficiency proton pump that increases ATP production by cyclic electron flow. *Journal of Biological Chemistry*, *292*(28), 11850–11860. https://doi.org/10.1074/jbc.M116.770792

Strand, D. D., D'Andrea, L., & Bock, R. (2019). The plastid NAD (P) H dehydrogenase-like complex: structure, function and evolutionary dynamics. *Biochemical Journal, 476(19)*, 2743-2756. https://doi.org/10.1042/BCJ20190365

Strenkert, D., Schmollinger, S., Gallaher, S. D., Salomé, P. A., Purvine, S. O., Nicora, C. D., … Merchant, S. S. (2019). Multiomics resolution of molecular events during a day in the life of *Chlamydomonas*. *Proceedings of the National Academy of Sciences of the United States of America*, *116*(6), 2374–2383. https://doi.org/10.1073/pnas.1815238116

Stroebel, D., Choquet, Y., Popot, J. L., & Picot, D. (2003). An atypical haem in the cytochrome

b6f complex. *Nature*, *426*(6965), 413–418. https://doi.org/10.1038/nature02155

Sukenik, A., Bennett, J., & Falkowski, P. (1987). Light-saturated photosynthesis - Limitation by electron transport or carbon fixation? *Biochimica et Biophysica Acta (BBA) - Bioenergetics*, *891*(3), 205–215. https://doi.org/10.1016/0005-2728(87)90216-7

Sültemeyer, D., Biehler, K., & Fock, H. P. (1993). Evidence for the contribution of pseudocyclic photophosphorylation to the energy requirement of the mechanism for concentrating inorganic carbon in *Chlamydomonas*. *Planta*, *189*(2), 235–242. https://doi.org/10.1007/BF00195082

Szymańska, R., Dłuzewska, J., Ślesak, I., & Kruk, J. (2011). Ferredoxin:NADP + oxidoreductase bound to cytochrome b 6f complex is active in plastoquinone reduction: Implications for cyclic electron transport. *Physiologia Plantarum*, *141*(3), 289–298. https://doi.org/10.1111/j.1399-3054.2010.01434.x

Tagawa, K., Tsujimoto, H. Y., & Arnon, D. I. (1963). Role of chloroplast ferredoxin in the energy conversion process of photosynthesis. *Proceedings of the National Academy of Sciences of the United States of America, 49(4),* 567. https://doi: 10.1073/pnas.49.4.567

Takahashi, H., Clowez, S., Wollman, F. A., Vallon, O., & Rappaport, F. (2013). Cyclic electron flow is redox-controlled but independent of state transition. *Nature Communications*, *4*. https://doi.org/10.1038/ncomms2954

Takahashi H., Schmollinger S., Lee J.-H., Schroda M., Rappaport F., Wollman F.-A., and Vallon O. (2016). PETO Interacts with Other Effectors of Cyclic Electron Flow in *Chlamydomonas*. *Molecular Plant*. 9, 558–568. http://dx.doi.org/10.1016/j.molp.2015.12.017

Takahashi, M., & Asada, K. (1988). Superoxide production in aprotic interior of chloroplast thylakoids. *Archives of Biochemistry and Biophysics*, *267*(2), 714–722. https://doi.org/10.1016/0003-9861(88)90080-X

Taubert, A., Jakob, T., & Wilhelm, C. (2019). Glycolate from microalgae: an efficient carbon source for biotechnological applications. *Plant Biotechnology Journal*, *17*(8), 1538–1546. https://doi.org/10.1111/pbi.13078

Terashima M., Specht M., & Hippler M. (2011). The chloroplast proteome: A survey from the *Chlamydomonas reinhardtii* perspective with a focus on distinctive features. *Current Genetics* 57: 151–168. https://doi.org/ 10.1016/j.jbiotec.2015.05.009

Tirumani, S., Gothandam, K. M., & J Rao, B. (2019). Coordination between photorespiration and carbon concentrating mechanism in *Chlamydomonas reinhardtii*: transcript and protein changes during light-dark diurnal cycles and mixotrophy conditions. *Protoplasma*, *256*(1), 117–130. https://doi.org/10.1007/s00709-018-1283-4

Trouillard, M., Meunier, B., & Rappaport, F. (2011). Questioning the functional relevance of mitochondrial supercomplexes by time-resolved analysis of the respiratory chain. *Proceedings of the National Academy of Sciences of the United States of America*, *108*(45). https://doi.org/10.1073/pnas.1109510108

Turina, P., Petersen, J., & Gräber, P. (2016). Thermodynamics of proton transport coupled ATP synthesis. *Biochimica et Biophysica Acta (BBA) - Bioenergetics*, *1857*(6), 653–664.

https://doi.org/10.1016/j.bbabio.2016.02.019

Vallon, O., Bulte, L., Dainese, P., Olive, J., Bassi, R., & Wollman, F. A. (1991). Lateral redistribution of cytochrome b6/f complexes along thylakoid membranes upon state transitions. *Proceedings of the National Academy of Sciences of the United States of America*, *88*(18), 8262–8266. https://doi.org/10.1073/pnas.88.18.8262

Vermeglio, A., Ravenel, J., & Peltier, G. (1990). Chlororespiration: A respiratory activity in the thylakoid membrane of microalgae and higher plants. In: Wiessner W., Robinson D.G., Starr R.C. (eds) *Cell Walls and Surfaces, Reproduction, Photosynthesis*. Experimental Phycology, vol 1. Springer, Berlin, Heidelberg. https://doi.org/10.1007/978-3-642-48652-4_14

Vicente, J. B., Gomes, C. M., Wasserfallen, A., & Teixeira, M. (2002). Module fusion in an A-type flavoprotein from the cyanobacterium *Synechocystis* condenses a multiple-component pathway in a single polypeptide chain. *Biochemical and Biophysical Research Communications*, *294*(1), 82–87. https://doi.org/10.1016/S0006-291X(02)00434-5

Voss, I., Sunil, B., Scheibe, R., & Raghavendra, A. S. (2013). Emerging concept for the role of photorespiration as an important part of abiotic stress response. *Plant Biology*, *15*(4), 713–722. https://doi.org/10.1111/j.1438-8677.2012.00710.x

Wada, S., Yamamoto, H., Suzuki, Y., Yamori, W., Shikanai, T., & Makino, A. (2018). Flavodiiron protein substitutes for cyclic electron flow without competing CO2 assimilation in rice. *Plant Physiology*, *176*(2), 1509–1518. https://doi.org/10.1104/pp.17.01335

Wang, J., Sommerfeld, M., & Hu, Q. (2009). Occurrence and environmental stress responses of two plastid terminal oxidases in *Haematococcus pluvialis* (Chlorophyceae). *Planta*, *230*(1), 191–203. https://doi.org/10.1007/s00425-009-0932-4

Wang, Y., Stessman, D. J., & Spalding, M. H. (2015). The CO2 concentrating mechanism and photosynthetic carbon assimilation in limiting CO2: How *Chlamydomonas* works against the gradient. *Plant Journal*, *82*(3), 429–448. https://doi.org/10.1111/tpj.12829

Weber A., Menzlaff E., Arbinger B., Gutensohn M., Eckerskom C., & Flugge U.I. (1995). The 2-Oxoglutarate/Malate Translocator of Chloroplast Envelope Membranes: Molecular Cloning of a Transporter Containing a 12-Helix Motif and Expression of the Functional Protein in Yeast Cells. *Biochemistry* 34: 2621–2627. https://doi.org/ 10.1016/j.jbiotec.2015.05.009

Wollman, F. A. (2001). State transitions reveal the dynamics and flexibility of the photosynthetic apparatus. *EMBO Journal*, *20*(14), 3623–3630. https://doi.org/10.1093/emboj/20.14.3623

Wei L., Derrien B, Gautier A., Houille-Vernes L., Boulouis A., Saint-Marcoux D., … & Wollman F.A. (2014). Nitric oxide-triggered remodeling of chloroplast bioenergetics and thylakoid proteins upon nitrogen starvation in *Chlamydomonas reinhardtii*. *Plant Cell* 26: 353–372. https://doi.org/ 10.1105/tpc.113.120121

Wu, D., Wright, D.A., Wetzel, C., Voytas, D.F., & Rodermel, S. (1999). The IMMUTANS variegation locus of *Arabidopsis* defines a mitochondrial alternative oxidase homolog that functions during early chloroplast biogenesis. *The Plant Cell*, 11(1):43-55. https://doi.org/10.1105/tpc.11.1.43

Yamamoto, H., Takahashi, S., Badger, M. R., & Shikanai, T. (2016). Artificial remodelling of

alternative electron flow by flavodiiron proteins in *Arabidopsis*. *Nature Plants*, *2*(3). https://doi.org/10.1038/NPLANTS.2016.12

Yamashita, E., Zhang, H., & Cramer, W. A. (2007). Structure of the Cytochrome b6f Complex: Quinone Analogue Inhibitors as Ligands of Heme cn. *Journal of Molecular Biology*, *370*(1), 39–52. https://doi.org/10.1016/j.jmb.2007.04.011

Yeh, H. L., Lin, T. H., Chen, C. C., Cheng, T. X., Chang, H. Y., & Lee, T. M. (2019). Monodehydroascorbate reductase plays a role in the tolerance of *Chlamydomonas reinhardtii* to photooxidative stress. *Plant and Cell Physiology*, *60*(10), 2167–2179. https://doi.org/10.1093/pcp/pcz110

Zhang, H., Whitelegge, J. P., & Cramer, W. A. (2001). Ferredoxin:NADP+ Oxidoreductase is a subunit of the chloroplast cytochrome b6f complex. *Journal of Biological Chemistry*, *276*(41), 38159–38165. https://doi.org/10.1074/jbc.M105454200

Zhang, Z., Huang, L., Shulmeister, V. M., Chi, Y. I., Kim, K. K., Hung, L. W., … Kim, S. H. (1998). Electron transfer by domain movement in cytochrome bc1. *Nature*, *392*(6677), 677–684. https://doi.org/10.1038/33612

2.2 Review 2: Comparing Diatom Photosynthesis with the Green Lineage: Electron Transport, Carbon Fixation and Metabolism

Comparing Diatom Photosynthesis with the Green Lineage: Electron Transport, Carbon Fixation and Metabolism

Short title: Photosynthesis in Diatoms versus Green Lineage

Authors:

Dany Croteau[1], Erik Jensen[1], Christian Wilhelm[2], Benjamin Bailleul[1#]

corresponding author

Affiliations:

[1]Institut de Biologie Physico-Chimique, Laboratory of Chloroplast Biology and Light Sensing in Microalgae, UMR7141 Centre National de la Recherche Scientifique (CNRS), Sorbonne Université, Paris, France.

[2]Institut für Biologie, Universität Leipzig, 0409 Leipzig, Germany.

Email: Dany Croteau: croteau@ibpc.fr

Erik Jensen: jensen@ibpc.fr

Christian Wilhelm: cwilhelm@rz.uni-leipzig.de

Benjamin Bailleul: bailleul@ibpc.fr

Abbreviations

2-PG	2-phosphoglycolate
3-PGA	3- phosphoglycerate
Δψ	Transthylakoidal electric gradient
ΔpH	Transthylakoidal proton gradient
ADP	Adenosine diphosphate
AEF	Alternative electron flows
AOX	Alternative oxidase
ATP	Adenosine triphosphate
CA	Carbonic anhydrases
CBB	Calvin-Benson-Bassham
CCM	Carbon concentrating mechanisms
CEF	Cyclic electron flow around PSI
Chl	Chlorophyll
Cyt.	Cytochrome
DDE	Diatoxanthin de-epoxidase
ECS	Electrochromic shift
EPYC	Essential pyrenoid component 1
ETC	Electron Transfer Chain
FCP	Fucoxanthin-Chl *a*/*c*-binding proteins
Fd	Ferredoxin
FLV	Flavodiiron protein
GAPDH	Glyceraldehyde 3-phospate dehydrogenase
LEF	Linear electron flow
LHC	Light-harvesting complexes
NADPH	Nicotinamide adenine dinucleotide phosphate
NDH	Nucleotide dehydrogenase
NPQ	Non-photochemical quenching
PC	Plastocyanin
pmf	Proton motive force
PQ/PQH$_2$	Plastoquinone/plastoquinol
PRK	Phosphoribulokinase
PSI	Photosystem I
PSII	Photosystem II
PTOX	Plastid terminal oxidase
qE	High energy quenching
RCA	Rubisco activase
ROS	Reactive oxygen species
Rubisco	Ribulose-1,5-bisphosphate carboxylase/oxygenase
RubP	Ribulose-1,5-bisphosphate
SLC4	Solute Carrier 4 Family
SOD	Superoxide dismutase
SQDG	Sulfoquinovosyldiacylglycerol
WWC	Water-to-water cycles
XC	Xanthophyll cycles

Abstract

Diatoms are an important group of eukaryotic phytoplankton responsible for about a quarter of CO_2 fixation on Earth. Oxygenic photosynthesis uses the same building blocks throughout the diversity, with highly conserved photosynthetic complexes and Calvin-Benson-Bassham cycle enzymes. However, many differences can be observed in the spatial organization of the photosynthetic apparatus and in the regulation of the photochemical and chemical phases of photosynthesis. Here we describe the similarities and differences between diatom photosynthesis and that of the green lineage. We focus on the spatial organization of photosynthetic complexes, on the different routes of photosynthetic electron transfers, on the regulation of CO_2 concentration and fixation, and on the orchestration of the general response of photosynthesis to environmental changes.

1.1 Introduction

Our understanding of oxygenic photosynthesis, performed by all photosynthetic eukaryotes including diatoms, has advanced enormously since the middle of the 20th century. However, almost all the original work on which our knowledge of photosynthesis is based has been carried out on cyanobacteria and eukaryotes from the green lineage, and mainly on a few model species which happened to be convenient to study, i.e., spinach, tobacco, *Arabidopsis*, *Chlamydomonas*, *Chlorella*, *Synechocystis*. Apart from the cyanobacteria and the green lineage, whose chloroplasts evolved from primary endosymbiosis with a cyanobacterium, a wide variety of microalgae acquired their plastids from a secondary or tertiary endosymbiosis (see chapter I). These dominate the Ocean, represent a large part of the biodiversity and thus promise new discoveries. In the current era of genomics, the rapidly expanding awareness of phylogenetic diversity begs the questions: *How much of the pioneer breakthroughs in photosynthesis are actually accurate in other photosynthetic groups? Are there novel photosynthetic mechanisms, regulatory modes or stress response strategies yet to be discovered?* From that perspective, exploring the diversity of photosynthesis is not just a way to fill a cabinet of curiosities but rather an opportunity to better understand the general constraints and degrees of freedom that intrinsically apply to oxygenic photosynthesis. This in turn could provide new opportunities to manipulate photosynthesis in plants and microalgae for agricultural or biotechnological purposes.

The biodiversity of photosynthesis is just beginning to be unveiled. The fragmented insights gathered so far allow us to formulate hypotheses, rather than providing comprehensive photophysiology fingerprints within (and between) most lineages. However, among multiple endosymbiosis microalgae, diatoms enjoy the most advanced investigation. Thanks to their central roles in biogeochemical cycling and trophic transfers (Tréguer *et al.,* 2018, 2021), diatoms have been the focus of increasing attention from the research community over the past decades. The accumulation of knowledge on the function and regulation of photosynthesis, the increase in genomic information and the rapid improvement of biomolecular tools (Falciatore *et al.,* 2020), now make diatoms a suitable secondary endosymbiotic group to challenge the "green paradigm" of eukaryotic oxygenic photosynthesis. Many aspects have already been covered by previous reviews on diatom photosynthesis (Wilhelm et al, 2006; Wang *et al.,* 2020; Roberts *et al.,* 2007; Lepetit *et al.,* 2022; Büchel *et al.,* 2022; Falciatore *et al.,* 2020). In this review, we propose to describe the known similarities and differences in diatom photosynthesis versus their green lineage counterparts. However, we first ought to acknowledge the gray areas

that hinder generalization of these observations as group-specific traits, one of which is the small number of model species on which our knowledge of diatom and green lineage photosynthesis is based. In diatoms, studies have been overwhelmingly concentrated at two extremes of their phylogenetic tree with very little work in between: the pennate *Phaeodactylum tricornutum* largely overweighting the centric *Thalassiosira pseudonana*. This bias is particularly problematic in diatom photosynthesis because of their immense phylogenetic diversity, vastly superior to that of Archaeplastida (Falciatore *et al.*, 2020). Important differences between the pennate and centric diatoms groups were revealed on topic more evenly studied, such as in the regulation of photoprotection via non-photochemical quenching (NPQ) (Grouneva *et al.*, 2009), the sub-unit composition of light-harvesting complexes (LHC) (Büchel 2020) and carbon concentrating mechanisms (CCMs) (Tsuji *et al.*, 2017). Therefore, caution should be exercised before expanding features only studied in *P. tricornutum* to other diatoms, especially to centric species. In this review, we have tried to use "diatoms" in the broader sense only when a given observation has been substantiated in at least one representative of both pennate and centric species.

Keeping this limitation in mind, we will focus in this review on the differences between diatom and green lineage regarding the different modes of photosynthetic electron transfer, carbon concentration and assimilation, and the global responses (sensors, regulators) of photosynthesis to environmental changes. This will come after a first section dedicated to the « skeleton » of oxygenic photosynthesis, i.e., what can be considered conserved across the phylogenetic diversity of oxygenic photosynthesis.

1.2 Conservation and diversity within oxygenic photosynthesis

Diatoms share the same building blocks with other organisms carrying out oxygenic photosynthesis: the structure-function of photosynthetic complexes involved in the photochemical phase of photosynthesis, as well as enzymes involved in the chemical phase, are highly conserved throughout the phylogenetic diversity. In oxygenic photosynthesis, the linear electron flow (LEF) involves two photosystems and results in the transfer of electrons from water, the primary electron donor, to the terminal acceptor, nicotinamide adenine dinucleotide phosphate (NADPH). Both photosystem II (PSII) and I (PSI), harvest light energy with their adjacent LHC and convert it into a charge separation (or photochemical event) leading to an oxidized chlorophyll (Chl) *a* molecule and a reduced acceptor molecule. From here starts an initial exergonic and short-distance electron transfer within the PSs. Ultimately, PSII transfers

electrons from the oxygen evolving complex, where water oxidation takes place, to a plastoquinone (PQ) in the stromal-facing Q_B pocket, while PSI catalyzes the transfer of electron from a lumen-soluble electron carrier, plastocyanin (PC) or cytochrome (cyt.) c_6, to ferredoxin (Fd). The Fd-$NADP^+$ reductase mediates electron transfer from (reduced) Fd to (oxidized) $NADP^+$ in the stroma, producing NADPH. The functioning in series of PSII and PSI is made possible by the intersystem electron transfer chain (ETC), which involves the PQ (and its reduced form, plastoquinol (PQH_2)), cyt. b_6f and the lumen soluble electron carrier (PC or cyt. c_6) that acts as a shuttle between cyt. b_6f and PSI (Hill & Bendall, 1960). The transfer of electrons is coupled with the pumping of protons across the thylakoid. This generates a proton motive force (pmf), which comprises an osmotic, proton gradient, component, ΔpH, and an electric component, $\Delta\psi$ (Mitchell 1966; Kramer *et al.*, 2003). The pmf is used by the chloroplast CF_1F_O-ATPase to synthesize adenosine triphosphate (ATP) by attaching a phosphate group to an adenosine diphosphate (ADP) molecule (Mitchell 1966; Boyer 1997). The end products of the photochemical phase of photosynthesis, ATP and NADPH, fuel the enzymatic reactions of the Calvin-Benson-Bassham (CBB) cycle to form intermediate compounds that will serve as precursors for the synthesis of much more complex molecules necessary for cellular metabolism (i.e., sugars, lipids, amino acids, nucleotides). The CBB cycle - also called the reductive pentose phosphate pathway - involves a series of 13 chemical reactions catalyzed by 11 enzymes. It begins with the fixation of CO_2 on ribulose-1,5-bisphosphate (RubP), a reaction catalyzed by the ribulose-1,5-bisphosphate carboxylase/oxygenase (Rubisco) that produces two molecules of 3- phosphoglycerate (3-PGA). Then, 3-PGA is reduced and converted into other triose phosphates which can be used further in cell metabolism, and be exported out of the plastid, or transformed to regenerate RubP, which will continue the cycle (Biel & Fomina, 2015).

Only a few of the fundamental players in photosynthesis are different between diatoms and the green lineage. One is the nature of the lumen carrier between cyt. b_6f and PSI. In the green lineage, the constitutive shuttle is the copper-containing PC whereas it is often the iron-containing cyt. c_6 in diatoms (Groussman *et al.*, 2015). However, this difference should be taken with caution: many species in the green lineage can replace PC with cyt. c_6 under copper stress (Sandmann *et al.*, 1983; Hill *et al.*, 1991). Most diatoms cannot synthesize PC, although it can however be found in diatoms adapted to low-iron environments. This is the case in *Thalassiosira oceanica*, a low iron specialist (Peers & Price, 2006; Lommer *et al.*, 2012), and the model polar species *Fragilariopsis cylindrus* has retained the PC gene (Blaby-Haas & Merchant, 2012). Another adaptation/acclimation to low iron includes replacing iron-

containing Fd with flavodoxin which uses flavin/copper as a cofactor instead of iron (Pierella Karlusich *et al.*, 2015).

The light-harvesting system also contrasts with very different pigment and protein composition from that of the green lineage. Briefly, diatoms use the LHC proteins that bind fucoxanthin and Chl *c*, in addition to Chl *a* (Büchel 2020). They are called FCPs (for fucoxanthin –Chl *a*/*c* binding proteins) as a distinction from the Chl *a*/*b* binding LHCs found in terrestrial plants and green algae. The two families have important differences regarding their pigmentation and structure, which are extensively covered in chapter VIII. Regardless of the molecular nature of the light-harvesting system, diatoms exhibit unique regulation of light absorption efficiency due to the large variations in cell size related to asexual and sexual cell divisions (see chapter IV). Cell size has a huge effect on a given Chl *a* molecule absorption *in vivo* because of the package effect (self-shading) inside the cell. In short, the larger the cell, the higher the package effect tends to be and the lower the absorption efficiency per Chl *a*. The absorption efficiency per Chl *a* decreases logarithmically with intracellular Chl *a* concentration (Blache et al., 2011), a relationship that scales allometrically across species/taxa (Fujiki & Taguchi, 2002, Finkel et al., 2004). The uniqueness of diatoms is that over a life cycle for which the cell volume decreases from 30 to 5 µm, the cells of the same species undergo a two-fold change in its absorption efficiency per Chl *a* (Wilhelm et al., 2014). Another peculiar optical property of diatoms concerns the way their frustule interacts with the light field to support photochemistry; another topic covered in chapter IV.

The downregulation of light-harvesting under conditions of excess light relies also on different molecular players. When light absorption outstrips photosynthetic capacity, excessive reduction of the photosynthetic ETC promotes the formation of reactive oxygen species (ROS) leading to PSI and PSII photodamages and photoinhibition (Sonoike 2011; Tiwari *et al.*, 2016; Barbato *et al.*, 2020; Campbell & Serôdio, 2020). To avoid this detrimental situation, most photosynthetic organisms evolved a set of processes able to down-regulate photochemistry in PSII by dissipating excess photons as heat. Consequently, the induction of these photoprotective mechanisms also result in a decrease of PSII Chl *a* fluorescence emission and they are collectively termed non-photochemical quenching (NPQ) (reviewed in (Lepetit & Goss, 2015)). Those processes are attributed to the build-up of a ΔpH across the membrane and/or the conversion of pigments via the xanthophylls cycle, as well as to the increase in photoinhibited PSII. Other components of NPQ involve the movement of LHCs (state transitions) or the sharing of excitons (spillover) between the two photosystems, two mechanisms apparently

absent in diatoms (see below). In both diatoms and green algae, the major NPQ component has historically been termed high energy quenching "qE" based on its faster kinetics, but we now know it relies on different molecular actors. In the green lineage qE involves a PSII subunit (PsbS in plants, LhcSR3 in green algae) and a reversible xanthophyll cycle based on violaxanthin (qE inactivated), the intermediary antheraxanthin and zeaxanthin (qE activated). Briefly, PSII from green photosynthetic organisms can switch from a light-harvesting mode to a heat-dissipation mode by altering the conformation of PsbS/LhcSR3 and the nature of their xanthophyll pigments. Diatom PSII can also switch to a heat-dissipation mode under conditions of excess light, but the key PSII subunit is LHCX (usually found with multiple isoforms), and the xanthophyll cycle involves diadinoxanthin and diatoxanthin (with no intermediate form). The mechanism and regulation of the xanthophyll cycle dependent NPQ also differs between diatoms and the green lineage (discussed in section 1.6).

Another potential source of difference – and a gray area in diatom photosynthesis- is the H^+/e^- coupling of the LEF. The transfer of electrons is coupled to the accumulation of protons in the lumen at two sites: the oxidation of water releases one proton per electron delivered to PSII and the Q cycle in the cyt. b_6f imposes the liberation of two protons per electron transferred from a PQ to PC^+ (or cyt. c_6^+). In the green lineage, the Q cycle being constitutive, this finally gives three protons accumulating in the lumen for each electron transferred through the LEF. Measurement of a net transfer of one positive charge during cyt. b_6f turnover under low pmf conditions suggests that the Q cycle also takes place in diatoms (Bailleul *et al.*, 2015), but its constitutive character remains to be demonstrated. The H^+/e^- coupling influences the ratio between ATP and NADPH produced by the LEF but is not its only determinant. The number of protons required to allow full rotation of CF_1F_O-ATPase (and synthesis of 3 ATP) depends on the number of *c* subunits in the rotor (Adachi et al., 2007; Hahn et al., 2018). Until now and among photosynthetic eukaryotes, this number has been experimentally evaluated at 14 only in spinach and pea (Seelert et al. 2000; Hahn et al. 2018). This means that for 2 electrons reaching NADPH, 6 protons accumulate in the lumen and lead to the synthesis of 1.28 ATP (6*3/14) in spinach (and likely in the green lineage). However, the number of *c*-ring subunits can vary between 8 and 15 across phyla when mitochondrial ATPases and photosynthetic cyanobacteria are included (Pogoryelov et al., 2007, Nesci et al. 2016) and the same stoichiometric diversity cannot be ruled out for chloroplastic CF_1F_O-ATPases, as suggested by early studies in *Chlamydomonas reinhardtii* (ref). The number of *c* subunits of the diatom CF_1F_O-ATPase is currently unknown, making the value of 1.28 ATP per NADPH produced by LEF putative in

diatoms.

Diatoms also exhibit peculiarity in the lipid content of their thylakoid membranes. In general, thylakoid membranes are composed of the two major neutral galactolipids - monogalactosyldiacylglycerol and digalactosyldiacylglycerol– and of the negatively charged sulfoquinovosyldiacylglycerol (SQDG) and phosphatidylglycerol (Vieler et al. 2007; Goss et al. 2009; Lepetit et al. 2012; Abida et al. 2015). These lipids are constitutive for all phototrophs and their stoichiometry defines the level of membrane fluidity and lipid-protein interactions (for recent review see Wilhelm *et al.,* 2020). Diatoms and green algae show a different ratio of neutral to charged lipids: neutral galactolipids make up 70–80% of total lipid in green algae (Murata & Siegenthaler, 1998) but only 50% in diatoms where the other half is represented by SQDG and phosphatidylglycerol (Goss et al. 2009; Lepetit et al. 2012; Abida et al. 2015). Moreover, in *P. tricornutum* or *C. meneghiniana* grown under high light, SQDG can even be the most abundant lipid in the thylakoids (Lepetit et al. 2012). Due to the different proportion of charged lipids, the surface charge distribution is clearly different in diatoms and green algae which results in different properties in protein-lipid interactions. For example, the key xanthophyll cycle enzyme violaxanthin de-epoxidase must be laterally separated from the SQDG-enriched lipid domain to be active (Goss *et al.*, 2007; Goss et al, 2009). Diatoms can additionally contain small amounts of diacylglycerylcarboxyhydroxymethylcholine and diacylglycerylhydroxymethyl-N,N,N-trimethyl-β-alanine whose specific functions are not known yet (Vieler et al., 2007; Canavate et al., 2016).

Differences in the light-harvesting system, the lipid composition, or the nature of the electron shuttle between cyt. b_6f and PSI, as well as the unknowns surrounding the H+/e- coupling and ATP/NADPH ratio produced by LEF in diatoms, should not mask the remarkable conservation of the basic units of energy transduction machinery in organisms carrying out oxygenic photosynthesis. This conservation argues for immense selective pressure to maintain strong homologies in photosynthetic reaction pathways among the diversity of photosynthetic eukaryotes (Falkowski *et al.*, 2008). Therefore, the functional biodiversity of photosynthesis is best appreciated not by wondering *what* these essential blocks (photosynthetic complexes, CBB cycle enzymes) are used for, but rather *how* they are spatially organized and *how* their activities are regulated (e.g., the nature of the sensors and regulators).

Indeed, in all photosynthetic eukaryotes photosynthesis is subject to the same constraint of great flexibility to respond to fluctuating environmental parameters. The availability of substrates, in particular CO_2 and light, changes over time (from second-to-seasonal scales), as does the

metabolic demand for ATP and NADPH. Thus, to answer *how* the same essential blocks lead to specificities of diatom photosynthesis compared to the green lineage, we will focus on (i) the spatial organization of photosynthetic complexes, (ii) the different modes of photosynthetic electron routes, (iii) the regulation of carbon concentration and assimilation system and, (iv) the integrated response of photosynthesis to varying environmental conditions. This last section will briefly mention the specificities of diatom photoprotection (already covered elsewhere: Lepetit et al., 2022; Büchel et al., 2022; Goss & Lepetit, 2015) and tackle how CCMs, regulation of the photosynthetic electron routes and photoprotection mechanisms are entangled.

1.3 Consequences of the secondary endosymbiosis and thylakoid ultrastructure

Due to their different evolutionary history (secondary versus primary endosymbiosis), diatoms and members of the green lineage show major architectural differences in their plastid organisation (see chapter VI). Diatom plastids are surrounded by four membranes (instead of two) (Fig. 1A), which implies different ways of importing and exporting molecules (Keeling, 2009). Moreover, in diatoms, thylakoids do not exhibit heterogeneous ultrastructure, as observed with thylakoid stacking in green algae or grana stacks in plants (Bedoshvili et al., 2009). Instead, the thylakoids run the length of the entire plastid by stacks of three (Bedoshvili et al, 2009; Pyszniak and Gibbs, 1992) (Fig. 1B). In plants, the heterogeneous ultrastructure of the thylakoids imposes a lateral segregation of the PSII, in grana, and PSI, in lamella (Dekker & Boekema, 2005). In diatoms, PSI and PSII immunolocalization studies and 3D reconstruction have shown that PSII are embedded at the junction of two thylakoids, which represents the two faces of the central thylakoid and the internal face of the two external thylakoids (Larkum & Vesk, 2003). While PSI are mainly found in the stromal faces of the two external thylakoids (Pysniak & Gibbs, 1992; Flori et al., 2017). This peculiar distribution of the photosystems is responsible for several features ascribed to diatom photosynthesis.

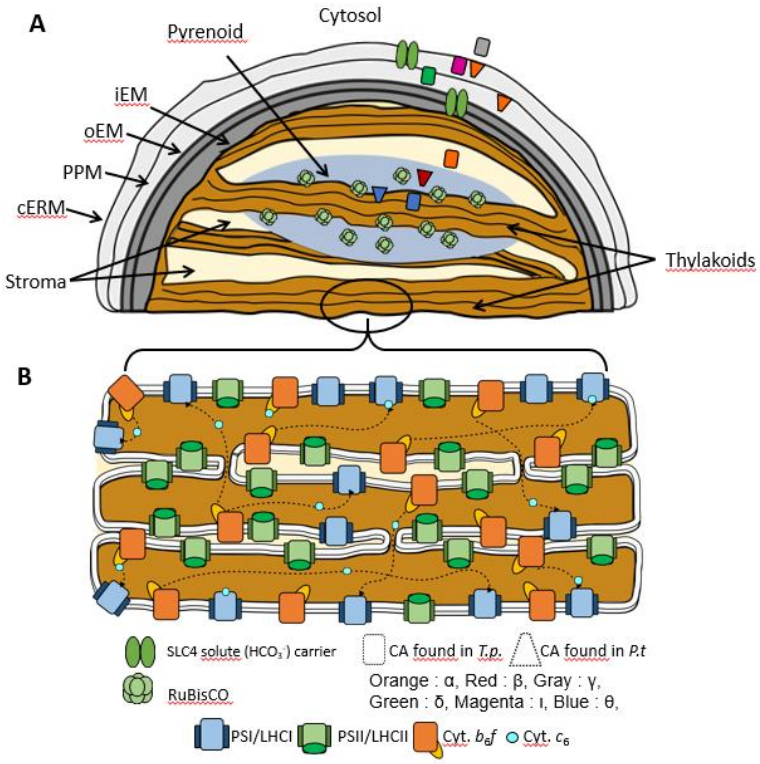

Figure 1: Schematic representation of diatoms' chloroplast. (**A**) chloroplast ultrastructure with ribulose-1,5-bisphosphate carboxylase/oxygenase (RubiscO) accumulated in the pyrenoid, the localization of the solute (HCO_3^-) carrier (SLC4) and the different carbonic anhydrases (CAs) that have been identified in *Thalassiosira pseudonana* (*T.p.*) and *Phaeodactylum tricornutum* (*P.t.*). (**B**) Distribution of photosynthetic complexes and luminal electron carriers in diatom's thylakoids. Photosystem (PS) II and PSI are more abundant in the internal and external thylakoidal membranes, respectively. The light harvesting complexes (LHC) system of each PS are represented as adjacent darker rectangles. Cytochrome (cyt.) b_6f is believed to be distributed roughly homogeneously (the ATP synthase is not represented for simplicity purposes). The dark dotted arrows represent the efficient long-range diffusion of the cyt. c_6, which was postulated to be facilitated by connections between thylakoids (Flori *et al.*, 2017). See text for more details. **Abbreviations:** cERM; chloroplast endoplasmic reticulum membrane, PPM; periplastidial compartment, oEM; outer envelope membrane, iEM; inner envelope membrane.

First, the homogeneous distribution of face-to-face PSIIs and PSIs along the stack ensures a rapid diffusion of the long-range electron carriers (PQ and cyt. c_6), which could be further facilitated by observed connections between thylakoids in *P. tricornutum* (Flori et al., 2017) (Fig. 1B). Diffusion of PC from cyt. b_6f to PSI represents an important limitation and potential regulatory nod for plant photosynthesis (Kirchhoff et al., 2011). Contrastingly, the electron transfer chain between the cyt. *f* and PSI remains in thermodynamic equilibrium in diatoms for an electron fluence one order of magnitude greater than that of plants (Flori et al., 2017),

indicating that the diffusion of electron carriers does not limit the global LEF rate at least in *Phaeodactylum* (Kirchoff et al, 2004; Kirchhoff et al. 2011; Flori et al, 2017).

Second, it should be noted that the thylakoid surface available for PSII (four internal thylakoid layers) exceeds that available for PSI (two external thylakoid layers). It is tempting to relate to reports that diatoms generally possess more PSII than PSI (while ≈1:1 is the go-to ratio in plants) (Raven et al., 2008, Strzepek et al, 2019). However, such a proposal must be taken with great caution. Indeed, such a consideration relies on a simplistic model where PSII and PSI would be exclusively embedded in the inner and outer thylakoid layers, respectively. In this simple model, the role and activity of the PSII in the PSI-deficient central thylakoid remains a puzzle that has not been properly addressed yet. Additionally, most PSII-to-PSI stoichiometries are based on immunoblots and do not represent the stoichiometry of functional photosystems, especially since, in several diatoms D1 (PsbA) has been found in entities which are not assembled/functional PSII (Levitan et al., 2019). The nature of those "D1 stocks" is not yet clear but they could be part of partially assembled PSIIs involved in the PSII repair cycle. The importance of this strategy may vary depending on cell size (Wu et al., 2011; Li et al., 2016) and/or light environment (Fischer et al., 2020) and between pennate and centric species (Lavaud et al., 2016).

In the green lineage, the PSII repair cycle largely depends on the segregation between active PSIIs and those that are inactive or undergoing repair (Järvi et al., 2015). In plants, the repair cycle involves a relatively long-range diffusion of inactivated PSII from the grana to the non-appressed regions. In diatoms, the PSII repair cycle is far from fully understood but cryo-electron tomography studies have begun to reveal heterogeneity in the spatial distribution of PSII complexes in thylakoids (Levitan et al., 2019; Jiang et al., 2021). These studies highlighted the existence of two pools of PSII complexes that may reflect that segregation between active and repairing PSIIs is also necessary in diatoms. Between a population of loosely distributed PSII patches and a second population arranged in semi-crystalline arrays of dimeric PSII cores, only the former displayed variable fluorescence (active photochemistry). The apparently inactive second dimeric PSII pool has therefore been proposed as a repair station for photodamaged complexes (Levitan et al., 2019).

The segregation between PSII and PSI is also important for the respective harvesting and conversion of light by the two photosystems. A process found in cyanobacteria and red algae, called spillover (Dekker & Boekema, 2005; Ley & Butler, 1977; Kowalczyk et al., 2013),

consists in the exchange of excitons between nearby PSII and PSI. Spillover leads to an increased functional absorption cross-section of PSI in conditions where PSII photochemical yield is low. In *P. tricornutum,* it has been shown that the ability of PSI to harvest excitons is independent of the activity of the PSII, excluding the possibility of spillover (Flori et al., 2017). It should be noted that another mode of balancing the light absorption by the two photosystems, called state transition, is present in the green lineage (Wollman 2001) and is related to the thylakoid stacking (Trissl & Wilhelm, 1993, Nagy et al., 2014). State transitions are thought to be absent in diatoms, although historical experimental evidence is now questioned (see further discussion on this topic in Lepetit *et al*., (2022)).

In sum, the lateral homogeneity of diatom thylakoids accompanies the face-to-face segregation of PSII and PSI. At least in *P. tricornutum*, this allows rapid electron transfer between PSII and PSI, and further segregation of PSII subpopulations. This appears to functionally replace the lateral segregation found in the green lineage both between PSII and PSI, and the long-range separation between active and inactivated PSII, while maintaining an efficient PSII repair cycle and avoiding spillover. Similar studies in other species are needed before these specificities can be generalized to diatoms as a group. Nevertheless, it remains tempting to propose that these features emerged to optimize energy transfers in the context of the particular organization of thylakoids into stacks of three (or four) in eukaryotes with secondary (or more) endosymbiosis plastids. Therefore, these features could be shared by diatoms and other secondary endosymbiosis eukaryotes.

1.4 Different modes of photosynthetic electron flows

The photochemical phase of photosynthesis is constrained by the same end goals regardless of the organisms. First, light absorption must be regulated based on the ability of cellular metabolism to consume its end products ATP and NADPH to avoid electron bottlenecks, otherwise leading to ROS production and photoinhibition. This situation is likely to occur under conditions of excess light, limiting CO_2 or chilling stress for instance, and a fine-tuning of the photosynthetic responses is required to avoid such harmful consequences. Even under optimal conditions, such a situation would occur if the photosynthetic ETC does not poise the right ATP/NADPH ratio to sustain metabolism and growth (Allen, 2002). Indeed, as discussed above, the ATP/NADPH ratio produced by the LEF is 1.28 assuming a constitutive Q cycle and the *c* subunits stoichiometry of the CF_1F_O ATPase typically found in plants. This value is lower than the ATP/NADPH ratio required for CO_2 fixation (1.5) and the difference becomes even

greater when ATP-consuming CCMs are considered (see section 1.5). This discrepancy results in an expected ATP deficit that, if not resolved, would lead to ever-accumulating NADPH. However, this naive view does not consider that CO_2 fixation is not the only future of NADPH and ATP. Many other metabolic pathways (reduction of nitrogen or sulfur, amino acids biosynthesis, thioredoxin regulation network…) use NADPH, ATP or both. Accordingly, it is accepted that the photochemical phase must demonstrate a certain level of flexibility regarding the ATP/NADPH produced to adapt to the sum of metabolic pathways using these energetic intermediates.

In the green lineage, such flexibility is assumed to be given by a network of alternative electron flows (AEFs), which are photosynthetic electron transfer pathways involving certain photosynthetic complexes, without supplying NADPH for CO_2 fixation. Here, we narrow the definition to electron fluxes participating in proton pumping across the thylakoid (i.e., involving PSII and/or cyt. b_6f), so that charge recombination or back-reactions in photosystems do not qualify as AEF (see review (Rutherford *et al.,* 2012)). These AEFs generate additional pmf without supplying NADPH to the CBB cycle and therefore increase the ATP/NADPH ratio (Eberhard *et al.*, 2008; Curien *et al.*, 2016; Alric & Johnson, 2017). Green lineage organisms possess multiple AEFs interacting through a complex regulatory network assumed to poise an adequate ATP/NADPH ratio for optimal functioning of the CBB cycle and other metabolic pathways downstream PSI (Eberhard et al., 2008; Curien et al., 2016; Croteau et al., 2023). But this is not the only reason AEFs improve resilience to various stresses (Eberhard et al., 2008; Alric & Johnson, 2017). When the photosynthetic ETC becomes over-reduced, the different AEFs act as electron valves allowing increased photochemistry in PSI and/or II (Chaux *et al.*, 2015; Curien *et al.*, 2016; Alric & Johnson, 2017). Moreover, as this additional output increases the pmf (and its ΔpH component), AEFs also provide photoprotection thanks to two ΔpH-dependent regulations. It drives NPQ induction (Munekage et al., 2002) and «photosynthetic control» (Sukenik et al., 1987), which are crucial processes to protect both PSII and PSI under light fluctuations (see section 1.7) (Dang *et al.*, 2014; Allahverdiyeva *et al.*, 2015; Chaux *et al.*, 2017; Storti *et al.*, 2019).

The main AEFs are generally divided into two categories discussed in the following sections: cyclic electron flow (CEF) around PSI (Shikanai 2014) and several water-to-water cycles (WWCs) culminating in O_2 reduction to water (Curien *et al.,* 2016). Although most of the molecular players involved in AEFs are not yet identified in diatoms, recent advances clearly show that the contribution of AEFs to total photosynthetic flux can be significant. This now

allows us to begin to put in perspective the role and extent of CEF and WWCs in diatoms compared to the green lineage (Fig. 2).

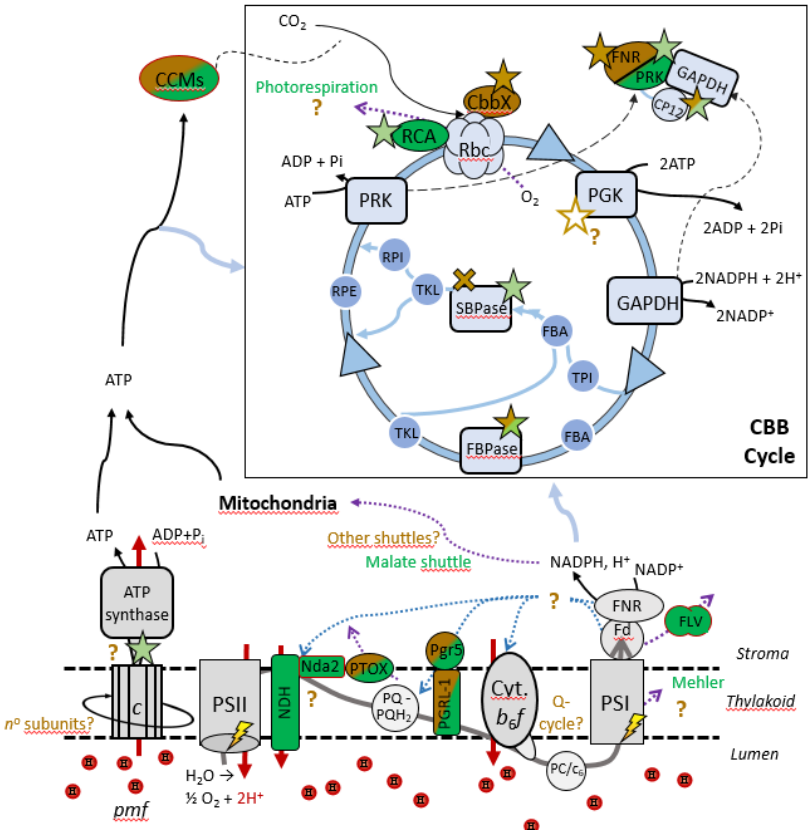

Figure 2: Schematic representation of the main differences in photosynthesis between diatoms and green organisms. Complexes/enzymes in grey and light blue are largely conserved in all organisms performing oxygenic photosynthesis. Proteins in green are present in green organisms only (red outline: present in some green organisms, but not angiosperms), the ones in green and brown are known to be present both in green organisms and in diatoms. The linear electron flow and proton transfer are shown with grey and red arrows, respectively. Known alternative electron flows (dashed lines: blue for Cyclic Electron Flow, purple for Water-to-water cycles) and their molecular actors, key redox regulations in the Calvin-Benson-Bassham (CBB) cycle and ATP synthase (stars) and open questions (question marks) are shown for green organisms (green) or diatoms (brown). The open brown star and brown cross indicate that the regulation is still unknown or absent, respectively, in diatoms. **Abbreviations:** CCMs; carbon concentrating mechanisms, Cyt.; cytochrome, FBAse; fructose-1,6-bisphosphatase, Fd; ferredoxin, Flv; flavodiiron proteins, FNR; Fd-NADP+ reductase, PC/c_6; plastocyanin or cytochrome c_6, GAPDH; glyceraldehyde 3-phospate dehydrogenase, Nda2; plastoquinone-reducing type II NADPH dehydrogenase, NDH; nucleotide dehydrogenase, Pgr5/PGRL-1; proton gradient (like), *pmf*; proton motive force, PQ; plastoquinone, PQH_2; plastoquinol, PRK; phosphoribulokinase, PS; photosystem, PTOX; plastid terminal oxidase, Rbc; ribulose-1,5-bisphosphate carboxylase/oxygenase, RCA; Rbc Activase. We refer the reader to the literature regarding the CBB for the complete name of all enzymes.

1.4.1. Cyclic electron flow around PSI

Through CEFs, electrons are redirected from PSI acceptors downstream of PSII, but whether it involves a Fd-PQ oxidoreductase (Hertle *et al.*, 2013) or electron injection in the cyt. b_6f without entering the PQ-pool (Joliot & Johnson, 2011; Nawrocki et al., 2019a) is still a matter of debate (Fig. 2). Two routes involving the PQ pool have been proposed. One is associated with the protein partners Pgr5/PGRL1 (Munekage et al., 2002; DalCorso et al. 2008; Hertle et al. 2013) and corresponds to the original reaction described by Arnon et *al.*, (1954). The other pathway depends on a type I nucleotide dehydrogenase (NDH) in plants (type II in green algae) which also injects electrons back into the PQ pool (Peltier *et al.*, 2016). While the "Pgr5" and "NDH" pathways can preferentially remedy to different stresses (Suorsa, 2015), they can also play a redundant role as confirmed by *Arabidopsis* mutants lacking either one or both routes (Munekage et al., 2004). Moreover, it is possible that the degree of reliance on one CEF pathway, rather than another, is taxa specific. It was recently demonstrated that the C_4 plant, *Flaveria bidentis*, is more affected by the suppression of the NDH-pathway than of the Pgr5-pathway (Ogawa et al. 2023), the opposite of what is observed in *Arabidopsi* (Munekage et al., 2004). Some argue in favor of a direct electron transfer through cyt. b_6f (Chain 1982) and this proposition gained support lately with emerging structural understanding of cyt. b_6f (Stroebel et al., 2003; Malone et al., 2019). Diatoms possess both PGR5 and PGRL1 (Grouneva et al., 2016) but not NDH (Oudot-Le Secq *et al.*, 2007). However, characterization of *P. tricornutum pgrl1* knockout and overexpressor revealed phenotypes inconsistent with the ones obtained in the green lineage (Zhou *et al.*, 2021).

When PSII is chemically inhibited, CEF can reach rates of ≈130 e^- s^{-1} PSI^{-1} in *Arabidopsis* (Joliot *et al.*, 2004). In *Chlamydomonas*, rates of ≈60 e^- s^{-1} PSI^{-1} have been reported (Nawrocki et al., 2019b) but can increase to ≈200 e^- s^{-1} PSI^{-1} when PSI, cyt. b_6f and PC are confined within supercomplexes under reducing conditions (Joliot *et al.*, 2022). Under non-stressful conditions, rates between 5 and 15 e^- s^{-1} PSI^{-1} are typically measured in diatoms (Maxwell & Biggins, 1976; Bailleul et al. 2015). Given these low rates, it has been proposed that CEF is not the constitutive regulator of the ATP/NADPH ratio in diatoms (Bailleul *et al.*, 2015) but some studies indicate that it may play an important role when diatom photosynthesis is faced with stressful conditions. Elevated CEF rates have been reported in iron-limited *T. pseudonana* (≈55 e^- s^{-1} PSI^{-1}) (Thamatrakoln et al., 2013) or in the polar *F. cylindrus* (≈25 e^- s^{-1} PSI^{-1}) (Goldman et al., 2015), suggesting that CEF is likely part of diatoms stress-response toolkit. It should be noted that all these rates measured with inhibited PSII are not representative of physiological conditions. The absence of an established and accepted protocol for the quantification of CEF under

physiological conditions is probably the main limitation to a comparative analysis of the importance of CEF in the green lineage and diatoms.

1.4.2. Water-to-water cycles

Electrons extracted from water can also be redirected to various AEFs leading to the photoreduction of O_2 to water than to the reduction of $NADP^+$ to supply CO_2 fixation. Thus, these WWCs are characterized by equal consumption and production of O_2 but can be measured by membrane inlet mass spectrometry using oxygen isotopes (Burlacot et al., 2020). They can also be detected by comparing PSII activity by Chl *a* fluorescence (which is the sum of LEF and WWCs) and net O_2 production (in which WWCs do not participate). Using such an approach, the extent of WWCs was compared in a diatom and a green alga, under different light conditions. The amount of WWCs was significantly lower in *P. tricornutum* than in *Chlorella vulgaris* under both fluctuating and non-fluctuating light (Wagner *et al.*, 2006). Interestingly, this led to greater efficiency in converting light energy to biomass in the diatom under fluctuating light simulating the vertical mixing that diatoms experience in the water column. No difference was observed under a non-fluctuating light regime (Wagner *et al.*, 2006). This probably indicates a more efficient management of photosynthetic pathways under dynamic light conditions. This is in line with the reputation of diatoms as specialists of turbulent waters (Margalef 1978) even though the adaptation of many species to stratified waters is now well recognized (Kemp & Villareal, 2018). Increasing O_2 consumption compared to dark respiration baseline in light-exposed diatoms is often reported (Weger et al. 1989; Wagner et al. 2006, 2016; Waring et al. 2010; Fisher and Halsey 2016). Furthermore, Fanesi et *al.*, (2016) showed that AEFs contribution to total photosynthetic flux is growth temperature- and species-dependent, observing variations between 10-30% in three freshwater diatoms. Nevertheless, none of these studies could determine unambiguously the relative extent of the different WWC pathways (listed in the following sections).

The first "historical" WWC was reported more than 70 years ago when Mehler (1951) observed the production of H_2O_2 by illuminated extracted thylakoids. Upon further investigation the first product of the Mehler reaction was identified as the superoxide radical $O_2^{\bullet-}$, which is instantaneously disproportionated to O_2 and H_2O_2 by the superoxide dismutase (SOD) and further recycled in the stroma to two water and two monodehydroascorbate molecules (Ogawa *et al.*, 1995; Asada, 1999). Only iron-containing and CuZn-containing SODs have been described in plant chloroplasts, but manganese-containing SOD has been found in the plastid of *T. pseudonana* (Wolfe-Simon, 2005). A NiSOD homolog has been identified in *P.*

tricornutum but whether it localizes in plastid and participates to the Mehler reaction is unknown (Cuvelier et al. 2010). The initial electron donor to O_2 has long been interpreted as reduced Fd when lacking $NADP^+$ acceptors (Furbank & Badger, 1983). But recent data suggest that reduced phylloquinone A, located within one of the two PSI electron transfer branches, is the main electron donor in the Mehler reaction (Santabarbara *et al.*, 2015; Kozuleva *et al.*, 2021) (Fig. 2). Due to its transient products, the impossibility to generate mutants lacking Mehler reaction and the difficulty in distinguishing it from other WWCs, the rate of the Mehler reaction is difficult to estimate and conflicting views exist depending on species and conditions. While such photoreduction of O_2 in the light has been attributed to Mehler reaction in diatoms (Waring et al., 2010), it is difficult to exclude a confusion with another WWC.

In the green lineage, except angiosperms, a major alternative oxidase generating another type of WWC are the flavodiiron (FLV) proteins (Chaux *et al.*, 2017; Storti *et al.*, 2019). The electron donors for FLVs is believed to be found downstream of phylloquinones, in the [4Fe-4S] clusters of the PSI (Jokel *et al.*, 2018; Sétif *et al.*, 2020). Interestingly, the contribution of FLVs to electron flow is crucial during the first few minutes of the dark-to-light transition, a timescale comparable to the redox activation of most CBB enzymes (Zimmer *et al.*, 2021). The FLV activity is much less discernable once steady-state is reached (Chaux *et al.*, 2017). Diatoms, like the rest of the red lineage, lack FLVs although homologs are found in *Symbiodinium* dinoflagellates (Shimakawa *et al.*, 2021)(Fig. 2).

Another type of WWC involves the shuttle of products of photosynthesis towards mitochondria, which are then respired (Curien *et al.*, 2016). With the definition we use here, such a light-dependent increase of mitochondrial respiration (but not the basal respiration already present in darkness) can be considered a WWC. In green lineage organisms, the malate-aspartate valve is particularly important for chloroplast-mitochondria coupling (Krömer & Heldt, 1991; Scheibe *et al.*, 2005; Kong *et al.*, 2018). The alternative oxidase (AOX) provides additional capacity to the respiratory electron transfer chain under stressful conditions or when the concentration of reducing equivalents is high, fueled by photosynthates or reducing power from photosynthesis (van Aken et al., 2009; Vishwakarma et al. 2014; Kaye et al., 2019). This creates a WWC since shuttled intermediates are first reduced in the chloroplast by electrons from the oxidation of water, then provide electrons in the mitochondrion for the reduction of O_2 catalyzed by AOX or cyt. *c* oxidase (complex IV).

This type of WWC has long been suspected in diatoms (Weger *et al.*, 1989), a suspicion that has been reinforced with the arrival of –omics techniques. Transcriptomic data from iron-

limited *P. tricornutum* suggest a role for the AOX in managing the excess reducing power generated in photosynthesis (Allen et al., 2008). In the same diatom, AOX knockdowns exhibit hypersensitivity to various stresses (Murik *et al.*, 2019). Even under non-stressful conditions, diatom photosynthesis appears to rely on efficient energetic interaction between organelles, where some photosynthesis-generated reducing power is redirected to the mitochondria and ATP is then imported back into the plastid (Bailleul et al, 2015). This model is based on the phenotype of the AOX knockdown lines (lower photosynthetic activity, increased NADPH and decreased ATP), as well as observations that 10% of electrons from PSII are rerouted to O_2-consuming processes and that an efficient exchange of ATP can occur between the two organelles (Bailleul *et al.*, 2015). This, combined with slow CEF rates (under chemical PSII inhibition and non-stressful oxic conditions), led to the hypothesis that this energetic interaction between mitochondria and chloroplast is the main *constitutive* AEF regulating ATP-to-NADPH ratio in diatoms, instead of CEF in the green lineage (Bailleul *et al.*, 2015; Flori *et al.*, 2017). A genome-scale metabolic network reconstruction for the marine diatom *P. tricornutum* confirmed the possibility of such an energetic interaction between the two organelles (Levering et al. 2016).

However, the molecular nature of these shuttles remains to be elucidated (Fig. 2). From genome-wide modeling, it has been proposed that a putative ornithine and a 2-oxoglutarate/oxaloacetate shunts might be active in diatoms (Levering et al. 2016; Broddrick et al. 2019) rather than the typical plant malate-shuttle (Scheibe et al., 2005). Other pathways could be related to the peculiar presence of energy-generating glycolysis enzymes within diatom mitochondria (Kroth et al. 2008; Bártulos et al. 2018). Finally, subcellular 3D imaging observations suggest increased physical interactions between mitochondrion and chloroplast in *P. tricornutum* compared to six distant phytoplankton species (including two Archaeplastida), could potentially favor exchange between organelles (Uwizeye et al., 2021). In the green alga *Dunaliella tertiolecta*, the use of spikes of C14 in nitrogen-limited conditions revealed that newly fixed carbon in the light had a very short lifetime and could be used as shuttles for reducing power (Halsey et al., 2011). Similar methodology could be useful in diatoms to better understand the nature of the shuttle molecules involved in this inter-organelle energetic interaction.

The plastid terminal oxidase (PTOX) is another important oxidase in the green lineage plastids which catalyzes the oxidation of reduced PQH_2 (Bennoun et al., 1982). Together with the chloroplast NDH (see CEF section), which non-photochemically reduces PQ into PQH_2, PTOX

completes a minimal respiratory process taking place in the thylakoid membrane. A key function of chlororespiration is to balance the redox state of the PQ pool in the dark (Nawrocki et al. 2015). Diatoms possess two copies of PTOX and evidence of PTOX activity under light has been reported (Dijkman & Kroon, 2002). However, diatoms do not possess NDH (Oudot-Le Secq *et al.*, 2007) (Fig. 2). Dark-activated NPQ is often reported in diatoms (Grouneva *et al.*, 2009; Lacour *et al.*, 2019; Croteau *et al.*, 2021) and it has previously been hypothesized that NPQ may be activated by a ΔpH generated by chlororespiratory activity (Jakob et al., 1999, 2001; Lavaud et al., 2002a; Cruz et al., 2011) . However, it is more likely that pmf in the dark results from CF_1F_O-ATP hydrolysis of ATP produced in diatom mitochondria (Bailleul et al., 2015), similar to what is observed in the green lineage (Finazzi & Rappaport, 1998; Buchert *et al.*, 2021). The combined activities of PTOX and PSII have been shown to represent an efficient WWC in prasinophytes, cyanobacteria and alpine plants (Bailey et al. 2008; Cardol et al. 2008; Streb et al. 2005) but this process seems limited to particular cases of adaptation to stressful conditions. This WWC appears to be negligible under light exposure in most cases in the green lineage (Nawrocki et al, 2015) and no report suggests otherwise in diatoms.

Finally, photorespiration, the oxygenase activity of the Rubisco, redirects photosynthetic electrons to O_2 instead of CO_2 fixation (Fig 2). It can therefore be considered a WWC which will be treated in section 1.5. It is important to note that the different WWCs, involving plastidial or mitochondrial oxidases, cannot be distinguished on the sole basis of MIMS measurements or by comparing Chl *a* fluorescence and net O_2 production. In the green lineage, the unambiguous attribution of light-driven O_2 consumption to a given oxidase was sometimes possible using mutants (e.g. KO mutant of FLV in *C. reinhardtii* (Chaux et al., 2017)). In the absence of an appropriate mutant, pharmacological approaches (e.g., inhibition of the mitochondrial respiration by appropriate inhibitors) can be used but are rarely fully conclusive.

1.4.3. Other AEFs

Of course, the fate of photosynthetic electrons is not limited to reducing CO_2 or alternatively, O_2. They are used for a variety of other chloroplast metabolic pathways, including the thioredoxin system, which is at play in the green lineage (Nikkanen & Rintamäki, 2019) as well as in diatoms (Weber et al, 2009; Kikutani et al, 2012). Reducing power is also needed for other basal metabolic needs, such as in nitrogen (Krapp *et al.*, 2014) or sulfur (Leustek *et al.*, 2000) assimilation. In diatoms, Lomas and Gilbert (1999) proposed such funnelling of photosynthetic electrons towards nitrogen assimilation could be particularly relevant for plastid redox poise as stored nitrate can serve as an alternate electron sink under stressing conditions. This was shown

by ammonium release increase in several diatom species undergoing high light stresses or low temperature shifts (Lomas *et al.*, 2000). Recent molecular insights support tight coupling between nutrients assimilation and redox balance in diatoms, notably a genome-scale metabolic model of *T. pseudonana* suggests excretion of sulfur compounds can also occur when nitrogen is limiting (Van Tol & Armbrust, 2021). Another type of AEF is the photoreduction of H^+ to H_2, which represent a critical electron sink in green algae allowing to resume photosynthesis during a transition from dark to light under anoxic conditions (reviewed in (Hemschemeier et al., 2023)). In diatoms, homologs of hydrogenases have only been found in *T. pseudonana*, but without maturation factors (Atteia et al., 2013). These hydrogenases do not seem to be fueled by photosynthetic ETC and could be involved in fermentation-like process rather than AEFs (Gain *et al.*, 2023).

Finally, a CEF around PSII providing photoprotection has been reported in diatoms (Lavaud *et al.*, 2002a; Wagner *et al.*, 2016) and chlorophytes (Falkowski *et al.*, 1986; Prasil *et al.*, 1996). However, it cannot be considered an AEF in the restricted definition used here as it does not increase the pmf, although it could play an important role in dissipation of excess light absorption in PSII. Recent studies however suggest that the involvement of a regulatory site (Qc) would allow proton pumping along the PSII-CEF (Gates et al, 2023).

1.5 Regulation of CO_2 concentration, CO_2 fixation and carbon metabolism

Carbon fixation, Rubisco and Calvin-Benson-Bassham cycle

As Rubisco is central to the CBB cycle providing carbon to form biomass, its regulation is crucial to adjust carbon metabolism to the photochemical phase of photosynthesis, even more so than its abundance (Raines, 2003). In the green lineage, the gene encoding Rubisco large subunit (*rbcL*) is encoded in the plastid genome, while the gene encoding its small subunit (*rbcS*) is in the nucleus, and hence the expression of Rubisco requires the coordination of both plastid and nuclear gene transcription (Sasaki et al, 1987; Suzuki & Makino 2012; Wostrikoff & Mackinder, 2023). In diatoms and other stramenopiles, both genes are encoded in the plastid genome (Liu et al., 2021; Oudot-Le Secq et al, 2007), suggesting that Rubisco activity is less regulated at the transcriptional level. Rubisco activation requires the carbamylation of a specific lysine residue and the binding of Mg^{2+} in its active site; both events are favored by high CO_2 and high pH (Jensen et al., 2017). Additionally, non-carbamylated Rubisco can be inhibited by RuBP and other sugar phosphates (Portis et al., 2008). In plants, the inhibitory RuBP is dissociated from Rubisco by Rubisco activase (RCA) at the cost of ATP consumption (Gontero

& Salvucci, 2014). The activity of RCA depends on the ATP/ADP ratio and redox regulations by thioredoxins at its C-terminus (Portis et al., 2008, Scafaro et al., 2019). There is no gene encoding RCA in diatoms (Fig. 2). In contrast, diatoms possess a plastid-encoded bacterial homolog of the CbbX gene (Fig. 2), also present in red algae (Jensen et al., 2017). The function of CbbX may be analogous to that of RCA as it also binds ATP, however, it seems to be regulated by RuBP binding on its C-terminus instead of being redox-regulated (Jensen et al, 2017; Mueller-Cajar et al, 2011).

A well-characterized regulatory mechanism in the CBB cycle of land plants and green algae is the one involving phosphoribulokinase (PRK), glyceraldehyde 3-phospate dehydrogenase (GAPDH) and the intrinsically disordered protein CP12 (Gontero et al, 2012; Michelet et al, 2013). Upon oxidation (i.e., in the dark), CP12 binds both PRK and GAPDH, forming a supra-molecular complex that inhibits both enzymes (Michelet et al., 2013). In light, CP12 is reduced by thioredoxins and the PRK-CP12-GAPDH complex is dissociated, leaving the enzymes active (Gontero et al., 2012). In contrast, diatoms might not have this type of regulation because no PRK-CP12-GAPDH complex has been successfully isolated so far (Fig. 2). However, another supra-molecular complex involving GAPDH, CP12 and Fd-$NADP^+$ reductase has been characterized in the pennate freshwater diatom *Asterionella formosa* (Mekhalfi et al., 2014).

In addition, putative homologs of CP12 have been found in *T. pseudonana* but their involvement in complex formation with other CBB cycle enzymes has not yet been confirmed (Shao et al., 2021). Inhibition of plastid GAPDH in the dark is crucial in land plants to avoid excessive NADPH consumption and futile cycles with the NADPH-producing oxidative phosphate pathway. But this latter pathway is not occurring in diatom plastid, therefore the redox regulation of GAPDH could be less important (Gruber & Kroth, 2017). Other CBB cycle enzymes, such as PRK and the sedoheptulose 1,7-bisphosphatase, possess N-terminal cysteine residues which are considered essential in their redox-regulation in lands plants and green algae. Those cysteines are too far apart to favor the formation of disulphide bonds in diatoms' PRK and are absent in sedoheptulose 1,7-bisphosphatase (Jensen et al., 2017; Launay et al, 2020). In contrast, the fructose-1,6-bisphosphatase is activated upon reduction in *P. tricornutum* (Michels et al., 2005), while data regarding phosphoglycerate kinase activation are still controversial (Bosco et al., 2012, Jensen et al, 2020b) (Fig. 2).

Type I Rubisco is able to fix CO_2 or O_2 at the same active site, which leads to the generation of different products. Photorespiration, which is the oxygenase activity of the Rubisco, is an essential carbon pathway in photosynthetic organisms of the green lineage. Fixation of O_2

instead of CO_2 generates a molecule of 3-PGA and a molecule of 2-phosphoglycolate (2-PG). Although Rubisco has 20-60 times higher affinity for CO_2 than for O_2, photorespiration occurs with a significant yield in air-saturated surface waters, at ambiant temperature, because of the higher concentration of dissolved CO_2 compared to O_2 (~250µM versus ~15µM) (Young et al, 2016). Since no net carbon is incorporated into cell metabolism and regeneration of the toxic 2-PG into 3-PGA is an energy-consuming process, photorespiration might seem a wasteful pathway. However, it has been shown that it is crucial to dissipate the excess of light energy used during photosynthesis that can lead to photoinhibition, and thus it may function as a safety valve in plants (Kozaki & Takeba, 1996; Villalobos-González et al., 2022). All the genes potentially involved in photorespiration are found in the genomes of *P. tricornutum* and *T. pseudonana*, with the exception of the glycerate kinase (Kroth et al. 2008), which could be replaced functionally by the photorespiratory 2-carbon oxidation cycle (Fabris et al., 2012). The reincorporation of 2-PG into the CBB cycle involves the glyoxylate pathway in diatoms, as in cyanobacteria (Kroth et al, 2008). Photorespiration under ambient CO_2 and O_2 conditions has been reported in diatoms (Schnitzler-Parker et al., 2004; Roberts et al, 2007; Shmitz et al. 2017) but the extent of this process remains unclear (Davis et al. 2017, Kroth & Matsuda, 2022). In the diatom *Thalassiosira weissflojii*, there is a positive correlation between the mRNA levels of the glycine decarboxylase and the formation of 2-PG with the activation of photorespiration when cells acclimated to low light are transferred to high light (Schnitzler-Parker et al., 2004). Thus, these markers could be helpful to monitor the initiation of the photorespiration pathway in marine environments. In diatoms, but also in green microalgae (Matsuda et al., 2011), photorespiration should be significantly reduced compared to land plants because of efficient CCMs increasing the CO_2/O_2 ratio in the vicinity of Rubisco.

Carbon concentration mechanisms and pyrenoid

Aquatic environments – unlike terrestrial ones – are much more limited in CO_2. In fact, at equilibrium with the atmosphere (i.e., currently around 400ppm and increasing), the concentration of CO_2 in the Ocean is only ~15µM on average, which accounts for less than 1% the amount of the total dissolved inorganic carbon (the most abundant form being bicarbonate, HCO_3^-) (Kim et al, 2006; Jensen et al, 2020a). Furthermore, the carboxylation half-saturation constant of Rubisco in microalgae is significantly higher than the average CO_2 concentration in the Ocean (Young et al, 2016; Heureux et al, 2017).

Despite these impediments, photosynthetic carbon fixation in microalgae is very efficient, being 10 to 50 times higher than that of terrestrial plants (Bhola et al, 2014). Indeed, most algae have

CCMs, which contribute to increasing the CO_2 concentration around Rubisco to levels close to saturation (Raven & Beardall, 2016). Both biophysical and biochemical processes can be involved in CCMs. Biochemical CCMs involve the prefixation of HCO_3^- to form C_4 intermediates (i.e., oxaloacetate) (von Caemmerer et al., 2017). Biochemical CCMs are less common in eukaryotic microalgae and have only been observed in few green microalgae, while their presence is still controversial in diatoms (Reinfelder et al., 2000; Kutska et al, 2014; Clement et al, 2017; Ewe et al, 2018; see however Yu et al, 2022). In contrast, a large majority of microalgae and cyanobacteria use biophysical CCMs, i.e., the active transport of HCO_3^- within cells and across cell compartments, and its conversion to CO_2 by carbonic anhydrases (CAs). In green algae, HCO_3^- is transported by "high-light activated 3" and "low CO_2-inducible 1" transporters across the plasma membrane, and by LCIA located in the chloroplast membrane (Yamano et al., 2015). In contrast, diatoms do not possess homologs to these transporters, but instead possess several genes encoding "solute carrier 4 family" (SLC4) proteins, which are closer to HCO_3^- transporters found in mammals (Nakajima et al., 2013). In *P. tricornutum*, some SLC4 homologs are induced under low CO_2 conditions (Matsuda et al., 2017), but this has not yet been studied in other diatom species. Homologs of SLC4 can be located either in the plasma or the plastid membranes. Indeed, among seven genes encoding for SCL4 HCO_3^- transporters, the N-terminal sequences of two of them contain signal and transit peptides for the endoplasmic reticulum and the plastid, respectively, in *P. tricornutum* and *T. pseudonana* (Matsuda et al., 2017) . Since diatoms have plastids surrounded by four membranes due to their secondary endosymbiosis origin, a more complex arrangement of HCO_3^- transporters is expected, although many components and driving forces of HCO_3^- transport (e.g., pH or ions) are still unknown.

Other important proteins of the CCMs are CAs. These ubiquitous enzymes catalyze the reversible hydration/dehydration reaction of CO_2. The reaction is essential for many processes in cells, including pH and redox homeostasis (Raven, 1995). Although all CAs catalyze the same reaction, they do not share an obvious evolutionary origin. Thus, CAs can be defined as a superfamily of metalloenzyme composed of several classes named with the Greek letters α-, β-, γ-, δ-, ζ-, η-, θ- and ι- (Jensen et al., 2020a). Their role in the CCMs of photosynthetic organisms is evidenced by their involvement in the efficiency of carbon fixation, their sensitivity to environmental CO_2 and their subcellular localization. The best-studied CAs are those belonging to classes α- and β- (DiMario et al., 2017; 2018), which are most common in non-photosynthetic eukaryotes including mammals and yeast but are also predominantly

present in higher plants and in green algae (Aspatwar et al., 2018). In the green alga *C. reinhardtii*, most CAs with a proposed role in CCMs belong to α- and -β classes and are found in the chloroplast stroma, thylakoid lumen and periplasmic space (Aspatwar et al., 2018). More recently, two mitochondrial β-CAs (CAH4 and CAH5) have been shown to be important for optimal photosynthesis and growth at low CO_2, probably by converting CO_2 from respiration back to HCO_3^- to be redirected into the chloroplast (Rai et al., 2021). Contrarily, diatoms have a more diversified set of CAs, which includes almost all classes discovered so far (Jensen et al, 2020a). Of the 8 existing CA classes, 4 of them (δ-, ζ-, θ- and ι) were discovered for the first time in diatoms. Both ι-CA and θ-CA were later identified in green microalgae but no homologs of the δ- and ζ- classes have been found in the green lineage. While most CAs use zinc as metal cofactor for activity, the δ- and ζ- classes can replace zinc with cobalt and cadmium, respectively. This could represent an environmental adaptation of diatoms to marine ecosystems, especially in zones where zinc is less abundant (Morel et al., 2020). The ι-CA class is also special, as some homologs prefer manganese over zinc, although completely metal-free homologs have also been described (Jensen et al, 2019; Del Prete et al., 2020; Hirakawa et al., 2021). While genes encoding for putative ι-CA are found in green algae, they have not yet been functionally characterized.

The pyrenoid is a membraneless organelle present in the plastids of most eukaryotic microalgae and serves primarily as a Rubisco confinement site and endpoint of CCMs. It is analogous -but not evolutionarily related- to the carboxysome found in cyanobacteria (Klanchui et al., 2017). Its structure and composition are very diverse in photosynthetic eukaryotes (Bedoshvili et al., 2009; Barrett et al., 2021). Most studies concerning algal pyrenoid have been carried out on *C. reinhardtii* (see He et al, 2023 for a review). The pyrenoid can be observed as a dense organelle structure surrounded by a sheath formed by two or more starch plates and is usually crossed by one or a few membranes extending from the thylakoid. It consists in a liquid-liquid phase separation formed by Rubisco aggregate (Barrett et al., 2021), which is packed and bound by a disordered protein, the essential pyrenoid component 1 (EPYC) (Mackinder et al., 2016). Although an essential role in Rubisco aggregation and pyrenoid formation has been established for EPYC in *C. reinhardtii,* there are no known homologs in other eukaryotic algae. The function of the diatom pyrenoid, on the contrary, has been much less studied. Most diatoms possess pyrenoids that have a thylakoid membrane running through the center (Bedoshvili et al, 2009). The presence of CAs in the lumen of a pyrenoid-crossing thylakoid appears to be a conserved feature of photosynthetic eukaryotes and suggests a direct involvement in CO_2

supply into the pyrenoid (Tsuji et al. 2017; Barrett et al. 2021; Nawaly et al. 2023). In fact, a α-class CA, CAH3, found at this location in *C. reinhardtii* is essential for growth in low/air CO_2 concentration and is also associated to PSII by facilitating the removal of protons after the oxidation of H_2O in the oxygen-evolving complex (Benlloch et al., 2015). Conversely, diatoms possess a θ-CA in the thylakoid crossing the pyrenoid, instead of one belonging to the α-class, which possibly has a similar dual role like that of *C. reinhardtii* (Kikutani et al. 2016; Tsuji et al. 2017). More recently, homologous CAs were also identified in *T. pseudonana*, suggesting a common broad distribution of this CA among divergent diatom groups (Nawaly et al., 2023). In *C. reinhardtii*, the LCIB protein has recently been proposed as an orthologous protein to the θ-CA, which is also located in the vicinity of the pyrenoid and may have a role in redirection of CO_2 from the chloroplast stroma to the pyrenoid (DiMario et al., 2018). The starch sheath seems to play an important role in the localization of the LCIB protein and in the efficiency of the CCMs in *C. reinhardtii* (Toyokawa et al., 2020), in contrast to diatoms which do not accumulate starch in the pyrenoid boundary, leaving open the question of a possible sheath with a different composition in diatoms.

Other metabolic pathways in the plastid

Diatoms possess both plastid and cytosolic glycolytic enzymes, like plants and green algae. In *C. reinhardtii*, the first/upper part of glycolysis (i.e., the consumption of ATP) occurs in the plastid while the second/lower part (i.e., the production of ATP and NADH) takes place only in the cytosol (Johnson & Alric, 2013). Studies of the genomes of *T. pseudonana* and *P. tricornutum* showed that most glycolysis enzymes have been duplicated and relocated (Kroth et al., 2008; Gruber & Kroth, 2017). Thus, diatoms also possess several isoenzymes of the second part of glycolysis located in the mitochondrion (Kroth et al., 2008). Although it is not clear why diatoms have a mitochondrial glycolysis pathway, it may be complementary to an ancestral bacterial-like Entner-Doudoroff glycolytic pathway, which leads to a lower ATP/NAD(P)H ratio in mitochondria and could have some energy-regulatory function (Kroth et al., 2008; Gruber & Kroth, 2017; Smith et al., 2012). Interestingly, *F. cylindrus* maintains high transcription of proteins involved in the lower glycolysis and the Enter-Doudoroff pathway for up to 4 months of darkness, which possibly help to survive the polar night and perhaps to promptly resume photosynthesis upon light return (Kennedy et al., 2020; Joli et al., 2023). Moreover, the presence of only the lower glycolysis in mitochondria could also facilitate the exchange of trioses phosphates produced from plastidial glycolysis or during the CBB cycle (Smith et al., 2012). Recently, it has been shown that a complete second part of the glycolytic-

gluconeogenic pathway is also present in diatom plastids, thanks to a plastid enolase and a bis-phospho-glycerate mutase resulting from a recent duplication of their mitochondrial isoform (Dorrell et al., 2022). This allows to feed the pyruvate hub with phospho-*enol*-pyruvate converted from 1,3-bis-phosphoglycerate produced by the CBB cycle. No phenotype in the photochemical phase of photosynthesis was associated to the loss of this pathway in enolase or bis-phospho-glycerate mutase knockout mutants (Dorrell et al., 2022).

A substantial difference between diatoms and the green lineage is carbon storage pathways. In diatoms, as well as in other chromalveolates, carbohydrates are accumulated as chrysolaminarin, a β-1,3-glucan, and stored in the cytosolic vacuole, unlike green algae which accumulate starch mainly in plastids. The chrysolaminarin content in diatoms varies with growth conditions, including nutrient and CO_2 availability (Jensen et al., 2020b; Yang et al., 2020). Over diatoms' cell cycle, chrysolaminarin levels generally remain constant, which means that the energy supply from the breakdown of carbohydrates is not exclusive to support cell growth (Hildebrand et al., 2017). This contrasts with *C. reinhardtii* which is believed to use the starch produced under light to support cell division during the night period (Ral et al., 2006; Vítová et al, 2011; 2014). Interestingly, while mutations impairing chrysolaminarin accumulation in diatoms do affect carbon metabolism, photosynthetic yields and plastid structure, they have a limited influence on growth rate (Hildebrand et al., 2017; Huang et al., 2018).

1.6 General response of photosynthesis to environmental stresses

The response of photosynthesis to environmental changes picks in the toolkit of regulatory mechanisms listed in this review. Depending on the nature of the shift/stress, CCMs, regulation of the CBB cycle enzymes, AEFs or photoprotection mechanisms are activated. This requires a conductor, a master regulator. In this section, we will discuss what is known about the orchestration of the photosynthetic responses to environmental stresses or acclimation processes in the green lineage and in diatoms.

While both $\Delta\psi$ and ΔpH (together forming the pmf) generated by photosynthetic electron flow are energetically equivalent in driving ADP phosphorylation by the CF_1F_O-ATP synthase (Hangarter & Good, 1982), they participate in different feedbacks governing the photosynthetic ETC. In the green lineage, the pH component, regulates the photochemical phase of photosynthesis and has been described as a "master regulator" of photosynthesis (Kramer et al, 2003: Armbruster et al. 2017; Davis et al. 2017). A major regulatory process governed by ΔpH

is the “energy-dependent” component qE of NPQ (Goss & Lepetit, 2015). Lumen acidification is the trigger for dimerization and activation of the violaxanthin de-epoxidase, which converts violaxanthin into zeaxanthin (Arnoux et al, 2009). A low luminal pH also induces a conformational change of PsbS/LhcSR3 mediated by the protonation of certain acidic residues exposed to the lumen (Goss & Lepetit, 2015). Lower luminal pH also makes the two stages of proton pumping across the thylakoid, at PSII and at cyt. b_6f, more difficult. As for the oxygen evolving complex, the $S_3 \rightarrow S_0$ step coupled to the release of protons is almost arrested *in vitro* at pH < 5 (Zaharieva *et al.*, 2011), which reinforces donor side limitation of PSII and sensitizes it to photodamages (Spetea *et al.*, 1997). Closer to physiological pH, lumen acidification slows the oxidation of PQH_2 in the Q_O site oxidation of cyt. b_6f in plants (Laisk *et al.*, 2005) and green algae (Finazzi & Rappaport, 1998). This phenomenon, called « photosynthetic control » plays an important role in PSI photoprotection under conditions of acceptor side limitation. By slowing down the cyt. b_6f turnover, « photosynthetic control » moves the limiting step of photosynthesis from downstream to upstream PSI, protecting it from photodamage. The ΔpH is considered a master regulator of photosynthesis because, not only does it regulate the turnover rate of PSII and cyt. b_6f, but (i) it is connected to AEFs and redox regulations through feedback loops which modulate the extent and composition of the pmf (Kramer et al., 2003; Croteau et al., 2023) and (ii), it also regulates CCMs. The modulation of the pmf depends on the redox regulation of the CF_1F_O ATPase through a cysteine couple permitting a disulfide formation under light. This cystein couple is present in a 9 amino acids segment of the γ subunits and can be reversibly reduced via thioredoxins. This thiol modulation, which modifies the quantity of pmf necessary for a given rate of ATP synthesis, is restricted to the green lineage (Buchert et al., 2017; Buchert et al., 2021; Kramer et al, 1990). The cystein couple responsible for this redox regulation is indeed absent in diatoms (Pancic & Strotmann, 1990; Ponomarenko, 2007). The effectiveness of CCMs in *C. reinhardtii* is strictly dependent on the amount of additional ATP produced by the activities of FLVs and CEF. The double mutant of PGRL1 and FLV (not the single mutants) show a decrease in carbon fixation rate under low inorganic carbon (Burlacot et al., 2022). For all these reasons, ΔpH is at the heart of orchestrating rapid responses to environmental changes (e.g., CO_2, light, temperature…) (Aguila Ruiz-Sola et al., 2023).

In the diatom *P. tricornutum*, the pH sensing associated to conformational changes of PsbS/LhcSR3 seems to be absent (Giovagnetti et al, 2021; Buck et al, 2021). Consequently, the fast (seconds scale) NPQ (qE) relaxation observed in the green lineage at the end of a high light

period is absent in *P. tricornutum*. Instead, the relaxation of qE follows the conversion of diatoxanthin back to diadinoxanthin by the diatoxanthin epoxidase, in a linear manner (Lavaud et al, 2002b; Goss et al, 2006). The XC is however dependent upon luminal pH through the activation of the diadinoxanthin de-epoxidase (DDE), but the characteristics of the XC are very different from that of plants (Goss & Lepetit, 2015). The DDE is activated at lower ΔpH (higher luminal pH) compared to the violaxanthin de-epoxidase from plants, it exhibits a broader pH optimum and is already active at pH 7 (Grouneva et al, 2006; Jakob et al, 2001). In brief, slight changes in the luminal pH are sufficient to generate high amounts of diatoxanthin in diatoms. Moreover, the regulation of the XC is at least as much regulated by the high-light inhibition of the diatoxanthin epoxidase as by the DDE (Blommaert et al, 2021). A hypothesis for this downregulation, yet to be explored in diatoms, could be via the production of H_2O_2 as recently shown for zeaxanthin epoxidase in spinach (Holzmann et la., 2022).

Because of the importance of ΔpH and because transient overshoot in Δψ under fluctuating light seems to increase the likelihood of charge recombination at PSII and damaging ROS production (Davis *et al.*, 2016), the partitioning between the osmotic and electric components of the pmf must be tightly controlled. In the green lineage, this partitioning can be measured experimentally using spectroscopic methods based on the electrochromic shift (ECS) of photosynthetic pigments (Witt et al, 1979; Bailleul et al, 2010). Indeed, the recovery of ΔpH is much slower than that of Δψ after a light-to-dark transition, due to the high proton buffering capacity of the lumen (Junge *et al.*, 1979). This results in a transitory negative ECS (a net decrease in the electric field across the thylakoid lasting a few hundreds miliseconds after a light-to-dark transition), a phenomenon sometimes called ECS inversion which allows the two components to be quantified (see (Kramer et al. 2003) for rational behind this reasoning). A suite of thylakoid ion channels is involved in controlling the relative extent of the two components of the pmf: including the H^+/K^+ antiporter KEA3, the voltage-dependent Cl^- transporter VCCN1 and the Cl^- channel ClCe (Armbruster et al., 2017; Dukic et al. 2019; Li et al. 2021; von Bismark et al, 2023 ; Herdean et al. 2016a/b). In *P. tricornutum*, KEA3 knockouts have been characterized and show higher pH-dependent xanthophyll cycle activity than wild type under moderate light, but not under high light where the ΔpH generated by photosynthesis may be sufficient to fully activate the diadinoxanthin de-epoxidase independently of KEA3 activity (Seydoux et al., 2022). Blast analysis also predict the presence of VCCN1 in the plastids of diatoms (Marchand et al., 2018). Interestingly, no ECS inversion is observed in *P. tricornutum* (Bailleul et al., 2015).

From this overview, it appears that the role of ΔpH is not as central in *P. tricornutum* as in the green lineage. However, this conclusion should be taken with caution due to the bias in favor of studies on *P. tricornutum*. Even though the linear relationship between NPQ and diatoxanthin seems to be a good faith rule in pennates (Barnett et al., 2015), the situation could be different in centric species. In *Opephora guenter-grassii*, the NPQ relaxes rapidly in a ΔpH-dependent manner and an ECS inversion is observed in line with a build-up of ΔpH (Blommaert et al., 2017). In *Cyclotella meneghiniana*, there is a heterogeneous NPQ that includes both a diatoxanthin-dependent NPQ like that of *P. tricornutum* and a strictly ΔpH-dependent component comparable to that of vascular plants (Grouneva et al., 2008). While the nature of the orchestrator of the short-term photosynthesis response in diatoms remains an enigma, such orchestration must be in play. For example, WWCs and photoprotection (NPQ) capacities are inversely proportional in three *Thalassiosira* species when shifted to high light stress (Fisher *et al.*, 2020).

Nevertheless, ΔpH is not the only sensor/regulator by which photosynthetic cells can detect the intensity of absorbed light; the redox state of the PQ-pool also carries useful information for the cell. The rate-limiting step of photosynthetic electron transport in the thylakoids is the Rieske movement in the cyt. b_6f complex (Wilhelm & Wild, 1984). Therefore, the redox state of the PQ pool gives a very good proxy for the saturation level of photosynthesis. This redox state is then a signal for several regulatory steps with both short term and long-term reactions (for review see (Foyer & Noctor, 2009)). In the short term, state transitions involve the STT7/STN7 kinase (Depège et al, 2003), activated when the Q_O site of the cyt b_6f is occupied by a (reduced) PQH_2 (Dumas et al., 2017). State transitions adjust the distribution of light between the two photosystems through the phosphorylation of LHCs by the STT7/STN7 kinase and their movement from one photosystem to the other (Wollman 2001). In diatoms, state transitions do not occur consistent with the lack of homologues for STT7/STN7 (Grouneva et al., 2013), likely because the absorption spectrum of FCPs in PSII and PSI is too similar (Lepetit et al., 2010). Although diatoms lack state transitions, the PQ redox state regulates light acclimation of the photosynthetic machinery over the long term (tens of minutes to hours), as in the green lineage (Lepetit et al., 2013).

For long-term responses, photosynthesis is also regulated by a light-sensing system involving an unexpected large array of photoreceptors with overlapping spectral sensitivities and functionalities. This is true for diatoms as well as higher plants, green algae, or other algal lineages (Kong & Okajima, 2016; Jaubert et al., 2017 and chapter V). However, light sensing

on land and in the aquatic environment faces quite different challenges. In plants, the red/far red light sensing phytochrome system integrated in a network of other photosensors, triggers the acclimation of the photosynthetic machinery at the molecular level. Phytochromes are present and involved in changes in gene expression in diatoms. However, no clear relationship with photosynthesis has been reported so far and phytochrome-dependent light-induced gene expression is not dependent on photosynthetic activity (Fortunato et al., 2016). In the open waters of aquatic environment, mixing can drastically change light intensity and quality in an unpredicted manner. It is no surprise that the photoreceptor network associated with light acclimation of photosynthesis is broad in diatoms. Diatoms have many photoreceptor genes, which can be divided into five classes (Jaubert et al., 2017). Among them, the cryptochromes (for review see Fortunato et al., 2015) and the aureochromes (Kroth et al., 2017) are of major importance on the regulatory function of algal photosynthesis.

Cryptochromes, which are composed of flavoproteins with a wide variety of light-dependent functions, including photolyases and blue-light activated DNA repair. Their action on photosynthesis acclimation is still enigmatic in diatoms. König et al (2017) showed that cryptochromes influence the transcription of FCP genes in the diatom *P. tricornutum*. But they are probably not direct blue light regulators of photosynthesis; instead, they influence photosynthesis through a network comprising other photoreceptors. One of the major components of this network are the various aureochrome photoreceptors, which are light-controlled transcription factors that can bind directly to DNA (Kroth et al., 2017). *P. tricornutum* is unable to acclimate to high light in the absence of blue light (Schellenberger-Costa et al. 2013a). Complementarily, inactivation of the Aureo 1A gene leads to complete loss of ability to acclimate to different light intensities (Schellenberger-Costa et al., 2013b). During a change from red to blue light, about 80% of 8000 identified genes are differentially expressed in *P. tricornutum*, demonstrating that the change in light color induces a complete reorganization of the cell, including major pathways such as protein biosynthesis, energy conversion or cell division. This metabolic reconstruction is completely blocked when the Aureo 1A gene is inactivated (Mann et al., 2020). This observation at the transcriptomic level is perfectly in line with the observation of differences in photosynthetic capacity and photoprotection (Mann et al., 2017). Metabolome data demonstrate that the change in light quality leads to a completely different carbon allocation pattern in the cells (Jungandreas et al., 2014). In summary, light acclimation is a very complex metabolic reorganization process that alters light absorption capacity, photoprotection, ROS management, electron sink regulation

and cell division processes. This complex regulation depends on extensive alterations in gene expression that are under the coordinated control of redox and photosensors. The concerted action of photoreceptors with a master modulator of photosynthesis in a comprehensive network is far from understood in diatoms.

1.7 Conclusion

At the scale of its smallest molecular building blocks, or from the perspective of its end goal, i.e., furnishing the metabolism with adequate ATP/NADPH, photosynthesis is very similar between green lineage and diatoms. The differences lie between, namely in *how* these building blocks organize themselves in a radically different organellar environment and *what* makes photosynthesis flexible enough to thrive in dynamic environments. If the current state of knowledge were sufficient to provide comprehensive fingerprints of "green" and diatom photosynthesis, we would like to ask questions such as: *Do differences improve fitness in environments where different groups/species dominate? Can photosynthesis biodiversity help us understand the global repercussions of climate change? Can we harness the power of biodiversity to boost photosynthesis-based biotechnology and increase crop yield?* We gave it our best shot and highlighted the organelle structure, AEF network, CO_2 uptake and metabolism, and regulatory networks as crucial distinctions between the two groups. But we remain far from a comprehensive understanding of photosynthesis in diatoms versus the green lineage, largely due to the limited number of species for which extensive physiological studies have been undertaken, especially in diatoms. As large-scale genomic initiatives such as TARA-Ocean (Sunagawa et al., 2020) or the "100 Diatom Genome Project" (Mock et al., 2022) move forward, it is imperative that functional studies on many and various diatom species keep pace with the expansion of -omics data to achieve ambitious goals such as answering the questions above.

Bibliography

1. Abida H, Dolch LJ, Meï C, Villanova V, Conte M, Block MA, Finazzi G, Bastien O, Tirichine L, Bowler C, et al. Membrane glycerolipid remodeling triggered by nitrogen and phosphorus starvation in Phaeodactylum tricornutum. Plant Physiology. 2015;167(1):118–136. doi:10.1104/pp.114.252395

2. Adachi K, Oiwa K, Nishizaka T, Furuike S, Noji H, Itoh H, Yoshida M, Kinosita K. Coupling of Rotation and Catalysis in F1-ATPase Revealed by Single-Molecule Imaging and Manipulation. Cell. 2007;130(2):309–321. doi:10.1016/j.cell.2007.05.020

3. Águila Ruiz-Sola M, Flori S, Yuan Y, Villain G, Sanz-Luque E, Redekop P, Tokutsu R, Küken A, Tsichla A, Kepesidis G, et al. Light-independent regulation of algal photoprotection by CO2 availability. Nature Communications. 2023;14(1):1977. https://www.nature.com/articles/s41467-023-37800-6. doi:10.1038/s41467-023-37800-6

4. Aken O Van, Giraud E, Clifton R, Whelan J. Alternative oxidase : a target and regulator of stress responses. 2009:354–361. doi:10.1111/j.1399-3054.2009.01240.x

5. Allahverdiyeva Y, Suorsa M, Tikkanen M, Aro EM. Photoprotection of photosystems in fluctuating light intensities. Journal of Experimental Botany. 2015;66(9):2427–2436. doi:10.1093/jxb/eru463

6. Allen AE, Laroche J, Maheswari U, Lommer M, Schauer N, Lopez PJ, Finazzi G, Fernie AR, Bowler C. Whole-cell response of the pennate diatom Phaeodactylum tricornutum to iron starvation. Proceedings of the National Academy of Sciences of the United States of America. 2008;105(30):10438–10443. doi:10.1073/pnas.0711370105

7. Allen JF. Photosynthesis of ATP-electrons, proton pumps, rotors, and poise. Cell. 2002;110(3):273–276. doi:10.1016/S0092-8674(02)00870-X

8. Alric J, Johnson X. Alternative electron transport pathways in photosynthesis: a confluence of regulation. Current Opinion in Plant Biology. 2017;37(i):78–86. doi:10.1016/j.pbi.2017.03.014

9. Armbruster U, Correa Galvis V, Kunz HH, Strand DD. The regulation of the chloroplast proton motive force plays a key role for photosynthesis in fluctuating light. Current Opinion in Plant Biology. 2017;37:56–62. http://dx.doi.org/10.1016/j.pbi.2017.03.012. doi:10.1016/j.pbi.2017.03.012

10. Arnon DI, Whatley FR, Allen MB. Photosynthesis by Isolated Chloroplasts. II. Photosynthetic Phosphorylation, the Conversion of Light into Phosphate Bond Energy. Journal of the American Chemical Society. 1954;76(24):6324–6329. doi:10.1021/ja01653a025

11. Arnoux P, Morosinotto T, Saga G, Bassi R, Pignol D. A structural basis for the ph-dependent xanthophyll cycle in arabidopsis thaliana. Plant Cell. 2009;21(7):2036–2044. doi:10.1105/tpc.109.068007

12. Asada K. The water-water cycle in chloroplasts: Scavenging of active oxygens and dissipation of excess photons. Annual Review of Plant Biology. 1999;50:601–639. doi:10.1146/annurev.arplant.50.1.601

13. Aspatwar A, Haapanen S, Parkkila S. An update on the metabolic roles of carbonic anhydrases in the model alga chlamydomonas reinhardtii. Metabolites. 2018;8(1). doi:10.3390/metabo8010022

14. Atteia A, Van Lis R, Tielens AGM, Martin WF. Anaerobic energy metabolism in unicellular photosynthetic eukaryotes. Biochimica et Biophysica Acta - Bioenergetics. 2013;1827(2):210–223. http://dx.doi.org/10.1016/j.bbabio.2012.08.002. doi:10.1016/j.bbabio.2012.08.002

15. Bailey S, Melis A, Mackey KRM, Cardol P, Finazzi G, van Dijken G, Berg GM, Arrigo K, Shrager J, Grossman A. Alternative photosynthetic electron flow to oxygen in marine Synechococcus.

Biochimica et Biophysica Acta - Bioenergetics. 2008;1777(3):269–276. doi:10.1016/j.bbabio.2008.01.002

16. Bailleul B, Berne N, Murik O, Petroutsos D, Prihoda J, Tanaka A, Villanova V, Bligny R, Flori S, Falconet D, et al. Energetic coupling between plastids and mitochondria drives CO2 assimilation in diatoms. Nature. 2015;524(7565):366–369. http://www.nature.com/doifinder/10.1038/nature14599. doi:10.1038/nature14599

17. Bailleul B, Cardol P, Breyton C, Finazzi G. Electrochromism: a useful probe to study algal photosynthesis. Photosynthesis Research. 2010;106(1–2):179–189. http://link.springer.com/10.1007/s11120-010-9579-z. doi:10.1007/s11120-010-9579-z

18. Barbato R, Tadini L, Cannata R, Peracchio C, Jeran N, Alboresi A, Morosinotto T, Bajwa AA, Paakkarinen V, Suorsa M, et al. Higher order photoprotection mutants reveal the importance of ΔpH-dependent photosynthesis-control in preventing light induced damage to both photosystem II and photosystem I. Scientific Reports. 2020;10(1):1–14. doi:10.1038/s41598-020-62717-1

19. Barnett A, Méléder V, Blommaert L, Lepetit B, Gaudin P, Vyverman W, Sabbe K, Dupuy C, Lavaud J. Growth form defines physiological photoprotective capacity in intertidal benthic diatoms. The ISME Journal. 2015;9(1):32–45. http://www.nature.com/doifinder/10.1038/ismej.2014.105. doi:10.1038/ismej.2014.105

20. Barrett J, Girr P, Mackinder LCM. Pyrenoids: CO2-fixing phase separated liquid organelles. Biochimica et Biophysica Acta - Molecular Cell Research. 2021;1868(5):118949. https://doi.org/10.1016/j.bbamcr.2021.118949. doi:10.1016/j.bbamcr.2021.118949

21. Bártulos CR, Rogers MB, Williams TA, Gentekaki E, Brinkmann H, Cerff R, Liaud MF, Hehl AB, Yarlett NR, Gruber A, et al. Mitochondrial glycolysis in a major lineage of eukaryotes. Genome Biology and Evolution. 2018;10(9):2310–2325. doi:10.1093/gbe/evy164

22. Bedoshvili YD, Popkova TP, Likhoshway Y V. Chloroplast structure of diatoms of different classes. Cell and Tissue Biology. 2009;3(3):297–310. doi:10.1134/S1990519X09030122

23. Benlloch R, Shevela D, Hainzl T, Grundström C, Shutova T, Messinger J, Samuelsson G, Elisabeth Sauer-Eriksson A. Crystal structure and functional characterization of photosystem II-associated carbonic anhydrase CAH3 in Chlamydomonas reinhardtii. Plant Physiology. 2015;167(3):950–962. doi:10.1104/pp.114.253591

24. Bennoun P. Evidence for a respiratory chain in the chloroplast. Proceedings of the National Academy of Sciences. 1982;79(14):4352–4356. http://www.pnas.org/cgi/doi/10.1073/pnas.79.14.4352. doi:10.1073/pnas.79.14.4352

25. Bhola V, Swalaha F, Ranjith Kumar R, Singh M, Bux F. Overview of the potential of microalgae for CO2 sequestration. International Journal of Environmental Science and Technology. 2014;11(7):2103–2118. doi:10.1007/s13762-013-0487-6

26. Biel K, Fomina I. Benson-Bassham-Calvin cycle contribution to the organic life on our planet. Photosynthetica. 2015;53(2):161–167. https://ps.ueb.cas.cz/artkey/phs-201502-0001_benson-bassham-calvin-cycle-contribution-to-the-organic-life-on-our-planet.php. doi:10.1007/s11099-015-0112-7

27. von Bismarck T, Korkmaz K, Ruß J, Skurk K, Kaiser E, Correa Galvis V, Cruz JA, Strand DD, Köhl K, Eirich J, et al. Light acclimation interacts with thylakoid ion transport to govern the dynamics of photosynthesis in Arabidopsis. New Phytologist. 2023;237(1):160–176. https://onlinelibrary.wiley.com/doi/10.1111/nph.18534. doi:10.1111/nph.18534

28. Blaby-Haas CE, Merchant SS. The ins and outs of algal metal transport. Biochimica et Biophysica

Acta - Molecular Cell Research. 2012;1823(9):1531–1552. http://dx.doi.org/10.1016/j.bbamcr.2012.04.010. doi:10.1016/j.bbamcr.2012.04.010

29. Blache U, Jakob T, Su W, Wilhelm C. The impact of cell-specific absorption properties on the correlation of electron transport rates measured by chlorophyll fluorescence and photosynthetic oxygen production in planktonic algae. Plant Physiology and Biochemistry. 2011;49(8):801–808. http://dx.doi.org/10.1016/j.plaphy.2011.04.010. doi:10.1016/j.plaphy.2011.04.010

30. Blommaert L, Chafai L, Bailleul B. The fine - tuning of NPQ in diatoms relies on the regulation of both xanthophyll cycle enzymes. Scientific Reports. 2021:1–17. https://doi.org/10.1038/s41598-021-91483-x. doi:10.1038/s41598-021-91483-x

31. Blommaert L, Huysman MJJ, Vyverman W, Lavaud J, Sabbe K. Contrasting NPQ dynamics and xanthophyll cycling in a motile and a non-motile intertidal benthic diatom. Limnology and Oceanography. 2017. doi:10.1002/lno.10511

32. Bosco MB, Aleanzi MC, Iglesias AÁ. Plastidic Phosphoglycerate Kinase from Phaeodactylum tricornutum: On the Critical Role of Cysteine Residues for the Enzyme Function. Protist. 2012;163(2):188–203. doi:10.1016/j.protis.2011.07.001

33. Boyer PD. The ATP synthase - A splendid molecular machine. Annual Review of Biochemistry. 1997;66:717–749. doi:10.1146/annurev.biochem.66.1.717

34. Broddrick JT, Du N, Smith SR, Tsuji Y, Jallet D, Ware MA, Peers G, Matsuda Y, Dupont CL, Mitchell BG, et al. Cross-compartment metabolic coupling enables flexible photoprotective mechanisms in the diatom Phaeodactylum tricornutum. New Phytologist. 2019;222(3):1364–1379. doi:10.1111/nph.15685

35. Büchel C. Light-Harvesting Complexes of Diatoms: Fucoxanthin-Chlorophyll Proteins. In: Outlove. 2020. p. 441–457. http://link.springer.com/10.1007/978-3-030-33397-3_16. doi:10.1007/978-3-030-33397-3_16

36. Büchel C, Goss R, Bailleul B, Campbell DA, Lavaud J, Lepetit B. Photosynthetic Light Reactions in Diatoms. I. The Lipids and Light-Harvesting Complexes of the Thylakoid Membrane. 2022. doi:10.1007/978-3-030-92499-7_15

37. Buchert F, Bailleul B, Hisabori T. A γ-subunit point mutation in Chlamydomonas reinhardtii chloroplast F1Fo-ATP synthase confers tolerance to reactive oxygen species. Biochimica et Biophysica Acta - Bioenergetics. 2017;1858(12):966–974. http://dx.doi.org/10.1016/j.bbabio.2017.09.001. doi:10.1016/j.bbabio.2017.09.001

38. Buchert F, Bailleul B, Joliot P. BBA - Bioenergetics Disentangling chloroplast ATP synthase regulation by proton motive force and thiol modulation in Arabidopsis leaves. BBA - Bioenergetics. 2021;1862(8):148434. https://doi.org/10.1016/j.bbabio.2021.148434. doi:10.1016/j.bbabio.2021.148434

39. Buck JM, Kroth PG, Lepetit B. Identification of sequence motifs in Lhcx proteins that confer qE-based photoprotection in the diatom Phaeodactylum tricornutum. Plant Journal. 2021;108(6):1721–1734. doi:10.1111/tpj.15539

40. Burlacot A, Burlacot F, Li-Beisson Y, Peltier G. Membrane Inlet Mass Spectrometry: A Powerful Tool for Algal Research. Frontiers in Plant Science. 2020;11(September):1–15. doi:10.3389/fpls.2020.01302

41. Burlacot A, Dao O, Auroy P, Cuiné S, Li-Beisson Y, Peltier G. Alternative photosynthesis pathways drive the algal CO2-concentrating mechanism. Nature. 2022;605(7909):366–371. doi:10.1038/s41586-022-04662-9

42. Von Caemmerer S, Ghannoum O, Furbank RT. C4 photosynthesis: 50 years of discovery and innovation. Journal of Experimental Botany. 2017;68(2):97–102. doi:10.1093/jxb/erw491

43. Campbell DA, Serôdio J. Photoinhibition of Photosystem II in Phytoplankton: Processes and Patterns. In: Photoinhibition of Photosystem II in Phytoplankton: Processes and Patterns. 2020. p. 329–365. http://link.springer.com/10.1007/978-3-030-33397-3_13. doi:10.1007/978-3-030-33397-3_13

44. Canãvate JP, Armada I, Riós JL, Hachero-Cruzado I. Exploring occurrence and molecular diversity of betaine lipids across taxonomy of marine microalgae. Phytochemistry. 2016;124:68–78. doi:10.1016/j.phytochem.2016.02.007

45. Cardol P, Bailleul B, Rappaport F, Derelle E, Béal D, Breyton C, Bailey S, Wollman FA, Grossman A, Moreau H, et al. An original adaptation of photosynthesis in the marine green alga Ostreococcus. Proceedings of the National Academy of Sciences of the United States of America. 2008;105(22):7881–7886. doi:10.1073/pnas.0802762105

46. Chain RK. Evidence for a reluctant-dependent oxidation of chloroplast cytochrome b-563. FEBS Letters. 1982;143(2):273–278. doi:10.1016/0014-5793(82)80115-4

47. Chaux F, Burlacot A, Mekhalfi M, Auroy P, Blangy S, Richaud P, Peltier G. Flavodiiron proteins promote fast and transient O2 photoreduction in chlamydomonas. Plant Physiology. 2017;174(3):1825–1836. doi:10.1104/pp.17.00421

48. Chaux F, Peltier G, Johnson X. A security network in PSI photoprotection: Regulation of photosynthetic control, NPQ and O2 photoreduction by cyclic electron flow. Frontiers in Plant Science. 2015;6(OCTOBER):1–7. doi:10.3389/fpls.2015.00875

49. Clement R, Jensen E, Prioretti L, Maberly SC, Gontero B. Diversity of CO2-concentrating mechanisms and responses to CO2concentration in marine and freshwater diatoms. Journal of Experimental Botany. 2017;68(14):3925–3935. doi:10.1093/jxb/erx035

50. Croteau D, Alric J, Bailleul B. The multiple routes of photosynthetic electron transfer in Chlamydomonas reinhardtii. In: The Chlamydomonas Sourcebook. Elsevier; 2023. p. 591–613. https://linkinghub.elsevier.com/retrieve/pii/B9780128214305000018. doi:10.1016/B978-0-12-821430-5.00001-8

51. Croteau D, Guérin S, Bruyant F, Ferland J, Campbell DA, Babin M, Lavaud J. Contrasting nonphotochemical quenching patterns under high light and darkness aligns with light niche occupancy in Arctic diatoms. Limnology and Oceanography. 2021;66(S1):S231–S245. doi:10.1002/lno.11587

52. Cruz S, Goss R, Wilhelm C, Leegood R, Horton P, Jakob T. Impact of chlororespiration on non-photochemical quenching of chlorophyll fluorescence and on the regulation of the diadinoxanthin cycle in the diatom Thalassiosira pseudonana. Journal of Experimental Botany. 2011;62(2):509–519. doi:10.1093/jxb/erq284

53. Curien G, Flori S, Villanova V, Magneschi L, Giustini C, Forti G, Matringe M, Petroutsos D, Kuntz M, Finazzi G. The water to water cycles in microalgae. Plant and Cell Physiology. 2016;57(7):1354–1363. doi:10.1093/pcp/pcw048

54. Cuvelier ML, Allen AE, Monier A, McCrow JP, Messie M, Tringe SG, Woyke T, Welsh RM, Ishoey T, Lee J-H, et al. Targeted metagenomics and ecology of globally important uncultured eukaryotic phytoplankton. Proceedings of the National Academy of Sciences. 2010;107(33):14679–14684. http://www.pnas.org/cgi/doi/10.1073/pnas.1001665107. doi:10.1073/pnas.1001665107

55. DalCorso G, Pesaresi P, Masiero S, Aseeva E, Schünemann D, Finazzi G, Joliot P, Barbato R, Leister

D. A Complex Containing PGRL1 and PGR5 Is Involved in the Switch between Linear and Cyclic Electron Flow in Arabidopsis. Cell. 2008;132(2):273–285. doi:10.1016/j.cell.2007.12.028

56. Dang K Van, Plet J, Tolleter D, Jokel M, Cuiné S, Carrier P, Auroy P, Richaud P, Johnson X, Alric J, et al. Combined increases in mitochondrial cooperation and oxygen photoreduction compensate for deficiency in cyclic electron flow in Chlamydomonas reinhardtii. Plant Cell. 2014;26(7):3036–3050. doi:10.1105/tpc.114.126375

57. Davis GA, Kanazawa A, Schöttler MA, Kohzuma K, Froehlich JE, Rutherford AW, Satoh-Cruz M, Minhas D, Tietz S, Dhingra A, et al. Limitations to photosynthesis by proton motive force-induced photosystem II photodamage. eLife. 2016;5:1–27. doi:10.7554/elife.16921

58. Davis GA, Rutherford AW, Kramer DM. Hacking the thylakoid proton motive force for improved photosynthesis: Modulating ion flux rates that control proton motive force partitioning into ΔΨ and ΔpH. Philosophical Transactions of the Royal Society B: Biological Sciences. 2017;372(1730). doi:10.1098/rstb.2016.0381

59. Dekker JP, Boekema EJ. Supramolecular organization of thylakoid membrane proteins in green plants. Biochimica et Biophysica Acta - Bioenergetics. 2005;1706(1–2):12–39. doi:10.1016/j.bbabio.2004.09.009

60. Depège N, Bellafiore S, Rochaix JD. Role of chloroplast protein kinase Stt7 in LHCII phosphorylation and state transition in Chlamydomonas. Science. 2003;299(5612):1572–1575. doi:10.1126/science.1081397

61. Dijkman NA, Kroon BMA. Indications for chlororespiration in relation to light regime in the marine diatom Thalassiosira weissflogii. Journal of Photochemistry and Photobiology B: Biology. 2002;66(3):179–187. doi:10.1016/S1011-1344(02)00236-1

62. DiMario RJ, Clayton H, Mukherjee A, Ludwig M, Moroney J V. Plant Carbonic Anhydrases: Structures, Locations, Evolution, and Physiological Roles. Molecular Plant. 2017;10(1):30–46. http://dx.doi.org/10.1016/j.molp.2016.09.001. doi:10.1016/j.molp.2016.09.001

63. DiMario RJ, Machingura MC, Waldrop GL, Moroney J V. The many types of carbonic anhydrases in photosynthetic organisms. Plant Science. 2018;268(July 2017):11–17. https://doi.org/10.1016/j.plantsci.2017.12.002. doi:10.1016/j.plantsci.2017.12.002

64. Dorrell RG, Liang Y, Gueguen N, Nonoyama T, Zhang Y, Zweig N, Fernie AR, Jouhet J, Maréchal E. A Plastidial Glycolytic-Gluconeogenic Switch of Mitochondrial Origin Enables Diatom Adaptations to High Latitudes. 2022. doi:10.1101/2022.09.08.507166

65. Dukic E, Herdean A, Cheregi O, Sharma A, Nzieng H. K+ and Cl− channels/transporters independently fne-tune photosynthesis in plants. Scientific Reports. 2019;9(May):1–12. https://www.nature.com/articles/s41598-019-44972-z.pdf. doi:https://doi.org/10.1016/0005-2728(79)90175-0

66. Dumas L, Zito F, Blangy S, Auroy P, Johnson X, Peltier G, Alric J. A stromal region of cytochrome b6f subunit IV is involved in the activation of the Stt7 kinase in Chlamydomonas. Proceedings of the National Academy of Sciences of the United States of America. 2017;114(45):12063–12068. doi:10.1073/pnas.1713343114

67. Eberhard S, Finazzi G, Wollman F-A. The Dynamics of Photosynthesis. Annual Review of Genetics. 2008;42(1):463–515. doi:10.1146/annurev.genet.42.110807.091452

68. Ewe D, Tachibana M, Kikutani S, Gruber A, Río Bártulos C, Konert G, Kaplan A, Matsuda Y, Kroth PG. The intracellular distribution of inorganic carbon fixing enzymes does not support the presence of a C4 pathway in the diatom Phaeodactylum tricornutum. Photosynthesis Research.

2018;137(2):263–280. doi:10.1007/s11120-018-0500-5

69. Fabris M, Matthijs M, Rombauts S, Vyverman W, Goossens A, Baart GJE. The metabolic blueprint of Phaeodactylum tricornutum reveals a eukaryotic Entner-Doudoroff glycolytic pathway. Plant Journal. 2012;70(6):1004–1014. doi:10.1111/j.1365-313X.2012.04941.x

70. Falciatore A, Jaubert M, Bouly JP, Bailleul B, Mock T. Diatom molecular research comes of age: Model species for studying phytoplankton biology and diversity[open]. Plant Cell. 2020;32(3):547–572. doi:10.1105/tpc.19.00158

71. Falkowski PG, Fenchel T, Delong EF. The microbial engines that drive earth's biogeochemical cycles. Science. 2008;320(5879):1034–1039. doi:10.1126/science.1153213

72. Falkowski PG, Fujita Y, Ley A, Mauzerall D. Evidence for Cyclic Electron Flow around Photosystem II in Chlorella pyrenoidosa . Plant Physiology. 1986;81(1):310–312. doi:10.1104/pp.81.1.310

73. Fanesi A, Wagner H, Becker A, Wilhelm C. Temperature affects the partitioning of absorbed light energy in freshwater phytoplankton. Freshwater Biology. 2016;61(9):1365–1378. doi:10.1111/fwb.12777

74. Finazzi G, Rappaport F. In vivo characterization of the electrochemical proton gradient generated in darkness in green algae and its kinetic effects on cytochrome b6f turnover. Biochemistry. 1998;37(28):9999–10005. doi:10.1021/bi980320j

75. Finkel Z, Irwin A, Schofield O. Resource limitation alters the 3/4 size scaling of metabolic rates in phytoplankton. Marine Ecology Progress Series. 2004;273:269–279. https://www.int-res.com/abstracts/meps/v273/p269-279/. doi:10.3354/meps273269

76. Fisher NL, Campbell DA, Hughes DJ, Kuzhiumparambil U, Halsey KH, Ralph PJ, Suggett DJ. Divergence of photosynthetic strategies amongst marine diatoms. PLoS ONE. 2020;15(12 December):1–27. http://dx.doi.org/10.1371/journal.pone.0244252. doi:10.1371/journal.pone.0244252

77. Fisher NL, Halsey KH. Mechanisms that increase the growth efficiency of diatoms in low light. Photosynthesis Research. 2016;129(2):183–197. doi:10.1007/s11120-016-0282-6

78. Flori S, Jouneau P-H, Bailleul B, Gallet B, Estrozi LF, Moriscot C, Bastien O, Eicke S, Schober A, Bártulos CR, et al. Plastid thylakoid architecture optimizes photosynthesis in diatoms. Nature Communications. 2017;8(May):15885. http://www.nature.com/doifinder/10.1038/ncomms15885. doi:10.1038/ncomms15885

79. Fortunato AE, Annunziata R, Jaubert M, Bouly JP, Falciatore A. Dealing with light: The widespread and multitasking cryptochrome/photolyase family in photosynthetic organisms. Journal of Plant Physiology. 2015;172:42–54. http://dx.doi.org/10.1016/j.jplph.2014.06.011. doi:10.1016/j.jplph.2014.06.011

80. Fortunato AE, Jaubert M, Enomoto G, Bouly JP, Raniello R, Thaler M, Malviya S, Bernardes JS, Rappaport F, Gentili B, et al. Diatom phytochromes reveal the existence of far-red-light-based sensing in the ocean. Plant Cell. 2016;28(3):616–628. doi:10.1105/tpc.15.00928

81. Foyer CH, Noctor G. Redox Regulation in Photosynthetic Organisms: Signaling, Acclimation, and Practical Implications. Antioxidants & Redox Signaling. 2009;11(4):861–905. http://www.liebertpub.com/doi/10.1089/ars.2008.2177. doi:10.1089/ars.2008.2177

82. Fujiki T, Taguchi S. Variability in chlorophyll a specific absorption coefficient in marine phytoplankton as a function of cell size and irradiance. Journal of Plankton Research. 2002;24(9):859–874. doi:10.1093/plankt/24.9.859

83. Furbank RT, Badger MR. Oxygen exchange associated with electron transport and photophosphorylation in spinach thylakoids. BBA - Bioenergetics. 1983;723(3):400–409. doi:10.1016/0005-2728(83)90047-6

84. Gain G, Berne N, Feller T, Godaux D, Cenci U, Cardol P. Induction of photosynthesis under anoxic condition in Thalassiosira pseudonana and Euglena gracilis: interactions between fermentation and photosynthesis. Frontiers in Plant Science. 2023.

85. Gates C, Ananyev G, Roy-Chowdhury S, Fromme P, Dismukes GC. Regulation of light energy conversion between linear and cyclic electron flow within photosystem II controlled by the plastoquinone/quinol redox poise. Photosynthesis Research. 2023;156(1):113–128. https://link.springer.com/10.1007/s11120-022-00985-w. doi:10.1007/s11120-022-00985-w

86. Giovagnetti V, Jaubert M, Shukla MK, Ungerer P, Bouly J-P, Falciatore A, Ruban A V. Biochemical and molecular properties of LHCX1, the essential regulator of dynamic photoprotection in diatoms. Plant Physiology. 2021:1–17. doi:10.1093/plphys/kiab425

87. Goldman JAL, Kranz SA, Young JN, Tortell PD, Stanley RHR, Bender ML, Morel FMM. Gross and net production during the spring bloom along the Western Antarctic Peninsula. New Phytologist. 2015;205(1):182–191. doi:10.1111/nph.13125

88. Gontero B, Maberly SC. An intrinsically disordered protein, CP12: Jack of all trades and master of the Calvin cycle. Biochemical Society Transactions. 2012;40(5):995–999. doi:10.1042/BST20120097

89. Gontero B, Salvucci ME. Regulation of photosynthetic carbon metabolism in aquatic and terrestrial organisms by Rubisco activase, redox-modulation and CP12. Aquatic Botany. 2014;118:14–23. http://dx.doi.org/10.1016/j.aquabot.2014.05.011. doi:10.1016/j.aquabot.2014.05.011

90. Goss R, Ann Pinto E, Wilhelm C, Richter M. The importance of a highly active and ΔpH-regulated diatoxanthin epoxidase for the regulation of the PS II antenna function in diadinoxanthin cycle containing algae. Journal of Plant Physiology. 2006;163(10):1008–1021. doi:10.1016/j.jplph.2005.09.008

91. Goss R, Latowski D, Grzyb J, Vieler A, Lohr M, Wilhelm C, Strzalka K. Lipid dependence of diadinoxanthin solubilization and de-epoxidation in artificial membrane systems resembling the lipid composition of the natural thylakoid membrane. Biochimica et Biophysica Acta - Biomembranes. 2007. doi:10.1016/j.bbamem.2006.06.006

92. Goss R, Lepetit B. Biodiversity of NPQ. Journal of Plant Physiology. 2015;172:13–32. doi:10.1016/j.jplph.2014.03.004

93. Goss R, Nerlich J, Lepetit B, Schaller S, Vieler A, Wilhelm C. The lipid dependence of diadinoxanthin de-epoxidation presents new evidence for a macrodomain organization of the diatom thylakoid membrane. Journal of Plant Physiology. 2009;166(17):1839–1854. doi:10.1016/j.jplph.2009.05.017

94. Grouneva I, Gollan PJ, Kangasjärvi S, Suorsa M, Tikkanen M, Aro EM. Phylogenetic viewpoints on regulation of light harvesting and electron transport in eukaryotic photosynthetic organisms. Planta. 2013;237(2):399–412. doi:10.1007/s00425-012-1744-5

95. Grouneva I, Jakob T, Wilhelm C, Goss R. A new multicomponent NPQ mechanism in the diatom Cyclotella meneghiniana. Plant and Cell Physiology. 2008;49(8):1217–1225. doi:10.1093/pcp/pcn097

96. Grouneva I, Jakob T, Wilhelm C, Goss R. Influence of ascorbate and pH on the activity of the diatom xanthophyll cycle-enzyme diadinoxanthin de-epoxidase. Physiologia Plantarum. 2006. doi:10.1111/j.1399-3054.2006.00613.x

97. Grouneva I, Jakob T, Wilhelm C, Goss R. The regulation of xanthophyll cycle activity and of non-photochemical fluorescence quenching by two alternative electron flows in the diatoms Phaeodactylum tricornutum and Cyclotella meneghiniana. Biochimica et Biophysica Acta - Bioenergetics. 2009;1787(7):929–938. http://dx.doi.org/10.1016/j.bbabio.2009.02.004. doi:10.1016/j.bbabio.2009.02.004

98. Grouneva I, Muth-Pawlak D, Battchikova N, Aro EM. Changes in relative thylakoid protein abundance induced by fluctuating light in the diatom thalassiosira pseudonana. Journal of Proteome Research. 2016;15(5):1649–1658. doi:10.1021/acs.jproteome.6b00124

99. Groussman RD, Parker MS, Armbrust EV. Diversity and evolutionary history of iron metabolism genes in diatoms. PLoS ONE. 2015;10(6):1–25. doi:10.1371/journal.pone.0129081

100. Gruber A, Kroth PG. Intracellular metabolic pathway distribution in diatoms and tools for genome-enabled experimental diatom research. Philosophical Transactions of the Royal Society B: Biological Sciences. 2017;372(1728). doi:10.1098/rstb.2016.0402

101. Hahn A, Vonck J, Mills DJ, Meier T, Kühlbrandt W. Structure, mechanism, and regulation of the chloroplast ATP synthase. Science. 2018;360(6389). doi:10.1126/science.aat4318

102. Halsey KH, Milligan AJ, Behrenfeld MJ. Linking time-dependent carbon-fixation efficiencies in Dunaliella Tertiolecta (Chlorophyceae) to underlying metabolic pathways. Journal of Phycology. 2011;47(1):66–76. doi:10.1111/j.1529-8817.2010.00945.x

103. Hangarter RP, Good NE. Energy thresholds for ATP synthesis in chloroplasts. BBA - Bioenergetics. 1982;681(3):397–404. doi:10.1016/0005-2728(82)90181-5

104. He S, Crans VL, Jonikas MC. The pyrenoid: the eukaryotic CO2-concentrating organelle. The Plant Cell. 2023 Jun 4:1–24. https://academic.oup.com/plcell/advance-article/doi/10.1093/plcell/koad157/7190196. doi:10.1093/plcell/koad157

105. Hemschemeier A, Posewitz MC, Happe T. Hydrogenases and hydrogen production. In: The Chlamydomonas Sourcebook. Elsevier; 2023. p. 343–367. https://linkinghub.elsevier.com/retrieve/pii/B9780128214305000080. doi:10.1016/B978-0-12-821430-5.00008-0

106. Herdean A, Nziengui H, Zsiros O, Solymosi K, Garab G, Lundin B, Spetea C. The Arabidopsis thylakoid chloride channel AtCLCe functions in chloride homeostasis and regulation of photosynthetic electron transport. Frontiers in Plant Science. 2016;7(FEB2016):1–15. doi:10.3389/fpls.2016.00115

107. Herdean A, Teardo E, Nilsson AK, Pfeil BE, Johansson ON, Ünnep R, Nagy G, Zsiros O, Dana S, Solymosi K, et al. A voltage-dependent chloride channel fine-tunes photosynthesis in plants. Nature Communications. 2016;7(May):1–11. doi:10.1038/ncomms11654

108. Hertle AP, Blunder T, Wunder T, Pesaresi P, Pribil M, Armbruster U, Leister D. PGRL1 Is the Elusive Ferredoxin-Plastoquinone Reductase in Photosynthetic Cyclic Electron Flow. Molecular Cell. 2013;49(3):511–523. http://dx.doi.org/10.1016/j.molcel.2012.11.030. doi:10.1016/j.molcel.2012.11.030

109. Heureux AMC, Young JN, Whitney SM, Eason-Hubbard MR, Lee RBY, Sharwood RE, Rickaby REM. The role of Rubisco kinetics and pyrenoid morphology in shaping the CCM of haptophyte microalgae. Journal of Experimental Botany. 2017;68(14):3959–3969. doi:10.1093/jxb/erx179

110. Hildebrand M, Manandhar-Shrestha K, Abbriano R. Effects of chrysolaminarin synthase knockdown in the diatom Thalassiosira pseudonana: Implications of reduced carbohydrate storage relative to green algae. Algal Research. 2017;23:66–77.

http://dx.doi.org/10.1016/j.algal.2017.01.010. doi:10.1016/j.algal.2017.01.010

111. Hill KL, Li HH, Singer J, Merchant S. Isolation and structural characterization of the Chlamydomonas reinhardtii gene for cytochrome c6: Analysis of the kinetic and metal specificity of its copper-responsive expression. Journal of Biological Chemistry. 1991;266(23):15060–15067. doi:10.1016/s0021-9258(18)98586-8

112. Hill R, Bendall F. Function of the two cytochrome components in chloroplasts: A working hypothesis. Nature. 1960;186(4719):136–137. doi:10.1038/186136a0

113. Hirakawa Y, Senda M, Fukuda K, Yu HY, Ishida M, Taira M, Kinbara K, Senda T. Characterization of a novel type of carbonic anhydrase that acts without metal cofactors. BMC Biology. 2021;19(1):1–15. doi:10.1186/s12915-021-01039-8

114. Holzmann D, Bethmann S, Jahns P. Zeaxanthin Epoxidase Activity Is Downregulated by Hydrogen Peroxide. Plant and Cell Physiology. 2022;63(8):1091–1100. doi:10.1093/pcp/pcac081

115. Huang W, Haferkamp I, Lepetit B, Molchanova M, Hou S, Jeblick W, Bártulos CR, Kroth PG. Reduced vacuolar β-1,3-glucan synthesis affects carbohydrate metabolism as well as plastid homeostasis and structure in Phaeodactylum tricornutum. Proceedings of the National Academy of Sciences of the United States of America. 2018;115(18):4791–4796. doi:10.1073/pnas.1719274115

116. Jakob T, Goss R, Wilhelm C. Activation of Diadinoxanthin De-Epoxidase Due to a Chiororespiratory Proton Gradient in the Dark in the Diatom Phaeodactylum tricornutum. Plant Biology. 1999;1(1):76–82. http://doi.wiley.com/10.1111/j.1438-8677.1999.tb00711.x. doi:10.1111/j.1438-8677.1999.tb00711.x

117. Jakob T, Goss R, Wilhelm C. Unusual pH-dependence of diadinoxanthin de-epoxidase activation causes chlororespiratory induced accumulation of diatoxanthin in the diatom Phaeodactylum tricornutum. Journal of Plant Physiology. 2001;158(3):383–390. doi:10.1078/0176-1617-00288

118. Järvi S, Suorsa M, Aro EM. Photosystem II repair in plant chloroplasts - Regulation, assisting proteins and shared components with photosystem II biogenesis. Biochimica et Biophysica Acta - Bioenergetics. 2015;1847(9):900–909. http://dx.doi.org/10.1016/j.bbabio.2015.01.006. doi:10.1016/j.bbabio.2015.01.006

119. Jaubert M, Bouly JP, Ribera d'Alcalà M, Falciatore A. Light sensing and responses in marine microalgae. Current Opinion in Plant Biology. 2017;37:70–77. doi:10.1016/j.pbi.2017.03.005

120. Jensen E, Clément R, Maberly SC, Gontero B. Regulation of the Calvin–Benson– Bassham cycle in the enigmatic diatoms: biochemical and evolutionary variations on an original theme. Pnas. 2017;372:2–5. https://royalsocietypublishing.org/doi/full/10.1098/rstb.2016.0401. doi:https://doi.org/10.1098/rstb.2016.0401

121. Jensen EL, Clement R, Kosta A, Maberly SC, Gontero B. A new widespread subclass of carbonic anhydrase in marine phytoplankton. ISME Journal. 2019;13(8):2094–2106. http://dx.doi.org/10.1038/s41396-019-0426-8. doi:10.1038/s41396-019-0426-8

122. Jensen EL, Maberly SC, Gontero B. Insights on the functions and ecophysiological relevance of the diverse carbonic anhydrases in microalgae. International Journal of Molecular Sciences. 2020;21(8). doi:10.3390/ijms21082922

123. Jensen EL, Yangüez K, Carrière F, Gontero B. Storage compound accumulation in diatoms as response to elevated CO2 concentration. Biology. 2020;9(1). doi:10.3390/biology9010005

124. Jiang J, Cheong KY, Falkowski PG, Dai W. Integrating on-grid immunogold labeling and cryo-electron tomography to reveal photosystem II structure and spatial distribution in thylakoid

membranes. Journal of Structural Biology. 2021;213(3):107746. https://doi.org/10.1016/j.jsb.2021.107746. doi:10.1016/j.jsb.2021.107746

125. Johnson X, Alric J. Central carbon metabolism and electron transport in chlamydomonas reinhardtii: Metabolic constraints for carbon partitioning between oil and starch. Eukaryotic Cell. 2013;12(6):776–793. doi:10.1128/EC.00318-12

126. Jokel M, Johnson X, Peltier G, Aro EM, Allahverdiyeva Y. Hunting the main player enabling Chlamydomonas reinhardtii growth under fluctuating light. Plant Journal. 2018;94(5):822–835. doi:10.1111/tpj.13897

127. Joli N, Concia L, Mocaer K, Guterman J, Laude J, Guerin S, Sciandra T, Bruyant F, Ait-Mohamed O, Beguin M, et al. Hypometabolism to survive the long polar night in the diatom Fragilariopsis cylindrus. bioRxiv. 2023:2023.01.14.524047. http://biorxiv.org/content/early/2023/01/15/2023.01.14.524047.abstract

128. Joliot P, Béal D, Joliot A. Cyclic electron flow under saturating excitation of dark-adapted Arabidopsis leaves. Biochimica et Biophysica Acta - Bioenergetics. 2004;1656(2–3):166–176. doi:10.1016/j.bbabio.2004.03.010

129. Joliot P, Johnson GN. Regulation of cyclic and linear electron flow in higher Plants. Proceedings of the National Academy of Sciences of the United States of America. 2011;108(32):13317–13322. doi:10.1073/pnas.1110189108

130. Joliot P, Sellés J, Wollman FA, Verméglio A. High efficient cyclic electron flow and functional supercomplexes in Chlamydomonas cells. Biochimica et Biophysica Acta - Bioenergetics. 2022;1863(8). https://reader.elsevier.com/reader/sd/pii/S0005272822003796?token=F4DCDCD660FC0D817E0060E1BC898BF1A3AA94C624AEE41EC3453BB3D1AB2537482E80C0E61C0BC7598BBB2B96BB768C&originRegion=eu-west-1&originCreation=20230314202527. doi:10.1016/j.bbabio.2022.148909

131. Jungandreas A, Costa BS, Jakob T, Von Bergen M, Baumann S, Wilhelm C. The acclimation of Phaeodactylum tricornutum to blue and red light does not influence the photosynthetic light reaction but strongly disturbs the carbon allocation pattern. PLoS ONE. 2014;9(8). doi:10.1371/journal.pone.0099727

132. Junge W, Ausländer W, McGeer AJ, Runge T. The buffering capacity of the internal phase of thylakoids and the magnitude of the pH changes inside under flashing light. BBA - Bioenergetics. 1979;546(1):121–141. doi:10.1016/0005-2728(79)90175-0

133. Kaye Y, Huang W, Clowez S, Saroussi S, Idoine A, Sanz-Luque E, Grossman AR. The mitochondrial alternative oxidase from Chlamydomonas reinhardtii enables survival in high light. Journal of Biological Chemistry. 2019;294(4):1380–1395. http://dx.doi.org/10.1074/jbc.RA118.004667. doi:10.1074/jbc.RA118.004667

134. Keeling PJ. Chromalveolates and the evolution of plastids by secondary endosymbiosis. Journal of Eukaryotic Microbiology. 2009;56(1):1–8. doi:10.1111/j.1550-7408.2008.00371.x

135. Kemp AES, Villareal TA. Progress in Oceanography The case of the diatoms and the muddled mandalas : Time to recognize diatom adaptations to strati fi ed waters. 2018;167(July):138–149. doi:10.1016/j.pocean.2018.08.002

136. Kennedy F, Martin A, Bowman JP, Wilson R, McMinn A. Dark metabolism: a molecular insight into how the Antarctic sea-ice diatom Fragilariopsis cylindrus survives long-term darkness. 2019. doi:10.1111/nph.15843

137. Kikutani S, Nakajima K, Nagasato C, Tsuji Y, Miyatake A, Matsuda Y. Thylakoid luminal Θ-

carbonic anhydrase critical for growth and photosynthesis in the marine diatom Phaeodactylum tricornutum. Proceedings of the National Academy of Sciences of the United States of America. 2016;113(35):9828–9833. doi:10.1073/pnas.1603112113

138. Kikutani S, Tanaka R, Yamazaki Y, Hara S, Hisabori T, Kroth PG, Matsuda Y. Redox regulation of carbonic anhydrases via thioredoxin in chloroplast of the marine diatom Phaeodactylum tricornutum. Journal of Biological Chemistry. 2012;287(24):20689–20700. http://dx.doi.org/10.1074/jbc.M111.322743. doi:10.1074/jbc.M111.322743

139. Kim JM, Lee K, Shin K, Kang JH, Lee HW, Kim M, Jang PG, Jang MC. The effect of seawater CO2 concentration on growth of a natural phytoplankton assemblage in a controlled mesocosm experiment. Limnology and Oceanography. 2006;51(4):1629–1636. doi:10.4319/lo.2006.51.4.1629

140. Kirchhoff H, Hall C, Wood M, Herbstová M, Tsabari O, Nevo R, Charuvi D, Shimoni E, Reich Z. Dynamic control of protein diffusion within the granal thylakoid lumen. Proceedings of the National Academy of Sciences of the United States of America. 2011;108(50):20248–20253. doi:10.1073/pnas.1104141109

141. Kirchhoff H, Schöttler MA, Maurer J, Weis E. Plastocyanin redox kinetics in spinach chloroplasts: Evidence for disequilibrium in the high potential chain. Biochimica et Biophysica Acta - Bioenergetics. 2004;1659(1):63–72. doi:10.1016/j.bbabio.2004.08.004

142. Klanchui A, Cheevadhanarak S, Prommeenate P, Meechai A. Exploring Components of the CO2-Concentrating Mechanism in Alkaliphilic Cyanobacteria Through Genome-Based Analysis. Computational and Structural Biotechnology Journal. 2017;15:340–350. https://doi.org/10.1016/j.csbj.2017.05.001. doi:10.1016/j.csbj.2017.05.001

143. Kong F, Burlacot A, Liang Y, Légeret B, Alseekh S, Brotman Y, Fernie AR, Krieger-Liszkay A, Beisson F, Peltier G, et al. Interorganelle communication: Peroxisomal MALATE DEHYDROGENASE2 connects lipid catabolism to photosynthesis through redox coupling in chlamydomonas. Plant Cell. 2018;30(8):1824–1847. doi:10.1105/tpc.18.00361

144. Kong SG, Okajima K. Diverse photoreceptors and light responses in plants. Journal of Plant Research. 2016;129(2):111–114. doi:10.1007/s10265-016-0792-5

145. König S, Juhas M, Jäger S, Kottke T, Büchel C. The cryptochrome—photolyase protein family in diatoms. Journal of Plant Physiology. 2017;217(June):15–19. http://dx.doi.org/10.1016/j.jplph.2017.06.015. doi:10.1016/j.jplph.2017.06.015

146. Kowalczyk N, Rappaport F, Boyen C, Wollman FA, Collén J, Joliot P. Photosynthesis in Chondrus crispus: The contribution of energy spill-over in the regulation of excitonic flux. Biochimica et Biophysica Acta - Bioenergetics. 2013;1827(7):834–842. http://dx.doi.org/10.1016/j.bbabio.2013.04.004. doi:10.1016/j.bbabio.2013.04.004

147. Kozaki A, Takeba G. Photorespiration protects C3 plants from photooxidation. Nature. 1996;384(December):557–560. http://www.ncbi.nlm.nih.gov/pubmed/7509040

148. Kozuleva M, Petrova A, Milrad Y, Semenov A, Ivanov B, Redding KE, Yacoby I. Phylloquinone is the principal Mehler reaction site within photosystem I in high light. Plant Physiology. 2021:1–11. doi:10.1093/plphys/kiab221

149. Kramer DM, Cruz JA, Kanazawa A. Balancing the central roles of the thylakoid proton gradient. Trends in Plant Science. 2003;8(1):27–32. doi:10.1016/S1360-1385(02)00010-9

150. Kramer DM, Wise RR, Frederick JR, Alm DM, Hesketh JD, Ort DR, Crofts AR. Regulation of coupling factor in field-grown sunflower: A Redox model relating coupling factor activity to the activities of other thioredoxin-dependent chloroplast enzymes. Photosynthesis Research.

1990;26(3):213–222. doi:10.1007/BF00033134

151. Krapp A, David LC, Chardin C, Girin T, Marmagne A, Leprince AS, Chaillou S, Ferrario-Méry S, Meyer C, Daniel-Vedele F. Nitrate transport and signalling in Arabidopsis. Journal of Experimental Botany. 2014;65(3):789–798. doi:10.1093/jxb/eru001

152. Krömer S, Heldt HW. On the Role of Mitochondrial Oxidative Phosphorylation in Photosynthesis Metabolism as Studied by the Effect of Oligomycin on Photosynthesis in Protoplasts and Leaves of Barley (Hordeum vulgare). Plant Physiology. 1991;95(4):1270–1276. https://academic.oup.com/plphys/article/95/4/1270-1276/6087001. doi:10.1104/pp.95.4.1270

153. Kroth PG, Chiovitti A, Gruber A, Martin-Jezeque V, Mock T, Parker MS, Stanley MS, Kaplan A, Caron L, Weber T, et al. A model for carbohydrate metabolism in the diatom Phaeodactylum tricornutum deduced from comparative whole genome analysis. PLoS ONE. 2008;3(1). doi:10.1371/journal.pone.0001426

154. Kroth PG, Matsuda Y. Carbohydrate Metabolism. In: The Molecular Life of Diatoms. Cham: Springer International Publishing; 2022. p. 465–492. https://link.springer.com/10.1007/978-3-030-92499-7_17. doi:10.1007/978-3-030-92499-7_17

155. Kroth PG, Wilhelm C, Kottke T. An update on aureochromes: Phylogeny – mechanism – function. Journal of Plant Physiology. 2017;217(June):20–26. doi:10.1016/j.jplph.2017.06.010

156. Kustka AB, Milligan AJ, Zheng H, New AM, Gates C, Bidle KD, Reinfelder JR. Low CO2 results in a rearrangement of carbon metabolism to support C4 photosynthetic carbon assimilation in Thalassiosira pseudonana. New Phytologist. 2014;204(3):507–520. doi:10.1111/nph.12926

157. Lacour T, Morin P-I, Sciandra T, Donaher N, Campbell DA, Ferland J, Babin M. Decoupling light harvesting, electron transport and carbon fixation during prolonged darkness supports rapid recovery upon re-illumination in the Arctic diatom Chaetoceros neogracilis. Polar Biology. 2019;42(10):1787–1799. http://link.springer.com/10.1007/s00300-019-02507-2. doi:10.1007/s00300-019-02507-2

158. Laisk A, Eichelmann H, Oja V, Peterson RB. Control of cytochrome b 6 f at low and high light intensity and cyclic electron transport in leaves. 2005;1708:79–90. doi:10.1016/j.bbabio.2005.01.007

159. Larkum AWD, Vesk M. Algal Plastids: Their Fine Structure and Properties. 2003. p. 11–28. http://link.springer.com/10.1007/978-94-007-1038-2_2. doi:10.1007/978-94-007-1038-2_2

160. Launay H, Huang W, Maberly SC, Gontero B. Regulation of Carbon Metabolism by Environmental Conditions: A Perspective From Diatoms and Other Chromalveolates. Frontiers in Plant Science. 2020;11(July):1–14. doi:10.3389/fpls.2020.01033

161. Lavaud J, Gorkom HJ Van, Etienne A-L. Photosystem II electron transfer cycle and chlororespiration in planktonic diatoms. Photosynthesis Research. 2002;74:51–59.

162. Lavaud J, Rousseau B, Gorkom HJ Van, Etienne A, Van Gorkom HJ, Etienne A, Gorkom HJ Van, Etienne A. Influence of the Diadinoxanthin Pool Size on Photoprotection in the Marine Planktonic Diatom Phaeodactylum tricornutum 1. Plant physiology. 2002;129:1398–1406. doi:10.1104/pp.002014.dissipation

163. Lavaud J, Six C, Campbell DA. Photosystem II repair in marine diatoms with contrasting photophysiologies. Photosynthesis Research. 2016;127(2):189–199. doi:10.1007/s11120-015-0172-3

164. Lepetit B, Campbell DA, Lavaud J, Büchel C, Goss R, Bailleul B. Photosynthetic Light Reactions in Diatoms. II. The Dynamic Regulation of the Various Light Reactions. The Molecular Life of Diatoms. 2022:423–464. doi:10.1007/978-3-030-92499-7_16

165. Lepetit B, Goss R, Jakob T, Wilhelm C. Molecular dynamics of the diatom thylakoid membrane under different light conditions. Photosynthesis Research. 2012;111(1–2):245–257. doi:10.1007/s11120-011-9633-5

166. Lepetit B, Sturm S, Rogato A, Gruber A, Sachse M, Falciatore A, Kroth PG, Lavaud J. High Light Acclimation in the Secondary Plastids Containing Diatom Phaeodactylum tricornutum is Triggered by the Redox State of the Plastoquinone Pool. Plant Physiology. 2013;161(2):853–865. http://www.plantphysiol.org/cgi/doi/10.1104/pp.112.207811. doi:10.1104/pp.112.207811

167. Lepetit B, Volke D, Gilbert M, Wilhelm C, Goss R. Evidence for the Existence of One Antenna-Associated, Lipid-Dissolved and Two Protein-Bound Pools of Diadinoxanthin Cycle Pigments in Diatoms. Plant Physiology. 2010;154(4):1905–1920. http://www.plantphysiol.org/cgi/doi/10.1104/pp.110.166454. doi:10.1104/pp.110.166454

168. Leustek T, Martin MN, Bick JA, Davies JP. Pathways and regulation of sulfur metabolism revealed through molecular and genetic studies. Annual Review of Plant Biology. 2000;51(1):141–165. https://www.annualreviews.org/doi/10.1146/annurev.arplant.51.1.141. doi:10.1146/annurev.arplant.51.1.141

169. Levering J, Broddrick J, Dupont CL, Peers G, Beeri K, Mayers J, Gallina AA, Allen AE, Palsson O, Zengler K. Genome-Scale Model Reveals Metabolic Basis of Biomass Partitioning in a Model Diatom. 2016:1–22. doi:10.1371/journal.pone.0155038

170. Levitan O, Chen M, Kuang X, Yu K, Jiang J, Banal M. Structural and functional analyses of photosystem II in the marine diatom Phaeodactylum tricornutum. 2019;116(35). doi:10.1073/pnas.1906726116

171. Ley AC, Butler WL. Energy transfer from photosystem II to photosystem I in Porphyridium cruentum. Biochimica et Biophysica Acta (BBA) - Bioenergetics. 1977;462(2):290–294. https://linkinghub.elsevier.com/retrieve/pii/000527287790127X. doi:10.1016/0005-2728(77)90127-X

172. Li G, Woroch AD, Donaher NA, Cockshutt AM, Campbell DA. A Hard Day's Night: Diatoms Continue Recycling Photosystem II in the Dark. Frontiers in Marine Science. 2016;3(November):1–10. http://journal.frontiersin.org/article/10.3389/fmars.2016.00218/full. doi:10.3389/fmars.2016.00218

173. Li M, Svoboda V, Davis G, Kramer D, Kunz HH, Kirchhoff H. Impact of ion fluxes across thylakoid membranes on photosynthetic electron transport and photoprotection. Nature Plants. 2021;7(7):979–988. http://dx.doi.org/10.1038/s41477-021-00947-5. doi:doi.org/10.1007/s11120-013-9817-2

174. Liu S, Xu Q, Liu K, Zhao Y, Chen N. Chloroplast Genomes for Five Skeletonema Species: Comparative and Phylogenetic Analysis. Frontiers in Plant Science. 2021;12(December). doi:10.3389/fpls.2021.774617

175. Lomas MW, Gilbert PM. Temperature regulation of nitrate uptake: A novel hypothesis about nitrate uptake and reduction in cool-water diatoms. Limnology and Oceanography. 1999;44(3 I):556–572. doi:10.4319/lo.1999.44.3.0556

176. Lomas MW, Rumbley CJ, Glibert PM. Ammonium release by nitrogen sufficient diatoms in response to rapid increases in irradiance. Journal of Plankton Research. 2000;22(12):2351–2366. doi:10.1093/plankt/22.12.2351

177. Lommer M, Specht M, Roy AS, Kraemer L, Andreson R, Gutowska MA, Wolf J, Bergner S V., Schilhabel MB, Klostermeier UC, et al. Genome and low-iron response of an oceanic diatom adapted to chronic iron limitation. Genome Biology. 2012;13(7). doi:10.1186/gb-2012-13-7-r66

178. Mackinder LCM, Meyer MT, Mettler-Altmann T, Chen VK, Mitchell MC, Caspari O, Rosenzweig ESF, Pallesen L, Reeves G, Itakura A, et al. A repeat protein links Rubisco to form the eukaryotic carbon-concentrating organelle. Proceedings of the National Academy of Sciences of the United States of America. 2016;113(21):5958–5963. doi:10.1073/pnas.1522866113

179. Malone LA, Qian P, Mayneord GE, Hitchcock A, Farmer DA, Thompson RF, Swainsbury DJK, Ranson NA, Hunter CN, Johnson MP. Cryo-EM structure of the spinach cytochrome b 6 f complex at 3.6 Å resolution. Nature. 2019;575(7783):535–539. http://dx.doi.org/10.1038/s41586-019-1746-6. doi:10.1038/s41586-019-1746-6

180. Mann M, Serif M, Jakob T, Kroth PG, Wilhelm C. PtAUREO1a and PtAUREO1b knockout mutants of the diatom Phaeodactylum tricornutum are blocked in photoacclimation to blue light. Journal of Plant Physiology. 2017;217(May):44–48. http://dx.doi.org/10.1016/j.jplph.2017.05.020. doi:10.1016/j.jplph.2017.05.020

181. Mann M, Serif M, Wrobel T, Eisenhut M, Madhuri S, Flachbart S, Weber APM, Lepetit B, Wilhelm C, Kroth PG. The Aureochrome Photoreceptor PtAUREO1a Is a Highly Effective Blue Light Switch in Diatoms. iScience. 2020;23(11):101730. https://doi.org/10.1016/j.isci.2020.101730. doi:10.1016/j.isci.2020.101730

182. Marchand J, Heydarizadeh P, Schoefs B, Spetea C. Ion and metabolite transport in the chloroplast of algae : lessons from land plants. Cellular and Molecular Life Sciences. 2018;75(12):2153–2176. https://doi.org/10.1007/s00018-018-2793-0. doi:10.1007/s00018-018-2793-0

183. Margalef R. Life-forms of phytoplankton as survival alternatives in an unstable environment. Oceanologica Acta. 1978;1:493–509.

184. Matsuda Y. Inorganic carbon utilization by aquatic photoautotrophs and potential usages of algal primary production. Photosynthesis Research. 2011;109(1–3):1–5. doi:10.1007/s11120-011-9683-8

185. Matsuda Y, Hopkinson BM, Nakajima K, Dupont CL, Tsuji Y. Mechanisms of carbon dioxide acquisition and CO2 sensing in marine diatoms: A gateway to carbon metabolism. Philosophical Transactions of the Royal Society B: Biological Sciences. 2017;372(1728). doi:10.1098/rstb.2016.0403

186. Maxwell PC, Biggins J. Role of Cyclic Electron Transport in Photosynthesis as Measured by the Photoinduced Turnover of P700 in Vivo. Biochemistry. 1976;15(18):3975–3981. doi:10.1021/bi00663a011

187. Mehler AH. Studies on reactions of illuminated chloroplasts. II. Stimulation and inhibition of the reaction with molecular oxygen. Archives of Biochemistry and Biophysics. 1951;34(2):339–351. http://www.sciencedirect.com/science/article/pii/0003986151900124. doi:10.1016/0003-9861(51)90012-4

188. Mekhalfi M, Amara S, Robert S, Carrière F, Gontero B. Effect of environmental conditions on various enzyme activities and triacylglycerol contents in cultures of the freshwater diatom, Asterionella formosa (Bacillariophyceae). Biochimie. 2014;101(1):21–30. doi:10.1016/j.biochi.2013.12.004

189. Meyer Zu Tittingdorf JMW, Rexroth S, Schäfer E, Schlichting R, Giersch C, Dencher NA, Seelert H. The stoichiometry of the chloroplast ATP synthase oligomer III in Chlamydomonas reinhardtii is not affected by the metabolic state. Biochimica et Biophysica Acta - Bioenergetics. 2004;1659(1):92–99. doi:10.1016/j.bbabio.2004.08.008

190. Michelet L, Zaffagnini M, Morisse S, Sparla F, Pérez-Pérez ME, Francia F, Danon A, Marchand CH,

Fermani S, Trost P, et al. Redox regulation of the Calvin-Benson cycle: Something old, something new. Frontiers in Plant Science. 2013;4(NOV):1–21. doi:10.3389/fpls.2013.00470

191. Michels AK, Wedel N, Kroth PG. Diatom plastids possess a phosphoribulokinase with an altered regulation and no oxidative pentose phosphate pathway. Plant Physiology. 2005;137(3):911–920. doi:10.1104/pp.104.055285

192. Mitchell P. chemiosmotic coupling in oxidative and photosynthetic phosphorylation. Biological Reviews. 1966;41(3):445–501. http://doi.wiley.com/10.1111/j.1469-185X.1966.tb01501.x. doi:10.1111/j.1469-185X.1966.tb01501.x

193. Mock T, Hodgkinson K, Wu T, Moulton V, Duncan A, van Oosterhout C, Pichler M. Structure and Evolution of Diatom Nuclear Genes and Genomes. In: The Molecular Life of Diatoms. Cham: Springer International Publishing; 2022. p. 111–145. https://link.springer.com/10.1007/978-3-030-92499-7_5. doi:10.1007/978-3-030-92499-7_5

194. Morel FMM, Lam PJ, Saito MA. Trace Metal Substitution in Marine Phytoplankton. Annual Review of Earth and Planetary Sciences. 2020;48:491–517. doi:10.1146/annurev-earth-053018-060108

195. Mueller-Cajar O, Stotz M, Wendler P, Hartl FU, Bracher A, Hayer-Hartl M. Structure and function of the AAA + protein CbbX, a red-type Rubisco activase. Nature. 2011;479(7372):194–199. http://dx.doi.org/10.1038/nature10568. doi:10.1038/nature10568

196. Munekage Y, Hashimoto M, Miyake C, Tomizawa KI, Endo T, Tasaka M, Shikanai T. Cyclic electron flow around photosystem I is essential for photosynthesis. Nature. 2004;429(6991):579–582. doi:10.1038/nature02598

197. Munekage Y, Hojo M, Meurer J, Endo T, Tasaka M, Shikanai T. PGR5 is involved in cyclic electron flow around photosystem I and is essential for photoprotection in Arabidopsis. Cell. 2002;110(3):361–371. doi:10.1016/S0092-8674(02)00867-X

198. Murata N, Siegenthaler P-A. Lipids in Photosynthesis: An Overview. In: Lipids in Photosynthesis: Structure, Function and Genetics. Dordrecht: Kluwer Academic Publishers; p. 1–20. http://link.springer.com/10.1007/0-306-48087-5_1. doi:10.1007/0-306-48087-5_1

199. Murik O, Tirichine L, Prihoda J, Thomas Y, Araújo WL, Allen AE, Fernie AR, Bowler C. Downregulation of mitochondrial alternative oxidase affects chloroplast function, redox status and stress response in a marine diatom. New Phytologist. 2019;221(3):1303–1316. doi:10.1111/nph.15479

200. Nagy G, Ünnep R, Zsiros O, Tokutsu R, Takizawa K, Porcar L, Moyet L, Petroutsos D, Garab G, Finazzi G, et al. Chloroplast remodeling during state transitions in Chlamydomonas reinhardtii as revealed by noninvasive techniques in vivo. Proceedings of the National Academy of Sciences of the United States of America. 2014;111(13):5042–5047. doi:10.1073/pnas.1322494111

201. Nakajima K, Tanaka A, Matsuda Y. SLC4 family transporters in a marine diatom directly pump bicarbonate from seawater. Proceedings of the National Academy of Sciences of the United States of America. 2013;110(5):1767–1772. doi:10.1073/pnas.1216234110

202. Nawaly H, Tanaka A, Toyoshima Y, Tsuji Y, Matsuda Y. Localization and characterization θ carbonic anhydrases in Thalassiosira pseudonana. Photosynthesis Research. 2023 Mar 2. https://link.springer.com/10.1007/s11120-023-01007-z. doi:10.1007/s11120-023-01007-z

203. Nawrocki WJ, Bailleul B, Cardol P, Rappaport F, Wollman FA, Joliot P. Maximal cyclic electron flow rate is independent of PGRL1 in Chlamydomonas. Biochimica et Biophysica Acta - Bioenergetics. 2019;1860(5):425–432. https://doi.org/10.1016/j.bbabio.2019.01.004.

doi:10.1016/j.bbabio.2019.01.004

204. Nawrocki WJ, Bailleul B, Picot D, Cardol P, Rappaport F, Wollman FA, Joliot P. The mechanism of cyclic electron flow. Biochimica et Biophysica Acta - Bioenergetics. 2019;1860(5):433–438. doi:10.1016/j.bbabio.2018.12.005

205. Nawrocki WJ, Tourasse NJ, Taly A, Rappaport F, Wollman F-A. The Plastid Terminal Oxidase: Its Elusive Function Points to Multiple Contributions to Plastid Physiology. Annual Review of Plant Biology. 2015;66(1):49–74. http://www.annualreviews.org/doi/10.1146/annurev-arplant-043014-114744. doi:10.1146/annurev-arplant-043014-114744

206. Nesci S, Trombetti F, Ventrella V, Pagliarani A. The c-Ring of the F1FO-ATP Synthase: Facts and Perspectives. Journal of Membrane Biology. 2016;249(1–2):11–21. doi:10.1007/s00232-015-9860-3

207. Nikkanen L, Rintamäki E. Chloroplast thioredoxin systems dynamically regulate photosynthesis in plants. Biochemical Journal. 2019;476(7):1159–1172. doi:10.1042/BCJ20180707

208. Ogawa K, Kanematsu S, Takabe K, Asada K. Attachment of CuZn-superoxide dismutase to thylakoid membranes at the site of superoxide generation (PSI) in spinach chloroplasts: Detection by immuno-gold labeling after rapid freezing and substitution method. Plant and Cell Physiology. 1995;36(4):565–573. doi:10.1093/oxfordjournals.pcp.a078795

209. Ogawa T, Kobayashi K, Taniguchi YY, Shikanai T, Nakamura N, Yokota A, Munekage YN. Two cyclic electron flows around photosystem I differentially participate in C4 photosynthesis. Plant Physiology. 2023;191(4):2288–2300. https://doi.org/10.1093/plphys/kiad032. doi:10.1093/plphys/kiad032

210. Oudot-Le Secq MP, Grimwood J, Shapiro H, Armbrust EV, Bowler C, Green BR. Chloroplast genomes of the diatoms Phaeodactylum tricornutum and Thalassiosira pseudonana: Comparison with other plastid genomes of the red lineage. Molecular Genetics and Genomics. 2007;277(4):427–439. doi:10.1007/s00438-006-0199-4

211. Pancic PG, Strotmann H. Structure of the nuclear encoded γ subunit of CF0CF1 of the diatom Odontella sinensis including its presequence. FEBS Letters. 1993;320(1):61–66. doi:10.1016/0014-5793(93)81658-M

212. Parker MS, Armbrust EV, Piovia-Scott J, Keil RG. Induction of photorespiration by light in the centric diatom Thalassiosira weissflogii (Bacillariophyceae): Molecular characterization and physiological consequences. Journal of Phycology. 2004;40(3):557–567. doi:10.1111/j.1529-8817.2004.03184.x

213. Peers G, Price NM. Copper-containing plastocyanin used for electron transport by an oceanic diatom. Nature. 2006;441(7091):341–344. doi:10.1038/nature04630

214. Peltier G, Aro E-M, Shikanai T. NDH-1 and NDH-2 Plastoquinone Reductases in Oxygenic Photosynthesis. Annual Review of Plant Biology. 2016;67(1):55–80. doi:10.1146/annurev-arplant-043014-114752

215. Pierella Karlusich JJ, Ceccoli RD, Graña M, Romero H, Carrillo N. Environmental selection pressures related to iron utilization are involved in the loss of the flavodoxin gene from the plant genome. Genome Biology and Evolution. 2015;7(3):750–767. doi:10.1093/gbe/evv031

216. Pogoryelov D, Klyszejko AL, Krasnoselska GO, Heller EM, Leone V, Langer JD, Vonck J, Müller DJ, Faraldo-Gómez JD, Meier T. Engineering rotor ring stoichiometries in the ATP synthase. Proceedings of the National Academy of Sciences of the United States of America. 2012;109(25). doi:10.1073/pnas.1120027109

217. Ponomarenko S V. Evolutionary modifications of molecular structure of ATP-synthase γ-subunit. Journal of Evolutionary Biochemistry and Physiology. 2007;43(5):467–475. doi:10.1134/S0022093007050027

218. Portis AR, Li C, Wang D, Salvucci ME. Regulation of Rubisco activase and its interaction with Rubisco. Journal of Experimental Botany. 2008;59(7):1597–1604. doi:10.1093/jxb/erm240

219. Prasil O, Kolber Z, Berry JA, Falkowski PG. Cyclic electron flow around Photosystem II in vivo. Photosynthesis Research. 1996;48(3):395–410. doi:10.1007/BF00029472

220. Del Prete S, Nocentini A, Supuran CT, Capasso C. Bacterial ι-carbonic anhydrase: a new active class of carbonic anhydrase identified in the genome of the Gram-negative bacterium Burkholderia territorii. Journal of Enzyme Inhibition and Medicinal Chemistry. 2020;35(1):1060–1068. https://doi.org/10.1080/14756366.2020.1755852. doi:10.1080/14756366.2020.1755852

221. Pyszniak AM, Gibbs SP. Immunocytochemical localization of photosystem I and the fucoxanthin-chlorophyll a / c fight-harvesting complex in the diatom Phaeodactylum tricornutum. Protoplasma. 1992;166(3–4):208–217.

222. Rai AK, Chen T, Moroney J V. Mitochondrial carbonic anhydrases are needed for optimal photosynthesis at low CO2levels in Chlamydomonas. Plant Physiology. 2021;187(3):1387–1398. doi:10.1093/plphys/kiab351

223. Raines CA. The Calvin cycle revisited. Photosynthesis Research. 2003;75(1):1–10. doi:10.1023/A:1022421515027

224. Ral JP, Colleoni C, Wattebled F, Dauvillée D, Nempont C, Deschamps P, Li Z, Morell MK, Chibbar R, Purton S, et al. Circadian clock regulation of starch metabolism establishes GBSSI as a major contributor to amylopectin synthesis in Chlamydomonas reinhardtii. Plant Physiology. 2006;142(1):305–317. doi:10.1104/pp.106.081885

225. Raven JA. Photosynthetic and non-photosynthetic roles of carbonic anhydrase in algae and cyanobacteria. Phycologia. 1995;34(2):93–101. https://www.tandfonline.com/doi/full/10.2216/i0031-8884-34-2-93.1. doi:10.2216/i0031-8884-34-2-93.1

226. Raven JA, Beardall J, Larkum AW. The Physiology of Microalgae. 2016. http://link.springer.com/10.1007/978-3-319-24945-2. doi:10.1007/978-3-319-24945-2

227. Raven JA, Evans MCW, Korb RE. The role of trace metals in photosynthetic electron transport in O2-evolving organisms. Photosynthesis Research. 1999;60(2–3):111–150. doi:doi.org/10.1023/A:1006282714942

228. Reinfelder JR, Kraepiel AML, Morel FMM. Unicellular C4 photosynthesis in a marine diatom. Nature. 2000;407(6807):996–999. doi:10.1038/35039612

229. Roberts K, Granum E, Leegood RC, Raven JA. Carbon acquisition by diatoms. Photosynthesis Research. 2007;93(1–3):79–88. doi:10.1007/s11120-007-9172-2

230. Rutherford AW, Osyczka A, Rappaport F. Back-reactions, short-circuits, leaks and other energy wasteful reactions in biological electron transfer: Redox tuning to survive life in O 2. FEBS Letters. 2012;586(5):603–616. http://dx.doi.org/10.1016/j.febslet.2011.12.039. doi:10.1016/j.febslet.2011.12.039

231. Sandmann G, Reck H, Kessler E, Böger P. Distribution of plastocyanin and soluble plastidic cytochrome c in various classes of algae. Archives of Microbiology. 1983;134(1):23–27. doi:10.1007/BF00429401

232. Santabarbara S, Bullock B, Rappaport F, Redding KE. Controlling electron transfer between the two cofactor chains of photosystem i by the redox state of one of their components. Biophysical Journal. 2015;108(6):1537–1547. http://dx.doi.org/10.1016/j.bpj.2015.01.009. doi:10.1016/j.bpj.2015.01.009

233. Saroussi S, Schushan M, Ben-Tal N, Junge W, Nelson N. Structure and Flexibility of the C-Ring in the Electromotor of Rotary FoF1-ATPase of Pea Chloroplasts. PLoS ONE. 2012;7(9):1–12. doi:10.1371/journal.pone.0043045

234. Sasaki Y, Nakamura Y, Matsuno R. Regulation of gene expression of ribulose bisphosphate carboxylase in greening pea leaves. Plant Molecular Biology. 1987;8(5):375–382. doi:10.1007/BF00015815

235. Scafaro1 AP, De Vleesschauwer D, Bautsoens N, Hannah MA, Den Boer B, Gallé A, Van Rie J. A single point mutation in the C-terminal extension of wheat Rubisco activase dramatically reduces ADP inhibition via enhanced ATP binding affinity. Journal of Biological Chemistry. 2019;294(47):17931–17940. http://dx.doi.org/10.1074/jbc.RA119.010684. doi:10.1074/jbc.RA119.010684

236. Scheibe R, Backhausen JE, Emmerlich V, Holtgrefe S. Strategies to maintain redox homeostasis during photosynthesis under changing conditions. Journal of Experimental Botany. 2005;56(416):1481–1489. doi:10.1093/jxb/eri181

237. Schellenberger Costa B, Jungandreas A, Jakob T, Weisheit W, Mittag M, Wilhelm C. Blue light is essential for high light acclimation and photoprotection in the diatom Phaeodactylum tricornutum. Journal of Experimental Botany. 2013;64(2):483–493. https://academic.oup.com/jxb/article-lookup/doi/10.1093/jxb/ers340. doi:10.1093/jxb/ers340

238. Schellenberger Costa B, Sachse M, Jungandreas A, Bartulos CR, Gruber A, Jakob T, Kroth PG, Wilhelm C. Aureochrome 1a Is Involved in the Photoacclimation of the Diatom Phaeodactylum tricornutum. PLoS ONE. 2013;8(9). doi:10.1371/journal.pone.0074451

239. Schmitz J, Srikanth N V., Hüdig M, Poschmann G, Lercher MJ, Maurino VG. The ancestors of diatoms evolved a unique mitochondrial dehydrogenase to oxidize photorespiratory glycolate. Photosynthesis Research. 2017;132(2):183–196. doi:10.1007/s11120-017-0355-1

240. Seelert H, Poetsch A, Dencher NA, Engel A, Stahlberg H, Müller DJ. Proton-powered turbine of a plant motor. Nature. 2000;405(6785):418–419. http://www.nature.com/articles/35013148. doi:10.1038/35013148

241. Sétif P, Shimakawa G, Krieger-Liszkay A, Miyake C. Identification of the electron donor to flavodiiron proteins in Synechocystis sp. PCC 6803 by in vivo spectroscopy. Biochimica et Biophysica Acta - Bioenergetics. 2020;1861(10):148256. https://doi.org/10.1016/j.bbabio.2020.148256. doi:10.1016/j.bbabio.2020.148256

242. Seydoux C, Storti M, Giovagnetti V, Matuszyńska A, Guglielmino E, Zhao X, Giustini C, Pan Y, Blommaert L, Angulo J, et al. Impaired photoprotection in Phaeodactylum tricornutum KEA3 mutants reveals the proton regulatory circuit of diatoms light acclimation. New Phytologist. 2022;234(2):578–591. doi:10.1111/nph.18003

243. Shao H, Huang W, Avilan L, Receveur-Bréchot V, Puppo C, Puppo R, Lebrun R, Gontero B, Launay H. A new type of flexible CP12 protein in the marine diatom Thalassiosira pseudonana. Cell Communication and Signaling. 2021;19(1):1–13. https://doi.org/10.1186/s12964-021-00718-x. doi:10.1186/s12964-021-00718-x

244. Shikanai T. Central role of cyclic electron transport around photosystem I in the regulation of

photosynthesis. Current Opinion in Biotechnology. 2014;26(Figure 1):25–30. http://dx.doi.org/10.1016/j.copbio.2013.08.012. doi:10.1016/j.copbio.2013.08.012

245. Shimakawa G, Shoguchi E, Burlacot A, Ifuku K, Che Y, Kumazawa M, Tanaka K, Nakanishi S. Coral symbionts evolved a functional polycistronic flavodiiron gene. Photosynthesis Research. 2021;(0123456789). https://doi.org/10.1007/s11120-021-00867-7. doi:10.1007/s11120-021-00867-7

246. Smith SR, Abbriano RM, Hildebrand M. Comparative analysis of diatom genomes reveals substantial differences in the organization of carbon partitioning pathways. Algal Research. 2012;1(1):2–16. http://dx.doi.org/10.1016/j.algal.2012.04.003. doi:10.1016/j.algal.2012.04.003

247. Sonoike K. Photoinhibition of photosystem I. Physiologia Plantarum. 2011;142(1):56–64. doi:10.1111/j.1399-3054.2010.01437.x

248. Spetea C, Hideg É, Vass I. Low pH accelerates light-induced damage of photosystem II by enhancing the probability of the donor-side mechanism of photoinhibition. Biochimica et Biophysica Acta - Bioenergetics. 1997;1318(1–2):275–283. doi:10.1016/S0005-2728(96)00145-4

249. Storti M, Alboresi A, Gerotto C, Aro EM, Finazzi G, Morosinotto T. Role of cyclic and pseudo-cyclic electron transport in response to dynamic light changes in Physcomitrella patens. Plant Cell and Environment. 2019;42(5):1590–1602. doi:10.1111/pce.13493

250. Streb P, Josse EM, Gallouët E, Baptist F, Kuntz M, Cornic G. Evidence for alternative electron sinks to photosynthetic carbon assimilation in the high mountain plant species Ranunculus glacialis. Plant, Cell and Environment. 2005;28(9):1123–1135. doi:10.1111/j.1365-3040.2005.01350.x

251. Stroebel D, Choquet Y, Popot JL, Picot D. An atypical haem in the cytochrome b6f complex. Nature. 2003;426(6965):413–418. doi:10.1038/nature02155

252. Strzepek RF, Boyd PW, Sunda WG. Photosynthetic adaptation to low iron, light, and temperature in Southern Ocean phytoplankton. Proceedings of the National Academy of Sciences. 2019;116(10):4388–4393. doi:10.1073/pnas.1810886116

253. Sukenik A, Bennett J, Falkowski P. Light-saturated photosynthesis - Limitation by electron transport or carbon fixation? BBA - Bioenergetics. 1987;891(3):205–215. doi:10.1016/0005-2728(87)90216-7

254. Sunagawa S, Acinas SG, Bork P, Bowler C, Babin M, Boss E, Cochrane G, de Vargas C, Follows M, Gorsky G, et al. Tara Oceans: towards global ocean ecosystems biology. Nature Reviews Microbiology. 2020;18(8):428–445. doi:10.1038/s41579-020-0364-5

255. Suorsa M. Cyclic electron flow provides acclimatory plasticity for the photosynthetic machinery under various environmental conditions and developmental stages. Frontiers in Plant Science. 2015;6(September):1–8. doi:10.3389/fpls.2015.00800

256. Suzuki Y, Makino A. Translational downregulation of RBCL is operative in the coordinated expression of Rubisco genes in senescent leaves in rice. Journal of Experimental Botany. 2013;64(4):1145–1152. doi:10.1093/jxb/ers398

257. Thamatrakoln K, Bailleul B, Brown CM, Gorbunov MY, Kustka AB, Frada M, Joliot PA, Falkowski PG, Bidle KD. Death-specific protein in a marine diatom regulates photosynthetic responses to iron and light availability. Proceedings of the National Academy of Sciences. 2013;110(50):20123–20128. http://www.pnas.org/cgi/doi/10.1073/pnas.1304727110. doi:10.1073/pnas.1304727110

258. Tiwari A, Mamedov F, Grieco M, Suorsa M, Jajoo A, Styring S, Tikkanen M, Aro EM. Photodamage of iron-sulphur clusters in photosystem i induces non-photochemical energy dissipation. Nature Plants. 2016;2(4). http://dx.doi.org/10.1038/nplants.2016.35.

doi:10.1038/NPLANTS.2016.35

259. Van Tol HM, Virginia Armbrust E. Genome-scale metabolic model of the diatom Thalassiosira pseudonana highlights the importance of nitrogen and sulfur metabolism in redox balance. 2021. http://dx.doi.org/10.1371/journal.pone.0241960. doi:10.1371/journal.pone.0241960

260. Toyokawa C, Yamano T, Fukuzawa H. Pyrenoid starch sheath is required for LCIB localization and the CO2-concentrating mechanism in green algae. Plant Physiology. 2020;182(4):1883–1893. doi:10.1104/PP.19.01587

261. Tréguer P, Bowler C, Moriceau B, Dutkiewicz S, Gehlen M, Aumont O, Bittner L, Dugdale R, Finkel Z, Iudicone D, et al. Influence of diatom diversity on the ocean biological carbon pump. Nature Geoscience. 2018;11(1):27–37. http://dx.doi.org/10.1038/s41561-017-0028-x. doi:10.1038/s41561-017-0028-x

262. Tréguer PJ, Sutton JN, Brzezinski M, Charette MA, Devries T, Dutkiewicz S, Ehlert C, Hawkings J, Leynaert A, Liu SM, et al. Reviews and syntheses: The biogeochemical cycle of silicon in the modern ocean. Biogeosciences. 2021;18(4):1269–1289. doi:10.5194/bg-18-1269-2021

263. Trissl HW, Wilhelm C. Why do thylakoid membranes from higher plants form grana stacks? Trends in Biochemical Sciences. 1993;18(11):415–419. doi:10.1016/0968-0004(93)90136-B

264. Tsuji Y, Nakajima K, Matsuda Y. Molecular aspects of the biophysical CO2-concentrating mechanism and its regulation in marine diatoms. Journal of Experimental Botany. 2017;68(14):3763–3772. doi:10.1093/jxb/erx173

265. Uwizeye C, Decelle J, Jouneau PH, Flori S, Gallet B, Keck JB, Bo DD, Moriscot C, Seydoux C, Chevalier F, et al. Morphological bases of phytoplankton energy management and physiological responses unveiled by 3D subcellular imaging. Nature Communications. 2021;12(1):1–12. http://dx.doi.org/10.1038/s41467-021-21314-0. doi:10.1038/s41467-021-21314-0

266. Vieler A, Wilhelm C, Goss R, Süß R, Schiller J. The lipid composition of the unicellular green alga Chlamydomonas reinhardtii and the diatom Cyclotella meneghiniana investigated by MALDI-TOF MS and TLC. Chemistry and Physics of Lipids. 2007;150(2):143–155. doi:10.1016/j.chemphyslip.2007.06.224

267. Villalobos-González L, Alarcón N, Bastías R, Pérez C, Sanz R, Peña-Neira Á, Pastenes C. Correction: Villalobos-González et al. Photoprotection Is Achieved by Photorespiration and Modification of the Leaf Incident Light, and Their Extent Is Modulated by the Stomatal Sensitivity to Water Deficit in Grapevines, (Plants, (2022), 11, (1050), 10.3. Plants. 2022;11(16). doi:10.3390/plants11162096

268. Vishwakarma A, Bashyam L, Senthilkumaran B, Scheibe R, Padmasree K. Physiological role of AOX1a in photosynthesis and maintenance of cellular redox homeostasis under high light in Arabidopsis thaliana. Plant Physiology and Biochemistry. 2014;81:44–53. doi:10.1016/j.plaphy.2014.01.019

269. Vitova M, Bisova K, Kawano S, Zachleder V. Accumulation of energy reserves in algae: From cell cycles to biotechnological applications. Biotechnology Advances. 2014;33(6):1204–1218. doi:10.1016/j.biotechadv.2015.04.012

270. Vítová M, Bišová K, Umysová D, Hlavová M, Kawano S, Zachleder V, Čížková M. Chlamydomonas reinhardtii: Duration of its cell cycle and phases at growth rates affected by light intensity. Planta. 2011;233(1):75–86. doi:10.1007/s00425-010-1282-y

271. Wagner H, Jakob T, Lavaud J, Wilhelm C. Photosystem II cycle activity and alternative electron transport in the diatom Phaeodactylum tricornutum under dynamic light conditions and nitrogen

limitation. Photosynthesis Research. 2016;128(2):151–161. doi:10.1007/s11120-015-0209-7

272. Wagner H, Jakob T, Wilhelm C. Balancing the energy flow from captured light to biomass under fluctuating light conditions. New Phytologist. 2006. doi:10.1111/j.1469-8137.2005.01550.x

273. Wang W, Zhao S, Pi X, Kuang T, Sui S, Shen J. Structural features of the diatom photosystem II–light-harvesting antenna complex. The FEBS Journal. 2020;287(11):2191–2200. https://onlinelibrary.wiley.com/doi/10.1111/febs.15183. doi:10.1111/febs.15183

274. Waring J, Klenell M, Bechtold U, Underwood GJC, Baker NR. Light-induced responses of oxygen photoreduction, reactive oxygen species production and scavenging in two diatom species. Journal of Phycology. 2010;46(6):1206–1217. doi:10.1111/j.1529-8817.2010.00919.x

275. Weber T, Gruber A, Kroth PG. The presence and localization of thioredoxins in diatoms, unicellular algae of secondary endosymbiotic origin. Molecular Plant. 2009;2(3):468–477. http://dx.doi.org/10.1093/mp/ssp010. doi:10.1093/mp/ssp010

276. Weger HG, Herzig R, Falkowski PG, Turpin DH. Respiratory losses in the light in a marine diatom: Measurements by short-term mass spectrometry. Limnology and Oceanography. 1989;34(7):1153–1161. http://doi.wiley.com/10.4319/lo.1989.34.7.1153. doi:10.4319/lo.1989.34.7.1153

277. Wilhelm C, Büchel C, Fisahn J, Goss R, Jakob T, LaRoche J, Lavaud J, Lohr M, Riebesell U, Stehfest K, et al. The Regulation of Carbon and Nutrient Assimilation in Diatoms is Significantly Different from Green Algae. Protist. 2006;157(2):91–124. doi:10.1016/j.protis.2006.02.003

278. Wilhelm C, Goss R, Garab G. The fluid-mosaic membrane theory in the context of photosynthetic membranes: Is the thylakoid membrane more like a mixed crystal or like a fluid? Journal of Plant Physiology. 2020;252(July):153246. https://doi.org/10.1016/j.jplph.2020.153246. doi:10.1016/j.jplph.2020.153246

279. Wilhelm C, Jungandreas A, Jakob T, Goss R. Light acclimation in diatoms: From phenomenology to mechanisms. Marine Genomics. 2014;16(1):5–15. http://dx.doi.org/10.1016/j.margen.2013.12.003. doi:10.1016/j.margen.2013.12.003

280. Wilhelm C, Wild A. The Variability of the Photosynthetic Unit in Chlorella II. The Effect of Light Intensity and Cell Development on Photosynthesis, P-700 and Cytochrome f in Homocontinuous and Synchronous Cultures of Chlorella. Journal of Plant Physiology. 1984;115(2):125–135. http://dx.doi.org/10.1016/S0176-1617(84)80059-0. doi:10.1016/S0176-1617(84)80059-0

281. Witt HT. Energy conversion in the functional membrane of photosynthesis. Analysis by light pulse and electric pulse methods. The central role of the electric field. BBA Reviews On Bioenergetics. 1979;505(3–4):355–427. doi:10.1016/0304-4173(79)90008-9

282. Wolfe-Simon F, Grzebyk D, Schofield O, Falkowski PG. The role and evolution of superoxide dismutases in algae. Journal of Phycology. 2005;41(3):453–465. doi:10.1111/j.1529-8817.2005.00086.x

283. Wollman FA. State transitions reveal the dynamics and flexibility of the photosynthetic apparatus. EMBO Journal. 2001;20(14):3623–3630. doi:10.1093/emboj/20.14.3623

284. Wostrikoff K, Mackinder LCM. Rubisco and inorganic carbon assimilation. In: The Chlamydomonas Sourcebook. Vol. 2. Elsevier; 2023. p. 223–271. https://linkinghub.elsevier.com/retrieve/pii/B9780128214305000158. doi:10.1016/B978-0-12-821430-5.00015-8

285. Wu H, Cockshutt AM, McCarthy A, Campbell DA. Distinctive Photosystem II Photoinactivation and Protein Dynamics in Marine Diatoms. Plant Physiology. 2011;156(4):2184–2195.

http://www.plantphysiol.org/cgi/doi/10.1104/pp.111.178772. doi:10.1104/pp.111.178772

286. Yamano T, Sato E, Iguchi H, Fukuda Y, Fukuzawa H. Characterization of cooperative bicarbonate uptake into chloroplast stroma in the green alga Chlamydomonas reinhardtii. Proceedings of the National Academy of Sciences of the United States of America. 2015;112(23):7315–7320. doi:10.1073/pnas.1501659112

287. Yang R, Wei D, Xie J. Diatoms as cell factories for high-value products: chrysolaminarin, eicosapentaenoic acid, and fucoxanthin. Critical Reviews in Biotechnology. 2020;40(7):993–1009. doi:10.1080/07388551.2020.1805402

288. Young JN, Heureux AMC, Sharwood RE, Rickaby REM, Morel FMM, Whitney SM. Large variation in the Rubisco kinetics of diatoms reveals diversity among their carbon-concentrating mechanisms. Journal of Experimental Botany. 2016;67(11):3445–3456. doi:10.1093/jxb/erw163

289. Yu G, Nakajima K, Gruber A, Rio Bartulos C, Schober AF, Lepetit B, Yohannes E, Matsuda Y, Kroth PG. Mitochondrial phosphoenolpyruvate carboxylase contributes to carbon fixation in the diatom Phaeodactylum tricornutum at low inorganic carbon concentrations. New Phytologist. 2022;235(4):1379–1393. doi:10.1111/nph.18268

290. Zaharieva I, Wichmann JM, Dau H. Thermodynamic limitations of photosynthetic water oxidation at high proton concentrations. Journal of Biological Chemistry. 2011;286(20):18222–18228. http://dx.doi.org/10.1074/jbc.M111.237941. doi:10.1074/jbc.M111.237941

291. Zhou L, Gao S, Wu S, Han D, Wang H, Gu W, Hu Q, Wang J, Wang G. PGRL1 overexpression in Phaeodactylum tricornutum inhibits growth and reduces apparent PSII activity. Plant Journal. 2020;1:1850–1857. doi:10.1111/tpj.14872

292. Zimmer D, Swart C, Graf A, Arrivault S, Tillich M, Proost S, Nikoloski Z, Stitt M, Bock R, Mühlhaus T, et al. Topology of the redox network during induction of photosynthesis as revealed by time-resolved proteomics in tobacco. Science Advances. 2021;7(51). https://www.science.org/doi/10.1126/sciadv.abi8307. doi:10.1126/sciadv.abi8307

Acknowledgments

D.C., E.J and B.B. acknowledge funding from the ERC Starting Grant PhotoPHYTOMICS (ERC-2016-STG grant # 715579) and the “Initiative d’ Excellence” Program from the French state (“DYNAMO” grant, ANR-11-LABX-0011-0). E.J also acknowledges the ANR Browncut (ANR-19-CE20-0020). B.B. also acknowledges the Centre National de la Recherche Scientifique.

Chapter 3

The molecular actors and mechanism of NPQ in pennate diatoms

3.1 NPQ models and assumptions behind variable fluorescence measurements

As mentioned in the general introduction on NPQ (Section 1.4) and in the second review of Chapter 2 (Croteau et al., 2024), NPQ in diatoms consists of two components: a relatively fast-relaxing component called qZ (Blommaert et al., 2021) and a slow-relaxing component related to photoinhibition-dependent quenching (qI). The qZ component requires both the de-epoxidation of xanthophyll pigments and the presence of Lhcx proteins. In *P. tricornutum* grown under non-stress conditions, only the DD/DT cycle and the Lhcx1 protein are constitutively present. It has been shown that Lhcx2/3 can functionally replace Lhcx1 (Buck et al., 2019) and that the VAZ-cycle can substitute for the DD/DT cycle (Giossi et al., 2024) under light stress conditions. However, this substitution does not occur with the experimental conditions used in this Chapter. Therefore, the main objective is to explore the interplay between DT and Lhcx1 and, their roles in NPQ generation. To achieve this, we used our "photoprotection-dial", which consists of a series of complemented Lhcx1-knockout mutants, accumulating the protein to varying extent and therefore, displaying varying NPQ capacities. We then modulated the de-epoxidation state (DES) of xanthophyll pigments of these strains with different light perturbations. This approach allowed the creation of Lhcx1 vs. DES matrices, in which we measured photochemical and non-photochemical PSII efficiencies, to gain a deeper understanding of the NPQ/qZ mechanism and the specific roles of Lhcx1 and DT.

This Chapter has a second objective. The concomitant measurements of the photochemical and non-photochemical efficiencies of PSII allow us to test the nature of non-photochemical quenching in PSII: does it behave as a homogeneous Stern-Volmer quencher? i.e., does NPQ compete with photochemistry the same way an exogenous quencher does with chlorophyll *a* fluorescence dissolved solution? Interestingly, investigating this question is also an adequate way to test in diatoms the validity of the theoretical framework (the "lake model") that is widely used in photosynthesis studies based on Chl *a* fluorescence (Kramer et al., 2004). From this point of view, it is important to recall the different assumptions underlying the "lake model" and the fluorescence-based parameters routinely used in photosynthesis, such as NPQ, Fv/Fm, and others.

Almost all variable fluorescence parameters are derived from the minimal and maximal F

levels, of which the physiological meanings is anchored in a set of assumptions. Therefore, any physiological interpretation of PSII fluorescence parameters is dependent on how much can be trusted assumptions that are considered reasonable approximation in most scenarios, but that are not absolute truths. The challenge in integrating this theoretical framework into practical work is to ensure that the experimental conditions and physiological assumptions used to interpret the results align with the limitations of this approach. For a full discussion of the limitations of the "lake model" and commonly used fluorescence parameters, see reviews by (Alexandrina Stirbet, 2011, Lazár, 2015). Below, I describe some of these assumptions and discuss some diatom-specific considerations that will be essential to keep in mind in this Chapter 3.

1. **Fluorescence emanating from PSI is considered negligible compared to PSII.** Although there is critical need for more thorough research on this topic, especially across different photosynthetic groups, two main claims support this approximation are **i)** PSI fluorescence contribution at room temperature is usually small compared to PSII (<25% of F_0) (Trissl et al., 1993), although it can sum up to 50% in organisms with high PSI:PSII stoichiometry like C4-plants (Genty et al., 1990, Pfündel et al., 2013). In microalgae, by comparison with plants, low re-absorption in the near-infrared and fairly similar fluorescence spectra between FCPI and FCPII (Herbstová et al., 2015), allow to measure F at shorter wavelength (around 690 nm) with better signal-to-noise ratio and less prone to PSI artefact. **ii)** PSI fluorescence is considered to be *non-variable*. This assumption stems from observation that closed RCI, e.i., $P700^+$, was as efficient a non-photochemical quencher as the pair P700-A_0 (open RCI) was a photochemical quencher (Butler, 1978). Meaning the yield of fluorescence (Φ_F) for PSI is independent of the redox state of its donor side (but an influence of the redox state on the PSI acceptor side on Φ_F has been recently suggested in plants (Schreiber, 2023)). Supporting this claim are also the F decays kinetics unaffected by the redox state of P700 (Il'ina et al., 1984, Hecks et al., 1994, Savikhin et al., 2000). Nevertheless, this concept remains challenged to this day, *in vivo* in specific conditions in plants (Schreiber, 2023), *in silico* (Lazár, 2013) and *in vitro* with purified PSI of green organisms (Telfer et al., 1978), cyanobacteria (Byrdin et al., 2000), and more recently, of the centric diatom *Chaetoceros gracilis* (Nagao et al., 2020). It is noteworthy that in most *in vitro* studies, P700 is chemically reduced before measuring exciton trapping efficiency and that the reducing agent itself can quench excited Chl *a* (Wientjes and Croce, 2012). By controlling for this bias (Wientjes and Croce, 2012) estimated a Φ_F approximately 4% higher for closed rather than open PSI of isolated *Arabidopsis* chloroplasts. In sum, if the Φ_F of PSI is non negligible and *non-variable*, it can be easily corrected by subtracting a fluorescence background signal to the measured values (Pfündel, 2021). In the instance where the Φ_F of PSI is non negligible and *variable*, data should reflect a complex case of heterogeneity (see below and (Lazár, 2013)).

2. **A lake model is assumed**. The lake versus puddle model argument revolves around the level of connectivity, or exciton sharing, between PSII reaction centres (RCIIs). In a **lake model**, *all* RCs are connected by a *common* pigment bed, and unrestricted exciton sharing will lead to a charge separation if at least one RC is open. In this extreme scenario, the theoretical curve of fluorescence rise would be a step function jumping from F_0 to F_M once the first photon after all Q_A have been reduced is absorbed. In the opposite **puddle model**, all RCIIs possess their individual light-harvesting antenna and there is no sharing of excitons between these independent photosynthetic units. In

this case, the chance of closing a RCII obeys a Poisson distribution and a first-order exponential saturation fluorescence rise is expected. Nevertheless, it is well known that experimental fluorescence curves are rather sigmoidal (Joliot, 1965, Delosme, 1967), indicating partial connectivity. Some intermediate, more complex, models suggest exciton migration is restricted within "packages" of RCIIs sharing the same antenna or that exciton transfers between individual (puddle-like) units are possible but restrained by a probability function (reviewed in (Stirbet, 2013)). Many PSII fluorescence parameters introduced in Section 1.3.2 are compatible with both lake and puddle models (Klughammer and Schreiber, 2008). This is the case for ΦPSII which has proven to be very robust when comparing $rETR_{II}$ to O_2 evolution as a function of light intensity (Genty et al., 1989). However, the meaning of other parameters such as NPQ depends on the type of photosynthetic unit. For instance, NPQ can be used as a measure of the concentration of a non-photochemical quencher only if a lake model is considered (Lavergne and Trissl, 1995, Kramer et al., 2004).

3. **De-excitation pathways rate constants do not change over the course of an experiment.** This means that k_F, k_H, k_P and k_{NPQ} (see Section 1.3.2) are intrinsic properties of the biological material investigated. They might change depending on growth and pre-treatments, but do not change over the course of a short (scale of minutes) experiment. Therefore, changes in the amplitude of different de-excitation pathways reflect variations in photochemical quencher concentration, but not in the associated rate constants (see Section 1.3.2). The fact that k_{NPQ} is often considered variable is simply a black box actually reflecting the limits of our understanding of both NPQ and the variable fluorescence model. In contrast, the amplitude of de-excitation due to NPQ can be expressed as the product of the (invariable) rate constant k_{NPQ} times the concentration of a quencher molecule Q in the Stern-Volmer model (1.22). Lately, some fundamental concerns were raised about the invariability of k_F and k_H (Garab et al., 2023). Moreover, there are common experimental conditions, sometimes voluntarily achieved, for which this assumption is false because PSII properties change over the course of the experiment. For example, if photoinhibition occurs or photoacclimation processes (gene transcription, protein synthesis) have enough time to take place. These cases should be treated as "dynamic heterogeneity" (see below), and it is up to the experimenters to interpret the results cautiously and use the appropriate controls.

4. **The measured sample is homogeneous** In the real world, any measured photosynthetic entity, whether a single cell, a leaf or a suspension of microalgae, cannot be strictly treated as a "lake model" because it is by inevitably composed of several patches of connected PSIIs. There are probably several patches of connected PSIIs in a thylakoid, several individual thylakoids in a cell, and several individual cells in a suspension. An implicit assumption which is made is that the many "lakes" in a sample share similar properties, i.e., similar rate constants for de-excitation pathways and homogeneous concentrations of Q_A and nonphotochemical quencher Q. However, two types of heterogeneity can be considered (reviewed by (Lavergne and Briantais, 1996)). Static heterogeneity refers to different subpopulations of PSIIs in the initial state of a sample, while dynamic heterogeneity emerges if changes in energy trapping properties occur unevenly across the PSII distribution over the course of an experiment. These two types of heterogeneity exist, even when considering only the heterogeneity within thylakoids regardless of intercellular variability. Let's consider static heterogeneity first. In green organisms, photosynthetic complexes are segregated with heterogeneous stoichiometry

across distinct thylakoid regions, the stacked grana, unstacked stroma lamella or grana margins in plants (Wollenberger et al., 1994), while distinctions between appressed and non-appressed domains are reported in green algae thylakoids despite the absence of grana (Wietrzynski et al., 2020). Varying photosynthetic complexes stoichiometry could impose unequal constraints on the photosynthetic ETC and ultimately produce sub-populations of PSII with different Q_A redox state or NPQ. Static heterogeneity can also be attributed to sub-populations of PSII bound to antennae of different sizes, the so-called α- and β-PSII for instance (Lavergne and Briantais, 1996). In diatoms, the thylakoid membranes are loosely arranged and no sub-populations of functional PSII have been reported, but PSII and PSI are more abundant in the internal and external thylakoidal membranes, respectively ((Flori et al., 2017, also discussed in (Croteau et al., 2024)). Let's now consider the case of dynamic heterogeneity, i.e., changes in PSII properties occur unevenly across the PSII distribution over the course of an experiment. A typical example is during acute light stress when some PSIIs suffer photodamages (reviewed in (Campbell and Serôdio, 2020, Campbell and Tyystjärvi, 2012)). Making matters even more complex, sub-populations of PSII can undergo different steps of the PSII clearance/repair cycles at different rates and further increase heterogeneity(Campbell and Tyystjärvi, 2012, G. Li et al., 2016).

Finally, when working with cultures of unicellular organisms, another possible source of heterogeneity (static or dynamic) could be physiological differences between the cells (even more critical with natural samples). It is usually assumed that all cells in a culture exhibit homogeneous properties when they are in exponential growth, however, this assumption has never been exhaustively challenged.

The work from this Chapter resulted in a scientific paper that has been accepted in the journal *Nature Communications* at the time of the deposit of this thesis.

3.2 Article: Pennate diatoms make Non Photochemical Quenching as simple as possible, but not simpler

Pennate diatoms make Non-Photochemical Quenching as simple as possible, but not simpler

Dany Croteau, Marianne Jaubert, Angela Falciatore, Benjamin Bailleul*

CNRS, Sorbonne Université, Institut de Biologie Physico-Chimique, Laboratoire de Photobiologie et Physiologie des Plastes et des Microalgues - P3M, UMR7141, F-75005 Paris, France

*Corresponding author: bailleul@ibpc.fr

Abstract

Studies of marine microalgal photosynthesis are heavily moulded on legacy research from organisms like *Arabidopsis* and *Chlamydomonas*, despite the differences between primary and secondary endosymbionts. Non-photochemical quenching (NPQ) protects photosystem II from excessive light and, in pennate diatoms, requires the xanthophyll pigment diatoxanthin and Lhcx proteins. Although NPQ's relationship with diatoxanthin is straightforward, the role of Lhcx proteins has been unclear and at the core of several conflicting NPQ models, often unnecessarily borrowing the complexity of models from green organisms. We used 14 *Phaeodactylum tricornutum* strains, including 13 transgenic lines with variable Lhcx1 expression levels, grew them under two non-stressful light conditions, and modulated diatoxanthin levels through short light stress. The resulting Lhcx1-diatoxanthin matrices were used to demonstrate that NPQ is proportional to the product of the Lhcx1 concentration and the proportion of diatoxanthin in the xanthophyll pool. This indicates that the interaction between diatoxanthin and Lhcx1 creates a homogeneous Stern-Volmer quencher responsible for NPQ. Additionally, we demonstrated that the photosynthetic unit in pennate diatoms follows a "lake" model, with discrepancies in the NPQ-photochemistry relationship arising from unconsidered assumptions, one possibility being cellular heterogeneity. This underscores pennate diatoms as natural reductionist system for studying marine photosynthesis.

Abbreviations

Δψ: transthylakoidal electric field

σPSII: functional absorption cross-section of PSII

Chl: chlorophyll

DD: diadinoxanthin

DES: De-Epoxidation State

DT: diatoxanthin

F_0: minimal fluorescence

F_0': minimal fluorescence in the presence of NPQ

F_M: maximal fluorescence

F_M': maximal fluorescence in the presence of NPQ

F_{MR}: maximal fluorescence at the end of fast-relaxing phase of NPQ relaxation

F_V/F_M: maximal quantum yield of PSII in the dark

F_V'/F_M': potential quantum yield of PSII in the dark in the presence of NPQ

F_V/F_{MR}: maximal quantum yield of PSII in the dark at the end of fast-relaxing phase of NPQ relaxation

IL: Intermittent Light

LL: Low Light

ML: Moderate Light

NPQ: Non-Photochemical Quenching

PS: photosystem

Q_A: Primary Quinone acceptor of Photosystem II

qE: energy-dependent quenching

qI: photoinhibition-related quenching

qZ: zeaxanthin-dependent quenching

$R_{exp/th}$: Ratio of experimental-to-theoretical F_V'/F_M'

SV: Stern-Volmer

56 **XC**: Xanthophyll Cycle

Introduction

By comparison with plants and green algae, the model pennate diatom *Phaeodactylum tricornutum* is, in many ways, a simplified system to appreciate the constraints and regulatory networks that outline photosynthesis. For instance, its four plastid membranes are loosely arranged and show no heterogeneous lateral segregation of photosynthetic complexes, both photosystem (PS) have similar absorption spectra and typically accumulate at roughly equivalent stoichiometry (see review [1]). Such features combined with growing molecular tools adapted to diatoms, make of *P. tricornutum* an ideal model to probe the specific challenges that apply to the oceanic fraction of photosynthesis [2] (≈50% of global primary production [3]), its adaptations to marine environments (specific light environment, HCO_3- as the main C source, no hydric stress, etc.) and its plasticity in the context of climate change. Indeed, phototrophs derived by secondary endosymbiosis events (mainly diatoms, haptophytes and dinoflagellates), and not primary endosymbionts of the green lineage, dominate photosynthesis in the Ocean. Strikingly, the main photosynthetic complexes are exceptionally well conserved across organisms and the universal goal of photosynthesis is to match light harvesting with NADPH/ATP demands in dynamic environments. Yet, to adapt to niche-specific challenges and fuel original metabolic pathways [4,5], a plethora of regulatory pathways and antenna proteins evolved across groups [6]. Still how this diversity affects functions remains often overlook as, rich of more than a century of research on *Arabidopsis,* common crops, *Chlamydomonas* and *Chlorella*, the "green paradigm" chiefly rules how photosynthesis experiments are conducted and interpreted regardless of the (eukaryotic) organism studied.

This is nicely exemplified by the case of non-photochemical quenching (NPQ). By increasing the proportion of PSII chlorophyll (Chl) *a* de-excitation through heat releasing pathways, NPQ is crucial to limit risks of generating destructive oxygen species leading to PSII photoinhibition and thus, deeply influence global carbon fluxes [7]. While NPQ is observed in virtually all phototrophs, it arises from collections of mechanisms, governed by a multitude of different molecular players and varying with acclimation conditions [6]. Several mechanisms are known to affect PSII fluorescence and muddle NPQ interpretation in plants, red algae and cyanobacteria, like state-transition [8], chloroplast movements [9], and PSII-to-PSI spillover [10]. Those mechanisms appear absent in *P. tricornutum* and all diatoms so far [11]. Moreover, in contrast to the compounded nature of NPQ in most organisms, *P. tricornutum*'s NPQ relaxes as a mono-exponential decay in darkness with a lifetime of ≈10 min (if the quenching associated with PSII

damages (qI) is avoided). In pennate (and some centric) diatoms, NPQ is linearly correlated to the de-epoxidized xanthophyll pigment diatoxanthin (DT) [12–18]. Diatoms possess a single-step xanthophyll cycle (XC) which converts diadinoxanthin (DD) into DT [19], versus the two-steps XC in other organisms [20,21]. The proportion of the xanthophyll pigments active in NPQ (i.e., DT) is called de-epoxidation state (DES) and is calculated as DT/(DD+DT)).

These features suggest that NPQ in *P. tricornutum* is a very simple process. The linear relationship between NPQ and DT resembles the behaviour of a homogeneous Stern-Volmer (SV) quencher Q in solution, where the extent of fluorescence quenching is expressed as its concentration $[Q]$ multiplied by its quenching rate constant (κ_{SV}). In photosynthesis, the "lake" model defines a photosynthetic unit containing numerous PSII complexes embedded in a common light-harvesting antenna and competing for excitons [22,23]. The yield of each process involved in excited Chl *a* relaxation (fluorescence, heat dissipation, photochemistry or NPQ) is then determined by the kinetic competition between their rate constants, the one of photochemistry being proportional to the concentration of open reaction centres with oxidized Q_A ($[Q_A]$) [24,25] (see Text S1 for details). Therefore, an SV-quencher in a lake model (hereafter called "SV-lake" model), predicts two equations relating NPQ to $[Q]$ (Equation 1) and to the photochemical yield of PSII (Equation 2):

Equation 1

$$\mathrm{NPQ} = {F_M}/{F_M'} - 1 = \kappa_{SV}[Q]$$

where F_M and F_M' are maximal fluorescence in darkness, before and following light perturbation, respectively.

Equation 2

$${F_V'}/{F_M'} = {F_V}/{F_M} \times \left(1 - f(NPQ)\right),$$

$$\text{with } f(NPQ) = \frac{\left(1-{F_V}/{F_M}\right)\times \mathrm{NPQ}}{\left(1+\left(1-{F_V}/{F_M}\right)\times \mathrm{NPQ}\right)}$$

Where F_V'/F_M' and F_V/F_M are maximum yield of PSII in the dark ($[Q_A] = 1$), with and without NPQ, respectively, and where f(NPQ) represents the expected relative decrease in F_V'/F_M' for a given value of NPQ. Considering that functional absorption cross-section (σPSII) and maximum quantum yield of PSII vary together and remain proportional as heat dissipation processes take place in the antenna [26], the relationship between σPSII and NPQ should also follow Equation 2

(see Text S1). The lake model is a theoretical simplification, in practice, photosynthetic samples are composed of non-connected domains (e.g., different cells, different thylakoids within a cell). However, multiple domains do not necessarily invalidate the lake model provided all domains in the sample behave as a "lake" and share homogeneous properties/parameters ([Q_A], [Q] and de-excitation pathways' rate constants). Many attempts were made for more precise, and complex, models, intermediate between the "lake" model and the "puddle" model which considers that each PSII has its own independent light-harvesting system [22,23]. Yet, the lake model provides immense descriptive and predictive power despite its simplicity and is used to derive a multitude of photosynthetic parameters (see Text S1).

Several groups tested the "SV-lake" model in *P. tricornutum*. Although the linear relationship between NPQ and DT (Equation 1) still holds, deviations from theory were reported regarding the relationship between NPQ and PSII photochemistry (Equation 2). In [12], the authors measured a larger than predicted non-photochemical quenching of minimal fluorescence (F_0', open PSII reaction centres), relative to the non-photochemical quenching of maximal fluorescence (F_M', closed reaction centres) (see Text S1). In [27], a higher than predicted F_V'/F_M' for a given NPQ, or an apparent "excess of PSII photochemistry", was reported. In both scenarios, the efficiency of the non-photochemical quencher appeared higher when reaction centres were open rather than closed, a pattern previously coined "economic quenching" in plants [28]. More recently, higher than predicted σPSII for a given NPQ was similarly interpreted as an "*antenna uncoupling*" model [29], another model inspired by plants [30,31], but intrinsically incompatible with an SV-lake model. Depending on models, the functional uncoupling of PSII antenna would either entirely explain Chl *a* fluorescence decrease [29], or act as the main mechanism among two quenching processes [27,32,33]. Due to the expected proportionality between σPSII and F_V'/F_M', the different observations (both σPSII and F_V'/F_M' higher than predicted) likely indicate a shared phenomenon (see Text S1) that seems *a priori* inconsistent with the SV-lake model.

Another challenge concerns the nature of the SV-quencher, which cannot be DT *alone* since the slope of the NPQ vs. DT relationship is highly variable between growth conditions [13,15,16,34–36]. Two explanations have been proposed, which are not mutually exclusive. First, a low luminal pH could "activate" DT by protonating the acidic residues of some protein partners [14,37], similar to the role of PsbS in plants [38] or LHCSR3 in *Chlamydomonas* [39]. Second, variations in the slope may

arise from differences in the proportion of xanthophylls associated to PSII antenna. Indeed, other xanthophyll pools have been described, including one soluble in the lipid phase and one associated to PSI [35,36,40]. Another argument against the original idea that DT *alone* acts as an SV-quencher [12,41] is the strict requirement of a second molecular effector for NPQ: Lhcx proteins [42,43], which are LHC stress-related sub-family close to LHCSR3 [44]. Each diatom species relies on a distinct array of Lhcx isoforms. *Phaeodactylum tricornutum* possesses four of them. Lhcx1-2-3 influence NPQ levels [29], but only Lhcx1 is constitutively expressed [42]. Unlike in plants, where high-energy quenching (qE) can occur in the absence of PsbS or in the absence of zeaxanthin [21], both Lhcx proteins and DT are mandatory for the reversible NPQ in *P. tricornutum* [29].

With PSII fluorescence as sole observable, all models and hypotheses presented above are doomed to self-referential dead-ends when it comes to determining whether apparent incongruities convey information about "real" photophysiological features or about the validity of the "SV-lake" model. Pennate diatoms could offer the exceptional opportunity to test the coherence of the "SV-lake" model via a second observable, [Q], provided its nature can be elucidated and measured. Due to its simplicity and predictive power grounded in established physical principles, identifying a natural system for which the "SV-lake" model applies without incoherencies would be a pivotal step in photosynthesis research. To strive towards these goals, identifying the nature of Q and testing the "SV-lake" model, we introduce a novel approach involving "molecular titration" of Lhcx1. We generated 13 transgenic strains which, together with *P. tricornutum* wildtype, can be seen as a continuum of Lhcx1 concentration rather than discrete entities. These strains were grown under two non-stressful growth conditions, leading to the expression of the Lhcx1 isoform only. We modulated the amount of DT with brief light stress, allowing us to explore NPQ (and other parameters such as σPSII or F_V'/F_M') in two Lhcx1×DES matrices defined by each growth condition. These data allowed us to establish robust phenomonological relationships between NPQ, DT and Lhcx1, identify a promising candidate for the homogeneous SV-quencher and revisit the validity of the "SV-lake" model in pennate diatoms.

Results

Varying Lhcx1 and diatoxanthin concentrations, everything else equal

Both Lhcx1 and DT influence NPQ levels [12,29], but their respective concentrations have never been modulated and quantified simultaneously under controlled conditions to develop a simple and comprehensive model unifying their respective involvement in NPQ. To do so, we used a "molecular titration" approach by cultivating wildtype (WT) *P. tricornutum* (Pt2, CCAP 1052/1A) and 13 transgenic strains (Lhcx1-KO and 12 Lhcx1-complemented (described in [45])), under two non-stressful growth conditions known to be associated with contrasted XC pigments and Lhcx1 accumulations (Fig. 1). Other isoforms are not or barely expressed in the absence of high light periods [42,45] or nutrient deprivation[46]. We first measured Lhcx1 accumulation in the 14 strains grown under intermittent light (IL) conditions using Western blots, as we had previously done for these strains grown under the low light (LL) conditions (first reported in [45]). Normalizing Lhcx1 accumulation to its maximal value (IL-grown complemented strain LtpM, for Lhcx1 Talen target site modified plasmid, strain M) provided a relative [Lhcx1] scale encompassing all strains and growth conditions, used for the colour code in the figures (see Methods). [Lhcx1] ranged from 0 to 0.37 ± 0.02 under LL and from 0 to 1 under IL, confirming larger pools of Lhcx1 under IL than LL. The WT displayed intermediate values of 0.07 ± 0.03 under LL, and 0.68 ± 0.11 under IL conditions (Fig. 1 and Fig. S1).

Then, we tested whether inter-strains baseline physiology was influenced by [Lhcx1]. Overall, under LL and IL, linear regression analysis indicated that broad changes in [Lhcx1] did not significantly influence (p.value>0.05) baseline physiological parameters (Table 1) like growth rates (only measured in LL), the maximum quantum yield (F_V/F_M) and functional absorption cross-section (σPSII) of PSII, and the light-harvesting pigments composition (Fig. 1d-g). However, F_V/F_M, σPSII and the content of fucoxanthin and Chl *c*, relative to Chl *a*, were all significantly higher (10-20%) under LL than IL (p.value<0.01, One-Way ANOVA) (Fig. 1 and Fig. S2). Unexpectedly, photoprotective pigments (xanthophylls and β-carotene) correlated significantly with [Lhcx1], which resulted in a significant increase of the xanthophyll-to-β-carotene ratio, by ≈100% under LL and ≈50% under IL, from lowest to highest [Lhcx1] (p.value < 0.01, Table 1 and Fig. 2b). This expands the space within which we can test NPQ models, as we have two independent Lhcx1-DES matrices associated to distinct PSII characteristics and light-harvesting

antenna. Nevertheless, for each growth condition, baseline physiology was largely unaffected by [Lhcx1], allowing us to explore variations of Lhcx1 and/or DT (using different light protocols, see below), everything else being roughly equal.

Relationships between NPQ, de-epoxidation state and Lhcx1

We first measured NPQ, using a fluorescence imaging system, and xanthophyll pigments by HPLC under steady-state conditions at different light intensities and at different relaxation times after a shift from high light to darkness (see Methods). To compare treatments with varying xanthophyll pools (Fig. 2), we correlated NPQ to DES, but all relationships with DT are found in Fig. S3 to S6. When NPQ relaxation was followed, we observed that the fully relaxed F_M' returns to a value very close to the initial dark-adapted F_M (Fig. S4a-b). This confirmed that only a fast-relaxing component of NPQ was significant in our experiments, allowing us to neglect contributions from photoinhibition-related quenching (qI) in our interpretation of the NPQ data.

As a function of light intensity, NPQ and DES followed sigmoidal curves [47] (Fig. 3a-d). As expected, larger [Lhcx1] resulted in larger capability to deploy NPQ among strains, and the relationship between maximal NPQ (NPQ_M, see Methods) and [Lhcx1] (Table 1) scaled near-perfectly across both growth conditions (R^2=0.97) (Fig. 2a). The other fitted parameters, the light intensity for half-saturation (*E*50NPQ) and the sigmoidal coefficient (*n*), also varied significantly (*p*.value < 0.05) with [Lhcx1] (Table 1 and see Methods). All strains appeared to converge towards a similar DES plateau of 40% for LL (Fig. 3e). Under IL, most strains did not reach saturated DES value at the highest light intensity, with only Lhcx1-KO stabilizing around 60% (Fig. 3f). Unsurprisingly, NPQ was strongly linearly correlated with DES (Fig. 3c-d) and DT (Fig. S3) for all strains and growth conditions; however, with very different slopes depending on their [Lhcx1]. Specifically, the slope of the NPQ vs. DES relationship was proportional to [Lhcx1] regardless of growth conditions (Fig. 3g). The robust relationship between NPQ, [Lhcx1] and DES, across strains, light intensities and growth conditions (despite significant variations between LL and IL PSII characteristics, see Fig. 1 and Fig. S2) prompted us to test its stability during transitory phases. Indeed, this relationship was maintained during NPQ relaxation in darkness for LL strains (Fig. S4-S5 and open symbols in Fig. 3f-g). For IL strains, NPQ relaxation in darkness was faster than in LL, and the NPQ/DES relationship deviated from strict proportionality for some strains, showing a trajectory that did not pass through the origin of the axes. This complicated the linear

fit (see Fig. S5 and Discussion). Overall, Lhcx1 appears to act as an NPQ enhancer for a given DES, so that NPQ could be expressed as 0.25 × [Lhcx1] × DES in our relative scale (Fig. 3h). Conversely, no strong relationship encompassing both growth conditions was found between NPQ, [Lhcx1] and DT (Fig. S6).

The phenomenological relationship between NPQ, [Lhcx1] and DES, remains robust across 9 strains, six light intensities, steady-state and transitory phases, and two different growth conditions (Fig. 3h). It supports the concept of a homogeneous Stern-Volmer non-photochemical quencher (*Q*), whose quenching coefficient is consistent across the two light conditions (see Discussion) and whose concentration corresponds to [Lhcx1] × DES for the Lhcx1 quantification used here. This conserved relationship provides significant insight into the nature and molecular mechanism of NPQ. First, it strongly argues against a composite nature for NPQ in *P. tricornutum* in contrast to *Chlamydomonas* or *Arabidopsis* [6]. It is hardly reconcilable (see Discussion) with complex NPQ models involving two quenching sites (e.g., [27,32,33]) direct pH regulation of LHCSR3/PsbS as in green organisms [38,39] or PSII antenna uncoupling [29]. Instead, this robust relationship supports the previous proposal [48] that a single component dominates rapidly reversible NPQ in pennate diatoms. This NPQ component being strictly proportional to the proportion of de-epoxidized xanthophyll, it is analogous to the strictly zeaxanthin-dependent and slowly relaxing component qZ, observed in *Arabidopsis* PsbS mutants [21,49] (see Discussion). Overall, these observations are compatible with a model where the SV-quencher *Q* is generated by DT interacting with Lhcx1. Assuming each Lhcx1 protein interacts with DD/DT (possibly via binding see [50] and Discussion) and that only the Lhcx1-DT complex generates *Q* and induces NPQ/qZ, then [*Q*] would be the product of [Lhcx1] (the concentration of xanthophyll interaction sites) and DES (the proportion of xanthophylls in the DT form) (Fig. 3i).

Relationships between photochemistry and NPQ and the SV-lake model

Given compelling results that NPQ/qZ behaves like an SV-quencher proportional to [Lhcx1]×DES in *P. tricornutum*, we decided to revisit the "SV-lake" model. This model predicts a unique relationship (Equation 2) between the potential quantum yield of PSII for photochemistry in the dark (F_V'/F_M') and NPQ level. Yet, previous studies have shown a consistent deviation from this relationship in *P. tricornutum*, indicating excess photochemistry (or excess σPSII) for a given NPQ [12,27,29]. We induced NPQ/qZ under 6 min of high light followed by concomitant monitoring

of NPQ/qZ relaxation and F_V'/F_M' recovery in darkness. The final part of this work focuses specifically on the relaxation of the NPQ in the dark, which allows us to mathematically separate the fast-relaxing component of NPQ from the slow-relaxing one. We achieved this by using, as a reference, the F_M' value at the end of the fast relaxation phase (see Methods), which was not possible in the first part of this work relying partly on steady-state NPQ values. To clarify that any minor contributions from slow-relaxing components of the NPQ, such as qI, is now excluded, we will henceforth refer to the fast-relaxing component as qZ rather than the more general and less precise term NPQ.

For comparison with previous studies, we focused on cultures acclimated to moderate light (ML) (40 µmol photons m^{-2} s^{-1}, 12:12 L:D) but LL and IL conditions were also investigated (Fig. S7-8). For ML-acclimated experiments, we selected the WT and six strains showing higher NPQ capacity than the WT under LL. The qZ reached values ranging from 2 to 4 between strains at light offset, and subsequently relaxed in darkness with a half-time of approximately 7 min (Fig. 4 and S7). To test the SV-lake model, we plotted the measured F_V'/F_M' as a function of the expected relative decrease in F_V'/F_M' due to qZ, given by the parameter $f(\mathrm{qZ})$ (instead of $f(\mathrm{NPQ})$ in Equation 2, see Methods). Like others before us [12,27], we observed that F_V'/F_M' in the early phase of qZ relaxation was larger than predicted by the SV-lake model (Fig 4b). Thus, plotting F_V'/F_M' against $f(\mathrm{qZ})$, which represents the expected relative decrease of F_V'/F_M' for a given qZ in the SV-lake model (see Equation 3 in Methods), produced a linear relationship (R^2=0.97) but, a slope of -0.68 rather than predicted -1 (Fig. 4c). We calculated the Ratio of experimental-to-theoretical F_V'/F_M', $R_{exp/th}$ (see Methods); it generally increased from 1 to 3 min after the dark transition, before reversing concomitantly with qZ relaxation (Fig. 4). The same trend was observed in strains acclimated to LL and IL (Fig. S7-8), but with smaller gap between experimental and theoretical values than in ML. Negative $R_{exp/th}$ values were also sometime observed in the first phase of the dark transition, which we interpret as PSII photochemical yield being limited by incomplete reoxidation of Q_A^- (Fig S7-8).

Having replicated observations made by others, we considered three possible explanations for this deviation from the theory. In addition to the *"PSII antenna uncoupling"* hypothesis [29] and the *"economic quenching"* hypothesis [27], we introduced a third one, the *"heterogeneity"* hypothesis, which suggests that the SV-lake model is valid locally, in each domain/cell, but with

different properties between domains. We hypothesized that the apparent "excess" PSII photochemistry might result from averaging many "lake" domains with varying properties, such as [Lhcx1] or F_V/F_M values (see empirical demonstration in Text S2). Such heterogeneity can either exist between PSII sub-populations within a cell [51] or between cells. Heterogeneity between cells is custom in microalga cultures and one way it can be visualise is by using flow cytometry and DAPI staining to measure DNA/cell and cell biovolume as markers of cell cycle phase distribution [52] (Fig 4d).

NPQ/qZ and PSII antenna uncoupling

We first examined the "*antenna uncoupling*" hypothesis. We used a similar protocol but with a fluorometer based on single turnover flashes as in [29], allowing to monitor both PSII functional cross-section (σPSII') and F_V'/F_M'in parallel to qZ relaxation, (see Methods). Consistent with [29], we observed that σPSII' decreased less than expected for a given qZ level (Fig. 5a). As noted previously, variations in σPSII' can indicate changes in the optical cross-section, i.e., the physical size of PSII antenna (i.e., "antenna uncoupling" [29]), changes in F_V'/F_M', or both. Additionally, we tracked the evolution of F_V'/F_M' relative to qZ and found a similar excess for photochemistry (Fig 5b). Throughout qZ relaxation, σPSII' remained proportional to F_V'/F_M' (Fig. 5c), implying a constant *optical* cross-section of PSII. This rejects the *"PSII antenna uncoupling"* hypothesis where NPQ stems (at least part of it) from changes in PSII optical cross-section due to physical uncoupling [27,29,32,33]. Furthermore, it indicates that deviations measured for both observables, σPSII' and F_V'/F_M', are synonymous ways of reporting the same phenomenon, whatever its underlying cause might be.

The effect of heterogeneity on the relationship between photochemical yield and NPQ/qZ.

At this point, we chose to explore the "*heterogeneity*" hypothesis. To simulate heterogeneity, we selected values compatible with our cytometry (Fig. 4d) and fluorescence measurements, as well as a level of heterogeneity in maximal qZ and F_V/F_M consistent with the single cell fluorescence reported in [53] (see full empirical demonstration in Text S2). The very good agreement between the fitted relationship and the experimental data (green line in Fig. 4c) demonstrates that intercellular heterogeneity can elucidate the deviation from the SV-lake model, without invaliding it.

To effectively distinguish between "*economic quenching*" and the "*heterogeneity*" hypotheses, we reasoned that "*economic quenching*" should be an inherent property of *Q*, independent of measurement protocols. In contrast, under the "*heterogeneity*" hypothesis, one would expect the deviation to vary depending on the degree of heterogeneity, which can be manipulated to some extent. A well-known source of heterogeneity is asynchronicity among cells in a given culture. A conventional protocol to synchronize cells involves incubating cultures in darkness for an extended period (40 h in *P. tricornutum* [52]), thereby reducing inter-cell heterogeneity as all cells complete their final cycle before reaching the same G1 phase. Indeed, flow cytometry and DAPI staining assays revealed clearly more uniform distribution in biovolume and cellular DNA after 40 h of dark incubation than for cultures sampled directly under ML (Fig. 4d and Fig. 6d). The same qZ relaxation experiment as under ML was performed after 40 hours of dark acclimation, 8 times with the same 7 strains. The reproducibility of the experiments after dark acclimation was lower than in ML, but in all 8 repetitions performed, a linear relationship was found (R^2=0.99) with slopes closer to the theoretical one than before dark acclimation (Fig. S8). Even more compelling was the observation that in four of the eight experiments (shown in Fig. 6c), the data showed an almost perfect agreement with the model, encompassing all seven measured strains. This demonstrates that more homogeneous cultures tend to deviate less from the SV-lake model and, that varying quenching efficiency between open or closed PSII centres is not an intrinsic feature of qZ.

Finally, we examined the SV-lake model using another pennate diatom, the araphid pennate *Plagiostriata* sp. (formerly *Leptocylindrus danicus* [54]). When acclimated to ML and subjected to the same protocol previously used on *P. tricornutum*, *Plagiostriata* sp. displayed qZ of approximately 2. During dark relaxation, F_V'/F_M' and qZ showed a linear relationship with a slope of -1.01 aligning almost perfectly with the SV-lake model (4 different experiments with 3 independent biological replicates each time) (Fig. 7). All those observations support the "*heterogeneity*" over the "*economic photoprotection*" hypothesis.

Discussion

To elucidate the nature and mechanism of reversible NPQ in pennate diatoms, we exploited the capability of generating, in *P. tricornutum*, transgenic lines with different Lhcx1 expression and NPQ capabilities but with similar growth, PSII photochemistry, and light-harvesting pigment

composition (Fig. 1). The only significant difference was the distribution of photoprotective xanthophylls normalized to β-carotene pigments, which strongly correlates with Lhcx1 levels (Fig. 2). This dependence suggests potential epistatic control of Lhcx1 over xanthophyll synthesis pathway, similar to the control PsbS exerts over zeaxanthin in *Arabidopsis* [38]. This "molecular titration" approach revealed a robust phenomenological relationship in which NPQ is proportional to [Lhcx1]×DES, valid across nine strains, with very different xanthophyll pool sizes, Lhcx1 concentrations, and NPQ capacities ranging from 0 to roughly 3 times the WT level. It remained valid in two growth conditions despite significant differences in pigment content, F_V/F_M and σPSII (Table 1). The substantial overlap between LL and IL on the NPQ vs DES*[Lhcx1] plot (Fig. 3h) suggests that the quencher *Q* has consistent quenching efficiency across the two growth conditions. We note however that exact comparison of *Q*'s efficiency in quenching Chl *a* fluorescence between LL and IL growth conditions would require expressing the concentration of *Q* per Chl a in PSII. This is not accessible here due to the quantification of Lhcx1 concentration via Western blot (it is normalized per (D2 + βCF1), see Methods). Nevertheless, this robust phenomenological relationship provides several valuable insights into the fundamental nature of NPQ. First, we can confidently attribute it to a single component and reject models proposing multiple quenching sites and mechanisms for NPQ in pennate diatoms, whether it be a direct role of luminal pH, PSII antenna uncoupling or a second quencher. In this work, we rejected the "*PSII antenna uncoupling*" hypothesis thanks to the observed proportionality between σPSII' and F_V'/F_M' during NPQ/qZ relaxation (Fig. 5). We propose that variations in σPSII', stemming from changes in F_V'/F_M', have been misattributed to changes in optical cross-section in previous works. Models involving multiple quenching sites might describe situations where the reversible qZ is accompanied by a slowly relaxing component, such as that related to PSII photodamage (qI) (a difficult bias to control for in fluorescence lifetime experiments [27,32,33]), which we ensured was absent from our protocols. The role of luminal pH in the NPQ of *P. tricornutum* seems limited to regulation of the diadinoxanthin de-epoxidase [48,55] without *direct* pH sensing as seen in green organisms where LHCSR3 and/or PsbS act as pH sensors [21,38,39]. Two recent studies support this distinction by showing that mutation of acidic residues in Lhcx1 –that are involved in pH sensing by LHCSR [56]- does not affect NPQ [45,50]. Our data reinforce this idea. Specifically, if the range of pH values examined here (sufficient to reach DES values from 0 to 60%) influenced NPQ independently of XC, this would disrupt the linear relationship we observe between NPQ and DES, but no such

deviation is observed. Given that qE traditionally refers to the fast-relaxing NPQ *directly* triggered by luminal pH-sensing antenna proteins, we conclude that qE does not accurately represent the fast-relaxing NPQ component in pennate diatoms. Instead, this component aligns more closely with zeaxanthin-dependent quenching (qZ), first described in *Arabidopsis* PsbS mutants [21,49]. Indeed, qZ is an NPQ component displaying slower relaxation than qE, as it depends on the conversion of the de-epoxidized pigment (zeaxanthin) back to the epoxidized form (violaxanthin). The strong correlation between fast-relaxing NPQ and DES in our work suggests that this NPQ component is better described by qZ than by qE [48], if the definition of qZ is broadened to "de-epoxidized xanthophyll-dependent quenching".

This robust relationship provides new information to ponder the molecular mechanism of NPQ/qZ and nature of the SV-quencher. Recent studies using different methods [57–59] argued that lutein acts as the nonphotochemical quencher in green organisms' qE by accepting excitation energy transfer from excited Chl *a*. Interestingly, excitation energy transfer to the S_1 state of zeaxanthin has also been suggested as the dominant quenching mechanism in *Nannochloropsis oceanica* [60]. While both *Nannochloropsis* and diatoms lack lutein, DT and zeaxanthin share an identical terminal ring structure (two in the case of zeaxanthin) to the one putatively involved in lutein's quenching activity. The comparison with *Nannochloropsis*, a closer relative to diatoms, is particularly relevant here because zeaxanthin, like DT for *P. tricornutum*, also requires interaction with an Lhcx protein to allow NPQ [20,60]. This interaction could simply be the binding of xanthophylls on Lhcx1, as supported by the latest biomolecular and structural knowledge of Lhcx1. Indeed, the mutation of a tryptophan residue conserved in all LHCSR and Lhcx proteins (Lhcx4 being a crucial exception) and located in the vicinity of a putative xanthophylls binding pocket, significantly impairs NPQ capacity in *P. tricornutum* [50]. Nevertheless, Lhcx1-DT binding is not the only possible mechanistic model for which DT interacting with Lhcx1 could form an SV-quencher. Like suggested for lutein with CP29 in plants [59], an Lhcx1 binding pocket could allow for more planar s-trans conformer of the xanthophyll, of which the S_1 state could form the quencher. Additionally, in *Arabidopsis*, zeaxanthin accumulates at the antenna periphery to induce quenching, rather than being converted from violaxanthin strongly protein-bound within the antenna [61]. The further observation that zeaxanthin-related quenching occurs in isolated membranes [62], but not in isolated complex, suggests that the peripheral zeaxanthin is weakly linked

411 and lost during the purification process [61]. In contrast, in *P. tricornutum*, isolated FCPs contain
412 both DD and DT [40] and are capable of quenching [63].

413 The "molecular titration" approach used here for Lhcx1 could also be applied to the other
414 isoforms providing NPQ capacity, Lhcx2 and Lhcx3 [29], to determine whether the quenching
415 efficiency of DT depends on the isoforms it interacts with. In this model, Lhcx1 would determine
416 the partition between xanthophylls involved in NPQ/qZ and other pools, and from there, the slope
417 of the NPQ vs. DT relationship. A similar idea was initially put forward by Schumann *et al.* [35], but
418 before discovering Lhcx proteins, this hypothesis could not be convincingly demonstrated since
419 both Lhcx concentrations and the size of xanthophylls pools vary with growth conditions [14]. We
420 can anticipate limits to the simple relationship between NPQ, Lhcx1 and DES: when the XC
421 enzymes are fast compared to the equilibrium time between the different pools of xanthophylls,
422 the DES measured experimentally (on total xanthophylls) could be different from the proportion
423 of DT interacting with Lhcx. We propose that this explains the deviation from proportionality
424 between qZ and DES in some of the strains grown in IL (Fig. S5), consistent with results from
425 [36,64]. In some IL-grown strains, some DT remains when NPQ is fully relaxed (Fig S5), likely
426 indicating that the qZ-involved xanthophyll pool undergoes faster epoxidation than the lipid-phase
427 soluble one. This interpretation is also supported by the absence of deviation in LL-grown cells,
428 where qZ relaxation (DT epoxidation) is two-fold slower, allowing more time for DES
429 equilibration between the xanthophyll pools.

430 The SV-lake model also predicts a unique relationship between the yields of photochemical
431 and non-photochemical processes (Equation 2) which is perfectly respected in the pennate diatom
432 *Plagiostriata* sp. (Fig. 7) and could be observed in 7 strains of *P. tricornutum* under certain
433 conditions (after acclimation to darkness for 40 hours) (Fig. 6). We also show that, without dark
434 acclimation in *P. tricornutum*, the potential photochemical yield and functional cross-section of
435 PSII exceed what is expected in an SV-lake model for a given level of qZ (Fig. 4c, Fig. 5). Similar
436 observations led to alternative models of "*economic quenching*" (in the case of excess F_V'/F_M'
437 [12,27]) or "*antenna uncoupling*" (in the case of excess σPSII [29]). If we excluded the "*antenna*
438 *uncoupling*" hypothesis, the discrepancy we observed remains compatible with the "*economic*
439 *quenching*" model. However, it is difficult to imagine another process that would compensate for
440 this discrepancy only in some contexts, like in *Plagiostriata* sp. or in *P. tricornutum* after 40 hours

of dark acclimation, so that the expected relationship in an SV-lake model is respected *by chance*. The most parsimonious interpretation is that the SV-lake model correctly describes the photosynthetic unit of pennate diatoms, but at least one implicit assumption behind Equation 2 is not satisfied when "excess" photochemistry is measured. One implicit assumption is that properties/parameters of the SV-lake model ($[Q_A]$, [Q], rate constants) are *homogeneous across all "lake" domains/cells* and *invariant during NPQ relaxation.* We demonstrated that realistic levels of heterogeneity (Text S2) between cells/domains obeying the SV-lake model could reproduce the apparent excess of photochemistry measured (Fig. 4c). Furthermore, experimental approaches promoting intercellular homogeneity (such as 40h incubation in darkness) eliminated this discrepancy (Fig. 6), strongly supporting the "*heterogeneity hypothesis*". If 40h incubation in darkness induces closer, but not always perfect, agreement with the SV-lake model (Fig. S8), it might be that intracellular heterogeneity remains (e.g., heterogeneous "PSII-lake" domains with different properties within a cell [51]). The possibility that parameters describing the lake model vary during the NPQ relaxation should however also be considered. Lately, questions have been raised regarding possible variations in the rate constant of PSII intrinsic losses [65]. We also recently observed a decrease in the trans-thylakoidal electric field ($\Delta\psi$) after a high light to dark transition (Croteau *et al.,* forthcoming), which could increase photochemical yield by reducing the probability of charge recombination [66,67]. Excess photochemistry under high NPQ/qZ conditions could also result from a temporarily more oxidized Q_A compared to the situation when qZ has fully relaxed. However, heterogeneity is our favourite hypothesis, a reasonable one that can naturally explain biases in F_V'/F_M' vs. NPQ/qZ relationships (always in the direction of excess photochemistry) without compromising the predictive power of the lake model. It is tempting to propose that the agreement with the lake model relates to the structural simplicity of pennate diatoms thylakoids, that are devoid of the grana stacks/lamella ultrastructure found in plants [68] or appressed/non-appressed domains found in green algae [69] and display limited PSII segregation [70].

Although its full range of validity remains to be explored, the SV-lake model can be seen as a null hypothesis to test intermediate models between lake and puddle models [23], models including heterogeneity (Text S2), additional quenching mechanisms or novel concepts [65]. The NPQ/qZ model presented here for pennate diatoms is remarkably simple compared to models for green organisms [71] or the recent model for *Nannochloropsis* [20] and offers unprecedented predictive

power. Considering other characteristics discussed in [1,11], we propose that *P. tricornutum* can be used as a "natural reductionist system" to improve our understanding of photosynthesis regulations. For example, xanthophyll cycle activity can be measured *in vivo* through chlorophyll fluorescence measurements [48]. We see great potential in generalizing the present approach - using a series of transgenic strains differing in the amount of Lhcx1 and xanthophylls, all other factors being equal - to study the orchestration of photosynthetic regulations in more detail. Using this "NPQ-dial" as an entry point allows to extract phenomenological laws describing how NPQ/qZ modulates various other aspects of photosynthesis, such as the redox state of various players the photosynthetic chain ($[Q_A]$ is conveniently assessed through the parameter qL in a lake model only [23]), the partition between cyclic and linear electron flows, or the susceptibility to PSII photodamage. Such approach has the potential to move diatoms from a footnote to photosynthesis research on green organisms and cyanobacteria, to organisms of predilection to tackle fundamental questions and strengthen our modelling capabilities.

Material and Methods

Culture and growth conditions

Wildtype *Phaeodactylum tricornutum* Bohlin CCAP 1052/1A (Pt2) and 13 transgenic Lhcx1 lines were grown in filtered (0.2 µm) seawater with added *f*/2 medium in 40 mL flasks. The transgenic lines consisted of the Lhcx1 knock-out strain (Ko6) and 12 complemented lines expressing different levels of Lhcx1 in the Ko6 background, first generated in [45]. The complemented strains are called LtpA, LtpB, etc. for Lhcx1 Talen target site modified plasmid strain A, B, C, etc. Cells were grown at 19°C under three different light conditions: low light (LL) (5 µmol photons m^{-2} s^{-1}) or medium light (ML) (40 µmol photons m^{-2} s^{-1}) both under a 12L:12D photoperiod, and intermittent light (IL) (cycles of 55 min dark and 5 min at 40 µmol photons m^{-2} s^{-1}) [12]. Cultures were monitored every 2-to-3-days for cell concentration using a Multisizer 3 Coulter counter (Beckman Coulter, CA, USA). For experiments, they were sampled in the exponential phase (between 0.7 and 1.5×10^6 mL^{-1}, always 4-to-5h into the light phase of the photoperiod), concentrated (10-15 times) by centrifugation (5000 RPM, 6 min), then left to recover on an agitator for 30 min under very low light (approximately 1 µmol photons m^{-2} s^{-1}). Cultures were rediluted approximately 10 times when reaching $2*10^6$ cells/mL to ensure they remained in

exponential phase. Growth rates were calculated as the slope of the ln-transformed concentration versus time (in days) in the exponential phase.

Western blotting and Lhcx1 protein quantification

Lhcx1 immunodetection on IL cultures was performed as previously done for LL cultures in (Fig. S14E in [45]), using a rabbit polyclonal anti-LHCSR antibody from *Chlamydomonas* (gifted from K. K. Niyogi, University of California, Berkeley, USA, dilution 1: 5 000) which can detect all of *P. tricornutum* Lhcx isoforms [33,42,46]. In this study, two proteins, instead of one, were used as loading control, the ATP synthase-βCF_1 and the PSII D2 subunits (detected thanks to the antibodies gifted by J-D. Rochaix, University of Geneva, Geneva, Switzerland, at a 1: 10 000 dilution each). Proteins were The different bands were quantified by Image lab v5.0 software (Bio-Rad) and values derived by the sum of the βCF_1 and D2 signals were used to calculate the Lhcx1 concentrations. This allowed comparisons of Lhcx1 concentrations between the two different growth conditions, LL and IL, and between wildtype and transgenic lines expressing different Lhcx1 content. Wildtype and the highest Lhcx1 expressor, LtpM, were blotted together on a same membrane (twice for each strain giving four calibration curves) (Fig. 1 and Fig. S1) for ranges of total protein loadings (between 1 and 10 µg). From the linear fitting of the Lhcx1 versus total protein loading obtained in LL and IL, we calculated a calibration factor of 2.49 ± 0.62 to account for the increase in Lhcx1 concentration from LL to IL. We normalized all LL Lhcx1 values from [45] between 0 and 1 and divided these values by the 2.49 calibration factor, so that LL and IL [Lhcx1] were then comparable on the same relative scale.

Pigment analysis

For pigment analysis, cells were concentrated 10-20 times by centrifugation and then let for 30 min under very low light (approximately 1 µmol photons m^{-2} s^{-1}) in 15 mL Falcon tube under gentle agitation. For dark-adapted cells, the sampling was done directly in the Falcon. For light acclimated cells, sampling was done directly in the plateholder in the fluorometer when steady-state NPQ is reached or during NPQ relaxation in darkness. 50 µL was sampled and immediately dropped in 950 µL of pure methanol, quickly vortexed (2 s) and flash frozen in liquid nitrogen before storage at -80°C. Pigment analysis was done following [72] protocol, with a Shimadzu Prominence- I LC-2030C 3D HPLC (Shimadzu Corporation, Kyoto, Japan) equipped with a Waters Nova-Pak C18 4 µm 3.9 × 150 mm column (Waters corporation, Milford, USA). In

our hands, Chl *a* degradation is inevitable even on a 4°C refrigerated plate, so we thawed and ran one sample at the time.

Fluorescence measurements: F_V/F_M, σPSII and NPQ calculation

For most fluorescence measurements, we used a fluorescence imaging system (SpeedZen, JbeamBio, France), allowing to measure multiple 60 µL samples in parallel, with a green actinic light (532 nm). Minimum (F_0) and maximal (F_M) fluorescence were measured on dark-adapted samples, before and after a saturating pulse of 250ms (5000 µmol photons m^{-2} s^{-1}, 532 nm), respectively, to calculate the maximal quantum yield of PSII $F_V/F_M = (F_M-F_0)/F_M$. When the minimal (F_0') and maximal (F_M') fluorescence were measured in the dark during NPQ relaxation, following a high light treatment, the potential quantum yield of PSII during NPQ relaxation was calculated as $F_V'/F_M' = (F_M'-F_0')/F_M'$. The maximum quantum yield at the end of the NPQ relaxation was calculated as $F_VR/F_MR = (F_MR-F_0R)/F_MR$ where F_0R and F_MR are the minimal and maximal fluorescence measured when NPQ is fully relaxed.

For NPQ measurements, we distinguished two situations depending on whether the protocol allowed to discern specifically the nonphotochemical quenching associated with the rapidly relaxing NPQ component qZ, or the sum of all NPQ components had to be considered (including the slowly relaxing component that we attribute to qI when NPQ relaxation could not be monitored). The qZ component we investigate in this paper is rapidly deployed (3 min under light) or relaxed (approximately 15 min in darkness), and fully relaxed in all treatments for which it was measured (Fig. S4 and S7).

To measure NPQ under steady-state illumination, the samples were exposed to seven increasing light-steps (75 to 750 µmol photons m^{-2} s^{-1}) for 3 min (sufficient to reach a steady-state) before measuring the light-acclimated F_M' at each light-step. We then calculated NPQ as 1 - F_M/F_M'. From these fluorescence values, the relationship between NPQ and light intensity (E) was fitted as in [47]: $NPQ = NPQ_M \times E^n / (E50NPQ^n + E^n)$, where NPQ_M is the extrapolated maximal NPQ value, $E50NPQ$ is the light intensity for NPQ half-saturation, and n is the sigmoidicity coefficient. For NPQ vs. pigment analysis, performed on 6 LL and 9 IL strains, this experiment was conducted by batch of five separated sub-samples which were each collected for further pigment analysis, whether it is at the end of different light-steps or at different times of relaxation in darkness following a light stress (450 µmol photons m^{-2} s^{-1}) of 6 min (see Fig. 3).

For the NPQ relaxation analysis, we first applied 6 min of light stress (750 µmol photons m^{-2} s^{-1}) to induce NPQ and then followed its relaxation in darkness, during 15 to 30 min depending on growth conditions. The monitoring of F_0' and F_M' began 15 s after transition to darkness and was measured every min afterwards untill full relaxation, from which we computed F_V'/F_M', F_VR/F_MR. To test the validity of Equation 2, we reasoned that the influence of slowly relaxing phenomena should be eliminated. Therefore, we used the situation at the end of the dark relaxation, instead of the dark-acclimated situation before the light stress, as a reference for maximal fluorescence (F_MR) and maximum quantum yield (F_VR/F_MR). This allowed us to calculate the reversible part of NPQ as qZ = 1 - F_MR/F_M', and to test the Equation 2 which was adapted from [73] and rewritten as:

Equation 3

$$\frac{F_V'/F_{M'}}{\left(F_{VR}/F_{MR}\right)} = 1 - f(qZ) \text{ where } f(qZ) = \frac{\left(1-F_{VR}/F_{MR}\right)\times \mathrm{qZ}}{\left(1+\left(1-F_{VR}/F_{MR}\right)\times \mathrm{qZ}\right)}$$

The experimental data for time in darkness ≥1.25 min was used to test the validity of Equation 3. The ratio between experimental and theoretical F_V'/F_M' was calculated as:

$$R_{exp/th} = \frac{F_V'/F_{M'}}{F_{VR}/F_{MR}\times(1-f(qZ))}.$$

For measurements of the functional cross-section of PSII (σPSII), we used a Fluorescence Induction and Relaxation (miniFIRe) fluorometer built by Max Gorbunov (Rutgers University, NJ, USA). In this setup, 3 mL of a sample were left to relax under low light as described above but without centrifugation. The sample was then transferred in a glass tube, then a single turnover flash of intense blue light (100 µs, 455 nm, 60 nm bandwidth) provided in parallel F_V/F_M or F_V'/F_M' measurements, as well as σPSII (dark acclimated before light treatment) or σPSII' (during NPQ relaxation in darkness) [26]. The optical cross-section of PSII was calculated as σPSII/(F_V/F_M) [74].

Flow cytometry

For six strains in ML, we collected two 15 mL samples. One was directly centrifuged (2500 rpm, 15 min, 4°C), while the other was incubated in a vented flask in darkness for 40 h before centrifugation. After centrifugation, cell pellets were fixed in cold 70% EtOH, and stored 48 h in darkness at 4°C. Prior to cytometry, cells were washed once in cold EtOH and once in PBS, then stained by diamidino-2-phenylindole (DAPI, final concentration of 0.5 ng/mL). After 45 min

incubation in darkness at room temperature, cells were washed with PBS again. Cytometric analysis was carried out with a MACSQuant Analyser flow cytometer (Miltenyi Biotec, Germany), at least 50 000 events were recorded per sample. The V1.A channel (408 nm excitation, 450/50 nm detection) was used to detect DAPI fluorescence, a proxy for cellular DNA content and forward scatter (FSC) was used to estimate biovolume. Cells in phase G1 are expected to show lower DAPI fluorescence and smaller biovolume compared to cells in phase S, G2 or M [52].

Curve fitting and data analysis

For statistical analysis, we were interested in trends through a [Lhcx1] dimension (continuous relative scale from 0 to 1) rather than in one-to-one inter-strain comparisons. All parameters were not measured in all strains and growth conditions, but we tried to select the most relevant [Lhcx1] for a given question. To test for significant influence of [Lhcx1] on a given parameter, we used linear regressions calculated over the mean value of the parameter in each strains/growth condition (for homogeneous weights between different [Lhcx1] coordinates when the number of biological replicates is heterogeneous between strains). All relationships are shown in Table 1 and all mean values ± SD in Table S1. We then compared the distribution of mean values of parameters among strains between growth conditions (LL and IL) (independent factors) to confirm that we were studying the effects of NPQ in two PSII-antenna-systems with significantly different features. We selected the dependent variables that did not directly include Lhcx1 or NPQ: F_V/F_M, σPSII, optical absorption cross-section of PSII, and concentration of different pigments (Table 1). To access significant mean differences between growth conditions for these variables we used a type III one-way Analysis of Variance (ANOVA) with Satterthwaite's method (R software, package *lmerTest*), to consider uneven number of strains used and the varying number of biological replicates between growth conditions and independent variable measured (Table S1).

Data availability

Data will be made deposited on Dryad shortly.

References

1. Croteau, D., Jensen, E., Wilhelm, C. & Bailleul, B. Comparing Diatom Photosynthesis with the Green Lineage: Electron Transport, Carbon Fixation and Metabolism. *Diatom Photosynthesis: From Primary Production to High-Value Molecules*, 1–44 (2024).

2. Russo, M. T., Rogato, A., Jaubert, M., Karas, B. J. & Falciatore, A. *Phaeodactylum tricornutum*: An established model species for diatom molecular research and an emerging chassis for algal synthetic biology. *Journal of Phycology* 59, 1114–1122 (2023).

3. Field, C. B., Behrenfeld, M. J., Randerson, J. T. & Falkowski, P. Primary production of the biosphere: integrating terrestrial and oceanic components. *Science* **281**, 237–240 (1998).

4. Allen, A. E. et al. Evolution and metabolic significance of the urea cycle in photosynthetic diatoms. *Nature* **473**, 203–207 (2011).

5. Dorrell, R. G. et al. Complementary environmental analysis and functional characterization of lower glycolysis-gluconeogenesis in the diatom plastid. *The Plant Cell* **36**, 3584–3610 (2024).

6. Goss, R. & Lepetit, B. Biodiversity of NPQ. *Journal of Plant Physiology* **172**, 13–32 (2015).

7. Álvarez, E., Thoms, S., Bracher, A., Liu, Y. & Völker, C. Modeling photoprotection at global scale: The relative role of nonphotosynthetic pigments, physiological state, and species composition. *Global Biogeochemical Cycles* **33**, 904–926 (2019).

8. Wollman, F.-A. State transitions reveal the dynamics and flexibility of the photosynthetic apparatus. The *EMBO journal* **20**, 3623 - 3630 (2001).

9. Kasahara, M. et al. Chloroplast avoidance movement reduces photodamage in plants. *Nature* **420**, 829–832 (2002).

10. Yokono, M., Murakami, A. & Akimoto, S. Excitation energy transfer between photosystem II and photosystem I in red algae: larger amounts of phycobilisome enhance spillover. *Biochimica et Biophysica Acta (BBA)-Bioenergetics* **1807**, 847–853 (2011).

11. Lepetit, B. et al. Photosynthetic Light Reactions in Diatoms. II. The Dynamic Regulation of the Various Light Reactions. *The Molecular Life of Diatoms.* 423–464 (2022).

12. Lavaud, J., Rousseau, B., van Gorkom, H. J. & Etienne, A.-L. Influence of the diadinoxanthin pool size on photoprotection in the marine planktonic diatom *Phaeodactylum tricornutum*. *Plant Physiology* **129**, 1398–1406 (2002).

13. Lavaud, J., Rousseau, B. & Etienne, A.-L. General features of photoprotection by energy dissipation in planktonic diatoms (Bacillariophyceae). *Journal of Phycology* **40**, 130–137 (2004).

14. Lavaud, J. & Lepetit, B. An explanation for the inter-species variability of the photoprotective non-photochemical chlorophyll fluorescence quenching in diatoms. *Biochimica et Biophysica Acta (BBA)-Bioenergetics* **1827**, 294–302 (2013).

15. Barnett, A. et al. Growth form defines physiological photoprotective capacity in intertidal benthic diatoms. *The ISME journal* **9**, 32–45 (2015).

16. Croteau, D. et al. Contrasting nonphotochemical quenching patterns under high light and darkness aligns with light niche occupancy in Arctic diatoms. *Limnology and Oceanography* **66**, S231–S245 (2021).

17. Lacour, T. et al. The role of sustained photoprotective non-photochemical quenching in low temperature and high light acclimation in the bloom-forming arctic diatom *Thalassiosira gravida*. *Frontiers in Marine Science* **5**, 354 (2018).

18. Giovagnetti, V., Flori, S., Tramontano, F., Lavaud, J. & Brunet, C. The velocity of light intensity increase modulates the photoprotective response in coastal diatoms. *PLoS One* **9**, e103782 (2014).

19. Olaizola, M., La Roche, J., Kolber, Z. & Falkowski, P. G. Non-photochemical fluorescence quenching and the diadinoxanthin cycle in a marine diatom. *Photosynthesis Research* **41**, 357–370 (1994).

20. Short, A. et al. Kinetics of the xanthophyll cycle and its role in photoprotective memory and response. *Nature Communications* **14**, 662 (2023).

21. Nilkens, M. et al. Identification of a slowly inducible zeaxanthin-dependent component of non-photochemical quenching of chlorophyll fluorescence generated under steady-state conditions in *Arabidopsis. Biochimica et Biophysica Acta (BBA)-Bioenergetics* **1797**, 466–475 (2010).

22. Lavergne, J. & Trissl, H.-W. Theory of fluorescence induction in photosystem II: derivation of analytical expressions in a model including exciton-radical-pair equilibrium and restricted energy transfer between photosynthetic units. *Biophysical Journal* **68**, 2474–2492 (1995).

23. Kramer, D. M., Johnson, G., Kiirats, O. & Edwards, G. E. New fluorescence parameters for the determination of QA redox state and excitation energy fluxes. *Photosynthesis Research* **79**, 209–218 (2004).

24. Butler, W. Chlorophyll fluorescence: a probe for electron transfer and energy transfer. *Photosynthesis I: Photosynthetic Electron Transport and Photophosphorylation*, 149–167 (1977).

25. Klughammer, C. & Schreiber, U. Complementary PS II quantum yields calculated from simple fluorescence parameters measured by PAM fluorometry and the Saturation Pulse method. *PAM Application Notes* **1**, 201–247 (2008).

26. Gorbunov, M. Y., Kolber, Z. S., Lesser, M. P. & Falkowski, P. G. Photosynthesis and photoprotection in symbiotic corals. *Limnology and Oceanography* **46**, 75–85 (2001).

27. Giovagnetti, V. & Ruban, A. V. Detachment of the fucoxanthin chlorophyll a/c binding protein (FCP) antenna is not involved in the acclimative regulation of photoprotection in the pennate diatom *Phaeodactylum tricornutum. Biochimica Et Biophysica Acta (BBA)-Bioenergetics* **1858**, 218–230 (2017).

28. Belgio, E. et al. Economic photoprotection in photosystem II that retains a complete light-harvesting system with slow energy traps. *Nature Communications* **5**, 4433 (2014).

29. Buck, J. M. et al. Lhcx proteins provide photoprotection via thermal dissipation of absorbed light in the diatom *Phaeodactylum tricornutum. Nature Communications* **10,** 4167 (2019).

30. Burke, J., Ditto, C. & Arntzen, C. Involvement of the light-harvesting complex in cation regulation of excitation energy distribution in chloroplasts. *Archives of Biochemistry and Biophysics* **187**, 252–263 (1978).

31. Nicol, L., Nawrocki, W. J. & Croce, R. Disentangling the sites of non-photochemical quenching in vascular plants. *Nature Plants* **5**, 1177–1183 (2019).

32. Miloslavina, Y. et al. Ultrafast fluorescence study on the location and mechanism of non-photochemical quenching in diatoms. *Biochimica et Biophysica Acta (BBA)-Bioenergetics* **1787**, 1189–1197 (2009).

33. Taddei, L. et al. Dynamic changes between two LHCX-related energy quenching sites control diatom photoacclimation. *Plant Physiology* **177**, 953–965 (2018).

34. Lepetit, B. et al. High light acclimation in the secondary plastids containing diatom *Phaeodactylum tricornutum* is triggered by the redox state of the plastoquinone pool. Plant Physiology **161**, 853–865 (2013).

35. Schumann, A., Goss, R., Jakob, T. & Wilhelm, C. Investigation of the quenching efficiency of diatoxanthin in cells of *Phaeodactylum tricornutum* (Bacillariophyceae) with different pool sizes of xanthophyll cycle pigments. *Phycologia* **46**, 113–117 (2007).

36. Lavaud, J., Materna, A. C., Sturm, S., Vugrinec, S. & Kroth, P. G. Silencing of the violaxanthin de-epoxidase gene in the diatom *Phaeodactylum tricornutum* reduces diatoxanthin synthesis and non-photochemical quenching. *PLoS One* **7**, e36806 (2012).

37. Ruban, A. et al. The super-excess energy dissipation in diatom algae: comparative analysis with higher plants. *Photosynthesis Research* **82**, 165–175 (2004).

38. Li, X.-P. et al. A pigment-binding protein essential for regulation of photosynthetic light harvesting. *Nature* **403**, 391–395 (2000).

39. Peers, G. et al. An ancient light-harvesting protein is critical for the regulation of algal photosynthesis. *Nature* **462**, 518–521 (2009).

40. Lepetit, B., Volke, D., Gilbert, M., Wilhelm, C. & Goss, R. Evidence for the existence of one antenna-associated, lipid-dissolved and two protein-bound pools of diadinoxanthin cycle pigments in diatoms. *Plant Physiology* **154**, 1905–1920 (2010).

41. Bilger, W. & Björkman, O. Role of the xanthophyll cycle in photoprotection elucidated by measurements of light-induced absorbance changes fluorescence and photosynthesis in leaves of *Hedera canariensis.* *Photosynthesis Research* **25**, 173–185 (1990).

42. Bailleul, B. et al. An atypical member of the light-harvesting complex stress-related protein family modulates diatom responses to light. *Proceedings of the National Academy of Sciences* **107**, 18214–18219 (2010).

43. Zhu, S.-H. & Green, B. R. Photoprotection in the diatom *Thalassiosira pseudonana*: role of LI818-like proteins in response to high light stress. *Biochimica et Biophysica Acta (BBA)-Bioenergetics* 1797, 1449–1457 (2010).

44. Dittami, S. M., Michel, G., Collén, J., Boyen, C. & Tonon, T. Chlorophyll-binding proteins revisited-a multigenic family of light-harvesting and stress proteins from a brown algal perspective. *BMC Evolutionary Biology* **10**, 1–14 (2010).

45. Giovagnetti, V. et al. Biochemical and molecular properties of LHCX1, the essential regulator of dynamic photoprotection in diatoms. *Plant Physiology* **188**, 509–525 (2022).

46. Taddei, L. et al. Multisignal control of expression of the LHCX protein family in the marine diatom *Phaeodactylum tricornutum. Journal of Experimental Botany* **67**, 3939–3951 (2016).

47. Serôdio, J. & Lavaud, J. A model for describing the light response of the nonphotochemical quenching of chlorophyll fluorescence. *Photosynthesis Research* **108**, 61–76 (2011).

48. Blommaert, L., Chafai, L. & Bailleul, B. The fine-tuning of NPQ in diatoms relies on the regulation of both xanthophyll cycle enzymes. *Scientific Reports* **11**, 12750 (2021).

49. Kress, E. & Jahns, P. The dynamics of energy dissipation and xanthophyll conversion in *Arabidopsis* indicate an indirect photoprotective role of zeaxanthin in slowly inducible and relaxing components of non-photochemical quenching of excitation energy. *Frontiers in Plant Science* **8**, 2094 (2017).

50. Buck, J. M., Kroth, P. G. & Lepetit, B. Identification of sequence motifs in Lhcx proteins that confer qE-based photoprotection in the diatom *Phaeodactylum tricornutum. The Plant Journal* **108**, 1721–1734 (2021).

734 51. Melis, A. & Homann, P. H. Heterogeneity of the photochemical centers in system II of chloroplasts.
735 *Photochemistry and Photobiology* **23**, 343– 350 (1976).

736 52. Huysman, M. J. et al. Genome-wide analysis of the diatom cell cycle unveils a novel type of cyclins
737 involved in environmental signaling. *Genome Biology* **11**, 1–19 (2010).

738 53. Annunziata, R. et al. Trade-off between sex and growth in diatoms: Molecular mechanisms and
739 demographic implications. *Science Advances* **8**, eabj9466 (2022).

740 54. Sato, S. et al. Genome-enabled phylogenetic and functional reconstruction of an araphid pennate
741 diatom *Plagiostriata* sp. CCMP470, previously assigned as a radial centric diatom, and its bacterial
742 commensal. *Scientific Reports* **10**, 9449 (2020).

743 55. Grouneva, I., Jakob, T., Wilhelm, C. & Goss, R. Influence of ascorbate and pH on the activity of the
744 diatom xanthophyll cycle-enzyme diadinoxanthin de-epoxidase. *Physiologia Plantarum* **126**, 205–211
745 (2006).

746 56. Liguori, N., Roy, L. M., Opacic, M., Durand, G. & Croce, R. Regulation of light harvesting in the green
747 alga *Chlamydomonas reinhardtii. Journal of the American Chemical Society* **135**, 18339–18342 (2013).

748 57. Zheng, M., Pang, X., Chen, M. & Tian, L. Ultrafast energy quenching mechanism of LHCSR3-dependent
749 photoprotection in *Chlamydomonas. Nature Communications* **15**, 4437 (2024).

750 58. Ruan, M. et al. Cryo-EM structures of LHCII in photo-active and photoprotecting states reveal allosteric
751 regulation of light harvesting and excess energy dissipation. *Nature Plants* **9**, 1547–1557 (2023).

752 59. Accomasso, D., Londi, G., Cupellini, L. & Mennucci, B. The nature of carotenoid S* state and its role in
753 the nonphotochemical quenching of plants. *Nature Communications* **15**, 847 (2024).

754 60. Park, S. et al. Chlorophyll–carotenoid excitation energy transfer and charge transfer in *Nannochloropsis*
755 *oceanica* for the regulation of photosynthesis. *Proceedings of the National Academy of Sciences* **116**,
756 3385–3390 (2019).

757 61. Xu, P., Tian, L., Kloz, M. & Croce, R. Molecular insights into Zeaxanthin-dependent quenching in higher
758 plants. *Scientific Reports* **5**, 13679 (2015).

759 62. Gilmore, A. M., Shinkarev, V. P., Hazlett, T. L. & Govindjee. Quantitative analysis of the effects of
760 intrathylakoid pH and xanthophyll cycle pigments on chlorophyll a fluorescence lifetime distributions and
761 intensity in thylakoids. *Biochemistry* **37**, 13582–13593 (1998).

762 63. Nagao, R. et al. Enhancement of excitation-energy quenching in fucoxanthin chlorophyll a/c-binding
763 proteins isolated from a diatom *Phaeodactylum tricornutum* upon excess-light illumination. *Biochimica et*
764 *Biophysica Acta (BBA)-Bioenergetics* **1862**, 148350 (2021).

765 64. Lavaud, J., Rousseau, B. & Etienne, A.-L. In diatoms, a transthylakoid proton gradient alone is not
766 sufficient to induce a non-photochemical fluorescence quenching. *FEBS letters* **523**, 163–166 (2002).

767 65. Garab, G., Magyar, M., Sipka, G. & Lambrev, P. H. New foundations for the physical mechanism of
768 variable chlorophyll a fluorescence. Quantum efficiency versus the light-adapted state of photosystem II.
769 *Journal of Experimental Botany* **74**, 5458–5471 (2023).

770 66. Davis, G. A. et al. Limitations to photosynthesis by proton motive force-induced photosystem II
771 photodamage. elife **5**, e16921 (2016).

772 67. Diner, B. & Joliot, P. Effect of the transmembrane electric field on the photochemical and quenching
773 properties of Photosystem II in vivo. *Biochimica et Biophysica Acta (BBA)-Bioenergetics* **423**, 479–498
774 (1976).

775 68. Pribil, M., Labs, M. & Leister, D. Structure and dynamics of thylakoids in land plants. *Journal of*
776 *Experimental Botany* **65**, 1955–1972 (2014).

777 69. Wietrzynski, W. et al. Charting the native architecture of *Chlamydomonas* thylakoid membranes with
778 single-molecule precision. *Elife* **9**, e53740 (2020).

779 70. Flori, S. et al. Plastid thylakoid architecture optimizes photosynthesis in diatoms. *Nature*
780 *Communications* **8**, 15885 (2017).

781 71. Bennett, D. I. et al. Models and mechanisms of the rapidly reversible regulation of photosynthetic light
782 harvesting. *Open Biology* **9**, 190043 (2019).

783 72. Berne, N., Fabryova, T., Istaz, B., Cardol, P. & Bailleul, B. The peculiar NPQ regulation in the
784 stramenopile *Phaeomonas* sp. challenges the xanthophyll cycle dogma. *Biochimica et Biophysica Acta*
785 *(BBA)-Bioenergetics* **1859**, 491–500 (2018).

786 73. Ruban, A. V. & Murchie, E. H. Assessing the photoprotective effectiveness of non-photochemical
787 chlorophyll fluorescence quenching: a new approach. *Biochimica et Biophysica Acta (BBA)-Bioenergetics*
788 **1817**, 977–982 (2012).

789 74. Mauzerall, D. & Greenbaum, N. L. The absolute size of a photosynthetic unit. *Biochimica et Biophysica*
790 *Acta (BBA)-Bioenergetics* **974**, 119–140 (1989).

791

Acknowledgements

We thank Francis-André Wollman for critical reading of the manuscript, as well as Johann Lavaud, Bernard Lepetit and Bernard Genty for fruitful discussions. We also thank K. K. Niyogi and J-D. Rochaix for the gifted antibodies and Chiara Giossi and Marcelo Orlando for help with the measurement of Chl *a* standard. D.C and B.B. acknowledge the support by the European Research Council (ERC) PhotoPHYTOMIX project (grant agreement No. 715579). D.C., B.B. and A.F. also acknowledge funding from the BrownCut Projet (ANR-19-CE20-0020). A.F acknowledges funding from Fondation Bettencourt-Schueller (Coups d'élan pour la recherche francaise-2018), the "Initiative d'Excellence" program (Grant "DYNAMO," ANR-11-LABX-0011-01) and by the EMBRC-FR-"Investissements d'avenir" program (ANR-10-INBS-02).

Author contributions

D.C. and B.B. designed the study. D.C. performed all biophysics measurements and D.C. and B.B. analysed the data. M.J and D.C. performed the Western blot analysis and analysed the results with support from A.F. The original draft of the manuscript was written by D.C. All the authors discussed the results and commented on the manuscript.

Competing Interest Statement

Authors declare that they have no competing interests.

Materials and Correspondence

Material request and correspondence should be addressed to B. B. (bailleul@ibpc.fr)

Figures

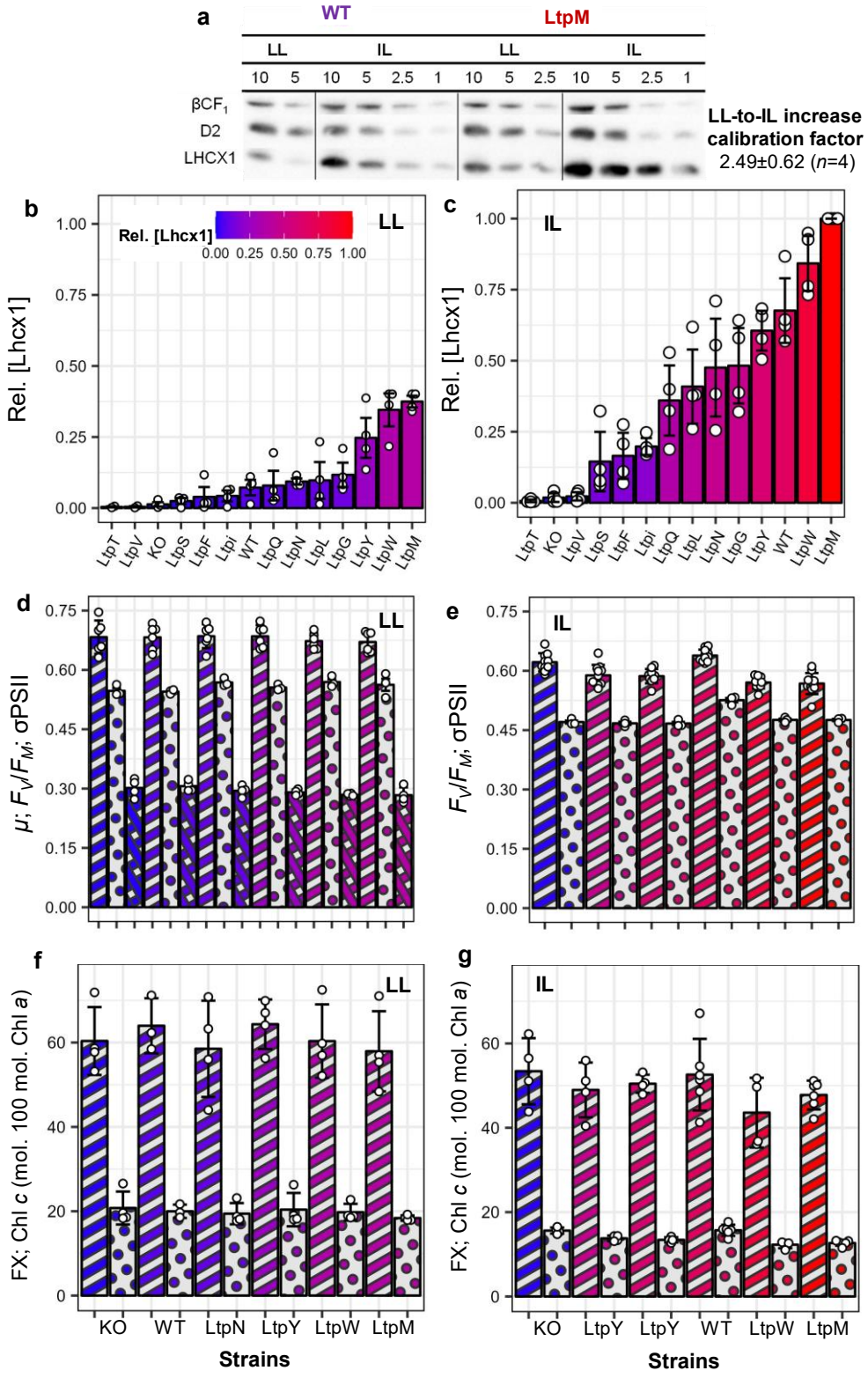
a
WT
LtpM
LL
IL
LL
IL
10 5 10 5 2.5 1 10 5 2.5 10 5 2.5 1
βCF1
D2
LHCX1
LL-to-IL increase
calibration factor
2.49±0.62 (n=4)
b
Rel. [Lhcx1]
LL
Rel. [Lhcx1]
0.00 0.25 0.50 0.75 1.00
1.00
0.75
0.50
0.25
0.00
LtpT LtpV KO LtpS LtpF Ltpi WT LtpQ LtpN LtpL LtpG LtpY LtpW LtpM
c
IL
Rel. [Lhcx1]
d
LL
μ; FV/FM; σPSII
0.75
0.60
0.45
0.30
0.15
0.00
e
IL
FV/FM; σPSII
f
LL
FX; Chl c (mol. 100 mol. Chl a)
60
40
20
0
KO WT LtpN LtpY LtpW LtpM
Strains
g
IL
FX; Chl c (mol. 100 mol. Chl a)
KO LtpY LtpY WT LtpW LtpM
Strains

Fig. 1 | Lhcx1 accumulation and baseline physiology of 14 *Phaeodactylum tricornutum* strains cultivated under two different light conditions.

Western blots on wildtype and Lhcx1 complemented strain LtpM, with different protein loadings (1-10 µg), were used to calculate changes in [Lhcx1] normalized to the sum of ATP synthase βCF1 and PSII-D2 subunit (see Methods), between low light (LL) and intermittent light (IL) conditions (**a**). The obtained scaling factor allowed to calculate a relative [Lhcx1] scale common to LL (**b**) and IL (**c**) growth conditions, shown on a 0-to-1 colour-scale (see text). Full blots for IL are shown in Fig. S1 whereas relative Lhcx1 quantifications in LL are taken from[45]. Baseline physiology parameters were measured under LL **(d)** and IL **(e)** on six strains exemplifying the [Lhcx1] gradient, including dark-acclimated quantum yield of PSII (F_V/F_M, single stripped bars), growth rate (μ, d^{-1}, X-stripped bars) and PSII functional absorption cross-section (σPSII, in $Å^2 \cdot 10^{-3}$, dotted bars)**.** Light-harvesting pigment composition was also measured under LL **(f)** and IL **(g)** (full dataset in Table S1 and Fig. S2), including fucoxanthin (FX) (single stripped bars) and chlorophyll (Chl) *c* (dotted bars) normalized to Chl *a*. Bars height represent mean ± SD and white dots represent all independent biological replicates measured. Linear regression results for mean parameters value vs. [Lhcx1] are in Table 1.

815

816

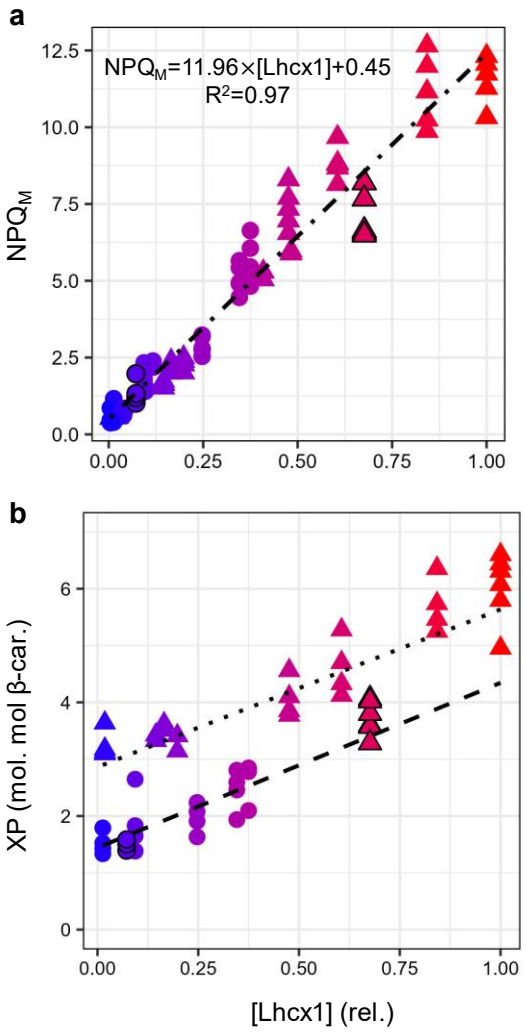

817

Fig. 2 | Lhcx1 dependence of maximal NPQ capacity and xanthophyll pigments pool.

Linear regression of extrapolated maximum NPQ (NPQ_M) (see Methods) vs. [Lhcx1] across both growth conditions (LL, circles; IL, triangles). The wildtype (WT) *Phaeodactylum tricornutum* (black outline symbols) and all 13 Lhcx1 mutants are shown (**a**). All biological replicates of xanthophyll pigment (XP) pool normalized to β-carotene (see Methods) vs. [Lhcx1] for both growth condition. The colour code is that used in Fig 1. Details for linear regressions in **b** are found in Table 1. All replicates measured on independent biological replicates are shown, the linear regressions are fitted on mean values per strain×growth conditions which can be found in Table S1.

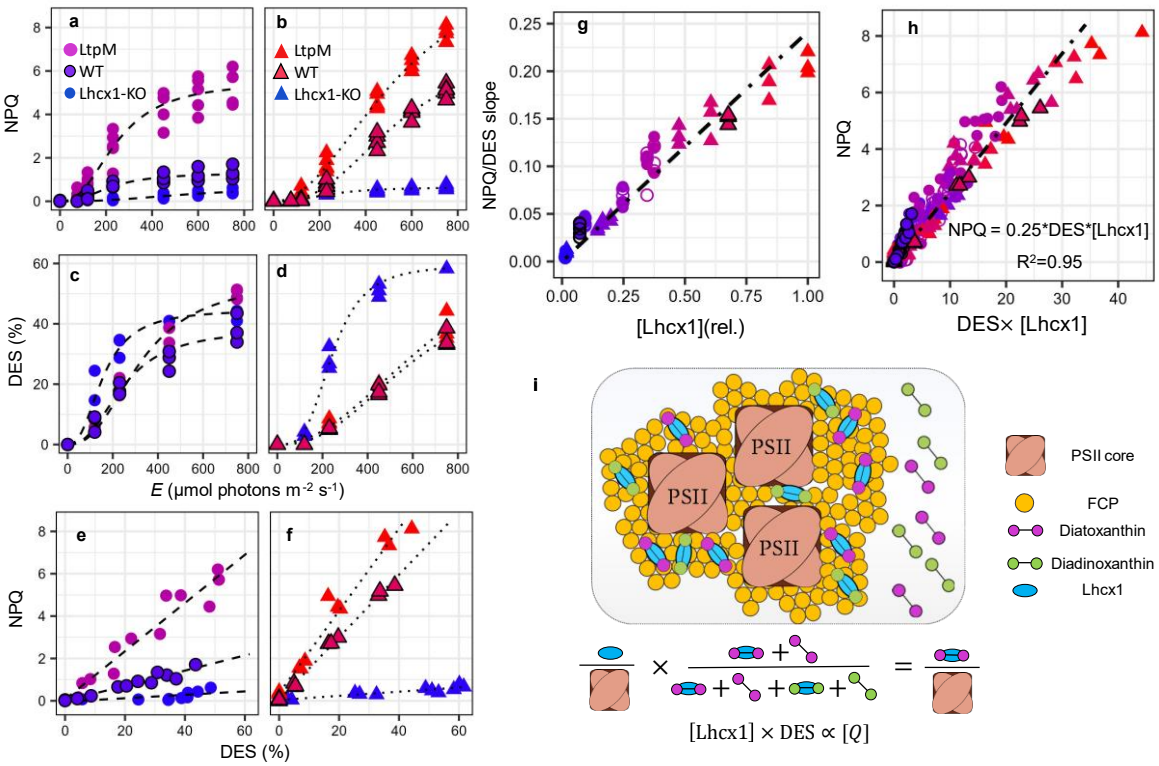

818

Fig. 3 | Relationships between NPQ, Lhcx1 and the de-epoxidation state (DES) support an "SV-lake" model in *Phaeodactylum tricornutum*.

The same colour code as in Fig 1-2 is used. NPQ vs. light intensity (*E*) (**a**, **b**) and DES vs. *E* relationship (**c**, **d**) in *P. tricornutum* wildtype (WT, black outline symbols), KO and the Lhcx1 overexpressor strain, LtpM grown under low light (LL, circle markers) (**a**, **c**) and intermittent light (IL, triangle markers) (**b**, **d**). Based on first 4 panels, the NPQ vs. DES relationship was plotted for LL (**e**) and IL (**f**). NPQ vs. DES slope determined in 9 strains at different steady-state light intensities (closed symbols, same protocol as for **e**-**f**) and during relaxation in the dark for 6 LL grown strains (open symbols, see Methods) are shown as a function of [Lhcx1] (**g**). For all 291 data points corresponding to experiments shown in panels **a**-to-**g**, are used for the linear regression of NPQ vs. DES×[Lhcx1] plotted in (**h**). Schematic representation of a working model wherein DT interacting with Lhcx1 is proportional to the concentration of a Stern-Volmer quencher (*Q*) for pennate diatoms' NPQ (**i**). The NPQ vs. DES (and DT) slopes for all strain×growth conditions in steady-state illumination are found in Fig. S3; the ones for the dark relaxation protocols in Fig. S4 and S5, and the equivalent of panels **g** and **h** when using DT instead of DES to access quenching efficiency in Fig. S6. Details on mean ± SD and number of biological replicates are found in Table S1.

819

820

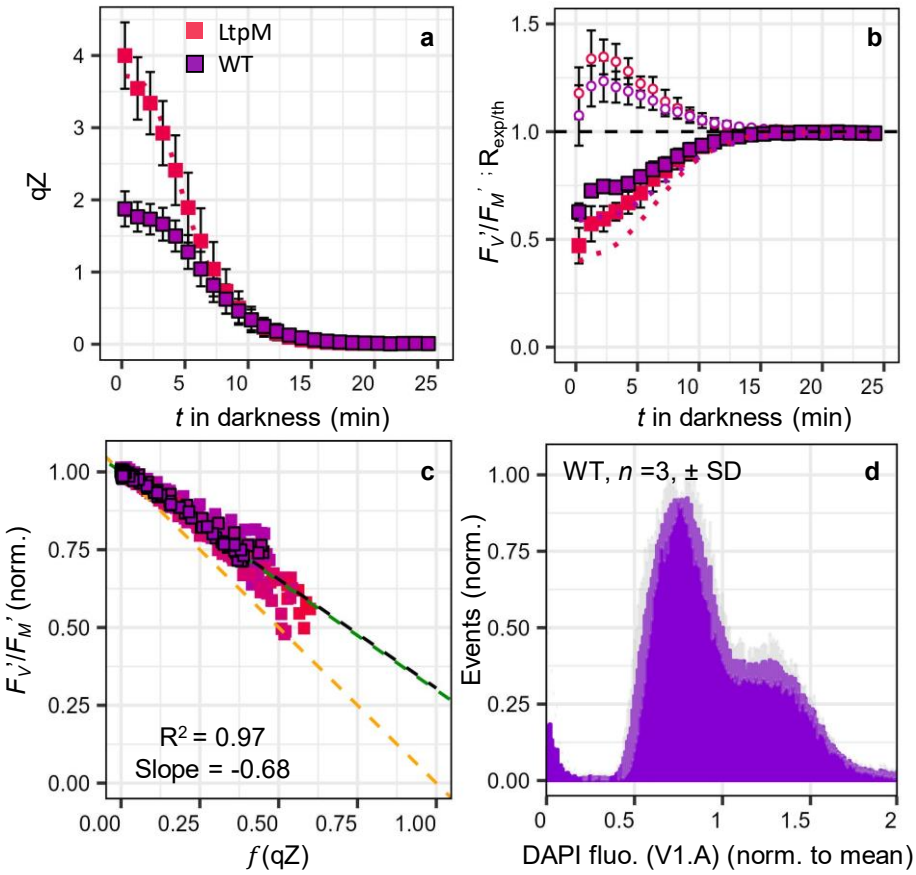

Fig. 4 | PSII photochemistry vs. NPQ/qZ relationship and the "SV-lake" model.

Relaxation kinetics of the rapidly reversible, diatoxanthin-dependent, qZ component of NPQ (**a**) and of the potential quantum yield of PSII (F_V'/F_M') (normalized to its value at the end of the relaxation) (**b**) in the dark after induction of qZ under high light (6 min, 750 µmol photons m^{-2} s^{-1}). Exemplary curves of mean ± SD of 4 independent biological replicates in *Phaeodactylum tricornutum* wildtype (WT, symbols with black outline) and complemented strain LtpM, grown under moderate light (ML, see Methods). The theoretical F_V'/F_M' according to the "SV-lake" model (dotted line) and the Ratio of experimental-to-theoretical F_V'/F_M' ($R_{exp/the}$, open circles) are shown in (**b**). Relationship between F_V'/F_M' and f(qZ) (relative decrease in F_V'/F_M' due to qZ) during dark relaxation, for all 651 data points corresponding to WT and LtpM (panels **a**, **b**) as well as five other strains (n=4 for WT, LtpG, LtpN, LtpQ and LtpW, and n=3 for LtpM and LtpY, individually shown in Fig S7-S8). The black dash line is the linear regression between F_V'/F_M' and f(qZ) and theoretical relationship according to the "SV-lake" model (orange dashed line) are shown. Since Lhcx1 was not quantified under ML, we used the maximum qZ reached to establish the colour scale in **a**, **b**, **c**. Histogram of the distribution of mean cellular DAPI fluorescence (V1. A channel) (proxy of DNA/cell) measured by flow cytometry in the WT (mean ± SD (grey shading), n = 3, cytometry results for 5 other mutant strains shown in Fig. S9) (**d**). The green dashed line in (**c**) represents the theoretically predicted F_V'/F_M' vs. f(qZ) relationship for a "heterogeneous SV-lake model" situation, compatible with the inter-cellular heterogeneity measured in (**d**) (see Text S2).

821

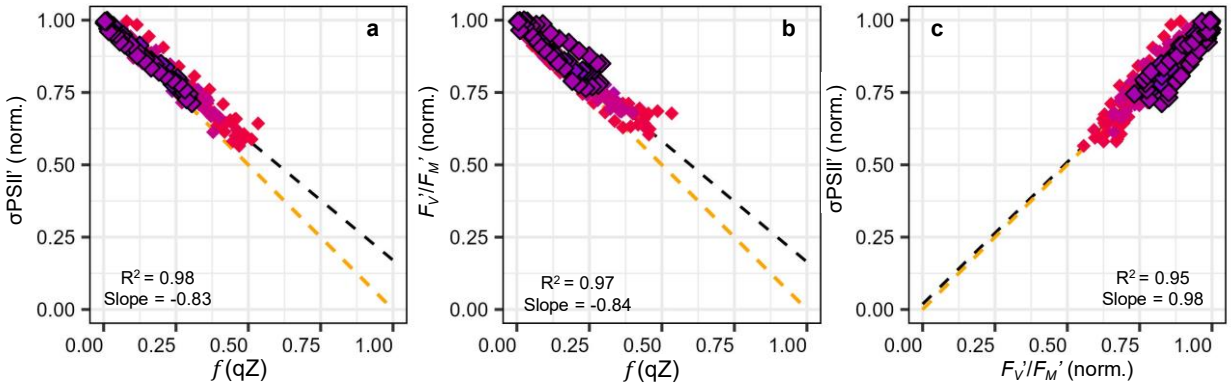

822

Fig. 5 | Relationships between NPQ/qZ, PSII photochemistry and functional absorption cross-section are incompatible with the "antenna uncoupling" hypothesis.

The PSII absorption functional cross-section (σPSII') and potential quantum yield for photochemistry (F_V'/F_M') were monitored during relaxation of the rapidly reversible, diatoxanthin-dependent, qZ component of NPQ in the dark and plotted vs. the relative decrease due to qZ (f(qZ)), in *Phaeodactylum tricornutum* wildtype (black outline symbols) and four other Lhcx1-mutant strains (LtpM, LtpN, LtpW, LtpY, see Fig. 1) grown under moderate light (ML) and priorly exposed to 6 min of high light (see Methods). The relationships between σPSII' and f(qZ) (**a**), between F_V'/F_M' and f(qZ) (**b**) and between σPSII' and F_V'/F_M' (**c**) are fitted by linear regressions (black dashed lines) and the theoretical relationships are displayed as orange dashed lines. The data combine 3 independent biological replicates for all strains (except 2 for LtpM), all 281 data points are shown. Since Lhcx1 was not quantified under ML, we used the maximum qZ reached to establish the colour scale.

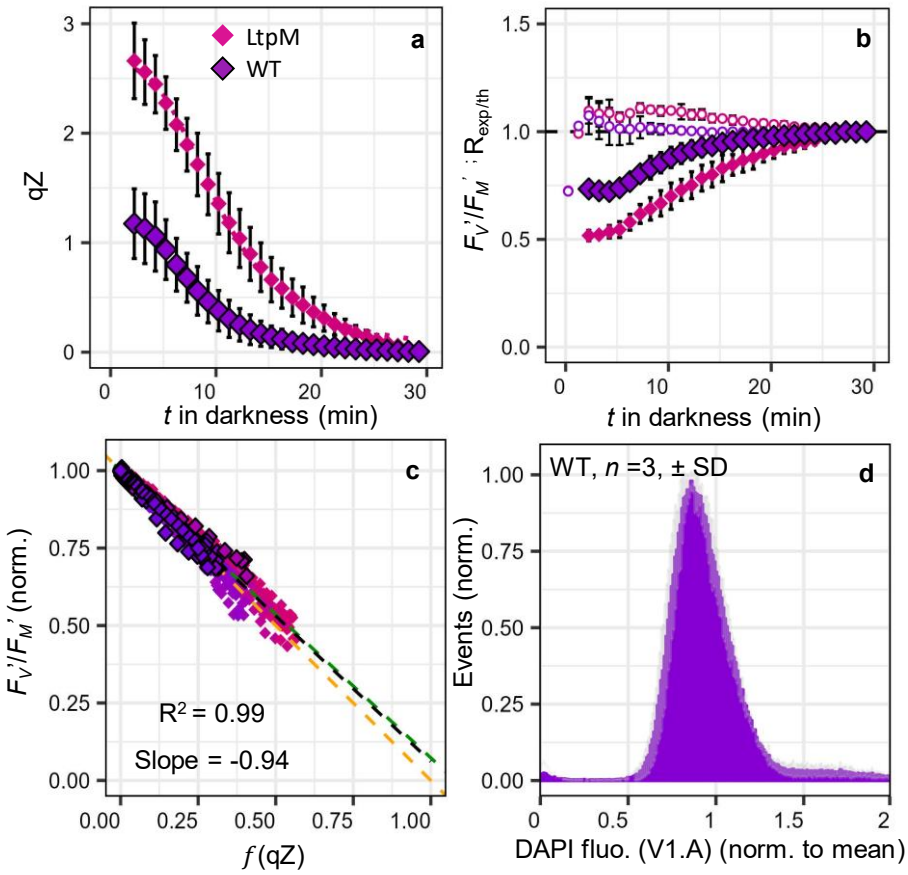

Fig. 6 | PSII photochemistry vs. NPQ/qZ relationship in homogeneous (synchronized) cell population meets expectations of the "SV-lake" model.

Relaxation kinetics of the rapidly reversible, diatoxanthin-dependent, qZ component of NPQ (**a**) and of the potential quantum yield of PSII (F_V'/F_M') (normalized to its value at the end of the relaxation) and of the Ratio between experimental and theoretical F_V'/F_M' ($R_{exp/th}$,open symbols) (**b**) in the dark after induction of qZ under high light (6 min, 750 µmol photons m^{-2} s^{-1}). Exemplary curves of mean ± SD of 4 independent biological replicates in *Phaeodactylum tricornutum* wildtype (WT, purple symbols with black outline) and complemented strain LtpM (pink symbols). Strains, grown in moderate light (ML), were incubated in the dark for 40 h to reduce physiological heterogeneity (see text) before measurements. The theoretical F_V'/F_M' according to "SV-lake" model (dotted line) and the Ratio of experimental-to-theoretical F_V'/F_M' ($R_{exp/th}$, open circles) are shown in (**b**). Relationship between F_V'/F_M' and f(qZ) (relative decrease in F_V'/F_M' due to qZ) during dark relaxation, for all 721 data points corresponding to WT and LtpM (panels **a**, **b**) as well as five other strains (n=4, for WT, LtpM, LtpN, LtpW and LtpY, and n=2 for LtpG and LtpQ, individually shown in Fig S7-S8). The black dash line is the linear regression between F_V'/F_M' and f(qZ) (relative decrease in F_V'/F_M' due to qZ) and theoretical relationship according to the "SV-lake" model (orange dashed line) are shown. Since Lhcx1 was not quantified under ML, we used the maximum qZ reached to establish the colour scale in **a**, **b**, **c**. Histogram of the distribution of mean cellular DAPI fluorescence (V1.A channel) (proxy of DNA/cell) measured by flow cytometry in WT acclimated to ML and then incubated in the dark for 40 h (mean ± SD (grey shading), n = 3, cytometry results for 5 other mutant strains are shown in Fig. S9) (**d**). The green dashed line in (**c**) represents the theoretically predicted F_V'/F_M' vs. f(qZ) relationship for a "heterogeneous SV-lake model" situation, compatible with the inter-cellular heterogeneity measured in (**d**) (see text and Text S2).

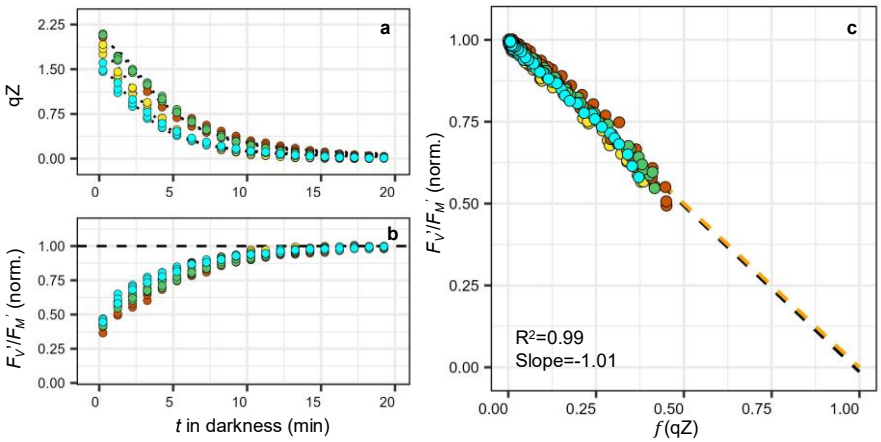

826

Fig. 7 | PSII photochemistry vs. NPQ/qZ relationship in the pennate diatom *Plagiostriata* sp. meets expectations of the "SV-lake" model.

Relaxation kinetics of the rapidly reversible, diatoxanthin-dependent, qZ component of NPQ (**a**) and of the potential quantum yield of PSII (F_V'/F_M') (normalized to its value at the end of the relaxation) (**b**) in the dark after induction of qZ under high light (6 min, 750 µmol photons m^{-2} s^{-1}) in the pennate diatom *Plagiostriata* sp. acclimated to moderate light (see Methods). The four colours represent four different experiments conducted at different times on biological triplicates (total n=12). Linear regression (black dashed line) of F_V'/F_M' vs. f(qZ) (relative decrease in F_V'/F_M' due to qZ) on all 240 data points and theoretical relationship according to the "SV-lake" model (orange dashed line) (**c**).

827

828 # Tables

Table 1| Lhcx1 concentration dependence of various physiological parameters in *Phaeodactylum tricornutum*. Outcomes of linear regression analysis for various physiological parameters vs. [Lhcx1], in *Phaeodactylum tricornutum* wildtype and Lhcx1-mutant strains cultivated under either low light (LL) or intermittent light (IL) growth conditions. Significant (*p*.value<0.05) are underlined in green and *N* is the number of strains accessed for a given parameter. Parameters for which one growth condition is underlined in blue, indicate that the mean of this parameter was significantly higher under this growth condition compared to the other (ANOVA-test, *p*.value<0.05, see Fig. S2). The growth rate (μ) for IL strains was not measured, xanthophyll pigments (XP) comprises diadinoxanthin (DD) plus diatoxanthin (DT), the de-epoxidation sate (DES) is calculated as DT/(DD+DT), the sigmoidicity parameter for nonphotochemical quenching (NPQ) induction (*n*) is globally fitted across all strains for LL (see Table S1) so its dependency to [Lhcx1] could not be tested, details on total biological replicates and mean ± SD for each strain and growth conditions are found in Table S1.

Physiological process	Parameter	Growth condition	Slope	*y*-intercept	R^2	*p*.value	*N*
Growth	μ	LL	-0.03	0.30	0.22	0.09	14
PSII Fluorescence	F_V/F_M	LL	-0.01	0.68	0.05	0.45	14
		IL	-0.02	0.61	0.16	0.15	14
	σPSII	LL	-0.44	563.61	1.58E-05	0.99	14
		IL	21.51	465.43	0.11	0.46	7
Light-harvesting pigments	FX/Chl a	LL	-4.12	61.70	0.05	0.66	6
		IL	-3.49	50.72	0.15	0.31	9
	Chl c/Chl a	LL	-3.37	20.42	0.38	0.19	6
		IL	-1.38	14.38	0.17	0.28	9
Photoprotective pigments	XP/Chl a	LL	9.94	6.34	0.85	0.01	6
		IL	5.37	15.31	0.91	5.59E-05	9
	β-car./Chl a	LL	-1.08	4.39	0.61	0.07	6
		IL	-1.34	5.00	0.68	0.01	9
	XP/β-car.	LL	2.94	1.43	0.81	8.75E-04	6
		IL	2.74	2.92	0.91	3.28E-03	9
NPQ induction	NPQ_M	LL	13.20	0.38	0.97	1.69E-10	14
		IL	11.97	0.38	0.96	4.53E-10	14
	E50NPQ	LL	275.64	133.86	0.44	0.02	11[a]
		IL	433.48	193.85	0.86	4.07E-05	11[a]
	*n*NPQ	IL	-2.07	3.87	0.82	1.26E-04	11[a]
NPQ vs. XP (induction)	*a*(NPQ/DES)	LL	0.27	0.01	0.97	4.34E-04	6
		IL	0.21	0.12	0.91	2.93E-03	9
	a(NPQ/DT)	LL	2.67	0.22	0.98	4.48E-07	6
		IL	1.05	0.10	0.95	7.46E-06	9
NPQ vs. XP (relaxation)	*a*(NPQ/DES)	LL	0.27	0.18	0.98	1.27E-04	6
		IL	0.16	0.19	0.90	8.01E-05	9
	a(NPQ/DT)	LL	2.45	0.23	0.91	3.24E-03	6
		IL	0.74	0.15	0.87	2.59E-04	9

Abbreviations: Dark-acclimated maximal quantum yield of PSII; F_V/F_M, PSII functional cross-section; σPSII, Fucoxanthin; FX, β-carotene, β-car., Fitted extrapolated maximum NPQ; NPQ_M, Light intensity for half-saturation of NPQ; E50NPQ

a: For three strains with relative [Lhcx1] ≈ 0, NPQ fitted parameters were removed from the linear regressions because NPQ induction was null.

3.3 Supplementary Information and Appendix

Pennate diatoms make NPQ as simple as possible, but not simpler

Dany Croteau, Marianne Jaubert, Angela Falciatore, Benjamin Bailleul*

CNRS, Sorbonne Université, Institut de Biologie Physico-Chimique, Laboratoire de Biologie du chloroplaste et perception de la lumière chez les microalgues, UMR7141, F-75005 Paris, France

*Corresponding author: bailleul@ibpc.fr

Supplementary Information

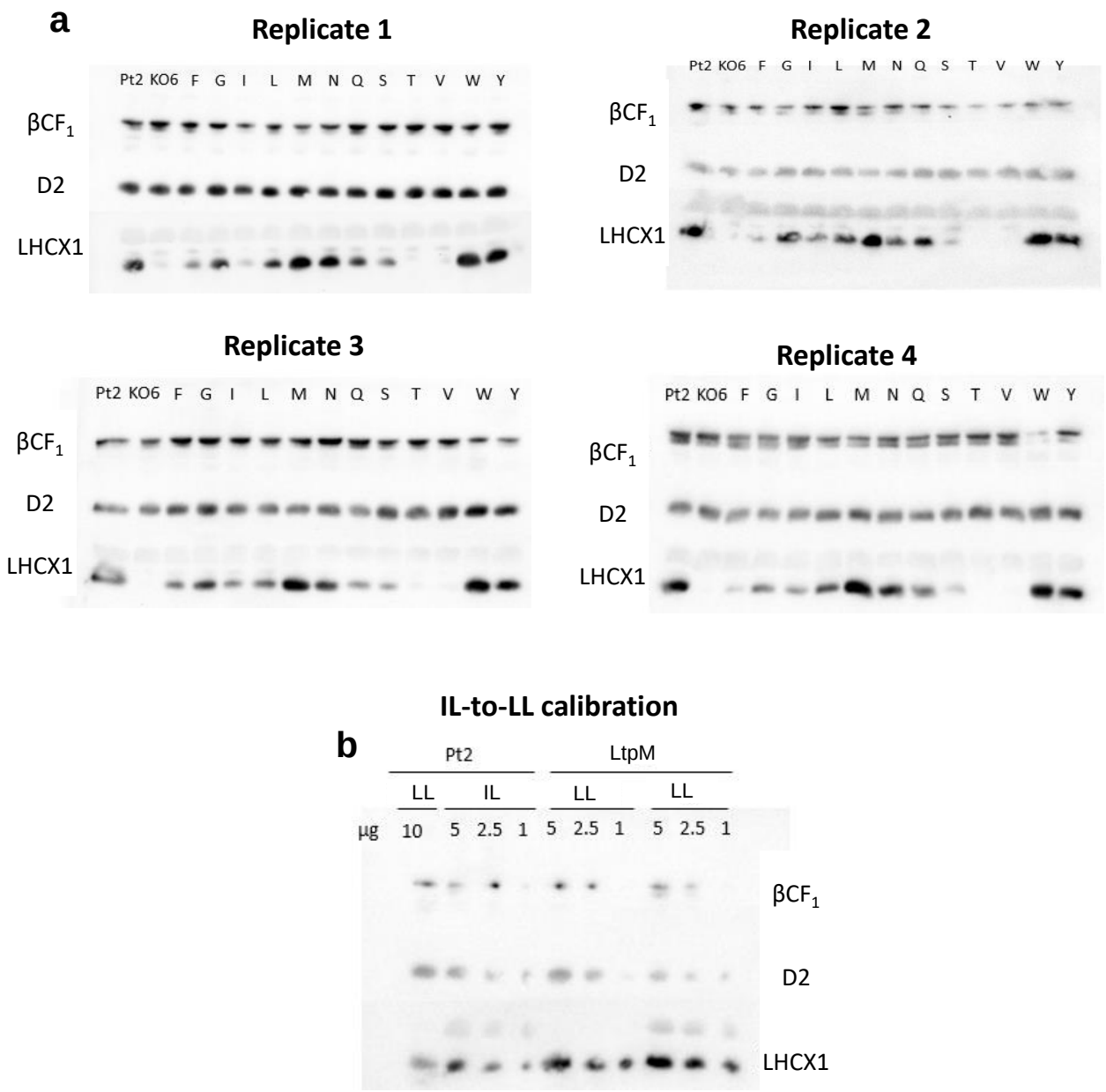

Fig. S1 | Quantification of Lhcx1 by Western blots in *Phaeodactylum tricornutum* strains cultivated under intermittent light (IL) and calibration with pre-existing Lhcx1 quantifications for cultivation under low light (LL).

Four replicates of Western blots for all 14 strains (only the last letter of all complemented lines is shown for clarity purposes) cultivated under IL for quantification of Lhcx1, ATP synthase βCF1 subunit and PSII-D2 subunit (**a**) Western blots for various total protein loadings (between 1 and 10 µg) in wildtype (WT) *Phaeodactylum tricornutum* and complemented strain LtpM cultivated under IL and LL used to calculate the factor of relative [Lhcx1] increase from LL-to-IL (**b**). Raw quantification by Western blots for LL were taken from previous works first published in Giovagnetti et al., 2022

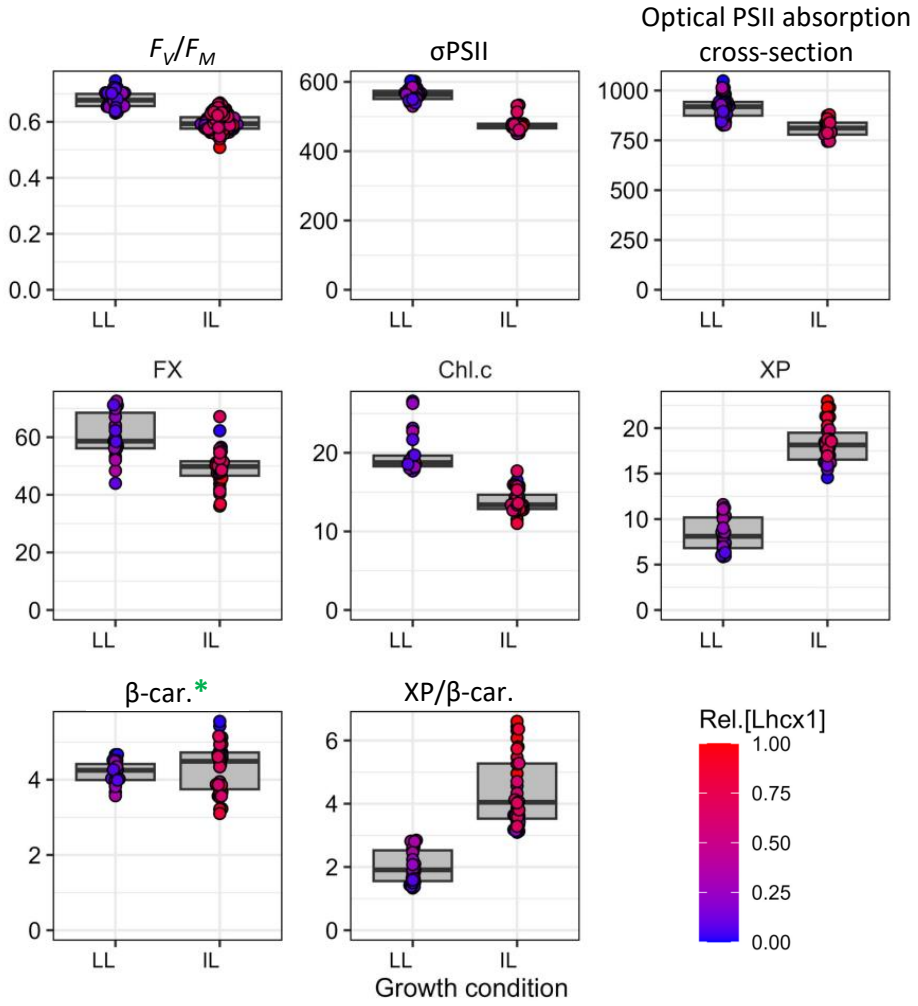

Variable	F_Value	P_Value
Fv/Fm	389.83	2.20E-46
σPSII	286.02	3.40E-24
Optical σPSII	59.30	1.81E-10
FX	36.64	1.50E-07
Chl.c	139.60	2.25E-16
XP	942.77	2.59E-33
β-car.	0.23	6.33E-01
XP/β-car.	363.89	4.93E-24

Fig. S2 | Physiological parameters under low light (LL) and intermittent light (IL) growth conditions in all *Phaeodactylum tricornutum* strains.

Boxplots comparing all values of physiological parameters (excluding Lhcx1 or NPQ-related parameters, see Fig. 1 and Table 1) and pigment content measured across wildtype and all Lhcx1-mutants *Phaeodactylum tricornutum* strains grouped by growth conditions to compare photoacclimation effects (color scales indicate the relative Lhcx1 concentration in the strain measured (see Fig. 1)). Significant differences between growth conditions were tested using one-way ANOVA with Satterthwaite's method (R software, package lmerTest), accounting for uneven strain numbers and biological replicates. Functional PSII absorption cross-section (σPSII) and optical PSII absorption cross-section are in $Å^2$. Pigment concentrations (fucoxanthin (FX), chlorophyll (Chl) c, xanthophyll pigments (XP, diadinoxanthin+ diatoxanthin), and β-carotene (β-car.)) are normalized to 100 mol. Chl a, except XP/β-car. (mol/mol). The only parameter showing no significant differences (β-car.) is marked with a green star and written in green in the table.

Figure S3

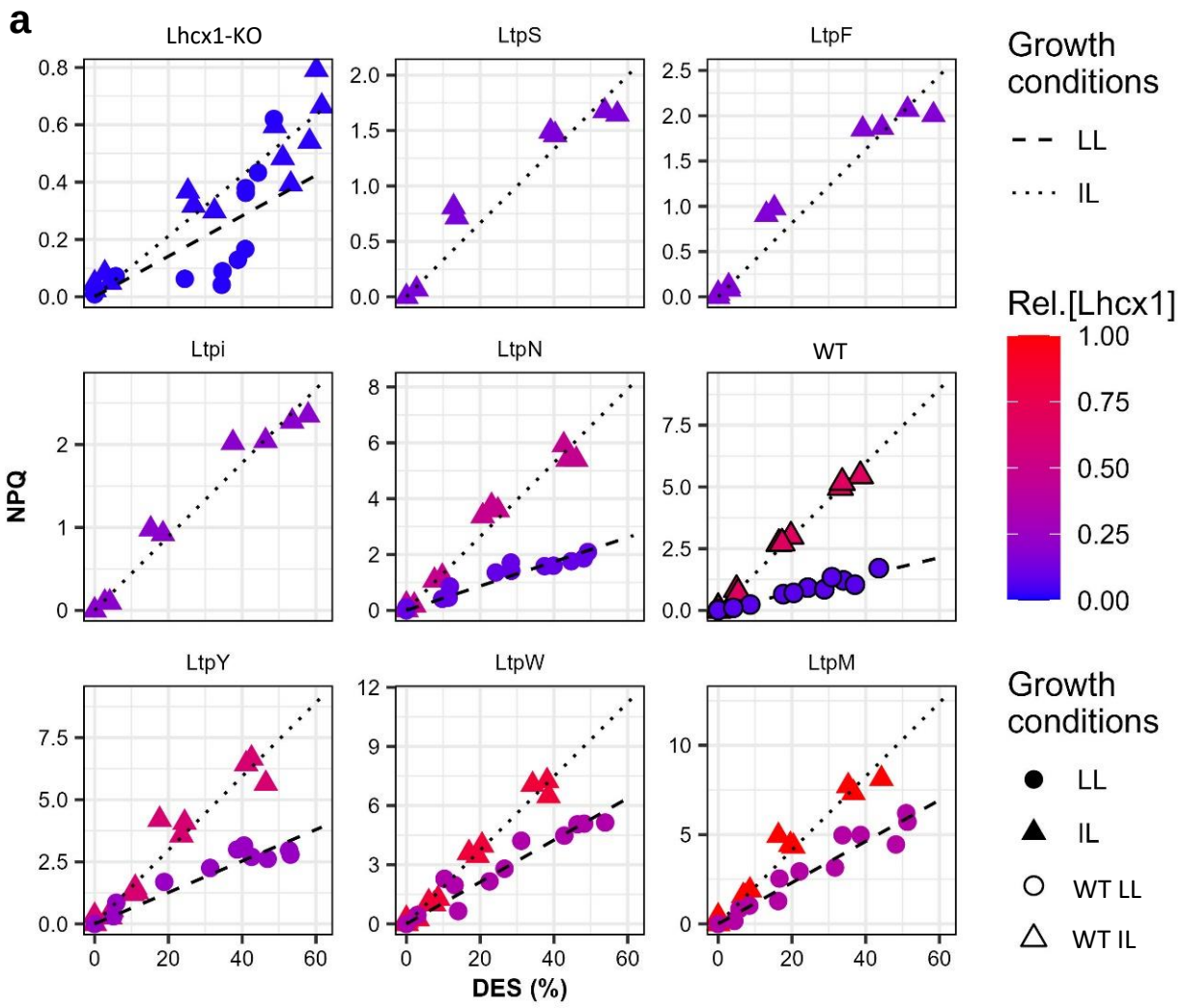

	Strains	Lhcx1	slope	SD	*n*
LL	KO	0.013	0.007	0.004	3
	WT	0.072	0.035	0.006	3
	LtpN	0.093	0.044	0.004	3
	LtpY	0.247	0.066	0.011	3
	LtpW	0.346	0.107	0.004	3
	LtpM	0.375	0.115	0.019	3
IL	KO	0.018	0.011	0.002	3
	LtpS	0.145	0.033	0.002	2
	LtpF	0.165	0.041	0.004	2
	Ltpi	0.198	0.045	0.003	2
	LtpN	0.476	0.132	0.010	3
	LtpY	0.606	0.150	0.021	3
	WT	0.676	0.150	0.005	3
	LtpW	0.842	0.188	0.019	3
	LtpM	1	0.208	0.012	3

Figure S3

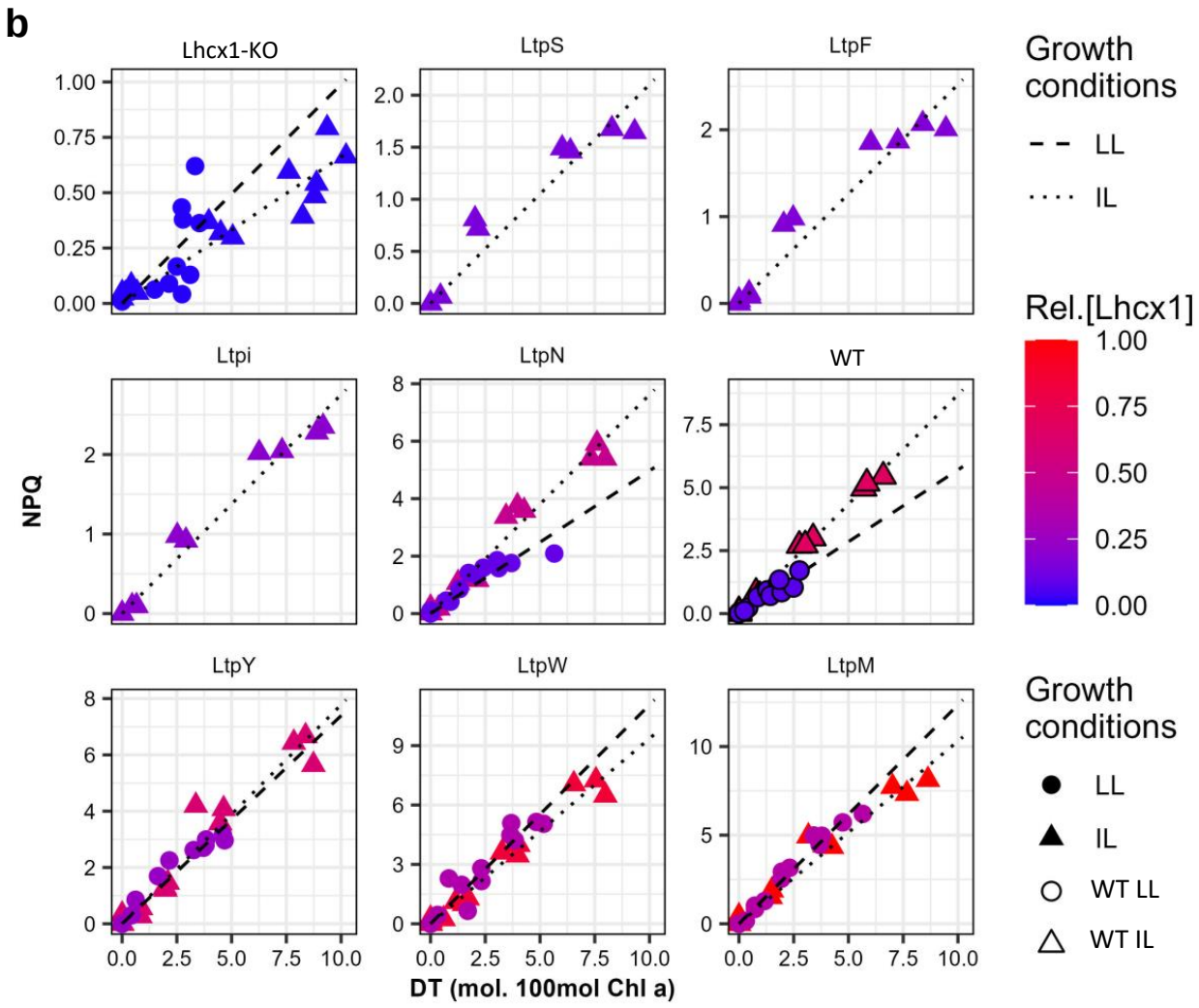

	Strains	Lhcx1	slope	SD	*n*
LL	Ko6	0.013	0.106	0.054	3
	Pt2	0.072	0.594	0.138	3
	LtpN	0.093	0.530	0.122	3
	LtpY	0.247	0.744	0.057	3
	LtpW	0.346	1.171	0.203	3
	LtpM	0.375	1.242	0.071	3
IL	Ko6	0.018	0.067	0.014	3
	LtpS	0.145	0.212	0.019	2
	LtpF	0.165	0.255	0.027	2
	Ltpi	0.198	0.276	0.011	2
	LtpN	0.476	0.764	0.046	3
	LtpY	0.606	0.786	0.101	3
	Pt2	0.676	0.872	0.027	3
	LtpW	0.842	0.952	0.131	3
	LtpM	1	1.035	0.067	3

Figure S3

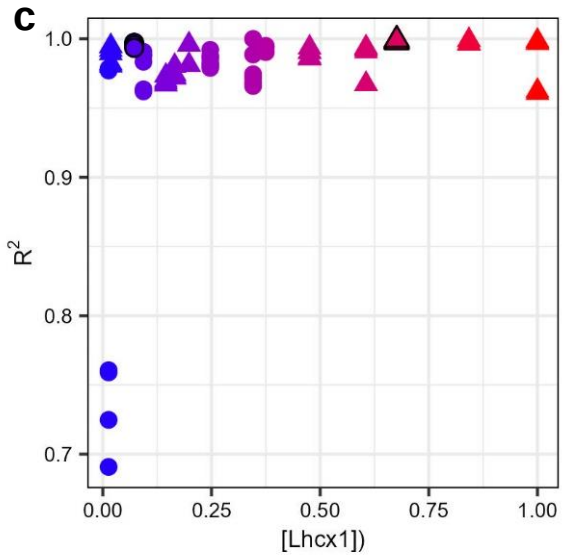

Fig. S3 | Slopes of the NPQ vs. DES or NPQ vs DT relationships, under steady-state light exposure, in all *Phaeodactylum tricornutum* strains.

All NPQ vs. DES (**a**) or NPQ vs DT (**b**) relationships measured in *P. tricornutum* wildtype (WT) and all Lhcx1-mutants strains under increasing light intensities at steady-state, following cultivation under low light (LL, circles) and intermittent light (IL, triangles) growth conditions. All individual experiments (comprising 5 data points) were fitted linearly and all obtained R^2 are plotted as a function of [Lhcx1] (**c**), with R^2>0.95 in all fits independently of Lhcx1 concentration, except in Lhcx1-KO**.** For all species*growth condition, the mean slope and are calculated shown under the plots in (**a**) and (**b**). These mean values of NPQ/DES and NPQ/DT slopes are used for the linear regressions vs. Lhcx1 concentration in Table 1 of the main manuscript.

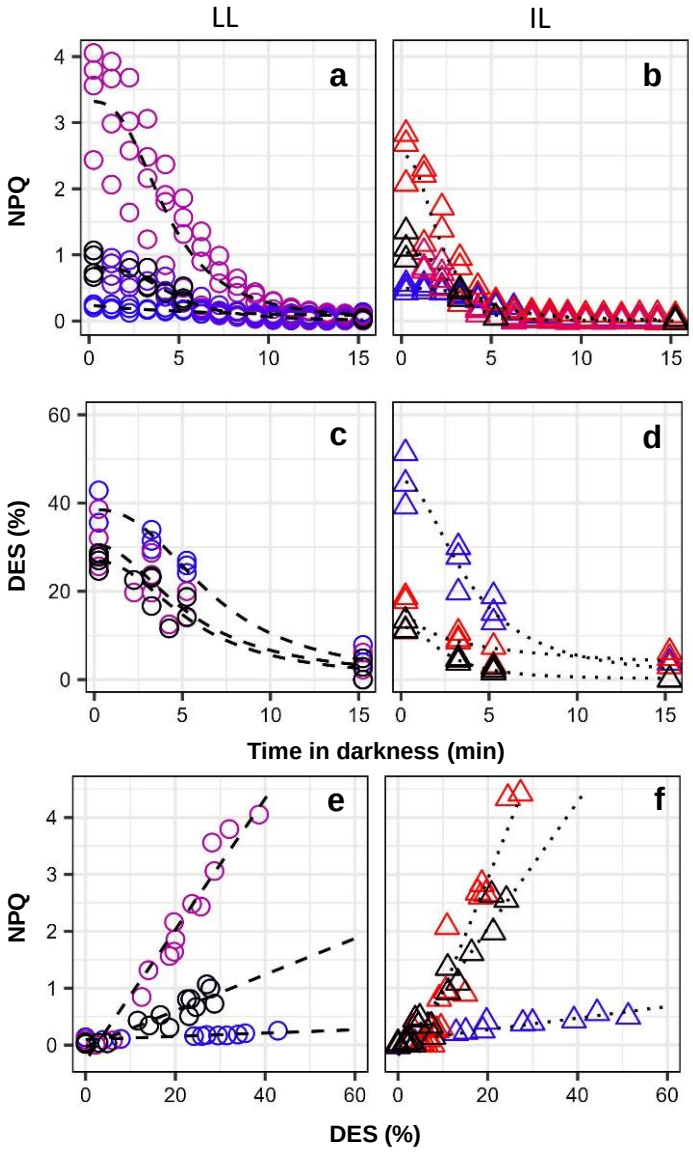

Fig. S4 | Relaxation of NPQ and DES in darkness in *Phaeodactylum tricornutum* wildtype and Lhcx1 mutants.

NPQ (**a, b**) and de-epoxidation state (DES) (**c, d**) relaxation kinetics in *P. tricornutum* wildtype (WT, black outline symbols), Lhcx1-KO (blue symbols) and the Lhcx1 overexpressor strain, LtpM (pink and red symbols), in the dark, after NPQ induction under 6 min of high light (450 µmol photons m^{-2} s^{-1}). Data for cells grown under low light (LL, open circles) (**a**, **c**) and intermittent light (IL, open triangles) (**b**, **d**) are shown. Based on the first 4 panels, the NPQ vs. DES linear relationships were plotted for LL (**e**) and IL (**f**). Relationships between NPQ. DES and diatoxanthin, in all replicates of all strains*growth conditions are shown in Fig. S5.

Figure S5

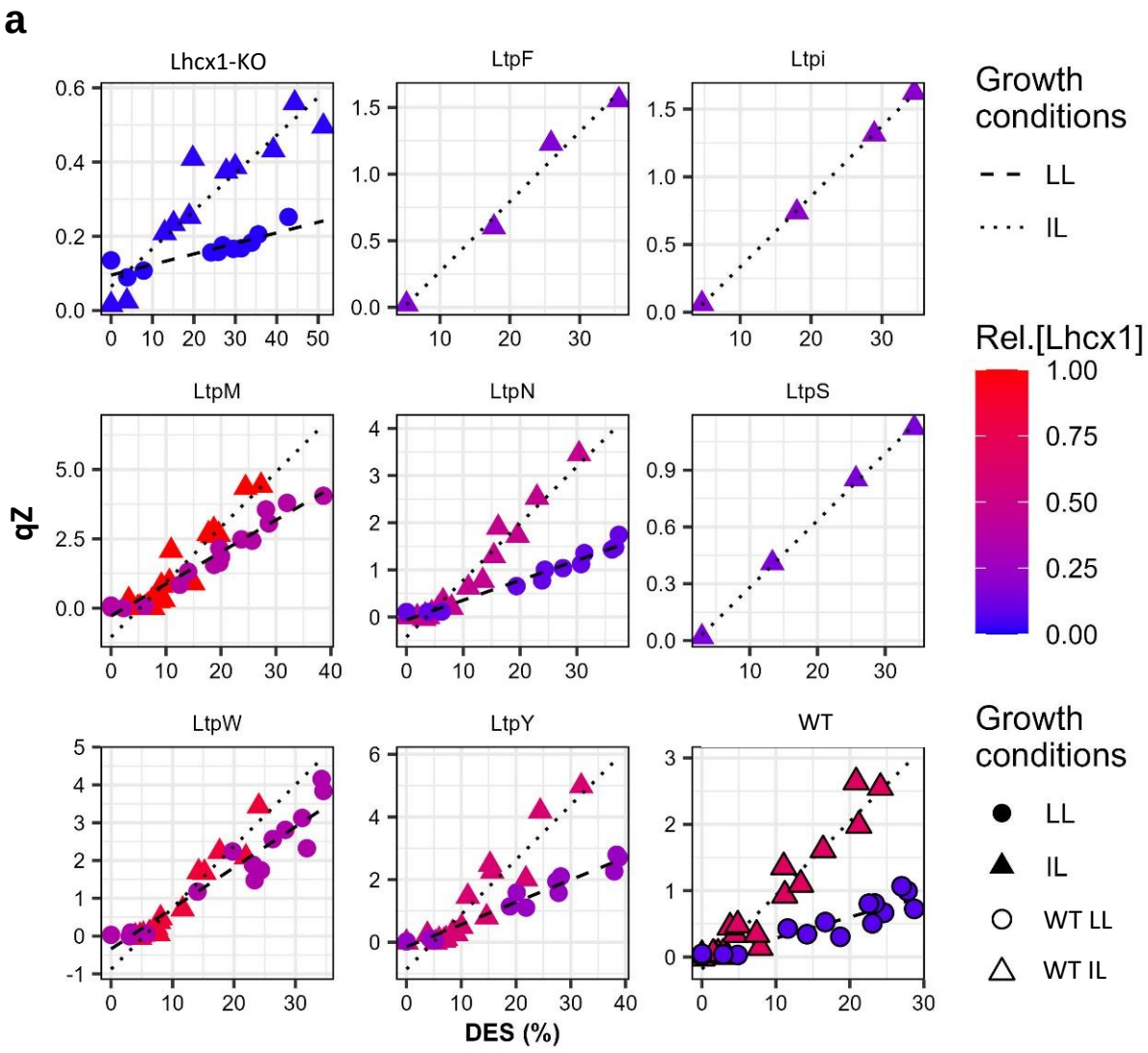

	Strains	Lhcx1	slope	SD	y0	SD	*n*
LL	Lhcx1-KO	0.013	0.005	0.000	0.043	0.020	3
	WT	0.072	0.031	0.007	-0.013	0.039	4
	LtpN	0.093	0.041	0.004	-0.032	0.053	3
	LtpY	0.247	0.069	0.007	-0.074	0.067	3
	LtpW	0.346	0.100	0.021	-0.187	0.144	4
	LtpM	0.375	0.110	0.013	-0.154	0.164	4
IL	Lhcx1-KO	0.018	0.011	0.002	0.030	0.023	3
	LtpS	0.145	0.034		-0.038		1
	LtpF	0.165	0.047		-0.119		1
	Ltpi	0.198	0.048		-0.087		1
	LtpN	0.476	0.106	0.021	-0.237	0.094	4
	LtpY	0.606	0.150	0.044	-0.477	0.412	4
	WT	0.676	0.106	0.021	-0.130	0.118	5
	LtpW	0.842	0.129	0.022	-0.451	0.136	4
	LtpM	1.000	0.175	0.021	-0.639	0.274	5

Figure S5

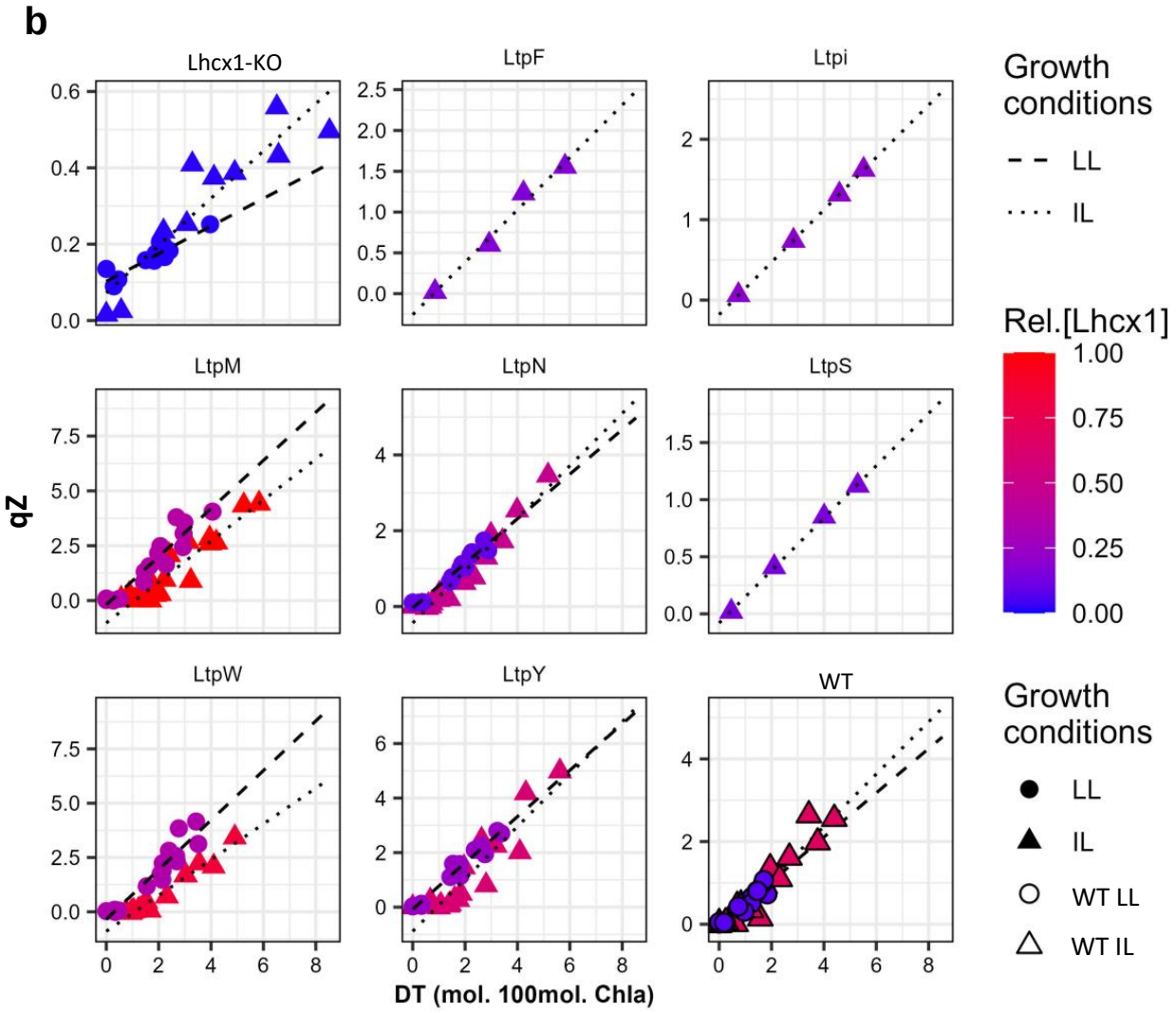

	Strains	Lhcx1	slope	SD	y0	SD	*n*
LL	Lhcx1-KO	0.013	0.065	0.018	0.045	0.023	3
	WT	0.072	0.515	0.093	-0.011	0.041	4
	LtpN	0.093	0.586	0.082	-0.030	0.059	3
	LtpY	0.247	0.856	0.087	-0.063	0.058	3
	LtpW	0.346	1.057	0.226	-0.180	0.140	4
	LtpM	0.375	1.102	0.255	-0.151	0.171	4
IL	Lhcx1-KO	0.018	0.072	0.015	0.031	0.024	3
	LtpS	0.145	0.220		-0.042		1
	LtpF	0.165	0.290		-0.119		1
	Ltpi	0.198	0.304		-0.085		1
	LtpN	0.476	0.593	0.116	-0.235	0.106	4
	LtpY	0.606	0.802	0.220	-0.467	0.400	4
	WT	0.676	0.625	0.116	-0.135	0.119	5
	LtpW	0.842	0.640	0.082	-0.446	0.131	4
	LtpM	1.000	0.853	0.078	-0.671	0.269	5

Figure S5

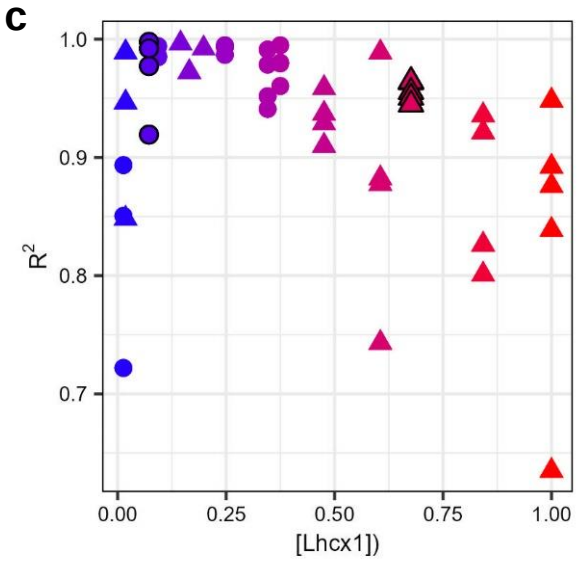

Fig. S5 | Slopes of the qZ component of NPQ vs. DES or, vs. DT relationships, during relaxation in darkness, in all *Phaeodactylum tricornutum* strains.

All relationships between the rapidly reversible, diatoxanthin-dependent, qZ component of NPQ vs. DES (**a**) or vs. DT (**b**) measured in *P. tricornutum* wildtype (WT) and all Lhcx1-mutants over different time points of qZ relaxation in darkness, following cultivation under low light (LL, circles) and intermittent light (IL, triangles) growth conditions. All individual experiments (comprising time=0 plus 4 time points of relaxation) were fitted linearly and all obtained R^2 are plotted as a function of [Lhcx1] in (**c**). For IL strains, there was a deviation from proportionality between qZ and DES or DT, leading to lower R^2 when fitted with a linear function (see Discussion). For all species*growth condition, the mean slope and SD are calculated and shown under the plots in (**a**) and (**b**). These mean values of qZ/DES and qZ/DT slopes are used for the linear regressions vs. Lhcx1 concentration in Table 1 of the main manuscript.

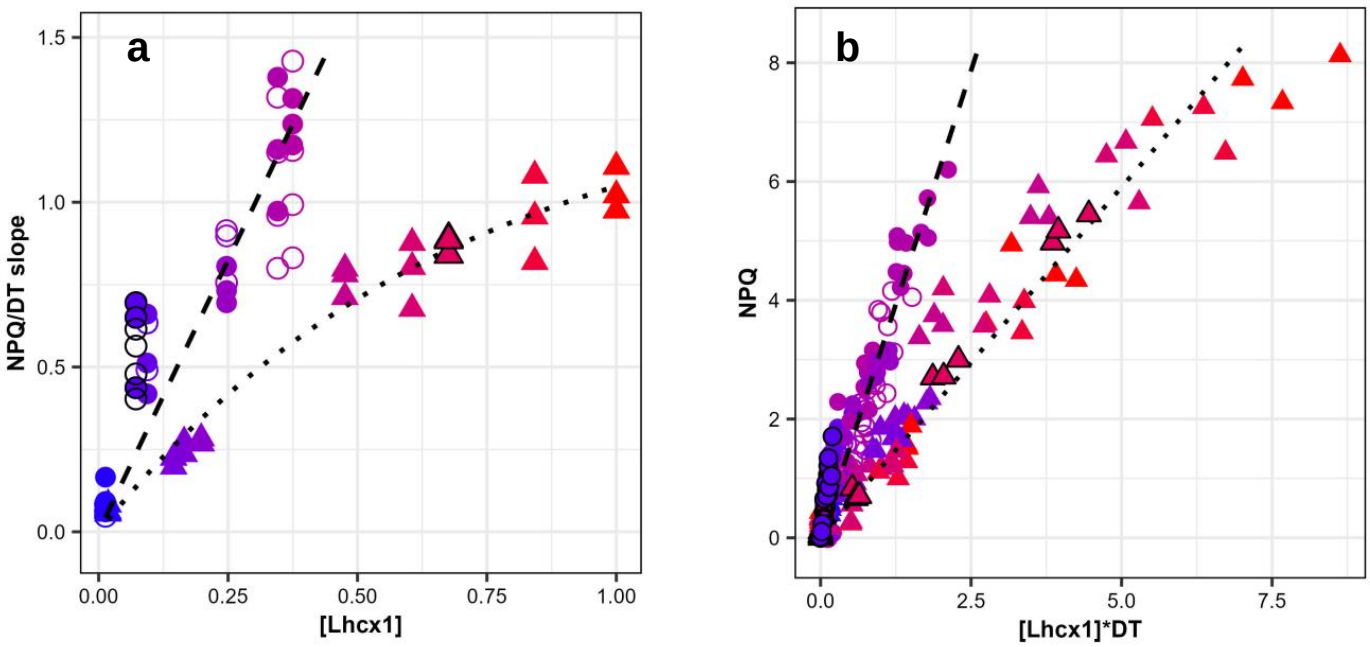

Fig. S6 | Relationships between NPQ, DT and Lhcx1 in all *Phaeodactylum tricornutum* strains.

The slopes of the NPQ/DT relationships measured under different light intensities at steady-state (closed symbols) and during NPQ relaxation in darkness (open symbols) are plotted against the relative Lhcx1 concentration (**a**). The panel **a** combines different *P. tricornutum* strains (black outline symbols represent wildtype) acclimated to low light (LL, circles) or intermittent light (IL, triangles). All 291 NPQ data points corresponding to the experiments from which the slopes in (**a**) were calculated are plotted vs. DT×[Lhcx1] (**b**).

Figure S7

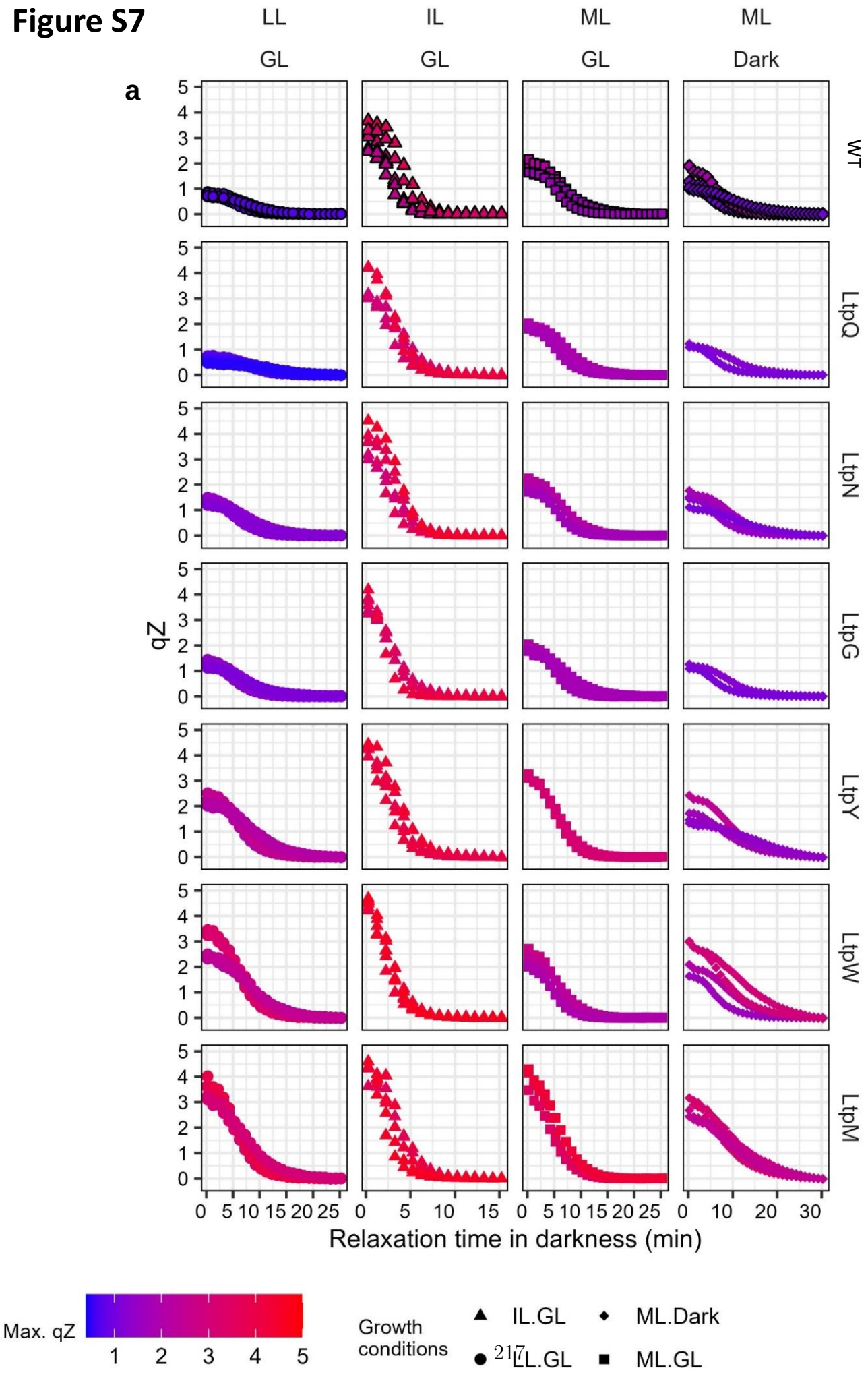
a
LL
GL
IL
GL
ML
GL
ML
Dark
WT
LtpQ
LtpN
LtpG
LtpY
LtpW
LtpM
qZ
0 5 10 15 20 25
0 5 10 15
0 5 10 15 20 25
0 10 20 30
Relaxation time in darkness (min)
Max. qZ
1 2 3 4 5
Growth conditions
IL.GL
ML.Dark
LL.GL
ML.GL

Figure S7

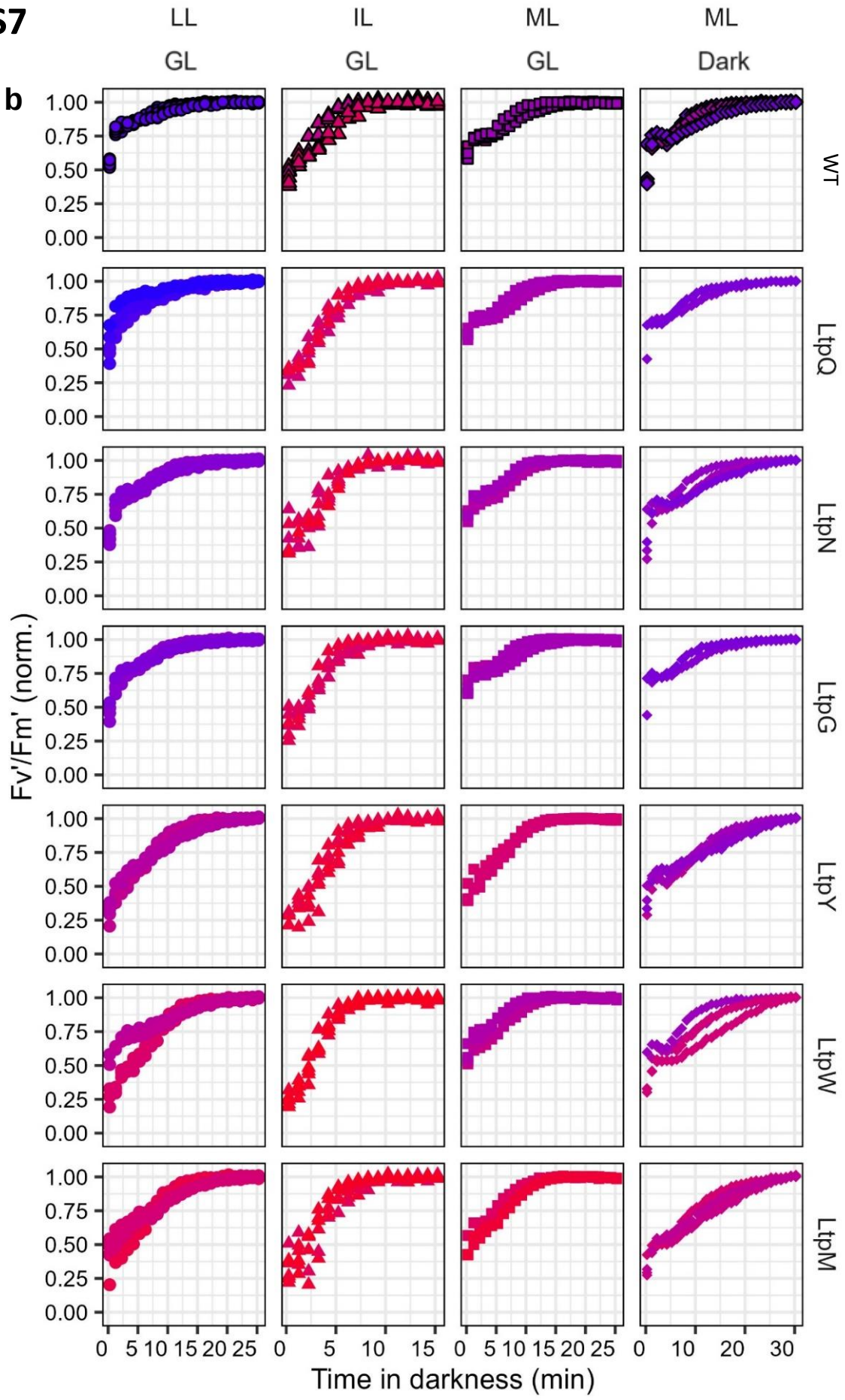
b
LL
GL
IL
GL
ML
GL
ML
Dark
WT
LtpQ
LtpN
LtpG
LtpY
LtpW
LtpM
Fv'/Fm' (norm.)
1.00
0.75
0.50
0.25
0.00
0 5 10 15 20 25
0 5 10 15
0 5 10 15 20 25
0 10 20 30
Time in darkness (min)

Figure S7

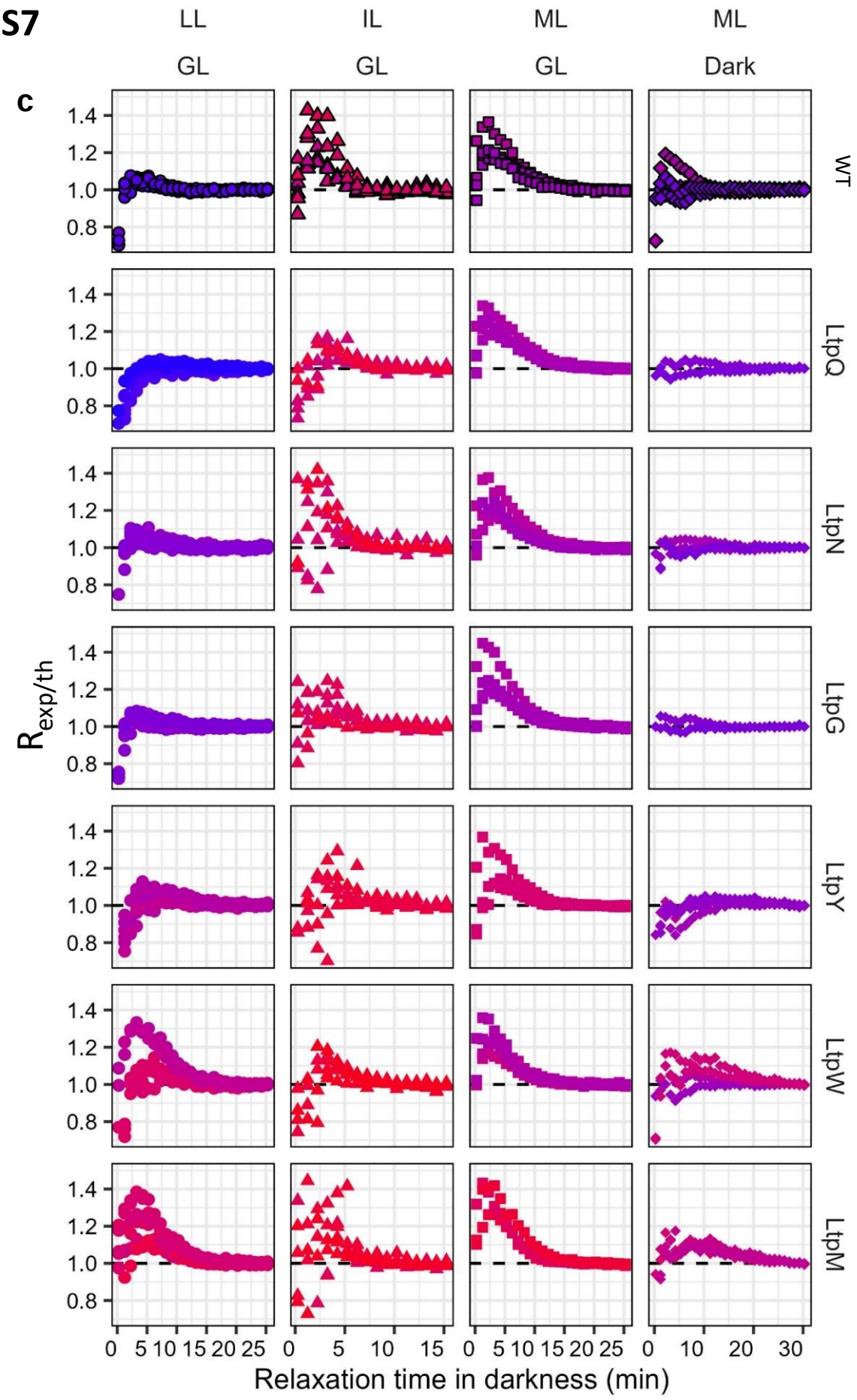
c
LL
GL
IL
GL
ML
GL
ML
Dark
WT
LtpQ
LtpN
LtpG
LtpY
LtpW
LtpM
$R_{exp/th}$
1.4
1.2
1.0
0.8
0 5 10 15 20 25
0 5 10 15
0 5 10 15 20 25
0 10 20 30
Relaxation time in darkness (min)

Fig. S7 | Time dependence of the qZ component of NPQ, F_V'/F_M' and the Ratio of experimental-to-theoretical F_V'/F_M' ($R_{exp/th}$) during relaxation in darkness, in all *Phaeodactylum tricornutum* strains.

For all strains and growth conditions (low light (LL), intermittent light (IL), moderate light (ML) under growth light (GL) or after 40h of dark acclimation (Dark)), the kinetics of the rapidly reversible, diatoxanthin-dependent, qZ component of NPQ relaxation (**a**), F_V'/F_M' normalized to its fully relaxed value (**b**), and $R_{exp/th}$ (**c**) were measured after qZ induction under high light (6 min, 600 (LL, IL) or 750 µmol photons m^{-2} s^{-1} (ML)). Raw data for LL growth conditions were used to derive similar parameters published in Giovagnetti et al., 2022 and are shown here after reanalysis in the context of testing the "SV-lake" model.

Figure S8

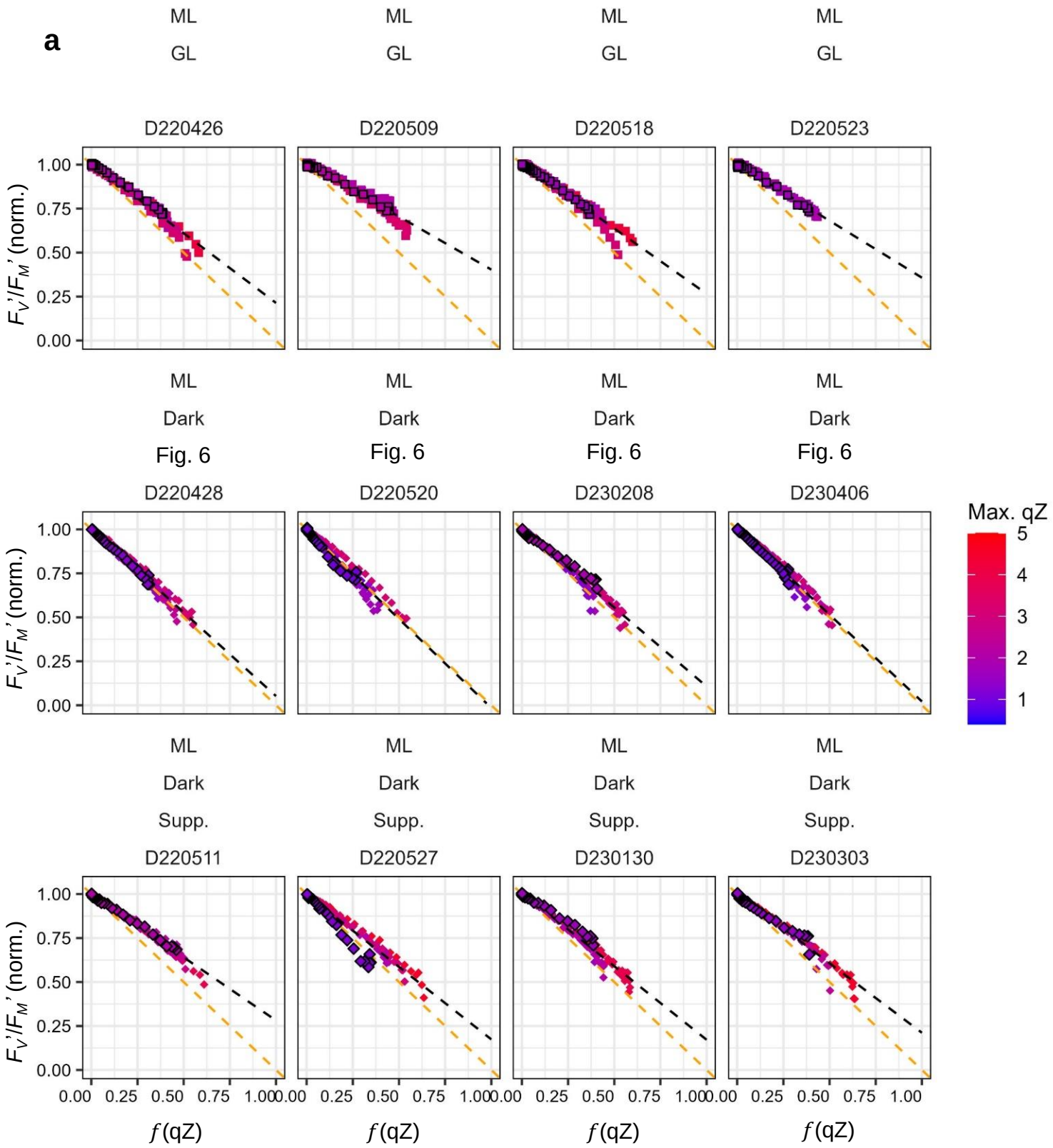
a
ML
GL
D220426
D220509
D220518
D220523
D220428
D220520
D230208
D230406
D220511
D220527
D230130
D230303
Dark
Supp.
Fig. 6
F_V'/F_M' (norm.)
f(qZ)
Max. qZ
0.00
0.25
0.50
0.75
1.00
1
2
3
4
5

Figure S8

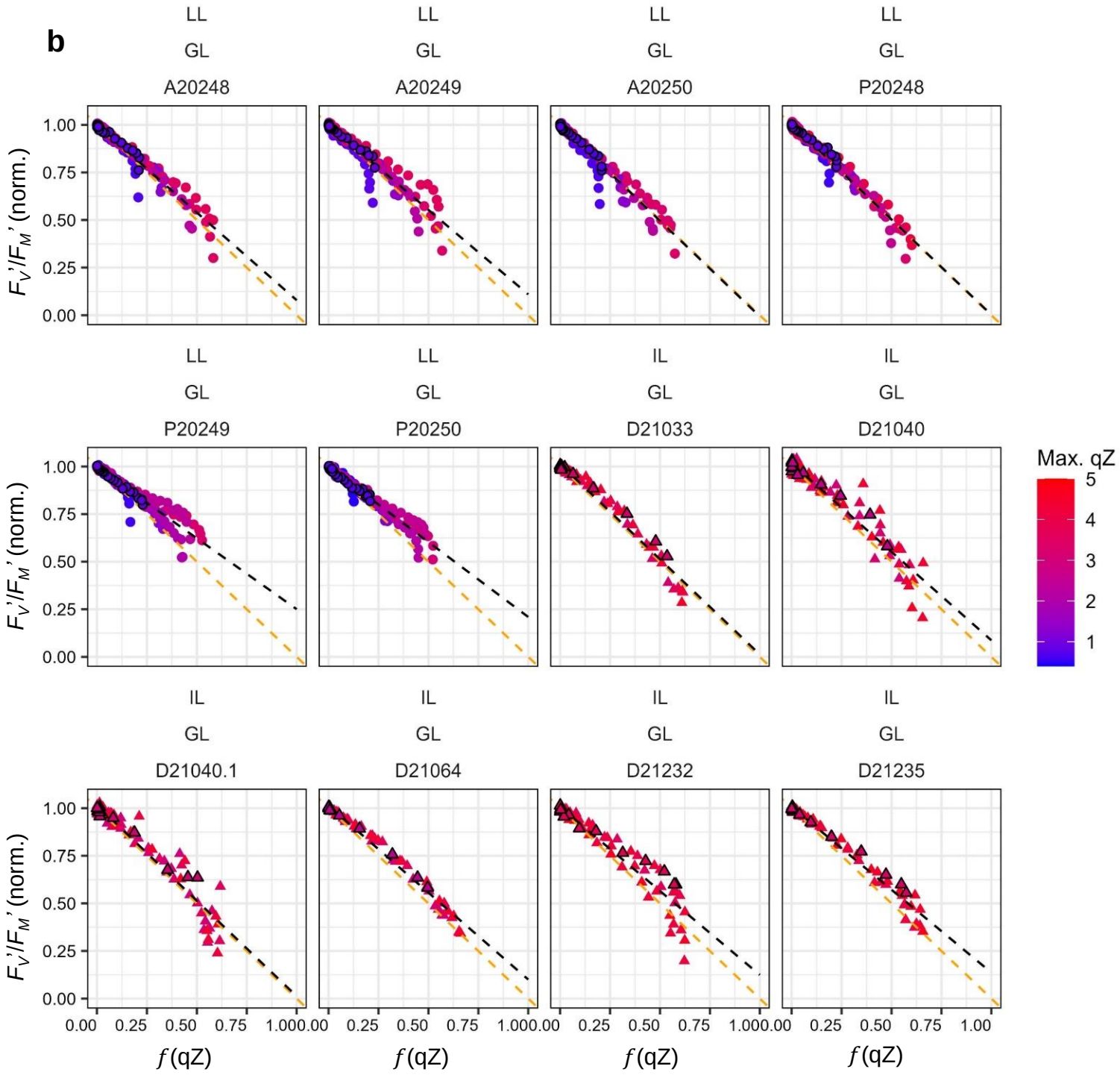
b
LL
GL
A20248
A20249
A20250
P20248
P20249
P20250
IL
D21033
D21040
D21040.1
D21064
D21232
D21235
F_V'/F_M' (norm.)
1.00
0.75
0.50
0.25
0.00
f(qZ)
Max. qZ
5
4
3
2
1

Figure S8

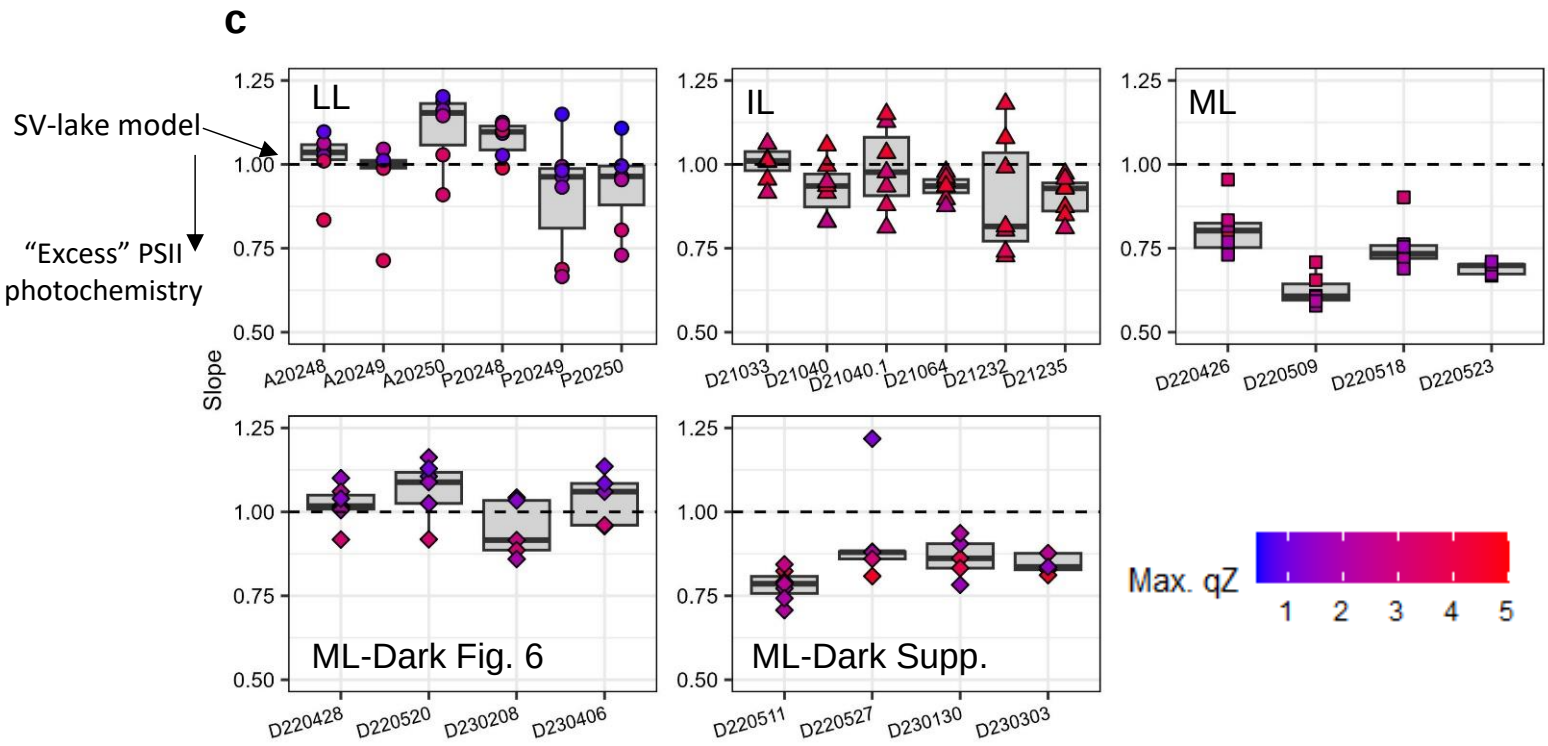

Fig. S8 | Normalized F_V'/F_M' vs. its relative decrease due to qZ (f(qZ)), in all *Phaeodactylum tricornutum* strains, for all experiments/days of measurements and growth conditions.

Every experiment, spanning 5 to 7 strains (including wildtype (black outline symbols)) cultivated under a same growth condition, for which the relationship between F_V'/F_M' and f(qZ) was tested is shown, with the dashed black line representing linear regression analysis ran on all strains together, compared to the theoretical slope of -1 (orange dashed lines). In (**a**) strains are acclimated to moderate light (ML), sampled directly under growth light (GL, squares) or after 40 h of "Dark" acclimation (diamonds), for which we distinguish experiments of near exact agreement with the Stern-Volmer (SV)-lake model theory shown in Fig. 6 and days of experiment where Dark treatment improved agreement with theory compared to ML-GL, but not fully. In (**b**) strains are acclimated to low light (LL, circles) and intermittent light (IL, triangles). The absolute value of the slope of linear regression ran on every individual strain for a given day of experiment and growth condition are shown in (**c**). Absolute slope value of 1 are expected by the SV-lake model, while absolute slope values below 1 represent "excess" of PSII photochemistry (see main manuscript).

Figure S9

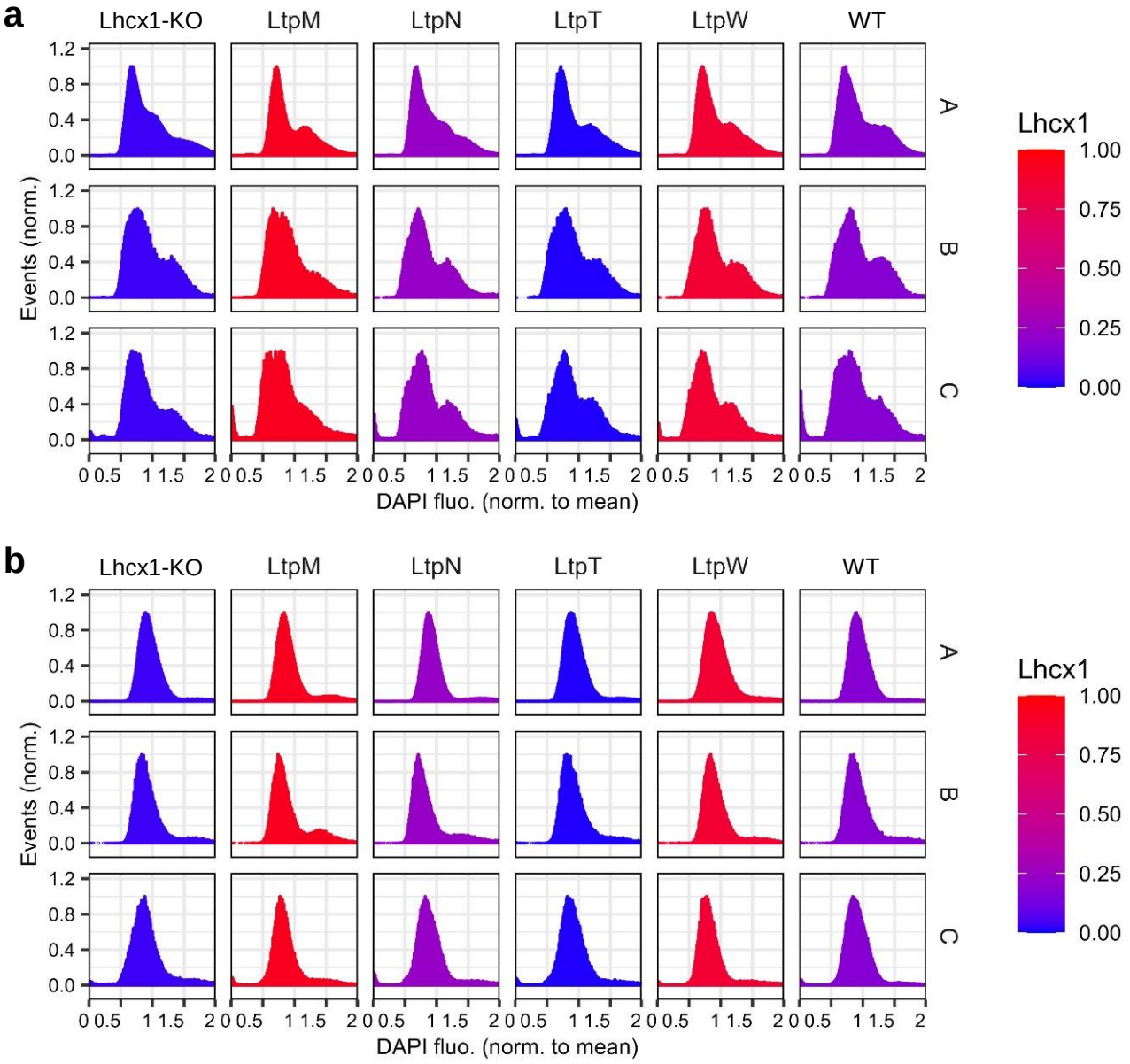
a
Lhcx1-KO
LtpM
LtpN
LtpT
LtpW
WT
A
B
C
Events (norm.)
DAPI fluo. (norm. to mean)
Lhcx1
1.00
0.75
0.50
0.25
0.00
b
Lhcx1-KO
LtpM
LtpN
LtpT
LtpW
WT
A
B
C
Events (norm.)
DAPI fluo. (norm. to mean)
Lhcx1
1.00
0.75
0.50
0.25
0.00

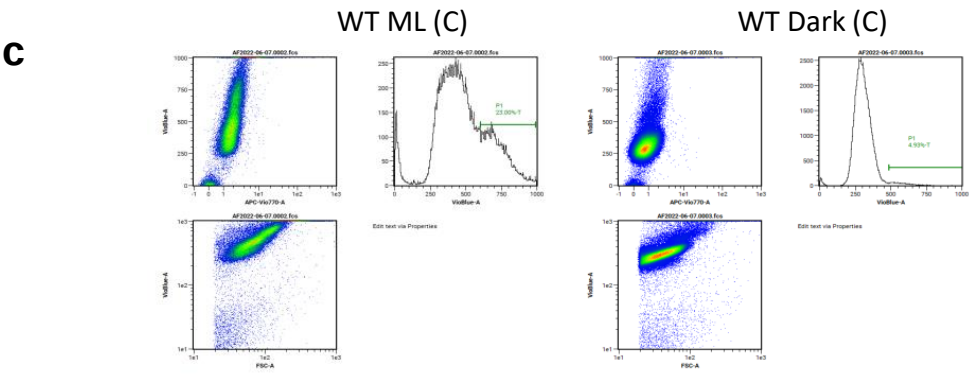
c
WT ML (C)
WT Dark (C)

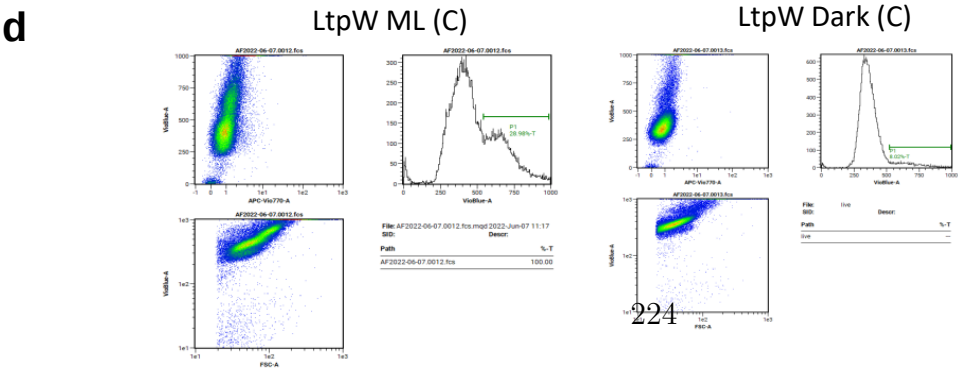
d
LtpW ML (C)
LtpW Dark (C)

Figure S9

e

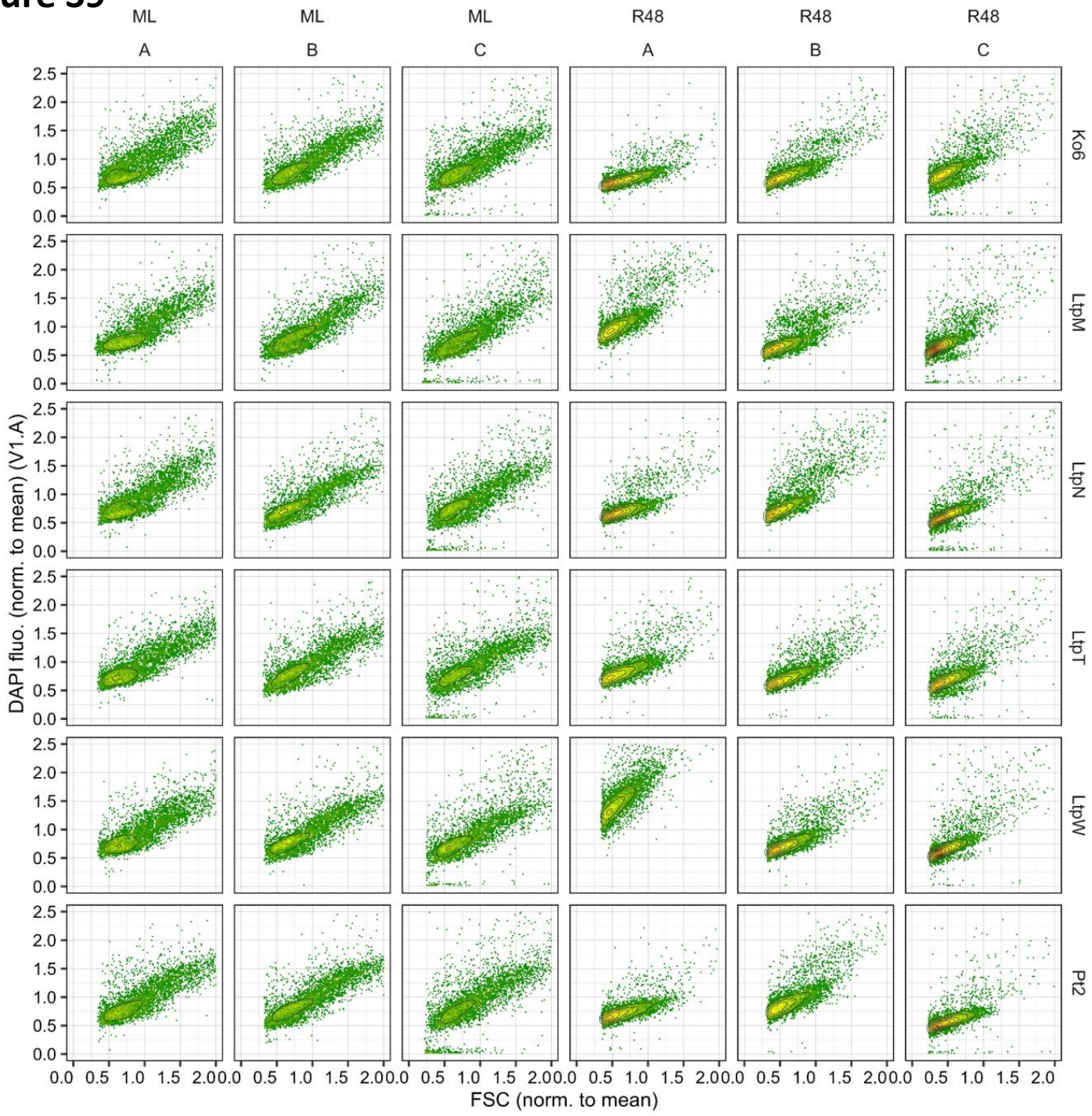

Fig. S9 | Assessing physiological heterogeneity with and without dark acclimation in *Phaeodactylum tricornutum* wildtype and different Lhcx1 mutants.

Cytograms showing events (≥ 50, 000 recorded) of DAPI-fluorescence (V1.A channel), a proxy of DNA content per cell, in cultures of different *P. tricornutum* strains grown under moderate light (ML) and sampled either directly under growth light (**a**) or after 40 h of "Dark" acclimation, before centrifugation and fixation in cold EtOH (**b**). This protocol commonly used to synchronize cells' physiology (see Methods and Huysman *et al.,* 2010) served as the basis to explore the "heterogeneous Stern-Volmer hypothesis" in Text S2. Examples of MACSquantify software output and gating on V1.A histogram to approximate the proportion of each population of wildtype (Replicate C) (**c**) and LtpW (Replicate C) for ML and Dark treatment (**d**). DAPI fluorescence vs. forward scatter (FSC) in all replicates (strain*Treatment), with the mean of both parameters being calculated over all events recorded for ML and Dark treatments, plot made with R software and binning set at 100 (**e**).

References

Giovagnetti, V. Jaubert, M, Shukla MK, Ungerer P, Bouly JP, Falciatore A, and Ruban AV. Biochemical and molecular properties of LHCX1, the essential regulator of dynamic photoprotection in diatoms. *Plant Physiology* **188**, 509–525 (2022).

Huysman MJ, Martens C, Vandepoele K, Gillard J, Rayko E, Heijde M, Bowler C, Inzé D, Peer Y, De Veylder L, *et al*. 2010. Genome-wide analysis of the diatom cell cycle unveils a novel type of cyclins involved in environmental signaling. *Genome Biology* **11**: R17.

In this Appendix, we outline the fundamental principles of the "lake" model and explain how photosynthetic parameters can be derived from chlorophyll *a* fluorescence measurements within this theoretical framework. Additionally, we expend this model to the situation where the regulated heat dissipation process (reversible non-photochemical quenching) is entirely attributed to a quencher Q of concentration [Q], and refer to this expanded model as the "SV-lake" model.

Within the "lake" model, the photosynthetic unit includes numerous photosystem II complexes embedded in a shared light-harvesting antenna, all competing for excitons (Lavergne & Trissl, 1995; Kramer *et al.*, 2004). The yield of each process involved in excited chlorophyll relaxation is then determined by the kinetic competition between these processes. The yields of fluorescence (Φ_F), intrinsic losses (sum of fluorescence and non-regulated heat, Φ_{NO}), photochemistry (Φ_{PSII}) and non-photochemical quenching (Φ_{NPQ}) are described by the following equations:

Equation 3	$\Phi_F = k_F / (k_F + k_H + kp \times [Q_A] + \kappa_{NPQ})$
Equation 4	$\Phi_{NO} = (k_F + k_H) / (k_F + k_H + k_p \times [Q_A] + \kappa_{NPQ})$
Equation 5	$\Phi_{PSII} = k_p \times [Q_A] / (k_F + k_H + k_p \times [Q_A] + \kappa_{NPQ})$
Equation 6	$\Phi_{NPQ} = \kappa_{NPQ} / (k_F + k_H + k_p \times [Q_A] + \kappa_{NPQ})$

Here, k_F, k_H, k_P and κ_{NPQ} represent the rate constants for radiative and non radiative dissipation, photochemical and non-photochemical quenching, respectively. The term $[Q_A]$ denotes the concentration of open reaction centers with oxidized Q_A.

Within this theoretical framework, fluorescence yield can provide valuable information about the photochemical and non-photochemical yields, provided that PSI fluorescence – considered minor and of constant yield- is not considered (Stirbet & Govindjee, 2011). The fluorescence measured from a photosynthetic sample in a given instrument can be expressed as the product of a factor α (describing the instrument and sample, *e.g.* the geometry in the instrument, percentage of fluorescence detected, number of photosynthetic units in the sample), the fluorescence yield (Φ_F) and the light irradiance E.

Equation 7	$F = \alpha \times E \times k_F / (k_F + k_H + kp[Q_A] + \kappa_{NPQ})$

From there, the fluorescence level can be derived in different situations: F_0 and F_m represent the fluorescence levels when all PSIIs are open ($[Q_A] = 1$) or closed (($[Q_A] = 0$) in the absence of NPQ, respectively, whereas F_0' and F_m' are their counterparts when NPQ is present.

Equation 8	$F_0 = \alpha \times E \times k_F / (k_F + k_H + kp)$
Equation 9	$F_m = \alpha \times E \times k_F / (k_F + k_H)$
Equation 10	$F_0' = \alpha \times E \times k_F / (k_F + k_H + kp + \kappa_{NPQ})$
Equation 11	$F_m' = \alpha \times E \times k_F / (k_F + k_H + \kappa_{NPQ})$

By combining equations 7 and 9, we find that that the yields of intrinsic losses, photochemistry or of non photochemical quenching can be derived such fluorescence measurements

Equation 12	$\Phi_{NO} = F/ F_m$
Equation 13	$\Phi_{PSII} = (F_m' – F) / F_m'$
Equation 14	$\Phi_{NPQ} = F / F_m' - F / F_m$

We can also calculate the maximum (F_v/F_m) or potential (F_v'/F_m') quantum yield of PSII for photochemistry by combining equations 8 to 11:

Equation 15	$F_v/F_m = (F_m – F_0)/F_m) = k_p / (k_F + k_H + k_p)$
Equation 16	$F_v'/F_m' = (F_m' – F_0')/F_m') = k_p / (k_F + k_H + k_p + \kappa_{NPQ})$

For a fluorophore in a homogeneous solution, the extent of fluorescence quenching by a quencher Q is expressed as the product of the quencher concentration and its quenching rate coefficient. The Stern-Volmer equation postulates a kinetic competition between radiative relaxation (fluorescence) and relaxation of the excited fluorophore by Q and expresses the NPQ as the product of the Stern-Volmer (SV) quencher Q and its quenching coefficient k_{SV}. For the photosynthetic unit, we call "SV-lake" model, the theoretical framework where the NPQ is entirely due to a non-photochemical quencher Q of concentration, behaving as a SV quencher:

Equation 17	$\kappa_{NPQ} = k_Q \times [Q]$

Combining equations 14 and 17 gives the equation 1 displayed in the main text:

Equation 1	$NPQ = F_m/ F_m' – 1 = k_Q/(k_F + k_H) \times [Q] = k_{SV}[Q]$

In a "SV-lake" model, the product of the SV quencher concentration and its coefficient of quenching can therefore be assessed through the sole measurements of fluorescence levels at closed reaction centers (F_m and F_m').

Every excited chlorophyll has an equal probability of encountering a photochemical or non-photochemical quencher is generally described by the "lake" model.

In the “lake” or “SV-lake” models, every excited chlorophyll has the same probability of encountering a photochemical or non-photochemical quencher and the yield of both processes is –again- given by the kinetic competition between them. It is ossible to determine the influence of NPQ on photochemistry. , The influence of NPQ on the fluorescence level at open reaction center (F_0', maximal yield for photochemistry) can be obtained by combining equations 8, 10 and 17:

Equation 18	$F_0/ F_0' - 1 = k_Q/(k_F + k_H + k_P) \times [Q] = k_{SV0}[Q]$

Combining equations 1 and 18 gives equation 17 which expresses the change in the efficiency of the SV quencher due to photochemistry:

Equation 19	$k_{SV0} / k_{SV} = F_0/ F_m$

Another way to express the interplay between photochemical and non-photochemical quenching is to calculate the influence of NPQ on the potential yield of PSII for photochemistry (F_v'/F_m'). Combining 15, 16 and 17, wich gives equation 20: t

Equation 20	$F_v'/F_m' = (F_v/F_m) / (1 + (1 - F_v/F_m) \times NPQ)$

We can define $f(NPQ)$ as the expected relative decrease of potential quantum yield of PSII for photochemistry due to NPQ (using the maximum quantum yield F_v/F_m as a reference):

Equation 21	$f(NPQ) = (F_v/F_m - F_v'/F_m')/(F_v/F_m)$ $= (1 - F_v/F_m) \times NPQ/(1 + (1 - F_v/F_m) \times NPQ)$

The combination of equations 20 and 21 provides the equation 2 from the main text, which we prefered to the equation 17 because it allows to confrount our experimental data (relationship between F_v'/F_m' and $f(NPQ)$) with a theoretical relationship which is linear. It is important to note that testing the validity of the “SV-lake” model through equation 21 (our work) is absolutely equivalent to testing it through equation 17 (as in Giovagnetti & Ruban, 2017) or through equation 19 (Lavaud *et al*., 2002). In another study (Buck *et al.*, 2019), the evolution of functional absorption cross-section (σPSII) was studied as a function of NPQ. Since the functional cross-section (σPSII) is the product of the optical cross-section of PSII (optical-σPSII) and the potential yield of PSII for photochemistry (F_v'/F_m') when NPQ represents

only heat-dissipation proceses in the antenna (Gorbunov *et al.*, 2001; Mauzerall & Greenbaum, 1989), the same NPQ-dependencies are expected for F_v'/F_m' or for σPSII.

3.4 Discussion and perspectives

The article above argues that NPQ in *P. tricornutum* and *Plagiostriata* sp., at least in the growth and experimental conditions tested, is exceptionally well described by a homogeneous SV-quencher model. We present, I hope, very compelling evidence that the quencher (Q) is proportional to DT interacting with Lhcx1 in PSII. Moreover, the work of Buck et al., suggests that Lhcx2 and Lhcx3 would provide the same environment to DT, although the DT quenching efficiency might then be different from the ones we obtained here . That is not to say that there are no conditions that can be found for which the SV-model is rejected, for example, see the effect of different inhibitors on NPQ in *P. tricornutum* (Lavaud and Kroth, 2006)). Neither do we ignore the wisdom of the famous aphorism "*All models are wrong but some are useful.*". At some level, the SV-model is incomplete and simply *wrong*, as all models are, but it is certainly very *useful*.

Molecular actors and quenching mechanisms

The strength of our argument is summarized in Fig.3g-h of the previous paper. A direct relationship between observables measured with three completely different methods (variable fluorescence, HPLC and immunoblots) and with such a large window of validity is hard to disregard and undoubtedly *useful*. Indeed, the phenomenological relationship remained consistent across a large dataset, including 9 strains, two contrasted growth conditions and using two independent experimental approaches to vary NPQ (under steady-state illumination of various intensities or over time of relaxation in darkness). For example, these Lhcx1 mutants can now provide an ideal control and null hypothesis to investigate the molecular mechanism of qZ. We remain agnostic about this mechanism for the moment, but combining the Lhcx1-mutants series with more sophisticated techniques, such as time-resolved fluorescence or transient absorption spectroscopy could yield very important results. Having a strong null hypothesis on the expected relative change in fluorescence or bleaching lifetime as a function of [Lhcx1] $\times$ DES, and expecting other signals to remain unchanged, would be a huge advantage when using techniques for which data interpretation is not as straightforward as with variable fluorescence. A very recent study using transient absorption spectroscopy, proposed the LHCSR3-dependent, qE, quenching site in *C. reinhardtii* was a lutein in S_1 state (Zheng et al., 2024). Provided the micro-sized cell fraction sample preparation protocol used by the authors can efficiently be applied on diatoms and other organisms containing four membranes plastids, there is a lot that could be done to push further our proposed model.

For one, diatoms, and other secondary endosymbionts, do not possess lutein so it would be interesting to investigate the nature of the quenching site. Beyond that, one of the most interesting questions surely is whether different molecular actors can foster the same quenching mechanism. Testing different molecular actors could involved *P. tricornutum* double-mutants (Buck et al., 2021) to use an approach similar to ours but with Lhcx3, *P. tricornutum* accumulating more than one isoforms or, even a Lhcx1 knockout prepared during the night period which should only accumulate the enigmatic Lhcx4. There is also the question of whether the VAZ cycle pigments are equivalent to DT when it comes to qZ quenching. In a ZEP3 mutants for which VAZ accumulation partially rescues qZ capacity, variable fluorescence analysis suggests qZ could be proportional to the number of de-epoxidized sites, independently of the nature of the pigment (DT, AX or ZX) (Giossi et al., 2024). There are also representatives from other groups showing a single qZ-NPQ component relying on the VAZ cycle which could be tested, like *Phaeomonas* sp. (Berne et al., 2018), but for which we unfortunately do not know the LHC actor(s). Also exists the very interesting case of

Nannochloropsis oceanica, surely the species from secondary endosymbiosis origin for which the NPQ has been the most studied with *P. tricornutum* (Park et al., 2019). *Nannochloropsis oceanica* possesses the VAZ cycle and a single Lhcx isoform, and the presence of both actors are obligatory for NPQ. The latest model explains its NPQ as a mixture of qE and qZ (to which AX and VX participate to a lesser extent than ZX) (Short et al., 2023). Using a similar molecular titration approach to ours with *N. oceanica* sole Lhcx isoform would be another promising way to test the phylogenetic limits of the model we put forward.

The lake model and assumptions of the variable fluorescence method

Regarding the lake model, it is of significant importance to be able to demonstrate it to work almost perfectly in a given species (in fact, two). Knowing the relationship between PSII photochemistry and qZ is extremely powerful, and it can now be used as a fulcrum to reach a deeper understanding of how qZ interacts with multiple other levels of photosynthesis regulations, which will be the focus of Chapter 4. Therefore, in this discussion, I will mainly focus on the circumstances under which we observed deviation from the model, namely the larger than predicted PSII photochemistry for a given qZ in the first minutes of the relaxation in the dark. It must be mentioned that in addition to the two conditions shown in the manuscript, moderate growth light and after 40 h of dark acclimation, a vast (almost obsessive!) number of hypotheses were tested, including the intensity and duration of the light stress, the spacing between saturating pulses, single and multiple turnover pulses, the colour of the actinic light (from four different fluorometers), additions of various concentrations of uncouplers or HCO_3^-, experimenting at different moments over the diurnal cycle, cold acclimation, among others... Besides with the 40h dark-acclimation presented in the manuscript, this phenomenon was stubbornly consistent. One hypothesis that we entertained for a while, and mentioned in the paper's discussion, is a transient decrease in $\Delta\psi$, as an anti-correlation between $\Delta\psi$ magnitude and PSII photochemistry is known (Diner and Joliot, 1976, Davis et al., 2016). Indeed, we also made the surprising observation of a $\Delta\psi$ collapse upon sudden dark transition in *P. tricorntutum*, which will be presented in Chapter 5. We finally concluded that the $\Delta\psi$ recovered over a shorter timescale than the deviation from the model, and therefore that it could not be the main explanation.

But it is noteworthy, that with the lake model as baseline hypothesis, we can now explore additive effects of other factors potentially influencing PSII photochemistry while maintaining the assumption that NPQ is strictly dependent upon $\kappa_{SV} \times [Q]$. Similarly, we thought about the recent discussion about part of the variable fluorescence rise being imputable to a shift from a "dark-adapted" to a "light-adapted" state of PSII during a multiple turnover pulse (Garab et al., 2023). Could it be responsible for the "excess of PSII photochemistry" we observed? This would require the contrast in fluorescence yield between "dark-adapted" PSIIs and "light-adapted" PSIIs to also be transiently affected upon sudden dark transition, bringing us back to square one. However, once again, pennate diatoms could be the ideal model to investigate further the incongruities regarding variable fluorescence rise raised in (Garab et al., 2023). Differences between "dark" and "light" adapted PSIIs have been proposed to be caused by dielectric relaxation processes based on works with purple bacteria (Sipka et al., 2022). In diatoms, the absolute $\Delta\psi$ prior to the pulse, which should influence dielectric relaxation processes, can be manipulated and quantified. Which would add a key observable to explore these questions (see Chapter 5). Nevertheless, the fact that we still measured "excess of PSII photochemistry" with a single turnover pulse (less prone to generate "light-adapted" PSIIs (Garab et al., 2023)) and that we could observe a perfect lake model-like relationship after prolonged dark-adaptation, is hard to reconcile with this theory

as it stands right now.

All in all, the heterogeneity hypothesis is our favourite because the deviation is simple to derive mathematically from the lake model with an SV-quencher, and always in the observed direction. Moreover, assuming all PSIIs, let alone cells, have the same photochemical properties is a strong hypothesis. We explored the idea of heterogeneity among cell with DAPI-staining cytometry and observed bi-modal populations (≈75-25% in terms of DNA content). Bi-modal distribution between contrasted PSII populations is exactly the kind distribution that exacerbate the most deviation from the expected F_V'/F_M' values as a function of qZ. While very heterogenous, multimodal populations, would tend to dampen contrasts (see Appendix I in the previous manuscript). Nevertheless, we have no way to measure photochemistry in these populations individually at the moment. The next step could be to play with mixtures of different concentrations and Lhcx1-mutant strains to see if the experimental curves are validated by theoretical calculations. Additionally, variable fluorescence at the single-cell level is rapidly improving and will allow to push this hypothesis further in the near future. The single-cell fluorometer we are testing at the lab does not achieve the signal-to-noise ratio to test the F_V'/F_M' versus qZ relationship directly yet, especially at very high NPQ level and in a relatively small cell like *P. tricornutum*. However, it could be interesting to investigate if we can identify ensembles of cells with different average properties roughly reflecting the heterogeneity measured by cytometry, with and without dark adaptation.

The heterogeneity hypothesis also brings up a much needed discussion about the common use of NPQ in the field as an indicator of less productive, or stressed, communities. Granted the nonlinear nature of the relationship between NPQ and fluorescence, by contrast with the linear one between Φ_{PSII} and fluorescence (see Section 1.3), and the heterogeneity within field samples, this approach yields surprisingly coherent results (Schuback et al., 2017, Ryan-Keogh and Thomalla, 2020, L. Lacour et al., 2023, Sezginer et al., 2023). A partial answer might be that strong NPQ is usually ascribed to nutrients deficiency stress responses, which can have relatively uniform effects on organisms from different phyla (Falkowski et al., 2017). An interesting scenario to test the limit case of how this nonlinear relationship could affect fluorescence parameters interpretation in natural heterogeneous samples is the one of allelopatic interactions. Allelopathy is the release of toxic secondary metabolites by photosynthetic organisms, that impede the growth of photosynthetic competitors. Allelopathy is extremely common in nature and toxic compounds often target photosynthesis and lead to increasing NPQ. Crucially, allelopathic effects are often taxa specific (Srivastava et al., 1998, Wolfram et al., 2015, Long et al., 2021). Therefore, using NPQ as photosynthetic "health index" in communities where strong allelopathic interactions are at play, should be very susceptible to the erroneous interpretation that a whole community has high NPQ (and is therefore "unhealthy"), when only a specific taxon is negatively affected by another one thriving. During my Ph.D., I had the chance of collaborating on a project on allelopathy which I will quickly overview in Chapter 5. Interestingly, NPQ was often the first sign that indicated the onset of allelopathic stress.

Conclusion

These discussion points illustrate the strength of having a simple model anchored in physical principles to explore further hypotheses, whether in the mechanisms of NPQ, its diversity among groups or test the limits of the "Q_A model" (Duysens and Sweer, 1963) for variable fluorescence. Alternative NPQ models in diatoms used incongruities with the "Q_A model" as basis for proposing more complex quenching dynamics than a classical Stern-Volmer quencher (Lavaud, Rousseau, van Gorkom, and Etienne, 2002, Giovagnetti and Ruban, 2017, Buck et

al., 2019). We believe it is more parsimonious to construe the same surprising observation made by the aforementioned reports and us, as a breach of the assumptions behind the "Q_A model", and maintain that Q behaves like a SV-quencher (previous Fig.3g-h). One of the premises of my Ph.D. was that *P. tricornutum* is a particularly convenient organism to work with. Many of the points listed as advantageous, simpler, features when working on *P. tricornutum* in Introduction, are strongly substantiated by the findings of this Chapter.

Chapter 4

NPQ as a regulator of photosynthetic processes in diatoms

4.1 Regulation of photosynthesis at the gene expression level

The regulation of photosynthesis involves a delicate interplay between short-term dynamic mechanisms and long-term acclimation processes, which are intricately linked to the organism's genetic makeup and environmental sensing systems. In Chapter 2, my co-authors and I reviewed the literature concerning the dynamic mechanisms that grant photosynthesis a "degree of freedom" and flexibility to thrive under ever changing environmental conditions. On short time scale, processes like qZ, qI quenching, cyclic electron flows (CEF) and pH-dependent photosynthetic control, are dynamically activated via different regulations such as disulfide bridge formation, phosphorylation, pH-dependent dimerization, etc. These processes are all directly responsive to the energy state of the plastid. In the next manuscript, we used our continuum of Lhcx1 expressing mutants as a qZ-dial to modulate the internal state of the cell by increasing light energy dissipation in PSII, everything else remaining roughly equal. This approach offers new perspectives and insights into many regulatory mechanisms, some of which have barely been described before in diatoms, such as CEF. However, the effectiveness of these short-term mechanisms depends heavily on the long-term regulatory processes that precede them, specifically, photoacclimation processes shaped by gene regulation responding to the cell's history. Through transcriptomics, this Chapter also investigates how qZ influences the initial onset of genic regulation upon a shift to high light.

Genic regulation relies on an intricate network of signalling pathways, in order to modulate the abundance of various molecular actors, this process optimizes the photosynthetic apparatus tuning to current and forecast (circadian regulation, for instance) conditions. For example, these regulations can entail increasing light-absorbing pigments upon low light shift, increasing detoxification machinery and photoprotective mechanisms upon high light shift, or enhancing membrane fluidity by modulating its lipid composition under chilling stress, etc. Internal and external cues are monitored through various sensors and interact with transcription factors that mediate the activation or repression of specific genes (Ait-Mohamed et al., 2020). Additionally, most photosynthetic genes are encoded in the nucleus, but their associated proteins are exported to various organelles to regulate their functions. This includes organelle possessing their own genomes, such as plastids and mitochondria (*anterograde signalling*). Conversely, signals originating from the plastid or other organelles that need to

be transmitted to the nucleus for appropriate regulation represent *retrograde signalling*. To achieve a holistic comprehension of photosynthesis regulation, it is crucial to decipher the roles of various sensors and gene expression patterns. Even more importantly, we must understand how converging signals within a complex network are integrated to orchestrate a cohesive response at the organismal level.

External sensing includes detecting changes in temperature and concentrations of nutrients, among others, but the light environment is especially crucial for photosynthesis (reviewed in diatoms in (Jaubert et al., 2022)). Diatoms possess a wide array of pigment-bound photoreceptors that modulate gene expression as a function of light intensity, quality and period. In terms of internal cues, ROS production by photochemistry is an important source of signal under stressful conditions like high light (Foyer, 2018). *A priori*, both $^1O_2$ predominantly produced by PSII, and H_2O_2 resulting from the Mehler reaction at PSI may lead to retrograde signalling and could trigger high light responses. Because of their very short lifetimes $^1O_2$ have been suggested to be less important than H_2O_2 as a signal molecule (Noctor and Foyer, 2016). However, a recent study in *Chlamydomonas* showed that $^1O_2$ generates indirect signalling through lipid peroxidation by-products (Pancheri et al., 2024). Another central regulation hub and source of retrograde signalling is the redox state of the PQ-pool. This is clearly demonstrated by using different inhibitors to oxidize or reduce the PQ-pool, which mimic the effects of low or high light at the PQ-pool level, even when the *actual* light intensity remains unchanged. This experiment was first performed with the green algae *Dunaliella tertiolecta* (Escoubas et al., 1995), but has since been repeated with diatoms (Lepetit et al., 2013), showing notably that accumulation of Lhcx isoforms and XC enzymes are triggered when PQ-pool reduction is favoured by addition of exogenous inhibitors. Finally, the glutathione-ascorbate metabolism, itself influenced by H_2O_2 and NADPH production, is crucial for plants healthy growth not only to maintain adequate concentrations of co-factors for various reactions, but also for its signalling functions (Foyer and Noctor, 2011). While the literature in diatoms is not as deep, it is likely also the case for this group (Rosenwasser et al., 2014, Van Creveld et al., 2015, Volpert et al., 2018).

A frontier in genic regulation studies is to develop protocols, representative of natural conditions (without the use of inhibitors) allowing to disentangle genes expression responding to changes in the external environment from responses to retrograde signalling. In this upcoming paper, we propose that this can be achieved with a high enough resolution of transcriptomic profiling along an "abiotic dimension" and an "internal state dimension". In our case, we used the time of high light exposure (abiotic) modulated by the magnitude of qZ (internal state). As mentioned in the first paragraph, we also used the ranging Lhcx1 concentration among mutants to unveil phenomenological relationships between NPQ/qZ extent and other regulatory mechanisms in *P. tricornutum*. We are in the final steps of finalizing the following manuscript which will be submitted before the end of the year.

4.2 Article: A photoprotection dial to unveil multi-level orchestration of photosynthetic regulations in diatoms

A photoprotection dial to unveil multi-level orchestration of photosynthetic regulations in diatoms

D. Croteau[1*], M. Jaubert[1], T. Quemar[1], A. Falciatore[1], A. Maes[2, 3], B. Bailleul[1*]

1. UMR7141, Institut de Biologie Physico-Chimique, Sorbonne Université / CNRS, 13 Rue Pierre et Marie Curie, 75005 Paris, France
2. UMR8226, Institut de Biologie Physico-Chimique, Sorbonne Université / CNRS, 13 Rue Pierre et Marie Curie, 75005 Paris, France
3. Plateforme de Génomique Fonctionnelle FR550, Institut de Biologie Physico-Chimique, Sorbonne Université / CNRS, 13 Rue Pierre et Marie Curie, 75005 Paris, France

[*] corresponding authors: dany.croteau@ibpc.fr, bailleul@ibpc.fr

Abstract

The comprehensive orchestration of photosynthetic regulatory modules represents the next frontier in photosynthesis research. In this study, we exploit the features of Non Photochemical Quenching (NPQ) in a variety of mutant strains of the diatom *Phaeodactylum tricornutum* expressing different levels of the NPQ-mandatory protein Lhcx1 to create a "photoprotection dial". Adjusting this "photoprotection dial" by varying light exposure and comparing strains allows to explore the interactions between NPQ, the redox state of the photosynthetic electron transport chain, photoinhibition or cyclic electron flow. The efficiency of non-photochemical losses in photosystem II shows a linear correlation with cyclic electron flow and an inverse relationship with photoinhibition. This approach not only provides informative phenomenological relationships between regulatory modules but also enables the study of how photosynthetic signals influence gene expression at the genome-wide scale. Approximately half of the genes responded to high light conditions in an Lhcx1-dependent manner, highlighting the role of photosynthetic signals in light-regulated gene expression. Clustering of genes based on exposure time under high light and/or photoprotection capacity provided clear insights, revealing clusters with invariant expression (e.g., housekeeping genes and cell cycle genes), groups strongly influenced by photoprotection (e.g., proteasomes, ribosomes and photoprotection-related genes) and groups modulated by light in an Lhcx1-independent manner (e.g., light absorption and photosynthetic complexes).

Abbreviations

PSII: Photosystem II

PSI: Photosystem I

NPQ: Non-Photochemical Quenching of chlorophyll fluorescence

PQ/PQH_2: Plastoquinone/Plastoquinol

ROS: Reactive Oxygen Species

HL: High Light

Lhcx: Light-Harvesting Complex X

Lhcr: Light-Harvesting Complex R

Lhcf: Light-Harvesting Complex F

qT: State transitions-dependent quenching

qZ: Xanthophyll-dependent quenching

qI: Photoinhibition-related quenching

qL: Fraction of open PSII reaction centers

LEF: Linear Electron Flow

CEF: Cyclic Electron Flow

AEF: Alternative Electron Flow

TEF: Total Electron Flow

Δ(TEF/LEF): Relative change in total electron flow proportion versus linear electron flow

ATP: Adenosine Triphosphate

ΦPSII: Yield of photochemistry,

ΦNPQ: Yield for dissipation by NPQ downregulation

ΦNO: Yield of other non-photochemical losses

YI: PSI yield of photochemistry

YND: PSI yield of non-photochemical energy dissipation due to donor side limitation

YNA: PSI yield of non-photochemical energy dissipation due to acceptor side limitation

P700: Photosystem I primary donor

c-t cyt. : c-type cytochromes (cytchrome c_6 + cytochrome *f*)

WT: wildtype

Pt: *Phaeodactylum tricornutum*

FCP: fucoxanthin chlorophyll-a/c protein

FPKM: fragments per kilobase of transcript per million fragments mapped

PCA: Principal Component Analysis

MC: meta-cluster

GO: Gene Ontology

PGAM: Phosphoglycerate Mutase

XC: Xanthophyll cycle

VDE: Violaxanthin deepoxidase

ZEP3: Zeaxanthin epoxidase 3

D1/D2: PsbA (D1) and PsbD (D2) proteins forming heterodimer in PSII

DT: Diatoxanthin

DD: Diadinoxantin

F_v/F_m: Maximum yield of PSII photochemistry in the dark

F_v'/F_m': Maximum yield of PSII photochemistry in the dark after light exposure

DNA: Deoxyribonucleic acid

^{t}RNA: Transfer ribonucleic acid

Introduction

To navigate changing environmental conditions and energetic demands, photosynthesis evolved a highly integrated network of feedback loops which act through electron flows, metabolic bifurcations, plastic gene expression and protein accumulation, among others. In the last decades, loss-of-function mutants stimulated an efficient reductionist approach to deduct the roles of different molecular actors or regulators by observing the functional consequences of their absence. However, there are intrinsic limits to this reductionist approach. *Grosso modo*, establishing clear causal relationships between genotype and phenotype is as straightforward as is narrow the scope of action of the protein encoded by the mutated gene (e.g., alternative electron flows mainly active under specific conditions (Chaux *et al.*, 2017; Nawrocki *et al.*, 2019)). By contrast, constitutive proteins are either vital or operate nested in flexible modules, where many actors can compensate each other and lead to cascade signalling steering physiology reorganization to buffer the deleterious effects of a dysregulated gene, or organism death can occur (Munekage *et al.*, 2004). Overcoming these "complex system problems" (self-organisation/system history, nonlinear/threshold responses, etc.) to gain a holistic understanding of regulations and their orchestration at the organismal level, is the new grail of photosynthesis research. If big data and system biology are approaches of choice to tackle such problems, mutagenesis and physiology studies could still grant valuable insights if creative experimental design tailored to address these questions are developed. Here, we present such an approach and unveil multi-level orchestration of the high light response in the model diatom *Phaeodactylum tricornutum*, by using a series of ranging Lhcx1 expressing mutants to provide a continuous gradient of photosystem II (PSII) photoprotection via Non Photochemical Quenching (NPQ) of chlorophyll (Chl) *a* fluorescence.

In a static view of photosynthesis, NPQ protects PSII by enhancing absorbed light energy dissipation as heat, which helps mitigating oxidative stress. However, photosynthesis is a dynamic process. Regulations do not happen in a vacuum but are rather connected through an intricate network of sensors, regulators and signalling pathways that constantly interact to fine-tune the system in response to both internal (metabolic state of the cell) and external (environmental) cues. Therefore, during a perturbation, tweaking one regulator should lead to profound repercussions on other regulatory modules across different levels simultaneously, themselves affecting others, and so forth. More NPQ, favouring heat dissipation over photochemistry in PSII everything else

remaining equal, should result in more oxidized PSII acceptors (Q_A and the plastoquinone (PQ) pool) and in a slower generation of reactive oxygen species (ROS) leading to photoinhibition (Laisk *et al.*, 1996). Yet, the PQ pool redox state and ROS production are crucial triggers of retrograde signalling (Escoubas *et al.*, 1995; Lepetit *et al.*, 2013; Foyer, 2018) which, if modulated by NPQ, should engender far-reaching consequences of their own. Formalizing these inferences into simple relationships is extremely challenging and is the focus of this study.

An hypothesis in plants suggests NPQ downregulating PSII reducing pressure, could be met by an increase in cyclic electron flux (CEF) around PSI, which boosts ATP output and help to cope with stressful conditions (Li *et al.*, 2018). In diatoms, translocation of reducing power to the mitochondria is hypothesized as the main constitutive alternative electron flux (AEF) to increase ATP output (Bailleul *et al.*, 2015). Nevertheless, enhanced CEF in stressful conditions has been reported (Thamatrakoln *et al.*, 2013; Goldman *et al.*, 2015; Gain *et al.*, 2023), thus CEF may be more dynamically regulated in diatoms. This begs the question, how does NPQ affect the relative activities of PSII and PSI: in a proportional manner (no change in CEF)? Or does CEF compensate transient decreases in linear electron flow (LEF)? In green organisms, oxidation of PSII core D1 and D2 proteins occurs during high light stress (Kale *et al.*, 2017). Photo-oxidation of PSII causes photoinhibition, i.e., the diminution of PSII photochemistry, while damaged PSII act as nonphotochemical quenchers (qI), leading to intricate effects between photochemistry and NPQ (Nawrocki *et al.*, 2021). Mechanisms contributing to NPQ are believed to protect PSII from photoinhibition, but contradictory views exist about the photoprotective nature of NPQ (Santabarbara *et al.*, 2001). In diatoms, qI and D1 degradation increase when the xanthophyll cycle necessary for NPQ is chemically inhibited during a light stress (Cartaxana *et al.*, 2013). However, refined protocols, without untargeted effects, are needed to establish quantitative relationships between NPQ, qI, photoinhibition, and the interplay between D1 degradation and its ATP-consuming repair cycle (Campbell & Tyystjärvi, 2012). Lastly, separating gene expression changes responding directly to light through photoreceptors from the ones responding to internal cues linked to photosynthesis, poses an additional layer of challenges, that has yet to be solved in any organism (Jaubert *et al.*, 2023).

In *P. tricornutum*, NPQ is unusually simple compared to its compounded nature in other organisms (Steen *et al.*, 2022; Short *et al.*, 2023). We recently demonstrated that the rapidly reversible part of

NPQ in *P. tricornutum* consists of a single component (qZ) strictly dependent upon the concentration of a nonphotochemical quencher. The later behaves as a homogeneous Stern-Volmer quencher and its amount is proportional to diatoxanthin (DT) interacting with Lhcx1 proteins in PSII antenna (Blommaert *et al.,* 2021, Croteau *et al.,* 2024). Through the xanthophyll cycle, DT concentration is swiftly regulated depending on the energy status of the plastid and modulates NPQ/qZ on the minute scale (Olaizola *et al.*, 1994; Goss & Jakob, 2010). In parallel, Lhcx1 is constitutively synthetized but its concentration, as well as that of the other isoforms Lhcx2 and Lhcx3, is adjusted on photoacclimative scales to pre-emptively optimize the capacity to reach higher NPQ level when triggered according to the cell history (Lepetit *et al.*, 2013; Taddei *et al.*, 2016). Beyond its mechanism, NPQ competition with other reactions in PSII is surprisingly well approximated by the theoretical "lake model" (Croteau *et al.,* 2024). This makes the estimation of many important parameters very reliable in *P. tricornutum*, such as such as the quantum yields of photochemistry (ϕPSII), non-regulated heat dissipation (ϕNO) and NPQ (ϕNPQ), and the concentration of open PSII reaction center (with oxidized secondary acceptor Q_A, qL). Another feature of *P. tricornutum* that fosters simpler fluorescence data interpretation and the robustness of these parameters is the absence of state transitions (reviewed in (Lepetit *et al.,* 2022)).

Recently, we introduced a series of *P. tricornutum* mutants with ranging Lhcx1 accumulation, already when grown in non-stressful conditions which do not trigger qZ. Therefore, this mutation is undetectable to the cells and offers the opportunity to work on various cultures with similar "system history" but equipped with a continuum of potential to downregulate PSII reducing pressure via qZ only *when* a stress occurs. Moreover, using several strains, up to 10 here, allows to model other processes as a function of qZ, and makes this approach incredibly robust to pleiotropic biases and noise, and able to detect potential nonlinear and threshold responses, which are limitations of one-on-one strain comparisons (e.g., wildtype versus knockout or overexpressor). We provide phenomenological relationships of the redox state of Q_A, photoinhibition and change in CEF as simple functions of qZ. Furthermore, by varying time in high light exposure (external cue) and qZ (modifying photosynthetic signals, internal cues), we could deconvolute the effects of external and internal cues on transcript profiles at the genome-wide scale. This unveiled that more than 50% of *P. tricornutum*'s genes is modulated by photoprotection (qZ magnitude) over high light response. We discuss how this powerful approach could be extended to other regulators and organisms, so that phenomenological relationships

between regulatory modules could be used as basic building blocks to develop phenomenological models of photosynthesis regulation.

Results

Effect of qZ on photosystems energy partitioning and redox state of intersystem chain

Ten *P. tricornutum* mutant strains with ranging Lhcx1 accumulation were grown under low light conditions which do not trigger qZ, therefore maintaining cultures in roughly equal photophysiological state, as characterized in (Croteau et al., 2024). The 10 strains were then exposed to an illumination of 570 µmol photons m^{-2} s^{-1} until a steady-state was reached, before characterizing energy partitioning in the two photosystems and the redox state of intermediary transporters (Fig. 1). This light intensity was chosen to maximize contrasts in NPQ/qZ, while reaching light-saturated regime for all strains (Fig. S1). Like our previous findings (Croteau al., 2024), NPQ was linearly correlated to Lhcx1 amount under saturating light exposure (Fig. 1a). This robust relationship will allow us in the next steps to estimate Lhcx1 amount in a given sample, based on NPQ/qZ, to define the *x*-axis and the colour scale. As a function of Lhcx1 amount, ϕPSII decreased only slightly (Fig. 1b), as expected in the light-saturating regime, where LEF is limited by non-photochemical steps (Sukenik *et al.,* 1987). Consequently, the increase in ϕNPQ from approximately 0 in Lhcx1-Ko to approximately 0.6 in overexpressors is compensated by a roughly equivalent decrease in ϕNO. The "lake model" approximates exceptionally well energy partitioning in pennate diatoms (Croteau et al., 2024), allowing accurate estimation of the concentration of open PSII reaction centers (with oxidized secondary acceptors Q_A) by the qL parameter (Kramer *et al.*, 2004). Over the Lhcx1 gradient, qL strongly increased (Fig. 1c). This reflects the different implications between fluxes and pools, as despite similar PSII activities among strains, the proportion of oxidized Q_A varied by 4-fold (as such, a similar variation in the redox state PQH_2/PQ is very likely). Therefore, we conclude that when NPQ is increased everything else being roughly equal, the shortening of PSII exciton lifetime by NPQ/qZ is compensated by the higher availability of the substrate Q_A to keep LEF roughly unaffected. While PSII is only involved in LEF, cyt. b_6f and PSI also participate in CEF. Indirect effects of NPQ/qZ on this portion of the electron transport chain are much less studied even though both processes are interconnected through feedback-loops with luminal pH (Munekage *et al.*, 2004) and possibly the PQ pool (Alric, 2015). Unexpectedly, the special chlorophyll pair of PSI, P700, became more

oxidized as Lhcx1 decreased, which is visualized through the YND parameter (see Methods), whereas acceptor side limitation was low and invariant between strains (Fig. 2d). The *c*-type cytochromes (*c*-t. cyt.), which comprise cytochrome *f* and cytochromes c_6, were almost fully oxidized at 570 µmol photons m^{-2} s^{-1} in all strains (Fig. S2) in agreement with their lower redox potential compared to P700/$P700^+$. Interestingly, the redox states of *c*-t. cyt. and of P700 were also in good agreement with thermodynamic equilibrium during transition from light to dark (Fig. S3, see also (Flori *et al.*, 2017)).

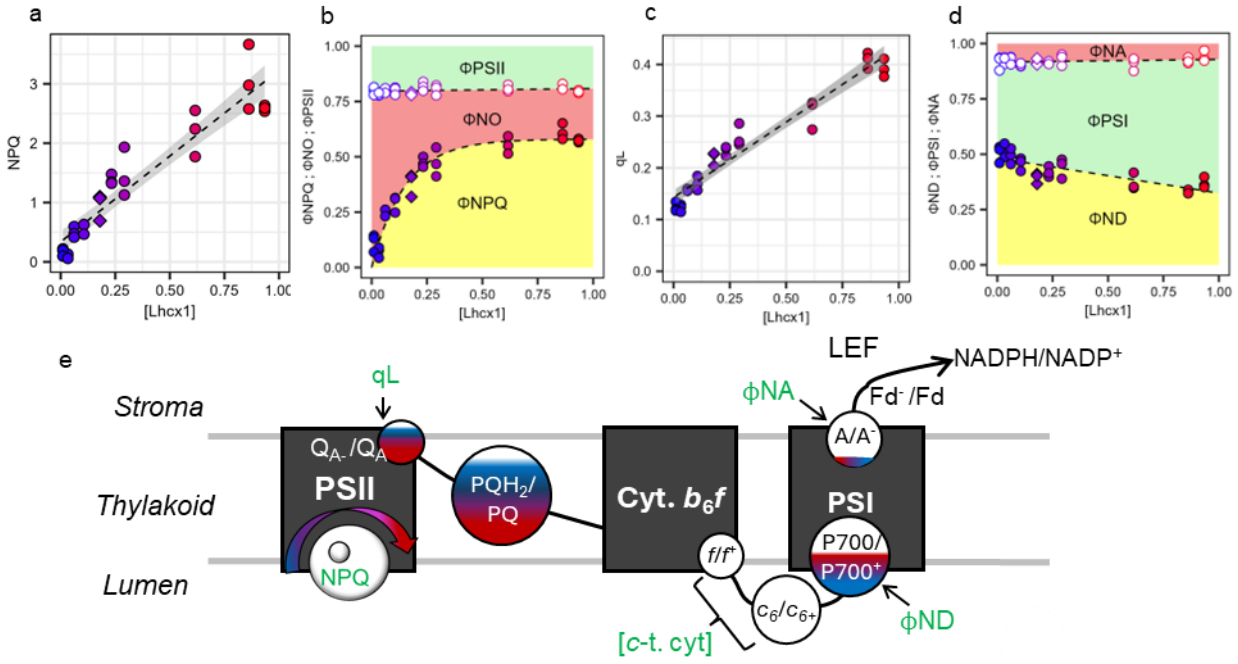

Fig. 1| Influence of Lhcx1 on Non Photochemical Quenching (NPQ), PSI and PSII photochemistry, and redox state of the intersystem electron chain in *Phaeodactylum tricornutum*. Diverse photophysiology parameters in 10 *Phaeodactylum tricornutum* strains (Pt2-WT in diamond symbols) with ranging Lhcx1 concentrations (color scale indicates Lhcx1 concentration, used consistently throughout the paper) measured under a steady-state condition at 570 µmol photons m^{-2} s^{-1}; NPQ (a), the quantum yields of photosystem (PS) II photochemistry (ϕPSII), non-regulated heat dissipation (ϕNO) and regulated heat dissipation (ϕNPQ) (b), the qL parameter (which approximates Q_A redox state in the lake model (Kramer et al., 2004)) (c), the quantum yields of PSI (ϕPSI), PSI donor side limitation (ϕND, which corresponds to the proportion of oxidized P700) and PSI acceptor side limitation (ϕNA, which approximates the proportion of reduced acceptors (A)) (d). The same experiment was conducted with parameters measured as a function of light intensity in three strains and is shown in Fig. S1. Schematic representation of the linear electron flow (LEF) redox-state of the photosynthetic electron transport chain as a function of Lhcx1/NPQ (fully oxidized *c*-type cytochromes (*c*-t cyt.) were measured in Fig. S2) (e). The NPQ dial represents the range of Lhcx1 mutants allowing to vary the efficiency of NPQ. The experimental data shown in panels a-d correspond to independent biological triplicates for all but one strain (*n*=2 for that strain).

Effect of qZ on partitioning between linear and cyclic electron flows

In line with this, an increase of the PSI yield (ϕPSI) with Lhcx1 amount was observed (Fig. 1d), which suggests that, in addition to LEF, an important Lhcx1-dependent CEF takes place. The relatively large increase in PSI activity compared to the small decrease in PSII activity as a function of Lhcx1 is corroborated by an intermediate increase of the photochemical rate (sum of both PS activities) with Lhcx1 (Fig 2a and b). If this is compatible with an increase of CEF as a function of qZ, measuring absolute CEF values is notoriously challenging and strictly speaking requires measuring simultaneously absorption cross-section of both PS in addition to their yields (Finazzi & Forti, 2004). However, since there are no state-transition in diatoms (Owens, 1986; Lepetit *et al.*, 2022), the absorption cross-sections of both photosystems are not susceptible to change during the short-term experiments used here. This allowed us to estimate relative changes in total electron flow (TEF, which comprises CEF) over LEF by introducing the new parameter Δ(TEF/LEF). This parameter is useful because it requires only measurements of PSII and PSI yields. In addition, it is insensitive to the absolute values of PSII and PSI absorption cross-sections or their stoichiometry as long as they remain constant throughout the experiment. We checked however that neither PSII/PSI stoichiometry, nor absorption cross-sections of the photosystems varied between strains (see Supplementary material). This simplified approach permits to demonstrate a linear relationship between the yield of photons dissipation via NPQ and Δ(TEF/LEF) (Fig. 2d). While the molecular actors of CEF remain unknown in diatoms (Lepetit *et al.*, 2022), the role of CEF under nutrient starvation (Thamatrakoln *et al.*, 2013), anoxic conditions (Gain *et al.*, 2023), or in cold environnement (Goldman *et al.*, 2015) has already been reported. This study adds light stress to this list, over which Δ(TEF/LEF) can be formalized as a function of the ϕNPQ due to qZ.

It is to note that CEF does not only compensate the decrease of LEF to allow a consistent PSI activity. At the contrary, the relative increase in ϕPSI with qZ exceeded the relative decrease in ϕPSII. This suggests an “active” upregulation of CEF with qZ possibly linked to the higher oxidation of the PQ pool or the luminal pH (although the total light-induced electrochemical gradient did not vary between strains (Fig. S5)). This intense acceleration of PSI activity with qZ, confirmed by measurements of the photochemical rate based on the independent observable ECS, is at first glance surprising in the light-saturating regime. To further confirm the link between qZ and CEF, we followed PSII and PSI activities in four different strains in the light-limiting regime,

following a high light treatment generating qZ. In these conditions, PSII activity recovered towards maximal value with time as the qZ generated under high light relaxed (Fig. 2). However, the activity of PSI remained roughly stable with time, resulting in a similar relationship between Δ(TEF/LEF) and the ϕNPQ due to qZ (Fig. 2j).

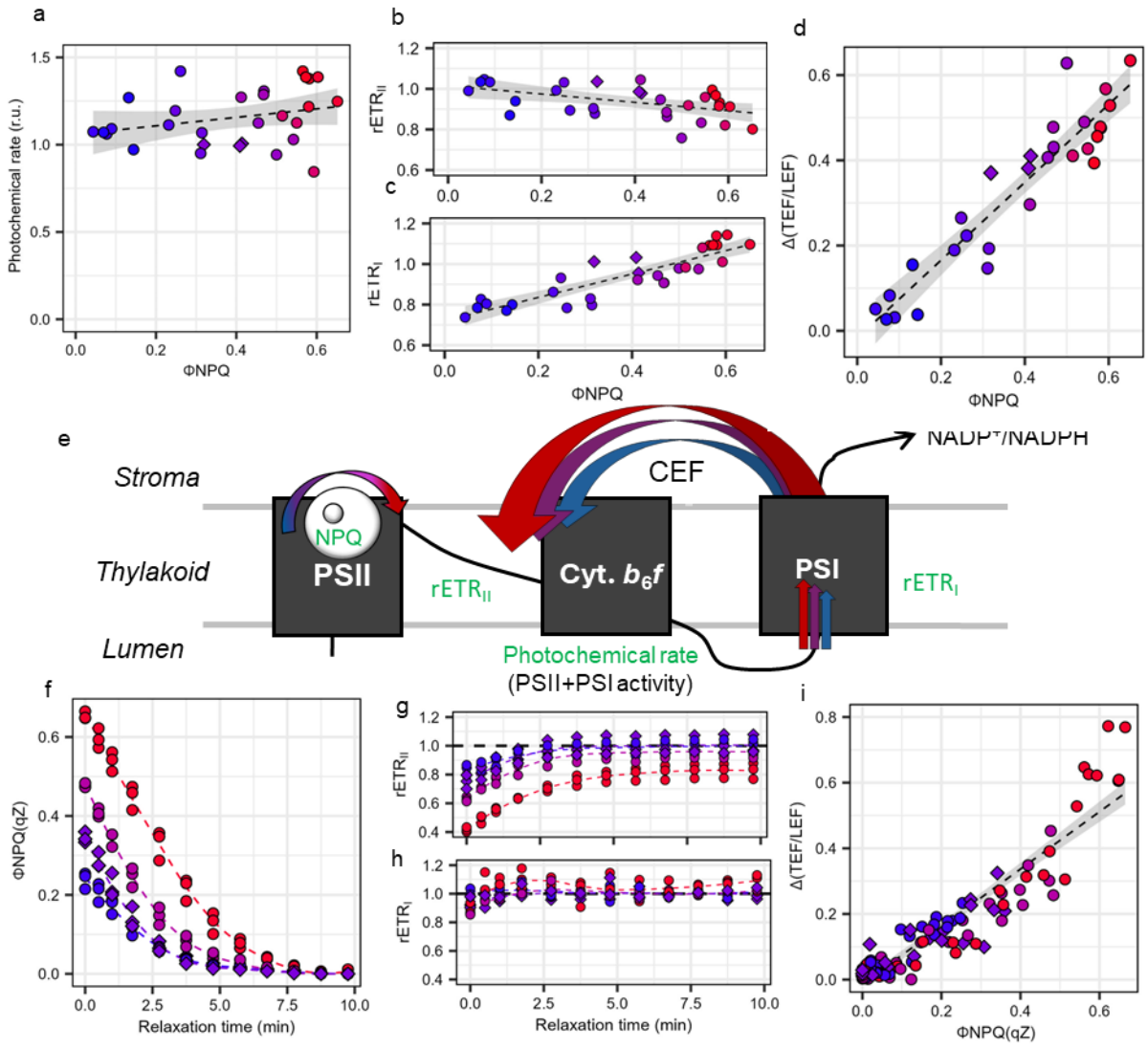

Fig. 2| Effect of Lhcx1-dependent qZ on cyclic electron flow (CEF) in *Phaeodactylum tricornutum*. Photochemical rate (photosystem (PS) I and II activity) measured by electrochromic shift, (a), relative electron flow of PSII ($rETR_{II}$) (b) and PSI ($rETR_{I}$) (c), all parameters are measured under steady-state 570 µmol photons m^{-2} s^{-1} illumination and are normalized to the mean value of the WT (diamond symbols). Calculation of the relative increase of total electron flow (TEF) due to CEF (Δ(TEF/LEF)) as a function of ϕNPQ (d). Schematic representation of photosynthetic electron flows under these conditions. The NPQ dial represents the range of Lhcx1 mutants allowing to vary the efficiency of NPQ and the arrows on the top of the scheme represent the amplitude of CEF (e). Relaxation of the qZ component of ϕNPQ under limiting light regime after its induction (f), parallel measurements of $rETR_{II}$ (g) and $rETR_{I}$ (h) allow to calculate a Δ(TEF/LEF) versus ϕNPQ under different conditions. The experimental data shown in panels a-d et f-i correspond to independent biological triplicates for each strain (except one strain for which *n*=2 in a-d). See Material and Methods for details.

Effect of qZ on photoinhibition, photoinhibition-associated quenching (qI) and D1 photodamage

Six strains were then used to study the interacting effects between qZ, the nonphotochemical quenching by damaged PSII (qI) and the recovery of the maximum quantum yield of PSII after light exposure (F_V'/F_M'Rec.). This was done over a prolonged light stress (1 h), followed by 30 min of low light recovery (see Methods and Fig. S6). To separate the overlapping effects of PSII photodamage and repair, the experiment was repeated with the addition of increasing concentrations of the chloroplast translation inhibitor lincomycin, therefore blocking D1 turnover. Final lincomycin concentrations of 0.4 and 0.8 µg mL^{-1} were saturating (Fig. S7) and those two treatments were averaged to represent inhibited PSII-repair conditions in Fig. 3. Like during light stress of shorter duration, there was no clear trend in ϕPSII between strains over 1h exposure, while the increase in ϕNPQ (development of qI or increase in qZ via *de novo* synthesis of molecular actors) was mirrored by a corresponding decrease in ϕNO (Fig. 3a and d). The effects of lincomycin were subtle during light stress but resulted in much slower, unfinished, kinetics of ϕNPQ relaxation and F_V'/F_M' recovery after 30 min under low light (Fig. 3b and e). Without saturating lincomycin, since PSII repair occurs throughout the experiment, the reversible NPQ reflects not only the relaxation of qZ but also includes the relaxation of photo-inhibition-associated quenching, qI. To account for this, we deconvoluted the fast (qZ) and slow (qI) components of the ϕNPQ at the end of the illumination, based on the biphasic NPQ relaxation in the dark (see Methods and Fig 3b). Photoinhibition significantly decreased as the contribution of qZ to ϕNPQ increased, irrespective of PSII repair, as illustrated by the impact of qZ on the loss of photochemistry (F_V'/F_M'Rec.) or photoinhibition associated quenching (qI, Fig 3c and f). As expected, inhibiting PSII repair with lincomycin resulted in higher qI contribution (Fig 3c) and loss of photochemistry (i.e., lower F_V'/F_M'Rec., Fig 3f). Whether photoinhibition was quantified by loss of photochemistry or its associated quencing, the photoprotective effect of PSII repair was higher around intermediate qZ values than for knockouts or overexpressors with the light stress intensity and duration used here (Fig. S10).

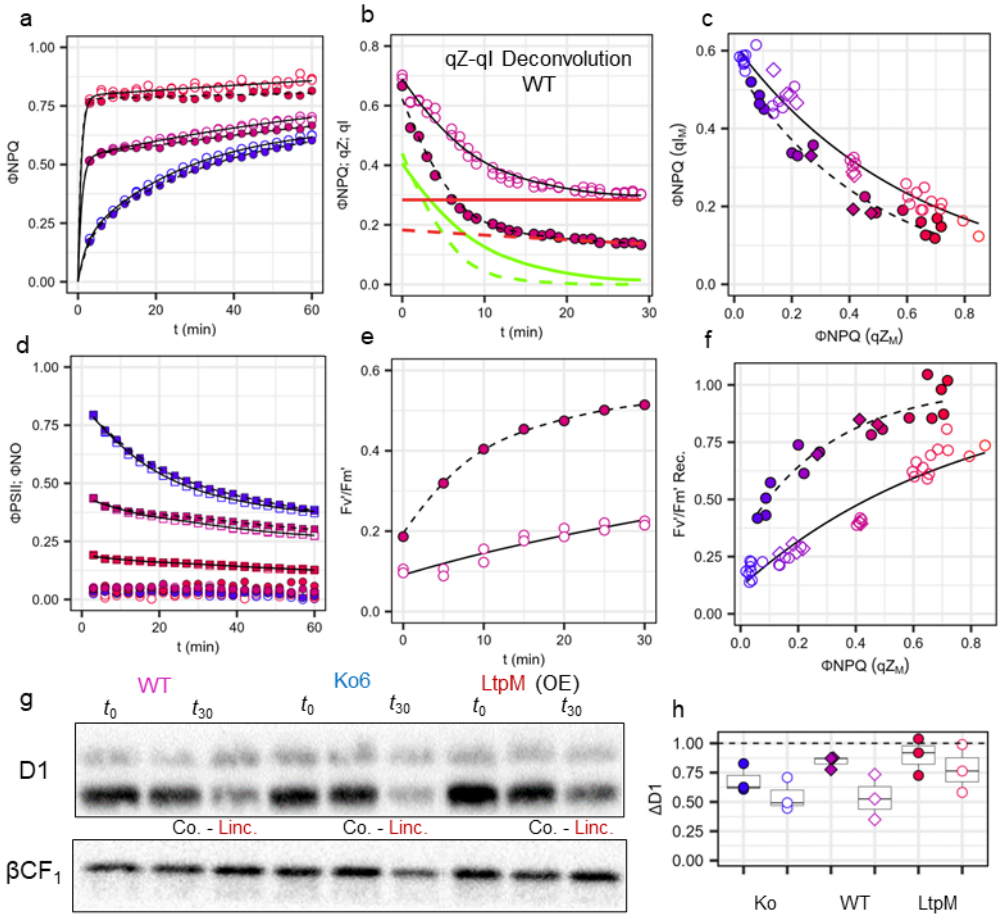

Fig. 3|Effects of Lhcx-dependent qZ on PSII photoinhibition in *P. tricornutum*. Various photosystem (PS) II parameters were monitored during a 1h high light (HL) period followed by 30 min of low light relaxation. Measurements in control (closed circles) and lincomycin (Linc.) treatments (average of 0.4 and 0.8 µg mL^{-1}, open circles) of the quantum yield of nonphotochemical quenching (ϕNPQ) in three strains with contrasted Lhcx1 concentrations (Ko, WT and one overexpressor (OE)) during HL stress (a) and ϕNPQ deconvoluted in its qZ (green) and qI (red) components during relaxation under low light (b), maximum contribution of qI to ϕNPQ (ϕNPQ (qI_M)) versus maximum contribution of qZ (ϕNPQ (qZ_M)) (c), quantum yield of PSII (ϕPSII) and non-regulated heat dissipation (ϕNO) during HL stress (d) and recovery of the maximum quantum yield of PSII in the dark (F_V'/F_M') measured at the end of seven 1 min dark windows over low light relaxation (e) and the relative recovery of F_V'/F_M' at the end of relaxation (F_V'/F_M'Rec.) versus ϕNPQ(qZ_M) (f). Western-blot of D1 and the ATP-synthase ($βCF_1$ subunit) content (loading control) before HL stress and after 30 min of low light recovery with and without addition of Linc. (0.4 µg mL^{-1}) and relative remaining D1 content compared to t_0 (ΔD1) (h). See Fig. S6 and Material and Methods for details about the protocols, saturating effect of Linc. in Fig. S7, full qZ/qI deconvolution in Fig. S8 and see triplicates of Western Blot membranes in Fig. S9. All experiments were done on three independent biological triplicates.

Immunoblotting of D1, sampled at the end of the 30 min recovery, showed similar patterns, with clearly less D1 detected in Lhcx1-Ko than in the wildtype (WT) or an overexpressor in the absence of lincomycin. The loss of D1 was greater in the absence of PSII repair and, again, this effect was maximal in the WT (Fig. 3i and j). The variations in D1 content among strains were not as exacerbated as with metrics of photoinhibition measured by fluorometry. However, it is well-known that diatoms can stock extra non-functional D1 which can be used for PSII repair even when plastid translation is inhibited, and complicates the relationship between D1 and F_V'/F_M'Rec. (Lavaud *et al.*, 2016). Overall, this experiment shows undeniably that qZ protects PSII from photodamage and slows down D1 degradation in *P. tricornutum*, without the ambiguity of possible side effects from a chemical agent.

Half of P. tricornutum genome's expression is modulated by qZ during high light stress

These results imply that well-characterized internal photosynthetic cues involved in retrograde signalling, such as the redox state of PQ pool (Escoubas *et al.*, 1995; Lepetit *et al.*, 2013; Agarwal *et al.*, 2023) or ROS (Foyer, 2018; Pancheri *et al.*, 2024), can vary as a function of qZ. More speculative photosynthetic signals, like the ATP/NADPH ratio (which may increase due to higher CEF) or the breakdown products of macromolecules, such as D1, or lipids peroxidation, might also be affected (Foyer, 2018; Pancheri *et al.*, 2024). Additionally, photosynthetic organisms evolved a diverse array of receptors that can sense abiotic cues and tune gene expression accordingly (Jaubert *et al.*, 2023). A recurrent, and unresolved, conundrum in photosynthesis regulation studies is to determine whether the expression of a given set of genes reacts to environmental sensing or to retrograde signalling. In this context, the integrated signals that regulate gene expression under high light stress can be divided into two dimensions: an "internal cue", consisting of qZ-modulated photosynthetic signals (represented by the maximum capacity for qZ, qZ_M), and an "external cue," represented by the duration of exposure to high light exposure (HL-t). This novel approach allows us to achieve three goals, **i)** investigating the whole-genome response to high light stress, **ii)** evaluating the importance of qZ in this response and, **iii)** distinguishing direct and indirect regulatory effects of light regulation on gene expression (Fig. 4). Summarily, we collected 50 transcriptomes from 6 six different strains over a 1h light stress (see Principal Component Analysis (PCA) (Fig. S11)). We uniformized the weight of the two

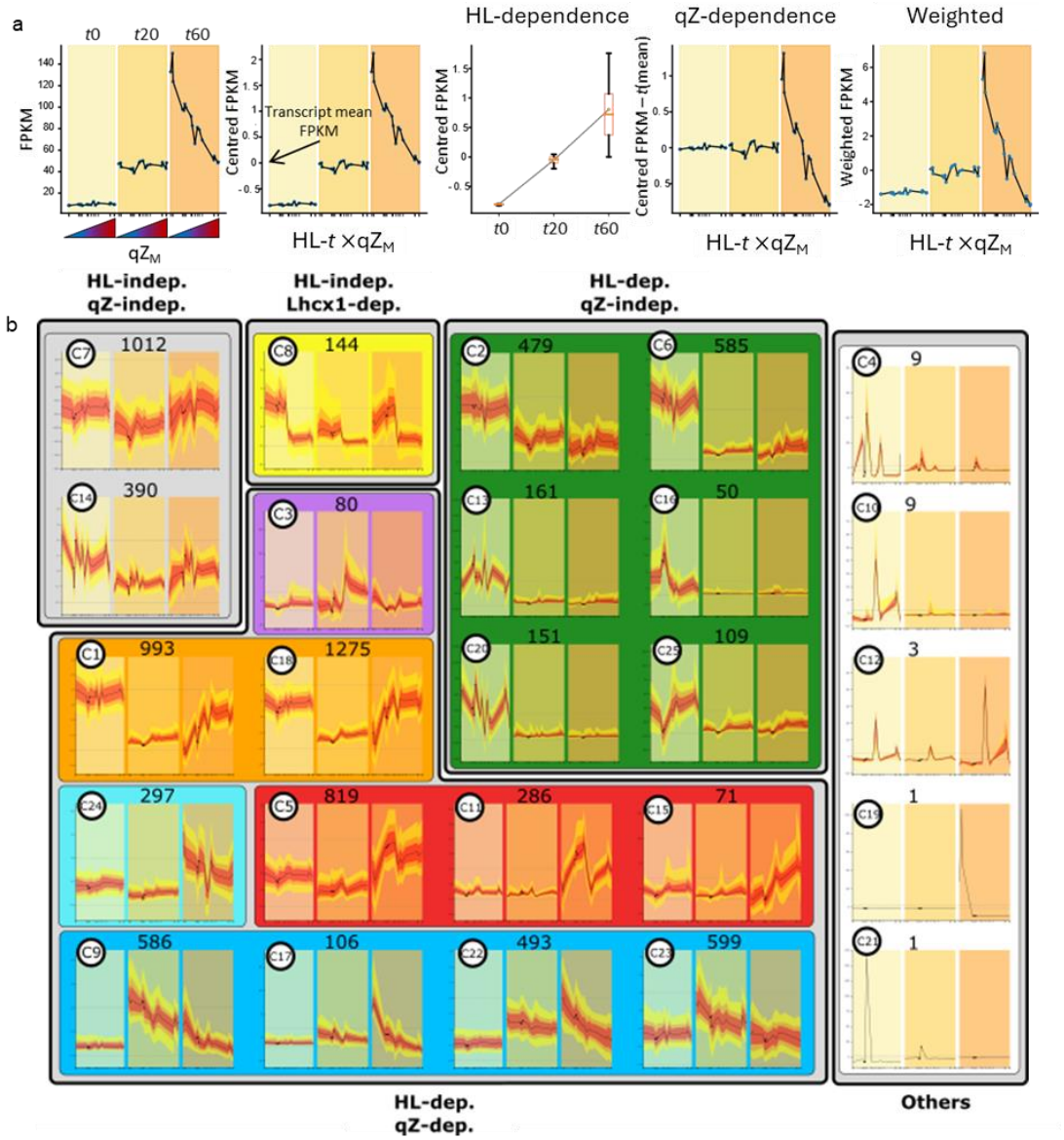

Fig. 4| Whole-genome clustering based on time of exposure to high light (HL-*t*) and photoprotection capacity (qZ_M). 50 transcriptomes (triplicates of 6 different strains) obtained at three time points during HL exposure, were used. Upper panels: CRTISO4 gene (cluster 17 clusters (c# top left of each panel below)) as example of the different steps to transform gene expression level (FPKM) as a function of HL-*t*×qZ_M (reversible nonphotochemical quenching component), into weighted FPKM, with equal weight accorded to HL-*t*-dependent variations and qZ_M-dependent variations (see Methods) (a). Weighted FPKM against HL-*t*×qZ_M for all genes among the 50 transcriptomes (if FPKM>10 in at least 2 samples) (see Principal Component Analysis (Fig. S12)) distributed in 25 clusters by K-means algorithm (see Elbow-test for number of clusters (Fig. S13)) with the number of genes per cluster written above the plot, the dots on the black line are WT samples (b). The black outline regroups clusters by their HL-*t* and Lhcx1/qZ_M dependence and clusters are further manually grouped by their overall patterns into metaclusters (MC) associated to a name and specific colour for the remaining of the paper written below the figure (HLr and HLi are HL-repressed and -induced, respectively). In Fig. S14 the HL-*t* and qZ_M dependence for all genes per cluster are provided.

dimensions (qZ_M and HL-*time*) before using a clustering algorithm (K-means) to group the different genes according to their *time*×qZ_M expression patterns (see Fig. 4 and Methods).

Of the 10,381 genes identified over RNA sequencing (BGI), 8,710 were used for data transformation (we excluded genes with very low across (FPKM<10) expressions see Methods) and clusterization in 25 clusters (using K-means, see Elbow test in Fig. S12). 1,425 genes were affiliated to clusters mostly invariant or noise (c7 and c14, upper left in Fig 4). Clusters dependent to HL-*time* and roughly independent to qZ_M regrouped 1,535 genes. Surprisingly, a small cluster (c8, 144 genes) was dependent on qZ_M irrelevantly of HL-*time*. However, most genes (5,605) were in clusters dependent to HL-*time* and qZ_M, which unveils that, even being conservative and considering the now ≈12,000 genes identified in *P. tricornutum*, close to 50% of its genome expression is modulated by photoprotection over HL stress. To facilitate further analyses, we manually regrouped the clusters into metaclusters (MC) according to their overall expressions patterns as a function of HL-*time*×qZ_M (see Fig. 4), but the lists of genes per cluster is found in Supplementals.

Expression of light absorption and photoprotection genes as a function of HL-time×qZ_M

We then corroborated the findings of our methods by searching the MC affiliation of genes involved in the light-harvesting process, which are known molecular actors of *P. tricornutum*'s high light response (Nymark *et al.,* 2009), namely the fucoxanthin-Chl *a*/*c*-binding proteins (FCP) of the Lhcf (major antenna proteins), Lhcr (red-algae PSI homologs), Lhcx families, as well as High-light induced proteins. All Lhcf, except Lhcf15, and 8 Lhcr were affiliated to MC1, which groups genes repressed by HL and not influenced by photoprotection (Fig. 5a). Of the 28 genes associated with the Chl biosynthesis pathway, 75% were also part of MC1 (including the newly discovered Chl *c* dioxygenase (Jiang *et al.*, 2023)) (Fig. 5d), confirming a uniform response of molecular actors involved in light absorption. Four Lhcr genes were previously observed to be unexpectedly induced upon HL shift (Nymark *et al.*, 2009). We show that these four Lhcr, plus Lhcr9 (not detected in the previous study), are part of the MC2, in which HL upregulation is countered by photoprotection (Fig 4 and Fig. 5b). Other high-light induced Lhcx isoforms Lhcx2-3 were also part of MC2, while the expression of the mysterious dark expressed Lhcx4 (Nymark *et al.*, 2013), was part of MC1 (Fig 5b). In the 44 genes associated with carotenoid and xanthophyll biosynthesis, 21 were part of MC1 and 16 were affiliated to MC2. Interestingly, from the

xanthophyll portion of the pathway, only the genes encoding VDE and ZEP3, regulating the xanthophyll cycle and therefore qZ in diatoms, were part of MC2, as well as the VDE-related

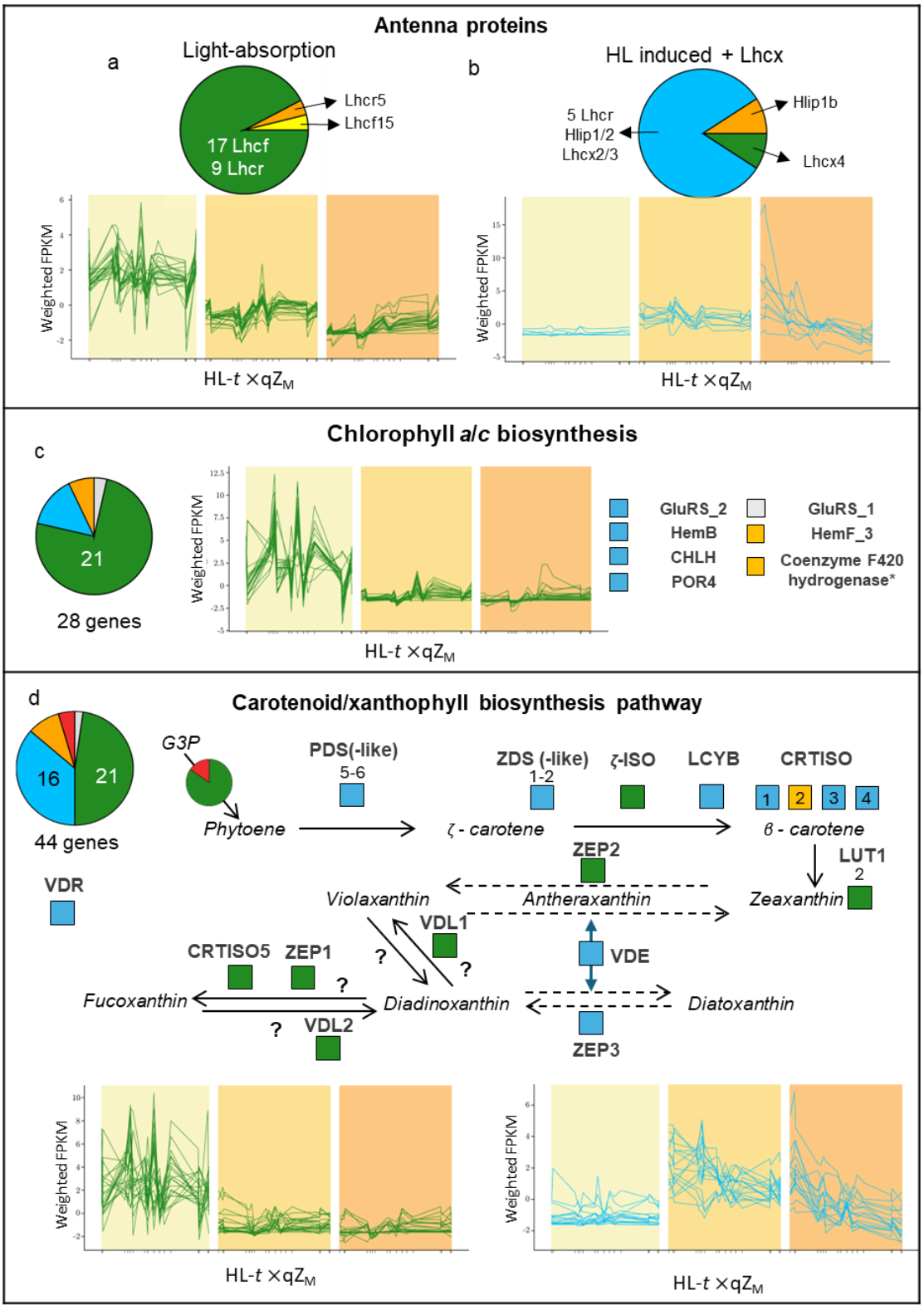

Fig. 5| Genes metaclusters (MC) affiliation and weighted FPKM profiles of antenna proteins and enzymes involved in pigment biosynthesis. Pie charts show gene MC affiliation (Fig. 4) for fucoxanthin-chlorophyll *a*/*c*-binding proteins (FCP) in *Phaeodactylum tricornutum*: (a) Light absorption, including all Lhcf (major antenna proteins) and nine Lhcr (red-algae photosystem I homologs) and their weighted FPKM versus high light (HL) exposure time and photoprotection capacity via the Lhcx1-dependent qZ (HL-$t\times qZ_M$) profiles (in MC1), (b) HL induced antenna proteins including five Lhcr (mostly based on Nymark *et al.,* 2009) and three Hlip and Lhcx isoforms (except Lhcx1)) and their weighted FPKM versus HL-$t\times qZ_M$ profiles (in MC2). Chlorophyll *a* and *c* biosynthesis genes MCs affiliation and their weighted FPKM profiles in MC1 and individual genes affiliated to other MCs (c). In (d), MC affiliation of 44 genes associated with carotenoid and xanthophyll biosynthesis and a simplified pathway representation proposed by Cao *et al.,* 2023. Only MC affiliations (13 genes) are shown from Glycerol-3-phosphate (G3P) to phytoene; numbers above coloured squares indicate the number of isoforms, and specific isoforms number are written within coloured squares when their MC differs. Dashed arrows represent xanthophyll cycles; violaxanthin de-epoxidase (VDE) catalyses both violaxanthin to zeaxanthin and diadinoxanthin to diatoxanthin de-epoxidation and zeaxanthin epoxidase 3 (ZEP3) placement is based on (Giossi *et al.,* 2024). Question marks indicate missing intermediate and unknown enzymes, and the VDE-related (VDR), of unknown function, is shown outside of the pathway. Weight FPKM profiles of carotenoid/xanthophyll biosynthesis genes affiliated to MC1 and MC2 are also shown. All gene information and cluster affiliations are provided in Supplementary data.

(VDR) with still unknown functions (genes encoding other VDE and ZEP isoforms were affiliated to MC1) (Fig. 5d).

Overall, the genes involved in light harvesting systems are largely dominated by the metaclusters MC1 and MC2. Genes involved in light absorption (chlorophyll and carotenoid biosynthesis, Lhcr and Lhcf) were mostly HL repressed and qZ-independent (MC1), whereas most of the ones involved in photoprotection (xanthophyll cycle, Lhcx and high-light induced Lhcs) were HL induced and qZ-countered (MC2).

Biological processes and sub-cellular localization associated with metaclusters

We then used Gene Ontology (GO) enrichment analysis to investigate if MCs, regrouping genes responding similarly to internal (qZ-modulated photosynthetic signals) and external (exposure time to HL) cues, could be associated to predominant molecular functions and/or biological processes. For four MCs, there was clear common themes in the enriched GOs for which we associated a general function (Fig. 6 and Fig. S14 for complete analysis). The invariant MC0 was enriched in processes related to “Housekeeping and cell division”, with significant enrichment in the GOs “cell division”, “mitotic sister chromatid segregation” and “microtubule movement” and encompassing many annotated histone and tyrosine kinase genes. In addition to genes related to light absorption (Fig 5), genes encoding subunits of photosynthetic complexes were strongly enriched in the HL-repressed MC1. Enriched GOs in MC3, whose transcription pattern was stable at 20 min and increased at 60 min in an inverse function of qZ_M, seemed almost uniquely linked

to proteolysis, and contained many genes encoding proteasomal complex subunits. MC5, grouping genes induced at 60 minutes with a positive effect of qZ_M (although with different dependencies between clusters), was very strongly associated with ribosome assembly and translation. The last two MCs were more diverse. On top of those associated with photoprotection, many genes associated to oxidoreduction reactions and ROS detoxification (see significant glutathione metabolism KEGG enrichment for instance (Fig. S14)) were found in MC2. The most functionally diverse MC was MC4, containing many genes associated to replication, transport and metabolism. Notably, we found in this cluster six of the seven bis-phospho-glycerate mutase and one of the three enolase (one PGAM and one enolase found in MC1) associated to the lower-half

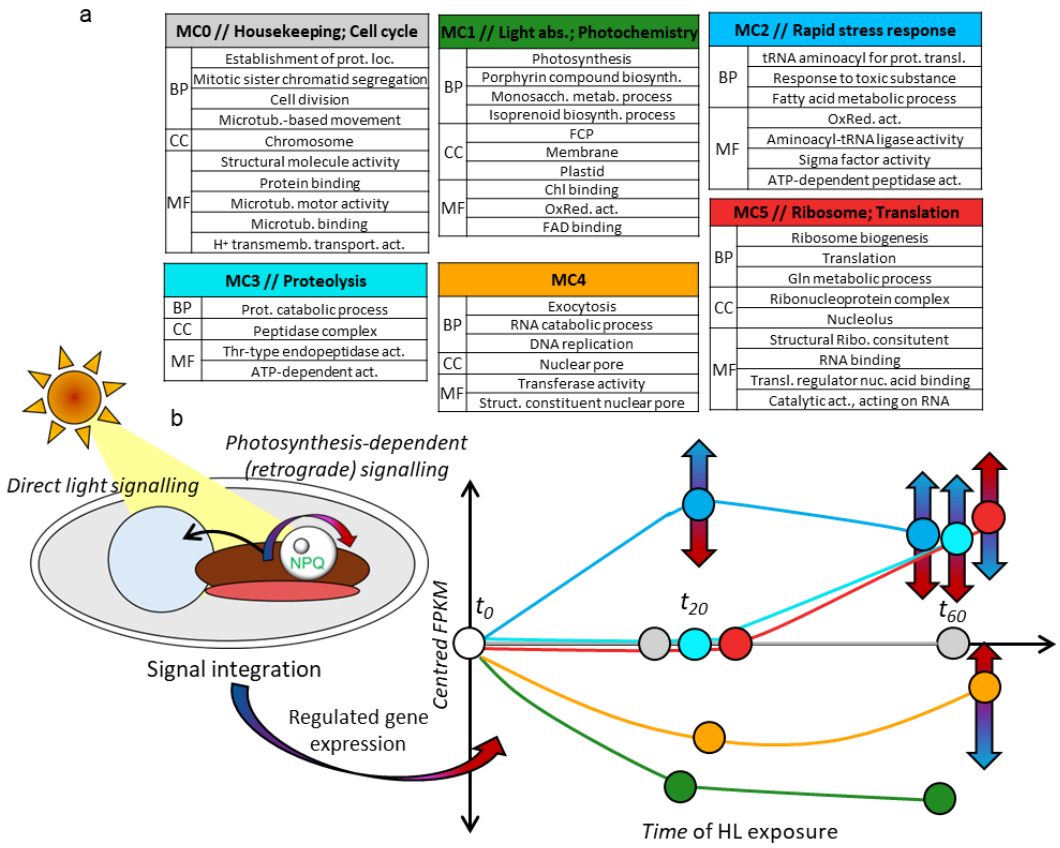

Fig. 6| Metaclusters (MC) gene ontology (GO) enrichment analysis and schematic representation of gene expression regulation during high light (HL) stress. GO enrichment per MC (Fig. 4) analysis (biological process (BP), cellular compartment (CC) and molecular function (MF)) performed with the g:Profiler platform (Raudvere et al., 2019) on *Phaeodactylum tricornutum* genes IDs based on the third version of the genome, shown for the six main MCs, five of which we could attribute a general function to. Only GO highlighted as main driver by g:Profiler algorithm are shown here to avoid redundancies (all enriched GOs and KEGGs, and their p-values provided in Fig. S15) (a). Schematized representation of signal perception and integration by *P. tricornutum* cells and resulting expression regulation of the genes belonging to the six main MCs, and their relative qZ_M-dependency (see also Fig. 4) over 1 h of HL exposure (b).

plastidglycolytic-gluconeogenesis pathway, characteristic of secondary endosymbiotic organisms (Dorrell *et al.*, 2024).

Using previous target localization analyses over *P. tricornutum*'s whole genome with various softwares (compiled in (Ait-Mohamed *et al.*, 2020) and see Methods), we investigated the potential link between the MC-affiliation of a gene and the predicted target of the corresponding encoded protein. Genes encoding proteins targeting the plastid were significantly more affiliated to MC1 (HL-repressed) and MC2 (HL-induced, qZ_M countered) (Fig. S15). Another striking pattern fitting nicely with the general function of MC0 (housekeeping, cell cycle) was its overrepresentation in predicted nucleus-targeted genes. We reran per cluster GO analysis on custom backgrounds containing only gene targeting a given compartment to see if additional insights could be gained that way. This mostly corroborated the analysis at the organismal level, but it revealed informative localization of certain molecular functions. The strong upregulation of aminoacyl tRNA synthetase (aaRS) genes of MC2 is particularly important in the plastid (as opposed to mitochondria or cytoplasm). Moreover, the proteolysis-enriched MC was more overrepresented in the cytoplasm, with many Clp protease/peptidase isoforms. Interestingly, the FtsH1 (and other isoforms) protease associated to PSII repair in the plastid was rather affiliated to MC2, showing its more immediate regulation at 20 min of HL, together with other actors of photoprotection (Fig. 5).

Discussion

Overall, we show that our Lhcx1 molecular titration approach, using a large series of mutants with equal initial state but ranging NPQ/qZ capacities, is uniquely efficient to unveil phenomenological relationships between important processes of photosynthesis regulation. Moreover, we were able to breakdown the information steering gene expression integrated by the cells during a high light stress into two dimensions, an environmental/external cue (exposure time in high light), and an internal cue mediated by qZ-modulated photosynthetic signaling. Impressively, we estimate that about half of *P. tricornutum* genome expression is modulated by qZ during the high light stress used here, indicating a widespread dialogue between photosynthetic signals and genic regulations. Our functional analysis of photosynthesis in the series of mutants provided several phenomenological relationships linking qZ and various photosynthetic parameters (redox states of Q_A, *c*-t. cyt. and P700, LEF versus CEF, photoinhibition). This allows to speculate about the state

of different internal sensors and source of retrograde signaling over the high light stress. Along with varied enrichment of genes associated to specific functions found in different clusters/MCs and their sub-cellular targets, we draw one of the most comprehensive and detailed portraits of high light stress response at the organismal level so far. In addition, thanks to its simplistic model in *P. tricornutum* (Croteau et al. 2024), we can quantify the effects of NPQ in tuning this high light response, one of the most studied and ubiquitous photosynthesis regulators. In the following sections, we discuss the HL response of the different clusters over time, starting with the short-term response (20 min) and then moving on to the long-term response (60 min).

Upon HL exposure, the most direct cue for gene regulations comes from direct light signalling, without influence from photoprotection. Here, we show that around 3,700 genes are downregulated in a qZ_M-independent manner at 20 min. This includes approximately 1,500 genes affiliated to MC1, encoding antenna proteins, photosynthetic complexes subunits, and pigment biosynthesis enzymes, and approximately 3,200 genes of various functions found in MC4. However, these two clusters evolve differently with time. After 60 min, the downregulation of genes affiliated to MC4 relaxes in a qZ_M-dependent manner, from no recovery for Lhcx1-Ko to partial recovery in the WT and full recovery to their initial expression in most overexpressors (Fig. 4). This pattern could be described as a gene expression fuse that temporarily shuts down transcription of a large number of genes during HL stress, with their expression levels returning to normal once qZ_M-dependent checkpoints are reached. This mechanism may provide time to coordinate and balance enzyme stoichiometry within a metabolic pathway or relieve downstream bottlenecks induced by HL. For genes related to light-absorption, a potential checkpoint might only be reach if light intensity decreases, in line with the absence of long-term relaxation of MC1.

Another short-term response is the upregulation of genes of MC2 at 20 min. However, in stark contrast with the behavior of the HL-repressed genes described above, this short-term response immediately shows a negative qZ_M-dependency. The counteracted effect of qZ_M on the induction at 20 min is small in clusters 17 and 22 (and then exacerbated after 60 min), and greater in clusters 9 and 23 (and then almost relaxed at 60 min) (Fig. 4). These two behaviors within the same MC might simply reflect that genes are HL-induced faster in clusters 9 and 23 than in clusters 17 and 22. The intense qZ_M-dependency of MC2 fits with its overall gene content, involved in rapid and finely tuned response to an external stress. Indeed, MC2 includes genes related to photoprotection

(XC-related genes, HLIP, Lhcx, FtsH1), redox signalling via many glutaredoxins (GLRX1, GLRXC1, GLRXC2, GLRXM1), thioredoxins (Trx-f, Trx-m, Trx-y), glutathione reductase (Gsr_1, Gsr_2) and detoxification enzymes involved in the glutathione peroxidase cycle (SOD1, GPX2), only to name characterized genes. An enrichment in the sigma transcription factor family was also found in MC2 (Fig. 6), which could be a promising avenue for future investigation aiming at deciphering the control of gene expression in response to high light in *P. tricornutum.*

This qZ_M-dependency also indicates the influence of photosynthetic signaling, in line with our functional data. The first physiological change upon high light stress is large acceleration of PS turnover, while the cyt. b_6f becomes limiting to electron transport. This leads to several short-term HL-dependent changes in photosynthesis that are strongly qZ-dependent: the reduction of Q_A and the PQ pool, favoring ROS production, and the oxidation of *c*-t cyt. and P700 (Fig. 1). Additionally, an active and qZ-dependent CEF upregulation appears, which is potentially mediated by the Q_A/PQ pool redox state (Fig. 2). Finally, a qZ-dependency of PSII photodamage was found over longer timescale, whether assessed by D1 accumulation, the decrease of F_V'/F_M', or the photoinhibition-dependent quenching qI. This results in a long list of potential photosynthetic sensors whose states change rapidly upon high light exposure in a manner modulated by qZ. Triggers of MC2 could therefore include the redox state of the PQ pool, which is already known to activate Lhcx expression (Lepetit *et al.*, 2013), oxidative stress possibly sensed in the stroma through the glutathione pool (Volpert *et al.*, 2018) and various types of ROS signaling. At this stage, we can only speculate about the precise source of such potential ROS signalling. The Mehler reactions at PSI, act as a release valve under acceptor limitation and generates H_2O_2 (Kozuleva *et al.*, 2021), an important signaling molecule for the stress response of diatoms, especially related to their nitrogen metabolism (Rosenwasser *et al.*, 2014). However, in our case, PSI acceptor side limitation did not increase in the absence of Lhcx1 (Fig. 1), although many of the genes encoding triggered by exogenous H_2O_2 addition in (Rosenwasser *et al.*, 2014) belong to MC2. We supposed that $^1O_2$ production by PSII is inversely proportional to qZ, but due to $^1O_2$ extremely short lifetime, a more likely indirect signaling mechanism could be lipid peroxidation by-products (Pancheri *et al.*, 2024). But it is hard to know if these would accumulate fast enough to influence MC2 after 20 min or should be more realistically associated to the slower response of MC3 (Fig. 4 and see below). Besides direct stress response, many MC2-affiliated genes may function to increase cell capacity to manage redox overload by: **i)** promoting oxidative phosphorylation, suggesting a trade-off

between CEF and plastid-mitochondria coupling in diatoms (Bailleul *et al.*, 2015)), **ii)** enhancing carbon fixation by upregulating carbon concentrating mechanisms, such as the three bestrophins ion channels (crucial in *Chlamydomonas* (Burlacot *et al.*, 2022)) and carbonic anhydrases (Jensen *et al.*, 2020) targeted to the plastid according to HECTAR/ASAFIND, and, **iii)** investing in redox sensitive nitrogen metabolism (Rosenwasser *et al.*, 2014), including 15 aminoacyl ligase tRNA targeted to the plastid.

Two MCs do not exhibit a short-term response and are only activated in the long-term. Genes in MC3 and MC5 are induced after 60 minutes of HL exposure, depending on qZ. In MC3, the long-term response is counteracted by qZ, while in MC5, it is exacerbated by qZ. As mentioned earlier, MC3 is the smallest MC (297 genes) and contains almost strictly genes related to protein catabolism. The counteracting effect of qZ indicates a profound stress underwent by strains lacking photoprotection, although none of the metacaspase protease family isoforms associated to cell death (Graff van Creveld *et al.*, 2021), were found in MC3. In addition to $^1O_2$ reaction products, other breakdown products, for instance of D1 (Foyer, 2018) could be involved in signalling, since the loss of D1 displayed long-term qZ-dependence. Since MC5 is strongly enriched in genes associated to ribosomes and growth, the exacerbating effect of qZ on their long-term induction might indicate that photoprotected cells can more rapidly use photosynthetic products provided by the light increase for metabolism and growth. It is difficult to speculate at this time about the internal sensors regulating this MC, as many different internal thresholds indicating favorable growth conditions could be involved. In addition, regulation could involve the release of inhibitory loops associated with other signaling pathways, such as sufficient light and/or controlled ROS levels.

To conclude, the Lhcx1 molecular titration approach introduced here allows to successfully overcome many complex problems that usually limit the conclusions that can be made from loss-of-function mutants. We believe this approach will continue to be extremely valuable in the future to pursue a system-approach to understanding orchestration of photosynthetic regulations. It could be used to investigate other high light responses in this *P. tricornutum* mutant series, such as alternative electron flows (Burlacot, 2023) or metabolomics under high light (Zhou *et al.*, 2022) for instance. It could also be used to target molecular actors involved in high light response that are suitable for a similar approach in other groups, Lhcx1 in *Nannochloropsis* naturally comes to

mind (Short *et al.*, 2023). Another interesting approach could be to explore other stress responses, such as nitrogen deficiency or heat stress, and to target non-constitutive genes involved in these responses, such as high-affinity nitrogen transporters or heat shock proteins. Finally, we believe the transcriptomic dataset presented here will be a very valuable resource for other researchers either curious about the expression of gene(s) encoding their protein(s) of interest during a high light stress or looking for novel molecular candidates within metaclusters, which represents genes subsets with increased likelihood of being associated to its labelled general function.

Material and Methods

Culture and growth conditions

Wildtype *P. tricornutum* Bohlin CCAP 1052/1A (Pt2) and 9 transgenic Lhcx1 lines previously characterized (Croteau et al., 2024) were grown in *f*/2 medium prepared from filtered (0.2 µm) seawater, in Erlenmeyers of 250 or 1000 mL depending on the volume required for a given set of experiments. Cells were grown under 5 µmol photons m^{-2} s^{-1} and 12: 12 photoperiod, those light conditions assuring the basal expression of only the Lhcx1 isoforms (Croteau et al., 2024). Temperature was maintained at 19°C for growth and all experiments. Cultures cell density was monitored every 3 days for cell concentration using a Multisizer 3 Coulter counter (Beckman Coulter, CA, USA) and dilution were performed to always maintain the cultures in exponential growth (0.7-to-1.5×10^6 cells mL^{-1}). All experiments began between 4 and 6 hours into the light phase of the photoperiod to improve reproducibility.

Fluorescence and spectroscopic measurements

For the *steady-state light exposure* experiments, samples of 50 mL were concentrated 10-fold by centrifugation (5000 RPM, 6 min), supplemented with ≈10% w/v Ficoll (to slowdown cell sedimentation during measurements), and then left to recover under gentle agitation and very low light (approximately 1 µmol photons m^{-2} s^{-1}) for at least 30 min. Experiments were conducted in a JTS-10 spectrophotometer (Biologic, France), allowing to measure Chl *a* variable fluorescence and absorption change signals at different wavelengths by equipping the detecting light with specific interference filters (3-8 nm bandwidth). Two absorption change signals were probed. First, the movement of electrons and protons across the thylakoid membrane generate an electric field which induces the electrochromic shift (ECS) of pigments absorption spectrum, whereby change in Δψ can be observed by probing the linear ECS (ECS_{lin}) (Bailleul *et al.*, 2010). Second, changes in the redox state of electron carriers, namely P700 and *c*-type cytochromes (*c*-t cyt., sum of cyt. *f* and cyt. c_6, replacing plastocyanin in diatoms) result in absorption changes in the green and far-red regions of the spectrum, respectively. The *c*-t cyt. and ECS_{lin} signals were obtained

through measuring transient absorption changes at 520, 554 and 566 nm with BG39 filter on the measuring and reference photodiodes (Schott (Mainz, Germany)) as in (Bailleul *et al.,* 2015) . Signals of interest were then calculated as *c*-t cyt. = [554]-0.4*([520]+[566]), and ECS_{lin}=[520]-0.25* *c*-t cyt. Absorption difference related to the redox changes of P700 was measured at 705 nm – 730 nm with a high pass RG695 filters on the measuring and reference photodiodes, the difference between the two wavelengths allowing to eliminate the scatter signals. For every biological replicate, a first sub-sample (1.3 mL) was used to measured absorption difference following a saturating single turnover flash from a dye laser (690 nm) allowing to obtain the ECS_{lin} signal corresponding to one single charge separation (CS) per PS, and the oxidation of 1 *c*-t cyt. per PSI. Those two values were used for normalization of ECS_{lin} and *c*-t cyt. The maximal absorption change signal corresponding to full oxidation of P700 (P_M) was then measured at the end of a 20 ms saturating pulse (red light, 660 nm, 6000 µmol photons m^{-2} s^{-1}) in the presence of 15 µM 3-(3,4-dichlorophenyl) 1,1-dimethylurea (DCMU).

Two new sub-samples (measured independently) were then exposed for 2 min to a 40 µmol photons m^{-2} s^{-1} actinic light (red light, 620 nm) to activate photosynthesis and then, for the next 3 min, one sub-sample remained under 40 µmol photons m^{-2} s^{-1} (control) and the other was exposed to a high light (HL) of 570 µmol photons m^{-2} s^{-1}. After 3 min, a pseudo-steady-state was reached and a series of measurements were performed sequentially as fast as possible (8 min in total, with at least 30 s between measurements that require a saturating pulse), always maintaining the actinic illumination except during the various measurements in dark windows (all <500 ms). Steady-state (F_s) and maximum fluorescence (F_M') under light were measured with a detecting light pulse before and after a 200 ms saturating pulse respectively. The quantum yields of the three energy dissipation pathways in PSII we calculated as: PSII photochemical conversion (ϕPSII) = (F_M'-F_s)/F_M', ϕNPQ = F_s/F_M'-F_s/F_M and non-regulated heat loss (ϕNO) = F_S/F_M . The fraction of open reaction centres (qL) were calculated as qL = (F_M'-F_s)/(F_M'-F_0') * F_0'/F_s, where F_0' is the minimum fluorescence in a sample during or after light exposure with all Q_A oxidized. In a model where NPQ is the result of a Stern-Volmer-like quenching process (qZ), F_0' can be theoretically extrapolated in under light as $F_0/(F_M-F_0)/F_M+F_0/F_M$') and qL estimates the redox-state of Q_A (i.e., the concentration of photochemical quencher) (Kramer *et al.*, 2004). A shorter pulse sequence (22 ms) was used to measure P700 redox-state, at steady-state under light before the pulse (P_S), more oxidized at the end of the pulse (P_M') and fully re-reduced in the dark after the pulse (P_0). The yield of PSI photochemistry was calculated as ϕPSI = (P_S-P_M')/(P_o-P_M'), and PSI donor side limitation (ϕND) as = -P_0/P_M and PSI acceptor side limitation (ϕNA) as = 1- ϕPSI-ϕND (Ferté, 2019). Relative electron flow at PSII ($rETR_{II}$= ϕPSII*E) estimates the linear electron flux (LEF) while relative electron flow at PSI ($rETR_I$= ϕPSI*E) is the sum of LEF and cyclic electron flow (CEF), or total electron flow (TEF). There was no effect of Lhcx1

accumulation on PS antenna functional size among the strains (Fig. S4) and in diatoms there are no rapid changes in absorption cross-sections (i.e., state-transition) (Lepetit *et al.*, 2022). Therefore, relative changes in the contribution of CEF to LEF due to NPQ can be estimated by comparing the yields of both PS in condition with and without NPQ (570 and 40 µmol photons m^{-2} s^{-1}, respectively) as:

$$\Delta(\text{TEF/LEF}) = \frac{\Phi\text{PSI}_{570}}{\Phi\text{PSII}_{570}} \times \frac{\Phi\text{PSII}_{40}}{\Phi\text{PSI}_{40}} - 1$$

For example, a Δ(TEF/LEF) of 0.4 in steady state under 570 µmol photons m^{-2} s^{-1} indicates that CEF contribution to TEF has increased by 40%, from the unknown (but ≈ among strains) baseline CEF contribution to TEF at 40 µmol photons m^{-2} s^{-1}. The same rationale can be use to compare CEF and LEF at the same light intensities but without and with NPQ, e.g., during its relaxation (see below). In a third sequence, the actinic light was shut off (during 175 ms, averaged 7 times with 2 s dead time between curves) to measure the photochemical rate (turnover rate of both photosystems) via the ECS_{lin} decay. At the light shut-off only PSI and PSII stop contributing to Δψ instantaneously, therefore the initial slope in ECS_{lin} decay reflect the photochemical rate per PS (Bailleul *et al.*, 2010). The ECS_{lin} decay was fitted as $ECS_T * e^{(-t/\tau)}$ where ECS_T is an approximation of the light induced electrochemical gradient (Avenson *et al.,* 2005), τ is the lifetime and the initial slope is calculated as ECS_T/τ. The number of oxidized *c*-t cyt. under 570 µmol photons m^{-2} s^{-1} was estimated as the amplitude of the change in the *c*-t cyt. signal from during 175 ms dark window, normalized to the laser flash signal. The equilibrium constant between P700/(P700+$P700^+$) and *c*-t cyt./(*c*-t cyt.+ *c*-t $cyt.^+$) was also calculated as in (Flori *et al.*, 2017) and see (Fig. S3)). This whole sequence of measurements was conducted on the 10 strains, and on three independent biological samples for each.

For three strains, WT, Lhcx1-Ko and one Lhcx1-OE (LtpW), a similar experiment was conducted but for which 10 sub-samples per strain where exposed to different light intensities (9 steps from 0 to 1000 µmol photons m^{-2} s^{-1}). In this case, an additional saturating pulse sequence was used to estimate the maximum proportion of *c*-t cyt. which can be oxidized with a saturating pulse, allowing to normalized *c*-t $cyt.^+$ to the fraction of total *c*-t cyt. This experiment served as rationale to identify 570 µmol photons m^{-2} s^{-1} as the optimal light intensity to use to maximize NPQ contrast between strains.

For the *transient NPQ relaxation and CEF experiment*, four strains (WT, Lhcx1-Ko and two Lhcx1-OE) were prepared as described above before measurements. In samples for which NPQ was gradually induced to its maximum value, the actinic light was abruptly switched down to 26 µmol photons m^{-2} s^{-1} before the relaxation of qZ and the recovery of ϕPSII was monitored in one sub-sample. The experiment was repeated to measure ϕPSI during the relaxation of NPQ in another sub-sample of the same biological

replicate. The relaxation kinetics of Δ(TEF/LEF) could be calculated as described above for all time points and replacing ϕPSI_{40} by the values measured when qZ had fully relaxed.

Photoinhibition and NPQ deconvolution analysis

To determine if qZ protects PSII against photoinhibition, a prolonged high light (HL) stress experiment was conducted in a fluorescence imaging system equipped with a green (532 nm) actinic light (SpeedZen, JbeamBio, France), allowing to measure multiple 60 µL samples in parallel on a same plate. Six strains, two low, two medium and two high Lhcx1 expressing strains, including WT and Lhcx1-Ko, were selected and prepared as described above. The samples were first exposed to 4 min of low light (35 µmol photons m^{-2} s^{-1}) and then let to relax in the dark 1 min before the maximum PSII yield in the dark was measured (F_V/F_M) (Fig. S6). Samples were then illuminated under HL (750 µmol photons m^{-2} s^{-1}) for 60 min and PSII fluorescence parameters were measured every 3 min. Samples were then let to recover over six low light/dark intervals (4: 1 min) like before the stress, during which PSII fluorescence parameters were measured every min. This protocol accelerates qZ relaxation and promotes PSII repair under low light, and allow to compare F_V/F_M before light stress and at its maximal recovered value (F_V'/F_M'Rec.) in standardized conditions which should allow to fully oxidized Q_A after 1 min of darkness. Each time a biological replicate was measured in six sub-samples in parallel, supplemented with increasing final concentration (0 to 0.8 mg mL^{-1}, 5 min before the start of the experiment) of lincomycin (Sigma-Aldrich), which inhibits chloroplast translation and therefore *de novo* synthesis of D1 for PSII repair. The average of treatments at 0.4 and 0.8 mg mL^{-1} lincomycin (saturated effect on F_V'/F_M'Rec.) were used as comparison with the control conditions.

Under moderate light stress, *P. tricornutum* exhibits a single qZ component of NPQ, proportional to DT bound to Lhcx1 and which relax under ≈10 min under low light or darkness (Croteau et al., 2024). Under longer light stress, photodamaged PSII centres cannot participate to electron transport but can act as nonphotochemical quenchers (qI), complexifying the relationship between total NPQ and F_V'/F_M' (Nawrocki *et al.*, 2021). To clarify the role of qZ in protecting PSII from photoinhibition and qI in diatoms, NPQ relaxation was fitted as the sum of a fast (qZ) and a slow (qI) monoexponential decay.

$$\varphi NPQ = qZ_M e^{t \times \tau z} + qI_M e^{t \times \tau I}$$

Where qZ_M and qI_M are the maximal contribution of each component to ϕNPQ, i.e., at the beginning of the relaxation, and τ_Z and τ_I are the decay rates of both component (see Fig. S8).

High light experiment for biochemistry and RNA sampling

A 60 min HL (600 µmol photons m^{-2} s^{-1}) stress followed by 30 min of recovery under low light (15 µmol photons m^{-2} s^{-1}) experiment was reproduced on an experimental setup allowing to work on large volumes of non-concentrated cultures always at $1*10^6$ c/mL (Erlen maintained agitated over a LED panel) and to sample biological material. To monitor PSII fluorescence parameters in parallel of these experiments, 1 mL sub-samples were let to relax 1 min in the dark in a home-made fluorometer before measing minimum and maximal fluorescence. The reversible-qZ portion of NPQ was estimated with the highest recovered value of F_M' post-stress as reference: F_M'Rec./F_M'-1, and used as independent variable for D1 and gene expression kinetics. To attempt to link D1 degradation to qI and F_V'/F_M'Rec., three strains (WT, Lhcx1-Ko and two Lhcx1-OE) were grown and maintained in exponential phase in volumes of 100 mL. A protein sample of 10 mL was collected before the experiment. Then, the culture was split in two, one was supplemented with lincomycin (final concentration 0.4 mg mL^{-1}) and another 10 mL sample was retrieved at the end of the experiment (after 30 min recovery under low light) for both treatments. Samples in Falcon were centrifuged 10 min (2500 RPM) at 4°C, rinsed in PBS and stored at -80°C. For RNA sampling, the same experiment (without lincomycin) was repeated on 350 mL cultures of six strains which were sampled (100 mL, filtered onto Whatman filter 589/2 and immediately frozen in liquid nitrogen) at t0, and at t20 and t60 of the HL treatment. At the same timepoints, 10 mL samples for pigment analysis were centrifuged and stored at -80°C.

Immunoblotting and RNA extraction

Immunodetection of D1 was performed following the same protocol as in (Giovagnetti *et al.,* 2022), using rabbit-polyclonal D1 (AS05 084, 1: 50,000) and ATPsynthase-βCF_1 (AS05 084, 1: 10,000 (loading control)) antibodies (Agrisera, Sweden). Total protein loading was of 10 µg to ensure the detection of both antibodies was in the linear range. RNA was extracted with TriPure Isolation Reagent (Roche) following the protocol provided by the company, further purified by an ammonium acetate precipitation, and finally treated with RQI DNaseI (Promega). cDNA libraries were prepared from extracts enriched in mRNA by oligo-T selection, and sequenced by the DNBseq platform at the Beijing Genomics Institute (*BGI* Group). Sequencing, mapping over *P. tricornutum* second version genome (Phatr, and transcripts quantification of the extracted RNA samples was outsourced to BGI (Hong Kong).

Analysis of transcriptomic data

Three biological replicates of six different strains with ranging maximal qZ values and sampled at three different timepoints (t=0, t=20 min and t=60 min) over a prolonged light stress were used for transcriptomic analysis. Total RNA was extracted as described, polyA enriched and sequenced at BGI by DNBseq. We retrieve 4.35Gb bases per sample with an average mapping using HISAT2 of 90.26 % on

PHATR2 genome (74 % uniquely mapped). The large number of transcriptomes retrieved (50, one outlier biological replicate of LtpW (overexpressor) was removed) and one sample of Ko6-t0 was lost during RNA extraction) allowed to develop a novel approach to decipher genes whose expression respond directly to abiotic cues (here light exposure over time) from those responding to physiological signals mediated by photosynthesis functioning and thus deeply influenced by qZ/Lhcx1 (shown in Fig. 4).

For every transcript, mRNA abundance is counted and first normalized by fragments per kilobase of transcript per million fragments mapped (FPKM) for each sample at t=0, t=20 min and t=60 min. Then FPKM are divided by the average expression of this transcript (on the 50 transcriptomes) and centred to zero, called centred FPKM. The average expression of the 16-18 samples at each time represents the time dependence of the HL-induced changes. The standard deviation of the 3 average values at t=0, 20 and 60 min is calculated as *std(t)*. The Lhcx1 effect is calculated by subtracting time dependence of the HL-induced changes to the centred FPKM at each time. The standard deviation of the 50 values after this subtraction is calculated as *std(Lhcx1)*. So that the clustering method gives equal importance to time and Lhcx1 dependences, we modified the gene expression profiles by giving the same weight to both dependencies. For this, the time dependence and the Lhcx1 dependence were divided by the average value of *std(t)* and *std(Lhcx1)*, respectively. Finally weighted FPKM are obtained by combining both normalized time and Lhcx1 dependencies. For K-means clustering, random seeding is used, and data are organized by ascending HL exposure time (0, 20, 60) and within each HL exposure time by strain showing ascending amount of Lhcx1, as estimated by the maximal capacity of qZ. The Elbow method did not show a clear break, and the number of clusters was set at 25 (Fig. S12).

Gene ontology (GO) enrichment analyses were done with the online platform g:Profiler (Raudvere *et al.*, 2019) using the gene id on *P. tricornutum* third genome version, with a significance threshold in adjusted p.value of 0.05, calculated according to the SCS methods (statistical domain scope limited to annotated genes). In Fig. 6 only GOs identified as a main drivers by the g:Profiler algorithm are shown, but all GOs and KEGGs, and their respective adjusted p.value are shown in Fig. S14. In some cases, we wanted to investigate GO enrichment in sub-MC associated to a specific cellular compartment. For such purposes, we used the protein target predictions of various softwares compiled in (Ait-Mohamed *et al.*, 2020). We assigned plastid targeting for genes identified as such by HECTAR or ASAFIND, both more specialized for secondary endosymbiotic organisms WoLF PSORT. We assigned mitochondria targeting for genes for which MITOFATES identified mitochondrial presequence or for WoLF PSORT consensus predicted location was mitochondria (251 had dual target prediction mitochondria and plastid). Other locations were predicted by WoLF PSORT consensus, if not

contradicting HECTAR, ASAFIND or MITOFATES. We grouped together “Cytoplasm” and “Cytoplasm_nucleus” predictions, and did not consider very small groups with less than 50 genes (“Golgi”, “Peroxisome”, etc)

Acknowledgements

The authors want to thank Pascal Campagne and Bernard Lepetit for fruitful discussions about the transcriptomic data and bioinformatic analysis. This research was supported by the European Research Council (ERC) PhotoPHYTOMIX project (grant agreement No. 715579) and the ANR ‘BrownCut’ (ANR-19-CE20-0020). AF was supported by funding from the Fondation Bettencourt-Schueller (Coups d’élan pour la recherche francaise-2018) and the “Initiative d’Excellence” program (Grant “DYNAMO,” ANR-11-LABX-0011-01).

References

Agarwal, Ananya, et al. "Light-dependent signal transduction in the marine diatom *Phaeodactylum tricornutum*". *Proceedings of the National Academy of Sciences*, vol. 120, no. 11, 2023, e2216286120.

Ait-Mohamed, Ouardia, et al. "PhaeoNet: a holistic RNAseq-based portrait of transcriptional coordination in the model diatom *Phaeodactylum tricornutum*". *Frontiers in Plant Science*, vol. 11, 2020, p. 590949.

Alric, Jean. The plastoquinone pool, poised for cyclic electron flow? *Frontiers in plant science*, vol. 6, 2015, p. 540.

Avenson, Thomas J, et al. "Integrating the proton circuit into photosynthesis: progress and challenges". *Plant, Cell & Environment*, vol. 28, no. 1, 2005, pp. 97–109.

Bailleul, Benjamin, et al. "Electrochromism: a useful probe to study algal photosynthesis". *Photosynthesis research*, vol. 106, 2010, pp. 179–89.

Bailleul, Benjamin, et al. "Energetic coupling between plastids and mitochondria drives CO2 assimilation in diatoms". *Nature*, vol. 524, no. 7565, 2015, pp. 366–69.

Blommaert, Lander, et al. "The fine-tuning of NPQ in diatoms relies on the regulation of both xanthophyll cycle enzymes". *Scientific Reports*, vol. 11, no. 1, 2021, p. 12750.

Burlacot, Adrien. "Quantifying the roles of algal photosynthetic electron pathways: a milestone towards photosynthetic robustness". *New Phytologist*, vol. 240, no. 6, 2023, pp. 2197–203.

Burlacot, Adrien, et al. "Alternative photosynthesis pathways drive the algal CO2-concentrating mechanism". *Nature*, vol. 605, no. 7909, 2022, pp. 366–71.

Campbell, Douglas A, and Esa Tyystjärvi. "Parameterization of photosystem II photoinactivation and repair". *Biochimica et Biophysica Acta (BBA)-Bioenergetics*, vol. 1817, no. 1, 2012, pp. 258–65.

Cartaxana, P, et al. "Photoinhibition in benthic diatom assemblages under light stress". *Aquatic Microbial Ecology*, vol. 70, no. 1, 2013, pp. 87–92.

Chaux, Frédéric, et al. "Flavodiiron proteins promote fast and transient O2 photoreduction in Chlamydomonas". *Plant physiology*, vol. 174, no. 3, 2017, pp. 1825–36.

Croteau, Dany, et al. "Pennate diatoms make Non Photochemical Quenching as simple as possible, but not simpler." *Research Square*, 2024.

Dorrell, Richard G, et al. "Complementary environmental analysis and functional characterization of lower glycolysis-gluconeogenesis in the diatom plastid". *The Plant cell*, 2024, koae168.

Escoubas, Jean-Michel, et al. "Light intensity regulation of cab gene transcription is signaled by the redox state of the plastoquinone pool." *Proceedings of the National Academy of Sciences*, vol. 92, no. 22, 1995, pp. 10237–41.

Ferté, Suzanne. "Exploring the diversity of cyclic electron flow around photosystem I in microalgae species". 2019. Sorbonne Université, PhD dissertation.

Finazzi, Giovanni, and Giorgio Forti. "Metabolic flexibility of the green alga *Chlamydomonas reinhardtii* as revealed by the link between state transitions and cyclic electron flow". *Photosynthesis Research*, vol. 82, 2004, pp. 327–38.

Flori, Serena, et al. "Plastid thylakoid architecture optimizes photosynthesis in diatoms". *Nature communications*, vol. 8, no. 1, 2017, p. 15885.

Foyer, Christine H. "Reactive oxygen species, oxidative signaling and the regulation of photosynthesis". *Environmental and experimental botany*, vol. 154, 2018, pp. 134–42.

Gain, Gwenaëlle, et al. "Induction of photosynthesis under anoxic condition in *Thalassiosira pseudonana* and Euglena gracilis: interactions between fermentation and photosynthesis". *Frontiers in Plant Science*, vol. 14, 2023, p. 1186926.

Giossi, Chiara E, et al. "Both major xanthophyll cycles present in nature can provide Non-Photochemical Quenching in the model diatom *Phaeodactylum tricornutum*". *bioRxiv*, 2024, pp. 2024–03.

Giovagnetti, Vasco, et al. "Biochemical and molecular properties of LHCX1, the essential regulator of dynamic photoprotection in diatoms". *Plant Physiology*, vol. 188, no. 1, 2022, pp. 509–25.

Goldman, Johanna AL, et al. "Gross and net production during the spring bloom along the Western Antarctic Peninsula". *New Phytologist*, vol. 205, no. 1, 2015, pp. 182–91.

Goss, Reimund, and Torsten Jakob. "Regulation and function of xanthophyll cycle-dependent photoprotection in algae". *Photosynthesis research*, vol. 106, 2010, pp. 103–22.

Graff van Creveld, Shiri, et al. "Biochemical characterization of a novel redox-regulated metacaspase in a marine diatom". *Frontiers in Microbiology*, vol. 12, 2021, p. 688199.

Jaubert, Marianne, et al. "Sensing and signalling in diatom responses to abiotic cues". *The Molecular Life of Diatoms*, 2022, pp. 607–39.

Jensen, Erik L, et al. "Insights on the functions and ecophysiological relevance of the diverse carbonic anhydrases in microalgae". *International Journal of Molecular Sciences*, vol. 21, no. 8, 2020, p. 2922.

Jiang, Yanyou, et al. "A chlorophyll c synthase widely co-opted by phytoplankton". *Science*, vol. 382, no. 6666, 2023, pp. 92–98.

Kale, Ravindra, et al. "Amino acid oxidation of the D1 and D2 proteins by oxygen radicals during photoinhibition of Photosystem II". *Proceedings of the National Academy of Sciences*, vol. 114, no. 11, 2017, pp. 2988–93.

Kozuleva, Marina, et al. "Phylloquinone is the principal Mehler reaction site within photosystem I in high light". *Plant Physiology*, vol. 186, no. 4, 2021, pp. 1848–58.

Laisk, Agu, et al. "Quantum yields and rate constants of photochemical and nonphotochemical excitation quenching (experiment and model)". *Plant Physiology*, vol. 115, no. 2, 1997, pp. 803–15.

Lavaud, Johann, et al. "Photosystem II repair in marine diatoms with contrasting photophysiologies". *Photosynthesis Research*, vol. 127, 2016, pp. 189–99.

Lepetit, Bernard, et al. "High light acclimation in the secondary plastids containing diatom *Phaeodactylum tricornutum* is triggered by the redox state of the plastoquinone pool". *Plant physiology*, vol. 161, no. 2, 2013, pp. 853–65.

Lepetit, Bernard, et al. "Photosynthetic light reactions in diatoms. II. The dynamic regulation of the various light reactions". *The molecular life of diatoms*, Springer, 2022, pp. 423–64.

Li, Lei, et al. "Mechanisms of photodamage and protein turnover in photoinhibition". *Trends in plant science*, vol. 23, no. 8, 2018, pp. 667–76.

Munekage, Yuri, et al. "Cyclic electron flow around photosystem I is essential for photosynthesis". *Nature*, vol. 429, no. 6991, 2004, pp. 579–82.

Nawrocki, Wojciech J, et al. "Chlororespiration controls growth under intermittent light". *Plant physiology*, vol. 179, no. 2, 2019, pp. 630–39.

Nawrocki, Wojciech J, et al. "Molecular origins of induction and loss of photoinhibition-related energy dissipation qI". *Science Advances*, vol. 7, no. 52, 2021, eabj0055.

Nymark, Marianne, et al. "An integrated analysis of molecular acclimation to high light in the marine diatom *Phaeodactylum tricornutum*". *PloS one*, vol. 4, no. 11, 2009, e7743.

Nymark, Marianne, et al. "Molecular and photosynthetic responses to prolonged darkness and subsequent acclimation to re-illumination in the diatom *Phaeodactylum tricornutum*". *PLoS one*, vol. 8, no. 3, 2013, e58722.

Olaizola, Miguel, et al. "Non-photochemical fluorescence quenching and the diadinoxanthin cycle in a marine diatom". *Photosynthesis Research*, vol. 41, 1994, pp. 357–70.

Owens, Thomas G. "Light-harvesting function in the diatom *Phaeodactylum tricornutum*: II. Distribution of excitation energy between the photosystems". *Plant Physiology*, vol. 80, no. 3, 1986, pp. 739–46.

Pancheri, Tina, et al. "Singlet-Oxygen-Mediated Regulation of Photosynthesis-Specific Genes: A Role for Reactive Electrophiles in Signal Transduction". *International Journal of Molecular Sciences*, vol. 25, no. 15, 2024, p. 8458.

Raudvere, Uku, et al. "g: Profiler: a web server for functional enrichment analysis and conversions of gene lists (2019 update)". *Nucleic acids research*, vol. 47, W1, 2019, W191–W198.

Rosenwasser, Shilo, et al. "Mapping the diatom redox-sensitive proteome provides insight into response to nitrogen stress in the marine environment". *Proceedings of the National Academy of Sciences*, vol. 111, no. 7, 2014, pp. 2740–45.

Santabarbara, S, et al. "The quenching of photosystem II fluorescence does not protect the D1 protein against light induced degradation in thylakoids". *FEBS letters*, vol. 505, no. 1, 2001, pp. 159–62.

Short, Audrey, et al. "Kinetics of the xanthophyll cycle and its role in photoprotective memory and response". *Nature Communications*, vol. 14, no. 1, 2023, p. 6621.

Steen, Collin J, et al. "Interplay between LHCSR proteins and state transitions governs the NPQ response in *Chlamydomonas* during light fluctuations". *Plant, cell & environment*, vol. 45, no. 8, 2022, pp. 2428–45.

Sukenik, Assaf, et al. "Light-saturated photosynthesis—limitation by electron transport or carbon fixation?" *Biochimica et Biophysica Acta (BBA)-Bioenergetics*, vol. 891, no. 3, 1987, pp. 205–15.

Taddei, Lucilla, et al. "Multisignal control of expression of the LHCX protein family in the marine diatom *Phaeodactylum tricornutum*". *Journal of experimental botany*, vol. 67, no. 13, 2016, pp. 3939–51.

Thamatrakoln, Kimberlee, et al. "Death-specific protein in a marine diatom regulates photosynthetic responses to iron and light availability". *Proceedings of the National Academy of Sciences*, vol. 110, no. 50, 2013, pp. 20123–28.

Volpert, Adi, et al. "Diurnal fluctuations in chloroplast GSH redox state regulate susceptibility to oxidative stress and cell fate in a bloom-forming diatom". *Journal of phycology*, vol. 54, no. 3, 2018, pp. 329–41.

Zhou, Lu, et al. "Transcriptomic and metabolic signatures of diatom plasticity to light fluctuations". *Plant Physiology*, vol. 190, no. 4, 2022, pp. 2295–314.

4.3 Supplementary Information

Supplementary Figures

A photoprotection dial to unveil multi-level orchestration of photosynthetic regulations in diatoms

D. Croteau[1*], M. Jaubert[1], T. Quemar[1], A. Falciatore[1], A. Maes[2,3], B. Bailleul[1*]

1. UMR7141, Institut de Biologie Physico-Chimique, Sorbonne Université / CNRS, 13 Rue Pierre et Marie Curie, 75005 Paris, France
2. UMR8226, Institut de Biologie Physico-Chimique, Sorbonne Université / CNRS, 13 Rue Pierre et Marie Curie, 75005 Paris, France
3. Plateforme de Génomique Fonctionnelle FR550, Institut de Biologie Physico-Chimique, Sorbonne Université / CNRS, 13 Rue Pierre et Marie Curie, 75005 Paris, France

[*] corresponding authors: dany.croteau@ibpc.fr, bailleul@ibpc.fr

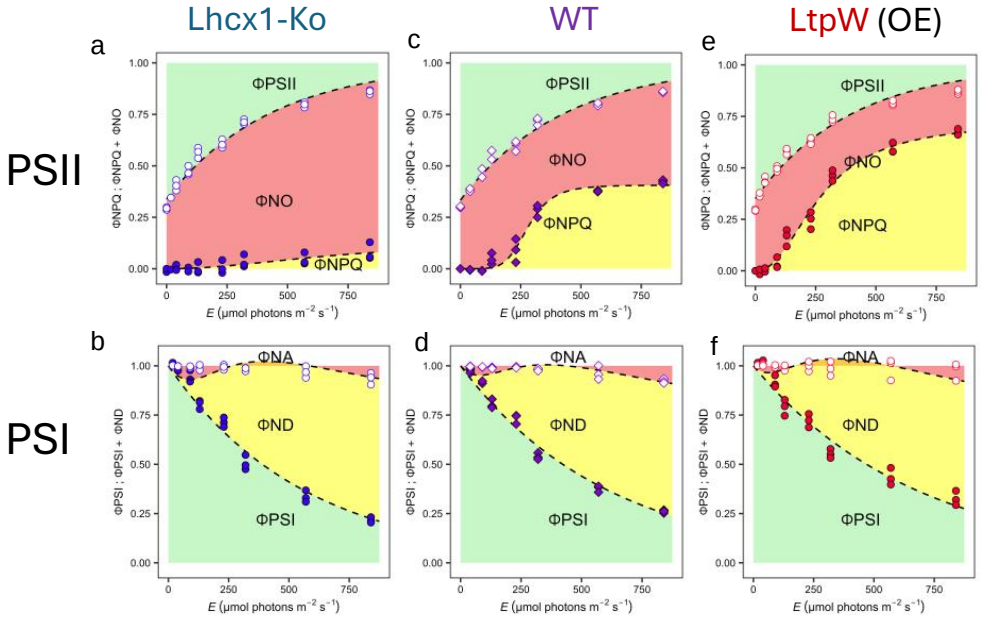

Fig. S1 | Light-dependence of PSII and PSI parameters in three representative strains: (Upper panels) Quantum yield of PSII photochemistry (ϕPSII), non-regulated heat dissipation (ϕNO) and ϕNPQ as a function of light intensity (*E*) were measured under steady-state 570 µmol photons m^{-2} s^{-1} illumination. During the same experiment (lower panels), the quantum yields of PSI (ϕPSI), PSI donor side limitation (ϕND, which corresponds to the proportion of oxidized P700) and PSI acceptor side limitation (ϕNA, which approximates the proportion of reduced acceptors) via the redox-state of P700 were also measured. The strains used are Lhcx1-Ko (a-b), WT (c-d) and the LtpW overexpressor (OE) (e-f). All panels show three independent biological replicates.

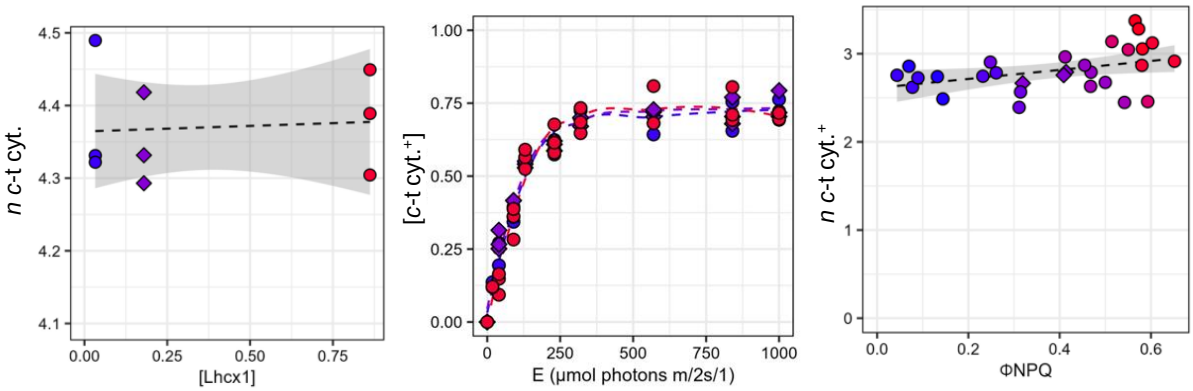

Fig. S2 | Light-induced oxidation of *c*-type cytochromes (*c*-t cyt.) and influence of Lhcx1-dependent qZ : Maximum number of *c*-t cyt. which can be oxidized in the dark with a saturating pulse (a) and the proportion of oxidized *c*-t cyt. under steady-state illumination as a function of light intensity *(E*) in Lhcx1-Ko, WT (diamond symbols) and Lhcx1 overexpressor (LtpW), showing that *c*-t cyt. oxidation saturates at 570 µmol photons m^{-2} s^{-1} (b). In (*c*) number of *c*-t cyt.$^{+}$ per PSI in the 10 strains with ranging Lhxc1 concentrations measured only under 570 µmol photons m^{-2} s^{-1} illumination. All panels show three independent biological replicates (except one strains for which n = 2 in (c)).

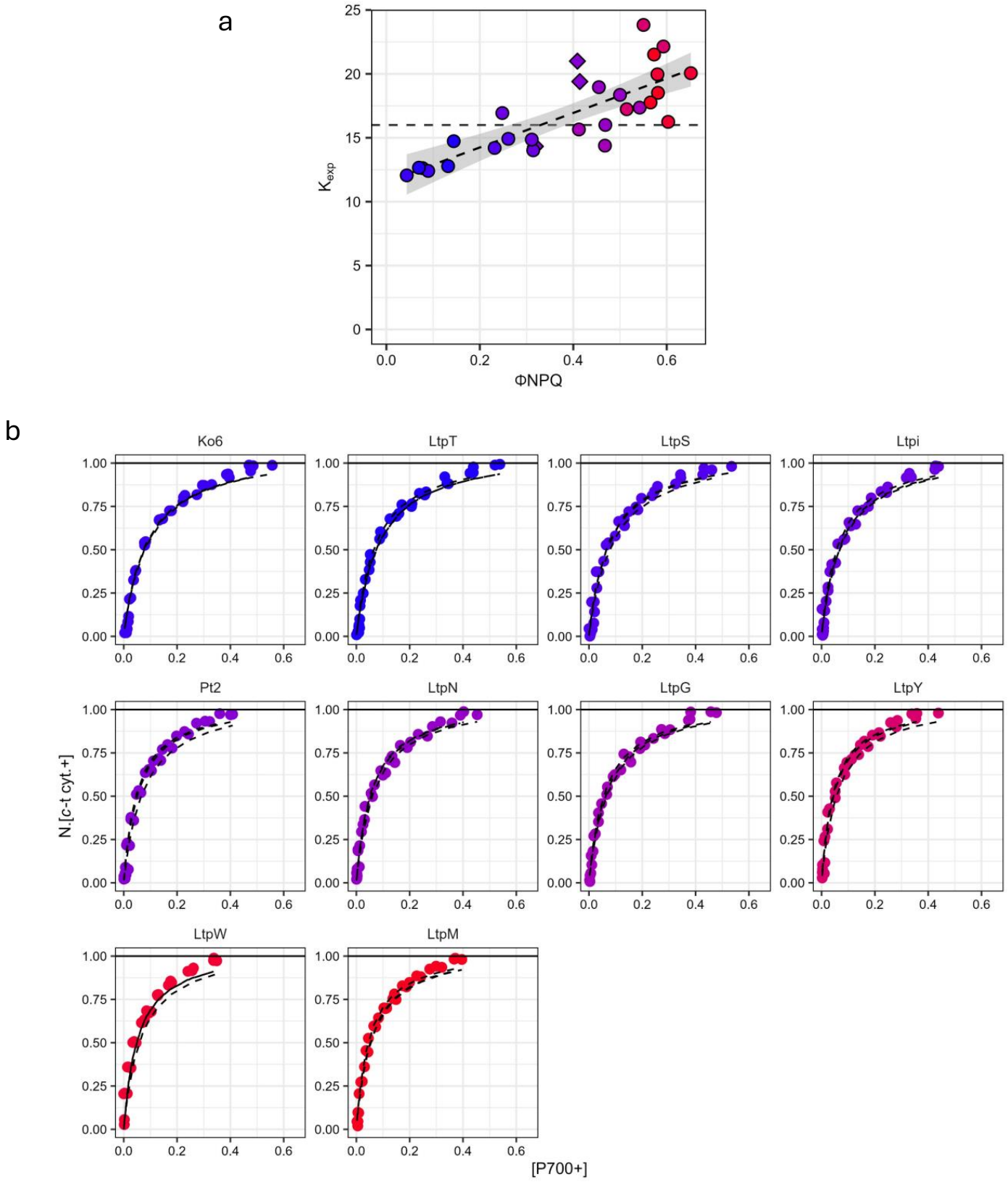

Fig. S3 | Influence of Lhcx1-dependent qZ on the equilibrium between redox state of P700 and *c*-type cytochromes (*c*-t cyt.): (a) The experimental equilibrium constant (K_{exp}) between *c*-t cyt. and P700 during their equilibrium in the dark, 175 ms dark windows, from steady-state 570 µmol photons m^{-2} s^{-1} illumination. K_{exp} is shown versus the quantum yield of nonphotochemical quenching (ϕNPQ) in 10 *Phaeodactylum tricornutum* strains with ranging Lhxc1 concentrations (WT diamond symbols). The theoretical K is 16 (horizontal dashed line). See Flori *et al.,* 2017 for more details. Because *c*-t cyt. oxidation versu light intensity saturated at 570 µmol photons m^{-2} s^{-1} (Fig. S2), we assumed all *c*-t cyt. were oxidized prior to reduction over 175 ms dark windows, shown for all strains/replicates in (b). All experiment were performed on three independent biological replicates (except LtpS for which n = 2).

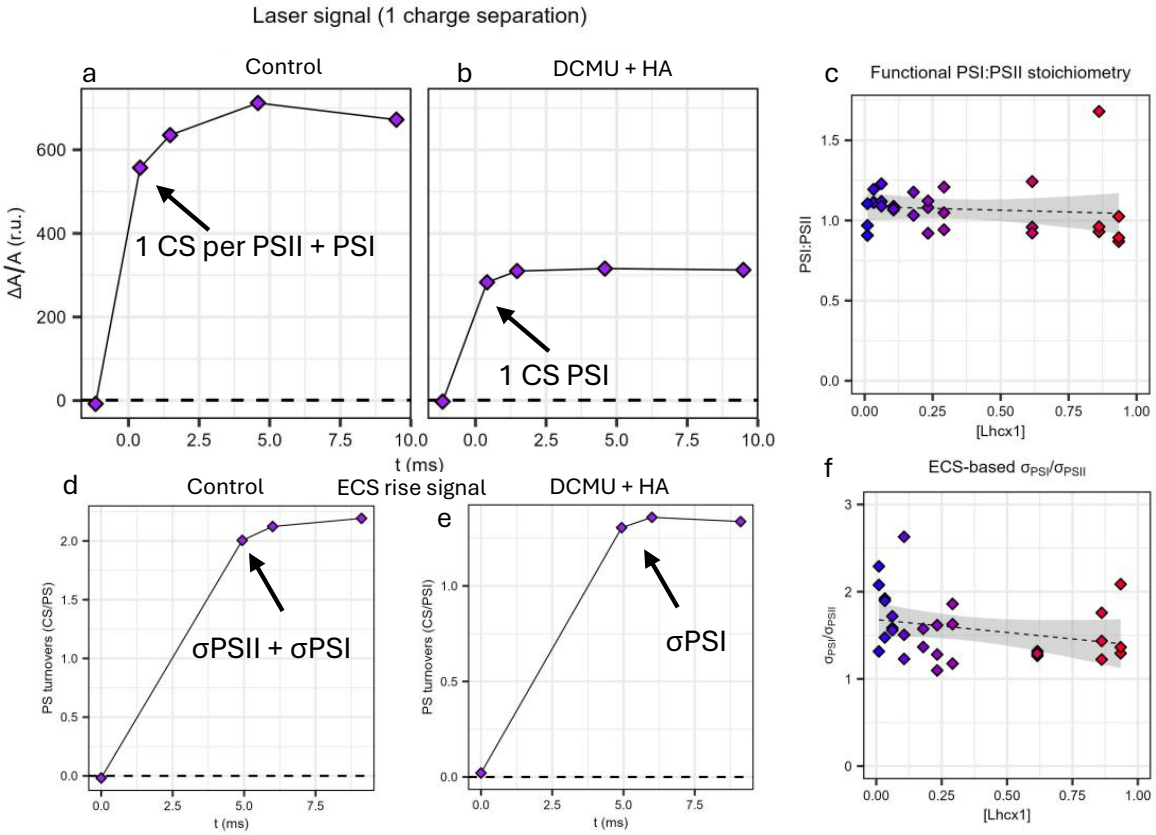

Fig. S4 | Photosystem (PS) I and II stoichiometry and antenna functional cross-section (σ) ratios for ranging Lhcx1 concentrations : Shown only for the WT, the absorbance change signal (ΔA/A) for the linear electrochromic shift (ECS_{lin}) following a laser flash inducing a single charge separation (CS) per photosystem (PS), in control conditions (a) and when PSII is inhibited by 3-(3,4-dichlorophenyl) 1,1-dimethylurea (DCMU) and hydroxylamine (HA) (b), and the stoichiometry of functional PSI-to-PSII in the 10 *Phaeodactylum tricornutum* strains with ranging Lhxc1 concentrations used in the paper (c). Shown only for the WT, dark-to-light ECS rise under moderate (130 µmol photons m^{-2} s^{-1}) light so that light absorption limits photochemistry and allows to measure the ECS-based functional cross-section (σ) of PSII+PSI (d) and PSI (when PSII is inhibited) in (e). To calculate the ratio between σPSI/σPSII in (f), σPSII was divided by Fv/Fm (0.71±0.01 across strains/replicates) to only take into account the fraction of absorbed light energy by PSII that participates to photochemistry (the rest is lost as heat) (see Ferté, 2019 for more details). Overall, we conclude from these measurements that there is no significant Lhcx1-dependent effects on PSI:PSII stoichiometry or σPSI/σPSII ratios among the 10 strains used. All measurements were repeated on three independent biological replicates (except one strains for which n = 2 in (c)).

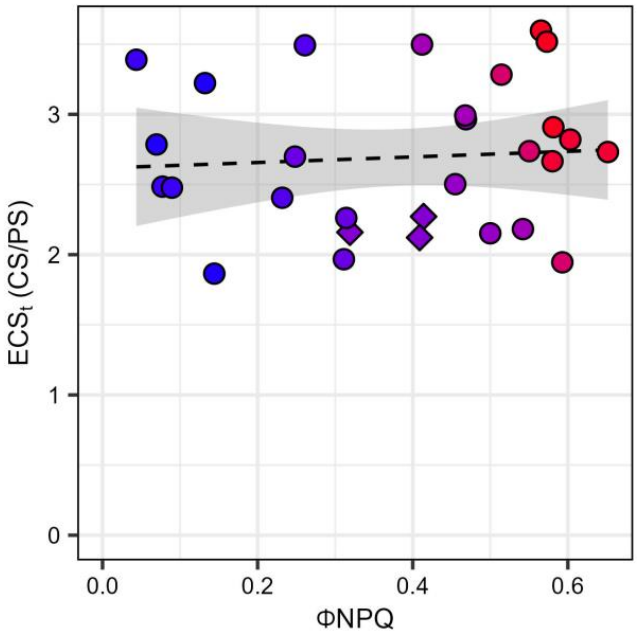

Fig. S5 | Influence of the Lhcx1-dependent qZ on the light-induced membrane potential: Light induced electrochemical proton gradient under 570 µmol photons m^{-2} s^{-1} illumination as measured by total electrochromic shift decay (ECS_t) (in charge separation (CS) per photosystem (PS) equivalence) over dark windows (see Avenson *et al.,* 2005 and Material and Methods), versus the quantum yield of nonphotochemical quenching (ϕNPQ) in 10 *Phaeodactylum tricornutum* strains (all measured with 3 independent biological replicates (except *n*=2 for one strain)) with ranging Lhxc1 concentrations (WT with diamond symbols).

Figure S6

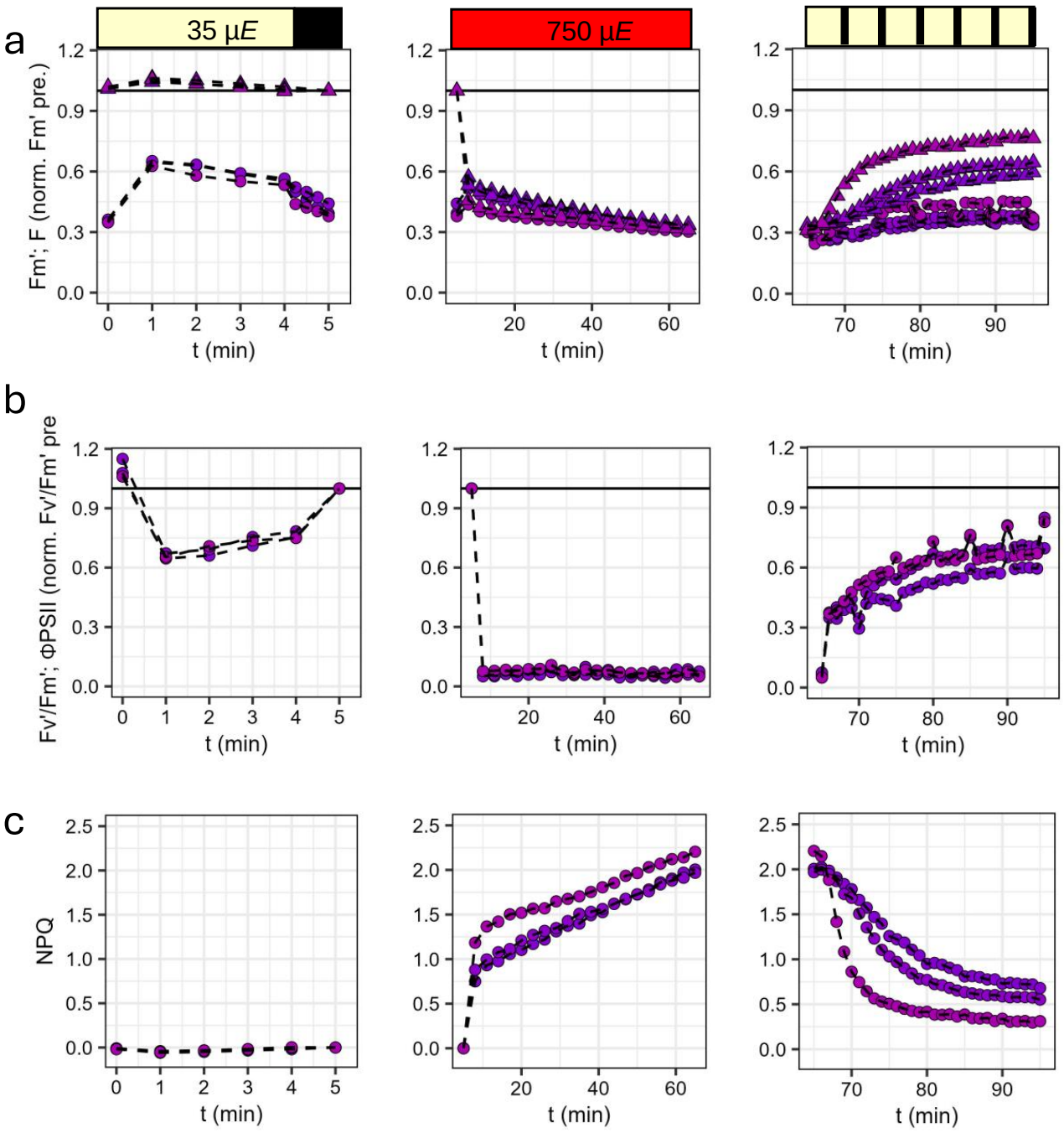
a
35 µE
750 µE
Fm'; F (norm. Fm' pre.)
t (min)
b
Fv'/Fm'; ΦPSII (norm. Fv'/Fm' pre
t (min)
c
NPQ
t (min)

Fig. S6 |Light protocol used to estimate the qZ-photoprotection against photoinhibition. Representation of the illumination protocol, shown only WT shown, used to test interactions between nonphotochemial quenching (NPQ) and photodamages/photoinhibition. We estimated the influence of NPQ-qZ on photoinhibition, via measurements of variations in the recovery of PSII quantum yield in the dark (F_V'/F_M') (Fig. 3 in the main manuscript) (and the slow relaxing photoinhibition quenching component, Fig. S8). First (left column), during 5 min of acclimation to low light (LL, 35 µmol photons m^{-2} s^{-1}) is used and followed by one min of darkness before measuring "pre."-stress fluorescence levels that will be used for normalization after recovery. Then (middle column), 60 min of exposure under 750 µmol photons m^{-2} s^{-1}. Finally (right column), recovery is monitored during 30 min separated in 6 LL/dark intervals (4 :1), allowing to measure F_V'/F_M' recovery in conditions comparable to the one measured at the end of LL acclimation. Minimum (F') and maximum (F'_M) fluorescence, F_V'/F_M' (a), F_V'/F_M' (b) and NPQ (c) are shown as example of the progression of the different parameters measured. See Material and Methods for more details.

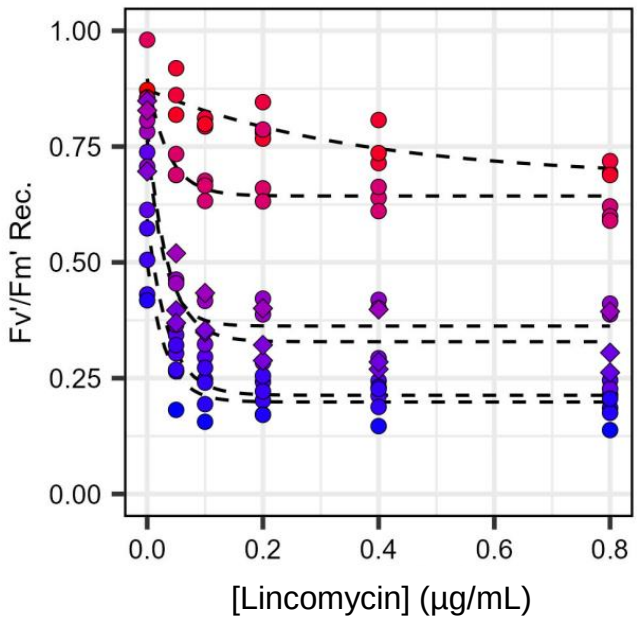

Fig. S7 | Lincomycin effect on high-light induced loss of PSII efficiency. The quantum yield of PSII in the dark at the end of low light recovery (F_v'/F_M'Rec.) following high light stress (see Fig. S6) is shown as a function of the concentration of lincomycin added right before the experiment. From this analysis, we concluded that concentrations 0.4 and 0.8 µg/mL are saturating, and we used these treatments for further analysis shown in Fig. 3. Experimental data correspond to independent biological triplicates in 6 strains (WT with diamonds).

Figure S8a:

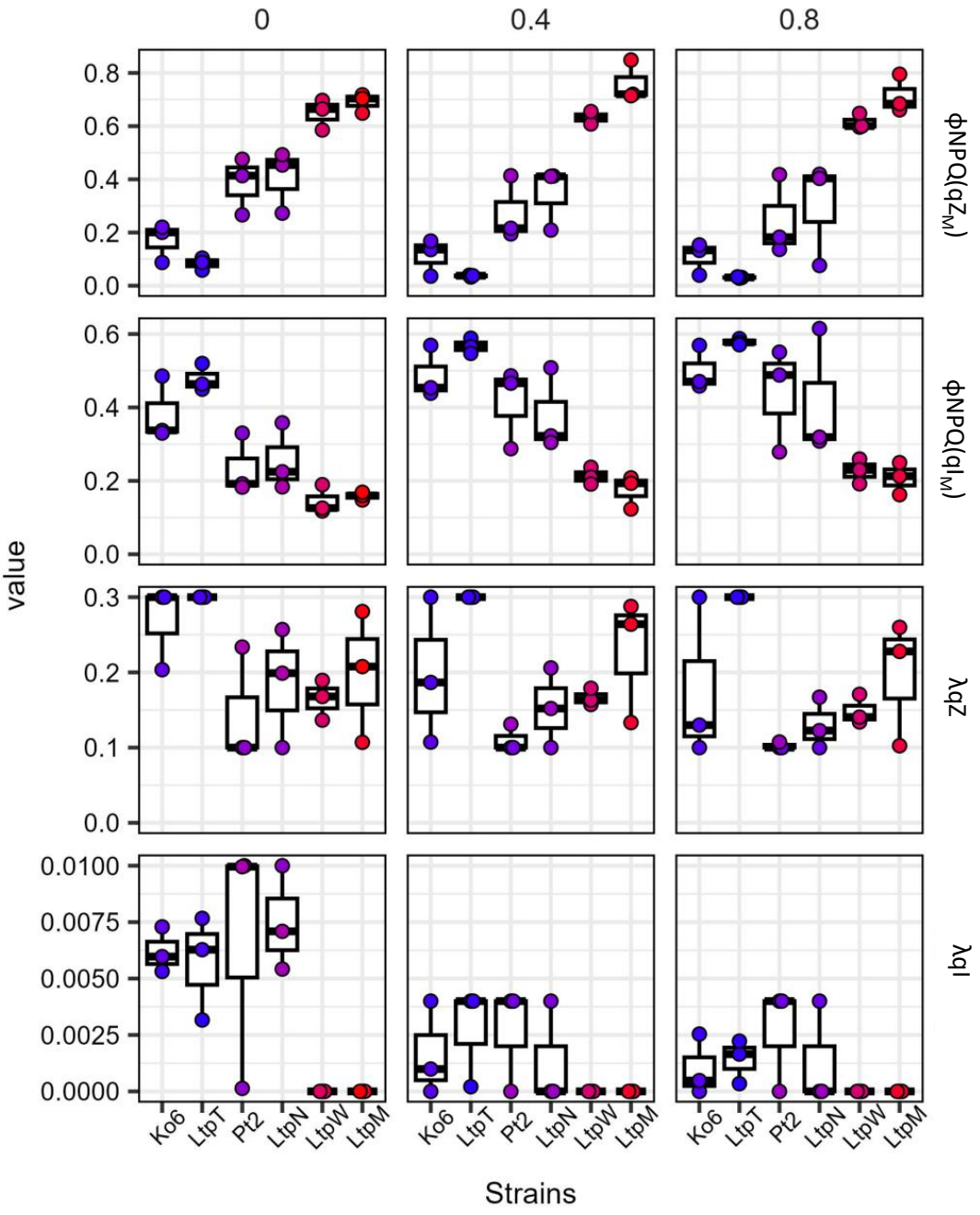
0
0.4
0.8
ΦNPQ(qZ_M)
ΦNPQ(qI_M)
λqZ
λqI
value
Strains
Ko6
LtpT
Pt2
LtpN
LtpW
LtpM

Figure S8b:

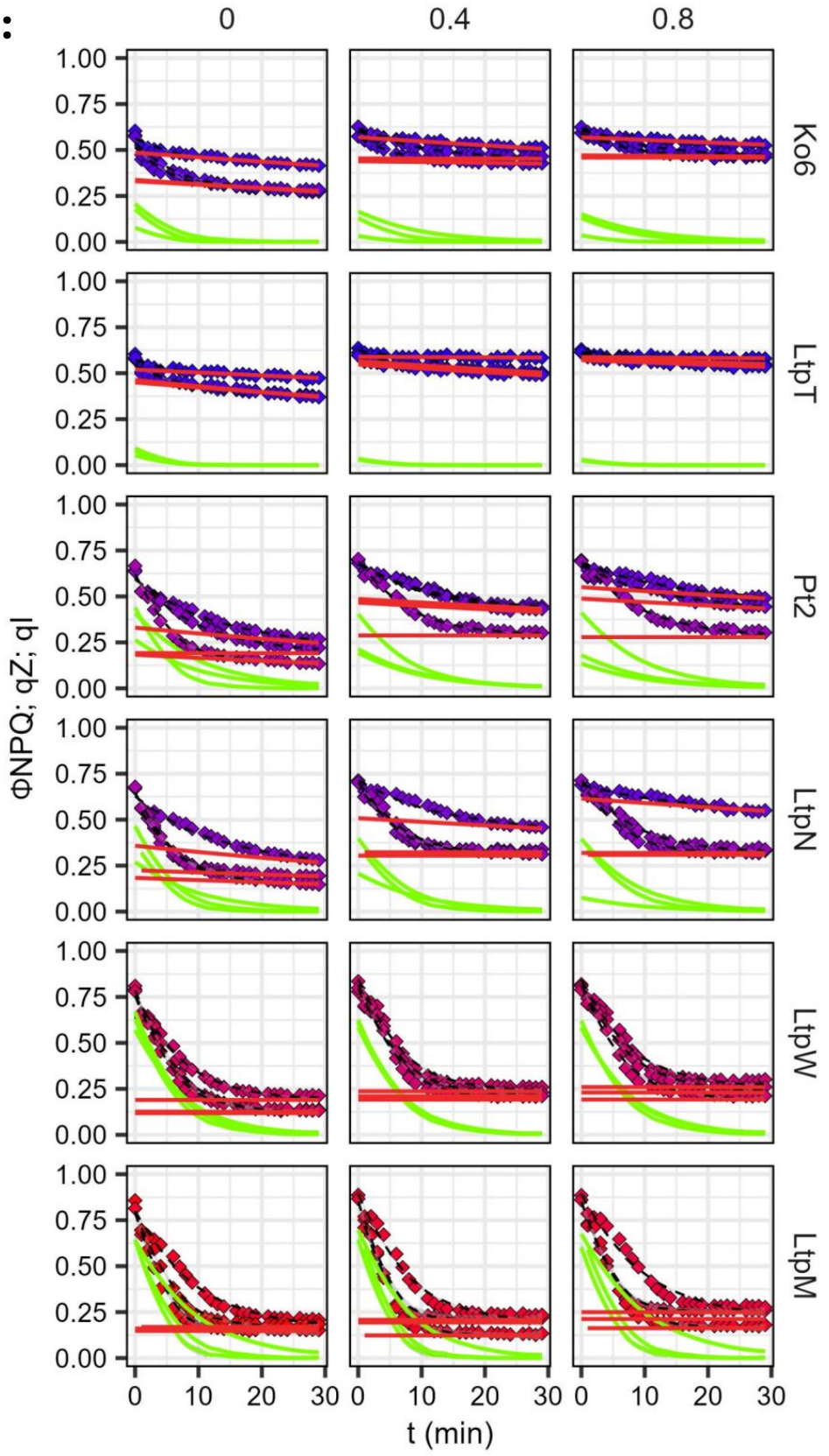

Fig. S8| Interplay between qZ and qI induced by 1h of high light illumination. To estimate the extent of Lhxc1-dependent (qZ) and photoinhibition-dependent (qI) quenching, the relaxation of the ϕNPQ was fitted as the sum of two monoexponential decay with the fast phase attributed to qZ and the slow phase attributed to qI (see Methods). Amplitudes of the qZ (top line), qI (second line) contributions to ϕNPQ, as well as their respective decay constant (λ, bottom two lines) are shown in panel (a). The deconvoluted qI and qZ fitted contributions are shown in panel (b). In both panels, results are shown as a function of for the different concentration of lincomycin (control: left, 0.4 µg/mL: middle, 0.8 µg/mL: right). Experimental data correspond to three independent biological replicates.

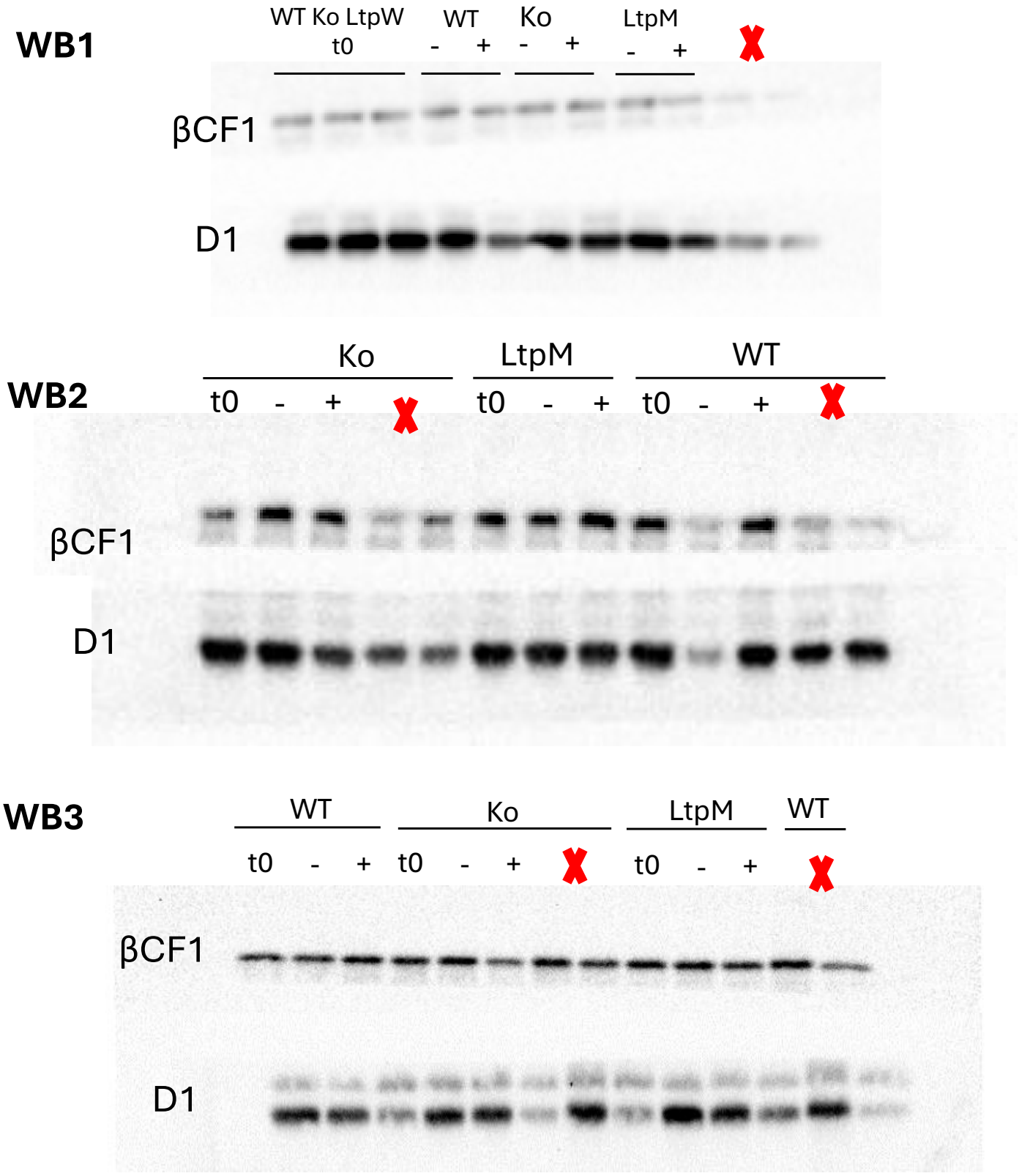

Fig. S9| Western blot membranes to measure the influence of Lhcx1-dependent qZ on D1 degradation due to high light stress. Biological independent triplicates of Western blots (WB) membranes used for measuring D1 PSII subunit with the ATP synthase βCF1 subunit as loading control. t0 is the initial conditions before light stress, + and –, represent with and without addition of 0.4 µg/mL of lincomycin, and are measured after 30 min of low light recovery following 1 h of high light stress (see Material and Methods). Symbols in red indicate extra material migrated in empty wells but not used in the paper. WB3 is shown in Fig. 3.

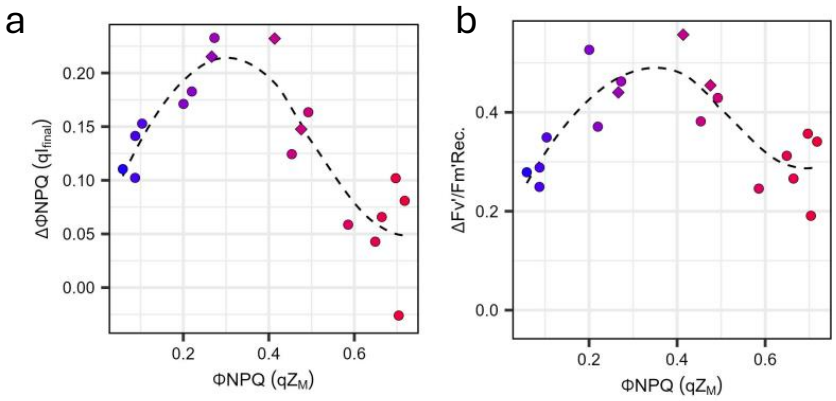

Fig. S10 | Interplay between the addition of lincomycin and Lhcx1-dependent qZ on PSII photoinhibition. The relative variation (Δ), between without and with addition of saturating concentration of lincomycin, of the qI component of ϕNPQ (see Fig. S8) (a) and of the quantum yield of PSII in the dark at the end of low light recovery (F_v'/F_M'Rec.) (b). Six *Phaeodactylum tricornutum* strains with ranging Lhcx1 expressions are used (WT with diamond symbols), with an independent biological triplicate measured in each.

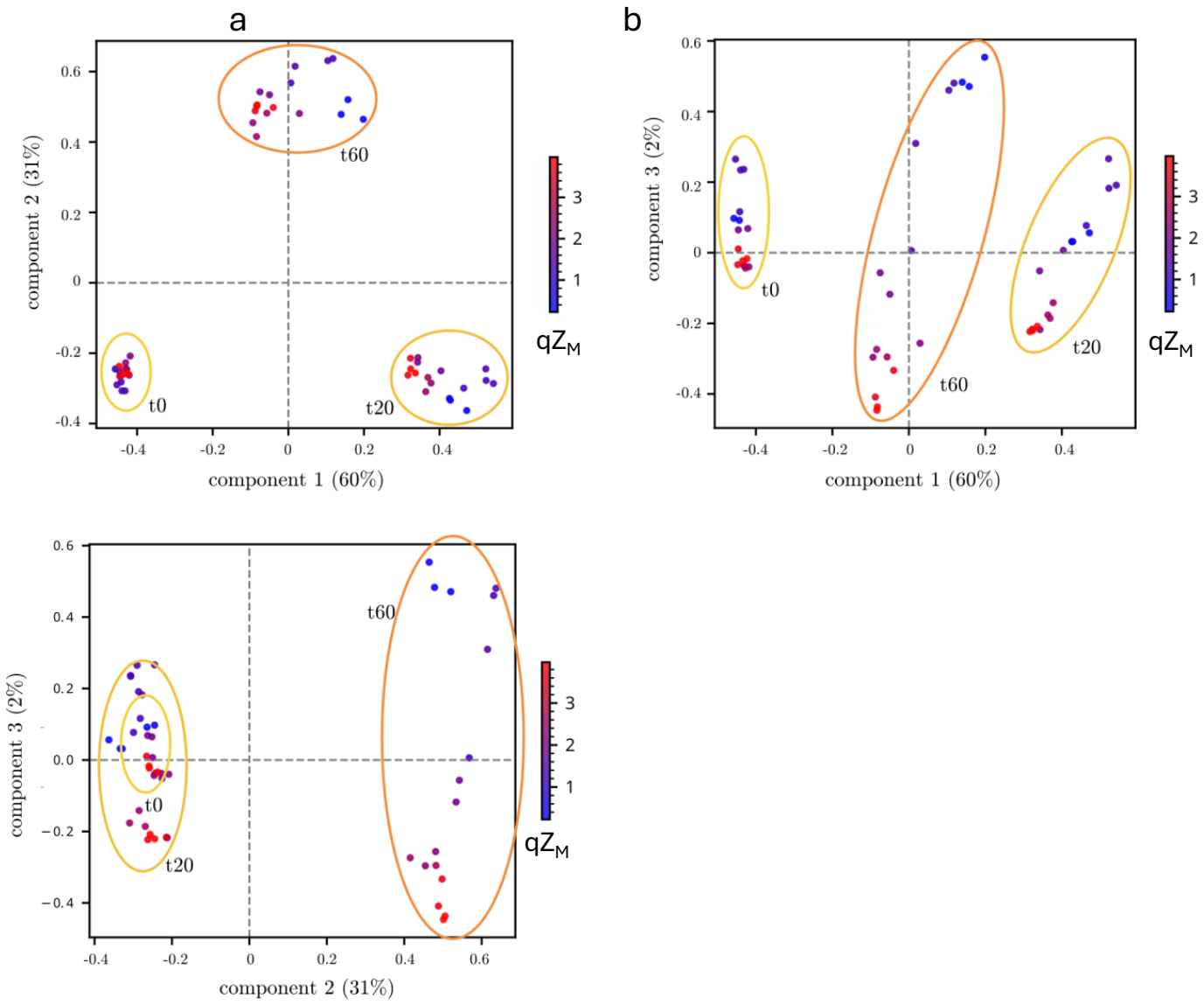

Fig. S11: Principal components analysis across the 50 transcriptomes collected at three time points (t0, t20 and t60) over high light stress on six strains of *Phaeodactylum tricornutum*, with ranging Lhcx1 accumulation determining qZ maximal capacities (qZ_M) and measured in independent biological triplicates.

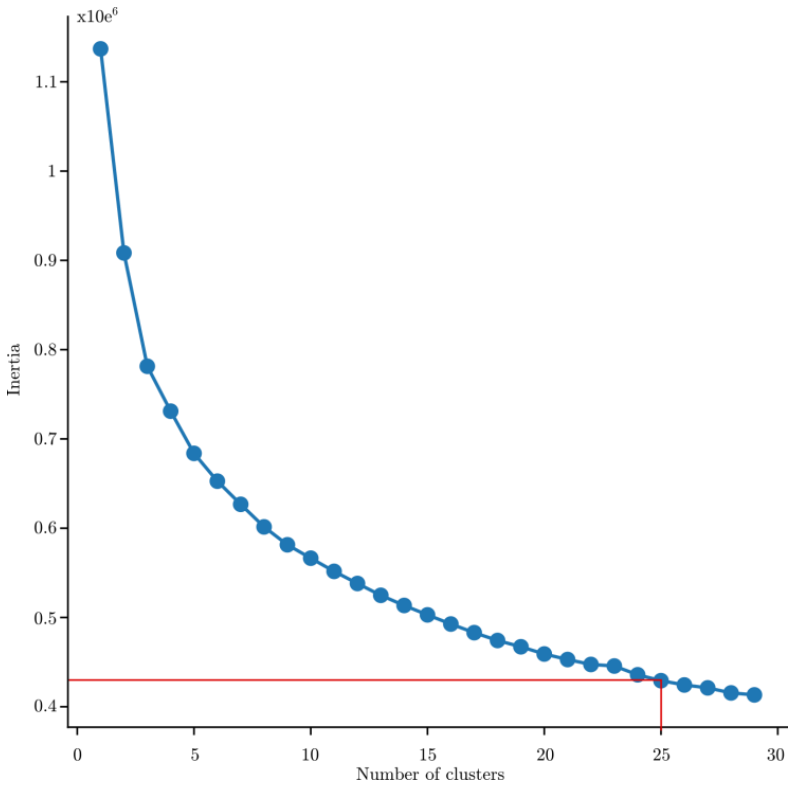

Fig. S12 | Results of the Elbow-test, performed to determine the number of clusters to use with K-means.

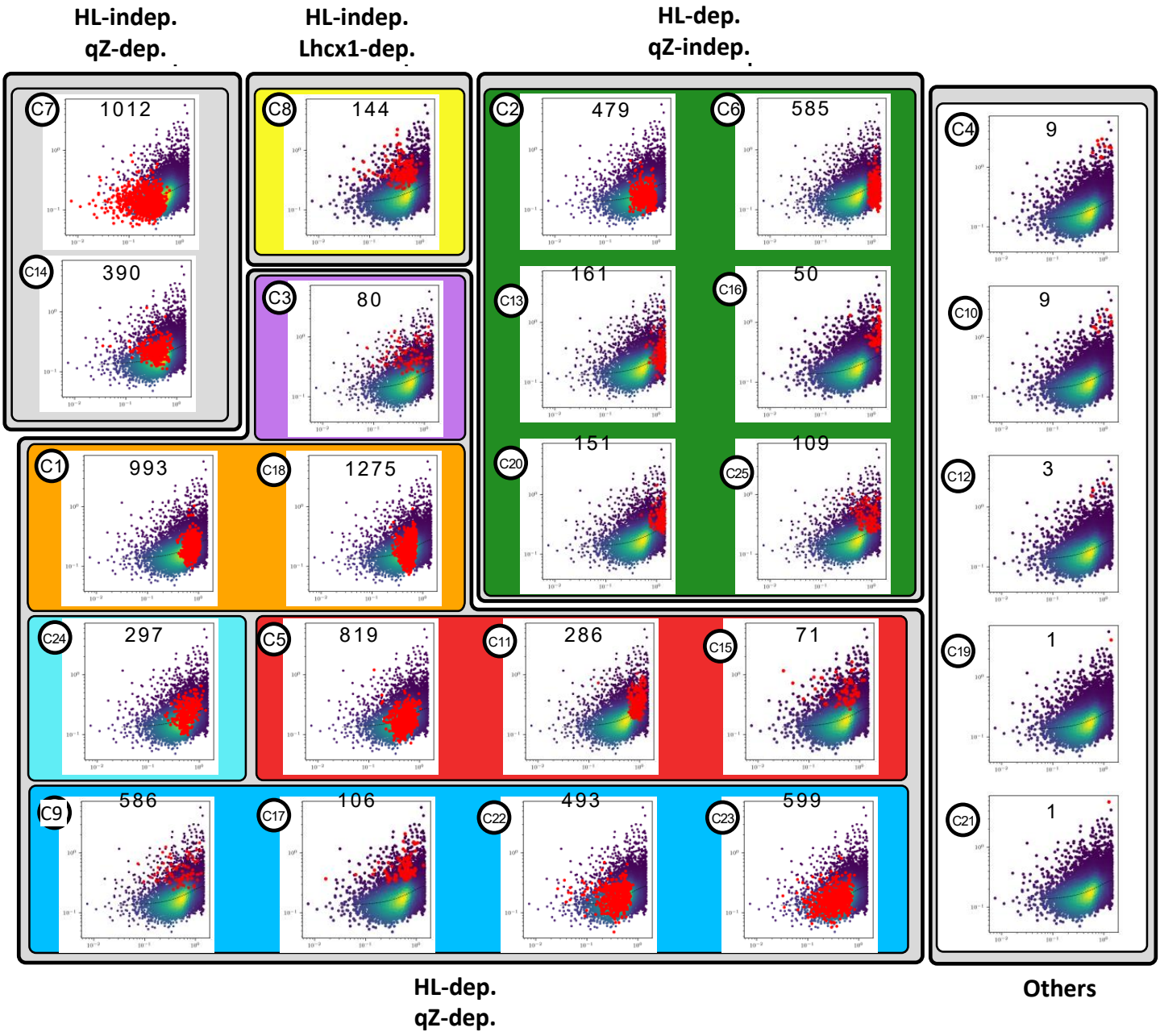

Fig. S13 | Relative importance of the exposure time to high light and of the Lhcx1-dependent qZ on the differential gene expression, cluster by cluster. For each cluster in Fig. 4b, the standard deviation due to qZ (y-axis) is plotted as a function of the standard deviation due to time of exposure (x-axis) for all genes of the transcriptomes (see Fig 4a and Material and Methods). All genes of a given the cluster indicated in red. This representation allows to reveal that, for instance, genes of cluster c8 are more influenced by the Lhcx1-dependent qZ than average across the 50 transcriptomes.

a

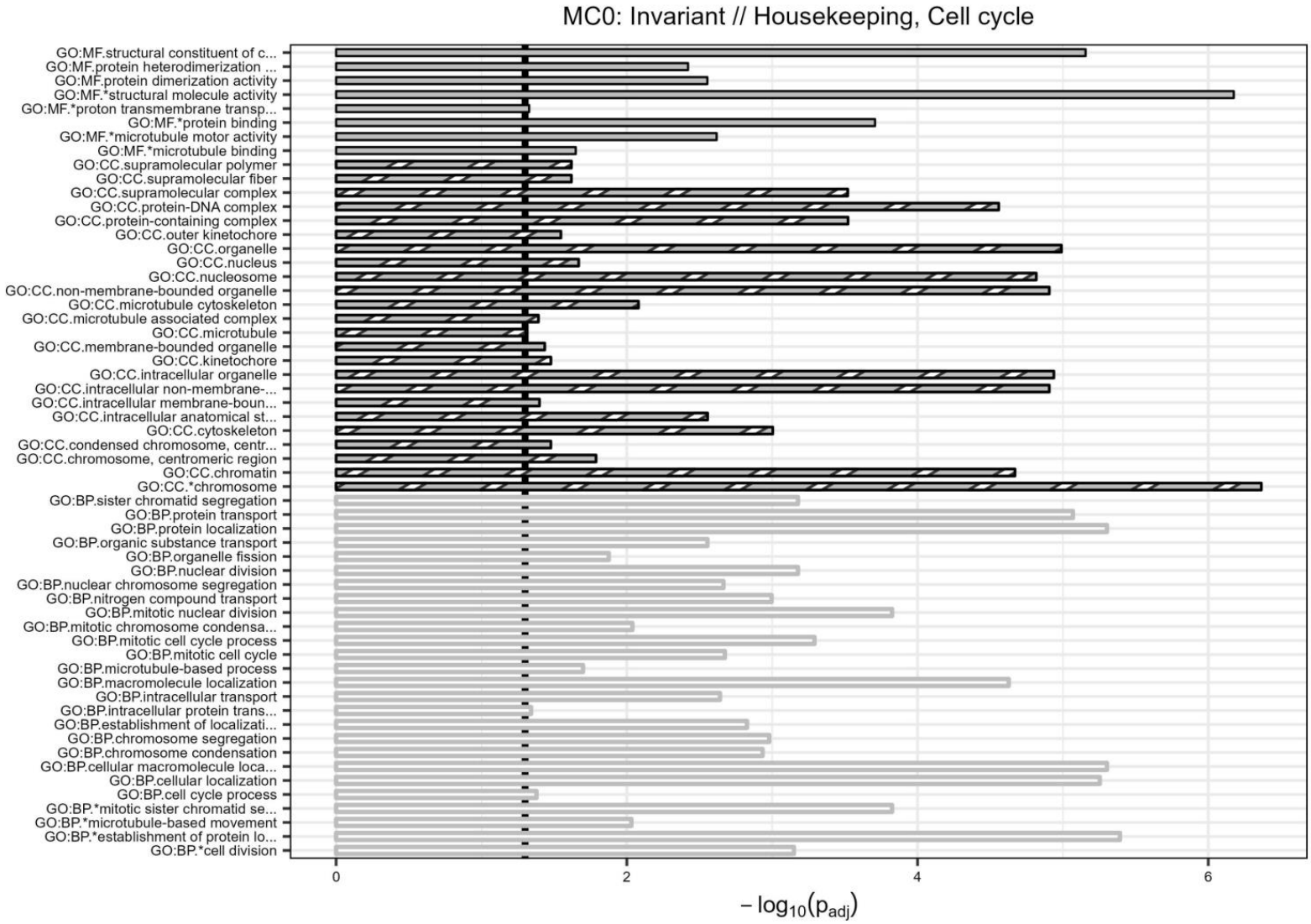

Fig. S14: Analysis of Gene ontology (GO) enrichment per Metacluster (MC). For the six main MCs defined in Fig. 4, the -$\log_{10}$ (adjusted p.value) of significantly enriched GOs (p.value<0.05, 1.3 vertical line on negative log scale), shown for enriched Biological Process (BP) (solid bars), Cellular Compartment (CC) (stripped bars) and Molecular Function (MF) (open baes). Analysis are performed with the g:Profiler platform (Raudvere *et al.,* 2019) with gene IDs based on *Phaeodactylum tricornutum* third version genome IDs (a-to-f). Asterisks next to bottom GOs for each categories indicate identification as main drivers by the g:Profiler algorithm (shown in Fig. 6). Above each graph is the main of the MC based on its qZ and time of high light exposure dependence and its gene content general function based on GO enrichment. In (g) enriched KEGG pathways with the same methods for the 6 main MCs.

b

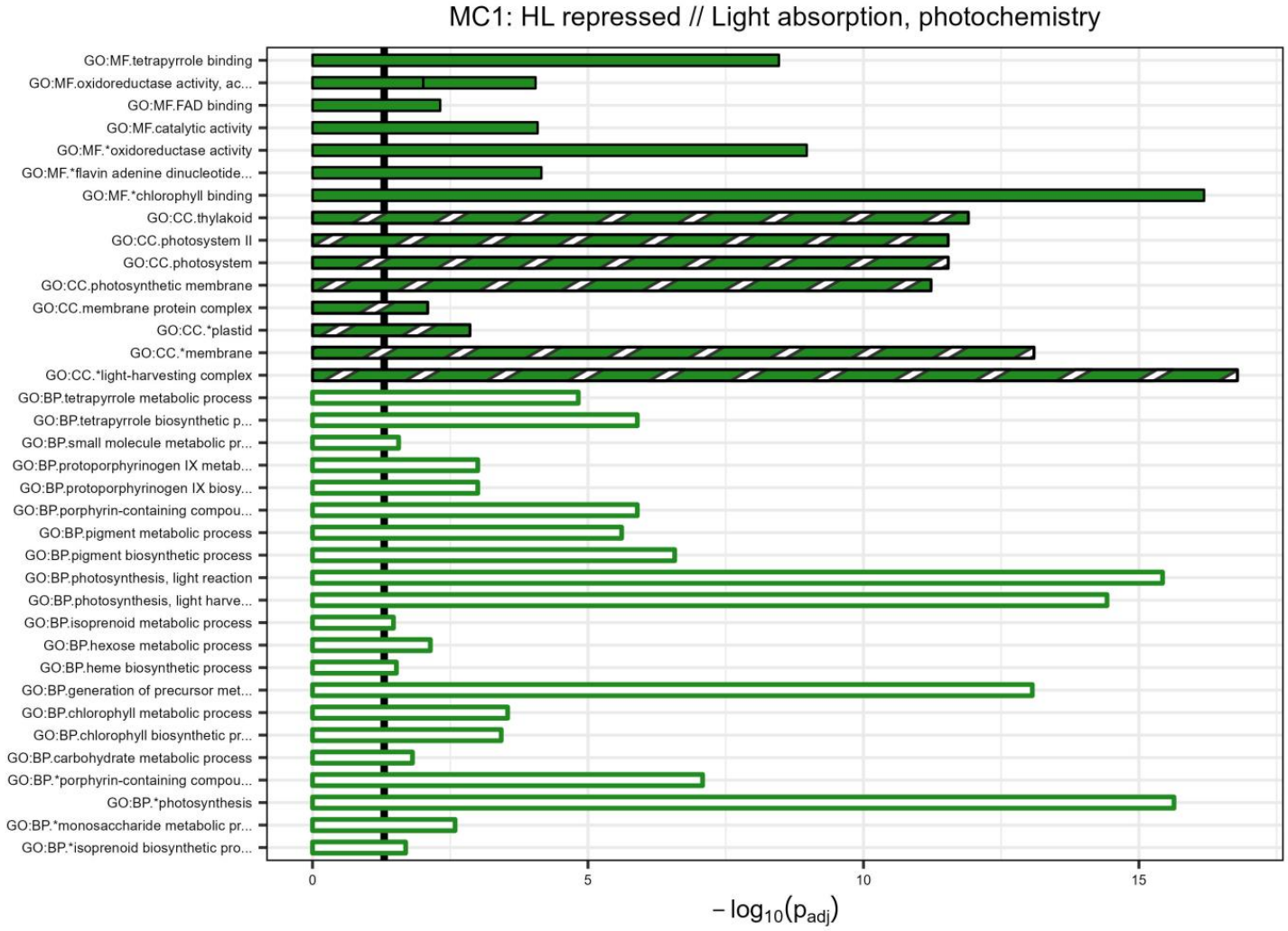
MC1: HL repressed // Light absorption, photochemistry
GO:MF.tetrapyrrole binding
GO:MF.oxidoreductase activity, ac...
GO:MF.FAD binding
GO:MF.catalytic activity
GO:MF.*oxidoreductase activity
GO:MF.*flavin adenine dinucleotide...
GO:MF.*chlorophyll binding
GO:CC.thylakoid
GO:CC.photosystem II
GO:CC.photosystem
GO:CC.photosynthetic membrane
GO:CC.membrane protein complex
GO:CC.*plastid
GO:CC.*membrane
GO:CC.*light-harvesting complex
GO:BP.tetrapyrrole metabolic process
GO:BP.tetrapyrrole biosynthetic p...
GO:BP.small molecule metabolic pr...
GO:BP.protoporphyrinogen IX metab...
GO:BP.protoporphyrinogen IX biosy...
GO:BP.porphyrin-containing compou...
GO:BP.pigment metabolic process
GO:BP.pigment biosynthetic process
GO:BP.photosynthesis, light reaction
GO:BP.photosynthesis, light harve...
GO:BP.isoprenoid metabolic process
GO:BP.hexose metabolic process
GO:BP.heme biosynthetic process
GO:BP.generation of precursor met...
GO:BP.chlorophyll metabolic process
GO:BP.chlorophyll biosynthetic pr...
GO:BP.carbohydrate metabolic process
GO:BP.*porphyrin-containing compou...
GO:BP.*photosynthesis
GO:BP.*monosaccharide metabolic pr...
GO:BP.*isoprenoid biosynthetic pro...
0
5
10
15
$-\log_{10}(p_{adj})$

c

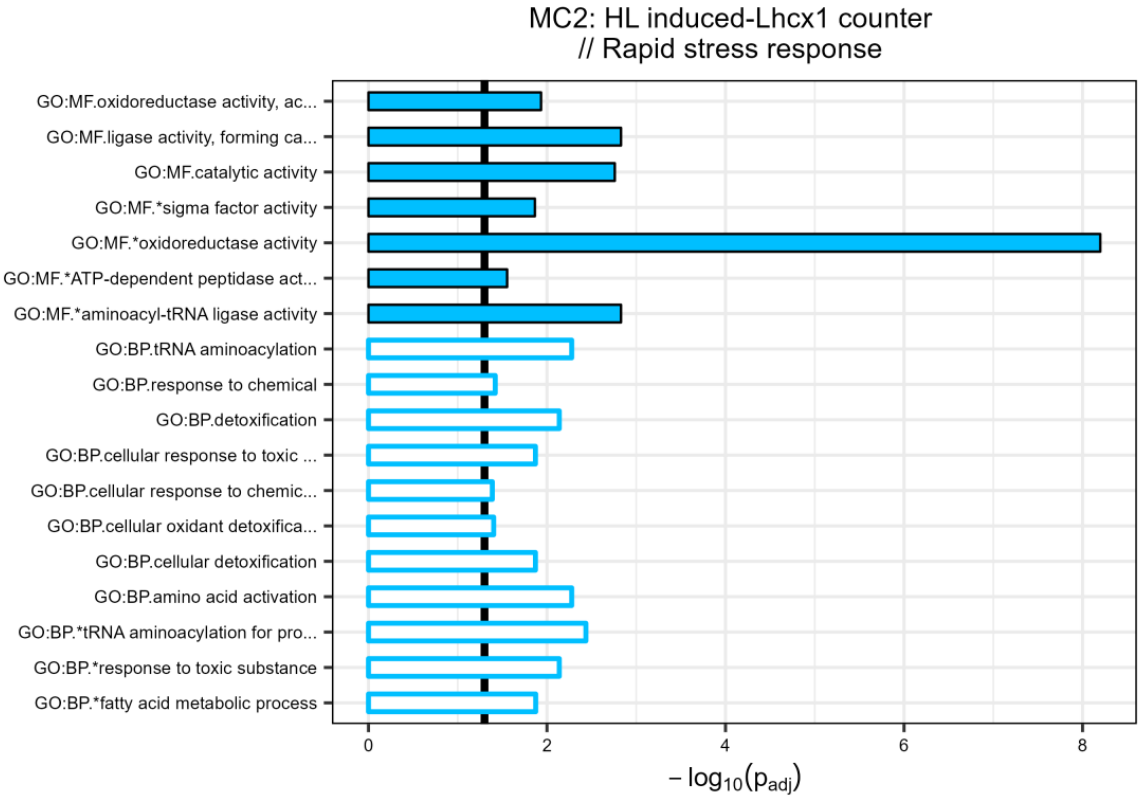
MC2: HL induced-Lhcx1 counter
// Rapid stress response
GO:MF.oxidoreductase activity, ac...
GO:MF.ligase activity, forming ca...
GO:MF.catalytic activity
GO:MF.*sigma factor activity
GO:MF.*oxidoreductase activity
GO:MF.*ATP-dependent peptidase act...
GO:MF.*aminoacyl-tRNA ligase activity
GO:BP.tRNA aminoacylation
GO:BP.response to chemical
GO:BP.detoxification
GO:BP.cellular response to toxic ...
GO:BP.cellular response to chemic...
GO:BP.cellular oxidant detoxifica...
GO:BP.cellular detoxification
GO:BP.amino acid activation
GO:BP.*tRNA aminoacylation for pro...
GO:BP.*response to toxic substance
GO:BP.*fatty acid metabolic process
0
2
4
6
8
$-\log_{10}(p_{adj})$

d

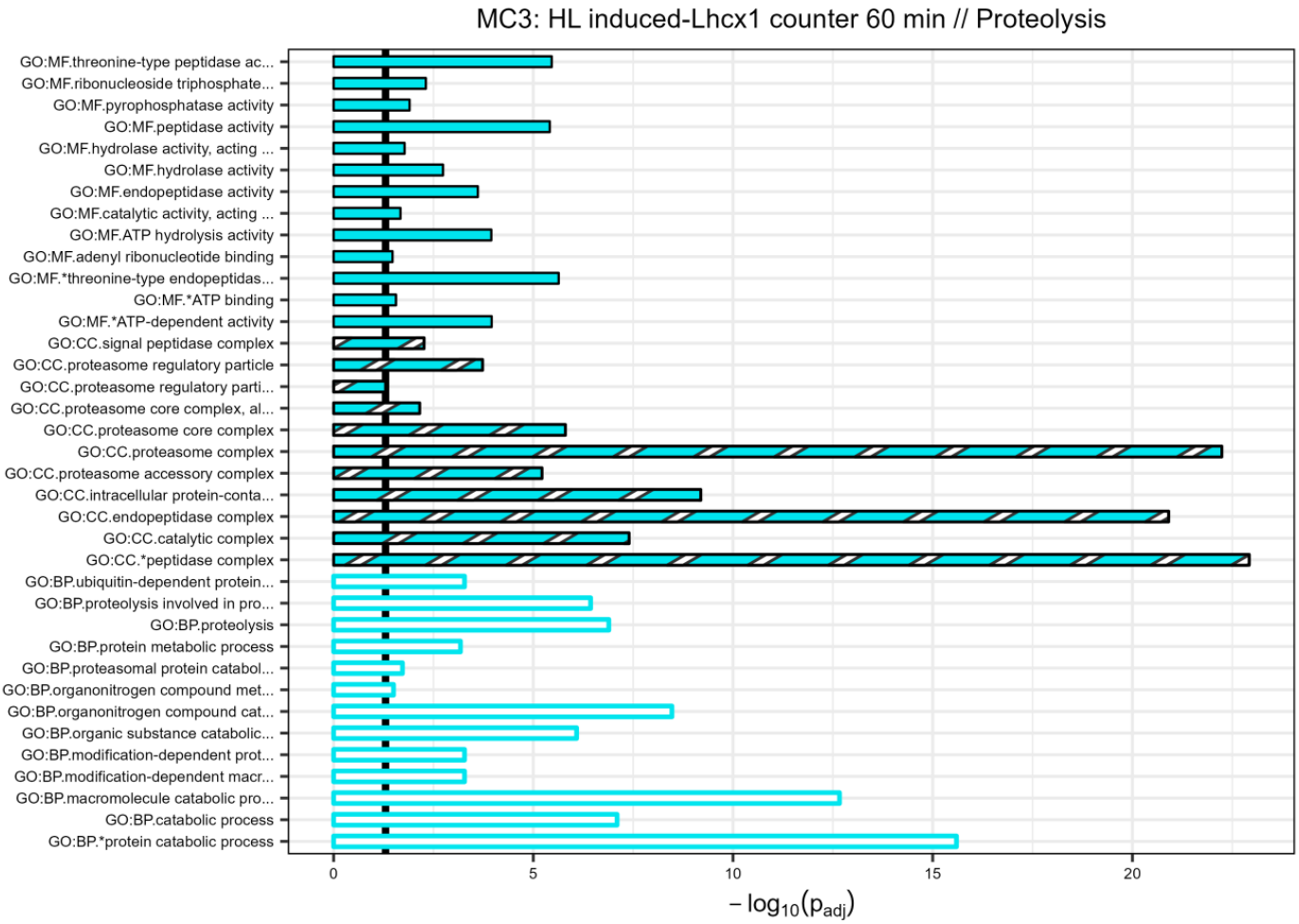
MC3: HL induced-Lhcx1 counter 60 min // Proteolysis
GO:MF.threonine-type peptidase ac...
GO:MF.ribonucleoside triphosphate...
GO:MF.pyrophosphatase activity
GO:MF.peptidase activity
GO:MF.hydrolase activity, acting ...
GO:MF.hydrolase activity
GO:MF.endopeptidase activity
GO:MF.catalytic activity, acting ...
GO:MF.ATP hydrolysis activity
GO:MF.adenyl ribonucleotide binding
GO:MF.*threonine-type endopeptidas...
GO:MF.*ATP binding
GO:MF.*ATP-dependent activity
GO:CC.signal peptidase complex
GO:CC.proteasome regulatory particle
GO:CC.proteasome regulatory parti...
GO:CC.proteasome core complex, al...
GO:CC.proteasome core complex
GO:CC.proteasome complex
GO:CC.proteasome accessory complex
GO:CC.intracellular protein-conta...
GO:CC.endopeptidase complex
GO:CC.catalytic complex
GO:CC.*peptidase complex
GO:BP.ubiquitin-dependent protein...
GO:BP.proteolysis involved in pro...
GO:BP.proteolysis
GO:BP.protein metabolic process
GO:BP.proteasomal protein catabol...
GO:BP.organonitrogen compound met...
GO:BP.organonitrogen compound cat...
GO:BP.organic substance catabolic...
GO:BP.modification-dependent prot...
GO:BP.modification-dependent macr...
GO:BP.macromolecule catabolic pro...
GO:BP.catabolic process
GO:BP.*protein catabolic process
0
5
10
15
20
− log10(padj)

e

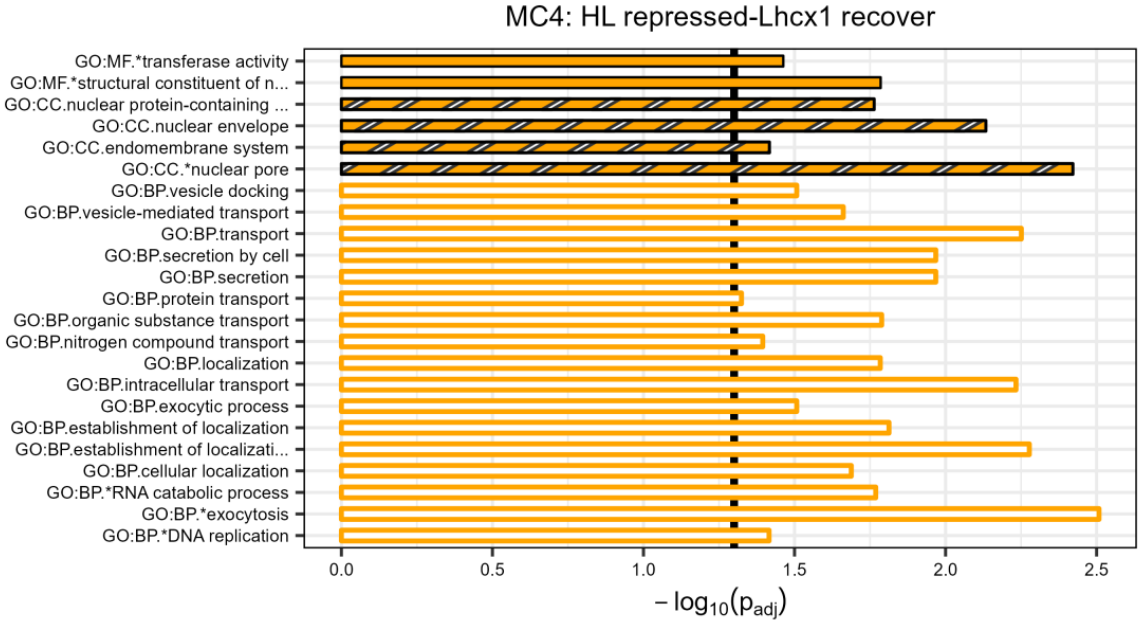
MC4: HL repressed-Lhcx1 recover
GO:MF.*transferase activity
GO:MF.*structural constituent of n...
GO:CC.nuclear protein-containing ...
GO:CC.nuclear envelope
GO:CC.endomembrane system
GO:CC.*nuclear pore
GO:BP.vesicle docking
GO:BP.vesicle-mediated transport
GO:BP.transport
GO:BP.secretion by cell
GO:BP.secretion
GO:BP.protein transport
GO:BP.organic substance transport
GO:BP.nitrogen compound transport
GO:BP.localization
GO:BP.intracellular transport
GO:BP.exocytic process
GO:BP.establishment of localization
GO:BP.establishment of localizati...
GO:BP.cellular localization
GO:BP.*RNA catabolic process
GO:BP.*exocytosis
GO:BP.*DNA replication
0.0
0.5
1.0
1.5
2.0
2.5
− log10(padj)

f

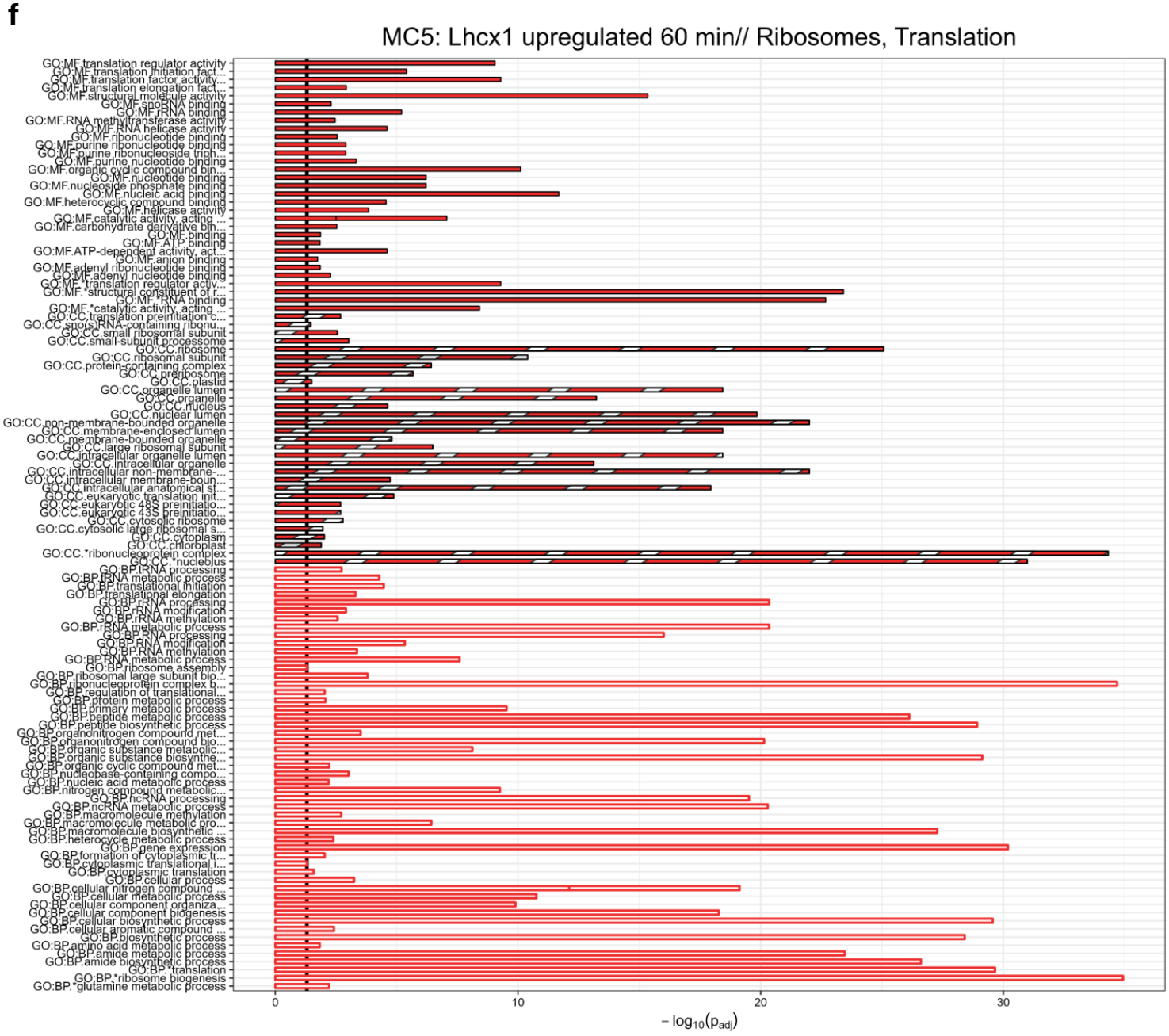

g

MC	term_name	term_id	-log$_{10}$(p$_{adj}$)	term_size	query_size	intersection_size	effective_domain_size
MC0-Invariant	Viral life cycle - HIV-1	KEGG:03250	2.22	13	156	8	993
MC1-HL repressed	Metabolic pathways	KEGG:01100	6.01	423	120	79	993
MC1-HL repressed	Biosynthesis of secondary metabolites	KEGG:01110	3.59	172	120	39	993
MC1-HL repressed	Fatty acid degradation	KEGG:00071	1.99	7	120	5	993
MC1-HL repressed	Valine, leucine and isoleucine degradation	KEGG:00280	1.67	19	120	8	993
MC2-HL induced/Lhcx1 countered	Metabolic pathways	KEGG:01100	3.71	423	169	98	993
MC2-HL induced/Lhcx1 countered	Glutathione metabolism	KEGG:00480	2.56	17	169	10	993
MC2-HL induced/Lhcx1 countered	Porphyrin metabolism	KEGG:00860	1.74	17	169	9	993
MC2-HL induced/Lhcx1 countered	Biosynthesis of cofactors	KEGG:01240	1.71	71	169	23	993
MC3-HL induced/Lhcx1 countered (60 min)	Proteasome	KEGG:03050	12.71	29	42	15	993
MC3-HL induced/Lhcx1 countered (60 min)	Protein processing in endoplasmic reticulum	KEGG:04141	1.60	30	42	6	993
MC4-HL repressed/Lhcx1 reversed (60min)	DNA replication	KEGG:03030	2.96	12	249	10	993
MC4-HL repressed/Lhcx1 reversed (60min)	Base excision repair	KEGG:03410	1.52	13	249	9	993
MC5-Lhcx1 upregulated (60 min)	Ribosome biogenesis in eukaryotes	KEGG:03008	15.44	45	215	36	993
MC5-Lhcx1 upregulated (60 min)	Ribosome	KEGG:03010	15.26	83	215	52	993

a

Compartment	Total	MC0	MC1	MC2	MC3	MC4	MC5
Plastid	1274	124	331	395	47	216	131
		-0.39	**0.46**	**0.51**	0.09	**-0.35**	**-0.24**
Mitochondria	1347	50	3	71	102	20	85
		-0.18	0.09	0.14	0.14	-0.06	0.05
Cytoplasm	1117	187	171	192	45	317	176
		0.04	-0.14	-0.16	0.19	0.09	0.17
Nucleus	2024	405	261	368	53	553	318
		0.24	**-0.27**	-0.11	**-0.23**	0.05	0.17
Plasma membrane	1029	165	210	182	31	302	103
		0.00	0.15	-0.14	-0.11	0.13	**-0.26**
Secreted	398	74	90	61	16	93	48
		0.16	**0.27**	**-0.25**	0.19	-0.10	-0.10
Cytoskeleton	53	8	0	8	11	5	14
		-0.06	-0.15	0.01	**1.79**	0.02	-0.02

b

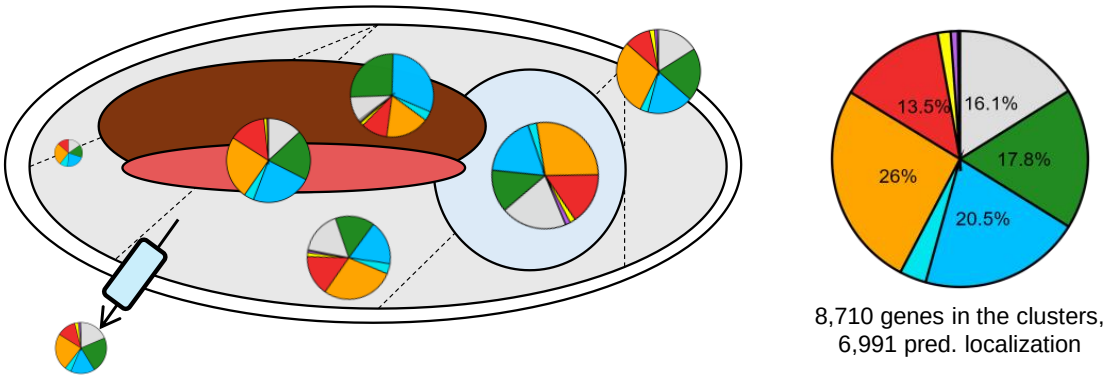

Fig. S15 | Distribution of the subcellular targets of the encoded protein among the different gene metacluster (MC). The subcellular targets for each encoded proteins were retrieved based on different prediction softwares and compiled by Ait-Mohammed *et al.,* 2020 (see also Material and Methods). In Table (a), the top number of each row indicates the number of genes for a given target compartment and MC combination, the bottom decimal number displays the relative deviation from the proportional number of genes expected for a homogeneous distributions of target compartments per MC, deviations larger than 20% are in bold, red for enriched and blue for underrepresented. In (b) schematized *Phaeodactylum tricornutum* cell with pie charts representing the pattern of MC distribution for this specific compartment, with the size of the pie charts representing the total number of genes. The blue circle represents the nucleus, the pink and brown horizontal ovals represent the mitochondrion and the plastid, respectively.

References

Ait-Mohamed O, Novák Vanclová AM, Joli N, Liang Y, Zhao X, Genovesio A, Tirichine L, Bowler C, Dorrell RG. PhaeoNet: a holistic RNAseq-based portrait of transcriptional coordination in the model diatom *Phaeodactylum tricornutum*. *Frontiers in Plant Science*. 2020 Oct 16;11:590949.

Avenson TJ, Kanazawa A, Cruz JA, Takizawa K, Ettinger WE, Kramer DM. Integrating the proton circuit into photosynthesis: progress and challenges. *Plant, Cell & Environment.* 2005 Jan;28(1):97-109.

Ferté S. *Exploring the diversity of cyclic electron flow around photosystem I in microalgae species* (Doctoral dissertation, Sorbonne Université).

Flori S, Jouneau PH, Bailleul B, Gallet B, Estrozi LF, Moriscot C, Bastien O, Eicke S, Schober A, Bártulos CR, Maréchal E. Plastid thylakoid architecture optimizes photosynthesis in diatoms*. Nature communications*. 2017 Jun 20;8(1):15885.

Raudvere U, Kolberg L, Kuzmin I, Arak T, Adler P, Peterson H, Vilo J. g: Profiler: a web server for functional enrichment analysis and conversions of gene lists (2019 update). *Nucleic acids research*. 2019 Jul 2;47(W1):W191-8.

4.4 Discussion and perspectives

In the article of this chapter we revealed many phenomenological relationships between qZ and other regulatory processes. Each of these phenomenological relationships can serve as individual vignette to highlight the strength of our Lhcx1-molecular titration. But perhaps even more impressively, we showed that when used in combination with a system biology approach, (i.e., transcriptomics), we were able to decipher the orchestration of the genome wide high light response. The success of this approach suggests it is very likely that valuable results would come-out of combining the Lhcx1 molecular titration with other 'omic approaches, for example targeted metabolomics. Also, I mentioned in Introduction (Section 1.5.1), there are good reasons to apprehend a less firm grip on a NPQ-dial anchored on a qE-component and a PsbS molecular titration in plants (or the hybrid qE/qZ NPQ of *Nannochloropsis* for instance (Short et al., 2023)). However, with 50% of *P. tricornutum*'s genome expression being modulated by qZ extent, which is largely exceeding our expectations, I now have little doubts that a similar approach with PsbS qE would lead to significant discoveries and offers some fresh perspectives on NPQ in the context of system-wide regulation. A striking fact is that a similar increase in Q_A oxidation, as the one we reported here, was shown in rice as a function of transgenic PsbS expression (Głowacka et al., 2018). I will return to these considerations in the general discussion in Chapter 6. What is more, a similar experiment in plants could also open the door to even more complex questions, like the transduction of photosynthesis-dependent signals to non-photosynthetic tissues (Foyer et al., 2003).

Alternative electron fluxes

A future avenue to investigate with our Lhcx1-mutant series is how qZ interacts with other alternative electron flux (AEF) on top of CEF, in particular, the energy coupling between plastid and mitochondria (Bailleul et al., 2015). As discussed in Croteau et al., 2024, plastid-mitochondria coupling is also at play in green organisms (and likely most phototrophs). The peculiar feature of plastid-mitochondria exchanges in diatoms is that it seems to be the constitutive prevalent AEF to boost ATP/NAPDH production, by contrast with cyclic electron flow (CEF) in green organisms (Munekage et al., 2004). In *Phaeodactylum*, the current model suggests that ≈10% of the electrons originating from water oxidation and travelling in the photosynthetic electron transfer chain are rerouted to mitochondrial oxidases. This proportion, which is consistent regardless of light intensity, is compatible with the constitutive lack of ATP resulting from the unbalance between electron/proton coupling in LEF and ATP/NADPH requirement for carbon fixation (J. F. Allen, 2003). However, this very (too?) simple model would benefit from being challenged by measurements of AEFs as a function of NPQ/qZ. Using membrane inlet mass spectroscopy (MIMS) it is possible to distinguish between O_2 evolution by PSII, and O_2 photoreduction by AEFs, including light-induced upregulation of mitochondrial respiration (Burlacot et al., 2020). With the now revealed qZ-dependent upregulation of CEF in *P. tricornutum*, the prospect of using MIMS to investigate interplays between CEF and plastid/mitochondria exchanges, as a function of qZ and over different illumination protocols, is very exciting. To go further one could even imagine varying HCO_3^- concentrations to study the role of these respective electron fluxes in fuelling carbon concentrating mechanisms, like is being done in *Chlamydomonas* (Burlacot and Peltier, 2023).

Photoinhibition quenching versus qZ

Another mechanism that we investigated in this paper is the photoprotective efficiency of qZ to avoid photoinhibition upon high light stress. Beyond a decrease in the recovery of quantum yield of PSII with lower qZ, we also saw the appearance of a larger photoinhibition-dependent quenching (qI) component. In qI, broken PSII centres act themselves as nonphotochemical quenchers, which in theory should protect the remaining active PSIIs and surrounding lipids from further damages. How qI interplays with other NPQ components is an extremely intricate process (Nawrocki et al., 2021), but the *P. tricornutum* Lhcx1-mutant series has all the features an experimenter could hope for to tackle this question. That is, a dial-like control on the level of qZ deployed, a single NPQ component which relaxes slowly, allowing the PQ-pool to get fully oxidized (stabilizing PSII potential photochemistry), before significant qZ relaxation takes. Moreover, the extent of qZ can also be explored in a single strain as a function of relaxation time. Finally, a validated lake model could be used to calculate theoretical PSII quantum yields, a null hypothesis testing if qI is not a simple bleaching effect for instance.

We made a step in the right direction with this paper, but we could not fully explore this gap in knowledge because, as a first step, we wanted to test whether qZ limits the extent of D1 photo-oxidation under high light stress in diatoms, which had never been done convincingly. Our preliminary experiments focused on finding the perfect conditions to maximize contrasts in PSII photoinhibition among WT, Lhcx1-Ko and Lhcx1-overexpressing strains. We thus opted for a rapid screening of multiple strains and lincomycin concentrations simultaneously with a camera fluorometer. Samples are subject to sedimentation in this device which can bias fluorescence measurements in a way that is not problematic for relative variations. However, it could undermine quantification of qZ and qI respective effects on maximal and minimal fluorescence levels. Moreover, qI relaxation is a very slow process and the camera fluorometer is also not ideal for gas exchanges over very long protocols. Nevertheless, we confirm that our biological model is a very promising avenue for the study of qI in secondary endosymbionts.

Relative and absolute measurements of CEF

We also took advantage of the absence of state transitions in diatoms to introduce a novel parameter Δ(TEF/LEF) allowing to calculate relative changes in CEF, which does not require knowledge of PSI and PSII antenna sizes or stoichiometries, and therefore remains, valid regardless of their unknown values. However, this approach does not allow us to determine whether there is a constitutive CEF. The fact that the trend of Δ(TEF/LEF) versus ΦNPQ passes through the origin suggests that the CEF to LEF ratio changes only through NPQ. For the Lhcx1-Ko, the ΦPSI/ΦPSII ratio, and thus the relative cyclic versus linear flow, is the same at 40 and 570 µmol photons m^{-2} s^{-1}. However, this does not rule out the possibility of a constitutive basal level of CEF (in addition to the chloroplast-mitochondria interaction), plus a variable component that depends only on NPQ. Nevertheless, Δ(TEF/LEF) already yields interesting surprises. For instance, CEF is often assumed to be a constant fraction of LEF under steady-state illumination in plants (Genty et al., 1990, Avenson et al., 2005) and green algae (Alric et al., 2010). Our results argue against this simple assumption in diatoms. Indeed, when we followed the yield of PSII and PSI as a function of light intensity, we observed that the yield of PSII decreases significantly more than that of PSI as light increases, and that this effect is exacerbated by a lack of qZ.

Chapter 5

NPQ as a target of regulation in diatoms, the role of the luminal pH and metabolic processes

This last Chapter of experimental results includes one of the initial questions of my Ph.D., which unfortunately could not be finalized as a manuscript in time for the writing of my thesis, and a rapid overview of collaborative works to which I participated over the course of my Ph.D. (one paper published, two under review, and in preparation for submission in the coming months).

5.1 Combining two ECS-based methods to gauge absolute proton motive force and its partitioning between $\Delta\psi$ and ΔpH in diatoms

The overall objective of my Ph.D. was to take advantage of simple photophysiological features of *P. tricornutum* and an original Lhcx1 molecular titration approach to unveil the orchestration of photosynthetic regulations in diatoms. Our strategy was to do so by focusing on the NPQ regulatory module and following these four steps (which are part of Fig. 5.1):

1. Proposing a working model for NPQ/qZ in *P. tricornutum* in which the role of both Lhcx1 and DT is accounted for (**Chapter 3**).

2. Validating that the assumptions of the lake model are mostly respected in *P. tricornutum* (**Chapter 3**).

3. Using these working model and hypotheses to provide phenomenological relationships describing the influence of NPQ/qZ on higher levels of photosynthesis regulations and make a first step towards describing photosynthesis regulation orchestrations in a secondary endosymbiotic organism (**Chapter 4**).

4. To close the regulatory loop, we wanted to study the regulation of NPQ itself by the luminal pH. Unfortunately, there is currently no method available to measure absolute values of ΔpH *in vivo*. However, thanks to some specific features of diatoms, it is theoretically possible to measure the ΔpH by combining two spectroscopic methods which have been previously demonstrated.

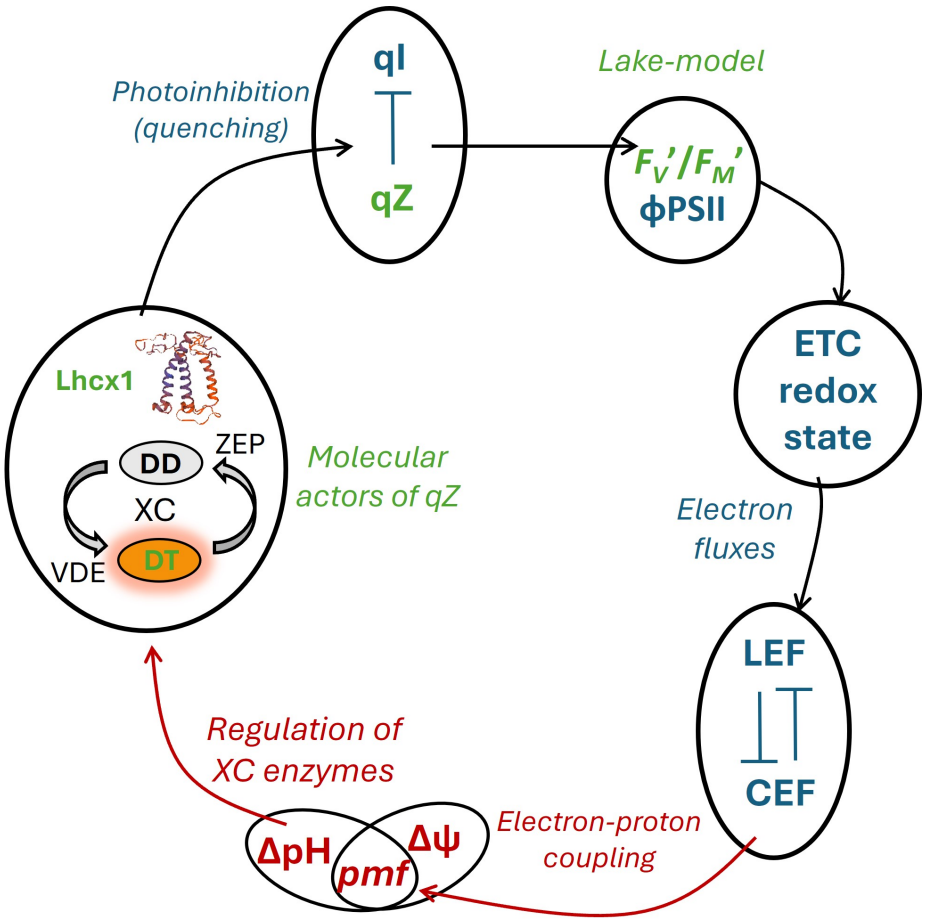

Figure 5.1: This figure is based on Fig. 1.15 and shows in red the portion NPQ as a target of regulation by ΔpH, i.e., the process that the method developed in this chapter aims at deciphering.

In the following section, I present a proof of concept for the methodology used to measure ΔpH in vivo in *P. tricornutum* (Point 4 above). The rationale for this project, as part of my Ph.D., was to "close the loop" of the NPQ regulatory module. Together with the existing literature on NPQ in *P. tricornutum*, the results of my thesis come closer to a comprehensive understanding of this regulatory process. This is particularly true for the generation and nature of nonphotochemical quenchers. The relationships between Lhcx1/DT and NPQ have been established (Chapter 3), and the light dependence of the DD to DT interconversion by the XC had been already documented previously by exploiting the linear relationship between NPQ and DT (Blommaert et al., 2021).

In addition, the effects of NPQ have been well characterized. The influence of NPQ on energy partitioning in PSII (Chapters 3 and 4) and its impact on the functioning of the electron transport chain, including the redox state of the intersystem chain, CEF and photoinhibition (Chapter 4), are now described by clear phenomenological relationships. It remains to be understood how the functioning of the photosynthetic electron chain determines DT concentrations. The missing link here is ΔpH, which is both determined by the coupling between proton pumping and photosynthetic electron fluxes and involved in the regulation of the diadinoxanthin de-epoxidase enzyme of the xanthophyll cycle.

To achieve a complete understanding of the NPQ regulatory module, developing a novel methodology to assess ΔpH *in vivo* is clearly the next step to move forward.

5.1.1 Using the ECS as a spectroscopic voltmeter of the thylakoid membrane

When photosynthesis functions, proton pumping in the lumen generates an electrochemical proton gradient (Mitchell, 1961), or proton motive force (pmf), which drives proton efflux in the stroma through the CF_1F_O-ATP synthase (and dissipation of the pmf). The pmf comprises and electric gradient ($\Delta\psi$) and a proton concentration gradient (ΔpH) component, which can be expressed as:

$$\text{pmf} = \Delta\psi_{\text{i-o}} + \frac{\ln(10) \cdot RT}{F}\Delta\text{pH}_{\text{o-i}} \tag{5.1}$$

Where $\Delta\psi_{\text{i-o}}$ and $\Delta\text{pH}_{\text{o-i}}$ are the electric and proton gradients, the difference between the inside (lumen) and the outside (stroma) compartments, R is the universal gas constant, T is the temperature in Kelvin and F is Faraday's constant. Due to a process called the "Stark effect", i.e., the shift of pigments absorption spectra when they are exposed to an electric field ($\vec{F}$), also called "electrochromic shift" (ECS) in the specific field of photosynthesis, the $\Delta\psi$ component can be straightforwardly measured through absorption difference spectroscopy (Duysens, 1954, Witt, 1979) (Fig. 5.2). As discussed in Section 1.2, a pigment jumps from its ground state (S_g) to an excited state (S_e) upon absorption of photon energy ΔE ($=\frac{hc}{\lambda}$). The $\vec{F}$ alters the energy difference between ground and excited states by changing the dipole moments ($\vec{\mu}_g, \vec{\mu}_e$) and by inducing dipole moments (polarization) ($\vec{\alpha}_g, \vec{\alpha}_e$), which is formalized in the following way:

$$\Delta\Delta E = -(\vec{\mu}_e - \vec{\mu}_0)\vec{F} - (\vec{\alpha}_e - \vec{\alpha}_0)\vec{F}^2 \tag{5.2}$$

For a single molecule in solution, the ΔΔE represents a homogeneous bandshift of the pigment absorption spectrum, and results in the characteristic double-wave shape ECS spectrum (Fig. 5.2). In photosynthesis, each photosynthetic pigment, and each transition from

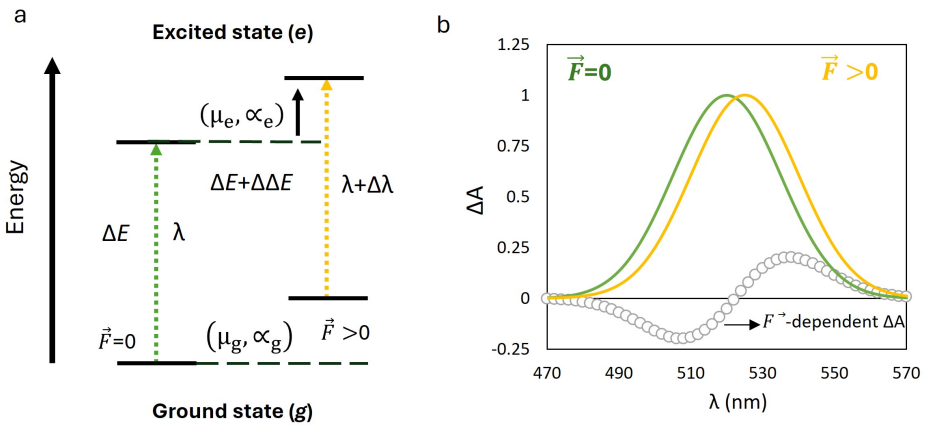

Figure 5.2: Application of an electric field $\vec{F}$ changes the energy difference between ground (g) and excited (e) of a pigment upon photon absorption. In green, the ΔE energy shift of a pigment absorbing a photon of a given λ, and in yellow the same pigment exposed to $\vec{F}$ absorbs a photon of wavelength $\lambda+\Delta\lambda$ (a). When absorption changes are measured, this gives a double-wave shape signal (the difference between absorption spectra of the pigment with and without $\vec{F}$), characteristic of the Stark effect or electrochromic shift (b). Adapted from Bailleul, Cardol, et al., 2010.

S_g to S_e within a pigment, participates to the absorption changes due to the Stark effect. This results in various ECS spectra of complex shapes across the phytodiversity (Bailleul, Cardol, et al., 2010). However, Equation 5.2 indicates that two components determine the total magnitude of the ECS: one, μ, depends linearly upon $\vec{F}$ and one, α, depends upon $\vec{F}^2$; these are the linear (ECS_{lin}) and quadratic (ECS_{quad}) components, respectively. In green organisms (at least wildtype strains), the ECS_{quad} is usually negligible (Joliot and Joliot, 1989). This means that absorption changes at a specific wavelength (not affected by absorption changes related to the redox state of electron carriers) can be probed as a linear spectroscopic voltmeter displaying relative changes in $\Delta\psi$. Multiple parameters informing on the functioning of the different photosynthetic ETC complexes and overall electron fluxes can be derived from ECS_{lin} amplitude and decay kinetics (Sacksteder and Kramer, 2000, Bailleul, Cardol, et al., 2010, see also Chapter 4). Therefore, having access to ECS_{lin} is tremendously useful, for example, to measure the turnover of both PS, their stoichiometry (Bailleul, Cardol, et al., 2010) or the thiol-regulation of the rate of the CF_1F_O-ATP synthase (Kramer and Crofts, 1989, Buchert et al., 2021). However, two features of the central role of the pmf in photosynthesis regulation are inaccessible when limited to this linear probe **i**) The ECS_{lin} represents only the *relative changes* in $\Delta\psi$, which does not take into account the already pre-existing pmf in the dark, observed in all photosynthetic organisms (Joliot and Joliot, 1989, Kramer and Crofts, 1989, Bailleul et al., 2015). **ii)** The partitioning between $\Delta\psi$ and ΔpH is unknown and can only be inferred via dedicated methods (like the ECS inversion method discussed below) based on various more or less strong assumptions. Those assumptions have been validated and backed up by *in silico* simulations for plants and *Chlamydomonas* (Kramer et al., 2003, Davis et al., 2017) but not yet for the large diversity of microalgae.

This second point is paramount as we have already seen in Chapter 1 & 2 that, although the $\Delta\psi$ and ΔpH equally contribute to fueling ATP synthesis, they play very different reg-

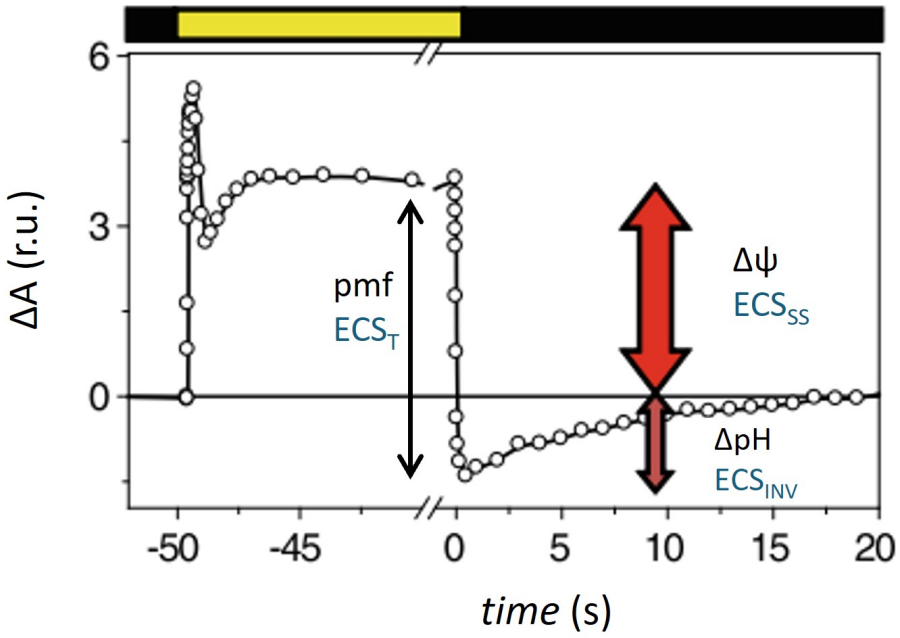

Figure 5.3: Change in absorption (ΔA) due to light-induced $\Delta\psi$ and concomitant variations in ECS_{lin} signal (with pre-existing dark $\Delta\psi$ arbitrarily set at 0) in the green algae *Chlorococcum ellipsoides* (taken and slightly modified from Bailleul, Cardol, et al., 2010). Parameters introduced by Cruz et al., 2001 (see text for explanations) are written in blue and their interpretation in terms of pmf partitioning are written in black.

ulatory roles. While $\Delta\psi$ pulls against photochemical charge separation and can decrease PS efficiency (Diner and Joliot, 1976), evidence for this phenomenon influencing photosynthesis output remains limited (but see (Davis et al., 2016)). On the other hand, the ΔpH is often described as a "master regulator" of photosynthesis (Kramer et al., 2003, Lepetit et al., 2022), with involvement in NPQ by regulating the xanthophyll cycle enzymes rates or the protonation of PsbS and LHCSR3, and the photosynthetic control of the Rieske protein turnover in cyt. b_6f, amongst many others (see for instance (Hoh et al., 2024)). The only proposed spectroscopic method to measure ΔpH *in vivo* at the moment, is based on the collapse of ECS_{lin} below its initial (dark) baseline upon switching off the actinic light. This produces an inversion of the ECS signal (ECS_{INV}), introduced in (Cruz et al., 2001 and now widely used in plant research (see Fig. 5.3). Briefly, when a sample is exposed to light, the pmf (both electric and pH components) increases until a steady-state value is reached, as protons are pumped into the lumen by photosynthetic activity. This results in an increase of ECS_{lin} to a steady-state (ECS_{SS}) value above the baseline reflecting the dark situation (Fig. 5.3). Upon light shut-off, rapid proton efflux through the CF_1F_O-ATP synthase and the concomitant activity of various ion channels, leads to the collapse of the $\Delta\psi$ (and therefore a diminution of ECS_{lin}). However, the ΔpH does not decrease with the same rate, because of the important pH buffering effect in the lumen. When the increase of ΔpH in the light is important, this can lead to a situation where after the light offset, $\Delta\psi$ becomes smaller than in the pre-illumination dark situation, as some of its amplitude has been "replaced" by ΔpH. This is visualized as a negative overshoot of ECS, which is used as a measure of the variation of the ΔpH induced by the illumination. Therefore, total light generated pmf is related to the total ECS signal as ECS_T=ECS_{SS} - ECS_{INV}, which is proportional ΔpH+$\Delta\psi$ increase in

the light. Over seconds-to-min after the extinction of the light, ΔpH and $\Delta\psi$ (thus ECS_{lin}) return to their initial value in the dark via the action of slower auxiliary ions transporters (Armbruster et al., 2014). Unfortunately, *P. tricornutum* usually shows no ECS_{INV}, or some of very small amplitude, and this method has not been validated in diatoms at the moment. In fact, the only report using this method in diatoms (with the centric *Opephora guenter-grassii* (Blommaert, 2017)) suggests the situation might be different in diatoms. In this section, I propose that through the combination of two previously demonstrated ECS-based methods, it is possible to assess the ΔpH *in vivo* in diatoms, without the need to access ECS_{INV}.

5.1.2 Method 1: Using the quadratic ECS probe of diatoms to determine absolute values of $\Delta\psi$

As mentioned above, the ECS_{lin} allows to measure relative changes in $\Delta\psi$. However, although the baseline is usually arbitrarily set to 0 during ECS measurements, it is well-known that there is usually a significant $\Delta\psi$ already present in the dark (from here onward called $\Delta\psi_d$). Therefore, if we want to express ECS_{lin} and $\Delta\psi$ in absolute values we get:

$$\Delta\psi = \Delta\psi_d + \Delta\Delta\psi \tag{5.3}$$

With appropriate normalization of ECS signals, and introducing the variation of $\Delta\psi$ relative to the dark situation ($\Delta\Delta\psi$), we find that ECS_{lin} is proportional to the difference between the ECS_{lin} signal in the light and in the dark:

$$ECS_{lin} \propto (\Delta\psi_d + \Delta\Delta\psi) - \Delta\psi_d \propto \Delta\Delta\psi \tag{5.4}$$

Contrary to green organisms, a large ECS_{quad} signal is observed in diatoms (Bailleul et al., 2015), as well as in other secondary endosymbionts like *Phaeomonas* sp. (Berne et al., 2018)(Fig. 5.4). Thus, doing the same for ECS_{quad} we obtain:

$$ECS_{quad} \propto (\Delta\psi_d + \Delta\Delta\psi)^2 - \Delta\psi_d^2 \tag{5.5}$$

Therefore measuring both ECS_{lin} and ECS_{quad} *in vivo* allows to solve this system of two equations with two unknown parameters:

$$ECS_{quad} = a \times (ECS_{lin} + \Delta\psi_d)^2 - a \times \Delta\psi_d^2 \tag{5.6}$$

Here, a is a constant representing an intrinsic feature of the photosynthetic apparatus of a given photosynthetic material on a given day of acclimation, it depends on the polarizability of the pigments participating to ECS_{quad} and on the mode of normalization of the ECS_{lin}. As mentioned above, $\Delta\psi_d$ is the pre-existing electric gradient in the dark. Therefore, measuring both ECS_{lin} and ECS_{lin} *in vivo* allows to calculate absolute values of $\Delta\psi_d$ and from there, absolute values of $\Delta\psi$ at any moment of a light perturbation. The deconvolution of the two components can theoretically be made with measurements under the same illumination protocol at two different wavelengths. In practice, the additional contributions of absorption changes due to oxidation-reduction of *c*-type cyt. makes it necessary to go through a three-wavelengths deconvolution as described in (Bailleul et al., 2015) and written below Fig.5.4. The determination of $\Delta\psi_d$ and absolute $\Delta\psi$ however still requires the determination of a. The privileged experimental strategy to find a is to use uncouplers to abolish $\Delta\psi_d$ and solve Equation 5.6 for $\Delta\psi_d \approx 0$. Once a is found in a given sub-sample, $\Delta\psi_d$ can be

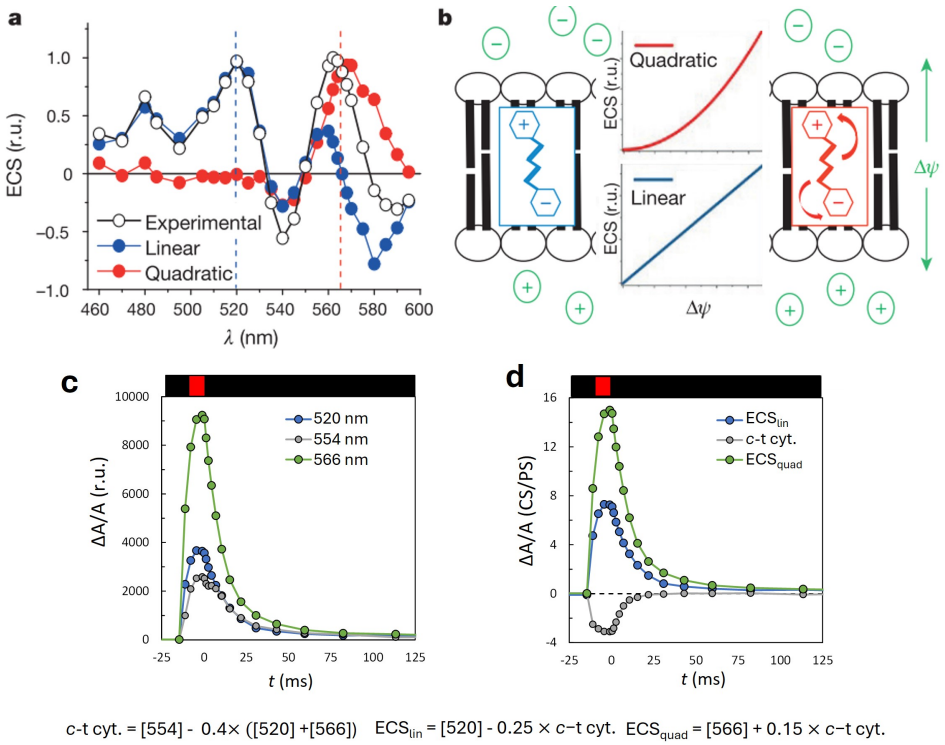

c-t cyt. = [554] - 0.4× ([520] +[566]) ECS_{lin} = [520] - 0.25 × c−t cyt. ECS_{quad} = [566] + 0.15 × c−t cyt.

Figure 5.4: The deconvoluted ECS spectra of *P. tricornutum* (a) and a schematic representation of the two ECS probes, arising from a shift in the dipole moment of polar pigments (linear) and light-induced polarization of polarizable pigments (quadratic) (b) (from Bailleul et al., 2015). In (c), a typical absorption difference signal (ΔA/A) measured over a saturating pulse (usually 15 ms, red bar) and its decay in the dark in *P. tricornutum*, measured at λ 520, 554 and 566 nm, is deconvoluted into c-t. cyt., ECS_{lin} and ECS_{quad} signals normalized to one charge separation (CS) per PS in (d) with the given equations.

directly calculated in different conditions provided both ECS_{lin} and ECS_{quad} are measured. If the ECS signal is calibrated to the signal generated by a laser flash inducing a single charge separation (CS) by PS, $\Delta\psi_d$ can be measured in CS/PS (1 CS/PS has been estimated to $\approx$ 20 mV (Bulychev and Vredenberg, 1976, Witt, 1979)). In green organisms (Finazzi and Rappaport, 1998, Joliot and Joliot, 2008) and in diatoms (Bailleul et al., 2015), the origin of the dark pmf (pmf_d) and thus, $\Delta\psi_d$, has been demonstrated to be the hydrolysis of mitochondrial ATP by the CF_1F_O-ATP synthase/hydrolase. Therefore, mitochondrial inhibitors (like antimycin A (AA) and salicylhydroxamic acid (SHAM)) are also commonly used to modulate the amplitude of the pmf_d and its two components (Bailleul et al., 2015).

5.1.3 Method 2: Using total pmf references to determine the pmf in the dark

Hence, with **Method 1** we show that absolute values of the electric component of the pmf can be measured in diatoms thanks to the presence of linear and quadratic ECS probes. From Equation 5.1, it is clear that combining this method with another one allowing us to gauge the pmf would provide a way to assess the ΔpH. This is the aim of this second method, which is based on the ECS response to an intense multiple-turnover saturating pulse of light and builds on previous work carried out mainly by Pierre and Anne Joliot.

Upon exposure to a saturating pulse, the ECS_{lin} signal rapidly ($\approx$ 15 ms) increases to a saturated value. The magnitude of the ECS increase reflects the increase of $\Delta\psi$, or $\Delta\Delta\psi$, between the dark value and the saturated one. After observing that $\Delta\Delta\psi$ can reach higher values before saturation with the addition of AA, Joliot & Joliot proposed that this was due to a decrease in the pre-existing pmf_d of mitochondrial origin, while the saturated value constantly represented the maximal pmf that can be stored in the lumen (from now on pmf_L for leak) (Joliot and Joliot, 2008). The hypothesized cause of this "leak" has changed over the years, but a saturated rotation rate of the ATP synthase F_1 subunit at pmf_L while the F_0 rotor continues to accelerate (proton slip) is currently favoured (Pierre Joliot personal communication). While the consumption of the light-induced $\Delta\Delta\psi$ roughly follows a mono-exponential decay (Avenson et al., 2005), the apparition of a bi-phasic decay is observed upon the addition of sufficient AA (or other pharmacological inhibitors of mitochondrial respiration, or uncouplers). The first phase, completed in roughly 100-200 ms, is interpreted to represent the rapid efflux of protons through the CF_1F_O-ATP synthase. While the second, much slower phase, is associated to passive leak of protons once the pmf dips below the activation threshold of the CF_1F_O-ATP synthase (or a small number of enzymes remain active) (Joliot and Joliot, 2008). This provides a second pmf reference value (together with pmf_L) which we will name pmf_i for "inactivation", previously determined to be around 110 mV in isolated chloroplasts (Junge et al., 1970). The strong argument in favour of these two thresholds (pmf_L and pmf_i) being absolute reference of pmf is that the "distance" (in terms of ECS) between the two was a constant, regardless of the pmf_d value and of the addition of inhibitors disturbing the partitioning between $\Delta\psi$ and ΔpH (Joliot and Joliot, 2008).

It is crucial to remember that these two reference values (pmf_i, pmf_L) relate to the pmf but that the observable used, ECS_{lin}, relates only to $\Delta\psi$ and is blind to the ΔpH. Nevertheless, it is assumed that the pmf generated during a short SP is strictly attributable to $\Delta\Delta\psi$ because of the large buffering effect of the lumen. Thus, the "opaque bottle analogy" is useful to understand the parameters that can be derived from this approach (Fig. 5.5). This analogy highlights that to determine the unknown volume of water in an opaque bottle, one could add water until it reaches its maximum capacity. Even if the exact overflow point is

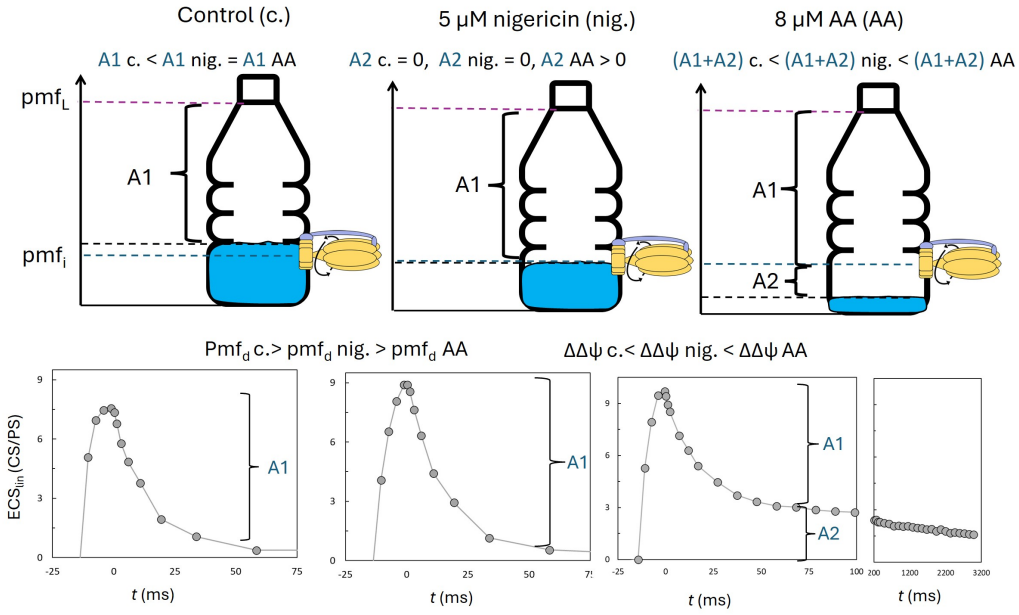

Figure 5.5: The opaque bottle analogy of the Joliot & Joliot method to probe the pmf in the dark. In control conditions (left column), the dark pmf (pmf_d) is above the ATP synthase pmf activation threshold value (pmf_i). Therefore, when the ECS_{lin} decays after the SP, only part of the amplitude of the phase 1 (A1) is visible. Upon addition of 5 µM of nigericin (nig.) (H^+/K^+ antiporter) (middle column), the ΔpH in the dark decreases, and so does the pmf_d, but here it remains roughly equal to pmf_i. Therefore, when the ECS_{lin} decays after the SP, the full A1 phase is visible (a larger ECS_{lin} than under control conditions is visible). Upon addition of 8 mM of antimycin A (AA) (right column), inhibition of mitochondria almost leads to the full dissipation of the pmf_d, which falls below the pmf_i. Therefore, when the ECS_{lin} decays after the SP, both the full A1 and par of the slow phase amplitude (A2) are visible, although A1 remains roughly equal to nigericin conditions.

unknown, the added volume can still be measured and expressed relative to this reference or leakage point. Similarly, the Joliot & Joliot method (**Method 2** from now on) consists of energizing the membrane with a strong light pulse and monitoring the increase in ECS until the pmf_L is reached (analogous to the maximum capacity), thus effectively measuring pmf_L-pmf_d (analogous to the added volume).

5.1.4 Outlining a convincing proof of concept for an *in vivo* ΔpH measurement method in diatoms

At this stage, the **Method 2** allows assessing values of pmf relative to the reference corresponding to the leak, or the maximal pmf that can be stored in the lumen. Similarly to **Method 1**, absolute values are then calculated using the pmf_L value which can only be obtained in a sub-sample for which the pmf_d is fully abolished with inhibitors. Therefore, the maximum possible amplitude of $\Delta\Delta\psi$ can be measured and its value now assigned to pmf_L. In particular, in this chapter we want to calculate absolute values of pmf, $\Delta\psi$ and ΔpH in the dark. This should be feasible by comparing the extent of $\Delta\Delta\psi$ over the saturating pulse with and without collapsing the pmf_d. Computing (pmf_L-0) minus ($\Delta\Delta\psi$ - pmf_d) indeed provides an absolute value of pmf_d in a sample of interest. Moreover, in the-

ory, using **Method 2** to estimate total pmf_d, combined with the quadratic ECS probe of diatoms, allows calculating $\Delta pH_d = pmf_d - \Delta\psi_d$. However, we first wanted to ensure that **Method 2** works in diatoms and that the values obtained for pmf_d are compatible with the one obtained for $\Delta\psi_d$ via **Method 1**. As customary with methodology development, this part of my Ph.D. was characterized by a lot of trials and errors. In the remaining of this section, I will focus on presenting data to validate a list of conditions that we wanted to check to make a convincing case that the described approach allows measuring reliable pmf_d and ΔpH_d values in diatoms.

1. The addition of chemicals induce the theoretically expected effects. For instance, adding nigericin, should decrease the pmf_d and ΔpH_d, but leave $\Delta\psi_d$ mostly unaffected.

2. Regardless of conditions, when over a saturating pulse generates a $\Delta\Delta\psi$ that reaches pmf_L and that pmf_i (and the corresponding experimental point identified) during an experiment, the difference between them should be constant. Indeed, they are two pmf references of the CF_1F_O-ATP synthase. This difference is experimentally visualized as the amplitude A1 of the fast ECS decay component (see Fig. 5.4c-d).

3. Assuming ΔpH_d can not be negative, pmf_d must always be larger or equal to $\Delta\psi_d$.

4. The method should yield theoretically sound values. For example, regarding the maximum pmf a biological membrane can sustain or luminal pH values within a range allowing for complexes to maintain their integrity (Kramer et al., 1999).

A final validation that should be made is to compare the relative changes in ΔpH and $\Delta\psi$ obtained with this approach to the ones observed with the ECS_{INV} method. Unfortunately, *P. tricornutum* only displays ECS inversion of very small amplitude and is not adequate to realize this validation. I will come back to this at the end of Section 5.1.9.

5.1.5 Material and methods

Wildtype *P. tricornutum* (Pt1) was grown agitated under 40 µmol photons m^{-2} s^{-1} (12:12 photoperiod) at 19°C in f/2 medium prepared from filtered (0.2 µm) seawater, in Erlenmeyer of 500 mL. On the day of the experiment, cultures were concentrated 10-fold by centrifugation (5000 RPM, 6 min), supplemented with ≈ 10% w/v Ficoll (to slow down cell sedimentation during measurements), and then left to recover under gentle agitation and very low light (approximately 5 µmol photons m^{-2} s^{-1}) for at least 45 min. Experiments were conducted in a JTS-10 spectrophotometer (Biologic, France), which can measure absorbance change (ΔA) spectroscopy and variable fluorescence. A laser flash sequence was first used to normalize the signal to a single CS/PS, this internal normalization allows comparison between samples measured on different cultures/days. To generate $\Delta\Delta\psi$, a LED (630 nm) saturating pulse of 10-to-20 ms (depending on conditions) was applied on the sample. The rise and decay of ΔA signal for a given treatment was always measured six times in total over three different wavelengths in this order 520, 554, 566, 566, 554, 520 nm, always waiting at least 30 s (and up to 2 min with certain chemicals) between saturating pulses. The *c*-type cyt., ECS_{lin} and ECS_{quad} signals were deconvoluted as described above, allowing to calculate both absolute $\Delta\psi$ (**Method 1**) and pmf_d (**Method 2**).

For **Method 2**, the ECS_{lin} decay was fitted as the sum of two mono-exponential functions, representing Phase 1 and 2, or active and inactive, of the CF_1F_O-ATP synthase.

$$\mathrm{ECS_{lin}} = A1e^{-\kappa_1 t} + A2e^{-\kappa_2 t} \tag{5.7}$$

Where A1 and A2 are the amplitudes of each phase, and κ their respective rate constants. Although there is theoretically no phase A2 when $\mathrm{pmf_d} > \mathrm{pmf_i}$, using Equation 5.7 to fit all curves regardless of $\mathrm{pmf_d}$ value proved to be more parsimonious (lower AIC than a single component mono-exponential decay) and less subjective. In the cases where A2 was around the value of control conditions, it was considered negligible. Because $\Delta\Delta\psi$ often slightly overshoots at the end of the pulse before the start of the decay kinetics, A1 is calculated as $\Delta\Delta\psi$ - A2. Maximum pmf capacity ($\mathrm{pmf_{max}}$) of a given sample is calculated by the addition of the sum of the largest A1 and A2 measured in a given sample over a titration with inhibitors allowing to fully dissipate the $\Delta\psi_\mathrm{d}$. In theory, this value should be equal to $\mathrm{pmf_L}$ in a sample for which the pmf in darkness is null (and no secondary effects impede maximal photochemistry). The value of $\mathrm{pmf_d}$ is calculated as $\mathrm{pmf_{max}}$ - A1, although under some high inhibitor concentrations, $\Delta\Delta\psi$ may not reach $\mathrm{pmf_L}$ (see below). Therefore, the incremental decrease in $\mathrm{pmf_d}$ induced by augmenting an inhibitor in concentration X to Y, equals A2($[X]$) - A2($[Y]$).

5.1.6 Validation of the method with nigericin and other pharmacological inhibitors titrations

The challenge here is to measure the absolute values of pmf and ΔpH in the dark, as there is already a simple and validated method to assess absolute $\Delta\psi$ in diatoms. Therefore, we concluded that titrating pmf and its two components with increasing concentrations of nigericin would be the best strategy for a proof of concept. According to theory, nigericin, a $\mathrm{H^+/K^+}$ antiporter, should reduce ΔpH, reduce pmf, and keep $\Delta\psi$ largely unchanged. The robust method of measuring $\Delta\psi$ can then be used as a precise control to confirm the invariance of $\Delta\psi$. Preliminary experiments (not shown) revealed that the effect of nigericin is sufficient to diminish $\mathrm{pmf_d}$ below $\mathrm{pmf_i}$ only when large concentrations are added, which also compromises photochemistry. Thus, undermining confidence that the $\Delta\Delta\psi$ reached represents the *true* $\mathrm{pmf_L}$ reference. Therefore, to investigate the dose-dependent effect of nigericin on the $\mathrm{pmf_d}$ and its partitioning, I first supplemented the samples with a low concentration of AA (3 µM) in background dose, decreasing the $\mathrm{pmf_d}$ slightly below $\mathrm{pmf_i}$ (Fig. 5.6). This allowed me to calculate the "ECS distance" between these two values, which should remain constant according to the assumptions behind the proposed method.

With both references $\mathrm{pmf_L}$ and $\mathrm{pmf_i}$ visible, I measured roughly unaffected $\Delta\psi_\mathrm{d}$ by the incremental addition of up to 5 µM of nigericin, while the pulse-induced $\Delta\Delta\psi$ increased (i.e., $\mathrm{pmf_d}$ decreased) by two CS/PS units. This is compatible with the mechanism of action of nigericin, a $\mathrm{H^+/K^+}$ antiporter, which is expected to decrease the ΔpH and $\mathrm{pmf_d}$, but not $\Delta\psi_\mathrm{d}$ (although by disturbing the mitochondrial electron transport chain, nigericin could indirectly affect the plastidal pmf). With increased background doses of AA (8 µM) and nigericin (12 µM), I started a SHAM titration, which inhibits the alternative oxidase (AOX)-dependent respiration and is needed to fully dissipate the $\mathrm{pmf_d}$ in *P. tricornutum* (Bailleul et al., 2015). Increasing SHAM concentrations led to a large reduction in $\Delta\psi_\mathrm{d}$ reaching values <1 CS/PS. However, at concentrations above 0.5 mM, SHAM also strongly disrupted photochemistry during the ECS increase (not shown), which resulted in a lower $\Delta\Delta\psi$ reached and also had complex uncoupling effects (as seen on the decay kinetics (Fig. 5.6h)). Because of that, the $\Delta\Delta\psi$ started to diminish. This highlights the necessity of using both references, $\mathrm{pmf_L}$ and

pmf_i, to determine pmf_d. Since to reach conditions where $\Delta\psi_d \approx 0$ (the secondary effects of SHAM do not alter the reliability of **Method 1**), it is necessary to add high inhibitor concentrations, to the point where $\Delta\Delta\psi$ does not confidently reach pmf_L due to inhibitor secondary effects.

The amplitude of pmf_L minus pmf_i should be a constant and is approximated here by the amplitude A1 of the fast component of the ECS relaxation after the saturating pulse. Accordingly, A1 values were computed for all inhibitors concentration combinations, also including a nigericin titration made with 8 µM AA in background dose (2 replicates), and other titration experiments realized during my Ph.D. (also with AA and the carbonyl cyanide m-chlorophenylhydrazone (CCCP) uncouplers) (Fig. 5.7). For each treatment, I normalized A1 and A2 over pmf_{max} (sum of the largest amplitude for each phase measured in a given sample). This revealed that while A2 increases from negligible level to up to 35% of pmf_{max}, A1 is largely invariant around 60% of pmf_{max}, at least over the intermediate A2 range (if SHAM is not completely hampering photochemistry (red dots in Fig. 5.7a and such treatments were discarded from b)). The fact that the sum of the largest A1 and A2 equals 95% rather than 100% highlights the challenge of measuring the maximum amplitude of both phases ($pmf_d \approx 0$) at the same time, due to secondary effects of pharmacological inhibitors, and that a small $\Delta\psi_d$ portion could not be abolished. Also, when pmf_d was about 5% of pmf_{max}, A1 was a bit lower. This could relate to a more dynamic intermediate state, where the oversimplistic function used to fit the CF_1F_O-ATP synthase kinetics might be less accurate. Indeed, many factors can influence the CF_1F_O-ATP synthase activity, like stromal pH, $[ATP]/[ADP+P_i]$ and counter ion fluxes, which cannot be captured by the functions used here. Worthy of note, the regulatory disulfide bridge on the γ-subunit of the ATP synthase found in green organisms (Kramer and Crofts, 1989, Buchert et al., 2021) is not present in diatoms, or at least in *P. tricornutum* (see in *Odontella sinensis* (Pancic and Strotmann, 1993)), although other redox modulations could exist (Carrillo et al., 2016). I did check for potential effects of common reducing agents (DTT and TCEP) which had no effect on *P. tricornutum*'s ECS decay kinetics. Overall, we conclude that pmf_L and pmf_i can be used as absolute pmf references in *P. tricornutum* under the growth and experimental conditions used here. Again, the method is for the moment aimed at measuring pmf, $\Delta\psi$ and ΔpH values in dark-acclimated situations, more controls are needed before the method can be used in superposition to a steady-state actinic light. The 60/40 ratio between A1 and A2 to form the pmf_{max} is also valuable. There exist different theoretical values which can be attributed to pmf_i and pmf_L, which will allow us to convert the relative variations in pmf, $\Delta\psi$ and ΔpH measured here into volts and pH units in the next section.

5.1.7 Theoretical consideration of the measured pmf, ΔpH and $\Delta\psi$ values

In *P. tricornutum* under the growth and experimental conditions used here, combining **Method 1** and **Method 2** suggests that the pmf_d magnitude is equivalent to the electric potential generated by 5.8 ± 0.4 CS/PS (pmf_{max} minus $\Delta\Delta\psi$ in control conditions) (Fig. 5.8). Additionally, the pmf_d is partitioned roughly evenly between $\Delta\psi$ (**Method 1**) and ΔpH (pmf_d minus $\Delta\psi_d$), which corroborates the hypothesis from (Kramer et al., 1999), based on the imperative of avoiding over-acidification of the lumen to preserve electron transport chain complexes integrity, and later backed up by *in silico* simulations (Kramer et al., 2003, Davis et al., 2017). It is also interesting that pmf_d is exactly half of the maximal pmf value sustainable by the thylakoid membrane of *P. tricornutum*. Moreover, regardless of inhibitors

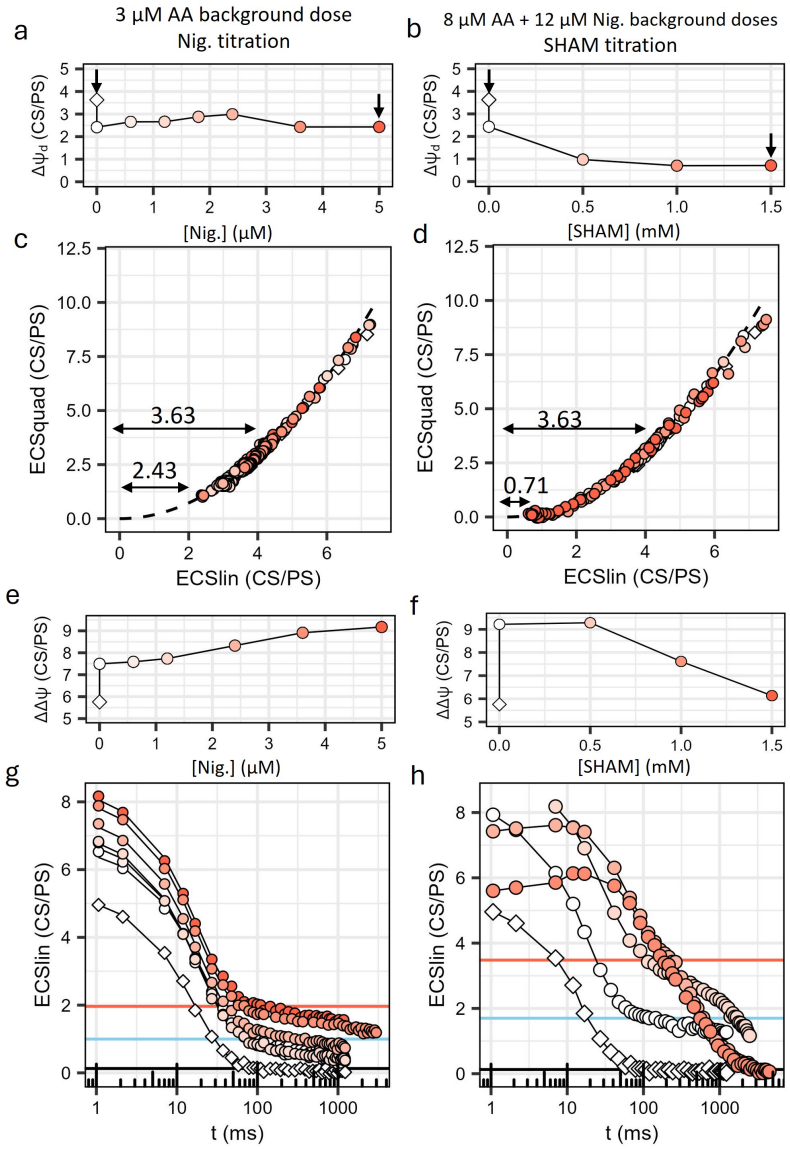

Figure 5.6: Parameters derived from **Method 1** over a nigericin (Nig.) and SHAM titrations. Variations in $\Delta\psi_{\mathrm{d}}$ as a function of Nig. (a) and SHAM concentrations (b) with different background doses of AA and/or Nig. In (c) and (d) the $\mathrm{ECS_{quad}}$ versus $\mathrm{ECS_{lin}}$ fitted parabola for the different inhibitor concentrations, with their maximum shifted by $\Delta\psi_{\mathrm{d}}$ so that all curves fall on the same a coefficient (see Section 5.1.2 and refer to Bailleul et al., 2015 for further details), the written values correspond to $\Delta\psi_{\mathrm{d}}$ for control conditions and with the highest inhibitor concentrations tested (arrows in the top panel). In (e) and (f) the $\Delta\Delta\psi$ and in (g) and (h) the complete $\mathrm{ECS_{lin}}$ decay kinetics in darkness (**Method 2** used on the same measurements) are shown. The black, blue and red horizontal lines are A2 in control, background dose of inhibitor(s) and highest inhibitor concentrations tested curves, respectively. Diamond symbols represent control condition and the colour scale indicates relative inhibitor concentrations. One replicate is shown here, but the experiment was repeated on three independent biological replicates with high reproducibility.

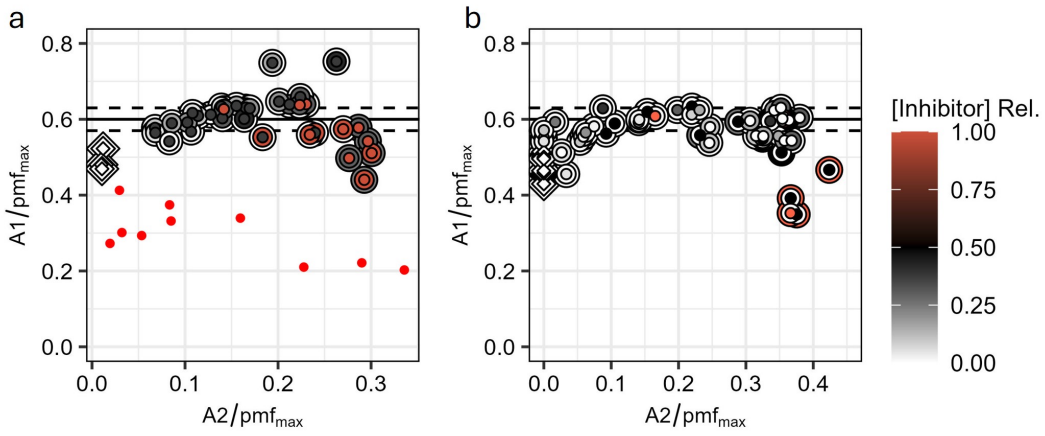

Figure 5.7: A1 versus A2 normalized to pmf_{max} for the three replicates of the experiment shown in Fig. 5.6 and 2 more replicates of the same experiment done with 8 µM AA as background dose and increasing concentration of nigericin (a). In (b) A1 versus A2 normalized to pmf_{max} in other inhibitor titration experiments done over the course of my Ph.D. Multiple circle symbols are overlaid to convey all the information about inhibitors concentrations. In (a), the largest (outer) symbols represent SHAM, the medium ones nigericin and the smallest (inner) ones AA. In (b), the largest symbols represent SHAM, the medium ones CCCP and the smallest ones AA. The color scale represents relative concentrations from minimal to maximal dosage used for a given inhibitor and diamond symbols are control treatments. The red dots in (a) are measurements for which high SHAM concentrations hampered photochemistry and artificially decreased A1. The horizontal lines represent 0.6 ± 0.05 (dotted lines).

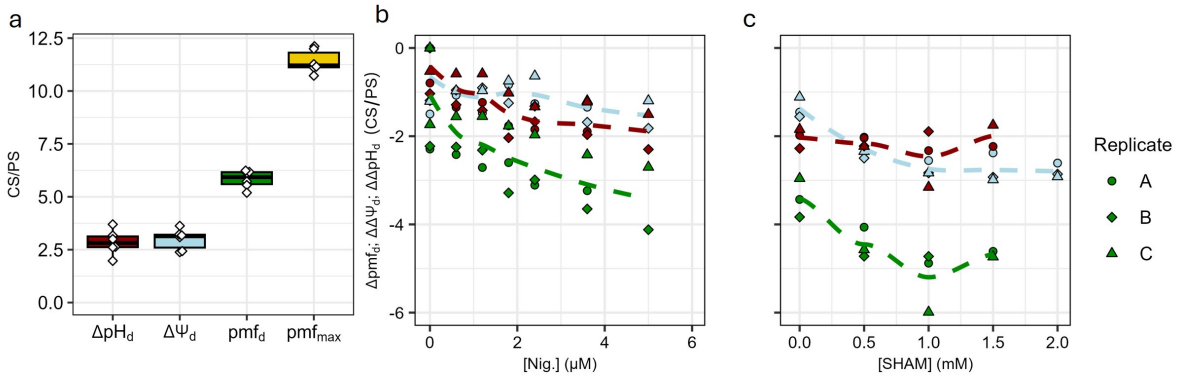

Figure 5.8: In dark/control conditions, the estimated pmf and its partitioning between ΔpH and Δpsi, and the pmf_{max} sustainable by the thylakoid membrane of *P. tricornutum* (a). In (b), are showed the incremental effects of nigericin addition with 3 µM AA in background dose and (c) the incremental effects of SHAM addition with 8 µM AA and 12 µM nigericin in background doses. In (a), six biological replicates are shown, the three used for the pharmacological inhibitors titrations showed in the other panels, and the control conditions of the three biological replicates used for the experiment presented in Section 5.1.8 and Fig. 5.9.

concentrations, the decrease in pmf_d was always larger than the one in $\Delta\psi_d$ (Fig. 5.8). This leaves us with a final point to examine for our proof of method to be completed, and it is the theoretical considerations of absolute values.

Granted a pmf_{max} equivalent to 11.4 ± 0.5 to CS/PS, we obtain a pmf_i of 4.6 (40% of pmf_{max} (Fig. 5.7)). Following the approach of (Davis and Kramer, 2020), we can convert these values into universal bioenergetics units by considering that the ATP synthase is active when the pmf exceeds the energy required for ATP synthesis (ΔG_{ATP}), estimated of 40 kJ/mol by (Giersch et al., 1980). In the case of the ATP synthase, its activation threshold is determined by the number of *c*-ring subunits (Equation 5.8), which is currently unknown in diatoms, I will thus consider 14 *c*-subunits as customary for photosynthetic eukaryotes from data on spinach and pea (Seelert et al., 2003, Hahn et al., 2018), but a stoichiometry of 13 cannot be ruled out in *Chlamydomonas* (Zu Tittingdorf et al., 2004). In:

$$\Delta G_{ATP} = n \cdot F \cdot \text{pmf} \tag{5.8}$$

n is the H^+/ATP ratio (4.67 for a 14 *c*-subunits rotor), giving a value of 88.8 mV for pmf_i, and 113.8 for the pmf_d found with our approach. This pmf_d value (>pmf_i) may reflect the extensive energy coupling between mitochondrial and plastidial electron chain in diatoms (Prihoda et al., 2012, Bailleul et al., 2015). For pmf_{max}, we obtain 222.1 mV, which is a little bit above the 180-200 mV potential a biological membrane is usually considered capable of sustaining (Teissie and Rols, 1993, Klingenberg, 2008). However, diatoms possess a unique lipid membrane composition, notably an increase of 20-to-30% in negatively charged lipids (sulfoquinovosyldiacylglycerol and phosphatidylglycerol) compared to green organisms (Lepetit et al., 2012, Wilhelm et al., 2020). It has yet to be investigated if this could increase the maximal potential the plastid thylakoidal membrane can sustain. It is also noteworthy that this renders 19.5 mV per CS, the exact value that had been estimated in pioneer studies on isolated thylakoids (Bulychev and Vredenberg, 1976, Witt, 1979). Moreover, from Equation

5.1 and considering a temperature of 291K, we can calculate a $\Delta\psi$ equivalence of 57.9 mV per pH unit. With a ΔpH of 54.4 mV, this gives 0.94 pH units, and considering a stromal pH of 8 (recently estimated by (Shimakawa et al., 2023) in *P. tricornutum*), a luminal pH of 7.1. This is perfectly in line with the more pH-sensitive VDE of diatoms still capable of de-epoxidation at pH 7, and the already active VDE in darkness, albeit with slow rates, estimated by (Blommaert et al., 2021). Finally, it is interesting to entertain the idea that diatoms might have a larger *c*-subunit stoichiometry than 14 (or perhaps smaller, and the pmf_i to pmf_{max} ratio reported here is off). I already mentioned that 222.1 mV is on the high end of plausible pmf_{max}. Moreover, simulations by (Davis and Kramer, 2020) associate large luminal pH (>6.5) to *c*-ring larger than 14. For the sake of argument, maintaining everything equal in the calculations above but increasing the number of *c*-subunits to 16, would give a more typical pmf_{max} of 194.3 kJ/mol, and would also lead to an increase in luminal pH to 7.2. However, there are many uncertainties in the above calculations, notably ΔG_{ATP} is sometimes estimated up to 50 kJ/mol and the stromal pH in plants is usually considered at 7.8. Moreover, our method itself has imperfections, notably in the fit used to determine amplitude A2. Despite these cautions to keep in mind, we conclude that this novel approach to probe absolute pmf and its partitioning *in vivo* in diatoms yields very sound values from a theoretical standpoint.

5.1.8 Relaxation of the pmf and ΔpH in darkness after high light stress

As mentioned above, more controls are required before using this new method on illuminated samples. The reasoning behind this precaution is that when part of PSI and PSII acceptors are reduced by light exposure, we are not convinced that the turnover of PSs during the short saturating pulse will be sufficient for the $\Delta\Delta\psi$ to reach the reference value corresponding to the *true* pmf_L. When pmf_i is visible, it is easy to test that the "ECS distance" between pmf_L and pmf_i is constant. However, it is not the case in most physiological situations where, in the absence of inhibitors, the pmf_d is maintained above pmf_i. Therefore, the first application we made of the method to understand photosynthesis regulation via the pmf and its partitioning in *P. tricornutum*, is to measure the kinetics of pmf in the dark, after a high light stress, as NPQ/qZ relaxes. One of the more pressing questions we wanted to address is "Does a persistent lower luminal pH, maintaining a high VDE de-epoxidation rate, explain the typical 10-to-15 min relaxation time of qZ in diatoms?".

In this paragraph, I briefly describe the protocol used to address the above question. For this experiment, I prepared seven sub-samples, one was used for laser normalization and determining *a* (coefficient of the **Method 1** parabola) using a AA+SHAM titration, and the six others were used for the light exposure protocols. The samples were exposed to 40 µmol µmol photons m^{-2} s^{-1} for five min, to activate the Calvin-Benson cycle, then to 840 µmol photons m^{-2} s^{-1} for six min to trigger NPQ/qZ. The relaxation of the pmf was then monitored (applying saturating pulses at different times). The five sub-samples were used to measure absorption change in this order 520, 554, 566, 554, 520 nm and the last one to measure variable fluorescence and NPQ/qZ.

In darkness after high light stress, we unexpectedly observed a transient collapse of the pmf_d (**Method 2**) between 45 s and 4 min from the light shut-off, making the distinctive ATP-synthase inactive phase strikingly visible (already visible in raw ECS data Fig. 5.9a, and green symbols Fig. 5.9c). This phenomenon was the most exacerbated at 1.25 min after dark transition, with the pmf_d decreasing 2.5 CS/PS below control values measured before the

light exposure protocol. This surprising observation was coherent with a decrease of 1 CS/PS in $\Delta\psi_d$ measured by **Method 1**. Our confidence in the validity of this observation is also supported by the fact that when A2 was visible, the active phase A1 stabilized around values, once again, close to 60% of pmf_{max} (Fig. 5.7). This is all the more impressive considering the drastically different experimental context between inhibitor titrations and the situation here, where the decrease of the pmf_d is due to physiological processes (of unknown nature at this stage). Reassured by coherent pmf_d and $\Delta\psi_d$ estimations, we calculated the evolution of the ΔpH_d and compared it to the relaxation kinetics of qZ. This showed that the evolution of ΔpH_d is exactly the opposite of what would be expected if the luminal pH was the limiting step for qZ relaxation. Indeed, ΔpH_d is at its lowest while qZ relaxation lags, and ΔpH_d starts increasing at the moment qZ relaxes (similar ΔpH_d relaxation kinetics were observed in Lhcx1-Ko and Lhcx1-overexpressor strains (with one replicate each, not shown)). This adds to evidence that the ΔpH is not as crucial in diatoms as in plants for the regulation of NPQ. Of course, the ΔpH is important to activate the VDE in the light. But, we show here that it relaxes back to its initial value (or even lower) in less than 20 seconds. Moreover, Lhcx1 does not seem to possess luminal residues reacting to ΔpH (Buck et al., 2021, Giovagnetti et al., 2022). In addition, changes in the net products of the XC seem to be more dependent upon variations in the rate of the ZEP, of large magnitudes (Blommaert et al., 2021), but for which the regulator(s) remain(s) unknown (see Section 1.4).

The cause of this abrupt collapse in pmf_d is unknown at the moment. One option is that a high ATP-requirement to sustain *P. tricornutum*'s metabolism, notably in carbon concentrating mechanisms (CCM) supporting the Calvin-Benson cycles in the pyrenoid (Burlacot and Peltier, 2023), results in a rapid exhaustion of ATP (including of mitochondrial origin), upon sudden transition from saturating light to darkness. Since the pmf is at equilibrium with the $[ATP]/[ADP+P_i]$ ratio, this would explain its transient collapse (Buchert et al., 2021). Regardless of the physiological reasons why the pmf (and its two components) transiently decrease at the offset of light, another question is which compartments are affected? Is the lumen transiently more basic? The stromal transiently more acid? Or both? The same question can be asked regarding the lumen and stroma charges, which together determine the $\Delta\psi$. First regarding the pH, it has previously been shown in plants (with fluorescent dyes) that the stromal pH increases during illumination, to varying extents (Werdan et al., 1975, Su and Lai, 2017), which theoretically would increase at least the ΔpH. Upon sudden transition to darkness after high light, the return of stromal pH to its pre-illumination value occurs in 3-to-4 min (Su and Lai, 2017, Aranda Sicilia et al., 2021). This is interesting as it shows the same time range of return to equilibrium between interdependent parameters in plants; with the stromal pH, and in diatoms; with the pmf and its partitioning, that we report here. Moreover, in *Arabidopsis*, the stroma alkalinization is partly dissipated in darkness by KEA1 and 2 H^+/K^+ antiporters (Aranda Sicilia et al., 2021), which opens the door to molecular candidates to investigate the nature of our observation with in *P. tricornutum* mutants. Also, huge elevation in stromal $[Ca^{2+}]$ have also been reported in *P. tricornutum* exposed to high light or H_2O_2 (Flori et al., 2023). Both a higher stromal pH and a more positively charged stroma, could have transient, and hardly predictable, effects on the pmf_d if the mechanisms from which they stemmed have slow reaction time versus the consumption of the pmf by the CF_1F_O-ATP synthase at the light shut-off. Finally, another mechanism which could influence the pmf over min timescale upon sudden transition to darkness in diatoms, is the conversion of HCO_3^- imported in the lumen into CO_2 by α-carbonic anhydrases in the vicinity of the pyrenoid (Kikutani et al., 2016, Nawaly et al., 2023). A transient maintenance of HCO_3^- pumping into the lumen at dark transition, coupled to its proton consuming conversion into

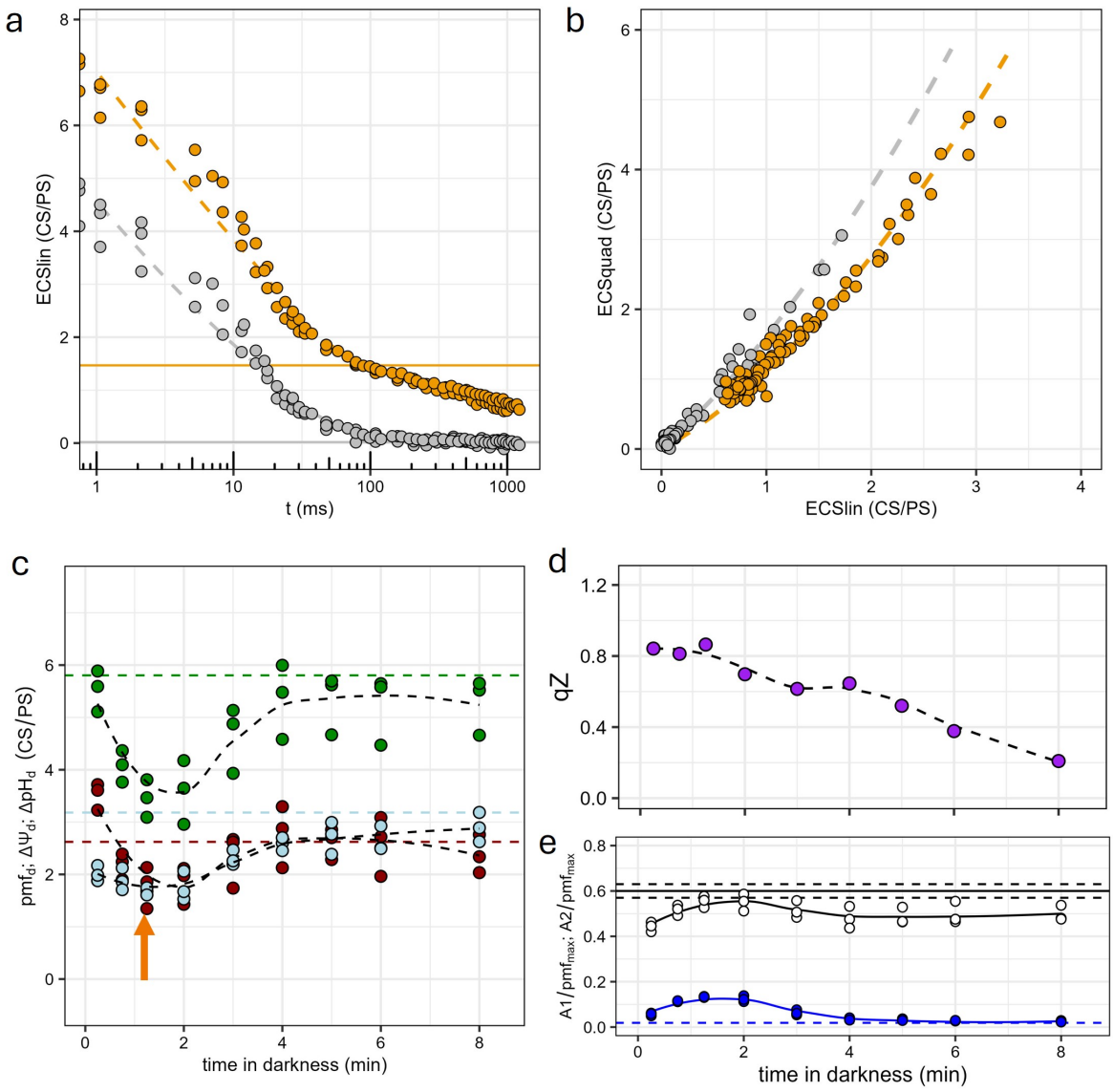

Figure 5.9: Raw data of ECS decay curves (n=3) after light pulse measured before high light exposure and 1.25 min after transition in the dark following high light exposure (a). In (b) the same data is used to show the widening of the parabola at 1,25 min, indicating a decrease in $\Delta\psi_d$ as per **Method 1** (see Section 5.1.2) (N.B., the parabolas are not $\Delta\psi_d$ shifted here (contrarily to Fig. 5.6) because the dynamic experimental conditions do not allow to measure the complete return of ECS to 0. Therefore differences in $\Delta\psi_d$ would be hardly visible between the curves if $\Delta\psi_d$-shifted). The complete relaxation kinetics of pmf_d, ΔpH_d and$\Delta\psi_d$ over 8 min in darkness after high light exposure, with the orange arrow corresponding to the above orange symbols (c) and one exemplary qZ relaxation curve measured over the same protocol (d). In (e), the A1 and A2 phase reflecting the ATP-synthase activity in each of the ECS dark decay curve fitted over the pmf relaxation experiment.

CO_2, could favour the decrease of both pmf components as $HCO_3^- + H^+ \leftrightarrow CO_2 + H_2O$. This hypothesis has huge implications for the potential usefulness of the method presented in this chapter in investigating another fundamental black box in the photosynthesis regulation of microalgae: the coupling between electron transport and CCMs (see (Burlacot and Peltier, 2023)). Interestingly, there is already a *P. tricornutum* RNAi mutant of α-carbonic anhydrase (Kikutani et al., 2016), that would be immensely convenient to use with our method to tackle this question.

5.1.9 Perspectives

I envision three avenues for the application of this new method allowing to measure absolute values of the pmf and its two components in diatoms. First, this research will provide a better understanding of regulation of the xanthophyll cycle and qZ by the luminal pH. Previous studies (Blommaert et al., 2021) have demonstrated that the XC can be monitored live and *in vivo* through the linear relationship between NPQ/qZ and the de-epoxidation state of xanthophyll pigments. By combining two non-invasive methods to assess the functioning of XC and ΔpH, we can test various hypotheses and models. In this study, we tested the validity of a hypothesis from the literature (Seydoux et al., 2022), which proposes that the slow relaxation of NPQ is kinetically driven by the relaxation of ΔpH. Specifically, we investigated the relaxation of NPQ/qZ and the pmf during the first minutes following a transition from bright light to dark. Our results show that NPQ remains in the relaxation lag phase even when the light-induced ΔpH has already dissipated and fallen below its pre-light initial value. This finding indicates that, at least under our experimental conditions, NPQ kinetics is not determined by ΔpH relaxation bur rather by the slow epoxidation of diatoxanthin into diadinoxanthin. Furthermore, measuring the de-epoxidation state and ΔpH immediately after switching off illumination of varying intensities could provide valuable insights into the pH regulation of XC. Although determining the exact role of ΔpH in the NPQ regulatory module is a challenging task that will require many years of study, I believe that the novel method developed here will be crucial in advancing this understanding, ultimately helping to "close the loop" on the NPQ regulatory module. Furthermore, In Chapter 3, we revealed an unexpected up-regulation of cyclic electron flow (CEF) as a function of qZ. It could be interesting to use the new method presented in this chapter to study the participation of CEF in generating the ΔpH, which then regulates NPQ. This could provide valuable insights into the feedback between these two critical regulatory mechanisms.

Finally, one could explore whether this method can be applied beyond *P. tricornutum*. Strictly speaking, this method requires the presence of linear and quadratic ECS signals. So far, the only microalgal groups where significant linear and quadratic components have been identified are diatoms and their sister groups. These components have been characterized in five diatom species in (Bailleul et al., 2015) and two additional ones since (Long et al., 2021, Dow et al., 2020). In groups phylogenetically related to diatoms, such as pinguiophytes (Berne et al., 2018) and raphidophytes (Benjamin Bailleul, personal communication), the presence of linear and quadratic components has also been observed. These groups are all candidates for *in vivo* ΔpH measurements. Furthermore, the presence of polarized and polarizable pigments in the photosynthetic antenna should not be considered a rare case. At least in theory, a linear and quadratic components should be present in all photosynthetic organisms, but with varying relative amplitudes, making their differentiation difficult. Anne and Pierre Joliot were able to visualize linear and quadratic probes in mutants of the model green microalgae *Chlorella sorokiniana* and *Chlamydomonas reinhardtii*, lacking PSII centres

and most of the chlorophyll antenna (Joliot and Joliot, 1989). This suggests that it is possible to develop such a tool in other lineages, provided that the pigment composition is modified by mutagenesis.

Another important aspect is the cross-validation of this method with another one. The only available spectroscopic method to date is based on the ECS inversion discussed before (Cruz et al., 2001, Avenson et al., 2005). Unfortunately, we do not see such ECS inversion in *P. tricornutum* (or of very small extent). This could reflect that the relaxation of the two pmf components or the buffering effect of the lumen are different in this species compared to green organisms. It could also be that there is no significant ΔpH building during high light illumination. This would explain why, already 20 s after light offset, we measure such a low ΔpH (Fig. 5.9). It would also be in line with the peculiar observation of a post-illumination pmf decrease. Additionally, one could wonder if the broader and higher pH-optimum for the catalytic rate of the VDE in diatoms (Jakob et al., 2001) is an adaptation to a lowered ability to generate high ΔpH? Perhaps in line with the relatively high lumen pH of 7.1 suggested in this chapter. This observation could reflect that proton pumping and ATP production is lagging behind electron transfer and NADPH production in diatoms, potentially because of slower or less efficient regulatory processes to accommodate the ATP/NADPH ratio to the metabolic demand (Croteau et al., 2024). For plants, but not green algae, the presence of the proton-pumping NDH-CEF pathway could partly explain how they can reach higher ΔpH (Peltier et al., 2016, Ogawa et al., 2023). Last, the surprising observation that nigericin does not inhibit NPQ/qZ in *P. tricornutum* also supports this idea (Grouneva et al., 2009, Seydoux et al., 2022).

Alternatively, we could use another diatom that exhibits both linear and quadratic ECS signals and ECS inversion to test the validity of our method. *Opephora guenter-grassii* is one such species in which ECS inversion has been observed (Blommaert, 2017), and where NPQ can be reduced in the presence of nigericin. However, an unexpected observation was made in this species (Blommaert, 2017): when NPQ and ECS inversion were monitored in the same sample with increasing amounts of nigericin, the responses of the two processes were hard to reconcile with theoretical expectations. As expected, NPQ decreased monotonically with increasing nigericin concentrations. But, while the amplitude of ECS inversion first increased at low nigericin concentrations, it started decreasing at higher concentrations. This non-monotone relationship between NPQ and ECS inversion raises doubts about the validity of the ECS inversion method in diatoms.

It is important to note that the ECS inversion method relies on a strong assumption: the pmf rapidly relaxes to its pre-illumination value immediately after light extinction. The interpretation of the $\Delta\psi$ inversion as equivalent to persistent ΔpH (both relative to their pre-illumination values) is only valid if the total pmf remains unchanged. We believe that in diatoms, at least in *P. tricornutum*, this assumption is not true. If the relaxation of the pmf to its pre-illumination value takes time (probably determined kinetically by the transfer of ATP from mitochondria to the plastid), the theoretical basis of the ECS inversion method may not be applicable to diatoms. Importantly, the unexpected observation of a collapse of the pmf upon sudden transition from high light to darkness (Fig. 5.9), does not require a quadratic ECS to be observed. Therefore, it would be feasible to look across different species/groups to find out if this observation can be reproduced, or even if it can be exacerbated under certain conditions. For instance, gas concentrations (or HCO_3^-) could be manipulated to investigate if the return of the pmf to pre-illumination depends upon mitochondrial respiration, or even carbon concentration mechanisms as discussed in the previous section. Another option to validate our method could be to use the fluorophore 9-aminoacridine (9-aa) (Schuldiner et al.,

1972), which has already been used in *P. tricornutum* (Seydoux et al., 2022). However, it is important to note that the localization of this fluorophore in the lumen has not yet been confirmed, so it cannot be considered as a reference method for luminal pH measurement at present.

5.2 Collaborative works

Over the course of my Ph.D., I also had the opportunity to contribute to several collaborative research efforts that led, or will lead, to the publication of scientific papers. These collaborations brought me to switch perspective, and look at photosynthesis not as research subject, but rather as a probe to investigate other processes outside of the scope of my personal project. One of those projects involved testing an innovative ECS-based method for measuring photosynthesis in mixtures, which we used to identify allelopathic interactions among 13 selected microalgae species, including *P. tricornutum*. The other three collaborations also involved *P. tricornutum*, in which we studied processes such as circadian rhythms, the potential interaction of photosynthesis with other plastid metabolic pathways, and the response of photosynthesis to pH changes of the external environment. In these projects, I applied my knowledge of Chl *a* variable fluorescence to study the photophysiology of *P. tricornutum*. My main goal in these collaborations was to seek for a photosynthesis-related phenotype in mutants of various proteins or across the entire circadian period. Moreover, these studies have provided valuable insights into the complex interactions between diatom photosynthesis and broader environmental and metabolic contexts.

5.2.1 Molecular components of the circadian-clock and its influence on photosynthesis in the diatom *P. tricornutum*

I will begin with the collaboration on circadian rhythms in *P. tricornutum*, as it provides a fitting conclusion to the work presented so far. In Chapter 3, I explored the mechanism of NPQ/qZ in *P. tricornutum*. In Chapter 4, the Lhcx1 mutants series was use as a qZ dial to investigate how qZ magnitude influences other regulatory processes constraining photosynthesis. In the current work, we investigate how, conversely, the circadian clock in *P. tricornutum* influences photosynthesis and once again identify the xanthophyll cycle and NPQ/qZ as the right-hand man of circadian clock, in charge of photosynthesis.

In the life of organisms, a key aspect is to ensure the proper temporal coordination of biological and physiological processes with periodic environmental signals, light/dark cycles being among the most obvious. However, the molecular mechanisms that regulate internal cellular rhythms in diatoms remain unknown. To address this issue, my co-authors first determined the optimal growth conditions to monitor circadian rhythms and then created knockout and overexpressor mutants of the putative clock component RITMO1 using CRISPR/Cas9 editing and ectopic gene overexpression.

We then compared circadian rhythms across various physiological parameters, including cellular fluorescence (measured by flow cytometry) and photophysiology (measured using a miniFIRe fluorometer) in these strains. Circadian rhythms are characterized by their ability to be entrained by periodic external cues (in this case, 16-h light/8-h dark cycles) and to persist for 2–3 days even after switching to continuous light (as shown in Fig. 5.10a). To determine whether RITMO1 is involved in the circadian clock, we looked for photosynthetic parameters that cycle under light/dark conditions and persist under continuous light in the

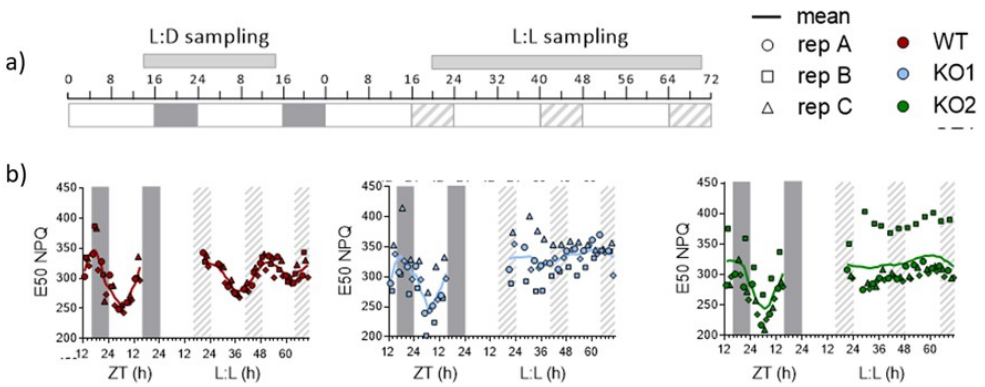

Figure 5.10: Schematic representation of sampling times for the analysis of WT, KO1, KO2, and OE1 cells grown under 16L:8D 50 µmol photons m^{-2} s^{-1} and subsequently exposed to L:L 30 µmol photons m^{-2} s^{-1}. Samples were collected continuously and measured one by one in the following order: WT, KO1, KO2, OE1 (not shown here) from replicate A to replicate D, with 15 minutes interval due to the measurement. Measurements were performed over 24 hours in L:D and 48 hours in L:L. In free running, samples were collected starting at L:L 16. (b) Evolution of E50NPQ, e.g., light intensity for which 50% of the maximum NPQ is reached under the sampling strategy presented in panel (a). Dots, squares, triangles, and diamonds represent the individual measures for biological replicates A to D, coloured dashed lines represent the moving average of all replicates (window of 4 hours). White and gray regions represent light and dark periods, gray dashed regions represent subjective nights in free-run conditions.

WT, but not in the RITMO1-Ko. Most photosynthetic parameters did not show oscillations in light/dark cycles or did not persist after switching to continuous light. However, a few did, including the PSII maximal efficiency (Fv/Fm) and NPQ/qZ-related parameters. The NPQ half-saturation intensity (E50NPQ, Fig. 5.10b) and the NPQ relaxation rate from high light to dark (not shown) showed the largest amplitude of oscillation, both in light/dark cycles and in continuous light. Interestingly, no significant persistent oscillations in NPQ parameters were detected in RITMO1-Ko mutants. This clearly indicates that the RITMO1 gene product is essential for the circadian rhythmicity of photosynthesis (as well as for cellular fluorescence and clock-controlled gene expression). The identification of RITMO1 as a component of the circadian clock in diatoms is an important step towards understanding how endogenous rhythmic regulations align with environmental rhythms in phytoplankton. The discovery that the photosynthetic parameters most controlled by the circadian rhythm are related to the light- and time- dependence of NPQ suggests a central role of the xanthophyll cycle in translating rhythms defined by the diatom internal clock into photosynthesis.

Manzotti A.*, Monteil R.*, Cheminant Navarro S., Hoguin A., **Croteau D.**, Jallet D., Daboussi F., Bouget F-Y., Jaubert M., Bailleul B., Bouly J-P., & Falciatore A. RITMO1 is a circadian clock component controlling rhythmic physiological processes in the marine diatom *Phaeodactylum tricornutum* (under review at New Phytologist). (* co-first authors)

5.2.2 Molecular determinants of pH homeostasis in *P. tricornutum*

Ionic and cellular pH homeostasis is a critical factor that regulates and influences metabolic reactions, protein stability, signalling pathways, and transport mechanisms. To maintain and balance intracellular ion concentrations, organisms must continuously sense and respond to changes in the extracellular environment and cellular compartments. Although this finely tuned system has been extensively studied in many organisms, such as plants and animals, the key regulators of intracellular homeostasis in diatoms have not yet been identified and characterized. Our collaborators at the Stazione Zoologica Anton Dohrn (Naples, Italy), who were initially interested in nitrogen acquisition by diatoms, created knockout mutants of putative low-affinity nitrate transporters in *P. tricornutum*. Unexpectedly, the *Ptnpf2* knockout (KO) mutant did not show phenotypic changes under low-nitrogen conditions but displayed distinct phenotypes when the external pH was suddenly altered. In line with this, *Ptnpf2* showed differential gene expression under varying pH conditions (Santin et al., 2021). Transcriptomic data was also obtained for WT and *Ptnpf2* KO strains at pH 7 and 8, as well as internal pH measurements. *Ptnpf2* KO mutants displayed higher internal pH values than WT 24 and 48 hours after shift to low pH, with values closer to those measured under normal pH conditions. This difference indicates a disruption of internal pH homeostasis in *Ptnpf2* KO mutants compared to other strains.

To infer the role of NPF2 in *P. tricornutum* metabolism and pH homeostasis, I studied the phenotype of *Ptnpf2-YFP* overexpressing (OE) and *Ptnpf2* KO strains in collaboration with Anna Santin, who visited the laboratory for three months. No growth differences were observed under normal pH conditions. However, after a shift from high to low pH (8 to 7), a 25% reduction in cell concentration was noted in *Ptnpf2* KO mutants within 24 hours, compared to WT and *Ptnpf2-YFP* OE strains. We also investigated this transient phenotype focusing on photosynthetic performance, particularly electron transport rate. A lower maximum relative electron transport rate ($rETR_M$) was observed in *Ptnpf2* KO mutants compared to WT at 3 and 24 hours after shifting to pH 7, an effect not observed at pH 8. We also analysed NPQ because of its close relationship with acidification of luminal pH. Although no differences were observed between strains at normal pH, *Ptnpf2* KO strains showed a significant increase in NPQ capacity compared to other strains after 24 and 48 hours after the shift to low pH. In general, NPQ responses were observed later (at 24 and 48 hours) compared to Fv/Fm and ETR responses (at 3 and 24 hours). This suggests acclimation responses in *Ptnpf2* KO strains to limit potential light stress by upregulating the synthesis of components involved in NPQ, such as xanthophyll cycle pigments and enzymes (Blommaert et al., 2021) and Lhcx proteins (Buck et al., 2019).

These molecular and functional genetic analyses provide new insights into NPF2 and its role as a key regulator of intracellular homeostasis. Collectively, our results demonstrate that *P. tricornutum* NPF2 protein is localized in a specific compartment between the four chloroplast membranes of diatoms, playing a crucial role in controlling photosynthesis and photoacclimation processes, as well as in maintaining intracellular pH homeostasis. Moreover, transcriptomic analyses of WT and NPF knockout mutants revealed a global regulation of stress-inducible genes, which are essential for maintaining redox homeostasis.

5.2.3 Functional characterization of lower glycolysis-gluconeogenesis mutants

For this collaboration, my supervisor and I, were contacted by Richard Dorrell, from Chris Bowler's lab at the Institut de Biologie de l'École Normale Supérieure to help for the characterization of the photosynthesis-related phenotype *P. tricornutum* strains. The complex evolutionary scheme of diatoms is best reflected by their intricate metabolism,in which various pathways of diverse origins intersecting in, often, unique ways. Moreover, diatoms are well-known for the extensive crosstalk and metabolites bifurcations between plastids and mitochondria (Prihoda et al., 2012, Bailleul et al., 2015, Broddrick et al., 2019). This project focused on two enzymes family, the phosphoglycerate mutase (PGAM) and phosphoglycerate enolase (Enolase, from here-onward), involved in the glycolysis–gluconeogenesis pathways. The interest for investigating the role of these proteins in diatoms was two-fold **i)** Their localization contrasts from the ones of plants. Diatoms realized the lower-half of the glycolysis in the mitochondria, by contrast to plants for which it is located in the cytosol (Kroth et al., 2008) and, **ii)** Environmental 'omic data suggest an important role for these proteins, especially at high latitudes.

Therefore, we grew these multiple strains, mutated in Enolase or PGAM isoforms, in conditions reflecting polar conditions, continuous light and low temperature. My role was to investigate for a photosynthetic phenotype in this strains using variable fluorescence. However, we did not find any significant photosynthesis phenotype (the reader is referred to the published paper (Dorrell et al., 2024) for the full details of the analysis done). More than a negative result, this is at the contrary an important finding since it indicate a robust network of redundant molecular actors with overlapping functions. Which could reflects the expansion of these enzymes families into multiple isoforms and their high expression in natural (high latitude) environments.

5.2.4 Deconvolution of photosynthesis in microalgal mixtures and application to allelopathy

My Ph.D. research focuses on the mechanistic aspects of photosynthesis regulation, where I have adopted a reductionist approach, downplaying the influence of external factors to light stress alone. I intentionally chose this approach because it allows for a clearer examination of the phenomenological relationships between regulatory modules and the interactions between photosynthetic processes, information that might be obscured in a more complex and less controlled system. However, aware of the limitation of such lab work on a model organism like *P. tricornutum*, I was happy to participate to a collective work aiming at investigating the response of microalgal consortia to stresses.

To adapt and thrive in diverse environments, algae rely on a variety of physiological, biochemical, and behavioural strategies to regulate and respond to abiotic stresses such as light, temperature, and nutrient availability. However, the fate of photosynthetic organisms is not solely determined by their ability to respond to abiotic changes. Biotic interactions also play an important role in the dynamics and structuring of microalgal communities. These interactions include relationships with bacteria, fungi, viruses, and other photosynthetic competitors, involving competition for nutrients and allelopathy, the release of toxic secondary metabolites. Allelopathy, which involves the direct inhibition of competing organisms by secondary metabolites, can have a significant impact on phytoplankton population dynamics, such as in some "red tides" produced by toxic dinoflagellates. Allelopathic effects have

been observed in all major phytoplankton clades, but the network of allelopathic interactions within phytoplankton, and the nature and targets of the secondary metabolites involved, remain largely unknown.

One reason for this is the difficulty of simultaneously measuring the physiological responses of each species in mixed cultures; traditional methods typically assess the effect of the supernatant of one species on the growth of another. This approach is not only time-consuming but also neglects some phenomena that require direct cell-to-cell contact, and is not well suited to the study of allelopathy in biofilms, for example. Although the targets of most allelopathic interactions in phytoplankton are not well known, it is likely that, as in higher plants, photosynthesis is the main target, including inhibition of photosynthetic electron transfer (at PSII or Rubisco), uncoupling of the transmembrane proton gradient, or inhibition of ATP synthase. Although knowledge of allelopathy in marine organisms is limited, the available evidence supports this hypothesis. For example, fischerellin A, an allelopathic compound produced by the cyanobacterium *Fischerella muscicola*, inhibits PSII activity in cyanobacteria and green algae (Srivastava et al., 1998). In addition, various aldehydes secreted by diatoms have been shown to affect the activity of the ATP synthase or some enzymes of the Calvin-Benson-Bassham cycle in other species (Wolfram et al., 2015).

To study these phenomena in marine microalgae, in the frame of the ERC PhotoPHYTOMICS granted to my supervisor, we collectively developed an innovative method based on ECS signals, i.e., changes in the absorption of photosynthetic pigments induced by the transthylakoid electric field generated during photosynthesis. The observation that ECS spectra are conserved within each clade but differ between clades (such as diatoms, chlorophytes, prasinophytes and dinoflagellates) led us to overcome an important methodological obstacle: we can now use these signals to deconvolute the photosynthetic activity of several microalgae in a mixture. The ability to extract the photosynthetic behaviour of individual species in a mixed culture and compare it to that in monoculture allowed us to identify the photosynthesis inhibition phenomena that occur when different microalgae are mixed and allelopathy is at play.

My contribution to this work took place during a five-week mission at the Roscoff Biological Station. We used strains from the Roscoff Culture Collection (https://www.roscoff-culture-collection.org/) to test allelopathic interactions within a 14 x 14 species matrix. Potential allelopathic effects were identified in about a third of the microalgae pairs. Notably, the dinoflagellate *Amphidinium carterae* demonstrated a strong allelopathic effect, completely inhibiting photosynthesis in 5 of the 13 other strains. I also used this opportunity to show that the photosynthesis and growth of *P. tricornutum* is not affected by *A. carterae*. With the microalgae mixture ECS deconvolution method, we also observed, unexpectedly, that photosynthesis in some microalgae (the haptophytes *E. huxleyii* and *T. lutea*, and the green algae *Chlorella* sp. and *Micromonas bravo*) is inhibited by the presence of *P. tricornutum*. To determine whether these effects were indeed mediated by secreted secondary metabolites, we compared these results with classical methods involving growth in co-culture vessels, where each species was placed in one of two glass vessels connected by a semi-permeable membrane that allows the passage of secondary metabolites but not of microalgae. This comparison confirmed that the growth inhibition observed over one week in these co-culture systems correlated perfectly with our 5-10 minute test based on photosynthesis in mixture.

A manuscript is in preparation which should be submitted before the end of 2025.

Croteau D.*, Ferté S.*, Israelievitch E.*, Peltekis A.*, Gachenot M., Cran L., Santabarbara S., Cardol P., Guillou L., & Bailleul B. An ECS-based method allows deconvolution of

photosynthetic activities in microalgal mixtures. (* co-first authors) (in preparation).

Chapter 6

General discussion and conclusion

In this general discussion, I would like to discuss three important points. First, if this thesis reveals insights into the general orchestration of photosynthesis regulation in pennate diatoms, we are still far from the detailed understanding of this orchestration in plants. I would therefore like to ponder the question of whether the general observation that the ΔpH playing the role of "master-regulator" in green organisms, also applies to diatoms? Second, I would like to think of the possibility of generalizing my findings to other less well-studied, secondary-endosymbiotic photosynthetic organisms, which typically form the major fraction of the phytoplankton. Last, I will discuss the role of NPQ supporting organisms' fitness and especially on growth, which is not a trivial question at all.

6.1 Is the ∆pH a master-regulator of photosynthesis in diatoms?

In the introduction, I defined the overarching objective of my thesis as "improving holistic understanding of photosynthesis regulations in diatoms and their orchestrations at the organismal level". The most straightforward way to understand the dynamics of how interacting phenomena are being orchestrated is to identify the conductor, or the "master-regulator". In green organisms, this conductor is commonly described to be the ΔpH (Kramer et al., 2003, Armbruster et al., 2017, see also the reviews of my co-authors and I in Chapter 2). At the moment I began my Ph.D., that question had only been explored with pharmacological inhibitors in diatoms (Ting and Owens, 1993, Lavaud and Kroth, 2006, Grouneva et al., 2009) and concepts found in plants were often ascribed to diatoms by homology rather than backed up with demonstration at the molecular level. This rapidly changed, first with the demonstration that for Lhcx1, the lumen exposed acidic residues do not seem involved in pH-sensing to induce NPQ (Buck et al., 2021, Giovagnetti et al., 2022), contrary to the case of PsbS or LHCSR3 (green organisms qE component of NPQ). Then, Seydoux et al., 2022 published the characterization of KEA3 mutants, and argued for a direct, and significant, role of the ΔpH in steering NPQ relaxation in the dark, at odds with (Blommaert et al., 2021) and my findings reported in the previous chapter (see Section 5.1.9). But even ignoring this point of contention, the simple fact that NPQ is dominated by a qZ, rather than a qE component, makes the ΔpH less critical in pennate diatoms than in green organisms for the regulation of photoprotection.

The second regulation feature of the ΔpH that inevitably has to be brought up in the "master-regulator" discussion, is the so-called "photosynthetic control" by which the luminal

pH slows down the Rieske protein movement and thus, the turnover of cyt. b_6f (Tikhonov, 2014). Crucially, the limiting step of electron transport under non-limiting light regimes is often at the cyt. b_6f (Wilhelm and Wild, 1984, Sukenik et al., 1987).

One of the big surprises of my Ph.D. was to observe a strong increase in relative cyclic electron flow (CEF) with increasing qZ under high light exposure. We also corroborated this observation by measuring a concomitant increase in photochemical rate, which estimates the sum of PSI and PSII activity at a given light intensity (Fig. 2 in Chapter 4). This raises questions about the way the two electron flows interact with each other. Both CEF and LEF share the same electron carriers besides the "cycling step" and PSII, which is only involved in LEF. Our experiment first shows that under high light, independently of qZ, the quantum yield of PSII, which determines LEF rate, decreases relatively more than does the quantum yield of PSI, on which both LEF and CEF depend. This already suggests compensation of a limited LEF under high light intensity by CEF. Even more striking is that although the LEF output remained roughly constant as a function of qZ across strains, Q_A oxidation (estimated via qL (Kramer et al., 2004)), and by extension the oxidation of the PQ-pool, increased (Fig. 2 in Chapter 4), and so did the CEF (higher in Lhcx1-overexpressors than in WT and Lhcx1-Ko). These two observations indicate competition between the two electron transport pathways. The CEF/LEF competition is typically expected to occur over the PQ-pool (J. F. Allen, 2003, Alric, 2015) or over the stromal pools of NAPDH and/or ferredoxin (Johnson, 2003, Alric et al., 2010). Although recent models argued against a regulation of CEF by the PQ-pool based on new structural insights about the cyt. b_6 (Nawrocki et al., 2021), our results are strikingly compatible with such a regulation mode.

Regardless of the site of competition between CEF and LEF, both should be subject to photosynthetic control as they share the PQH_2 oxidation step in cyt. b_6. Our results suggest that CEF either evades photosynthetic control, or that changes in luminal pH as a function of qZ (under 570 µmol photons m^{-2} s^{-1} illumination) are such that PQH_2 oxidation is not the limiting step to total electron flux, and that CEF is favoured over LEF, possibly by a more oxidized PQ-pool. At first glance, this could simply indicate that the pH reached under saturating light regime is not acidic enough to exert photosynthetic control in diatoms. Fundamental differences in the (not resolved for diatoms) structure of cyt. b_6f could be contemplated, but the structure of mandatory complexes tends to be strictly conserved by comparison with the diversity of regulation modes seen among photosynthetic groups (Falkowski et al., 2008). Of interest is the protonation of the Rieske protein histidine residue involved in gating photosynthetic control which occurs at pH below 6.2 (Tikhonov, 2014). The points raised in the previous discussion (Section 5.1) suggest it is not out of question that even under high light, luminal pH in *P. tricornutum* remains around this tipping point, and allows some leeway to the rate of PQH_2 oxidation, which could be influenced by the level of qZ (note that this is usually not considered in organisms relying on PsbS or LHCSR3 for NPQ because low luminal pH is taken for granted when NPQ is high, a shaky assumption in *P. tricornutum*). However, higher CEF is usually associated to an increase in ΔpH (Munekage et al., 2002) (suggesting lower luminal pH in Lhcx1 overexpressing strains), which actually helps to set photosynthetic control in motion (and trigger NPQ). This is usually interpreted as a crucial regulation to avoid PSI acceptor side limitation, which leads to critical PSI photodamages (PSI is devoid of repair cycle) (Sonoike, 2011). However, if indeed ATP generation lags behind electron transfer in diatoms, as suggested in the previous Section 5.1.9), a CEF-dependent ΔpH increase could be completely buffered in diatoms.

This raises the question of whether the stromal "cycling step" could limit electron flow (as contemplated before (Alric, 2010)) and perhaps, partly explain the CEF up-regulation we

observed as a function of qZ? A stromal redox poise to electron flow, has been reported before in plants (Johnson, 2003, Hald et al., 2008), with a pH midpoint of 7.7. Thus, within ideal range for modulation by stromal pH fluctuation under light in *P. tricornutum* (Shimakawa et al., 2023). Also interesting is that such a pathway is predicted to be mediated by a thioredoxin (Johnson, 2003). Many thioredoxin genes showed up-regulated expression under high light, but qZ-countered, in our transcriptomic experiment (metacluster 2 in Chapter 4), including some with plastid as predicted subcellular target. However, this would open the door to a higher susceptibility of diatoms to PSI acceptor side limitation, which has never been observed (see Chapter 4) or, in fact, thoroughly investigated. An interesting alternative electron flow which could enhance robustness against PSI acceptor side limitation in diatoms, is their capacity to funnel electron towards the reduction of stored NO_3^- to ammonium (McCarthy et al., 2017), which can be excreted outside of the cell (Lomas and Glibert, 1999, Lomas et al., 2000). This mechanism is also exacerbated by cold stress, typical conditions associated to PSI photodamages (Sonoike, 2011).

Before continuing it is worth reminding that I am already treading on highly speculative grounds, but I was told my thesis conclusion is the last time I will be as free to do so! But, in all seriousness, what makes these ideas even worth mentioning here, is at the heart of my Ph.D., we have the perfect experimental model to test these hypotheses. That is, the Lhcx1-molecular titration of *P. tricornutum* mutants, *and* a unique method to gauge *in vivo* the ΔpH (Chapter 5). For instance, the pH-dependency of cyt. b_6f turnover was characterized *in vivo* thanks to a *C. sorokiniana* antenna mutant, which displays the quadratic ECS probe that allows to estimate luminal pH (Finazzi and Rappaport, 1998). This work can now be undertaken in diatoms. Together with our Lhcx1-mutant series, it could hopefully set the stage to investigate trade-offs between regulations of electron flow via the PQ-pool (accurately estimated by qL in *P. tricornutum*), the ΔpH and the yield of PSI acceptor side limitation (ΦNA). All in all, I am raising questions about if it is wise to consider a monolithic, ΔpH-dependent, constraint on electron flow under physiological conditions? And is it possible that the points I am raising here reflect diatoms versus green organisms discrepancies? I will not dare consider the whole literature on Viridiplantae here, but I want to end by highlighting an example in the green algae *Chlamydomonas reinhardtii* with which I am familiar.

A previous Ph.D. candidate under Benjamin Bailleul, Suzanne Ferté, investigated the diversity of CEF regulation in three microalgae under the same 130 µmol photons m^{-2} s^{-1} illumination. A DCMU titration was used to gradually decrease PSII available acceptor concentration, thus decreasing LEF (estimated via ΦPSII), to compare it to the resulting variation in LEF+CEF (estimated via ΦPSI) (Ferté, 2019). In *C. reinhardtii*, this experiment revealed a competition model between both fluxes, by which CEF could fully compensate for the decrease in LEF. This is very interesting to compare to the experiment in *P. tricornutum* that I reported in Chapter 4, where I showed that for higher qZ, everything else being roughly equal, Q_A oxidation also increased, but LEF remains roughly constant. In this case, we see an *upregulation* of CEF, meaning that CEF did not only take the "space" left behind by a decreasing LEF, but rather increased as a function of qZ (N.B., photochemical rate increased together with higher CEF, which was not the case for (Ferté, 2019)). Like mentioned above, a more oxidized PQ-pool could partake in this regulation. Moreover, for the sake of argument, let's take for granted that luminal pH remained above the required level to make PQH_2 oxidation the limiting step of electron transport in *P. tricornutum*, as well as in *C. reinhardtii* with DCMU impeding PSII water-oxidation and the moderate light intensity used (Ferté, 2019). Then, the most significant difference between the two experiments is the constant LEF transferring reducing power to the stroma in *P. tricornutum*. Putatively,

this could be what allows CEF up-regulation, while in the DCMU experiment, production of reducing power is artificially decreased, until complete abolishment, by DCMU addition for CEF to increase. Perhaps, what makes visible in *P. tricornutum*a glimpse of this hypothetical regulation triangle, the redox state of PQ- and NADPH-pool, and the ΔpH, is not a diatoms versus green discrepancy. Rather, it might be related to a lower accumulation of ΔpH under light in microalgae (including Chlorophyceae), due to important ATP consumption and luminal protons uptake by carbon concentrating mechanisms (Kikutani et al., 2016, Burlacot and Peltier, 2023).

6.2 Applying our findings beyond *P. tricornutum* and pennate diatoms

Another important research avenue that opens up with this thesis, more precisely in Chapter 3, is whether the qZ component of NPQ is widespread in the phytodiversity. More specifically, can we, in most phytoplankton species, identify a nonphotochemical quencher dependent on the activity of the xanthophyll cycle and behaving as a Stern-Volmer homogeneous quencher? In *P. tricornutum*, we demonstrated that the simple relationship:

$$\mathrm{qZ} = \kappa_{\mathrm{SV}} \times [\mathrm{Lhcx1}] \times \mathrm{DES} \tag{6.1}$$

is a good approximation of total NPQ. But, is it the same for a large fraction of phytodiversity or is this simple case an oddity? There is already a lot in the literature to start hypothesizing about the question. Let's start with pennate diatoms. For a given species, it is regularly reported that the NPQ/DT slope decreases for growth under high, more stressful, light intensity compared to growth under moderate light intensity. This has been usually interpreted as an increase of xanthophyll cycle pigments in the lipid membranes playing an antioxidant role. Now, we can additionally wonder if changes in the NPQ/DES slope reflect changes in Lhcx content (of any isoform behaving like Lhcx1-2-3 of *P. tricornutum*) (Buck et al., 2019, 2021). In fact, it is the observation of a smaller NPQ/DT slope together with a constant NPQ/DES slope in *P. tricornutum* grown under moderate light compared to lower growth light, that led Schumann and al., to first propose that changing NPQ/DT slopes, or DT quenching efficiency, reflect DT partitioning among different pools and that only the one interacting with PSII could participate in NPQ (Schumann et al., 2007). There is also the case of the "natural Lhcx1 knockdown" *P. tricornutum* ecotype, Pt4, isolated in the Baltic Sea. Pt4 has been reported to have lower NPQ than Pt1 for the same de-epoxidation state (DES) (Bailleul, Rogato, et al., 2010). In another study, by comparison with Pt2 (almost identical to Pt1), Pt4 displayed higher DES but equal NPQ (Lavaud and Lepetit, 2013). What were question marks in these original papers now seem almost self-explanatory, more DES is required for equal NPQ/qZ (or Q) if the interaction site with Lhcx is less abundant (although, like in the manuscript of Chapter 3, it is important to note that changes in PSII cross-section size would need to be access to solidify this hypothesis). What happens if we try to expand this hypothesis to reinterpret published data in other pennate diatom species? In previous work undertaken during my M.Sc., my collaborators and I presented the variations in NPQ/DT slopes between five Arctic diatoms species (comprising two pennates), which overall decreased from low to moderate growth light acclimation (Croteau et al., 2021). Returning to this data set, we can now look at the NPQ/DES slopes (not shown in the original paper) with new insights (Fig. 6.1). Rather than decreasing, the NPQ/DES

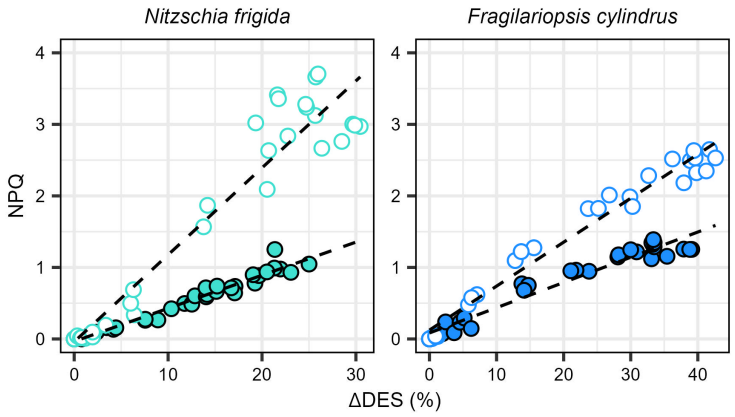

Figure 6.1: The NPQ/ΔDES slope (DT is always persistent in Arctic diatoms, therefore only light-induced DES variations are considered), in the sea-ice low light specialist *Nitzschia frigia* (turquoise) and the sea-ice/planktonic *Fragilariopsis cylindrus* (blue), closed symbols are measured in strains acclimated to low light growth and open symbols to moderate light growth.

slopes increased with more intense growth light intensity, which would indicate either higher Lhcx1 concentration or accumulation of isoforms with higher capacities to make DT an efficient quencher (κ_{SV}). Moreover, the relative growth light intensity-dependent increase in the NPQ/DES slope is higher in the sea-ice low light specialist *Nitzschia frigia* than in the sea-ice/planktonic *Fragilariopsis cylindrus*. This is compatible with a more pronounced stress response and mobilisation of Lhcx proteins in *N. frigida*, the only of the two species which showed growth photoinhibition under the moderate growth light intensity.

As mentioned in Chapter 3, things often appear more complicated in centric diatoms (Grouneva et al., 2008, Dong et al., 2015). As the generation of the first Lhcx knockouts in *T. pseudonana* has been recently reported, the present model offers a robust null hypothesis for more scrupulous studies of NPQ in a model centric species (Nakayasu et al., 2024). However, surprisingly considering a more distant phylogenetic relationship, Equation 6.1 could be a more powerful tool to unravel NPQ, and its influence over other regulatory processes, in haptophytes (see also the case of *Phaeomonas* sp., a Pinguiophyceae, i.e., sister group to stramenopile (Berne et al., 2018)). First in the model haptophyte species *Tisochrysis lutea*, the patterns of NPQ behaviour, with respect to different Lhcx isoforms and DT/DES, is reminiscing of what is usually observed in pennate diatoms (Pajot et al., 2022, Pajot et al., 2023, T. Lacour et al., 2023). A simple Stern-Volmer nonphotochemical quencher model would also permit to test if echinenone contributes to NPQ in *T. lutea*. This is an interesting question considering that the obligatory orange-carotenoid-protein partner of echinenone for NPQ in cyanobacteria (Kusama et al., 2015), appears mysteriously absent in *T. lutea* (T. Lacour et al., 2023). Moreover, during a rapid screening of our microalgae collection at the lab, it was common to find haptophyte species showing a single NPQ component decaying mono-exponentially in the dark, compatible with qZ at the phenomenological level (Fig. 6.2). Interestingly, this could be observed in representatives of both major haptophytes classes, Pavlovophyceae (*Exanthemacrysis* sp. and *Pavlova lutheri*) and Prymnesiophyceae (*T. lutea*), but unfortunately not *Emiliania huxleyi* (not shown), one of the largest contribut-

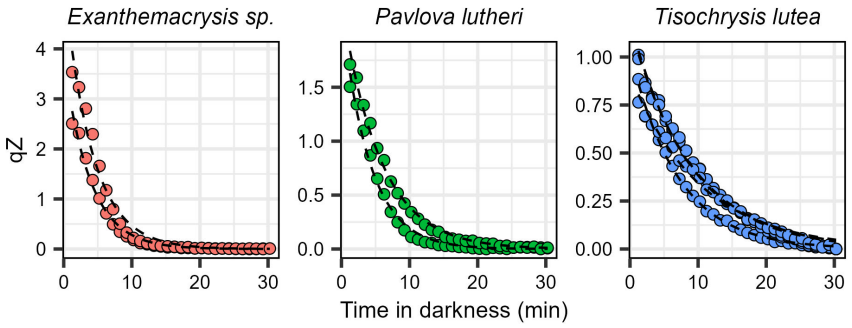

Figure 6.2: Single NPQ component relaxing in the dark after high light exposure as a mono-exponential decay, compatible with a qZ mechanism in three different haptophyte species .

ing species to oceanic primary production.

It is important to note that we do not conclude from this work that *P. tricornutum*, and the other species/groups mentioned to date, are the only microalgae for which NPQ is well represented by qZ. We suggest qZ is likely an important component in many marine microalgae, including centric diatoms. But we show that, by *chance*, pennate diatoms (and possibly many haptophytes) are *convenient* models to investigate qZ since it is the only NPQ component present, in addition to the slowly-reversible qI.

Another facet of my work worth considering in the context of microalgae diversity, is the introduction of the new parameter Δ(TEF/LEF) to investigate relative changes in CEF over LEF. The importance of CEF in photosynthesis regulation has been made abundantly clear over this thesis, but it is largely ignored in studies of secondary endosymbionts. One reason could stem from legacy of research on cyanobacteria and green organisms over which CEF has acquired a reputation of being a notoriously elusive parameter to gauge. The reason is that measuring absolute values of CEF requires measuring simultaneously absorption cross-section of both PS in addition to their yields (Finazzi and Forti, 2004). However, we showed that because diatoms seem to not possess state transitions (Owens, 1986), we can circumvent this problem by measuring relative changes in CEF only by measuring PS quantum yields and computing Δ(TEF/LEF) (see Methods in Chapter 4), assuming both PS cross-section are unlikely to change during the course of an experiment. At least lab settings, ΦPSII and ΦPSI are easily measurable in commercial instruments such as Joliot-type spectrometers (commercialized by BioLogix, KS, USA) or Dual-Pam (Walz, Germany). Therefore this parameter could be used in other pennate diatoms from now on. Indeed, the experiment we showed in the bottom panels of Fig. 2 in Chapter 4, does not require an intricate molecular titration restricted to model organisms. The effect of the magnitude of qZ over Δ(TEF/LEF) can be explored over qZ slow relaxation under low light in any wildtype strain, as we showed in the pennate diatom *Plagiostriata* sp. (Fig. 6.3). This protocol could be used to test qZ-dependent competition between CEF and LEF following acclimation to various growth conditions (temperature, light intensity, nutrients availability, etc.,) in different groups for example.

Additionally, the prevalence of state transitions among the phytodiversity is not a question that has been properly addressed yet. Indeed, research on state transitions occupy a large portion of photosynthesis regulation studies in green organisms, especially in green algae with mixotroph metabolism. State transitions are regulated by the redox state of the PQ-pool, which is strongly affected by mixotrophy. This make state transitions, once again

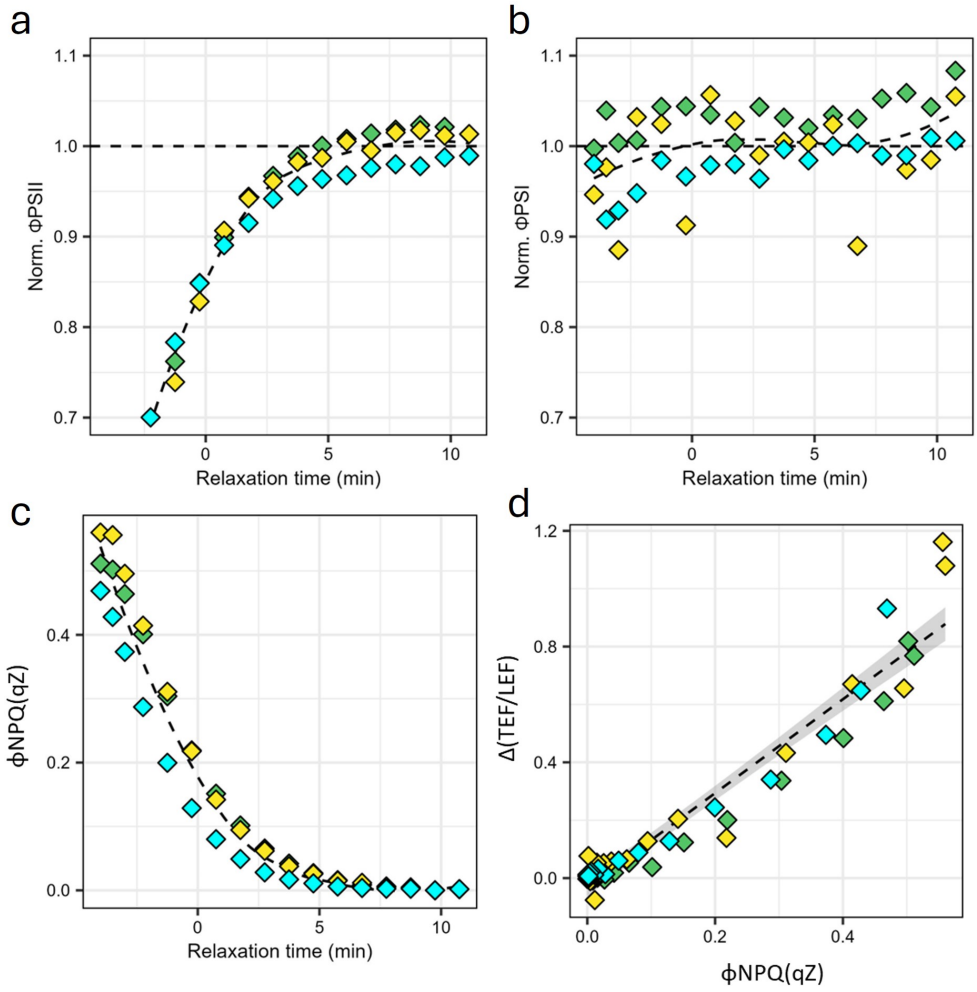

Figure 6.3: After exposure to high light and NPQ/qZ deployment in the pennate diatoms *Plagiostriata* sp. (grown under 60 µmol photons m^{-2} s^{-1} 12:12 photoperiod), the recovery of ΦPSII (a) and ΦPSI under low light are shown (b) normalized to their respective values once qZ is fully relaxed, relaxation of the qZ component of ΦNPQ (c) and the linear relationship between Δ(TEF/LEF) and ΦNPQ(qZ). Three independent biological replicates are shown in different colours.

by *chance*, a particularly convenient mechanism to study in mixotroph green algae (Wollman, 2001, Lucker and Kramer, 2013). The same can be said for cyanobacteria in which respiration and photosynthesis share some complexes embedded in a common membrane (Calzadilla and Kirilovsky, 2020). One can surely finds sporadic reports of state transitions in some haptophytes (Stamatakis et al., 2019) or cryptophytes (Cheregi et al., 2015) in the literature, but the phenotype on which this conclusion is made can be quite heterogeneous. A rigorous screening of multiple representatives of different, non-green, eukaryotic microalgae groups, with benchmark protocols to modulate the redox state of the PQ-pool and explore the existence of state transitions would be extremely valuable. Convergence in photosynthesis regulation mechanisms among groups is, in and of itself, interesting, but there is more at stake here. Maybe, the reputation of CEF being a "notoriously elusive parameter to measure" is not warranted for most species/groups forming the phytoplankton? At least when it comes to relative changes between the two fluxes, perhaps the Δ(TEF/LEF) parameter is valid, that is, if enough experimental evidence suggest state transitions are rare in secondary endosymbiotic organisms.

6.3 The unclear role of NPQ in supporting growth and concluding remarks

One of the most fundamental question that ought to be addressed at some point during this thesis is the place of NPQ in supporting growth. At first glance, NPQ (like some other alternative electron fluxes, for instance photorespiration) is a "waste" of light energy, dissipated as heat. Because nonphotochemical reactions (in the Calvin–Benson–Bassham cycle for instance) tend to be slower than photochemistry, and because of photoacclimation processes, light is rarely limiting photosynthetic growth in nature (although there are some cases like polar regions or shaded plants below a dense canopy). Accordingly, NPQ is commonly viewed as making organisms more fit to dynamic environments by enabling them to control reduction pressure on PSII and to limit oxidative stress, when electron transfers and proton pumping outpace metabolic needs upon sudden shift in environmental conditions. I described in Chapter 3 how qZ strictly downregulates PSII *functional* cross-section. However, in parallel to triggering NPQ deployment, environmental variations are signals integrated by the organism, which steers gene expression and photoacclimative processes. These processes evolved to minimize the risk of detrimental mismatch between the photochemical and nonphotochemical phases of photosynthesis and avoid photodamages to support growth and reproductive success of organisms. For example, the size of PSII *optical* cross-section can be decrease by reduced synthesis of light absorbing pigments and carbon fixing enzymes abundance can be increase under a more intense light environment. Moreover, we saw that NPQ itself comprehensively modulates triggers of gene expression upon high light shift (Chapter 4), which can affect the expression of the genes encoding the NPQ molecular actors themselves. All of this form complex networks of regulation and feedback loops investigated over the course of my Ph.D. These "complex system problems" (Section 1.5.1) make quantifying the role of NPQ in supporting growth under dynamic light conditions particularly challenging.

Nevertheless, after praising the strength of our experimental approach, it would have been unfortunate to shy away from attempting to find a growth phenotype in our series of Lhcx1-mutants. Even though my supervisor had warned me that many attempts had failed (using only a wildtype and a Lhcx1 knockdown mutant, but in turbidostats constant conditions) because of the redundant roles of the different isoforms of Lhcx. Indeed, one of the caveats

to our molecular titration approach is that over longer stress, we expect to see appearance of other Lhcx isoforms (Lhcx2-3), or shift in xanthophyll cycle enzymes output, dampening the qZ contrasts across our mutant series. In a first experiment, I selected six complemented lines (no wildtype or Lhcx1-Ko for an even "pleiotropic playing field") with ranging Lhcx1 expression. 24 h after re-diluting cultures by a factor five (all from exponential growth phase), I started applying a high light stress (HL) of 1 h/600 µmol photons m^{-2} s^{-1} to the strains before returning them to their usual low light (LL) conditions, for four consecutive days. This intermittent HL stress was chosen to imitate the protocol used for the photoinhibition and transcriptomic experiments used in Chapter 4, and to hopefully limit increases in qZ capacities among strains due to photoacclimation. Unfortunately, or perhaps as expected, I did not observe any clear Lhcx1-dependent growth phenotype (Fig. 6.4). However, less expected, it seemed like NPQ compensation by Lhcx isoforms, or by any other means, had nothing to do with the absence of a growth phenotype between strains. When comparing maximum qZ capacity prior to the first HL stress (Day 1) and the last one (Day 4), all strains displayed a similar and small upward shift in maximal qZ (Fig. 6.4d).

Because all the strains showed increased growth rates under intermittent stress conditions, I thought that maybe the benefits of extra light resource during HL stress could outweigh the negative consequences and potentially hide a growth phenotype. Indeed, the LL conditions we used to grow our Lhcx1-mutant series were chosen to avoid the expression of other Lhcx isoforms, but is growth limiting. I did a second experiment (not shown), in which the strains were grown under LL, exposed to the same 1 h HL stress, but then returned to a 50 µmol photons m^{-2} s^{-1} (growth saturating light intensity). This experiment was done only over one day to avoid extensive photoacclimative processes muddling the conclusions that could be drawn. However, this alternative protocol also did not reveal a Lhcx1-dependent growth phenotype, and the data of these experiments slept in a lost folder for 2 years, until the writing of this discussion... Is NPQ really crucial to avoid the deleterious effects on growth of punctual HL stress in *P. tricornutum*? At least in nutrient replete and roughly optimal lab-conditions, I propose it may not be.

Another relevant example comes from work related to the development of microalgae based-biotechnology. In Perin et al., 2023, different strains of *Nannochloropsis* (*oceanica* and *gaditana*) with mutated genes of NPQ molecular actors are used to compare with the productivity of a WT in extremely dense cultures ("industrial representative conditions"). The mutant strains are either fully lacking NPQ, *vde* and *lhcx1* KOs, or a *zep* overexpressing (OE) strains, which possess a lower maximal NPQ capacity and more rapid NPQ relaxation compared to the WT. Under "industrial representative conditions", growth is light-limited by very high optical density of the cultures, but the cells are exposed to sudden burst of HL (up to 1,200 m^{-2} s^{-1}) when agitation brings them to the surface of the culture vessel. The paper focuses on the significant gain in productivity of *zep* OE versus the WT, explained by a faster NPQ relaxation and less wasted energy when cells move back towards light-limiting conditions, which is a very interesting result. However, another less discussed result is perhaps more surprising, i.e., the fact that the *lhcx1* KO maintained the same productivity (measured in biomass) as the *zep* OE, and therefore higher than the WT (Fig. 6.5). Even more puzzling, parameters commonly used for non-invasive estimation of photosyntheis productivity (variable fluorescence (ETR and qL) and O_2 evolution) were lower in NPQ deprived strains, confirming that the loss of NPQ indeed increased stress on the photosynthetic apparatus (Fig. 6.5). These experiments were carried out in a species with a single Lhcx isoform, over multiple days and exposed to large and frequent light fluctuations. All in all, this seems to argue against a direct role for NPQ in supporting higher growth *even* under light fluctua-

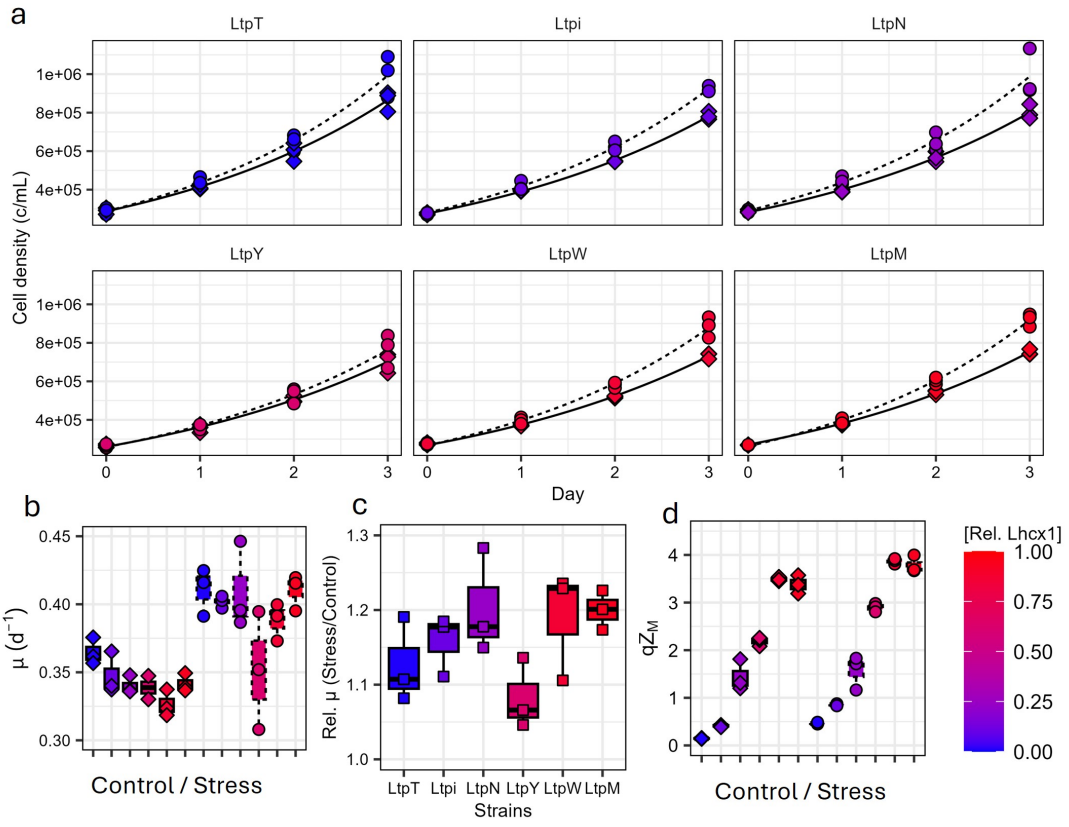

Figure 6.4: Growth experiment over four days for which "Stress" refers to punctual daily high light stress (1 h/600 µmol photons m^{-2} s^{-1}) while "Control" refers to cultures that remained under low intensity growth light meanwhile. Six complemented strains with increasing relative Lhcx1 concentrations are used. (a) Shows cell density against time in days, (b) shows the four days growth rate of the different strains (Control and Stress conditions are left and right, respectively), (c) shows relative growth rate variations between control and stress conditions and, (d) shows maximal qZ after three days of growth for Control cultures and the ones that underwent daily high light Stress. Diamond symbols and dashed lines represented Control conditions and circle symbols and solid lines represent Stress conditions. The blue-to-red colour scale represents relative Lhcx1 concentration in a given strain. The experiment was conducted on three independent biological replicates per strain.

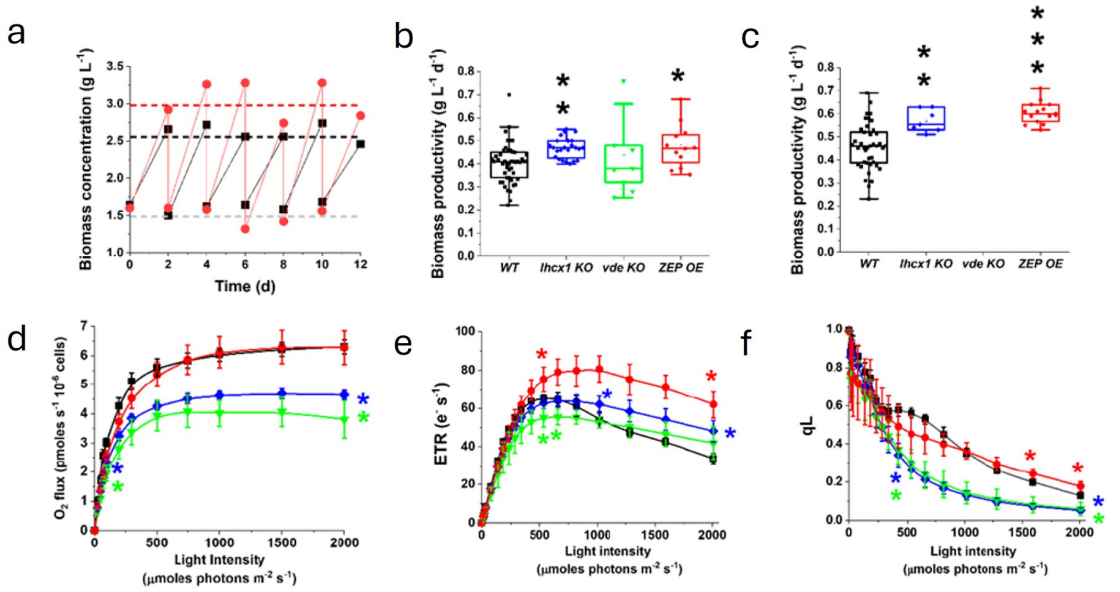

Figure 6.5: Successive dilutions representing *N. gaditana* WT and NPQ-mutant strains grown under very high ("industrial representative conditions") concentrations investigated by (Perin et al., 2023) (a). Biomass productivity under 400 (b) and 1,200 µmol photons m^{-2} s^{-1} growth light intensity (c). The *vde* Ko has reduced productivity versus WT, and both *zep* OE and *lhcx1* Ko have increased productivity versus WT (Fig. 5 in the original paper). Different photosynthetic parameters investigated in all strains, O_2 evolution (d), PSII electron transport (e) and qL (f) (see Fig. S5 in Perin et al., 2023 for details).

tions[1], in conditions where other factors influencing growth are closed to optimal, (nutrients replete and 22°C for instance). Therefore, should it be said that *zep* overexpression increased productivity? Or that it rescued a loss of productivity imputable to NPQ?

The literature in plants is broad and I certainly can not do an exhaustive review of all attempts to reveal NPQ-dependent growth phenotype, but certain examples are highly relevant to this discussion. For instance, slight decrease in growth and CO_2 assimilation under fluctuating light conditions have been reported in PsbS overexpressing (increasing NPQ) lines of *Arabidopsis* (Głowacka et al., 2018) and rice (Hubbart et al., 2012) (but see also (Logan et al., 2008)). Alternatively, (Schiphorst et al., 2023) struggled to find fluctuating light conditions for which *Arabidopsis* PsbS KO growth slowed down and raised similar points to the ones I am discussing here. They ultimately found combinations of light fluctuations and chilling stress that did reduce growth in a PsbS-dependent fashion, and discussed the possibility of PSI photodamages (favoured by low temperatures (Sonoike, 2011)). However, with extensive bioengineering efforts, i.e., transgenic expression of *A. thaliana*'s VDE, ZEP and PsbS in rice, a significant increase in productivity was achieved under fluctuating light, both artificial in greenhouse, and natural in field (Kromdijk et al., 2016). Therefore these mutants are affected in both qE and qZ to accelerate NPQ relaxation during shading events, which seems to enhance growth under fluctuating light. However, cost-benefits discussions about optimal NPQ dynamics should not be strictly centred around energy balance and damage avoidance. In Chapter 4, we saw how much information-rich are photosynthesis-dependent

[1]To be very rigorous the benefits of secondary photoprotective effects of xanthophyll pigment increase in the *lhcx1* KO would also need to be controlled for here.

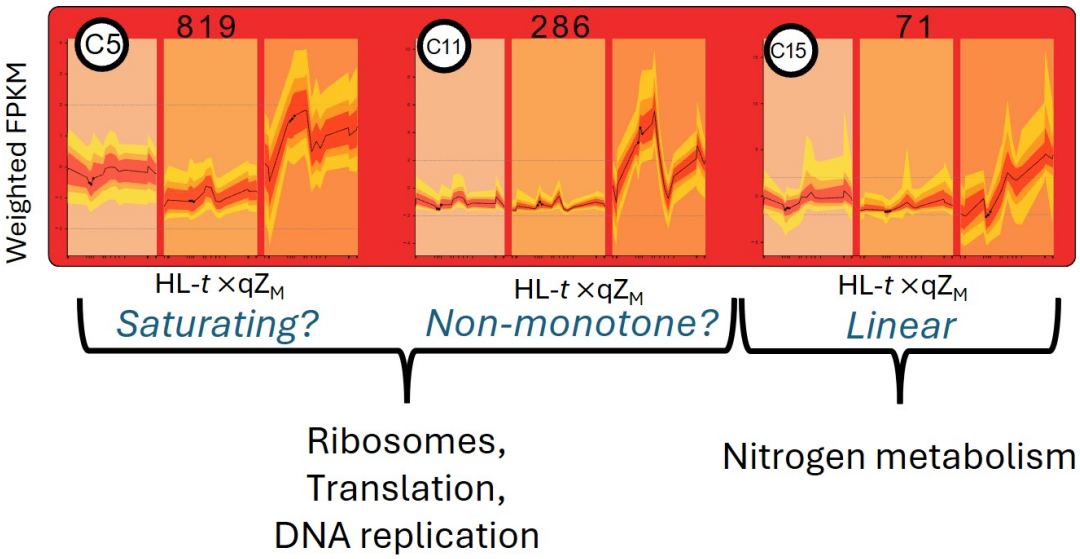

Figure 6.6: Discrepancy in qZ-dependent phenomenological relationships at the cluster level in metacluster 5 (see Chapter 4).

signals for gene expression in *P. tricornutum*. Perhaps, in some cases when abiotic conditions are mostly favourable to tolerate and recover from (some) photodamages, the optimal way to deal with sudden light bursts is to integrate the extremely intricate photosynthetic signals that co-evolved with NPQ of natural-level?

In the aforementioned (Głowacka et al., 2018), the authors suggested that the negative relationships between growth and PsbS could be imputable to a "chloroplast-derived signal for stomatal opening in response to light". Moreover, the trigger of this signal could be related to the redox state of the PQ-pool as they showed a similar positive relationship between NPQ and qL as we did with *P. tricornutum* in Chapter 4. In introduction, I mentioned the phenomenological relationships patterns that one may expect to observe between NPQ and other regulators (Fig. 1.14), and one of them was non-monotone relationships. In the transcriptomic analysis of Chapter 4, we focused on monotone relationships and analysis by metaclusters rather than individual clusters[2]. One peculiar situation drew my attention. In the clusters we regrouped into metacluster 5, described as invariant after 20 minutes of high light exposure and induced in a qZ-dependent manner after 60 minutes of illumination, one could argue upon closer examination, for three different types of phenomenological relationships (without seriously undermining the accuracy of the general description we made of this metacluster). A saturating (cluster 5), a non-monotone (cluster 11) and a small cluster of 71 genes increasing linearly with qZ (cluster 71) (Fig. 6.6).

What is relevant here, is the general function we assigned to metacluster 5 from GO enrichment analysis is "Ribosome; Translation". However, upon reanalysing at the cluster level, it became clear that this characterization is accurate only for clusters 5 and 11. Meaning that the expression of genes in metacluster 5 that we associated with pointing towards enhanced capacity to exploit high light bursts for growth, saturated beyond WT-level of qZ (cluster 5), or worse, declined (cluster 11). By contrast, genes whose expression increased linearly with qZ were very much enriched in nitrogen metabolism related processes. For example, the

[2]This is a huge dataset for which we still need some time to fully process. This decision may change before the submission of the manuscript

plastidial ferredoxin-nitrite reductase is found in cluster 5, together with significant (p.value < 0.05) KEGG enrichment in "Nitrogen metabolism", "Arginine biosynthesis" and "Biosynthesis of amino acids". A lot has been said about the interplays between carbon and nitrogen metabolism, and the crucial role of photosynthetic signals in plants (see the works of Foyer (Foyer et al., 2003, Foyer et al., 2012), and more). But to my knowledge, it has never been reported/considered that unbridled NPQ could disrupt the harmonious orchestration between carbon and nitrogen metabolism. While still speculative, I propose that the upregulation of genes related to nitrogen metabolism in cluster 15 might be mediated by elevated NPQ favouring a more oxidized PQ-pool, and higher cyclic electron flow (CEF). In this scenario, perhaps excessive NPQ causes CEF to out-compete nitrate reduction on the acceptor side of PSI? This observation may illustrate how overexpressing a regulatory process in a complex system can lead to indirect and counter-intuitive effects.

Bibliography

Agarwal, A., Levitan, O., Cruz de Carvalho, H., & Falkowski, P. G. (2023). Light-dependent signal transduction in the marine diatom *Phaeodactylum tricornutum*. *Proceedings of the National Academy of Sciences*, *120*(11), e2216286120.

Ait-Mohamed, O., Novák Vanclová, A. M., Joli, N., Liang, Y., Zhao, X., Genovesio, A., Tirichine, L., Bowler, C., & Dorrell, R. G. (2020). Phaeonet: A holistic rnaseq-based portrait of transcriptional coordination in the model diatom *Phaeodactylum tricornutum*. *Frontiers in Plant Science*, *11*, 590949.

Alexandrina Stirbet, G. (2011). On the relation between the kautsky effect (chlorophyll a fluorescence induction) and photosystem ii: Basics and applications of the ojip fluorescence transient. *Journal of Photochemistry and Photobiology B: Biology*, *104*(1-2), 236–257.

Allen, A. E., Dupont, C. L., Oborník, M., Horák, A., Nunes-Nesi, A., McCrow, J. P., Zheng, H., Johnson, D. A., Hu, H., Fernie, A. R., et al. (2011). Evolution and metabolic significance of the urea cycle in photosynthetic diatoms. *Nature*, *473*(7346), 203–207.

Allen, J. F. (2003). Cyclic, pseudocyclic and noncyclic photophosphorylation: New links in the chain. *Trends in Plant Science*, *8*(1), 15–19.

Alric, J. (2010). Cyclic electron flow around photosystem i in unicellular green algae. *Photosynthesis Research*, *106*, 47–56.

Alric, J. (2015). The plastoquinone pool, poised for cyclic electron flow?

Alric, J., Lavergne, J., & Rappaport, F. (2010). Redox and atp control of photosynthetic cyclic electron flow in chlamydomonas reinhardtii (i) aerobic conditions. *Biochimica et Biophysica Acta (BBA)-Bioenergetics*, *1797*(1), 44–51.

Amstutz, C. L., Fristedt, R., Schultink, A., Merchant, S. S., Niyogi, K. K., & Malnoë, A. (2020). An atypical short-chain dehydrogenase–reductase functions in the relaxation of photoprotective qh in *Arabidopsis*. *Nature plants*, *6*(2), 154–166.

Aranda Sicilia, M. N., Sanchez Romero, M. E., Rodriguez Rosales, M. P., & Venema, K. (2021). Plastidial transporters kea1 and kea2 at the inner envelope membrane adjust stromal ph in the dark. *New Phytologist*, *229*(4), 2080–2090.

Armbrust, E. V., Berges, J. A., Bowler, C., Green, B. R., Martinez, D., Putnam, N. H., Zhou, S., Allen, A. E., Apt, K. E., Bechner, M., et al. (2004). The genome of the diatom *Thalassiosira pseudonana*: Ecology, evolution, and metabolism. *Science*, *306*(5693), 79–86.

Armbruster, U., Carrillo, L. R., Venema, K., Pavlovic, L., Schmidtmann, E., Kornfeld, A., Jahns, P., Berry, J. A., Kramer, D. M., & Jonikas, M. C. (2014). Ion antiport accelerates photosynthetic acclimation in fluctuating light environments. *Nature communications*, *5*(1), 5439.

Armbruster, U., Galvis, V. C., Kunz, H.-H., & Strand, D. D. (2017). The regulation of the chloroplast proton motive force plays a key role for photosynthesis in fluctuating light. *Current Opinion in Plant Biology*, *37*, 56–62.

Aro, E.-M., Virgin, I., & Andersson, B. (1993). Photoinhibition of photosystem ii. inactivation, protein damage and turnover. *Biochimica et Biophysica Acta (BBA)-Bioenergetics*, *1143*(2), 113–134.

Avenson, T. J., Kanazawa, A., Cruz, J. A., Takizawa, K., Ettinger, W. E., & Kramer, D. M. (2005). Integrating the proton circuit into photosynthesis: Progress and challenges. *Plant, Cell & Environment*, *28*(1), 97–109.

Bailleul, B., Berne, N., Murik, O., Petroutsos, D., Prihoda, J., Tanaka, A., Villanova, V., Bligny, R., Flori, S., Falconet, D., et al. (2015). Energetic coupling between plastids and mitochondria drives co2 assimilation in diatoms. *Nature*, *524*(7565), 366–369.

Bailleul, B., Cardol, P., Breyton, C., & Finazzi, G. (2010). Electrochromism: A useful probe to study algal photosynthesis. *Photosynthesis research*, *106*, 179–189.

Bailleul, B., Rogato, A., de Martino, A., Coesel, S., Cardol, P., Bowler, C., Falciatore, A., & Finazzi, G. (2010). An atypical member of the light-harvesting complex stress-related protein family modulates diatom responses to light. *Proceedings of the National Academy of Sciences*, *107*(42), 18214–18219.

Baker, N. R., & Rosenqvist, E. (2004). Applications of chlorophyll fluorescence can improve crop production strategies: An examination of future possibilities. *Journal of experimental botany*, *55*(403), 1607–1621.

Barnett, A., Méléder, V., Blommaert, L., Lepetit, B., Gaudin, P., Vyverman, W., Sabbe, K., Dupuy, C., & Lavaud, J. (2015). Growth form defines physiological photoprotective capacity in intertidal benthic diatoms. *The ISME journal*, *9*(1), 32–45.

Baroli, I., & Niyogi, K. K. (2000). Molecular genetics of xanthophyll–dependent photoprotection in green algae and plants. *Philosophical Transactions of the Royal Society of London. Series B: Biological Sciences*, *355*(1402), 1385–1394.

Bar-On, Y. M., Phillips, R., & Milo, R. (2018). The biomass distribution on earth. *Proceedings of the National Academy of Sciences*, *115*(25), 6506–6511.

Beer, A., Gundermann, K., Beckmann, J., & Büchel, C. (2006). Subunit composition and pigmentation of fucoxanthin- chlorophyll proteins in diatoms: Evidence for a subunit involved in diadinoxanthin and diatoxanthin binding. *Biochemistry*, *45*(43), 13046–13053.

Beer, A., Juhas, M., & Büchel, C. (2011). Influence of different light intensities and different iron nutrition on the photosynthetic apparatus in the diatom *Cyclotella meneghiniana* (bacillariophyceae) 1. *Journal of Phycology*, *47*(6), 1266–1273.

Behrenfeld, M. J., & Boss, E. S. (2014). Resurrecting the ecological underpinnings of ocean plankton blooms. *Annual review of marine science*, *6*(1), 167–194.

Bennoun, P., Spierer-Herz, M., Erickson, J., Girard-Bascou, J., Pierre, Y., Delosme, M., & Rochaix, J. .-. (1986). Characterization of photosystem ii mutants of chlamydomonas reinhardii lacking the psba gene. *Plant molecular biology*, *6*, 151–160.

Berne, N., Fabryova, T., Istaz, B., Cardol, P., & Bailleul, B. (2018). The peculiar npq regulation in the stramenopile *Phaeomonas* sp. challenges the xanthophyll cycle dogma. *Biochimica et Biophysica Acta (BBA)-Bioenergetics*, *1859*(7), 491–500.

Betts, H. C., Puttick, M. N., Clark, J. W., Williams, T. A., Donoghue, P. C., & Pisani, D. (2018). Integrated genomic and fossil evidence illuminates life's early evolution and eukaryote origin. *Nature ecology & evolution*, *2*(10), 1556–1562.

Bilcke, G., Osuna-Cruz, C. M., Santana Silva, M., Poulsen, N., D'hondt, S., Bulankova, P., Vyverman, W., De Veylder, L., & Vandepoele, K. (2021). Diurnal transcript profiling of the diatom *Seminavis robusta* reveals adaptations to a benthic lifestyle. *The plant journal*, *107*(1), 315–336.

Bilger, W., & Schreiber, U. (1986). Energy-dependent quenching of dark-level chlorophyll fluorescence in intact leaves. *Photosynthesis Research*, *10*(3), 303–308.

Bilger, W., & Björkman, O. (1990). Role of the xanthophyll cycle in photoprotection elucidated by measurements of light-induced absorbance changes, fluorescence and photosynthesis in leaves of *Hedera canariensis*. *Photosynthesis research*, *25*, 173–185.

Blommaert, L. (2017). *Photoprotection in intertidal benthic diatoms* [Doctoral dissertation, Ghent University].

Blommaert, L., Chafai, L., & Bailleul, B. (2021). The fine-tuning of npq in diatoms relies on the regulation of both xanthophyll cycle enzymes. *Scientific Reports*, *11*(1), 12750.

Blommaert, L., Huysman, M. J., Vyverman, W., Lavaud, J., & Sabbe, K. (2017). Contrasting npq dynamics and xanthophyll cycling in a motile and a non-motile intertidal benthic diatom. *Limnology and Oceanography*, *62*(4), 1466–1479.

Blommaert, L., Vancaester, E., Huysman, M. J., Osuna-Cruz, C. M., D'hondt, S., Lavaud, J., Lepetit, B., Winge, P., Bones, A. M., Vandepoele, K., et al. (2020). Light regulation of lhcx genes in the benthic diatom seminavis robusta. *Frontiers in Marine Science*, *7*, 192.

Bojko, M., Olchawa-Pajor, M., Goss, R., Schaller-Laudel, S., Strzałka, K., & Latowski, D. (2019). Diadinoxanthin de-epoxidation as important factor in the short-term stabilization of diatom photosynthetic membranes exposed to different temperatures. *Plant, Cell & Environment*, *42*(4), 1270–1286.

Bonente, G., Ballottari, M., Truong, T. B., Morosinotto, T., Ahn, T. K., Fleming, G. R., Niyogi, K. K., & Bassi, R. (2011). Analysis of lhcsr3, a protein essential for feedback de-excitation in the green alga *Chlamydomonas reinhardtii*. *PLoS biology*, *9*(1), e1000577.

Bowler, C., Allen, A. E., Badger, J. H., Grimwood, J., Jabbari, K., Kuo, A., Maheswari, U., Martens, C., Maumus, F., Otillar, R. P., et al. (2008). The *Phaeodactylum* genome reveals the evolutionary history of diatom genomes. *Nature*, *456*(7219), 239–244.

Bradbury, J. (2004). Nature's nanotechnologists: Unveiling the secrets of diatoms. *PLoS Biology*, *2*(10), e306.

Bradbury, M., & Baker, N. R. (1984). A quantitative determination of photochemical and non-photochemical quenching during the slow phase of the chlorophyll fluorescence induction curve of bean leaves. *Biochimica et Biophysica Acta (BBA)-Bioenergetics*, *765*(3), 275–281.

Bricaud, A., Claustre, H., Ras, J., & Oubelkheir, K. (2004). Natural variability of phytoplanktonic absorption in oceanic waters: Influence of the size structure of algal populations. *Journal of Geophysical Research: Oceans*, *109*(C11).

Broddrick, J. T., Du, N., Smith, S. R., Tsuji, Y., Jallet, D., Ware, M. A., Peers, G., Matsuda, Y., Dupont, C. L., Mitchell, B. G., et al. (2019). Cross-compartment metabolic coupling enables flexible photoprotective mechanisms in the diatom *Phaeodactylum tricornutum*. *New Phytologist*, *222*(3), 1364–1379.

Buchert, F., Bailleul, B., & Joliot, P. (2021). Disentangling chloroplast atp synthase regulation by proton motive force and thiol modulation in *Arabidopsis* leaves. *Biochimica et Biophysica Acta (BBA)-Bioenergetics*, *1862*(8), 148434.

Buck, J. M., Kroth, P. G., & Lepetit, B. (2021). Identification of sequence motifs in lhcx proteins that confer qe-based photoprotection in the diatom *Phaeodactylum tricornutum*. *The Plant Journal*, *108*(6), 1721–1734.

Buck, J. M., Sherman, J., Bártulos, C. R., Serif, M., Halder, M., Henkel, J., Falciatore, A., Lavaud, J., Gorbunov, M. Y., Kroth, P. G., et al. (2019). Lhcx proteins provide photoprotection via thermal dissipation of absorbed light in the diatom *Phaeodactylum tricornutum*. *Nature Communications*, *10*(1), 4167.

Buck, J. M., Wünsch, M., Schober, A. F., Kroth, P. G., & Lepetit, B. (2022). Impact of lhcx2 on acclimation to low iron conditions in the diatom *Phaeodactylum tricornutum*. *Frontiers in Plant Science*, *13*, 841058.

Bulychev, A., & Vredenberg, W. (1976). Effect of ionophores a23187 and nigericin on the light-induced redistribution of mg2+, k+ and h+ across the thylakoid membrane. *Biochimica et Biophysica Acta (BBA)-Bioenergetics*, *449*(1), 48–58.

Burki, F., Roger, A. J., Brown, M. W., & Simpson, A. G. (2020). The new tree of eukaryotes. *Trends in ecology & evolution*, *35*(1), 43–55.

Burlacot, A., Burlacot, F., Li-Beisson, Y., & Peltier, G. (2020). Membrane inlet mass spectrometry: A powerful tool for algal research. *Frontiers in Plant Science*, *11*, 1302.

Burlacot, A., & Peltier, G. (2023). Energy crosstalk between photosynthesis and the algal co2-concentrating mechanisms. *Trends in Plant Science*, *28*(7), 795–807.

Butler, W. L. (1978). Energy distribution in the photochemical apparatus of photosynthesis. *Annual Review of Plant Physiology*, *29*(1), 345–378.

Butler, W. L., & Strasser, R. J. (1977). Tripartite model for the photochemical apparatus of green plant photosynthesis. *Proceedings of the National Academy of Sciences*, *74*(8), 3382–3385.

Byrdin, M., Rimke, I., Schlodder, E., Stehlik, D., & Roelofs, T. A. (2000). Decay kinetics and quantum yields of fluorescence in photosystem i from *Synechococcus elongatus* with p700 in the reduced and oxidized state: Are the kinetics of excited state decay trap-limited or transfer-limited? *Biophysical Journal*, *79*(2), 992–1007.

Calzadilla, P. I., & Kirilovsky, D. (2020). Revisiting cyanobacterial state transitions. *Photochemical & Photobiological Sciences*, *19*(5), 585–603.

Campbell, D. A., & Serôdio, J. (2020). Photoinhibition of photosystem ii in phytoplankton: Processes and patterns. In *Photosynthesis in algae: Biochemical and physiological mechanisms* (pp. 329–365). Springer.

Campbell, D. A., & Tyystjärvi, E. (2012). Parameterization of photosystem ii photoinactivation and repair. *Biochimica et Biophysica Acta (BBA)-Bioenergetics*, *1817*(1), 258–265.

Cardona, T. (2015). A fresh look at the evolution and diversification of photochemical reaction centers. *Photosynthesis research*, *126*, 111–134.

Carrillo, L. R., Froehlich, J. E., Cruz, J. A., Savage, L. J., & Kramer, D. M. (2016). Multilevel regulation of the chloroplast atp synthase: The chloroplast nadph thioredoxin reductase c (ntrc) is required for redox modulation specifically under low irradiance. *The Plant Journal*, *87*(6), 654–663.

Carvalho, F., Kohut, J., Gorbunov, M., Schofield, O., & Oliver, M. J. (2016). Mapping antarctic phytoplankton physiology using autonomous gliders. *OCEANS 2016 MTS/IEEE Monterey*, 1–6.

Cavalier-Smith, T. (1998). A revised six-kingdom system of life. *Biological Reviews*, *73*(3), 203–266.

Cheregi, O., Kotabová, E., Prášil, O., Schröder, W. P., Kaňa, R., & Funk, C. (2015). Presence of state transitions in the cryptophyte alga guillardia theta. *Journal of experimental botany*, *66*(20), 6461–6470.

Chua, N.-H., & Bennoun, P. (1975). Thylakoid membrane polypeptides of *Chlamydomonas reinhardtii*: Wild-type and mutant strains deficient in photosystem ii reaction center. *Proceedings of the National Academy of Sciences*, *72*(6), 2175–2179.

Collakova, E., Yen, J. Y., & Senger, R. S. (2012). Are we ready for genome-scale modeling in plants? *Plant science*, *191*, 53–70.

Croce, R., & Van Amerongen, H. (2014). Natural strategies for photosynthetic light harvesting. *Nature Chemical Biology*, *10*(7), 492–501.

Croce, R., Zucchelli, G., Garlaschi, F. M., Bassi, R., & Jennings, R. C. (1996). Excited state equilibration in the photosystem i- light-harvesting i complex: P700 is almost isoenergetic with its antenna. *Biochemistry*, *35*(26), 8572–8579.

Croteau, D., Alric, J., & Bailleul, B. (2023). The multiple routes of photosynthetic electron transfer in *Chlamydomonas reinhardtii*. In *The chlamydomonas sourcebook* (pp. 591–613). Elsevier.

Croteau, D., Guérin, S., Bruyant, F., Ferland, J., Campbell, D. A., Babin, M., & Lavaud, J. (2021). Contrasting nonphotochemical quenching patterns under high light and darkness aligns with light niche occupancy in arctic diatoms. *Limnology and Oceanography*, *66*, S231–S245.

Croteau, D., Jensen, E., Wilhelm, C., & Bailleul, B. (2024). Comparing diatom photosynthesis with the green lineage: Electron transport, carbon fixation and metabolism. *Diatom Photosynthesis: From Primary Production to High-Value Molecules*, 1–44.

Cruz, J. A., Sacksteder, C. A., Kanazawa, A., & Kramer, D. M. (2001). Contribution of electric field ($\Delta\psi$) to steady-state transthylakoid proton motive force (pmf) in vitro and in vivo. control of pmf parsing into $\Delta\psi$ and Δph by ionic strength. *Biochemistry*, *40*(5), 1226–1237.

Dal Bosco, C., Lezhneva, L., Biehl, A., Leister, D., Strotmann, H., Wanner, G., & Meurer, J. (2004). Inactivation of the chloroplast atp synthase γ subunit results in high nonphotochemical fluorescence quenching and altered nuclear gene expression in *Arabidopsis thaliana*. *Journal of Biological Chemistry*, *279*(2), 1060–1069.

Davis, G. A., Kanazawa, A., Schöttler, M. A., Kohzuma, K., Froehlich, J. E., Rutherford, A. W., Satoh-Cruz, M., Minhas, D., Tietz, S., Dhingra, A., et al. (2016). Limitations to photosynthesis by proton motive force-induced photosystem ii photodamage. *elife*, *5*, e16921.

Davis, G. A., & Kramer, D. M. (2020). Optimization of atp synthase c–rings for oxygenic photosynthesis. *Frontiers in Plant Science*, *10*, 1778.

Davis, G. A., Rutherford, A. W., & Kramer, D. M. (2017). Hacking the thylakoid proton motive force for improved photosynthesis: Modulating ion flux rates that control proton motive force partitioning into Δ ψ and Δph. *Philosophical Transactions of the Royal Society B: Biological Sciences*, *372*(1730), 20160381.

Delosme, R., Joliot, P., & Lavorel, J. (1959). Sur la complementarite de la fluorescence et de lemission doxygene pendant la periode dinduction de la photosynthese. *COMPTES RENDUS HEBDOMADAIRES DES SEANCES DE L ACADEMIE DES SCIENCES*, *249*(15), 1409–1411.

Delosme, R. (1967). Etude de l'induction de fluorescence des algues vertes et des chloroplastes au début d'une illumination intense. *Biochimica et Biophysica Acta (BBA)-Bioenergetics*, *143*(1), 108–128.

Demmig, B., & Björkman, O. (1987). Comparison of the effect of excessive light on chlorophyll fluorescence (77k) and photon yield of o 2 evolution in leaves of higher plants. *Planta*, *171*, 171–184.

Demmig-Adams, B., Ebbert, V., Zarter, C. R., & Adams, W. W. (2006). Characteristics and species-dependent employment of flexible versus sustained thermal dissipation and photoinhibition. *Photoprotection, photoinhibition, gene regulation, and environment*, 39–48.

Dinc, E., Tian, L., Roy, L. M., Roth, R., Goodenough, U., & Croce, R. (2016). Lhcsr1 induces a fast and reversible ph-dependent fluorescence quenching in lhcii in *Chlamydomonas reinhardtii* cells. *Proceedings of the National Academy of Sciences*, *113*(27), 7673–7678.

Diner, B., & Joliot, P. (1976). Effect of the transmembrane electric field on the photochemical and quenching properties of photosystem ii in vivo. *Biochimica et Biophysica Acta (BBA)-Bioenergetics*, *423*(3), 479–498.

Dittami, S. M., Michel, G., Collén, J., Boyen, C., & Tonon, T. (2010). Chlorophyll-binding proteins revisited-a multigenic family of light-harvesting and stress proteins from a brown algal perspective. *BMC Evolutionary Biology*, *10*, 1–14.

Dong, Y.-L., Jiang, T., Xia, W., Dong, H.-P., Lu, S.-H., & Cui, L. (2015). Light harvesting proteins regulate non-photochemical fluorescence quenching in the marine diatom *Thalassiosira pseudonana*. *Algal Research*, *12*, 300–307.

Dorrell, R. G., & Smith, A. G. (2011). Do red and green make brown?: Perspectives on plastid acquisitions within chromalveolates. *Eukaryotic cell*, *10*(7), 856–868.

Dorrell, R. G., Zhang, Y., Liang, Y., Gueguen, N., Nonoyama, T., Croteau, D., Penot-Raquin, M., Adiba, S., Bailleul, B., Gros, V., et al. (2024). Complementary environmental analysis and functional characterization of lower glycolysis-gluconeogenesis in the diatom plastid. *The Plant cell*, koae168.

Dow, L., Stock, F., Peltekis, A., Szamosvári, D., Prothiwa, M., Lapointe, A., Böttcher, T., Bailleul, B., Vyverman, W., Kroth, P. G., et al. (2020). The multifaceted inhibitory effects of an alkylquinolone on the diatom *Phaeodactylum tricornutum*. *ChemBioChem*, *21*(8), 1206–1216.

Dumas, L., Zito, F., Blangy, S., Auroy, P., Johnson, X., Peltier, G., & Alric, J. (2017). A stromal region of cytochrome b 6 f subunit iv is involved in the activation of the stt7 kinase in *Chlamydomonas*. *Proceedings of the National Academy of Sciences*, *114*(45), 12063–12068.

Duysens, L. (1954). Reversible changes in the absorption spectrum of *Chlorella* upon irradiation. *Science*, *120*(3113), 353–354.

Duysens, L., & Sweer, H. (1963). Mechanism of two photochemical reactions in algae as studied by means of fluorescence. *Studies on Microalgae and Photosyunthetic Bacteria. Special issue of Plant Cell Physiol.*, 353–372.

Escoubas, J.-M., Lomas, M., LaRoche, J., & Falkowski, P. G. (1995). Light intensity regulation of cab gene transcription is signaled by the redox state of the plastoquinone pool. *Proceedings of the National Academy of Sciences*, *92*(22), 10237–10241.

Esteban, R., Becerril, J. M., & García-Plazaola, J. I. (2009). Lutein epoxide cycle, more than just a forest tale. *Plant signaling & behavior*, *4*(4), 342–344.

Falciatore, A., Jaubert, M., Bouly, J.-P., Bailleul, B., & Mock, T. (2020). Diatom molecular research comes of age: Model species for studying phytoplankton biology and diversity. *The Plant Cell*, *32*(3), 547–572.

Falkowski, P. G., Fenchel, T., & Delong, E. F. (2008). The microbial engines that drive earth's biogeochemical cycles. *Science*, *320*(5879), 1034–1039.

Falkowski, P. G., Fujita, Y., Ley, A., & Mauzerall, D. (1986). Evidence for cyclic electron flow around photosystem ii in *Chlorella pyrenoidosa*. *Plant Physiology*, *81*(1), 310–312.

Falkowski, P. G., Lin, H., & Gorbunov, M. Y. (2017). What limits photosynthetic energy conversion efficiency in nature? lessons from the oceans. *Philosophical Transactions of the Royal Society B: Biological Sciences*, *372*(1730), 20160376.

Fan, M., Li, M., Liu, Z., Cao, P., Pan, X., Zhang, H., Zhao, X., Zhang, J., & Chang, W. (2015). Crystal structures of the psbs protein essential for photoprotection in plants. *Nature structural & molecular biology*, *22*(9), 729–735.

Ferté, S. (2019). *Exploring the diversity of cyclic electron flow around photosystem i in microalgae species* [Doctoral dissertation, Sorbonne Université].

Field, C. B., Behrenfeld, M. J., Randerson, J. T., & Falkowski, P. (1998). Primary production of the biosphere: Integrating terrestrial and oceanic components. *science*, *281*(5374), 237–240.

Finazzi, G., & Forti, G. (2004). Metabolic flexibility of the green alga *Chlamydomonas reinhardtii* as revealed by the link between state transitions and cyclic electron flow. *Photosynthesis Research*, *82*, 327–338.

Finazzi, G., & Rappaport, F. (1998). In vivo characterization of the electrochemical proton gradient generated in darkness in green algae and its kinetic effects on cytochrome b 6 f turnover. *Biochemistry*, *37*(28), 9999–10005.

Flameling, I. A., & Kromkamp, J. (1998). Light dependence of quantum yields for psii charge separation and oxygen evolution in eucaryotic algae. *Limnology and Oceanography*, *43*(2), 284–297.

Fleischmann, M. M., Ravanel, S., Delosme, R., Olive, J., Zito, F., Wollman, F.-A., & Rochaix, J.-D. (1999). Isolation and characterization of photoautotrophic mutants of *Chlamydomonas reinhardtii* deficient in state transition. *Journal of Biological Chemistry*, *274*(43), 30987–30994.

Flombaum, P., Gallegos, J. L., Gordillo, R. A., Rincón, J., Zabala, L. L., Jiao, N., Karl, D. M., Li, W. K., Lomas, M. W., Veneziano, D., et al. (2013). Present and future global distributions of the marine cyanobacteria *Prochlorococcus* and *Synechococcus*. *Proceedings of the National Academy of Sciences*, *110*(24), 9824–9829.

Flori, S., Dickenson, J., Gaikwad, T., Cole, I., Smirnoff, N., Helliwell, K., Brownlee, C., & Wheeler, G. (2023). Diatoms exhibit dynamic chloroplast calcium signals in response to high light and oxidative stress. *bioRxiv*, 2023–08.

Flori, S., Jouneau, P.-H., Bailleul, B., Gallet, B., Estrozi, L. F., Moriscot, C., Bastien, O., Eicke, S., Schober, A., Bártulos, C. R., et al. (2017). Plastid thylakoid architecture optimizes photosynthesis in diatoms. *Nature Communications*, *8*(1), 15885.

Flori, S., Jouneau, P.-H., Finazzi, G., Maréchal, E., & Falconet, D. (2016). Ultrastructure of the periplastidial compartment of the diatom *Phaeodactylum tricornutum*. *Protist*, *167*(3), 254–267.

Foyer, C. H. (2018). Reactive oxygen species, oxidative signaling and the regulation of photosynthesis. *Environmental and Experimental Botany*, *154*, 134–142.

Foyer, C. H., Neukermans, J., Queval, G., Noctor, G., & Harbinson, J. (2012). Photosynthetic control of electron transport and the regulation of gene expression. *Journal of Experimental Botany*, *63*(4), 1637–1661.

Foyer, C. H., & Noctor, G. (2011). Ascorbate and glutathione: The heart of the redox hub. *Plant Physiology*, *155*(1), 2–18.

Foyer, C. H., Parry, M., & Noctor, G. (2003). Markers and signals associated with nitrogen assimilation in higher plants. *Journal of Experimental Botany*, *54*(382), 585–593.

Garab, G., Magyar, M., Sipka, G., & Lambrev, P. H. (2023). New foundations for the physical mechanism of variable chlorophyll a fluorescence. quantum efficiency versus the light-adapted state of photosystem ii. *Journal of Experimental Botany*, *74*(18), 5458–5471.

Geel, C., Versluis, W., & Snel, J. F. (1997). Estimation of oxygen evolution by marine phytoplankton from measurement of the efficiency of photosystem ii electron flow. *Photosynthesis Research*, *51*, 61–70.

Genty, B., Briantais, J.-M., & Baker, N. R. (1989). The relationship between the quantum yield of photosynthetic electron transport and quenching of chlorophyll fluorescence. *Biochimica et Biophysica Acta (BBA)*, *990*(1), 87–92.

Genty, B., Harbinson, J., Briantais, J.-M., & Baker, N. R. (1990). The relationship between non-photochemical quenching of chlorophyll fluorescence and the rate of photosystem 2 photochemistry in leaves. *Photosynthesis Research*, *25*, 249–257.

Giersch, C., Heber, U., Kobayashi, Y., Inoue, Y., Shibata, K., & Heldt, H. W. (1980). Energy charge, phosphorylation potential and proton motive force in chloroplasts. *Biochimica et Biophysica Acta (BBA)-Bioenergetics*, *590*(1), 59–73.

Giossi, C. E., Wünsch, M. A., Dautermann, O., Schober, A. F., Buck, J. M., Kroth, P. G., Lohr, M., & Lepetit, B. (2024). Both major xanthophyll cycles present in nature can provide non-photochemical quenching in the model diatom *Phaeodactylum tricornutum*. *bioRxiv*, 2024–03.

Giovagnetti, V., Flori, S., Tramontano, F., Lavaud, J., & Brunet, C. (2014). The velocity of light intensity increase modulates the photoprotective response in coastal diatoms. *PLoS One*, *9*(8), e103782.

Giovagnetti, V., Jaubert, M., Shukla, M. K., Ungerer, P., Bouly, J.-P., Falciatore, A., & Ruban, A. V. (2022). Biochemical and molecular properties of lhcx1, the essential regulator of dynamic photoprotection in diatoms. *Plant Physiology*, *188*(1), 509–525.

Giovagnetti, V., & Ruban, A. V. (2017). Detachment of the fucoxanthin chlorophyll a/c binding protein (fcp) antenna is not involved in the acclimative regulation of photoprotection in the pennate diatom *Phaeodactylum tricornutum*. *Biochimica Biophysica Acta (BBA)-Bioenergetics*, *1858*(3), 218–230.

Głowacka, K., Kromdijk, J., Kucera, K., Xie, J., Cavanagh, A. P., Leonelli, L., Leakey, A. D., Ort, D. R., Niyogi, K. K., & Long, S. P. (2018). Photosystem ii subunit s overexpression increases the efficiency of water use in a field-grown crop. *Nature Communications*, *9*(1), 868.

Godaux, D., Bailleul, B., Berne, N., & Cardol, P. (2015). Induction of photosynthetic carbon fixation in anoxia relies on hydrogenase activity and proton-gradient regulation-like1-mediated cyclic electron flow in *Chlamydomonas reinhardtii*. *Plant Physiology*, *168*(2), 648–658.

Gorbunov, M. Y., & Falkowski, P. G. (2022). Using chlorophyll fluorescence to determine the fate of photons absorbed by phytoplankton in the world's oceans. *Annual Review of Marine Science*, *14*(1), 213–238.

Gorbunov, M. Y., Kolber, Z. S., Lesser, M. P., & Falkowski, P. G. (2001). Photosynthesis and photoprotection in symbiotic corals. *Limnology and Oceanography*, *46*(1), 75–85.

Goss, R., & Jakob, T. (2010). Regulation and function of xanthophyll cycle-dependent photoprotection in algae. *Photosynthesis Research*, *106*, 103–122.

Goss, R., & Lepetit, B. (2015). Biodiversity of npq. *Journal of plant physiology*, *172*, 13–32.

Grouneva, I., Jakob, T., Wilhelm, C., & Goss, R. (2008). A new multicomponent npq mechanism in the diatom *Cyclotella meneghiniana*. *Plant and cell physiology*, *49*(8), 1217–1225.

Grouneva, I., Jakob, T., Wilhelm, C., & Goss, R. (2009). The regulation of xanthophyll cycle activity and of non-photochemical fluorescence quenching by two alternative electron flows in the diatoms *Phaeodactylum tricornutum* and *Cyclotella meneghiniana*. *Biochimica et Biophysica Acta (BBA)-Bioenergetics*, *1787*(7), 929–938.

Groussman, R. D., Parker, M. S., & Armbrust, E. V. (2015). Diversity and evolutionary history of iron metabolism genes in diatoms. *PLoS One*, *10*(6), e0129081.

Hager, A. (1966). Die zusammenhänge zwischen lichtinduzierten xanthophyll-umwandlungen und hill-reaktion. *Berichte der Deutschen Botanischen Gesellschaft*, *79*(11), 94–107.

Hahn, A., Vonck, J., Mills, D. J., Meier, T., & Kühlbrandt, W. (2018). Structure, mechanism, and regulation of the chloroplast atp synthase. *Science*, *360*(6389), eaat4318.

Hald, S., Nandha, B., Gallois, P., & Johnson, G. N. (2008). Feedback regulation of photosynthetic electron transport by nadp (h) redox poise. *Biochimica et Biophysica Acta (BBA)-Bioenergetics*, *1777*(5), 433–440.

Harbinson, J., & Foyer, C. H. (1991). Relationships between the efficiencies of photosystems i and ii and stromal redox state in co2-free air: Evidence for cyclic electron flow in vivo. *Plant Physiology*, *97*(1), 41–49.

Harbinson, J., Genty, B., & Baker, N. R. (1990). The relationship between co 2 assimilation and electron transport in leaves. *Photosynthesis Research*, *25*, 213–224.

Harbinson, J., Prinzenberg, A. E., Kruijer, W., & Aarts, M. G. (2012). High throughput screening with chlorophyll fluorescence imaging and its use in crop improvement. *Current Opinion in Biotechnology*, *23*(2), 221–226.

Havaux, M., Dall'Osto, L., & Bassi, R. (2007). Zeaxanthin has enhanced antioxidant capacity with respect to all other xanthophylls in *Arabidopsis* leaves and functions independent of binding to psii antennae. *Plant physiology*, *145*(4), 1506–1520.

Havaux, M., & Niyogi, K. K. (1999). The violaxanthin cycle protects plants from photooxidative damage by more than one mechanism. *Proceedings of the National Academy of Sciences*, *96*(15), 8762–8767.

Hecks, B., Wulf, K., Breton, J., Leibl, W., & Trissl, H.-W. (1994). Primary charge separation in photosystem i: A two-step electrogenic charge separation connected with p700+ a0-and p700+ a1-formation. *Biochemistry*, *33*(29), 8619–8624.

Herbstová, M., Bína, D., Koník, P., Gardian, Z., Vácha, F., & Litvín, R. (2015). Molecular basis of chromatic adaptation in pennate diatom *Phaeodactylum tricornutum*. *Biochimica et Biophysica Acta (BBA)-Bioenergetics*, *1847*(6-7), 534–543.

Hill, R., & Bendall, F. (1960). Function of the two cytochrome components in chloroplasts: A working hypothesis. *Nature*, *186*(4719), 136–137.

Hoh, D., Froehlich, J. E., & Kramer, D. M. (2024). Redox regulation in chloroplast thylakoid lumen: The pmf changes everything, again. *Plant, Cell & Environment*, *47*(8), 2749–2765.

Hohmann-Marriott, M. F., & Blankenship, R. E. (2011). Evolution of photosynthesis. *Annual review of plant biology*, *62*(1), 515–548.

Holzmann, D., Bethmann, S., & Jahns, P. (2022). Zeaxanthin epoxidase activity is downregulated by hydrogen peroxide. *Plant and Cell Physiology*, *63*(8), 1091–1100.

Hopes, A., & Mock, T. (2015). Evolution of microalgae and their adaptations in different marine ecosystems. *eLS*, *3*, 1–9.

Horton, P. (1996). Nonphotochemical quenching of chlorophyll fluorescence. *Light as an energy source and information carrier in plant physiology*, 99–111.

Hubbart, S., Ajigboye, O. O., Horton, P., & Murchie, E. H. (2012). The photoprotective protein psbs exerts control over co2 assimilation rate in fluctuating light in rice. *The Plant Journal*, *71*(3), 402–412.

Il'ina, M. D., Krasauskas, V. V., Rotomskis, R. J., & Borisov, A. Y. (1984). Difference picosecond spectroscopy of pigment-protein complexes of photosystem i from higher plants. *Biochimica et Biophysica Acta (BBA)-Bioenergetics*, *767*(3), 501–506.

Jahns, P., & Holzwarth, A. R. (2012). The role of the xanthophyll cycle and of lutein in photoprotection of photosystem ii. *Biochimica et Biophysica Acta (BBA)-Bioenergetics*, *1817*(1), 182–193.

Jakob, T., Goss, R., & Wilhelm, C. (2001). Unusual ph-dependence of diadinoxanthin de-epoxidase activation causes chlororespiratory induced accumulation of diatoxanthin in the diatom *Phaeodactylum tricornutum*. *Journal of Plant Physiology*, *158*(3), 383–390.

Jaubert, M., Duchêne, C., Kroth, P. G., Rogato, A., Bouly, J.-P., & Falciatore, A. (2022). Sensing and signalling in diatom responses to abiotic cues. *The Molecular Life of Diatoms*, 607–639.

Jiang, Y., Cao, T., Yang, Y., Zhang, H., Zhang, J., & Li, X. (2023). A chlorophyll c synthase widely co-opted by phytoplankton. *Science*, *382*(6666), 92–98.

Johnson, G. N. (2003). Thiol regulation of the thylakoid electron transport chain a missing link in the regulation of photosynthesis? *Biochemistry*, *42*(10), 3040–3044.

Joliot, P. (1965). Cinétiques des réactions liées a l'émission d'oxygène photosynthétique. *Biochimica et Biophysica Acta (BBA)-Biophysics including Photosynthesis*, *102*(1), 116–134.

Joliot, P., & Joliot, A. (1989). Characterization of linear and quadratic electrochromic probes in *Chlorella sorokiniana* and *Chlamydomonas reinhardtii*. *Biochimica et Biophysica Acta (BBA)-Bioenergetics*, *975*(3), 355–360.

Joliot, P., & Joliot, A. (2008). Quantification of the electrochemical proton gradient and activation of atp synthase in leaves. *Biochimica et Biophysica Acta (BBA)-Bioenergetics*, *1777*(7-8), 676–683.

Junge, W., Rumberg, B., & Schröder, H. (1970). The necessity of an electric potential difference and its use for photophosphorylation in short flash groups. *European Journal of Biochemistry*, *14*(3), 575–581.

Kanazawa, A., Chattopadhyay, A., Kuhlgert, S., Tuitupou, H., Maiti, T., & Kramer, D. M. (2021). Light potentials of photosynthetic energy storage in the field: What limits the ability to use or dissipate rapidly increased light energy? *Royal Society Open Science*, *8*(12), 211102.

Kasahara, M., Kagawa, T., Oikawa, K., Suetsugu, N., Miyao, M., & Wada, M. (2002). Chloroplast avoidance movement reduces photodamage in plants. *Nature*, *420*(6917), 829–832.

Kaur, D., Khaniya, U., Zhang, Y., & Gunner, M. (2021). Protein motifs for proton transfers that build the transmembrane proton gradient. *Frontiers in chemistry*, *9*, 660954.

Kautsky, H., & Hilsch, A. (1931). Wechselwirkung zwischen angeregten farbstoff-molekülen und sauerstoff. *Berichte Der Dtsch Chem Gesellschaft*, *64*, 2677–2683.

Kikutani, S., Nakajima, K., Nagasato, C., Tsuji, Y., Miyatake, A., & Matsuda, Y. (2016). Thylakoid luminal θ-carbonic anhydrase critical for growth and photosynthesis in the

marine diatom *Phaeodactylum tricornutum*. *Proceedings of the National Academy of Sciences*, *113*(35), 9828–9833.

Kindle, K. L. (1990). High-frequency nuclear transformation of *Chlamydomonas reinhardtii*. *Proceedings of the National Academy of Sciences*, *87*(3), 1228–1232.

Kirchhoff, H., Schöttler, M. A., Maurer, J., & Weis, E. (2004). Plastocyanin redox kinetics in spinach chloroplasts: Evidence for disequilibrium in the high potential chain. *Biochimica et Biophysica Acta (BBA)-Bioenergetics*, *1659*(1), 63–72.

Klingenberg, M. (2008). The adp and atp transport in mitochondria and its carrier. *Biochimica et Biophysica Acta (BBA)-Biomembranes*, *1778*(10), 1978–2021.

Klughammer, C., & Schreiber, U. (1994). Saturation pulse method for assessment of energy conversion in ps i. *Planta*, *192*, 261–268.

Klughammer, C., & Schreiber, U. (2008). Complementary ps ii quantum yields calculated from simple fluorescence parameters measured by pam fluorometry and the saturation pulse method. *PAM application notes*, *1*(2), 201–247.

Kohzuma, K., Dal Bosco, C., Kanazawa, A., Dhingra, A., Nitschke, W., Meurer, J., & Kramer, D. M. (2012). Thioredoxin-insensitive plastid atp synthase that performs moonlighting functions. *Proceedings of the National Academy of Sciences*, *109*(9), 3293–3298.

Kolber, Z. S., Prášil, O., & Falkowski, P. G. (1998). Measurements of variable chlorophyll fluorescence using fast repetition rate techniques: Defining methodology and experimental protocols. *Biochimica et Biophysica Acta (BBA)-Bioenergetics*, *1367*(1-3), 88–106.

Krall, J., & Edwards, G. E. (1990). Quantum yields of photosystem ii electron transport and carbon dioxide fixation in c4 plants. *Functional Plant Biology*, *17*(5), 579–588.

Kramer, D. M., & Crofts, A. R. (1989). Activation of the chloroplast atpase measured by the electrochromic change in leaves of intact plants. *Biochimica et Biophysica Acta (BBA)-Bioenergetics*, *976*(1), 28–41.

Kramer, D. M., Cruz, J. A., & Kanazawa, A. (2003). Balancing the central roles of the thylakoid proton gradient. *Trends in plant science*, *8*(1), 27–32.

Kramer, D. M., Johnson, G., Kiirats, O., & Edwards, G. E. (2004). New fluorescence parameters for the determination of qa redox state and excitation energy fluxes. *Photosynthesis research*, *79*, 209–218.

Kramer, D. M., & Sacksteder, C. A. (1998). A diffused-optics flash kinetic spectrophotometer (dofs) for measurements of absorbance changes in intact plants in the steady-state. *Photosynthesis research*, *56*, 103–112.

Kramer, D. M., Sacksteder, C. A., & Cruz, J. A. (1999). How acidic is the lumen? *Photosynthesis research*, *60*, 151–163.

Krause, G. (1974). Changes in chlorophyll fluorescence in relation to light-dependent cation transfer across thylakoid membranes. *Biochimica et Biophysica Acta (BBA)-Bioenergetics*, *333*(2), 301–313.

Kress, E., & Jahns, P. (2017). The dynamics of energy dissipation and xanthophyll conversion in *Arabidopsis* indicate an indirect photoprotective role of zeaxanthin in slowly inducible and relaxing components of non-photochemical quenching of excitation energy. *Frontiers in Plant Science*, *8*, 2094.

Krieger-Liszkay, A., Fufezan, C., & Trebst, A. (2008). Singlet oxygen production in photosystem ii and related protection mechanism. *Photosynthesis research*, *98*, 551–564.

Kromdijk, J., Głowacka, K., Leonelli, L., Gabilly, S. T., Iwai, M., Niyogi, K. K., & Long, S. P. (2016). Improving photosynthesis and crop productivity by accelerating recovery from photoprotection. *Science*, *354*(6314), 857–861.

Kroth, P. G., Chiovitti, A., Gruber, A., Martin-Jezequel, V., Mock, T., Parker, M. S., Stanley, M. S., Kaplan, A., Caron, L., Weber, T., et al. (2008). A model for carbohydrate metabolism in the diatom *Phaeodactylum tricornutum* deduced from comparative whole genome analysis. *PloS one*, *3*(1), e1426.

Krug, L. A., Platt, T., Sathyendranath, S., & Barbosa, A. B. (2017). Ocean surface partitioning strategies using ocean colour remote sensing: A review. *Progress in Oceanography*, *155*, 41–53.

Kunkel, T. A. (1985). Rapid and efficient site-specific mutagenesis without phenotypic selection. *Proceedings of the National Academy of Sciences*, *82*(2), 488–492.

Kusama, Y., Inoue, S., Jimbo, H., Takaichi, S., Sonoike, K., Hihara, Y., & Nishiyama, Y. (2015). Zeaxanthin and echinenone protect the repair of photosystem ii from inhibition by singlet oxygen in *Synechocystis* sp. pcc 6803. *Plant and Cell Physiology*, *56*(5), 906–916.

Küster, L., Lücke, R., Brabender, C., Bethmann, S., & Jahns, P. (2023). The amount of zeaxanthin epoxidase but not the amount of violaxanthin de-epoxidase is a critical determinant of zeaxanthin accumulation in *Arabidopsis thaliana* and *Nicotiana tabacum*. *Plant and Cell Physiology*, *64*(10), 1220–1230.

Lacour, L., Llort, J., Briggs, N., Strutton, P. G., & Boyd, P. W. (2023). Seasonality of downward carbon export in the pacific southern ocean revealed by multi-year robotic observations. *Nature Communications*, *14*(1), 1278.

Lacour, T., Babin, M., & Lavaud, J. (2020). Diversity in xanthophyll cycle pigments content and related nonphotochemical quenching (npq) among microalgae: Implications for growth strategy and ecology. *Journal of Phycology*, *56*(2), 245–263.

Lacour, T., Robert, E., & Lavaud, J. (2023). Sustained xanthophyll pigments-related photoprotective npq is involved in photoinhibition in the haptophyte *Tisochrysis lutea*. *Scientific Reports*, *13*(1), 14694.

Lavaud, J., & Kroth, P. G. (2006). In diatoms, the transthylakoid proton gradient regulates the photoprotective non-photochemical fluorescence quenching beyond its control on the xanthophyll cycle. *Plant and Cell Physiology*, *47*(7), 1010–1016.

Lavaud, J., & Lepetit, B. (2013). An explanation for the inter-species variability of the photoprotective non-photochemical chlorophyll fluorescence quenching in diatoms. *Biochimica et Biophysica Acta (BBA)-Bioenergetics*, *1827*(3), 294–302.

Lavaud, J., Rousseau, B., & Etienne, A.-L. (2002). In diatoms, a transthylakoid proton gradient alone is not sufficient to induce a non-photochemical fluorescence quenching. *FEBS Letters*, *523*(1-3), 163–166.

Lavaud, J., Rousseau, B., & Etienne, A.-L. (2004). General features of photoprotection by energy dissipation in planktonic diatoms (bacillariophyceae). *Journal of Phycology*, *40*(1), 130–137.

Lavaud, J., Rousseau, B., van Gorkom, H. J., & Etienne, A.-L. (2002). Influence of the diadinoxanthin pool size on photoprotection in the marine planktonic diatom *Phaeodactylum tricornutum*. *Plant Physiology*, *129*(3), 1398–1406.

Lavergne, J., & Trissl, H.-W. (1995). Theory of fluorescence induction in photosystem ii: Derivation of analytical expressions in a model including exciton-radical-pair equilibrium and restricted energy transfer between photosynthetic units. *Biophysical journal*, *68*(6), 2474–2492.

Lavergne, J., & Briantais, J.-M. (1996). Photosystem ii heterogeneity. *Oxygenic photosynthesis: the light reactions*, 265–287.

Lazár, D. (2013). Simulations show that a small part of variable chlorophyll a fluorescence originates in photosystem i and contributes to overall fluorescence rise. *Journal of Theoretical Biology*, *335*, 249–264.

Lazár, D. (2015). Parameters of photosynthetic energy partitioning. *Journal of Plant Physiology*, *175*, 131–147.

Lepetit, B., Campbell, D. A., Lavaud, J., Büchel, C., Goss, R., & Bailleul, B. (2022). Photosynthetic light reactions in diatoms. ii. the dynamic regulation of the various light reactions. In *The molecular life of diatoms* (pp. 423–464). Springer.

Lepetit, B., Goss, R., Jakob, T., & Wilhelm, C. (2012). Molecular dynamics of the diatom thylakoid membrane under different light conditions. *Photosynthesis research*, *111*, 245–257.

Lepetit, B., Sturm, S., Rogato, A., Gruber, A., Sachse, M., Falciatore, A., Kroth, P. G., & Lavaud, J. (2013). High light acclimation in the secondary plastids containing diatom *Phaeodactylum tricornutum* is triggered by the redox state of the plastoquinone pool. *Plant physiology*, *161*(2), 853–865.

Lepetit, B., Volke, D., Gilbert, M., Wilhelm, C., & Goss, R. (2010). Evidence for the existence of one antenna-associated, lipid-dissolved and two protein-bound pools of diadinoxanthin cycle pigments in diatoms. *Plant physiology*, *154*(4), 1905–1920.

Li, G., Woroch, A. D., Donaher, N. A., Cockshutt, A. M., & Campbell, D. A. (2016). A hard day's night: Diatoms continue recycling photosystem ii in the dark. *Frontiers in Marine Science*, *3*, 218.

Li, X.-P., BjoÈrkman, O., Shih, C., Grossman, A. R., Rosenquist, M., Jansson, S., & Niyogi, K. K. (2000). A pigment-binding protein essential for regulation of photosynthetic light harvesting. *Nature*, *403*(6768), 391–395.

Li, X.-P., Müller-Moulé, P., Gilmore, A. M., & Niyogi, K. K. (2002). Psbs-dependent enhancement of feedback de-excitation protects photosystem ii from photoinhibition. *Proceedings of the National Academy of Sciences*, *99*(23), 15222–15227.

Logan, B., Terry, S., & Niyogi, K. (2008). *Arabidopsis* genotypes with differing levels of psbs expression differ in photosystem ii quantum yield, xanthophyll cycle pool size, and aboveground growth. *International Journal of Plant Sciences*, *169*(5), 597–604.

Lohr, M., & Wilhelm, C. (1999). Algae displaying the diadinoxanthin cycle also possess the violaxanthin cycle. *Proceedings of the National Academy of Sciences*, *96*(15), 8784–8789.

Lomas, M. W., & Glibert, P. M. (1999). Temperature regulation of nitrate uptake: A novel hypothesis about nitrate uptake and reduction in cool-water diatoms. *Limnology and Oceanography*, *44*(3), 556–572.

Lomas, M. W., Rumbley, C. J., & Glibert, P. M. (2000). Ammonium release by nitrogen sufficient diatoms in response to rapid increases in irradiance. *Journal of Plankton Research*, *22*(12), 2351–2366.

Long, M., Peltekis, A., González-Fernández, C., Hegaret, H., & Bailleul, B. (2021). Allelochemicals of *Alexandrium minutum*: Kinetics of membrane disruption and photosynthesis inhibition in a co-occurring diatom. *Harmful Algae*, *103*, 101997.

Lubitz, W., Chrysina, M., & Cox, N. (2019). Water oxidation in photosystem ii. *Photosynthesis research*, *142*(1), 105–125.

Lucker, B., & Kramer, D. M. (2013). Regulation of cyclic electron flow in *Chlamydomonas reinhardtii* under fluctuating carbon availability. *Photosynthesis research*, *117*, 449–459.

Lupette, J., Jaussaud, A., Seddiki, K., Morabito, C., Brugière, S., Schaller, H., Kuntz, M., Putaux, J.-L., Jouneau, P.-H., Rébeillé, F., et al. (2019). The architecture of lipid droplets in the diatom *Phaeodactylum tricornutum*. *Algal Research*, *38*, 101415.

Makita, H., & Hastings, G. (2018). Photosystem i with benzoquinone analogues incorporated into the a 1 binding site. *Photosynthesis research*, *137*, 85–93.

Malkin, S., & Kok, B. (1966). Fluorescence induction studies in isolated chloroplasts i. number of components involved in the reaction and quantum yields. *Biochimica et Biophysica Acta (BBA)-Biophysics including Photosynthesis*, *126*(3), 413–432.

Mascoli, V., Liguori, N., Xu, P., Roy, L. M., van Stokkum, I. H., & Croce, R. (2019). Capturing the quenching mechanism of light-harvesting complexes of plants by zooming in on the ensemble. *Chem*, *5*(11), 2900–2912.

Mauzerall, D., & Greenbaum, N. L. (1989). The absolute size of a photosynthetic unit. *Biochimica et Biophysica Acta (BBA)-Bioenergetics*, *974*(2), 119–140.

McCarthy, J. K., Smith, S. R., McCrow, J. P., Tan, M., Zheng, H., Beeri, K., Roth, R., Lichtle, C., Goodenough, U., Bowler, C. P., et al. (2017). Nitrate reductase knockout uncouples nitrate transport from nitrate assimilation and drives repartitioning of carbon flux in a model pennate diatom. *The Plant Cell*, *29*(8), 2047–2070.

Medlin, L. K. (2016). Evolution of the diatoms: Major steps in their evolution and a review of the supporting molecular and morphological evidence. *Phycologia*, *55*(1), 79–103.

Mitchell, P. (1961). Coupling of phosphorylation to electron and hydrogen transfer by a chemi-osmotic type of mechanism. *Nature*, *191*(4784), 144–148.

Mitchell, P., & Moyle, J. (1967). Chemiosmotic hypothesis of oxidative phosphorylation. *Nature*, *213*(5072), 137–139.

Mock, T., Hodgkinson, K., Wu, T., Moulton, V., Duncan, A., van Oosterhout, C., & Pichler, M. (2022). Structure and evolution of diatom nuclear genes and genomes. In *The molecular life of diatoms* (pp. 111–145). Springer.

Mock, T., Otillar, R. P., Strauss, J., McMullan, M., Paajanen, P., Schmutz, J., Salamov, A., Sanges, R., Toseland, A., Ward, B. J., et al. (2017). Evolutionary genomics of the cold-adapted diatom *Fragilariopsis cylindrus*. *Nature*, *541*(7638), 536–540.

Moustafa, A., Beszteri, B., Maier, U. G., Bowler, C., Valentin, K., & Bhattacharya, D. (2009). Genomic footprints of a cryptic plastid endosymbiosis in diatoms. *science*, *324*(5935), 1724–1726.

Müller, N. (1874). Untersuchungen über die diffusion der atmosphärischen gase und die gasausscheidung unter verschiedenen beleuchtungs-bedingungen. *Jahrbucher fur Wissenschaftliche Botanik*, *9*, 36–49.

Munekage, Y., Hashimoto, M., Miyake, C., Tomizawa, K.-I., Endo, T., Tasaka, M., & Shikanai, T. (2004). Cyclic electron flow around photosystem i is essential for photosynthesis. *Nature*, *429*(6991), 579–582.

Munekage, Y., Hojo, M., Meurer, J., Endo, T., Tasaka, M., & Shikanai, T. (2002). Pgr5 is involved in cyclic electron flow around photosystem i and is essential for photoprotection in *Arabidopsis*. *Cell*, *110*(3), 361–371.

Nagao, R., Yokono, M., Ueno, Y., Shen, J.-R., & Akimoto, S. (2020). Excitation-energy transfer and quenching in diatom psi-fcpi upon p700 cation formation. *The Journal of Physical Chemistry B*, *124*(8), 1481–1486.

Nakayasu, M., Akimoto, S., Yoneda, K., Ikuta, S., Shimakawa, G., & Matsuda, Y. (2024). Different functions of lhcx isoforms in photoprotective mechanism in the marine diatom *Thalassiosira pseudonana*. *bioRxiv*, 2024–04.

Nakov, T., Beaulieu, J. M., & Alverson, A. J. (2018). Accelerated diversification is related to life history and locomotion in a hyperdiverse lineage of microbial eukaryotes (diatoms, bacillariophyta). *New Phytologist*, *219*(1), 462–473.

Naranjo, B., Mignée, C., Krieger-Liszkay, A., Hornero-Méndez, D., Gallardo-Guerrero, L., Cejudo, F. J., & Lindahl, M. (2016). The chloroplast nadph thioredoxin reductase c, ntrc, controls non-photochemical quenching of light energy and photosynthetic electron transport in *Arabidopsis*. *Plant, Cell & Environment*, *39*(4), 804–822.

Nawaly, H., Tanaka, A., Toyoshima, Y., Tsuji, Y., & Matsuda, Y. (2023). Localization and characterization θ carbonic anhydrases in *Thalassiosira pseudonana*. *Photosynthesis Research*, *156*(2), 217–229.

Nawrocki, W. J., Liu, X., & Croce, R. (2020). *Chlamydomonas reinhardtii* exhibits de facto constitutive npq capacity in physiologically relevant conditions. *Plant physiology*, *182*(1), 472–479.

Nawrocki, W. J., Liu, X., Raber, B., Hu, C., De Vitry, C., Bennett, D. I., & Croce, R. (2021). Molecular origins of induction and loss of photoinhibition-related energy dissipation qi. *Science Advances*, *7*(52), eabj0055.

Nawrocki, W. J., Santabarbara, S., Mosebach, L., Wollman, F.-A., & Rappaport, F. (2016). State transitions redistribute rather than dissipate energy between the two photosystems in *Chlamydomonas*. *Nature plants*, *2*(4), 1–7.

Nicol, L., & Croce, R. (2021). The psbs protein and low ph are necessary and sufficient to induce quenching in the light-harvesting complex of plants lhcii. *Scientific Reports*, *11*(1), 7415.

Nilkens, M., Kress, E., Lambrev, P., Miloslavina, Y., Müller, M., Holzwarth, A. R., & Jahns, P. (2010). Identification of a slowly inducible zeaxanthin-dependent component of non-photochemical quenching of chlorophyll fluorescence generated under steady-state conditions in *Arabidopsis*. *Biochimica et Biophysica Acta (BBA)-Bioenergetics*, *1797*(4), 466–475.

Noctor, G., & Foyer, C. H. (2016). Intracellular redox compartmentation and ros-related communication in regulation and signaling. *Plant Physiology*, *171*(3), 1581–1592.

Novák Vanclová, A. M., Nef, C., Füssy, Z., Vancl, A., Liu, F., Bowler, C., & Dorrell, R. G. (2024). New plastids, old proteins: Repeated endosymbiotic acquisitions in kareniacean dinoflagellates. *EMBO reports*, *25*(4), 1859–1885.

Nürnberg, D. J., Morton, J., Santabarbara, S., Telfer, A., Joliot, P., Antonaru, L. A., Ruban, A. V., Cardona, T., Krausz, E., Boussac, A., et al. (2018). Photochemistry beyond the red limit in chlorophyll f–containing photosystems. *Science*, *360*(6394), 1210–1213.

Nymark, M., Valle, K. C., Hancke, K., Winge, P., Andresen, K., Johnsen, G., Bones, A. M., & Brembu, T. (2013). Molecular and photosynthetic responses to prolonged darkness and subsequent acclimation to re-illumination in the diatom *Phaeodactylum tricornutum*. *PLoS one*, *8*(3), e58722.

Ogawa, T., Kobayashi, K., Taniguchi, Y. Y., Shikanai, T., Nakamura, N., Yokota, A., & Munekage, Y. N. (2023). Two cyclic electron flows around photosystem i differentially participate in c4 photosynthesis. *Plant Physiology*, *191*(4), 2288–2300.

Ohnishi, N., Allakhverdiev, S. I., Takahashi, S., Higashi, S., Watanabe, M., Nishiyama, Y., & Murata, N. (2005). Two-step mechanism of photodamage to photosystem ii: Step 1 occurs at the oxygen-evolving complex and step 2 occurs at the photochemical reaction center. *Biochemistry*, *44*(23), 8494–8499.

Olaizola, M., La Roche, J., Kolber, Z., & Falkowski, P. G. (1994). Non-photochemical fluorescence quenching and the diadinoxanthin cycle in a marine diatom. *Photosynthesis Research*, *41*, 357–370.

Olaizola, M., & Yamamoto, H. Y. (1994). Short-term response of the diadinoxanthin cycle and fluorescence yield to high irradiance in *Chaetoceros muelleri* (bacillariophyceae). *Journal of Phycology*, *30*(4), 606–612.

Owens, T. G. (1986). Light-harvesting function in the diatom *Phaeodactylum tricornutum*: Ii. distribution of excitation energy between the photosystems. *Plant Physiology*, *80*(3), 739–746.

Pajot, A., Lavaud, J., Carrier, G., Garnier, M., Saint-Jean, B., Rabilloud, N., Baroukh, C., Bérard, J.-B., Bernard, O., Marchal, L., et al. (2022). The fucoxanthin chlorophyll a/c-binding protein in *Tisochrysis lutea*: Influence of nitrogen and light on fucoxanthin and chlorophyll a/c-binding protein gene expression and fucoxanthin synthesis. *Frontiers in Plant Science*, *13*, 830069.

Pajot, A., Lavaud, J., Carrier, G., Lacour, T., Marchal, L., & Nicolau, E. (2023). Light-response in two clonal strains of the haptophyte *Tisochrysis lutea*: Evidence for different photoprotection strategies. *Algal Research*, *69*, 102915.

Pancheri, T., Baur, T., & Roach, T. (2024). Singlet-oxygen-mediated regulation of photosynthesis-specific genes: A role for reactive electrophiles in signal transduction. *International Journal of Molecular Sciences*, *25*(15), 8458.

Pancic, P. G., & Strotmann, H. (1993). Structure of the nuclear encoded γ subunit of cf0cf1 of the diatom *Odontella sinensis* including its presequence. *FEBS letters*, *320*(1), 61–66.

Park, S., Steen, C. J., Lyska, D., Fischer, A. L., Endelman, B., Iwai, M., Niyogi, K. K., & Fleming, G. R. (2019). Chlorophyll–carotenoid excitation energy transfer and charge transfer in *Nannochloropsis oceanica* for the regulation of photosynthesis. *Proceedings of the National Academy of Sciences*, *116*(9), 3385–3390.

Peers, G., Truong, T. B., Ostendorf, E., Busch, A., Elrad, D., Grossman, A. R., Hippler, M., & Niyogi, K. K. (2009). An ancient light-harvesting protein is critical for the regulation of algal photosynthesis. *Nature*, *462*(7272), 518–521.

Peltier, G., Aro, E.-M., & Shikanai, T. (2016). Ndh-1 and ndh-2 plastoquinone reductases in oxygenic photosynthesis. *Annual review of plant biology*, *67*(1), 55–80.

Perin, G., Bellan, A., Michelberger, T., Lyska, D., Wakao, S., Niyogi, K. K., & Morosinotto, T. (2023). Modulation of xanthophyll cycle impacts biomass productivity in the marine microalga *Nannochloropsis*. *Proceedings of the National Academy of Sciences*, *120*(25), e2214119120.

Perozeni, F., Beghini, G., Cazzaniga, S., & Ballottari, M. (2020). *Chlamydomonas reinhardtii* lhcsr1 and lhcsr3 proteins involved in photoprotective non-photochemical quenching have different quenching efficiency and different carotenoid affinity. *Scientific reports*, *10*(1), 21957.

Petersen, J., Ludewig, A.-K., Michael, V., Bunk, B., Jarek, M., Baurain, D., & Brinkmann, H. (2014). *Chromera velia*, endosymbioses and the rhodoplex hypothesis—plastid evolution in cryptophytes, alveolates, stramenopiles, and haptophytes (cash lineages). *Genome biology and evolution*, *6*(3), 666–684.

Pfündel, E. E. (2021). Simultaneously measuring pulse-amplitude-modulated (pam) chlorophyll fluorescence of leaves at wavelengths shorter and longer than 700 nm. *Photosynthesis research*, *147*(3), 345–358.

Pfündel, E. E., Klughammer, C., Meister, A., & Cerovic, Z. G. (2013). Deriving fluorometer-specific values of relative psi fluorescence intensity from quenching of f 0 fluorescence

in leaves of *Arabidopsis thaliana* and *Zea mays*. *Photosynthesis research*, *114*(3), 189–206.

Pierella Karlusich, J. J., Ibarbalz, F. M., & Bowler, C. (2020). Phytoplankton in the tara ocean. *Annual Review of Marine Science*, *12*(1), 233–265.

Pinnola, A., Dall'Osto, L., Gerotto, C., Morosinotto, T., Bassi, R., & Alboresi, A. (2013). Zeaxanthin binds to light-harvesting complex stress-related protein to enhance non-photochemical quenching in *Physcomitrella patens*. *The Plant Cell*, *25*(9), 3519–3534.

Prihoda, J., Tanaka, A., de Paula, W. B., Allen, J. F., Tirichine, L., & Bowler, C. (2012). Chloroplast-mitochondria cross-talk in diatoms. *Journal of Experimental Botany*, *63*(4), 1543–1557.

Pruitt, R. E., & Meyerowitz, E. M. (1986). Characterization of the genome of *Arabidopsis thaliana*. *Journal of Molecular Biology*, *187*(2), 169–183.

Redekop, P., Rothhausen, N., Rothhausen, N., Melzer, M., Mosebach, L., Dülger, E., Bovdilova, A., Caffarri, S., Hippler, M., & Jahns, P. (2020). Psbs contributes to photoprotection in *Chlamydomonas reinhardtii* independently of energy dissipation. *Biochimica et Biophysica Acta (BBA)-Bioenergetics*, *1861*(5-6), 148183.

Redekop, P., Sanz-Luque, E., Yuan, Y., Villain, G., Petroutsos, D., & Grossman, A. R. (2022). Transcriptional regulation of photoprotection in dark-to-light transition—more than just a matter of excess light energy. *Science Advances*, *8*(22), eabn1832.

Rosenwasser, S., Graff van Creveld, S., Schatz, D., Malitsky, S., Tzfadia, O., Aharoni, A., Levin, Y., Gabashvili, A., Feldmesser, E., & Vardi, A. (2014). Mapping the diatom redox-sensitive proteome provides insight into response to nitrogen stress in the marine environment. *Proceedings of the National Academy of Sciences*, *111*(7), 2740–2745.

Ruban, A. V., Berera, R., Ilioaia, C., Van Stokkum, I. H., Kennis, J. T., Pascal, A. A., Van Amerongen, H., Robert, B., Horton, P., & Van Grondelle, R. (2007). Identification of a mechanism of photoprotective energy dissipation in higher plants. *Nature*, *450*(7169), 575–578.

Ruiz-Sola, M. Á., Flori, S., Yuan, Y., Villain, G., Sanz-Luque, E., Redekop, P., Tokutsu, R., Küken, A., Tsichla, A., Kepesidis, G., et al. (2023). Light-independent regulation of algal photoprotection by co2 availability. *Nature communications*, *14*(1), 1977.

Rutherford, A. W., Osyczka, A., & Rappaport, F. (2012). Back-reactions, short-circuits, leaks and other energy wasteful reactions in biological electron transfer: Redox tuning to survive life in o2. *FEBS Letters*, *586*(5), 603–616.

Ryan-Keogh, T. J., & Thomalla, S. J. (2020). Deriving a proxy for iron limitation from chlorophyll fluorescence on buoyancy gliders. *Frontiers in Marine Science*, *7*, 275.

Sacksteder, C. A., & Kramer, D. M. (2000). Dark-interval relaxation kinetics (dirk) of absorbance changes as a quantitative probe of steady-state electron transfer. *Photosynthesis Research*, *66*, 145–158.

Santabarbara, S., Bullock, B., Rappaport, F., & Redding, K. E. (2015). Controlling electron transfer between the two cofactor chains of photosystem i by the redox state of one of their components. *Biophysical Journal*, *108*(6), 1537–1547.

Santin, A., Caputi, L., Longo, A., Chiurazzi, M., Ribera d'Alcalà, M., Russo, M. T., Ferrante, M. I., & Rogato, A. (2021). Integrative omics identification, evolutionary and structural analysis of low affinity nitrate transporters in diatoms, dinpfs. *Open Biology*, *11*(4), 200395.

Savikhin, S., Xu, W., Chitnis, P. R., & Struve, W. S. (2000). Ultrafast primary processes in ps i from *Synechocystis* sp. pcc 6803: Roles of p700 and a0. *Biophysical Journal*, *79*(3), 1573–1586.

Schiphorst, C., Koeman, C., Caracciolo, L., Staring, K., Theeuwen, T. P., Driever, S. M., Harbinson, J., & Wientjes, E. (2023). The effects of different daily irradiance profiles on *Arabidopsis* growth, with special attention to the role of psbs. *Frontiers in Plant Science*, *14*, 1070218.

Schreiber, U. (1986). Detection of rapid induction kinetics with a new type of high-frequency modulated chlorophyll fluorometer. *Current Topics in Photosynthesis*, 259–270.

Schreiber, U. (2023). Light-induced changes of far-red excited chlorophyll fluorescence: Further evidence for variable fluorescence of photosystem i in vivo. *Photosynthesis Research*, *155*(3), 247–270.

Schuback, N., Hoppe, C. J., Tremblay, J.-É., Maldonado, M. T., & Tortell, P. D. (2017). Primary productivity and the coupling of photosynthetic electron transport and carbon fixation in the arctic ocean. *Limnology and Oceanography*, *62*(3), 898–921.

Schuldiner, S., Rottenberg, H., & Avron, M. (1972). Determination of Δph in chloroplasts: 2. fluorescent amines as a probe for the determination of Δph in chloroplasts. *European Journal of Biochemistry*, *25*(1), 64–70.

Schumann, A., Goss, R., Jakob, T., & Wilhelm, C. (2007). Investigation of the quenching efficiency of diatoxanthin in cells of *Phaeodactylum tricornutum* (bacillariophyceae) with different pool sizes of xanthophyll cycle pigments. *Phycologia*, *46*(1), 113–117.

Schweizer, T., Kubach, H., & Koch, T. (2021). Investigations to characterize the interactions of light radiation, engine operating media and fluorescence tracers for the use of qualitative light-induced fluorescence in engine systems. *Automotive and Engine Technology*, *6*(3), 275–287.

Seelert, H., Dencher, N. A., & Müller, D. J. (2003). Fourteen protomers compose the oligomer iii of the proton-rotor in spinach chloroplast atp synthase. *Journal of Molecular Biology*, *333*(2), 337–344.

Serif, M., Lepetit, B., Weißert, K., Kroth, P. G., & Bartulos, C. R. (2017). A fast and reliable strategy to generate talen-mediated gene knockouts in the diatom *Phaeodactylum tricornutum*. *Algal Research*, *23*, 186–195.

Seydoux, C., Storti, M., Giovagnetti, V., Matuszyńska, A., Guglielmino, E., Zhao, X., Giustini, C., Pan, Y., Blommaert, L., Angulo, J., et al. (2022). Impaired photoprotection in *Phaeodactylum tricornutum* kea3 mutants reveals the proton regulatory circuit of diatoms light acclimation. *New Phytologist*, *234*(2), 578–591.

Sezginer, Y., Campbell, D., Pillai, S., & Tortell, P. (2023). Fluorescence-based primary productivity estimates are influenced by non-photochemical quenching dynamics in arctic phytoplankton. *Frontiers in Microbiology*, *14*, 1294521.

Shelake, R. M., Pramanik, D., & Kim, J.-Y. (2019). Evolution of plant mutagenesis tools: A shifting paradigm from random to targeted genome editing. *Plant Biotechnology Reports*, *13*, 423–445.

Shimakawa, G., Yashiro, E., & Matsuda, Y. (2023). Mapping of subcellular local ph in the marine diatom *Phaeodactylum tricornutum*. *Physiologia Plantarum*, *175*(6), e14086.

Short, A., Fay, T. P., Crisanto, T., Mangal, R., Niyogi, K. K., Limmer, D. T., & Fleming, G. R. (2023). Kinetics of the xanthophyll cycle and its role in photoprotective memory and response. *Nature Communications*, *14*(1), 6621.

Simionato, D., Basso, S., Zaffagnini, M., Lana, T., Marzotto, F., Trost, P., & Morosinotto, T. (2015). Protein redox regulation in the thylakoid lumen: The importance of disulfide bonds for violaxanthin de-epoxidase. *FEBS Letters*, *589*(8), 919–923.

Sipka, G., Nagy, L., Magyar, M., Akhtar, P., Shen, J.-R., Holzwarth, A., Lambrev, P., & Garab, G. (2022). Light-induced reversible reorganizations in closed type ii reaction

centre complexes: Physiological roles and physical mechanisms. *Open Biology*, *12*(12), 220297.

Smith, S. R., Dupont, C. L., McCarthy, J. K., Broddrick, J. T., Oborník, M., Horák, A., Füssy, Z., Cihlář, J., Kleessen, S., Zheng, H., et al. (2019). Evolution and regulation of nitrogen flux through compartmentalized metabolic networks in a marine diatom. *Nature Communications*, *10*(1), 4552.

Sonoike, K. (2011). Photoinhibition of photosystem i. *Physiologia plantarum*, *142*(1), 56–64.

Srivastava, A., Jüttner, F., & Strasser, R. J. (1998). Action of the allelochemical, fischerellin a, on photosystem ii. *Biochimica et Biophysica Acta (BBA)-Bioenergetics*, *1364*(3), 326–336.

Stamatakis, K., Broussos, P.-I., Panagiotopoulou, A., Gast, R. J., Pelecanou, M., & Papageorgiou, G. C. (2019). Light-adaptive state transitions in the ross sea haptophyte *Phaeocystis antarctica* and in dinoflagellate cells hosting kleptoplasts derived from it. *Biochimica et Biophysica Acta (BBA)-Bioenergetics*, *1860*(1), 102–110.

Stiller, J. W., Schreiber, J., Yue, J., Guo, H., Ding, Q., & Huang, J. (2014). The evolution of photosynthesis in chromist algae through serial endosymbioses. *Nature Communications*, *5*(1), 5764.

Stirbet, A. (2013). Excitonic connectivity between photosystem ii units: What is it, and how to measure it? *Photosynthesis research*, *116*, 189–214.

Stransky, H., & Hager, A. (1970). The carotenoid pattern and the occurrence of the light induced xanthophyll cycle in various classes of algae: Vi. chemosystematic study. *Archiv für Mikrobiologie*, *73*, 315–323.

Su, P.-H., & Lai, Y.-H. (2017). A reliable and non-destructive method for monitoring the stromal ph in isolated chloroplasts using a fluorescent ph probe. *Frontiers in plant science*, *8*, 2079.

Sukenik, A., Bennett, J., & Falkowski, P. (1987). Light-saturated photosynthesis—limitation by electron transport or carbon fixation? *Biochimica et Biophysica Acta (BBA)-Bioenergetics*, *891*(3), 205–215.

Taddei, L., Chukhutsina, V. U., Lepetit, B., Stella, G. R., Bassi, R., van Amerongen, H., Bouly, J.-P., Jaubert, M., Finazzi, G., & Falciatore, A. (2018). Dynamic changes between two lhcx-related energy quenching sites control diatom photoacclimation. *Plant Physiology*, *177*(3), 953–965.

Taddei, L., Stella, G. R., Rogato, A., Bailleul, B., Fortunato, A. E., Annunziata, R., Sanges, R., Thaler, M., Lepetit, B., Lavaud, J., et al. (2016). Multisignal control of expression of the lhcx protein family in the marine diatom *Phaeodactylum tricornutum*. *Journal of experimental botany*, *67*(13), 3939–3951.

Teissie, J., & Rols, M.-P. (1993). An experimental evaluation of the critical potential difference inducing cell membrane electropermeabilization. *Biophysical journal*, *65*(1), 409–413.

Telfer, A., Barber, J., Heathcote, P., & Evans, M. (1978). Variable chlorophyll a fluorescence from p-700 enriched photosystem i particles dependent on the redox state of the reaction centre. *Biochimica et Biophysica Acta (BBA)-Bioenergetics*, *504*(1), 153–164.

Tian, L., Nawrocki, W. J., Liu, X., Polukhina, I., Van Stokkum, I. H., & Croce, R. (2019). Ph dependence, kinetics and light-harvesting regulation of nonphotochemical quenching in *Chlamydomonas*. *Proceedings of the National Academy of Sciences*, *116*(17), 8320–8325.

Tibiletti, T., Auroy, P., Peltier, G., & Caffarri, S. (2016). *Chlamydomonas reinhardtii* psbs protein is functional and accumulates rapidly and transiently under high light. *Plant physiology*, *171*(4), 2717–2730.

Tikhonov, A. N. (2014). The cytochrome b6f complex at the crossroad of photosynthetic electron transport pathways. *Plant Physiology and Biochemistry*, *81*, 163–183.

Ting, C. S., & Owens, T. G. (1993). Photochemical and nonphotochemical fluorescence quenching processes in the diatom *Phaeodactylum tricornutum*. *Plant Physiology*, *101*(4), 1323–1330.

Tréguer, P., Bowler, C., Moriceau, B., Dutkiewicz, S., Gehlen, M., Aumont, O., Bittner, L., Dugdale, R., Finkel, Z., Iudicone, D., et al. (2018). Influence of diatom diversity on the ocean biological carbon pump. *Nature Geoscience*, *11*(1), 27–37.

Tréguer, P. J., & De La Rocha, C. L. (2013). The world ocean silica cycle. *Annual review of marine science*, *5*(1), 477–501.

Trissl, H.-W., Gao, Y., & Wulf, K. (1993). Theoretical fluorescence induction curves derived from coupled differential equations describing the primary photochemistry of photosystem ii by an exciton-radical pair equilibrium. *Biophysical journal*, *64*(4), 974–988.

Troiano, J. M., Perozeni, F., Moya, R., Zuliani, L., Baek, K., Jin, E., Cazzaniga, S., Ballottari, M., & Schlau-Cohen, G. S. (2021). Identification of distinct ph-and zeaxanthin-dependent quenching in lhcsr3 from *Chlamydomonas reinhardtii*. *Elife*, *10*, e60383.

Turina, P., Petersen, J., & Gräber, P. (2016). Thermodynamics of proton transport coupled atp synthesis. *Biochimica et Biophysica Acta (BBA)-Bioenergetics*, *1857*(6), 653–664.

Van Creveld, S. G., Rosenwasser, S., Schatz, D., Koren, I., & Vardi, A. (2015). Early perturbation in mitochondria redox homeostasis in response to environmental stress predicts cell fate in diatoms. *The ISME Journal*, *9*(2), 385–395.

Van den Berg, T. E., & Croce, R. (2022). The loroxanthin cycle: A new type of xanthophyll cycle in green algae (chlorophyta). *Frontiers in Plant Science*, *13*, 797294.

Vancaester, E., Depuydt, T., Osuna-Cruz, C. M., & Vandepoele, K. (2020). Comprehensive and functional analysis of horizontal gene transfer events in diatoms. *Molecular Biology and Evolution*, *37*(11), 3243–3257.

Vass, I. (2012). Molecular mechanisms of photodamage in the photosystem ii complex. *Biochimica et Biophysica Acta (BBA)-Bioenergetics*, *1817*(1), 209–217.

Verhoeven, A., García-Plazaola, J. I., & Fernández-Marín, B. (2018). Shared mechanisms of photoprotection in photosynthetic organisms tolerant to desiccation or to low temperature. *Environmental and Experimental Botany*, *154*, 66–79.

Viola, S., Bailleul, B., Yu, J., Nixon, P., Sellés, J., Joliot, P., & Wollman, F.-A. (2019). Probing the electric field across thylakoid membranes in cyanobacteria. *Proceedings of the National Academy of Sciences*, *116*(43), 21900–21906.

Viola, S., Roseby, W., Santabarbara, S., Nürnberg, D., Assunção, R., Dau, H., Sellés, J., Boussac, A., Fantuzzi, A., & Rutherford, A. W. (2022). Impact of energy limitations on function and resilience in long-wavelength photosystem ii. *Elife*, *11*, e79890.

Volpert, A., Graff van Creveld, S., Rosenwasser, S., & Vardi, A. (2018). Diurnal fluctuations in chloroplast gsh redox state regulate susceptibility to oxidative stress and cell fate in a bloom-forming diatom. *Journal of phycology*, *54*(3), 329–341.

von Bismarck, T., Korkmaz, K., Ruß, J., Skurk, K., Kaiser, E., Correa Galvis, V., Cruz, J. A., Strand, D. D., Köhl, K., Eirich, J., et al. (2023). Light acclimation interacts with thylakoid ion transport to govern the dynamics of photosynthesis in *Arabidopsis*. *New Phytologist*, *237*(1), 160–176.

von Bismarck, T., Wendering, P., Perez de Souza, L., Ruß, J., Strandberg, L., Heyneke, E., Walker, B. J., Schöttler, M. A., Fernie, A. R., Nikoloski, Z., et al. (2023). Growth in fluctuating light buffers plants against photorespiratory perturbations. *Nature Communications*, *14*(1), 7052.

Weis, E., & Berry, J. A. (1987). Quantum efficiency of photosystem ii in relation to 'energy'-dependent quenching of chlorophyll fluorescence. *Biochimica et Biophysica Acta (BBA)-Bioenergetics*, *894*(2), 198–208.

Werdan, K., Heldt, H. W., & Milovancev, M. (1975). The role of ph in the regulation of carbon fixation in the chloroplast stroma. studies on co2 fixation in the light and dark. *Biochimica et Biophysica Acta (BBA)-Bioenergetics*, *396*(2), 276–292.

Wientjes, E., & Croce, R. (2012). Pms: Photosystem i electron donor or fluorescence quencher. *Photosynthesis research*, *111*, 185–191.

Wietrzynski, W., Schaffer, M., Tegunov, D., Albert, S., Kanazawa, A., Plitzko, J. M., Baumeister, W., & Engel, B. D. (2020). Charting the native architecture of *Chlamydomonas* thylakoid membranes with single-molecule precision. *Elife*, *9*, e53740.

Wilhelm, C., & Wild, A. (1984). The variability of the photosynthetic unit in *Chlorella* i. the effect of vanadium on photosynthesis, productivity, p700 and cytochrome f in undiluted and homocontinuous cultures of *Chlorella*. *Journal of plant physiology*, *115*(2), 115–124.

Wilhelm, C., Goss, R., & Garab, G. (2020). The fluid-mosaic membrane theory in the context of photosynthetic membranes: Is the thylakoid membrane more like a mixed crystal or like a fluid? *Journal of Plant Physiology*, *252*, 153246.

Witt, H. (1979). Energy conversion in the functional membrane of photosynthesis. analysis by light pulse and electric pulse methods: The central role of the electric field. *Biochimica et Biophysica Acta (BBA)-Reviews on Bioenergetics*, *505*(3-4), 355–427.

Wolfram, S., Wielsch, N., Hupfer, Y., Mönch, B., Lu-Walther, H.-W., Heintzmann, R., Werz, O., Svatoš, A., & Pohnert, G. (2015). A metabolic probe-enabled strategy reveals uptake and protein targets of polyunsaturated aldehydes in the diatom *Phaeodactylum tricornutum*. *Plos one*, *10*(10), e0140927.

Wollenberger, L., Stefansson, H., Yu, S.-G., & Albertsson, P.-Å. (1994). Isolation and characterization of vesicles originating from the chloroplast grana margins. *Biochimica et Biophysica Acta (BBA)-Bioenergetics*, *1184*(1), 93–102.

Wollman, F.-A. (2001). State transitions reveal the dynamics and flexibility of the photosynthetic apparatus. *The EMBO journal*.

Xu, P., Chukhutsina, V. U., Nawrocki, W. J., Schansker, G., Bielczynski, L. W., Lu, Y., Karcher, D., Bock, R., & Croce, R. (2020). Photosynthesis without β-carotene. *Elife*, *9*, e58984.

Yamamoto, H. Y. (1979). Biochemistry of the violaxanthin cycle in higher plants. In *Carotenoids℃ 5* (pp. 639–648). Elsevier.

Yamamoto, H., Nakayama, T., & Chichester, C. (1962). Studies on the light and dark interconversions of leaf xanthophylls. *Archives of Biochemistry and Biophysics*, *97*(1), 168–173.

Yokono, M., Murakami, A., & Akimoto, S. (2011). Excitation energy transfer between photosystem ii and photosystem i in red algae: Larger amounts of phycobilisome enhance spillover. *Biochimica et Biophysica Acta (BBA)-Bioenergetics*, *1807*(7), 847–853.

Yoon, H. S., Hackett, J. D., Van Dolah, F. M., Nosenko, T., Lidie, K. L., & Bhattacharya, D. (2005). Tertiary endosymbiosis driven genome evolution in dinoflagellate algae. *Molecular Biology and Evolution*, *22*(5), 1299–1308.

Zheng, M., Pang, X., Chen, M., & Tian, L. (2024). Ultrafast energy quenching mechanism of lhcsr3-dependent photoprotection in *Chlamydomonas*. *Nature Communications*, *15*(1), 4437.

Zhu, S.-H., & Green, B. R. (2010). Photoprotection in the diatom *Thalassiosira pseudonana*: Role of li818-like proteins in response to high light stress. *Biochimica et Biophysica Acta (BBA)-Bioenergetics*, *1797*(8), 1449–1457.

Zu Tittingdorf, J. M. M., Rexroth, S., Schäfer, E., Schlichting, R., Giersch, C., Dencher, N. A., & Seelert, H. (2004). The stoichiometry of the chloroplast atp synthase oligomer iii in *Chlamydomonas reinhardtii* is not affected by the metabolic state. *Biochimica et Biophysica Acta (BBA)-Bioenergetics*, *1659*(1), 92–99.